

MASSACHUSETTS INSTITUTE OF TECHNOLOGY

The RESEARCH LABORATORY *of* ELECTRONICS

PROGRESS REPORT

NO. 132

JANUARY 1-DECEMBER 31, 1989

AD-A225 355

1

DTIC

ELECTE

JUL 24 1990

DTIC

Approved for Release

Dissemination

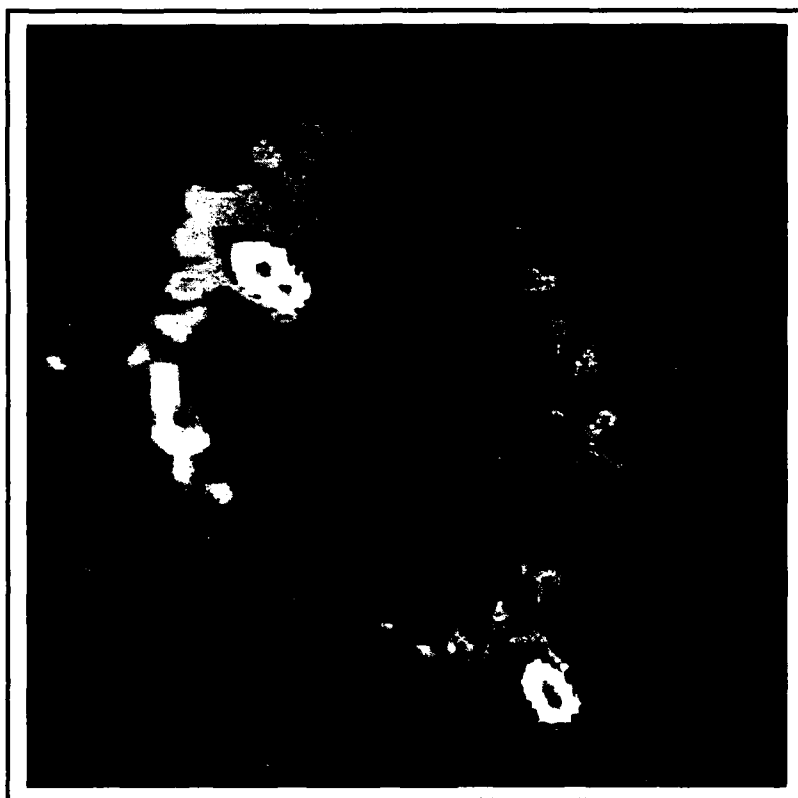
RLE Progress Report

No. 132

January 1 - December 31, 1989

Submitted by

Professor Jonathan Allen
Professor Daniel Kleppner



**Research Laboratory of Electronics
Massachusetts Institute of Technology
Cambridge, MA 02139 USA**

Accession For	
NTIS CRA&I	<input checked="" type="checkbox"/>
DTIC TAB	<input type="checkbox"/>
Unannounced	<input type="checkbox"/>
Justification	
By <i>No charge</i>	
Distribution <i>per lti</i>	
Availability Codes	
Dist	Avail and/or Special
<i>A-1</i>	

RLE Progress Report No. 132

Cover and title page: Shown is the image of an Einstein ring gravitational lens. The data represented in blue was acquired with a Very Large Array (VLA) telescope operated by the National Radio Astronomy Observatory in New Mexico. The line drawing on top is a calculation of the appearance of an Einstein ring based on light propagation through a gravitational field. Symmetry of a ring makes a system such as this one particularly attractive as an astrophysics laboratory. Some of Professor Jacqueline N. Hewitt's research is aimed at exploiting this (see page 231 of this report).

Our special thanks to the following staff members of the RLE Communications Group: Mary J. Ziegler for her exceptional editing, formatting, and scanning; Mary S. Greene for proofreading and preparation of the publications and personnel chapters; and Rita C. McKinnon for her help with proofreading. We also want to thank David W. Foss, Manager of the RLE Computer Facility, for his technical assistance and Donna M. Ticchi, RLE Administrative Officer, for her help with the personnel sections of this report.

We thank the faculty, staff, and students of RLE for their generous cooperation.

Editor:	Barbara Passero
Design and Illustration:	Robert H. Priest
Printer:	CSA Press, Hudson, Massachusetts
Photography:	John F. Cook
Typesetting:	This report was produced with IBM's BookMaster Software. Mylar negatives were printed on an IBM 4250-II electro-erosion printer.

©Massachusetts Institute of Technology. 1990. All rights reserved.

Table of Contents

INTRODUCTION	1
PART I SOLID STATE PHYSICS, ELECTRONICS AND OPTICS	
Section 1 Materials and Fabrication	5
Chapter 1 Submicron Structures Technology and Research	7
<i>Professor Henry I. Smith</i>	
1.1 Submicron Structures Laboratory	7
● 1.2 Microfabrication at Linewidths of 100nm and Below	7
1.3 Improved Mask Technology For X-Ray Lithography	9
● 1.4 Study of Electron Transport in Si MOSFETs with Deep-Submicron Channel Lengths	9
● 1.5 Studies of Electronic Conduction in One-Dimensional Semiconductor Devices	10
● 1.6 Surface Superlattice Formation in Silicon Inversion Layers Using 0.2 μm -Period Grating-Gate Field-Effect Transistors	12
1.7 Study of Surface Superlattice Formation in GaAs/GaAlAs Modulation Doped Field-Effect Transistors	13
● 1.8 Study of One-Dimensional Subbands and Mobility Modulation in GaAs/AlGaAs Quantum Wires	14
● 1.9 Arrays of Field-Effect-Induced Quantum Dots	14
1.10 Planar-Resonant-Tunneling Field-Effect Transistors (PRESTFETs)	16
● 1.11 Submicrometer-Period Gold Transmission Gratings for X-Ray Spectroscopy and Atom-Beam Interferometry	17
1.12 High-Dispersion, High-Efficiency Transmission Gratings for Astrophysical Spectroscopy	17
1.13 Epitaxy via Surface-Energy-Driven Grain Growth	18
Chapter 2 Microstructural Evolution in Thin Films of Electronic Materials	21
<i>Professor Carl V. Thompson</i>	
● 2.1 Modeling of Microstructural Evolution in Thin Films	21
● 2.2 Reliability and Microstructures of Interconnects	22
2.3 Epitaxial Grain Growth	23
2.4 Heteroepitaxy in Lattice Mismatched Systems	24
2.5 Kinetics of Thin Film Silicide Formation	24
2.6 Coarsening of Particles on a Planar Substrate	25
2.7 Thin Film Zone Melting Recrystallization of Silicon	25
2.8 Capillary Instabilities in Thin Solid Films	25
2.9 Focused Ion Beam Induced Deposition	25
2.10 Protective Coatings for Integrated Circuits in an In Vitro Environment	26

Table of Contents

Chapter 3	Focused Ion Beam Fabrication	29
	<i>Dr. John Melngailis</i>	
3.1	Focused Ion Beam Fabrication	29
3.2	Development of Focused Ion Beam Implantation and Lithography	29
3.3	Frequency Tunable Gunn Diodes Fabricated by Focused Ion Beam Implantation	30
3.4	NMOS Transistors with Focused Ion Beam Implanted Channel Regions	30
3.5	GaAs MESFETs Fabricated with Focused Ion Beam Channel Implants	31
3.6	Focused Ion Beam Exposure of Resists	31
3.7	Focused Ion Beam Induced Deposition of Low Resistivity Gold Structures	31
3.8	Fundamental Properties of Ion Induced Deposition	32
3.9	In-Situ Measurement of Gas Adsorption and Ion Induced Deposition	32
3.10	Focused Ion Beam induced Deposition of Platinum	33
Chapter 4	Chemical Reaction Dynamics at Surfaces	35
	<i>Professor Sylvia T. Ceyer</i>	
4.1	Chemical Reaction Dynamics on Semiconductor Surfaces	35
4.2	Collision Induced Dissociative Chemisorption of CH_4 on Ni(111) by Inert Gas Atoms: The Mechanism for Chemistry with a Hammer	36
4.3	Collision Induced Desorption	37
4.4	Synthesis of Benzene from Methane	38
4.5	The Structure and Chemistry of CH_3 and CH Radicals and Isotopic Variants Adsorbed on Ni(111)	38
4.6	High Resolution Electron Energy Loss Spectroscopy of H on Ni(111)	39
Chapter 5	Measurement of Electron-phonon Interactions Through Large-amplitude Phonon Excitation	41
	<i>Professor Keith A. Nelson</i>	
5.1	Introduction	41
5.2	High Repetition-rate Signals and Resonant Responses of Crystalline Solids	41
Chapter 6	Chemical Beam Epitaxy of Compound Semiconductors	47
	<i>Professor Leslie A. Kolodziejski</i>	
6.1	Chemical Beam Epitaxy Facility	47
6.2	Controlled Substitutional Doping of ZnSe Grown by Chemical Beam Epitaxy	49
6.3	Laser-Assisted Chemical Beam Epitaxy of Wide Bandgap Blue/Green II-VI Semiconductors	50
Chapter 7	High-Frequency InAlAs/InGaAs Metal-Insulator-Doped Semiconductor Field-Effect Transistors (MIDFETs) for Telecommunications	53
	<i>Professor Jesus A. del Alamo</i>	
7.1	Introduction	53
7.2	Experiments	54
7.3	Device Results	54
Chapter 8	Novel Superconducting Tunneling Structures	59
	<i>Professor John M. Graybeal</i>	
8.1	Project Description	59

Table of Contents

Chapter 9	Heterostructures for High Performance Devices	61
	<i>Professor Clifton G. Fonstad, Jr.</i>	
9.1	Introduction	61
● 9.2	Computer Controlled Growth of Lattice-Matched InGaAlAs Heterostructures on InP	61
9.3	InGaAlAs Multiple Quantum Well Heterostructures for Guided Wave Optics	62
9.4	MBE-Grown InGaAlAs/InP Long-Wavelength Laser Diodes for Narrow Linewidth Applications	63
● 9.5	InGaAlAs Strained-Layer Heterostructures on 111 GaAs and InP for Optical for Modulator Applications	64
9.6	Molecular Beam Epitaxial Growth on (h11) Vicinal Surfaces	65
● 9.7	Pseudomorphic AlAs/InAs/InGaAs Resonant Tunneling Structures	65
● 9.8	Three-Terminal Quantum Well Base/Tunnel Barrier Devices	66
9.9	Design and Fabrication of GaAlAs Heterostructure Laser Diodes for Monolithic Integration with Si Circuits	66
9.10	Microbridge Suspension of Monolithic GaAlAs Heterostructures Grown on Si by MBE	67
9.11	Damage-Free In-Situ UHV Etching and Cleaning of III-V Heterostructures Using Molecular Beams	68
Section 2	Optics and Devices	71
Chapter 1	Optics and Quantum Electronics	73
	<i>Professor Hermann A. Haus, Professor Erich P. Ippen, Professor James G. Fujimoto, Professor Peter L. Hagelstein, Dr. Santanu Basu, Dr. Jyhpyng Wang</i>	
● 1.1	The Nonlinear Waveguide Interferometer	73
1.2	Picosecond Optical Signal Sampling	74
● 1.3	Nonlinear Dynamics in Active Semiconductor Waveguides	75
● 1.4	Saturation Characteristics of Semiconductor Optical Amplifiers	76
● 1.5	Femtosecond Studies of Metallic and High Tc Superconductors	76
● 1.6	Suppressed and Enhanced Spontaneous Emission from Microcavities	77
● 1.7	New Ultrashort Pulse Laser Technology	78
● 1.8	Ultrafast Processes in Waveguide Devices	80
● 1.9	Image Potential and Electron Dynamics in Metals	82
1.10	Laser Medicine	83
1.11	Developmental Status of a Table-top XUV Laser at 194 Angstrom	86
1.12	Status of Zig-zag Slab Laser Development	88
1.13	Whisper Gallery Mirror Design	89
1.14	Polarizing Cavities for the Extreme Ultraviolet	90
1.15	Unstable Resonators for XUV Lasers	92
1.16	Advances in Conjugate Gradient Algorithm Development	93
1.17	Frequency Upconversion of Extreme UV Radiation	94
1.18	X-ray Detectors Based on the Quantum Well Nonlinearity	96
1.19	A Simple Line Shape Model for GaAs Multiple Quantum Wells	96
1.20	Coherent Fusion Theory	98
Chapter 2	Novel Processes and Materials for Infrared Nonlinear Optics	103
	<i>Professor Peter A. Wolff, Dr. Sunny Y. Auyang</i>	
2.1	Project Description	103

Table of Contents

Section 3	Surfaces and Interfaces	107
Chapter 1	Statistical Mechanics of Surface Systems and Quantum-Correlated Systems	109
	<i>Professor A. Nihat Berker</i>	
• 1.1	Introduction	109
• 1.2	Finite-Temperature Phase Diagram of Vicinal Si(100) Surfaces	109
• 1.3	Absence of First-Order Phase Transitions in Physical Surface Systems	109
• 1.4	New Orderings in Systems with Competing Interactions	110
Chapter 2	X-Ray Diffuse Scattering	111
	<i>Professor Robert J. Birgeneau</i>	
• 2.1	Introduction	111
• 2.2	Metal Surface Studies	111
• 2.3	Semiconductor Surface Studies	112
• 2.4	Rare Gases in Graphite	113
Chapter 3	Semiconductor Surface Studies	115
	<i>Professor John D. Joannopoulos</i>	
• 3.1	Introduction	115
• 3.2	Thermal Amplitudes of Surface Atoms	115
• 3.3	Heteroepitaxial Growth	118
Chapter 4	Ultralow Temperature Studies of Nanometer Size Semiconductor Devices	121
	<i>Professor Marc A. Kastner</i>	
• 4.1	Project Description	121
Chapter 5	The Quantum Hall Effect in Narrow MOSFETs	123
	<i>Professor Patrick A. Lee</i>	
• 5.1	Project Description	123
Chapter 6	Epitaxy and Step Structures on Semiconductor Surfaces	125
	<i>Professor Simon G.J. Mochrie</i>	
• 6.1	Project Description	125
PART II	APPLIED PHYSICS	
Section 1	Atomic, Molecular and Optical Physics	129
Chapter 1	Quantum Optics and Photonics	131
	<i>Professor Shaoul Ezekiel</i>	
1.1	Microwave Phase Dependent Optical Absorption	131
1.2	A New Approach to Microwave Excitation of Atomic Beams	132
1.3	Stimulated Brillouin Fiberoptic Gyroscope	136

Table of Contents

Chapter 2	Basic Atomic Physics	139
	<i>Professor Daniel Kleppner, Professor David E. Pritchard</i>	
● 2.1	Experimental Study of Small Ensembles of Atoms in a Microwave Cavity	139
2.2	Rydberg Atoms in a Magnetic Field	143
2.3	Millimeter-Wave Measurement of the Rydberg Constant	146
● 2.4	Precision Mass Spectroscopy of Ions	148
2.5	Neutral Atom Trap	153
Chapter 3	Small Angle X-Ray and Neutron Scattering - Its Application to Supramolecular Solutions	157
	<i>Professor Sow-Hsin Chen</i>	
3.1	Interlayer Diffusion in Langmuir-Blodgett Films	157
3.2	Thermodynamics of Protein/Surfactant Complex in Aqueous Solution and Reptation Mechanism for Protein/SDS Polyacrylamide Gel Electrophoresis	158
3.3	Phase Separation in a Lipid/Water/Urea Micellar System	160
3.4	Ion Distribution and Solubilization in Reverse Micelles	160
3.5	Ion Distribution around DNA Molecules	160
3.6	Structural Study of Vesicles Formed from a New Bolaamphiphile	161
3.7	Photon Correlation Spectroscopy and Its Applications: Dynamic Transition at the Percolation Threshold of a Three-Component Microemulsion	163
Section 2	Plasma Physics	165
Chapter 1	Plasma Dynamics	167
	<i>Professor George Bekefi, Professor Abraham Bers, Professor Bruno Coppi, Professor Miklos Porkolab, Riccardo Betti, Dr. Paolo Detragiache, Dr. Ronald C. Englade, Dr. Stanley C. Luckhardt, Dr. Stefano Migliuolo, Dr. Abhay K. Ram, Dr. Linda E. Sugiyama</i>	
1.1	Relativistic Electron Beams	167
1.2	Plasma Wave Interactions - RF Heating and Current Generation	169
1.3	Physics of Thermonuclear Plasmas	181
1.4	Investigation of Electron Cyclotron Resonance Plasma Production in the Versator II Tokamak	191
Section 3	Electromagnetics	195
Chapter 1	Electromagnetic Wave Theory and Applications	197
	<i>Professor Jin Au Kong, Dr. Sami M. Ali, Dr. Robert T. Shin, Dr. Ying-Ching E. Yang</i>	
● 1.1	Electromagnetic Waves in Multilayer Media	197
1.2	Remote Sensing of Earth Terrain	202
1.3	Remote Sensing of Sea Ice	208
1.4	SAR Image Interpretation and Simulation	212
1.5	Microwave and Millimeter Wave Integrated Circuits	215
1.6	High-Speed Integrated Circuit Interconnects	218
1.7	ILS/MLS Frequency Management Assessment	220

Table of Contents

Section 4 Radio Astronomy 223

Chapter 1 Radio Astronomy 225

*Professor Bernard F. Burke, Professor David H. Staelin, Professor Jacqueline N. Hewitt,
Dr. Philip W. Rosenkranz*

1.1	Galactic and Extragalactic Research	225
1.2	Gravitational Lens Search	225
1.3	Orbiting VLBI	229
1.4	Development of an Undergraduate Laboratory	230
1.5	Radio Interferometry of Nearby dMe Stars	231
1.6	Gravitational Lenses as Astrophysical Laboratories	231
1.7	Tiros-N Satellite Microwave Sounder	231
1.8	Long-Baseline Astrometric Interferometer	232
1.9	Nonthermal Radio Emission from the Jovian Planets	232
1.10	High-Resolution Passive Microwave Imaging of Atmospheric Structure	233
1.11	Characterization of Dolphin Whistles	234
1.12	Rapid Precision Net-Form Manufacturing	234

PART III SYSTEMS AND SIGNALS

Section 1 Digital Signal Processing 239

Chapter 1 Signal Processing Research Program 241

Professor Alan V. Oppenheim

1.1	Introduction	241
1.2	Algorithmic Fault Tolerance in Digital Signal Processing	241
1.3	Active Noise Cancellation Using the EM Algorithm	243
1.4	Iterative Maximum Likelihood Time Delay and Doppler Estimation Using Stationary Signals	244
1.5	Estimation and Correction of Geometric Distortions in Side-Scan Sonar Images	245
1.6	An Algorithm Design Environment for Signal Processing	245
1.7	Compiling Signal Processing Algorithms into Architectures	246
1.8	Vector Quantization with Adaptive Structured Codebooks	247
1.9	The Application of Complex Approximation Algorithms to the Design of Robust Range-Dependent Beamformers	249
1.10	Analysis and Applications of an Adaptively Trained Recurrent Neural Network	249
1.11	A Code-Division, Multiple Beam Sonar Imaging System	250
1.12	Back-projection with Fourier Series Expansion and FFT	250
1.13	Iterative Algorithms for Parameter Estimation from Incomplete Data and Their Applications to Signal Processing	251
1.14	Equalization (Identification) of Non-Minimum Phase Systems	251
1.15	Signal Processing with 1/f Processes Using Wavelets	252

Chapter 2 Speech Processing Research Program 253

Professor Jae S. Lim

2.1	Introduction	253
2.2	Development of a 1.5 Kbps Speech Vocoder	253
2.3	A New Method for Representing Speech Spectrograms	254
2.4	A Dual Excitation Speech Model	254
2.5	Image Texture Modeling	255
2.6	Speech Enhancement Techniques for the Dual Excitation Vocoder Model	255

Table of Contents

Chapter 3	Advanced Television Research Program	257
	<i>Professor Jae S. Lim, Professor William F. Schreiber</i>	
3.1	Advanced Television Research Program	257
3.2	Adaptive Amplitude Modulation for Transform Coefficients	258
3.3	Transform Coding for High Definition Television	259
3.4	Filter Design for Multirate Filter Banks	260
3.5	Adaptive Spatiotemporal Filtering	260
3.6	Signal Processing for Advanced Television Systems	261
3.7	Adaptive Frequency Modulation for Satellite Television Systems	261
3.8	Subband Coding for Channel-Compatible Transmission of High-Definition Television	262
3.9	Channel Equalization and Interference Reduction Using Adaptive Amplitude Modulation and Scrambling	263
3.10	A Novel QMF Design Algorithm	264
Chapter 4	Computer-Aided Fabrication System Structure	265
	<i>Professor Donald E. Troxel</i>	
4.1	Introduction	265
4.2	Computer-Aided Fabrication Environment	265
Chapter 5	Optical Propagation and Communication	267
	<i>Professor Jeffrey H. Shapiro, Dr. Robert H. Rediker, Dr. Ngai C. Wong</i>	
5.1	Introduction	267
5.2	Squeezed States of Light	267
5.3	Laser Radar System Theory	269
5.4	Fiber-Coupled External-Cavity Semiconductor High Power Laser	271
5.5	Analog Processing of Optical Wavefronts Using Integrated Guided-Wave Optics	272
Chapter 6	Custom Integrated Circuits	275
	<i>Professor Jonathan Allen, Professor John L. Wyatt, Jr., Professor Srinivas Devadas, Professor Jacob White</i>	
● 6.1	Custom Integrated Circuits	275
6.2	The Vision Chip Project	279
6.3	Techniques for Logic Synthesis, Testing and Design-for-Testability	283
6.4	Mixed Circuit/Device Simulation	288
6.5	Circuit Simulation Algorithms for Specialized Applications	289
6.6	Numerical Simulation of Short Channel MOS Devices	290
6.7	Efficient Capacitance Extraction Algorithms	291
6.8	Parallel Numerical Algorithms	292
6.9	Integrated Circuit Reliability	292
Chapter 7	Neurophysiology and Neural Computation	295
	<i>Professor Jerome Y. Lettvin</i>	
7.1	Abstracts of Doctoral Dissertations	295
7.2	Abstract of Masters Thesis	296

Table of Contents

PART IV LANGUAGE, SPEECH AND HEARING

Section 1	Speech Communication	299
Chapter 1	Speech Communication	301
	<i>Professor Kenneth N. Stevens, Dr. Joseph S. Perkell, Dr. Stefanie Shattuck-Hufnagel</i>	
1.1	Introduction	302
1.2	Studies of the Acoustics, Production and Perception of Speech Sounds	302
1.3	Studies and Models of the Perception and Production of Syllables, Words, and Sentences	306
1.4	Basic Speech Physiology	309
1.5	Speech Production of Cochlear Implant Patients	310
1.6	Phonatory Function Associated with Misuse of the Vocal Mechanism	310
1.7	Computer Facilities	311
Section 2	Sensory Communication	313
Chapter 1	Auditory Psychophysics and Aids for the Deaf	315
	<i>Professor Louis D. Braida, Nathaniel I. Durlach, Dr. William M. Rabinowitz, Dr. Charlotte M. Reed, Dr. Patrick M. Zurek</i>	
1.1	Introduction	315
1.2	Binaural Hearing	315
1.3	Hearing Aid Research	315
1.4	Tactile Communication of Speech	315
1.5	Multimicrophone Hearing Aids	315
1.6	Cochlear Prostheses	316
1.7	Hand Function	316
Section 3	Auditory Physiology	319
Chapter 1	Signal Transmission in the Auditory System	321
	<i>Professor Lawrence S. Frishkopf, Professor Nelson Y.S. Kiang, Professor William T. Peake, Professor William M. Siebert, Professor Thomas F. Weiss, Dr. Bertrand Delgutte, Dr. Donald K. Eddington, Dr. John J. Guinan, Dr. Robert A. Levine</i>	
1.1	Introduction	321
1.2	Signal Transmission in the External- and Middle-Ear	321
1.3	Cochlear Mechanisms	324
1.4	Regeneration of Primary-Auditory Neurons In Vitro	325
1.5	Stimulus Coding in the Auditory Nerve	326
1.6	Middle-Ear Muscle Reflex	327
1.7	Cochlear Efferent System	328
1.8	The Generators of the Brainstem Auditory Evoked Potential	329
1.9	Cochlear Implants	330
1.10	Anatomical Basis for the Relationships between Binaural Hearing and Brainstem Auditory Evoked Potentials in Humans	331

Section 4	Linguistics	335
Chapter 1	Linguistics	337
	<i>Professor Noam Chomsky, Professor Morris Halle</i>	
1.1	Introduction	337
1.2	Abstracts of Doctoral Dissertations	337
APPENDICES		
Appendix A	RLE Publications and Meeting Papers	343
A.1	Meeting Papers Presented	343
A.2	Published Meeting Papers	350
A.3	Meeting Papers Accepted For Publication	354
A.4	Published Journal Articles	355
A.5	Journal Articles Accepted for Publication	363
A.6	Journal Articles Submitted for Publication	366
A.7	Books/Chapters in Books	367
A.8	RLE Publications	368
A.9	Theses	369
A.10	Miscellaneous Publications	371
Appendix B	Current RLE Personnel	373
Appendix C	RLE Research Support Index	379
PROJECT STAFF AND SUBJECT INDEX		383

Introduction

The Research Laboratory of Electronics

The Research Laboratory of Electronics (RLE) was established in 1946 as the Institute's first interdepartmental laboratory. Originally organized under the joint sponsorship of the Departments of Physics and Electrical Engineering, RLE has broadened its interests to cover a wide range of research.

The RLE environment provides both the freedom of action essential in an academic institution and the availability of large-scale laboratory facilities and services required by researchers. RLE's interdisciplinary setting offers many opportunities for creative and collaborative research. By fostering this powerful combination of research and education, RLE effectively penetrates beyond the horizon of new ideas and information.

RLE Progress Report

RLE Progress Report Number 132 describes research programs at RLE for the period January 1 through December 31, 1989. Each chapter of the *Progress Report* contains both a statement of research objectives and a summary of research efforts for research projects listed. Faculty, research staff, students and others who participated in these projects are identified at the beginning of each project, along with sources of funding.

There are three appendices at the end of the report: Appendix A is a bibliography of RLE publications and papers presented by RLE staff during 1989; Appendix B is a roster of current RLE staff; and Appendix C is an index of RLE sponsors. In addition, the Project Staff and Subject Index provides access to the information in this report. *RLE*

RLE Progress Report Number 132 was produced by the RLE Communications Office. Further inquiries may be addressed to:

Research Laboratory of Electronics
Communications Office
Building 36-412
Massachusetts Institute of Technology
Cambridge, Massachusetts 02139
(617) 253-2566

Part I Solid State Physics, Electronics and Optics

Section 1 Materials and Fabrication

Section 2 Optics and Devices

Section 3 Surfaces and Interfaces

Section 1 Materials and Fabrication

Chapter 1 Submicron Structures Technology and Research

**Chapter 2 Microstructural Evolution in Thin Films
 of Electronic Materials**

Chapter 3 Focused Ion Beam Fabrication

Chapter 4 Chemical Reaction Dynamics at Surfaces

**Chapter 5 Measurement of Electron-phonon
 Interactions Through Large-amplitude
 Phonon Excitation**

**Chapter 6 Chemical Beam Epitaxy of Compound
 Semiconductors**

**Chapter 7 High-Frequency InAlAs/InGaAs Metal-Insulator-
 Doped Semiconductor Field-Effect Transistors
 (MIDFETs) for Telecommunications**

Chapter 8 Novel Superconducting Tunneling Structures

Chapter 9 Heterostructures for High Performance Devices

Chapter 1. Submicron Structures Technology and Research

Academic and Research Staff

Professor Henry I. Smith, Professor Dimitri A. Antoniadis, James M. Carter, Professor Jesus A. del Alamo, Professor Marc A. Kastner, Professor Terry P. Orlando, Dr. Mark L. Schattenburg, Professor Carl V. Thompson

Visiting Scientists and Research Affiliates

C.T. Liu,¹ Irving Plotnik,² T.P. Smith,³ Dr. Dan Tsui¹

Graduate Students

Sergio A. Ajuria, Phillip F. Bagwell, Martin Burkhardt, William Chu, Lawrence A. Clevenger, Kathleen R. Early, Cris Eugster, Jerrold A. Floro, Reza A. Ghanbari, Khalid Ismail, Eva Jiran, Harold Kahn, Yao-Ching Ku, Yachin Liu, Hai Longworth, Udi Meirav, Paul G. Meyer, Alberto Moel, Joyce E. Palmer, Samuel L. Park, Hui Meng Quek, John H.F. Scott-Thomas, Ghavam Shahidi, Siang-Chun The, Anthony Yen

Undergraduate Students

JoAnne Gutierrez, Kenneth Lu, Pablo Munguia, Lisa Su, Flora S. Tsai, Vincent Wong, Howard Zolla

Technical and Support Staff

Donna Martinez, Timothy McClure

1.1 Submicron Structures Laboratory

The Submicron Structures Laboratory at MIT develops techniques for fabricating surface structures with linewidths in the range from nanometers to micrometers, and uses these structures in a variety of research projects. These projects of the laboratory, which are described briefly below, fall into four major categories: development of submicron and nanometer fabrication technology; nanometer and quantum-effect electronics; crystalline films on non-lattice-matching substrates; and periodic structures for x-ray optics, spectroscopy and atomic interferometry.

1.2 Microfabrication at Linewidths of 100 nm and below

Sponsors

Joint Services Electronics Program
Contract DAAL03-89-C-0001
National Science Foundation
Grant ECS 87-09806

Project Staff

Martin Burkhardt, James M. Carter, William Chu, Kathleen Early, Reza A. Ghanbari, Yao-Ching Ku, Alberto Moel, Hui Meng Quek, Dr. Mark L. Schattenburg, Professor Henry I. Smith, Siang-Chun The, Anthony Yen

¹ Princeton University, Princeton, New Jersey.

² Hampshire Instruments, Westboro, Massachusetts.

³ IBM T.J. Watson Research Center, Yorktown Heights, New York.

A variety of techniques for fabricating structures with characteristic dimensions of $0.1\ \mu\text{m}$ (100 nm) and below are investigated. These include: x-ray nanolithography, holographic lithography, achromatic holographic lithography, electron-beam lithography, focused-ion-beam lithography, reactive-ion etching, electroplating, and liftoff. Development of such techniques is essential if we are to explore the rich field of research applications in the deep-submicron and nanometer domains.

X-ray nanolithography is of special interest because it can provide high throughput and broad process latitude at linewidths of 100 nm and below, something that cannot be achieved with scanning-electron-beam or focused-ion-beam lithography alone. We are developing a new generation of x-ray masks made from inorganic membranes (Si , Si_3N_4 , and SiC) in order to eliminate pattern distortion. To achieve multiple-mask alignment compatible with 50 nm linewidths, we will fix the mask-sample gap at $4\ \mu\text{m}$, translate the mask piezoelectrically, and detect alignment to $< 10\ \text{nm}$ by a dual-grating interferometric scheme. Phase-shifting x-ray masks should permit us to achieve 50 nm linewidths at such gaps. In previous studies we showed that a pi-phase-shifting mask improves process latitude by increasing the irradiance slope at feature edges. For linewidths below 50 nm we bring the mask membrane into soft contact with the substrate by electrostatic means. A variety of techniques are used to pattern the x-ray masks including e-beam lithography, focused-ion-beam lithography (FIBL), holographic lithography and sidewall shadowing.

Since the early research on x-ray lithography, it was believed that photoelectrons, released when x-ray photons are absorbed, severely limit the resolution of x-ray lithography for linewidths below 100 nm. For example, it was estimated that using the Al_K x-ray ($\lambda = 0.834\ \text{nm}$, $E = 1.5\ \text{keV}$), it would not be possible to reliably achieve linewidths below 100 nm. We explored this issue experimentally and found previous estimates to be in error. Figure 1 shows that a 30 nm wide line on an x-ray mask is faithfully replicated with no measurable linewidth change using any one of three x-ray wavelengths, Al_K

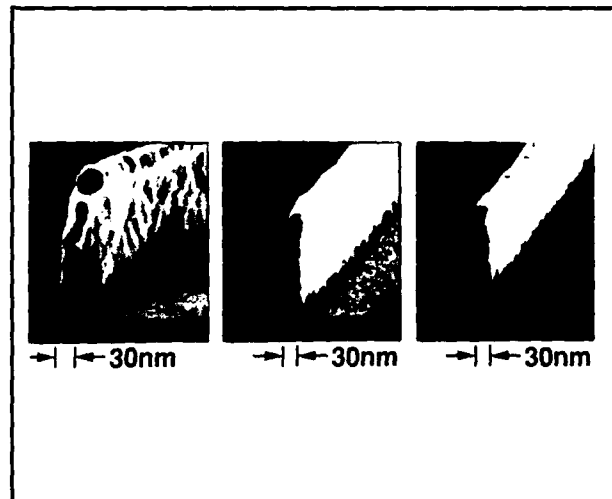


Figure 1. Replication in PMMA of a 30 nm-wide gold absorber line with (a) C_K ($\lambda = 4.5\ \text{nm}$), (b) Cu_L ($\lambda = 1.3\ \text{nm}$), and (c) Al_K ($\lambda = 0.83\ \text{nm}$).

(0.834 nm), Cu_L (1.33 nm), or C_K (45 nm). The implication is that for linewidths down to $\sim 10\ \text{nm}$, diffraction and not photoelectron range is the factor that will limit resolution.

A new type of achromatic holographic lithography (AHL) was developed that enables us to achieve 100 nm-period gratings (50 nm nominal linewidth). Previously, 200 nm was the minimum period achievable. The AHL scheme is illustrated in figure 2, and the exposure results shown in figure 3. This technology will be used to make gratings for x-ray spectroscopy and atom beam interferometry, and to fabricate new classes of quantum-effect electronic devices.

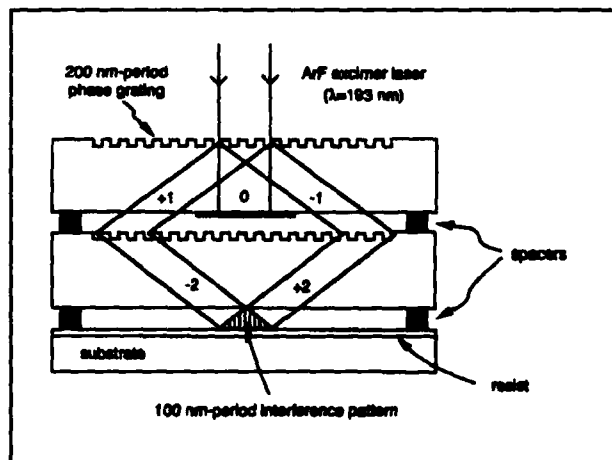


Figure 2. Schematic of the achromatic holographic configuration.

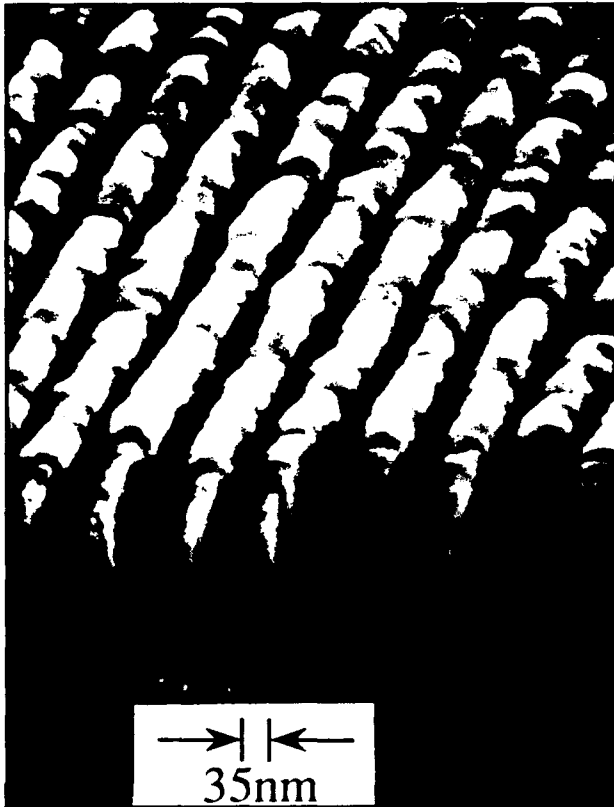


Figure 3. Scanning electron micrograph of 100 nm-period grating lines after exposure, shadow evaporation of nickel and reactive ion etching in an oxygen plasma.

1.3 Improved Mask Technology for X-Ray Lithography

Sponsors

Semiconductor Research Corporation
Contract 87-SP-080
Hampshire Instruments Corporation

Project Staff

Yao-Ching Ku, Kenneth Lu, Professor Henry I. Smith, Lisa Su, JoAnne Gutierrez, Flora S. Tsai

In order to utilize x-ray lithography in the fabrication of submicron integrated electronics, distortion in the x-ray mask must be eliminated. Distortion can arise from stress in the absorber, which is usually gold or tungsten. Tungsten is preferred because it is a closer match in thermal expansion to Si, SiC and other materials used as mask membranes. However, W is usually under high stress when deposited by evaporation or sputtering. Earlier, we demonstrated that for

a given type of substrate, zero stress (i.e., less than 5×10^7 dynes/cm²) can be achieved by controlling the sputtering pressure to within one-tenth of a millitorr. We are now developing a computer-controlled system for monitoring in situ, during deposition, the stress in sputtered W on x-ray mask membranes. Stress is determined from the resonant frequency of the membrane.

We have also investigated a number of materials as mask membranes including: Si, Si₃N₄, SiC, and laminates of Si₃N₄/poly Si/Si₃N₄ and SiO₂/Si₃N₄/SiO₂. The strongest membranes were Si rich Si₃N₄. A 1.2 μ m thick membrane of this material can sustain a full atmosphere pressure differential across a span of 20 mm. There is a concern, however, that Si₃N₄ will undergo stress changes during the heavy x-ray irradiation anticipated in IC production. We are investigating this issue as well as novel approaches to enhance the durability of Si membranes.

1.4 Study of Electron Transport in Si MOSFETs with Deep-Submicron Channel Lengths

Sponsor.

Joint Services Electronics Program
Contract DAAL03-89-C-0001

Project Staff

Professor Dimitri A. Antoniadis, Gregory A. Carlin, Paul G. Meyer, Ghavam Shahidi, Professor Henry I. Smith, Siang-Chun The

Electronic conduction in sub-100 nm channel length Si MOSFETs is being studied in order to observe non-stationary transport effects, i.e., effects arising from rapid spatial variation of the electric field, and the resulting disparity between the actual carrier temperature and the temperature that would correspond with the given field at steady-state conditions. In simple terms, non-stationary effects are observed when transit times across the very short channels become comparable to, or shorter than, energy relaxation times. Previous work has produced NMOS devices with channel lengths down

to 60 nm and gate oxides as thin as 2.5 nm. The devices were fabricated with a combination of x-ray nanolithography and optical projection lithography. Electron velocity overshoot and a reduction of hot-electron effects, as measured from the substrate current, were observed in these devices.

Our focus has now shifted to the fabrication of self-aligned deep-submicron MOSFETs. These devices will use polysilicon gates and cobalt salicidation (self-aligned silicidation). The aim is to reduce parasitic source and drain resistances and gate-source overlaps. This will permit a clearer observation of the non-stationary effects, e.g., in both substrate and gate currents, and will enable us to push device switching speed.

Deep-submicron self-aligned silicided NMOS devices have been successfully fabricated using optical projection lithography followed by partial photoresist ashing to define small features. Devices with effective channel lengths down to 230 nm were fabricated using this technique. As in the non-self-aligned device process, both boron and indium were used as implant species to control punchthrough and threshold voltage. The sheet resistance of the source-drain regions was reduced by silicidation from 110 to 13.6 Ohms per square, and source-drain contact resistances on the devices were reduced from 52 to 10.7 Ohms.

The self-aligned NMOS process is undergoing further development to include x-ray nanolithography for gate polysilicon patterning. This has included the development of inorganic x-ray mask technology to avoid distortion and achieve precise alignment. A simple optical scheme to align x-ray masks to substrates to less than 1 μm has also been developed. The absorber on the x-ray mask will be patterned using a combination of optical lithography and focused-ion-beam (FIB) lithography. In addition, an effort is being made to further improve consistency and control in the salicidation process.

Work is also in progress to develop a corresponding deep-submicron self-aligned PMOS process. This should give us 100 nm-channel-length CMOS circuits fabricated by a technology compatible with commercial mass production.

1.5 Studies of Electronic Conduction in One-Dimensional Semiconductor Devices

Sponsors

Joint Services Electronics Program
Contract DAAL03-89-C-0001
National Science Foundation
Grant ECS-85-03443

Project Staff

Professor Dimitri A. Antonaidis, Stuart B. Field, Professor Marc A. Kastner, Udi Meirav, Samuel L. Park, John H.F. Scott-Thomas, Professor Henry I. Smith

Sophisticated processing techniques and advanced lithography have allowed us to enter what we believe is a fundamentally new regime in the study of electronic conduction in one-dimensional systems. A slotted-gate MOSFET structure (figure 4) was used to produce an electron gas at the Si/SiO₂ interface beneath the gap in the lower-gate. This was done by biasing the upper gate positively, while keeping the slotted gate just below threshold. Fringing fields around the lower gate confined the electron gas to a width substantially narrower (~ 25 nm) than the distance separating the two halves of the slotted gate (~ 70 nm). The slotted gate was produced using x-ray nanolithography and liftoff. It was composed of refractory metals to allow a subsequent high temperature anneal. This anneal removed damage created by the e-beam evaporation of the refractory metal, so that the electron gas had a mobility of 15,000 cm² / V-sec at 4.2K. The electrical conductance of the 1-D gas was measured as a function of the upper gate voltage for temperatures less than 1K, and a surprising series of periodic oscillations was seen in the conductance (figure 5). Changing the gate voltage can be thought of as changing the number of electrons per unit length of electron gas. Since the conductance is thermally activated, the oscillations reflect a periodic change in the activation energy of the electron gas as the electron density is changed. Computer simulations solving Poisson's equation and the single particle Schrodinger

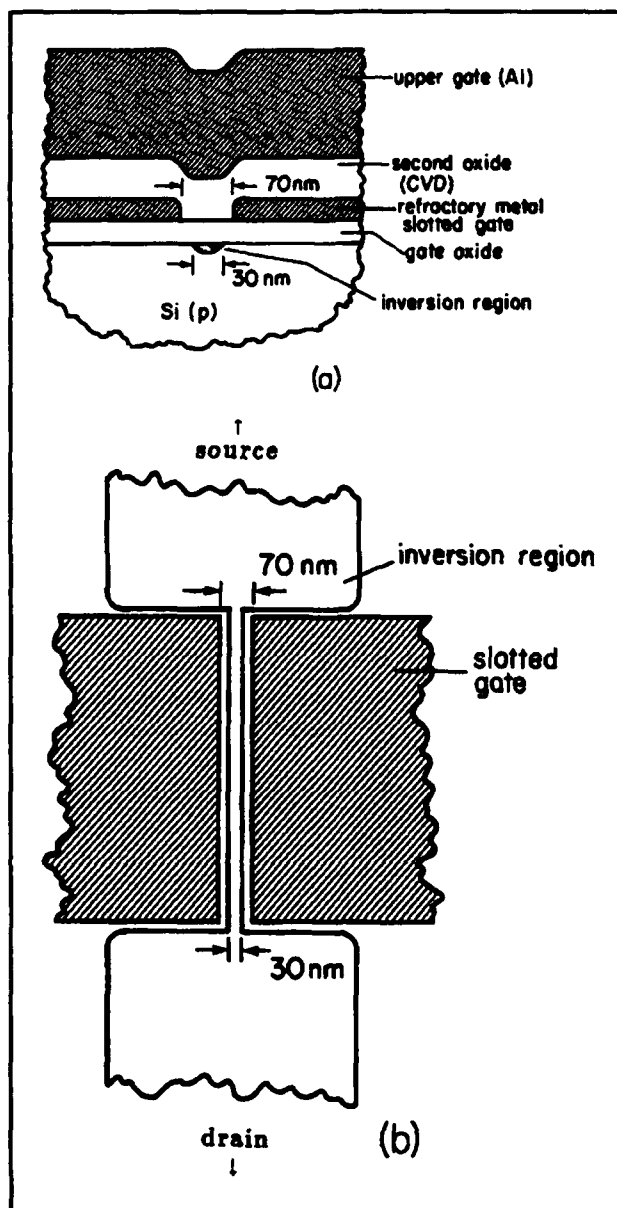


Figure 4. (a) Schematic cross section and (b) top view of the slotted-gate device. The inversion layer, formed by the positively biased upper gate is confined by the lower gate. The thermal oxide and refractory metal lower gate are both 30 nm thick, and the chemical vapor deposition oxide is 45 nm thick. The width of a narrow inversion layer is exaggerated in (b).

wave equation strongly suggest that the electron gas is dynamically one-dimensional when the oscillations are most strongly seen. That is, the electrons are in the lowest quantum energy level of the potential well created by the fringing fields of the slotted gate.

A one-dimensional electron gas will form a charge density wave (CDW) when the electron-electron interaction is the dominant energy. This is the same regime that the device is in when the oscillations are seen. In a CDW, electrons are spaced periodically. This minimizes the total energy of the electron gas. Impurities in the device can pin the CDW. Two impurities in the conducting channel would in turn strongly pin and weakly pin the CDW as the electron density of the gas is changed. This corresponds to commensurability and incommensurability of the CDW with the spacing of the impurities, and results in oscillatory behavior of the conductance with electron density. The period of the oscillations varies randomly from device to device, with no dependence on length. The period changes in the same device when it is heated to room temperature and then cooled. This strongly suggests that mobile impurity atoms are doing the pinning. It should be stressed that these oscillations are seen with no magnetic field, implying

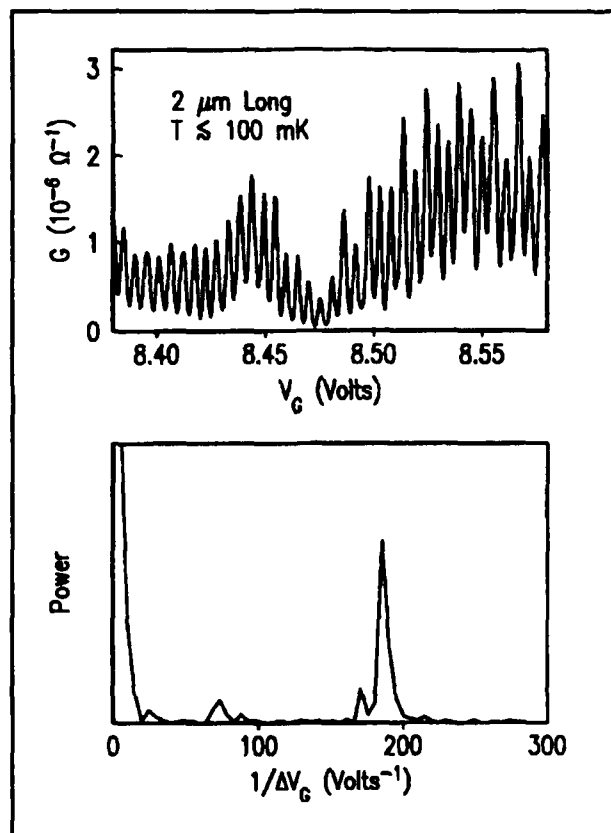


Figure 5. Top panel: Conductance G versus gate voltage V_G for a $2\ \mu\text{m}$ -long inversion layer. Bottom panel: Fourier power spectrum of the top panel data.

that the phenomenon is fundamentally different from phenomena requiring Landau quantization (such as the Quantum Hall Effect). Also, the effect seems to require a many-body theory (i.e., one incorporating electron-electron interactions).

1.6 Surface Superlattice Formation in Silicon Inversion Layers Using 0.2 μm -Period Grating-Gate Field-Effect Transistors

Sponsors

Joint Services Electronics Program
Contract DAAL03-89-C-0001
U.S. Air Force - Office of Scientific Research
Grant AFOSR-88-0304

Project Staff

Professor Dimitri A. Antoniadis, Phillip F. Bagwell,
Professor Marc A. Kastner, Professor Terry P. Orlando, Professor Henry I. Smith, Anthony Yen

We have been studying distinctly quantum mechanical effects in electrical conduction using the silicon grating-gate field-effect transistor (GGFET). The Si GGFET is a dual stacked-gate MOS-type structure in which the gate closest to the inversion layer (bottom gate) is a 200 nm period grating made of refractory metal. A SiO_2 insulating layer separates the grating gate and the inversion layer from a second continuous aluminum gate (top gate). Two types of electronic devices are possible in this geometry: (1) a lateral surface superlattice (LSSL) GGFET in which carrier conduction is perpendicular to the grating lines; and (2) a quasi-one-dimensional (Q1D) GGFET which confines carriers to move in narrow inversion strips beneath the grating lines.

Here we describe our observation of a transition from conduction through ~ 300 multiple parallel quantum wires to conduction in a 2D electron gas (standard MOSFET) using the Q1D GGFET. We can induce such a dimensional transition by varying the two gate voltages of the GGFET. When a strong magnetic field is applied perpendicular to the plane of the inversion layer at temperatures below 4.2K, we observe a large negative

transconductance whose onset voltage marks the transition from 1D to 2D conduction.

This is shown in figure 6, where the transition from 1D to 2D behavior occurs at a top-gate voltage around zero volts. The significant observation is that with a magnetic field perpendicular to the plane of the channel, adding more electrons to the MOSFET actually reduces the device conductance at the 1D to 2D transition point. The oscillations below the transition point are due to magnetoelectric subbands, while those above the transition are due to Shubnikov de Haas oscillations as the Landau levels pass through the Fermi level. This striking dimensional transition in a magnetic field has never been observed before.

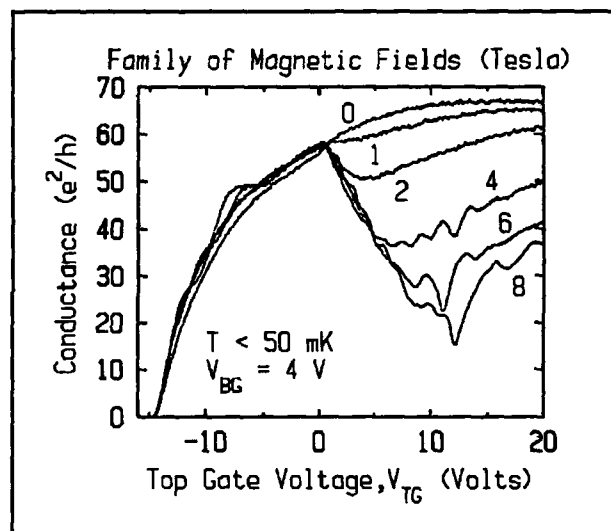


Figure 6. Plot of the conductance of a quasi-1D grating-gate MOSFET as a function of the top gate voltage, for several values of the perpendicular magnetic field. At a top gate voltage around zero volts there is a transition from 1D to 2D conduction with an attendant strong negative transconductance.

The origin of the unusual magnetoresistance effects that we have observed is still unclear. At the magnetic fields where the effect becomes prominent, the cyclotron radius is much smaller than the width of the quantum wires, so a semiclassical explanation involving an interplay of the cyclotron radius and wire width is probably inappropriate. Also, the two terminal magnetoresistance measurements significantly complicate interpretation of the data. A noninvasive four-terminal measurement would be ideal, but it is not clear that such a measurement is pos-

sible. Finally, the exact way in which the current feeds into the source contact from the bulk device may also be important. At higher magnetic fields where the magneto-conductance oscillations begin to appear, conduction takes place through edge states. These edge states may also play a role in giving rise to the effect.

1.7 Study of Surface Superlattice Formation in GaAs/GaAlAs Modulation Doped Field-Effect Transistors

Sponsor

U.S. Air Force - Office of Scientific Research
Grant AFOSR-88-0304

Project Staff

Professor Dimitri A. Antoniadis, Martin Burkhardt, William Chu, Professor Jesus A. del Alamo, Reza A. Ghanbari, Khalid Ismail, Professor Marc A. Kastner, Professor Terry P. Orlando, Professor Henry I. Smith, Anthony Yen

We have used the modulation-doped field-effect transistor (MODFET) as a test vehicle for studying quantum effects such as electron back diffraction in a GaAs/AlGaAs material system. In a conventional MODFET the current transport is modulated by a continuous gate between source and drain. In our studies, we have used Schottky metal gratings and grids for the gate, as illustrated in figure 7. Such gates produce a periodic potential modulation in the channel.

The grid was produced by x-ray nanolithography and liftoff. The x-ray mask of the grid was produced by two successive x-ray exposures, at 90 degrees to one another, using a master mask that was fabricated via holographic lithography. The latter yields coherent gratings over areas several centimeters in diameter. A new technique was developed that yields grating and grid patterns only in the channel region between source and drain. This has simplified the overall process and enhanced its reliability.

The MODFET is normally on, that is, a negative gate bias of about -0.2 V must be applied to pinch off conductance from source to drain. As the gate bias is raised

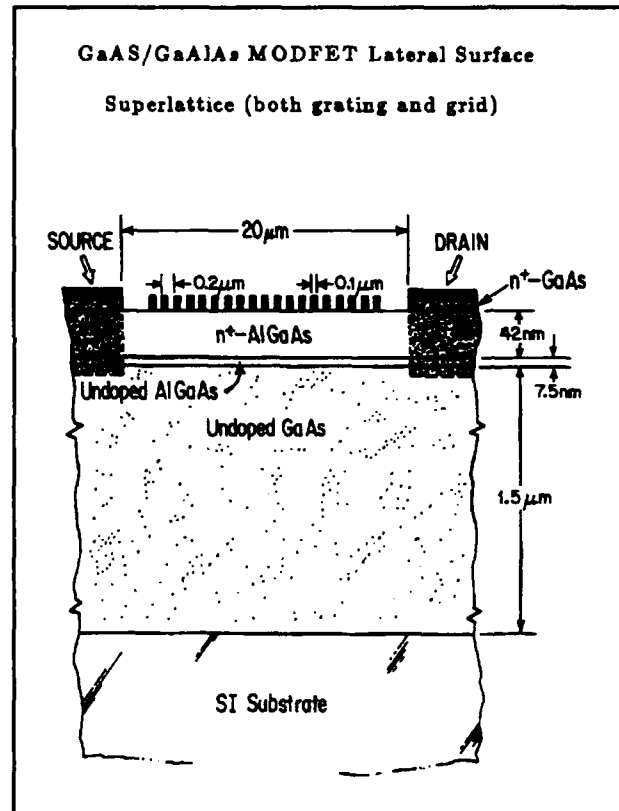


Figure 7. Schematic cross section of a grid-gate MODFET device. Contacts to the grid are made by pads off to the sides of the conduction channel.

above this threshold point, the height of the periodic potential modulation is reduced and, simultaneously, the Fermi energy is raised (or, equivalently, the electron wavelength is reduced) in the 2D electron gas residing at the AlGaAs/GaAs interface. When the electron wavelength phase-matches the periodic potential, electron back-diffraction occurs provided the inelastic length (i.e., the coherence or phase breaking length) is longer than the grating-period. Such back diffraction is manifested by a drop in the conductance. A stronger back diffraction effect is observed in the case of a grid because true minigaps are formed. The measurements of conductance modulation of grating and grid-gate MODFETs agrees with theoretical predictions. In the grid gate devices it was also possible to observe negative differential resistance which might be due to sequential resonant tunneling.

We plan to decrease the periodicity of the gratings and grids by a factor of two, to 100 nm period. For devices with such fine grating

periodicity the superlattice effect should become more pronounced and observable at higher temperatures. We will also conduct magnetotransport measurements with devices of 100 and 200 nm periodicity.

1.8 Study of One-Dimensional Subbands and Mobility Modulation in GaAs/AlGaAs Quantum Wires

Sponsors

Joint Services Electronics Program
Contract DAAL03-89-C-0001
U.S. Air Force - Office of Scientific Research
Grant AFOSR-88-0304

Project Staff

Professor Dimitri A. Antoniadis, Phillip F. Bagwell, William Chu, Professor Jesus A. del Alamo, Reza A. Ghanbari, Khalid Ismail, Professor Marc A. Kastner, Professor Terry P. Orlando, Professor Henry I. Smith, Anthony Yen

In order to study one-dimensional conductivity in the AlGaAs/GaAs modulation-doped structure without the conductance fluctuations normally associated with single microscopic systems, we fabricated arrays of 100 parallel quantum wires (MPQW). The measured Hall mobility in the 2-D electron gas at the AlGaAs/GaAs interface was 250,000 cm²/Vs at 4.2K. The multiple quantum wires were produced by x-ray nanolithography, liftoff of Ti/Au, and ion etching of the AlGaAs. The charge concentration in the quantum wires could be increased by applying a positive bias to a back-side contact or by illumination. (There was no persistent photocurrent in these samples).

Figure 8 shows the measured drain-source current versus backgate bias for the quantum wires (solid line) and for an equivalent 2-D device (dashed line). To explain the structure, we have developed a semi-classical model to calculate the conductivity of these devices. As seen in the dotted line in figure 8, our calculations match the measured data quite well.

Based on our calculations, we conclude that the observed mobility modulation is associated with populating the quasi-one-di-

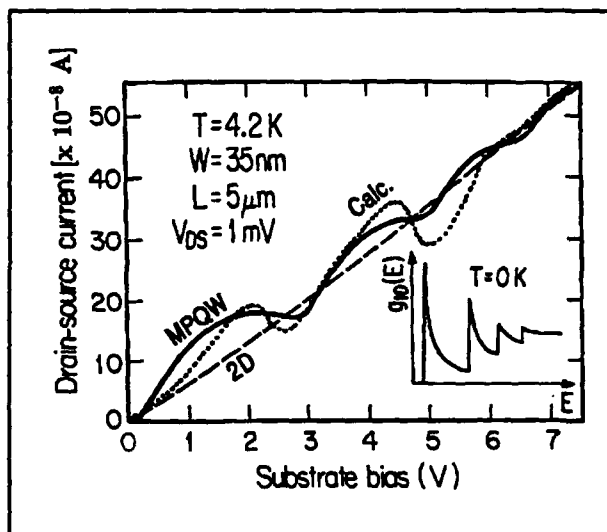


Figure 8. Drain-source current (I_{DS}) as a function of substrate bias (V_{SUB}) for the multiple parallel quantum wires (solid line) and scaled down 2D channel (dashed line). The inset shows the theoretical density of states in a Q1D wire at 0 K. The dotted line is an analytical calculation.

dimensional subbands. The negative differential transconductance regions arise when higher subbands begin to be populated. Currently, we are working on fabricating new versions of these devices that allow for control of the confining potential, and hence the position of the subbands, by use of a top gate. It is hoped that these devices will verify the validity of our model.

1.9 Arrays of Field-Effect-Induced Quantum Dots

Sponsors

Joint Services Electronics Program
Contract DAAL03-89-C-0001
U.S. Air Force - Office of Scientific Research
Grant AFOSR-88-0304

Project Staff

Professor Dimitri A. Antoniadis, Martin Burkhardt, William Chu, Professor Jesus A. del Alamo, Reza A. Ghanbari, Khalid Ismail, Professor Marc A. Kastner, C.T. Liu, Professor Terry P. Orlando, Professor Henry I. Smith, T.P. Smith, Professor Dan Tsui

A metal grid on a modulation-doped AlGaAs/GaAs substrate (depicted in figure

9a) produces a two-dimensional periodic potential modulation at the AlGaAs/GaAs interface via the Schottky effect. If a gate electrode is attached to the grid, the potential can be further modified with an external voltage source. By changing the gate voltage from positive to negative values, the potential seen by the electrons located at the AlGaAs/GaAs interface can be varied from uniform (in which case the electrons behave as a 2-D electron gas) to weakly coupled zero-D quantum wells (figure 9b) to isolated zero-D quantum dots (figure 9c). We have made such structures, with spatial periods of 200 nm in both orthogonal directions using technology similar to that described in Section 1.7, but now the grid gate occupies an area of several square millimeters. The isolated quantum dots and the attendant zero-dimensional electronic subbands were examined in collaboration with D. Tsui at Princeton University using far-infrared (FIR) cyclotron resonance. Transitions between the discrete energy levels in the quantum dots were observed as a function of magnetic field. Results were in agreement with a theoretical model.

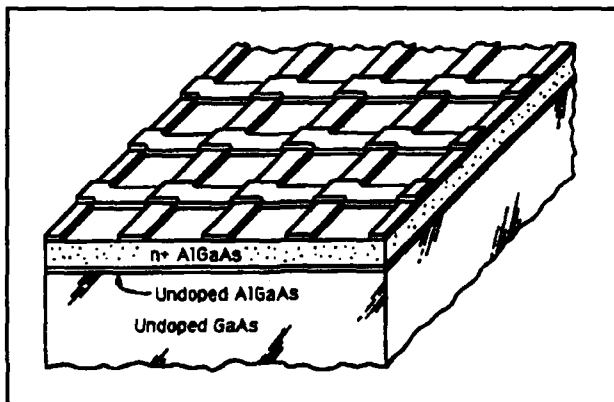


Figure 9a. Metal grid gate on a modulation-doped AlGaAs/GaAs substrate.

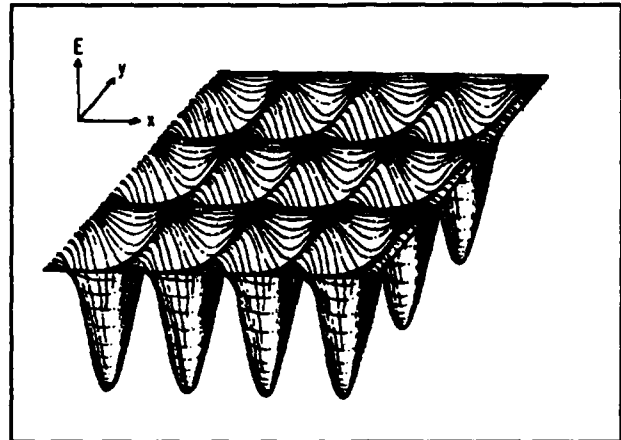


Figure 9b. Depiction of potential seen by electrons at the AlGaAs/GaAs interface for weakly coupled quantum dots.

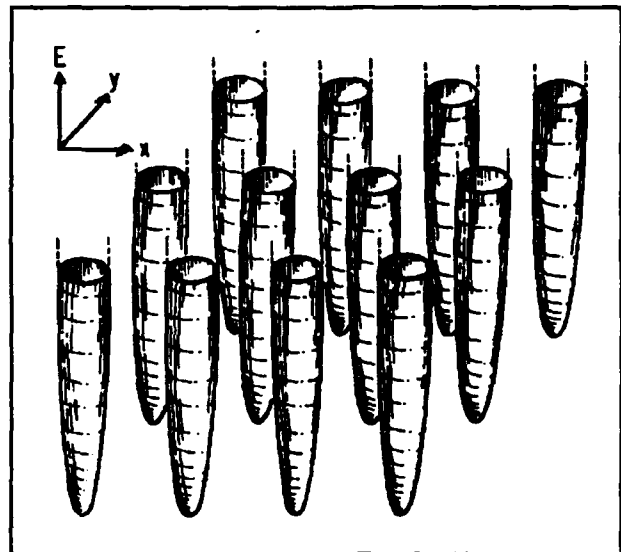


Figure 9c. Potential for the case of isolated quantum dots.

In collaboration with T.P. Smith and K. Ismail at IBM we applied a magnetic field perpendicular to the plane of the grid gate and measured magnetocapacitance as the gate voltage was swept, changing the electronic system from two-dimensional to coupled quantum wells, to isolated quantum dots. The normal oscillations due to Landau level filling are strongly suppressed when the Fermi level lines up with the minibandgaps. Thus, these measurements give important confirmation of the miniband structure we observed earlier in transport. In the weakly-coupled-quantum-dot regime the magnetocapacitance oscillations show evidence of fractal behavior when the number of flux

quanta per unit cell of our grid is a rational number (i.e., $1/2$, $1/3$, $3/5$, etc.).

We are currently fabricating a new set of grid-gate MODFETS, using an improved fabrication process and will study their transport, capacitance, and absorption properties as a function of magnetic field.

1.10 Planar-Resonant-Tunneling Field-Effect Transistors (PRESTFETs)

Sponsor

U.S. Air Force - Office of Scientific Research
Grant AFOSR-85-0154

Project Staff

Professor Dimitri A. Antoniadis, William Chu, Khalid Ismail, and Professor Henry I. Smith

Encouraged by the observation of negative differential resistance in the surface-superlattice MODFET (Section 1.7), we have proceeded to fabricate and test a double-barrier MODFET shown schematically in figure 10. Under the gate electrodes, the energy level diagram is as sketched in figure 11. With proper biasing, resonant tunneling should be observable, hence the name of the device PRESTFET (Planar-Resonant Tunneling Field-Effect Transistor).

Three types of measurements were performed (at 4.2 K) on a PRESTFET device in which the gate electrodes were 60 nm long and separated by 60 nm: (1) gate electrodes are connected together, the drain-to-source voltage is held fixed (< 5 mV), and the gate voltage is swept; (2) the electrodes are connected together and the intensity of an illuminating LED is scanned; (3) one gate bias is fixed while the other is swept.

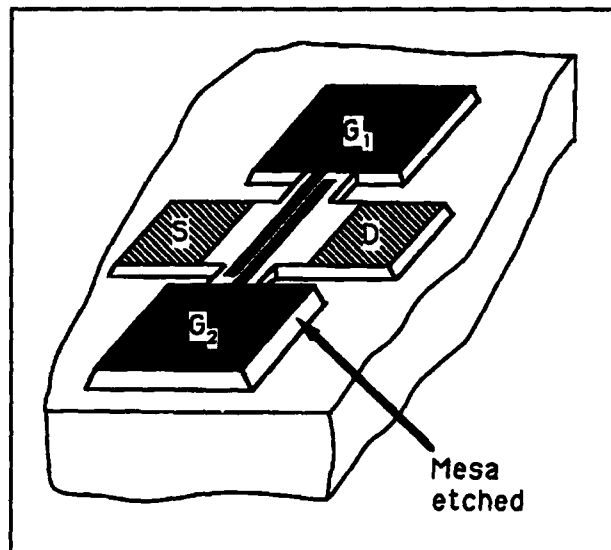


Figure 10. Sketch of the layout of a 4-terminal, double-barrier, planar-resonant-tunneling field-effect transistor (PRESTFET).

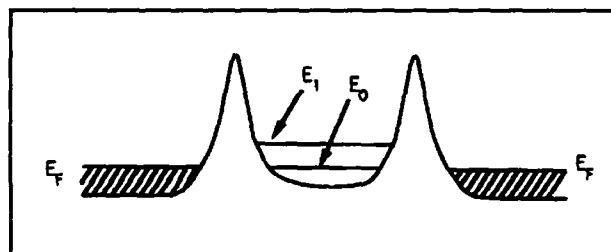


Figure 11. Energy level diagram of a symmetric, double-barrier PRESTFET.

In all three cases, clear resonances were observed in the drain-to-source current. In figure 12, a plot of the results of the third experiment is shown. The results of these three measurements provide clear evidence that resonant tunneling occurs through the quantized well states.

We are currently fabricating PRESTFET devices with even finer electrodes and developing a high-throughput PRESTFET fabrication process using x-ray nanolithography.

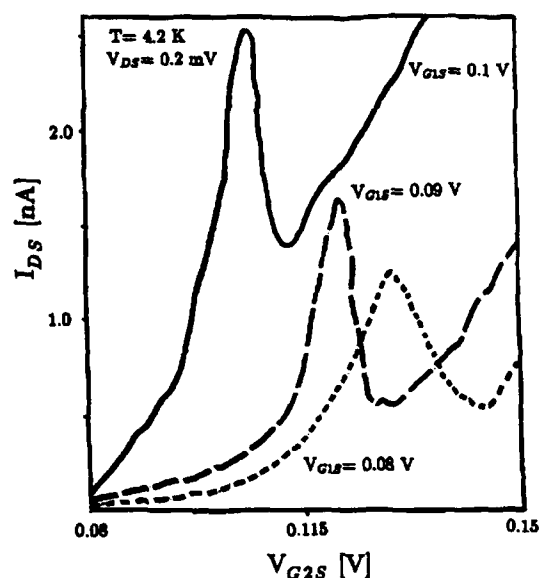


Figure 12. Drain-source current as a function of bias on gate 2 for three different bias conditions, below threshold, on gate 1.

1.11 Submicrometer-Period Gold Transmission Gratings for X-Ray Spectroscopy and Atom-Beam Interferometry

Sponsor

Joint Services Electronics Program
Contract DAAL03-89-C-0001
X-Opt., Incorporated

Project Staff

Dr. Mark L. Schattenburg, Professor Henry I. Smith

Gold transmission gratings with periods of 0.2 to 1.0 μm , and thicknesses ranging from 0.1 to 1 μm are fabricated using x-ray lithography and electroplating. The x-ray masks are made with holographic lithography. Transmission gratings are either supported on thin (1 μm) membranes or are made self-supporting by the addition of crossing struts. They are supplied to external laboratories for spectroscopy of the x-ray emission from a variety of sources. Over 15 laboratories around the world are using MIT-supplied gratings, and this project constitutes the sole source for these diffractors. Self-supporting transmission gratings in both gold and thin-film chromium are being provided to Pro-

fessor David Pritchard's group for use in experiments to study the diffraction of neutral sodium atoms by gratings. The sodium atoms have a de Broglie wavelength of ~ 17 pm. Clear demonstrations of atomic diffraction have been made with these gratings. The gratings can also be used to divide and recombine an atomic beam coherently, and may provide the easiest route to the realization of an atom wave interferometer.

1.12 High-Dispersion, High-Efficiency Transmission Gratings for Astrophysical X-Ray Spectroscopy

Sponsor

National Aeronautics and Space Administration
Contract NAS8-36748

Project Staff

Professor Claude R. Canizares, Dr. Mark L. Schattenburg, Professor Henry I. Smith

Gold gratings with spatial periods of 0.1 to 1.0 μm make excellent dispersers for high resolution x-ray spectroscopy of astrophysical sources in the 100 eV to 10 keV band. These gratings are planned for use in the Advanced X-Ray Astrophysics Facility (AXAF) that will be launched in the mid-1990s. In the region above 3 keV, the requirements of high dispersion and high efficiency dictate the use of the finest period gratings with aspect ratios approaching 10 to 1. To achieve this, we first expose a grating pattern in 1.0 μm -thick PMMA over a gold plating base using x-ray nanolithography. Gold is then electroplated into the spaces of the PMMA to a thickness up to 1 μm . Flight prototype gratings have been fabricated and undergone space-worthiness tests. In the initial stage of this program we used the carbon K x-ray ($\lambda = 4.5$ nm) which required that the mask and substrate be in contact to avoid diffraction. This, in turn, caused distortion of the grating. To avoid this problem we are developing a new technology of microgap x-ray nanolithography using the copper L x-ray ($\lambda = 1.33$ nm) and Si_3N_4 membrane masks.

1.13 Epitaxy via Surface-Energy-Driven Grain Growth

Sponsor

AT&T Bell Laboratories
U.S. Air Force - Office of Scientific Research
Grant AFOSR-85-0154

Project Staff

Jerold A. Floro, Professor Henry I. Smith, Professor
Carl V. Thompson

Epitaxial grain growth (EGG) in polycrystalline thin films on single crystal substrates is being investigated as an alternative process for obtaining and studying epitaxy. EGG can produce smoother epitaxial films than in conventional epitaxy and in some cases may yield lower defect densities as well. In addition, EGG can produce unique non-lattice-matched orientations not observed in conventional epitaxy. Thin film epitaxy is conventionally obtained by vapor deposition at low rate onto a single-crystal substrate held at elevated temperature, resulting in a single-crystal film as-deposited. In contrast, we deliberately deposit films at high rates and low temperatures in an ultra-high vacuum electron-beam evaporator in order to obtain polycrystalline films. These films can then be annealed in situ to promote epitaxial grain growth.

EGG occurs because the anisotropic film/single-crystal substrate interfacial energy selects one film crystallographic orientation as having the lowest total free energy. Grains in this orientation thus have the largest driving force for growth and will predominate as the system coarsens.

We are currently studying EGG in model systems known to exhibit conventional epitaxy, e.g., Au, Al, Cu, and Ag films on mica and alkali halide substrates. The following results have been obtained: (1) EGG occurs in all these systems, (2) in the case of Au on mica EGG results in a smoother, lower defect density film than a corresponding conventional epitaxial film, (3) the final orientation selected by EGG is determined by the energy of the film's free surface as well as the film/substrate interface, (4) the final orientation selected by EGG is not neces-

sarily the same orientation observed in conventional epitaxy, implying that conventional epitaxial orientations can be metastable. In the case of Au on (100) NaCl, (111) epitaxial Au grains grow, whereas conventional epitaxy yields a (100) film.

We have developed a coarsening theory which is applicable to epitaxial grain growth. This theory derives a growth law for interface-controlled coarsening of coplanar disks, including terms accounting for surface energy anisotropy. This growth law may then be used to computationally solve the continuity equation for grains in size space in order to monitor the time evolution of the grain size and orientation distribution. Use of an appropriate interface energy function will allow comparison with experiment.

1.14 Publications

1.14.1 JSEP Publications

Antoniadis, D.A. "Surface Superlattice and Quasi-One-Dimensional Devices in GaAs." Paper presented at the Meeting of the American Physical Society, St. Louis, Missouri, March 20-24, 1989.

Antoniadis, D.A., K. Ismail, and H.I. Smith. "Lateral Surface Superlattices and Quasi-One-Dimensional Structures in GaAs." Presented at the "Science and Engineering of 1- and 0-Dimensional Semiconductors." NATO Advanced Research Workshop, Cadiz, Spain, March 29-April 1, 1989.

Chu, W., A. Yen, K. Ismail, M.I. Shepard, H.J. Lezec, C.R. Musil, J. Melngailis, Y.-C. Ku, J.M. Carter, and H.I. Smith. "Sub-100 nm X-ray Mask Technology using Focused-Ion-Beam Lithography." *J. Vac. Sci. Technol. B* 7:1583-1585 (1989).

Early, K., M.L. Schattenburg, and H.I. Smith. "Absence of Resolution Degradation in X-Ray Lithography for λ from 4.5 nm to 0.83 nm." Paper presented at the Microcircuit Engineering '89, Cambridge, England, September 26-28, 1989.

Field, S.B., J.H.F. Scott-Thomas, M.A. Kastner, H.I. Smith, and D.A. Antoniadis. "Conductance Oscillations Periodic in the Density of a One-Dimensional Electron Gas." Paper presented at the Meeting of the American Physical Society, St. Louis, Missouri, March 20-24, 1989.

Ismail, K., W. Chu, A. Yen, D.A. Antoniadis and H.I. Smith, "Negative Transconductance and Negative Differential Resistance in a Grid-Gate Modulation-Doped Field-Effect Transistor." *Appl. Phys. Lett.* 54:460 (1989).

Ismail, K., D.A. Antoniadis, and H.I. Smith. "Lateral Resonant Tunneling in a Double-Barrier Field-Effect Transistor." *Appl. Phys. Lett.* 55, 589 (1989).

Ismail, K., D.A. Antoniadis, and H.I. Smith. "One-Dimensional Subbands and Mobility Modulation in GaAs/AlGaAs Quantum Wires." *Appl. Phys. Lett.* 54:1130 (1989).

Ismail, K., W. Chu, R. Tiberio, A. Yen, H.J. Lezec, M.I. Shepard, C.R. Musil, J. Melngailis, D.A. Antoniadis, and H.I. Smith. "Resonant Tunneling Across and Mobility Modulation Along Surface-Structured Quantum Wells." *J. Vac. Sci. Technol. B* 7:2025-2029 (1989).

Ismail, K., D.A. Antoniadis, H.I. Smith, C.T. Liu, K. Nakamura, and D.C. Tsui. "A Lateral-Surface Superlattice Structure on GaAs/AlGaAs for Far-Infrared and Magneto-Capacitance Measurements." *J. Vac. Sci. Technol. B* 7:2000-2002 (1989).

Ismail, K., T.P. Smith, W.T. Masselink and H.I. Smith. "Magnetic Flux Commensurability in Coupled Quantum Dots." *Appl. Phys. Lett.* 55:2766-2768 (1989).

Ismail, K. *The Study of Electron Transport in Field-Induced Quantum Wells on GaAs/GaAlAs*. Ph.D. diss., Dept. of Electr. Eng. and Comput. Sci., MIT, 1989.

Ku, Y.C., H.I. Smith, and I. Plotnik. "Low Stress Tungsten Absorber for X-Ray Masks." Paper presented at the Microcir-

cuit Engineering '89, Cambridge, England, September 26-28, 1989.

Liu, C.T., K. Nakamura, D.C. Tsui, K. Ismail, D.A. Antoniadis, and H.I. Smith. "Magneto-Optics of a Quasi Zero-Dimensional Electron Gas." *Appl. Phys. Lett.* 55:168 (1989).

Liu, C.T., D.C. Tsui, M. Shayegan, K. Ismail, D.A. Antoniadis, and H.I. Smith. "Observation of Landau Level Splitting of a Two-Dimensional Electron Gas in a Two-Dimensional Surface Superlattice." Submitted *Phys. Rev. Lett.*

Liu, C.T., K. Nakamura, D.C. Tsui, K. Ismail, D.A. Antoniadis, and H.I. Smith. "Far-Infrared Transmission Measurements on Grid-Gate GaAs/AlGaAs Lateral-Surface-Superlattice Structures." *J. Surface Sci.* (1989). Forthcoming.

Liu, C.T., K. Nakamura, D.C. Tsui, K. Ismail, D.A. Antoniadis, and H.I. Smith. "Far-Infrared and Magneto-Capacitance Measurements on GaAs/AlGaAs Lateral Surface Superlattice." Paper presented at the Meeting of the American Physical Society, St. Louis, Missouri, March 20-24, 1989.

Meyer, P.G. *Fabrication of Deep Submicron MOSFETs using a Self-Aligned Cobalt Disilicide Process*. S.M. thesis, Dept. of Electr. Eng. and Comput. Sci., MIT, 1989.

Moel, A., M.L. Schattenburg, J.M. Carter, and H.I. Smith. "Microgap Control in X-Ray Nanolithography." *J. Vac. Sci. Technol. B* 7:1692-1695 (1989).

Schattenburg, M.L., C.R. Canizares, and H.I. Smith. "X-Ray/VUV Transmission Gratings for Astrophysical and Laboratory Applications." *Physica Scripta* 4: 13-20 (1990).

Scott-Thomas, J.H.F., S.B. Field, M.A. Kastner, H.I. Smith, and D.A. Antoniadis. "Conductance Oscillations Periodic in the Density of a One-Dimensional Electron Gas." *Phys. Rev. Lett.* 62:583 (1989).

Shahidi, G. *Non-Stationary Transport Effects in Deep Sub-Micron Channel Si*

MOSFETs. Ph.D. diss., Dept. of Electr. Eng. and Comput. Sci., MIT, 1989.

Smith, H.I., K. Ismail, W. Chu, A. Yen, Y.C. Ku, and D.A. Antoniadis. "X-Ray Nanolithography and Quantum-Effect Electronics." Molecular Electronics-Science and Technology, Engineering Foundation Conferences, Keauhou Kona, Hawaii, February 19-24, 1989.

Smith, H.I., K. Ismail, W. Chu, A. Yen, Y.C. Ku, M.L. Schattenburg, and D.A. Antoniadis. "Fabrication of Quantum-Effect Electronic Devices Using X-Ray Nanolithography." In *Proceedings of the International Symposium on Nanostructure Physics and Fabrication*, pp. 57-65. Eds. W.P. Kirk and M.A. Reed. New York: Academic Press, 1989.

Smith, H.I., K. Ismail, M.L. Schattenburg, and D.A. Antoniadis. "Sub- 100 nm Electronic Devices and Quantum-Effects Research using X-Ray Nanolithography." Paper presented at the Microcircuit Engineering '89, Cambridge, England, September 26-28, 1989.

Smith, H.I. "X-Ray Lithography and Nanostructure Fabrication." Paper presented at the Meeting of the American Physical Society, St. Louis, Missouri, March 20-24, 1989.

Thompson, C.V., J. Floro, and H.I. Smith. "Epitaxial Grain Growth in Thin Metal Films." Submitted to *J. Appl. Phys.*

Yen, A., R.A. Ghanbari, E.H. Anderson, and H.I. Smith. "Fabrication of 100 nm-Period Gratings using Achromatic Holographic Lithography." Paper presented at the Microcircuit Engineering '89, Cambridge, England, September 26-28, 1989.

1.14.2 Other Publications

Ajuria, S.A. *Photon Enhanced Grain Growth*. S.M. thesis, Dept. of Mat. Sci. and Eng., MIT, 1989.

Bagwell, P.F., and T.P. Orlando. "Landauer's Conductance Formula and its Generaliza-

tion to Finite Voltages." *Phys. Rev. B* 40:1450 (1989).

Bagwell, P.F., and T.P. Orlando. "Broadened Conductivity Tensor and Density of States for a Superlattice Potential in 1, 2, and 3 Dimensions." *Phys. Rev. B* 40:3735 (1989).

Bagwell, P.F., and T.P. Orlando. "Finite Voltage Tunneling in Ballistic Devices." Paper presented at the Meeting of the American Physical Society, St. Louis, Missouri, March 20-24, 1989.

Carpenter, R. *Material Characterization Techniques for SOI Devices*. S.M. thesis, Dept. of Electr. Eng. and Comput. Sci., MIT, 1989.

Clevenger, L.A. *Controlled and Explosive Silicidation of Metal/Amorphous-Silicon Multilayer Thin Films*. Ph.D. diss., Dept. of Mat. Sci. and Eng., MIT, 1989.

Meirav, U., M.A. Kastner, M. Heiblum, and S.J. Wind, "One-dimensional Electron Gas in GaAs: Periodic Conductance Oscillations as a Function of Density." *Phys. Rev. B* 40:5871-5874 (1989).

Orlando, T.P., P.F. Bagwell, R.A. Ghanbari, K. Ismail, and D.A. Antoniadis. "Quantum Device Modeling with the Convolution Method." To appear as part of a chapter in *Electronic Properties of Multilayers and Low Dimensional Semiconductor Structures*. Eds. J.M. Chamberlain, L. Eaves, and J.C. Portal. London, Plenum Press: 1990.

Palmer, J.E. *Evolution of Microstructures in Ultra-Thin Films of GaAs and CaF₂ on Single Crystal Silicon*. Ph.D. diss., Dept. of Electr. Eng. and Comput. Sci., MIT, 1989.

Quek, H.M. *An Investigation of Graphoepitaxy in Thin Au and Bi Films*. S.M. thesis, Dept. of Mat. Sci. and Eng., MIT, 1989.

Chapter 2. Microstructural Evolution in Thin Films of Electronic Materials

Academic and Research Staff

Professor Carl V. Thompson, Dr. Paul Evans, Professor Clifton G. Fonstad, Jr., Dr. En Ma, Dr. John Melngailis, Professor Henry I. Smith

Visiting Scientists and Research Affiliates

Chenson K. Chen,¹ Dr. Roberto R. DeAvillez,² David J. Edell,³ Harold J. Frost,⁴ David A. Smith,⁵ King-N. Tu⁵

Graduate Students

Sergio A. Ajuria, Geoffrey Burns, Jaeshin Cho, Lawrence A. Clevenger, Andrew D. Dubner, Jerrold A. Floro, James S. Im, Eva Jiran, Harold Kahn, Yachin Liu, Hai Longworth, Joyce E. Palmer, Hui Meng Quek, Jaesang Ro

Undergraduate Student

Howard Zolla

Technical and Support Staff

Celia Slattery

2.1 Modeling of Microstructural Evolution in Thin Films

Sponsors

Joint Services Electronics Program
Contract DAAL03-89-C-0001
National Science Foundation
U.S. Air Force - Office of Scientific Research
Contract AFOSR 85-0154

Project Staff

Professor Carl V. Thompson, Harold J. Frost,
Jerrold A. Floro, Yachin Liu

We are developing analytic models for normal, secondary and epitaxial grain growth

in continuous thin films as well as particle coarsening in discontinuous films. The effects of surface or interface energy anisotropy play especially important roles in these processes. We have developed computer models for film formation by crystal nucleation and growth to impingement under a variety of conditions. The topology and geometry of grain structures have been shown to strongly depend on the conditions of film formation. We have also developed computer simulations for two-dimensional normal grain growth and secondary grain growth.

We are developing analytic models and computer simulations in parallel with experimental studies in model systems. Computer

¹ MIT Lincoln Laboratory.

² Pontificia Universidade Catolica, Department of Materials Science and Metallurgy, Rio de Janeiro, Brazil.

³ Harvard-MIT Health Sciences Program.

⁴ Thayer School of Engineering, Dartmouth College, Hanover, New Hampshire.

⁵ IBM, Thomas J. Watson Research Center.

simulations have allowed us to explain microstructural features which are generally characteristic of thin films, including: (1) stagnation of normal grain growth, (2) development of lognormal distributions of grain sizes and (3) abnormal grain growth which leads texture development or epitaxy. Grain growth models also provide a theoretical context for research on microstructure engineering using impurities, ion bombardment, substrate-surface-topography and precipitates.

Publications

Thompson, C.V. "Coarsening of Particles on a Planar Substrate: Interface Energy Anisotropy and Application to Grain Growth in Thin Films." *Acta Metall.* 36:2929 (1988).

Thompson, C.V. "Observations of Grain Growth in Thin Films." In *Microstructural Science for Thin Film Metallizations in Electronic Applications*, 115. Eds. J. Sanchez, D.A. Smith, and N. Delanerolle. Warrendale, Pennsylvania: the Minerals, Metals, and Materials Society, 1988.

2.2 Reliability and Microstructures of Interconnects

Sponsors

Joint Services Electronics Program
Contract DAAL03-89-C-0001
Semiconductor Research Corporation

Project Staff

Jaeshin Cho, Harold Kahn, Hai Longworth, Professor Carl V. Thompson

We are investigating the use of precipitates to produce metallic films and interconnects with engineered microstructures. We deposit initially layered alloy films (e.g., films deposited in a sandwich structure with a pure W layer between pure Al layers). When heated, precipitates form in the center of these films. These precipitates lead to a drag force which impedes grain boundary motion and

suppresses normal grain growth. Eventually, at elevated temperatures, a minor fraction of the grains begin to break free of the precipitates and grow abnormally. This can ultimately lead to very large grains and also changes in the crystallographic texture of films. With this technique, it is possible to control the grain sizes, the distribution of grain sizes, and the distribution of grain orientations over very broad ranges. We have now observed these effects in a number of aluminum alloy systems including Al-Cu-Cr, Al-Ag-Cr, Al-Mn-Cr, Al-Mn, and Al-W.

We are also developing new techniques which allow statistical characterization of failure of contacts and interconnects for silicon-based integrated circuit technology. We are using these techniques to correlate failure rates and mechanisms with microstructures of interconnect lines and contact diffusion barriers. We are investigating techniques for controlling microstructures in order to improve contact and interconnect reliability, especially under conditions which can lead to electromigration.

We have recently shown that interconnect lines with bimodally distributed grain sizes have drastically reduced reliabilities. Also, for lines with monomodally distributed (uniform) grain sizes, increasing the grain size (relative to line width) results in an increase of both the median time to electromigration-induced failure and the lognormal standard deviation in the time to failure, see figures 1-3. The net result, in large populations of lines with monomodal grain size distributions, is little or no change in the time to the first failure. We have explained these results in terms of a "failure unit model" in which grain boundaries are taken to be the individual units which are responsible for the reliability of a line. The successful application of this model indicates the importance of the properties of individual grain boundaries in controlling interconnect reliability. We are now investigating the statistical reliability of lines with single, controlled grain boundaries in order to understand in detail the type of microstructural features which limit interconnect reliability.

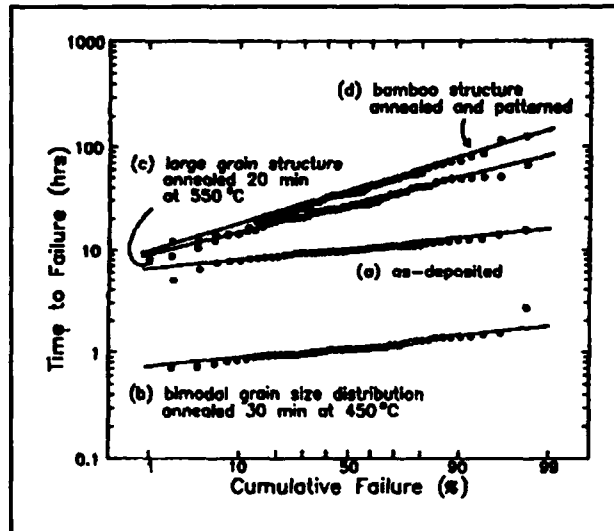


Figure 1. Distribution of failure times for 2.2- μm -wide, Al-2%Cu-0.3%Cr lines: (a) as-deposited (MTTF = 9.8 h, DTF = 0.197), (b) after annealing for 30 min. at 450°C to develop a bimodal grain size distribution (MTTF = 1.08 h, DTF = 0.223), (c) after annealing for 20 min. at 550°C to obtain mono-modally distributed large grains (MTTF = 26.3 h, DTF = 0.465), and (d) after annealing for 20 min at 550°C before patterning, to obtain bamboo microstructures (MTTF = 35.0 h, DTF = 0.580).

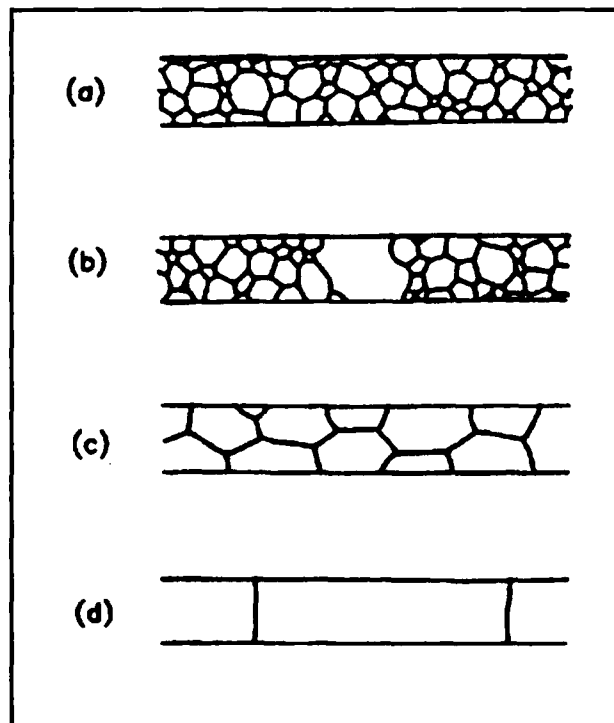


Figure 2. Sketches of the microstructures of the lines described in Figure 1, based on transmission electron microscopy.

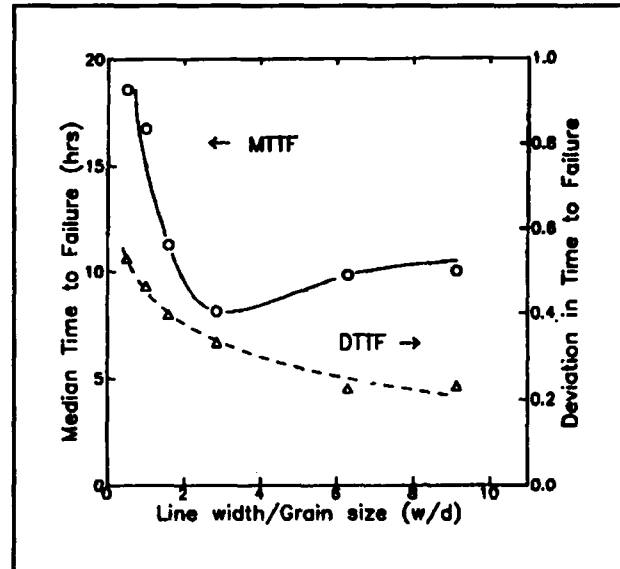


Figure 3. Median time to failure and deviation in the time to failure vs. linewidth/grain size ratio for Al-2%Cu-0.3%Cr lines with monomodally distributed grain sizes.

Publication

Cho, J., and C.V. Thompson. "The Grain Size Dependence of Electromigration Induced Failures in Narrow Interconnects." *Appl. Phys. Lett.* 54:2577 (1989).

2.3 Epitaxial Grain Growth

Sponsors

AT & T
U.S. Air Force - Office of Scientific Research
Contract AFOSR 85-0154

Project Staff

Jerrold A. Floro, Professor Carl V. Thompson, Professor Henry I. Smith

In the past year, we demonstrated that grain growth in polycrystalline films on single crystal substrates can lead to epitaxial films. This new approach to obtaining heteroepitaxial films can lead to ultrathin films with reduced defect densities compared to films deposited using conventional techniques. In epitaxial grain growth, ultrathin polycrystalline films are deposited on single crystal substrates. When these polycrystalline films are heated to elevated temperatures, epitaxial grains with low

film-substrate interface energies grow and consume misoriented grains. Because the initial polycrystalline films are deposited at low temperatures, fully continuous ultrathin films can be obtained. Conventional Volmer-Weber epitaxy which is carried out at higher deposition temperatures can not be used to obtain equivalently thin epitaxial films. We have developed kinetic analyses for epitaxial grain growth and are testing these analyses through experiments on model systems, including Au and Ag films on mica and NaCl. The ultimate goal of our research is to develop a general understanding of when and how epitaxial grain growth can be used as a route to low-defect-density ultra thin heteroepitaxial films in film/substrate systems with large lattice mismatches.

2.4 Heteroepitaxy in Lattice Mismatched Systems

Sponsor

U.S. Air Force - Office of Scientific Research
Contract AFOSR 85-0154

Project Staff

Joyce E. Palmer, Jerrold A. Floro, Geoffrey Burns,
Professor Carl V. Thompson, Professor Clifton G.
Fonstad

Heteroepitaxial growth of films with poor lattice matching with single crystal substrates often leads to films with high bulk as well as interface defect densities. When atom by atom or layer growth occurs, bulk defects are generally generated during strain accommodation well after film nucleation and the early stages of film growth. Alternatively, strain accommodation can occur through formation of low energy interfaces during competitive growth of grains or nuclei which initially have a variety of orientations. We are investigating these post-nucleation epitaxial processes in continuous and discontinuous films. Model systems include GaAs-on-silicon and epitaxial metals on alkali halide crystals.

2.5 Kinetics of Thin Film Silicide Formation

Sponsor

International Business Machines Corporation

Project Staff

Lawrence A. Clevenger, Dr. En Ma, Dr. Roberto R. DeAvillez, Professor Carl V. Thompson, King-N. Tu

There is considerable current interest in the use of refractory metals or refractory metal silicides as interconnects, as gate materials in MOS devices and for low contact resistance diffusion barriers at metal-silicon contacts in integrated circuits. One method of silicide formation is through reaction of metallic thin films with silicon substrates or polycrystalline silicon films. This application raises fundamental questions about the rate and products of thin film metal-silicon reactions. There are four critical parameters in analysis and modeling of these reactions; interdiffusivities, free energy changes, surface energies and interface reaction constants. Of these, the first two parameters are fairly well understood and can be predicted. The purpose of this project is to develop a better understanding and predictive capability for the last two parameters. Surface energies are being determined through silicide precipitation experiments and the kinetics of thin films reactions are being studied through thermal, TEM, and X-ray analysis of reactions in multilayer thin films.

We have found that in Pt/amorphous-Si, Ni/ α -Si, V/ α -Si and Ti/ α -Si multilayer films, an amorphous silicide is the first phase to form. These phases are thermodynamically stable only if crystalline silicide formation is kinetically suppressed. We have also detected evidence for nucleation at the early stages of the formation of crystalline silicides. These results suggest that phase selection in thin film reactions is governed by nucleation barriers.

We have also observed explosive reactions in multilayer metal/ α -Si films. These reactions can propagate in a room temperature ambient at velocities over 20 meters per second. This self-rapid-thermal-annealing process results in homogeneous films composed of the stable high temperature crystalline silicide.

2.6 Coarsening of Particles on a Planar Substrate

Sponsor

National Science Foundation

Project Staff

Yachin Liu, Professor Carl V. Thompson

Very small particles on a planar substrate can exchange material by atomic diffusion of the particle constituent on the substrate surface. This generally leads to an increase in the average particle size and spacing and can also lead to the development of restricted crystallographic orientations. This process can be very important in the early stages of the formation of a thin film. We have developed a theory to describe the evolution of particle sizes and orientations and are testing this theory by experimentally characterizing particle coarsening in model systems.

2.7 Thin Film Zone Melting Recrystallization of Silicon

Sponsor

International Business Machines Corporation

Project Staff

Paul Evans, James S. Im, Chenson K. Chen, Professor Carl V. Thompson

Techniques for producing device-quality single-crystal films of semiconductors on insulator (SOI) are of interest for multilayer or multimaterial integrated circuits, display devices and low-cost, high-efficiency solar cells. Such films can be obtained through directional solidification of confined thin films (zone melting recrystallization, ZMR). While there are analogies to bulk crystal growth, in ZMR there are also phenomena and mechanisms unique to thin-film solidification of radiatively heated silicon. Direct observation of dynamic and static liquid-solid interfaces complements theoretical modeling of solidification. We are studying these phenomena in order to develop means of controlling and optimizing thin film growth by ZMR.

We are also using ZMR to prepare thin film bicrystals in order to study the electronic properties of grain boundaries in silicon. We will correlate electronic properties with structural features, as revealed using high resolution electron microscopy.

2.8 Capillary Instabilities in Thin Solid Films

Project Staff

Eva Jiran, Professor Carl V. Thompson

Very thin metallic and semiconductor films ($\leq 200\text{\AA}$) are being used in an increasing variety of applications. Most solid films are used on substrates with which they would, in equilibrium, form non-zero contact angles. Therefore, even solid films tend to become discontinuous or bead in order to reduce their total film/substrate interface energy. This phenomena occurs in both continuous and patterned films. The rate of solid state beading is a strong function of the dimensions of a film or line as well as the microstructure of the film or line. For example, the beading rate rapidly increases with decreasing film thickness. We are experimentally characterizing the kinetics of beading of thin films of gold on SiO_2 . Film patterning allows independent study of both hole formation and hole growth.

2.9 Focused Ion Beam Induced Deposition

Sponsor

International Business Machines Corporation

Project Staff

Jaesang Ro, Andrew D. Dubner, Dr. John Melngailis, Professor Carl V. Thompson

It is now possible to produce ion beams with diameters as small as 500\AA . This permits use of focused ion beams for high spatial resolution implantation, sputtering and deposition. In principal, the latter can be used in integrated circuit mask repair or high resolution direct writing of interconnects. We are investigating the mechanisms of ion-beam-

induced chemical vapor deposition from metal-bearing gases.

2.10 Protective Coatings for Integrated Circuits in an In Vitro Environment

Sponsor

National Institutes of Health

Project Staff

David J. Edell, Professor Carl V. Thompson

We are investigating the use of various coating materials to prevent Na diffusion into integrated circuits to be used in biomedical applications. We are correlating processing conditions, microstructural characteristics and diffusion barrier properties to develop standard methodologies for deposition and characterization of protective coatings.

2.11 Publications

Ajuria, S.A. *Photon Enhanced Grain Growth*. S.M. thesis. Dept. of Mater. Sci. and Eng., MIT, 1989.

Atwater, H.A., and C.V. Thompson. "The Role of Point Defects in Ion-Bombardment-Enhanced and Dopant-Enhanced Grain Growth in Silicon Thin Films." *J. Nucl. Instrum. Meth. Phys. Res. B* 39:64 (1989).

Blauner, P.G., J.S. Ro, Y. Butt, C.V. Thompson, and J. Melngailis. "Direct Writing of Metallic Submicron Features Using Focused Ion Beams." *Materials Research Society Symposium Proceedings* 129: 483 (1989).

Clevenger, L.A., C.V. Thompson, and K.-N. Tu. "Controlled and Explosive Reactions in Nickel/Silicon Multilayer Thin Films." In *Materials Research Society International Meeting on Advance Materials* 10:431 (1989).

Clevenger, L.A., C.V. Thompson, and R.R. de Avillez. "Kinetics and Thermodynamics of Amorphous Silicide Formation in Nickel/-

Amorphous-Silicon Multilayer Thin Films." *Proceedings of the Spring 1989 MRS Meeting, Symposium D, San Diego, California*. Forthcoming.

Clevenger, L.A., C.V. Thompson, A.J. Judas, and J.L. Olson. "Metastable Reactions and Explosive Silicidation in Nickel/-Amorphous-Silicon Multilayer Thin Films." In *Selected Topics in Electronic Materials*, 23. Ed. B.R. Appleton et al. Materials Research Society, 1989.

Clevenger, L.A. *Controlled and Explosive Silicidation of Metal/Amorphous-Silicon Multilayer Thin Films*. Ph.D. diss. Dept. of Mater. Sci. and Eng. MIT, 1989.

Coffey, K.R., L.A. Clevenger, K. Barmak, D.A. Rudman, and C.V. Thompson. "Experimental Evidence for Nucleation During Thin Film Reactions." *Appl. Phys. Lett.* 55:852 (1989).

DeAvillez, R.R., L.A. Clevenger, and C.V. Thompson. "Relaxation Phenomena in Evaporated Amorphous Silicon Films." *J. Mater. Res.* 4:1057 (1989).

Im, J.S. *Experimental and Theoretical Investigation of Interface Morphologies Observed in Directional Solidification of Thin Si Films*. Ph.D. diss. Dept. of Mater. Sci., and Eng., MIT, 1989.

Palmer, J.E., G. Burns, C.G. Fonstad, and C.V. Thompson. "The Effect of As₄ Overpressure on Initial Growth of Gallium Arsenide on Silicon by MBE." *Appl. Phys. Lett.* 55:990 (1989).

Palmer, J.E. *Evolution of Microstructure in Ultra-Thin Films of GaAs and CaF₂ on Single Crystal Silicon*. Ph.D. diss. Dept. of Electr. Eng. and Comput. Sci., MIT, 1989.

Phillips, J.M., J.E. Palmer, N.E. Hecker and C.V. Thompson. "The Effect of Annealing on the Structure of Epitaxial CaF₂ Films on Si(100)." *Proceedings of the Spring 1989 Materials Research Society Meeting, Symposium D, San Diego, California, April 1989*. Forthcoming.

Quek, H.M. *An Investigation of Graphoepitaxy in Thin Au and Bi Films.* S.M. thesis. Dept. of Mater. Sci. and Eng., MIT, 1989.

Spaepen, F., and C.V. Thompson. "Calorimetric Studies of Reactions in Thin Films and Multilayers." *Appl. Surf. Sci.* 38:1 (1989).



Professor Carl V. Thompson checks a zone meter that was constructed in his laboratory.



Principal Research Scientist Dr. John Melngailis uses focused ion beams for patterned deposition from adsorbed gas molecules and for patterned implantation or lithography.

Chapter 3. Focused Ion Beam Fabrication

Academic and Research Staff

Dr. John Melngailis, Dr. Patricia G. Blauner, Dr. Tao Tao, Mark I. Shepard

Visiting Scientists and Research Affiliates

Dr. Khalid Ismail,¹ Professor Herbert D. Kaesz,² Leonard J. Mahoney,³ Dr. Alfred Wagner,¹ Ziling Xue²

Graduate Students

Andrew D. Dubner, Jeung-Soo Huh, Henri J. Lezec, James E. Murguia, Christian R. Musil, Jaesang Ro

Undergraduate Students

Yousaf Butt, Susan Zamani

Technical and Support Staff

Donna Martinez

3.1 Focused Ion Beam Fabrication

Research in focused ion beam applications is being conducted on two types of machines. The first system has mass separation and can produce beams of the dopants of Si and GaAs with diameters below 0.1 μm . This system, which is used for ion implantation and lithography, operates at voltages up to 150 kV, has sophisticated pattern generation software, and can accept up to five inch substrates. The second, simpler system has no mass separation and is operated with Ga^+ ions at energies up to 50 keV and minimum beam diameters of 0.06 μm . It is mounted on an ultrahigh vacuum system and has a sample stage which can be heated. This system is mainly used for ion induced deposition and milling.

3.2 Development of Focused Ion Beam Implantation and Lithography

Sponsor

U.S. Army Research Office
Contract DAAL03-88-K-0108

Project Staff

James E. Murguia, Mark I. Shepard, Christian R. Musil, Henri J. Lezec, Susan Zamani, Dr. John Melngailis

To apply ion beam implantation and lithography to integrated circuit fabrication, one must align the pattern to be written to existing features on the wafer. One must also generate this pattern from computer aided design. Accordingly, we have developed and refined the capability to transfer the patterns of any given level of an integrated circuit layout from the computer-aided design software in use at MIT, called

¹ IBM Research Division, Yorktown Heights, New York.

² University of California, Los Angeles.

³ MIT Lincoln Laboratory.

MAGIC, to the focused ion beam system. Different ion doses or dose gradients can be assigned to each rectangle of the design. This permits a wafer to be processed to a given step in the standard integrated circuits facility, transferred to the focused ion beam for implantation or for ultrafine lithography, and then transferred back to complete the fabrication.

Alignment is carried out by imaging alignment marks on the wafer using the scanning ion microscope mode. In addition, beam deflection routines have been developed which calibrate beam deflection, stage motion, and correct for axis non-orthogonality. We have placed features on a wafer aligned to $\pm 0.1 \mu\text{m}$. The overall capability that we have developed is essential to our implantation and lithography projects.

3.3 Frequency Tunable Gunn Diodes Fabricated by Focused Ion Beam Implantation

Sponsor

U.S. Army Research Office
Contract DAAL03-88-K-0108

Project Staff

Henri J. Lezec, Dr. Khalid Ismail, Mark I. Shepard, Leonard J. Mahoney, Professor Dimitri A. Antoniadis, Dr. John Melngailis

We have developed frequency tunable Gunn diodes which consist of two contacts on a GaAs surface. A conducting channel, which has a gradient of doping in the direction of current flow, runs between the two contacts. The frequency can be tuned from 6 to 23 GHz by varying the bias voltage by about 12 V. The power output of the devices is in the -3 to -4 dBm range. A Gunn diode with uniform doping shows very little variation of frequency with bias. Many gradients of doping were implanted by programming the focused ion beam system appropriately. In

addition, measurements were made of the percent of activation as a function of implanted dose. Since this percentage decreases with increasing dose, a linear gradient of dose does not imply a linear gradient of doping or of resistivity. The devices have been modeled using a computer program based on the Boltzmann transport equation. The tunable Gunn diodes may prove useful for special radars such as those used in collision avoidance.

3.4 NMOS Transistors with Focused Ion Beam Implanted Channel Regions

Sponsor

U.S. Army Research Office
Contract DAAL03-88-K-0108

Project Staff

James E. Murguia, Mark I. Shepard, Christian R. Musil, Professor Dimitri A. Antoniadis, Dr. John Melngailis

NMOS transistors with gate lengths from $1.6 \mu\text{m}$ to $10 \mu\text{m}$ were fabricated in the integrated circuits facility. Focused ion beam implantation was substituted for the threshold and punch-through control implants. Both boron and arsenic were implanted and both the geometry of the implant and the dose were varied. A total of 1,920 combinations of variables were fabricated in duplicate on the wafer. Four wafers were processed to verify reproducibility. NMOS transistors with a line implant (0.1 to $0.2 \mu\text{m}$ wide) adjacent to the source were compared to devices with no implant. A small increase in transconductance and a large increase in output conductance were observed. This resulted in a factor of twenty increase in open circuit gain. This result demonstrates the use of the focused ion beam to economically explore novel device concepts over a wide range of variables.

3.5 GaAs MESFETs Fabricated with Focused Ion Beam Channel Implants

Sponsors

Hughes Research Laboratories Fellowship
U.S. Army Research Office
Contract DAAL03-88-K-0108

Project Staff

Christian R. Musil, Leonard J. Mahoney, Mark I. Shepard, Dr. John Melngailis

We expect GaAs MESFETs with a gradient of doping from source to drain to show improved performance. This is of particular interest for short gates. We have designed and fabricated a mask set to explore a wide variety of transistor structures. The contacts and longer gates will be fabricated by conventional optical lithography using these masks. Ultra short gates (below $0.1\ \mu\text{m}$) will be fabricated using the focused ion beam to expose the resist. The penetration of ions into the substrate during the resist exposure is an undesirable side effect. A technique to overcome this has been developed and tested using a film of Si_3N_4 on the GaAs substrate under the resist. The film prevents ion penetration and damage, yet can be etched to apply the contact.

3.6 Focused Ion Beam Exposure of Resists

Sponsor

SEMATECH

Project Staff

Jeung-Soo Huh, James E. Murguia, Professor Herbert H. Sawin, Dr. John Melngailis

The goal of this program is to generate known resist profiles for the purpose of studying their effect on plasma etched features. Optical lithography can be used down to about $1\ \mu\text{m}$. Below that, focused ion beam lithography will be used. So far, we have exposed features down to $0.05\ \mu\text{m}$ in PMMA in $0.3\ \mu\text{m}$ thick resist with vertical sidewalls. These were made into x-ray lithography masks in collaboration with the MIT

Submicron Structures Laboratory. We are seeking other focused ion beam resists besides PMMA. We have used Shipley SAL 601 negative resist to also expose features down to $0.1\ \mu\text{m}$. However, this is less desirable since profile control in negative resists is difficult. Microport 2400 which is a positive e-beam resist was also tried but was found to have a small exposure window, i.e., less than a factor of two between threshold exposure and cross linking. Other candidates are being considered. The profile development will be modelled using TRIM programs for ion penetration and SAMPLE for resist dissolution.

3.7 Focused Ion Beam Induced Deposition of Low Resistivity Gold Structures

Sponsors

Charles S. Draper Laboratory
Contract DL-H-261827
U.S. Army Research Office
Contract DAAL03-87-K-0126

Project Staff

Dr. Patricia G. Blauner, Jaesang Ro, Yousaf Butt, Professor Carl V. Thompson, Dr. John Melngailis

A local gas ambient is created in vacuum on a sample surface by aiming a gas feed capillary tube at the surface in close proximity. For gold depositions we use a gas of $\text{C}_7\text{H}_7\text{F}_6\text{O}_2\text{Au}$. Deposition occurs when a focused ion beam is scanned on the surface in the area of the gas ambient. Ion induced deposition permits fabrication of deposited features at dimensions much finer than those achieved by laser induced deposition. Ion induced deposition is already in commercial use for repair of photolithography masks. If conducting films can be deposited, this process will be used for local repair and restructuring of integrated circuits. Also, if high aspect ratio structures (thick with steep side walls) can be deposited, the repair of x-ray lithography mask will become possible.

We have deposited gold lines down to $0.1\ \mu\text{m}$ width and patches $3 \times 3\ \mu\text{m}$ of $1\ \mu\text{m}$ thickness with steep side walls. The microstructure of the gold films has been studied by transmission electron microscopy. The

films grow in discontinuous, ball-like structures at the early stages and in columns as they thicken. Some features have been deposited on actual x-ray lithography masks and tested at the Fraunhofer Institute in Berlin. In spite of the structure, the x-ray opacity of films 0.8 μm thick was found to be sufficient for normal mask exposure.

When the substrate is heated to about 120°C, the structure of the deposited films is observed to change. In addition, the resistivity is found to drop from a value of $\sim 1000 \mu\Omega\text{cm}$ to a value below $10 \mu\Omega\text{cm}$, i.e., near the bulk value for gold of $2.4 \mu\Omega\text{cm}$. This is the first deposition of low resistivity metal film by this process. Low resistivity is needed for application of focused ion beam induced deposition to integrated circuit restructuring and repair.

3.8 Fundamental Properties of Ion Induced Deposition

Sponsors

Charles S. Draper Laboratory
Contract DL-H-261827
U.S. Army Research Office
Contract DAAL03-87-K-0126

Project Staff

Jaesang Ro, Professor Carl V. Thompson, Dr. John Melngailis

The ion induced deposition of gold from dimethylgold hexafluoro acetylacetonate has been studied using noble gas ions from an implanter. Although the instantaneous current density in a focused ion beam is about five orders of magnitude higher than that from a broad implanter beam, the fundamental principles of the process are the same. In the case of a focused ion beam, the beam is usually scanned rapidly over a given area so that the average current density is more nearly comparable. In going from Ne to Xe, the yield (atoms deposited/incident ion) is found to increase. The yield correlates better with nuclear stopping power than with electronic stopping power. In addition, the sputtering yield for each ion species was measured.

The mechanism by which the ion transfers energy to a molecule adsorbed on the surface is not clear. It is not direct ion-molecule impact because the cross section is too large. The substrate must participate. We are attempting to model the process using the TRIM program to calculate the energy distribution of surface atoms as a function of distance from the point of ion impact. The yield measurements are being carried out at room temperature, where the films are known to contain carbon, as well as at 120°C (where the films are much purer and their resistivities are nearly equal to the bulk gold values).

3.9 In-Situ Measurement of Gas Adsorption and Ion Induced Deposition

Sponsors

IBM General Technologies Division
IBM Research Division

Project Staff

Andrew D. Dubner, Dr. Alfred Wagner, Professor
Carl V. Thompson, Dr. John Melngailis

We have constructed a special apparatus to measure gas adsorption and ion induced deposition. The apparatus consists of an ultrahigh vacuum chamber with an ion gun having energies from 0.1 to 10 keV. The sample is a quartz crystal microbalance which can measure the gas adsorption as well as the film growth during ion induced deposition. The gas used is dimethylgold hexafluoro acetylacetonate ($\text{C}_7\text{H}_7\text{F}_6\text{O}_2\text{Au}$) and a monolayer is found to be adsorbed above 1 mTorr pressure. If the sample is cooled below room temperature and the gas pressure is raised above 100 mTorr, then a thicker layer of adsorbate is formed. The yield of atoms deposited per incident ion can be rapidly measured. The cross section for decomposition was found to be $2 \times 10^{-13} \text{ cm}^2$ for 5 keV Ar^+ ions. The deposition is a competition between sputtering and gas molecule decomposition. Contrary to our observations of ion induced deposition with high energy beams (30-100 keV) at these lower energies, relatively pure gold films can be deposited even at room temperature.

3.10 Focused Ion Beam Induced Deposition of Platinum

Sponsors

Charles S. Draper Laboratory
Contract DL-H-261827
U.S. Army Research Office
Contract DAAL03-87-K-0126

Project Staff

Dr. Tao Tao, Ziling Xue, Professor Herbert D. Kaesz, Dr. John Melngailis

Focused ion beam induced deposition of platinum from a precursor gas of (Methylcyclopentadienyl) - Platinumtrimethyl has been demonstrated. This organometallic is solid at room temperature with a vapor pressure of 0.06 Torr. A Ga^+ ion beam at 35 keV has been used. The resistivity and composition of the film and the deposition yield have been studied as a function of ion current density, line dose, substrate temperature, geometry, and supplementary hydrogen pressure. Yield varied from 0.2 to 30, and resistivity varied from 70 to 700 $\mu\Omega\text{cm}$ depending on the conditions. The lowest resistivity was observed at the highest current density: 0.22 nA at 500 cm/sec scan speed repeated over a 350 μm long line. The minimum linewidth observed so far is 0.3 μm , and the deposited platinum is found to be smooth. Auger analysis showed the films to contain carbon. The addition of hydrogen gas supplied to the same area by a second nozzle was found to have little effect on yield or resistivity. Although the deposition of gold from an organometallic precursor on a heated substrate results in low resistivity films, in the case of platinum this is not observed; in fact deposition yield drops to zero as the temperature is raised.

Deposition was also carried out in a focused ion beam milled groove 0.65 μm deep. The yield was found to be 34 at the bottom of the groove and decreased as the groove was filled in.

Focused ion beams induced deposition of platinum is of interest for circuit restructuring and repair because (1) the films have the lowest resistivity reported so far for deposition at room temperature and (2) platinum, unlike gold, is compatible with silicon device

fabrication. Platinum deposition is also expected to be useful for x-ray lithography mask repair because the x-ray absorption of platinum is slightly higher than that of gold or tungsten.

Publications

Blauner, P.G., J.S. Ro, Y. Butt, C.V. Thompson, and J. Melngailis. "The Microstructure of Gold Films Written by Focused Ion Beam Induced Deposition." *Mat. Res. Soc. Symp. Proc.* 129 (1989).

Blauner, P.G., J.S. Ro, Y. Butt, and J. Melngailis. "Focused Ion Beam Fabrication of Submicron Gold Structures." *J. Vac. Sci. Technol. B* 7: 609 (1989).

Blauner, P.G., Y. Butt, J.S. Ro, C.V. Thompson, and J. Melngailis. "Focused Ion Beam Induced Deposition of Low Resistivity Gold Films." *J. Vac. Sci. Technol. B* 7: 1816 (1989).

Chu, W., A. Yen, K. Ismail, M.I. Shepard, H.J. Lezec, C.R. Musil, J. Melngailis, Y.C. Ku, J.M. Carter, and H.I. Smith. "Sub-100 nm X-Ray Mask Technology Using Focused-Ion-Beam Lithography." *J. Vac. Sci. Technol. B* 7: 1583 (1989).

Dubner, A.D., and A. Wagner. "In-Situ Measurement of Ion Beam Induced Deposition of Gold." *Mat. Res. Soc. Symp. Proc.* 147: 155 (1989).

Dubner, A.D., and A. Wagner. "In-Situ Measurement of Ion Beam Induced Deposition of Gold." *J. Appl. Phys.* 65(9): 3636 (1989).

Dubner, A.D., and A. Wagner. "The Role of Gas Adsorption in Ion-Beam-Induced Deposition of Gold." *J. Appl. Phys.* 66(2): 870 (1989).

Dubner, A.D., and A. Wagner. "Mechanism of Ion Beam Deposition of Gold." *J. Vac. Sci. Technol. B* 7: 1950 (1989).

Ismail, K., W. Chu, R.T. Tiberio, A. Yen, H.J. Lezec, M.I. Shepard, C.R. Musil, J. Melngailis, D.A. Antoniadis, and H.I. Smith. "Resonant Tunneling Across and

Mobility Modulation Along Surface-Structured Quantum Wells." *J. Vac. Sci. Technol. B* 7: 2025 (1989).

Melngailis, J. "Focused Ion Beam Lithography and Implantation." *Proceedings of 8th Biennial University/Government/Industry Microelectronics Symposium*. June 1989.

Melngailis, J. and P.G. Blauner. "Focused Ion Beam Induced Deposition." *Mat. Res. Soc. Symp. Proc.* 147 (1989) (Proceedings of Spring Meeting San Diego, Symposium on Ion Beam Processing of Advanced Electronic Materials, April 1989).

Chapter 4. Chemical Reaction Dynamics at Surfaces

Academic and Research Staff

Professor Sylvia T. Ceyer, Dr. Kenneth B. Laughlin, Dr. Kevin J. Maynard

Graduate Students

John D. Beckerle, David J. Gladstone, Andrew D. Johnson, Marianne McGonigal, Michelle Schulberg, Qingyun Yang

Undergraduate Student

Gerald Cain

4.1 Chemical Reaction Dynamics on Semiconductor Surfaces

Sponsor

Joint Services Electronics Program
Contract DAAL03-89-C-0001

Project Staff

Professor Sylvia T. Ceyer, Dr. Kenneth B. Laughlin,
David J. Gladstone, Marianne McGonigal,
Michelle Schulberg, Gerald Cain

The etching of semiconductor materials in halocarbon plasma environments is a complex chemical process. The plasma is used to produce species that are highly reactive with the semiconductor surface. Because many different reactive species, including radicals, ions, and highly excited neutral molecules are produced in a plasma, the mechanism of the etching reaction is difficult to probe. Our program is aimed at using molecular beam reactive scattering techniques to systematically examine the role of each of these species in the etching process.

The initial goal of this project was to measure the barrier to F_2 dissociative chemisorption on Si(100). Contrary to popular belief, we found essentially no barrier to the dissociation of F_2 on the unfluorinated surface. The dissociative chemisorption of F_2 on Si(100) proceeds with unit probability for translational energies of the incident F_2 molecules as low as 0.5 kcal/mol. However, there is a substantial barrier to dissociation above fluorine coverages of 0.5 monolayer. Higher

fluorine coverages sufficient to produce the etch product SiF_4 require a higher translational energy of the F_2 molecule. We have observed efficient etching of Si(100) at 300 K for an incident kinetic energy of F_2 of 15 kcal/mol. The angular and translational energy distributions of the SiF_4 — as measured in our newly constructed scattering apparatus consisting of two beams incident on a surface and a rotatable, triply differentially pumped quadrupole mass spectrometer — indicate that the last step of the reaction is the thermal desorption of the product SiF_4 molecule.

We have established that silicon can be etched without the use of molecules incident with energies of hundreds of electron volts, such as those present in plasma etching environments. Molecular beam techniques utilize molecules with energies only slightly higher than thermal (<1 eV), and therefore do not introduce radiation damage or defects into the Si lattice, which is a typical result of plasma etching. We are continuing our work on this system to understand the lack of F_2 energy dependence on the formation of a second reaction product, SiF_2 .

We have also recently observed a new kind of mechanism for dissociative chemisorption. In the limit of zero fluorine coverage, we observed that the Si surface strips one of the fluorine atoms from the incident F_2 molecule, leaving the other fluorine atom to scatter into the gas phase. Although this stripping reaction is analogous to the well-known stripping reactions in gas phase chemical reaction dynamics, this is the first observation of its kind from a surface.

Publications

Ceyer, S.T., D.J. Gladstone, M. McGonigal and M.T. Schulberg, "Molecular Beams: Probes of the Dynamics of Reactions on Surfaces." in *Physical Methods of Chemistry*. 2nd ed. Eds. B.W. Rossiter, J.F. Hamilton and R.C. Baetzold. New York: Wiley, 1990. In press.

Gladstone, D.J., M.T. Schulberg, K.B. Laughlin, M. McGonigal and S.T. Ceyer. "Design of a Power Supply for Resistive Heating of Semiconductor Crystals."

Gladstone, D.J. *Reaction Dynamics of Fluorine with Silicon (100): Design of a Molecular Beam Surface Reactive Scattering Chamber*. Ph.D. diss. Department of Chemistry, MIT, 1989.

Laughlin, K.B., D.J. Gladstone, M. McGonigal and S.T. Ceyer. "Dynamics of the Reaction of F_2 with Si(100)." Paper presented at the Dynamics of Gas-Surface Interactions, Gordon Conference, August, 1989.

McGonigal, M., M.T. Schulberg, D.J. Gladstone, K.B. Laughlin, S.T. Ceyer. "Reactions of F_2 with Si(100)." Paper presented at Materials Research Society, Boston, December, 1989.

McGonigal, M. *Reactive Chemisorption of Molecular Fluorine on Si(100)*. Ph.D. diss. Department of Chemistry, MIT, 1989.

Schulberg, M.T., M. McGonigal, D.J. Gladstone, K.B. Laughlin, S.T. Ceyer. "The Etching of Si(100) with a Molecular Beam of F_2 ." Paper presented at the American Vacuum Society, Boston, October, 1989.

4.2 Collision Induced Dissociative Chemisorption of CH_4 on Ni(111) by Inert Gas Atoms: The Mechanism for Chemistry with a Hammer

Sponsors

MIT Energy Laboratory - Synthetic Fuels Center
National Science Foundation
Grant CHE 85-08734
Petroleum Research Fund
Contract 19014-AC5

Project Staff

Professor Sylvia T. Ceyer, John D. Beckerle, Andrew D. Johnson, Qingyun Yang

We observed that the dissociation of CH_4 physisorbed on Ni(111) at 46 K is induced by the impact of incident inert gas atoms. We studied the dynamics and mechanism of this new process — collision induced dissociative chemisorption — using molecular beam techniques coupled with ultrahigh vacuum electron spectroscopies. The absolute cross section for collision induced dissociation is measured over a wide range of kinetic energies (28–109 kcal/mol) and incident angles of Ne, Ar and Kr atom beams. The cross section displays a complex dependence on the energy of the impinging inert gas atom, characteristic of neither total nor normal energy scaling. Quantitative reproduction of the complex dependence of the cross section on the Ar and Ne incident energy by a two-step, dynamical model establishes the mechanism for collision induced dissociation.

Collision induced dissociation occurs by the impulsive transfer of kinetic energy upon collision of Ar or Ne with CH_4 , followed by the translationally activated dissociative chemisorption of the CH_4 upon its subsequent collision with the Ni surface. The dependence of the probability of activated dissociation on the resultant CH_4 normal energy, derived from the fit of the model to the experimental cross section, is in excellent agreement with the results of a previous study of the translationally activated dissociative chemisorption of CH_4 on Ni(111). We have shown that collision induced activation and translational activation are consistent

mechanisms for providing energy to CH_4 , surmounting the barrier to dissociative chemisorption.

Publications

Beckerle, J.D., A.D. Johnson, Q.Y. Yang and S.T. Ceyer. "Collision Induced Dissociative Chemisorption of CH_4 on $\text{Ni}(111)$ by Inert Gas Atoms: The Mechanism for Chemistry with a Hammer." *J. Chem. Phys.* 91: 5756 (1989).

Ceyer, S.T. "Translational and Collision Induced Activation of CH_4 on $\text{Ni}(111)$: Phenomena Connecting UHV Surface Science to High Pressure Heterogeneous Catalysis." *Langmuir* 6:82 (1990).

Ceyer, S.T. "The Mechanism for CH_4 Dissociation and the Synthesis of C_6H_6 from CH_4 on $\text{Ni}(111)$." Paper presented at the Pacifichem '89 Conference, American Chemical Society, Honolulu, Hawaii, December, 1989.

Ceyer, S.T. "Dynamics of Sticky Collisions with a Surface: Splats and Hammers." Paper presented at the National Symposium on Frontiers of Science, National Academy of Science, Irvine, CA March, 1989.

Ceyer, S.T. "Dynamics of Activated Dissociative Chemisorption and Collision Induced Desorption of CH_4 on $\text{Ni}(111)$." Paper presented at the Debye Symposium, American Chemical Society Meeting, Dallas, April, 1989.

Ceyer, S.T. "Dynamics of Sticky Collisions with a Surface: Splats and Hammers." Paper presented at the Ninth International Summer Institute in Surface Science, University of Wisconsin at Milwaukee, August, 1989.

Ceyer, S.T. "Dynamics of Collision Induced Dissociation and Desorption of CH_4 on $\text{Ni}(111)$." American Institute Chem. Eng. Meeting, San Francisco, November, 1989.

4.3 Collision Induced Desorption

Sponsors

MIT Energy Laboratory - Synthetic Fuels Center
National Science Foundation
Grant CHE 85-08734
Petroleum Research Fund
Contract 19014-AC5

Project Staff

Professor Sylvia T. Ceyer, John D. Beckerle, Andrew D. Johnson, Qingyun Yang

The desorption of CH_4 physisorbed on $\text{Ni}(111)$ is observed to be induced by collision with Ar atoms incident with energies less than 2 eV. The absolute cross section for collision induced desorption is measured as a function of the kinetic energy and incident angle of the Ar beam. The mechanism for desorption is shown to involve a direct and impulsive, bimolecular collision between Ar and CH_4 . Molecular dynamics simulations show that the energy and incident angle dependence of the desorption cross section are the consequence of two competing dynamical effects.

Publications

Beckerle, J.D., A.D. Johnson and S.T. Ceyer, "Observation and Mechanism of Collision Induced Desorption: CH_4 on $\text{Ni}(111)$," *Phys. Rev. Lett.* 62: 685 (1989).

Ceyer, S.T. "Dynamics of Sticky Collisions with a Surface: Splats and Hammers." Paper presented at the National Symposium on Frontiers of Science, National Academy of Science, Irvine, CA, March, 1989.

Ceyer, S.T. "Dynamics of Activated Dissociative Chemisorption and Collision Induced Desorption of CH_4 on $\text{Ni}(111)$." Paper presented at the Debye Symposium, American Chemical Society Meeting, Dallas, April, 1989.

Ceyer, S.T. "Dynamics of Sticky Collisions with a Surface: Splats and Hammers." Paper presented at the Ninth International Summer Institute in Surface Science, Uni-

versity of Wisconsin at Milwaukee, August, 1989.

Ceyer, S.T. "Dynamics of Collision Induced Dissociation and Desorption of CH_4 on $\text{Ni}(111)$." American Institute Chem. Eng. Meeting, San Francisco, November, 1989.

Ceyer, S.T. "Dynamics of Sticky Collisions with a Surface: Splats and Hammers." Paper presented at Workshop on Dynamics of Surface Reactions, Copenhagen, Denmark, May, 1989.

4.4 Synthesis of Benzene from Methane

Sponsors

MIT Energy Laboratory - Synthetic Fuels Center
National Science Foundation
Grant CHE 85-08734
Petroleum Research Fund
Contract 19014-AC5

Project Staff

Professor Sylvia T. Ceyer, Dr. Kevin Maynard, Andrew D. Johnson, Qingyun Yang

With the knowledge gained from our studies of methane activation about the microscopic origins for the pressure gap, we have been able to develop a scheme for bypassing the high pressure requirement. This scheme involves raising the energy of the incident molecule or collisionally inducing dissociation. In this way, we have been able to perform a high pressure reaction at low pressure: the synthesis of C_6H_6 from CH_4 . In addition, because this reaction is carried out at low pressure, we have been able to identify the adsorbed intermediates by high resolution electron energy loss spectroscopy and to determine the mechanism of this reaction.

The synthesis is effected by exposing a monolayer of CH_4 physisorbed on $\text{Ni}(111)$ at 47 K to a beam of Kr atoms. The collision of the incident Kr with the physisorbed CH_4 distorts the CH_4 from its tetrahedral configuration, thereby lowering the barrier to dissociation into an adsorbed methyl radical and an adsorbed hydrogen atom. As the surface temperature is raised to 230 K, all the

adsorbed CH_3 dissociates to CH and the CH recombines to form adsorbed C_2H_2 . Some of the C_2H_2 trimerizes to adsorbed C_6H_6 and at 410 K and 425 K, respectively, the atomically adsorbed hydrogen desorbs as H_2 and some of the chemisorbed C_6H_6 desorbs. The gas phase benzene is detected mass spectrometrically in a thermal desorption experiment. Although the maximum thermal desorption yield for benzene is 1.5 percent at a crystal heating rate of 17 K/S, the gas phase hydrocarbon selectivity of this synthesis for benzene production is 100 percent. This is the first observation of a reaction of CH_4 to form a gas phase, higher hydrocarbon over a metallic catalyst at the low pressures commensurate with a UHV environment.

Publications

Ceyer, S.T. "Bridging the Gap Between Surface Science and High Pressure Processes." Langmuir Award Lecture presented at the American Chemical Society, Miami, Florida, September, 1989.

Maynard, K.J., Q.Y. Yang, A.D. Johnson and S.T. Ceyer, "The Synthesis of C_6H_6 from CH_4 ." Paper presented at the American Vacuum Society, Boston, October, 1989.

Yang, Q.Y., A.D. Johnson, K.J. Maynard and S.T. Ceyer. "Synthesis of Benzene from Methane over a $\text{Ni}(111)$ Catalyst." *J. Am. Chem. Soc.* 111: 8748 (1989).

4.5 The Structure and Chemistry of CH_3 and CH Radicals and Isotopic Variants Adsorbed on $\text{Ni}(111)$

Sponsors

MIT Energy Laboratory - Synthetic Fuels Center
National Science Foundation
Grant CHE 85-08734
Petroleum Research Fund
Contract 19014-AC5

Project Staff

Professor Sylvia T. Ceyer, Qingyun Yang, Andrew D. Johnson, Dr. Kevin Maynard

We present a detailed analysis of the vibrational spectra of CH_3 , CH_2D and CD_3 adsorbed on $\text{Ni}(111)$ and of the products of its reactions. Molecular beam techniques effect the synthesis of adsorbed methyl radicals from CH_4 , CH_3D or CD_4 . Because we can measure these spectra at both higher resolution (30 cm^{-1}) and higher sensitivity (5×10^6 counts/sec), we have been able to observe both new features and also to carry out a symmetry analysis. The CH_3 radical is shown to be adsorbed with C_{3v} symmetry on a threefold hollow site. The symmetric C-H stretch mode of CH_3 and the overtone of the asymmetric deformation mode are shown to be in Fermi resonance. At temperatures above 150 K, CH_3 dissociates to form adsorbed CH.

Confirmation for the assignment of the spectrum to a CH species is found in the spectrum measured after thermal decomposition of CH_2D . This species decomposes to a mixture of adsorbed CH and CD. The frequencies of the C-H and C-D stretch modes are identical to the frequencies of these species produced from the decomposition of CH_3 and CD_3 . The adsorption site of the CH species is determined to be a threefold hollow site and the geometry of the $\text{Ni}_3\text{-C-H}$ is determined to be pyramidal. At temperatures above 230 K, carbon-carbon bond formation between the CH species is observed to yield C_2H_2 . Low coverages of C_2H_2 are shown conclusively to dissociate to C_2H and C_2 species at 400 K in contrast to a literature report of C_2H_2 dissociation to adsorbed CH. At temperatures above 380 K, high coverages of C_2H_2 result in trimerization to adsorbed benzene. The relative stabilities of the C_1 species on $\text{Ni}(111)$ are determined to be $\text{CH}_2 < \text{CH}_3 < \text{CH}$.

Publications

Yang, Q.Y. *The Chemistry of CH_4 on $\text{Ni}(111)$* . Ph.D. diss. Dept. of Chemistry, MIT, 1989.

4.6 High Resolution Electron Energy Loss Spectroscopy of H on $\text{Ni}(111)$

Sponsors

MIT Energy Laboratory - Synthetic Fuels Center
National Science Foundation
Grant CHE 85-08734
Petroleum Research Fund
Contract 19014-AC5

Project Staff

Professor Sylvia T. Ceyer, Qingyun Yang, Andrew D. Johnson, Dr. Kevin Maynard

A high resolution electron energy loss spectrum of half of a monolayer of $\text{H}(\text{D})$ adsorbed on $\text{Ni}(111)$ has been measured with sufficient intensity and resolution to allow seven vibrational loss features to be observed: $\nu_{\text{asy}} = 745, 790\text{ cm}^{-1}$; $\nu_{\text{sym}} = 1085, 1105\text{ cm}^{-1}$; $2\nu_{\text{asy}} = 1260, 1400\text{ cm}^{-1}$; $2\nu_{\text{sym}} = 2180\text{ cm}^{-1}$. The assignments of the fundamentals are based on the measured anharmonicity and angular distributions of the vibrational loss features.

The splitting of the ν_{asy} and ν_{sym} modes is explained by the local potential difference of H adsorbed on the fcc and hcp threefold sites. The absence of dispersion of these modes, as evidenced by measurements of the spectra at Σ of the Brillouin zone, indicate that dynamical coupling between the hydrogen atoms on neighboring sites is not operative to within the resolution of this experiment.

The splitting of the overtone of the asymmetric Ni-H stretch mode is due to a transition of each of the two different hydrogen atoms to the second vibrationally excited state. The observation of two distinct vibrational frequencies corresponding to the hydrogen atoms adsorbed on two threefold sites, whose structures differ only in the presence of a Ni atom in the second layer, confirms the previously proposed structure for the $(2 \times 2)2\text{H}$ overlayer. Since this is the first observation of any experimentally determined distinction in the physical properties of hcp and fcc threefold sites on any metal surface, these results provide a critical test of theory.

Publications

Yang, Q.Y., A.D. Johnson and S.T. Ceyer, "High Resolution Electron Energy Loss Spectroscopy of H on Ni(111)." Paper presented at American Vacuum Society, Boston, October, 1989.

Yang, Q.Y. *The Chemistry of CH₄ on Ni(111)*. Ph.D. diss. Dept. of Chemistry, MIT, 1989.



Professor Sylvia T. Ceyer with the molecular beam surface scattering apparatus.

Chapter 5. Measurement of Electron-phonon Interactions Through Large-amplitude Phonon Excitation

Academic and Research Staff

Professor Keith A. Nelson

Visiting Scientists and Research Affiliates

Dan E. Leaird,¹ Dr. Andrew M. Weiner¹

Graduate Student

Gary P. Wiederrecht

5.1 Introduction

Sponsor

Joint Services Electronics Program
Contract DAALO3-89-C-0001

The main goal of this project is to measure the strengths of electron-phonon interactions in semiconductors to understand the effect of these interactions on electron mobility at different temperatures. A secondary goal — extremely important for ultrafast electronics — is to determine the responses of electronic materials to input signals which are both fast (i.e., pulses of short duration) and high in repetition rate (i.e., many short pulses in rapid succession).

5.2 High Repetition-rate Signals and Resonant Responses of Crystalline Solids

We have successfully characterized the electronic and vibrational responses of a wide variety of solids to single femtosecond pulses. With earlier JSEP support, we demonstrated that ultrashort optical pulses passing through nearly any material initiate coherent vibrational oscillations that influence the material's transient optical and electrical responses. This finding is important for fast electronics because it indicates the

response of materials to fast electrical and optical signals. The material's response to sufficiently short signal duration (i.e., optical or electrical pulse duration) can include transient vibrational oscillations, negatively affecting its usefulness in possible applications such as information processing.

At the same time, the initiation of coherent lattice vibrational oscillations with ultrashort pulses provides us with a unique spectroscopic tool. We can record femtosecond time-resolved "stop-action" spectroscopic observations of coherently vibrating crystal lattices, permitting characterization of well defined, nonequilibrium crystal structures at various stages of vibrational distortion. Characterization of the effects of lattice vibrations (phonons) on electronic energy levels is of particular importance in semiconductors since temperature-dependent carrier mobilities are influenced by electron-phonon interactions.

Figure 1 shows the typical effects of a single ultrashort pulse on a crystalline solid. A femtosecond pulse exerts an "impulse" force on lattice vibrational modes, initiating vibrational oscillations. These oscillations influence the material's optical and electrical properties. The Terahertz-frequency oscillations in the data (shown in figure 1) correspond to individual lattice vibrational oscillation cycles, observed in real-time.

¹ Bell Communications Research (Bellcore).

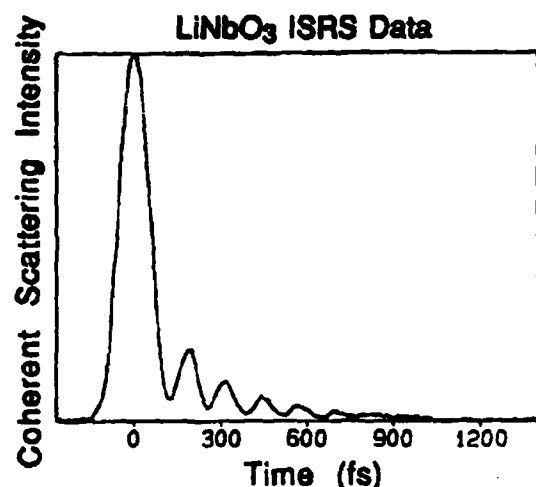


Figure 1. Impulsive stimulated Raman scattering (ISRS) data in which optic phonon oscillations and decay in lithium niobate are monitored. In this noncentrosymmetric crystal, the optic phonon mode is both Raman and IR active, and is strongly coupled to the polariton mode associated with infrared light propagation. The phonon oscillations induced through ISRS are therefore accompanied by IR radiation at the same frequency. Femtosecond pulses have therefore been used to excite phonons and also to produce tunable Terahertz-frequency (far-IR) radiation. The phonon frequency and damping rate depend on the ISRS scattering angle.

We are monitoring the material responses to high-density signals instead of a single signal for two main reasons. First, in any real-world high-speed signal-processing application, it is essential to process signals which are not only short in duration but also frequent, i.e., signals with high information density. It is important, therefore, to understand the differences between a material's response to one isolated pulse and its response to many pulses in rapid succession, the latter being far more relevant to applications.

Second, the data in figure 1 illustrate our ability to use short light pulse to control solid-state structure and behavior in a very precise way. We can use pulses to literally move ions or molecules in crystals toward or away from each other. In addition, we can monitor the motions and their effects in real time. Unfortunately, the extent of our optical control is limited because, with a single pulse, we can only move material very small distances — less than 10^{-3} Å. These small dis-

tances have dramatic effects in signal processing, as figure 1 illustrates. However, if we could drive lattice vibrations much harder — for example, to amplitudes exceeding 0.1 Å — we could induce permanent structural changes in solids, fabricate new materials, etc. We could also characterize electron-phonon interactions over a wide range of phonon displacements.

To measure material responses to high repetition-rate sequences of femtosecond pulses, we first needed to generate the pulse sequences. We could have approached this problem by splitting a single femtosecond pulse many times with partial reflectors and aiming all the resulting beams into a sample with desired timing. This extremely cumbersome approach would have involved dozens of partial and high reflectors, lenses, and precision delay lines. Instead, we chose to collaborate with scientists at Bellcore who have

Femtosecond Pulse Sequence

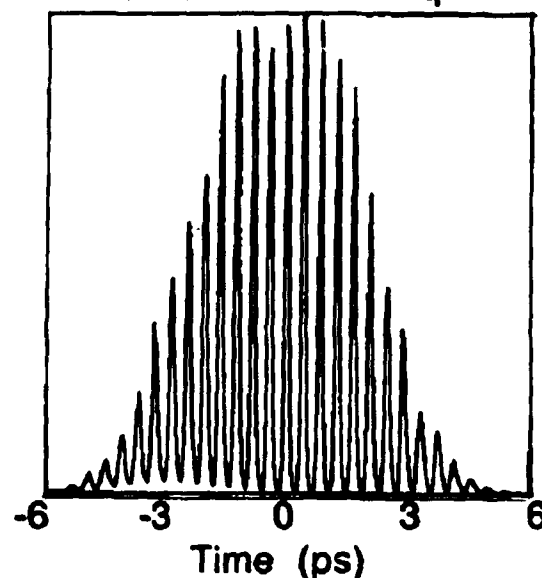


Figure 2. Cross-correlation trace of a sequence of femtosecond pulses at Terahertz repetition rates produced through pulse-shaping techniques. A single femtosecond pulse was passed through two gratings, two lenses, and a spatially varying mask to produce the output shown. The output can be used to exert repetitive "impulsive" driving forces on selected vibrational modes to achieve larger amplitudes than can be driven with a single pulse.

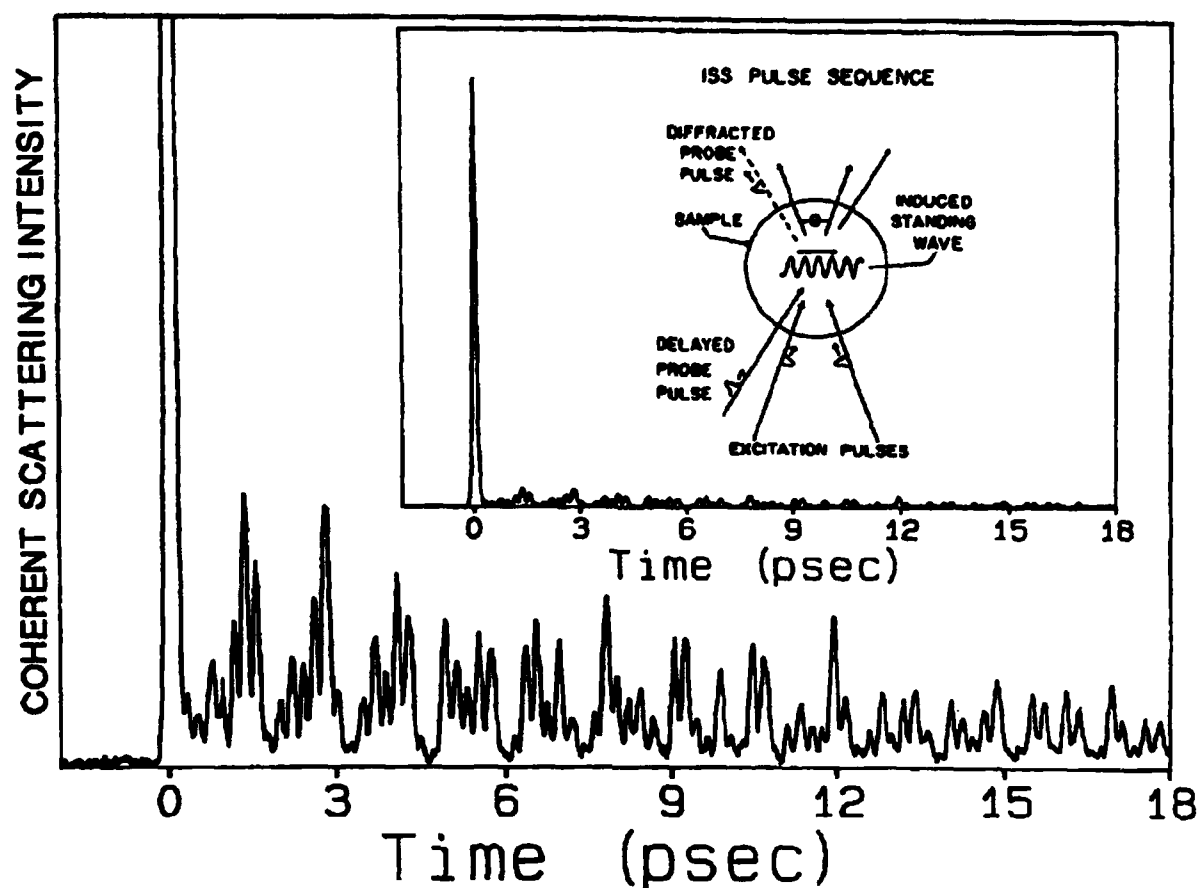


Figure 3. ISRS data from the α -perylene organic molecular crystal. Several phonon modes are excited by the femtosecond excitation pulses. This gives rise to the characteristic "beating" pattern which contains sum and difference frequencies. The "spike" at $t = 0$ is due to the essentially instantaneous electronic response of the crystal to the excitation pulses. The inset shows that the vibrational signal intensity is only about 4% that of the spike. In some signal processing applications (especially those involving threshold devices), the comparatively slow response due to vibrations could be disregarded.

recently developed femtosecond optical "pulse-shaping" techniques through which a single femtosecond pulse can be converted into a sequence with the desired timing. In this technique, a single pulse, passed through a simple optical network consisting of only two lenses, two gratings, and a spatially varying mask, yields a pulse sequence similar to the one shown in figure 2. Sequences with different temporal profiles are selected by changing the mask.

Figures 3 and 4, respectively, show crystal-line responses to single- and multiple-pulse excitation. For the initial demonstration, we used an organic molecular crystal since its

vibrational and electronic properties were well understood. Figure 3 shows the response to a single femtosecond pulse. The "impulse" force exerted by the pulse drives several lattice vibrational modes whose simultaneous oscillations yield the "beating" pattern in the data. The "spike" in the data at $t = 0$ is caused by the instantaneous electronic response of the crystals to the excitation pulses. The signal due to lattice vibrations is only about 4 percent as strong as that due to the electronic response. In some signal processing applications, this "slow" signal could be disregarded, using instead the ultrafast electronic response as the basis for a rapid switch.

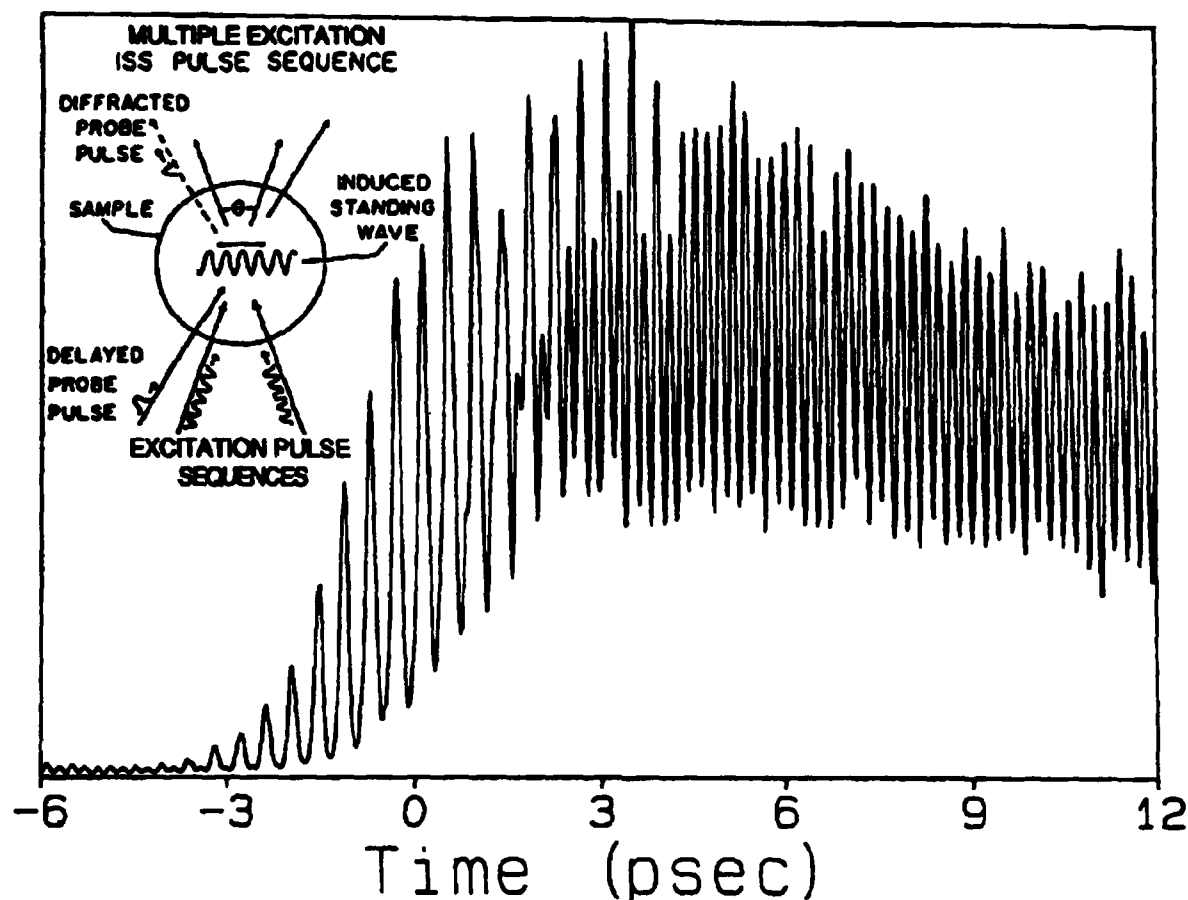


Figure 4. ISRS data from the perylene crystal driven by the pulse sequence shown in figure 2, which is tuned to drive the 80 cm^{-1} lattice vibrational mode. At first the signal is dominated by the instantaneous electronic response of the sample to each of the pulses in the sequence. After about 10 pulses, signal due to repetitively driven lattice vibrations is apparent. Signal from the vibrational mode grows stronger with each successive pulse, eventually reaching intensity levels comparable to the strongest electronic response. Selective amplification of the 80 cm^{-1} mode has been demonstrated. The strong response due to the amplified vibrational mode could not be ignored in any signal processing application.

Figure 4 shows the crystal's response to the sequence of pulses shown in figure 2. We have crafted this sequence so that the time between pulses (419 fs) is precisely equal to the oscillation period of one of the lattice vibrational modes. The impulse forces exerted by the pulses resonantly drive this mode in a manner analogous to repetitively pushing a child on a swing so that larger oscillation amplitudes are reached in time. The data show that for the first several pulses, the intense "spike" due to the electronic response dominates the signal. After about 10 pulses, however, the amplified vibrational response is apparent. By the end of the pulse sequence ($t > 3\text{ ps}$), the signal due to

vibrations is as intense as the strongest electronic "spike." This illustrates one important difference between the response of the material to high-density input signals versus the response to a single pulse. *We could not ignore the long-lived vibrational response in any real-life signal-processing application.*

The results also illustrate the increased optical control over the sample afforded by judicious multiple-pulse excitation. In this case, through repetitive excitation, we increased the vibrational amplitude by almost a factor of 10. Amplification is also highly mode-selective, since the pulse sequence is timed to drive only one of the lattice

vibrations. This is clear from the single-frequency oscillations in the data, as compared to the beating pattern in figure 3 that results from excitation of several vibrational modes.

At present, we are beginning experiments in which these techniques are applied to semiconductors. We expect to drive large-amplitude vibrational responses and to observe their effects on electronic energy levels. This will permit characterization of the electron-phonon interactions. Another very interesting application will be to multiple quantum well structures. Repetitive excitation should lead to large-amplitude responses of acoustic-like phonons which traverse a single well in the time between pulses of the sequence.

It is worth noting that our primary outside collaborator in this project, Dr. Andrew M. Weiner, performed research for his Ph.D. under the supervision of Professor Erich P. Ippen. Under earlier JSEP support, we collaborated with Dr. Weiner and Professor Ippen to conduct some of the first femtosecond time-resolved spectroscopy experiments on molecular crystals.

Our work in this area is widely recognized within the ultrafast optics and electronics community. *Optics News* described our research in a summary of 1989 highlights, and an article in *Science* is forthcoming. At present, we are preparing more detailed reports.

Publications

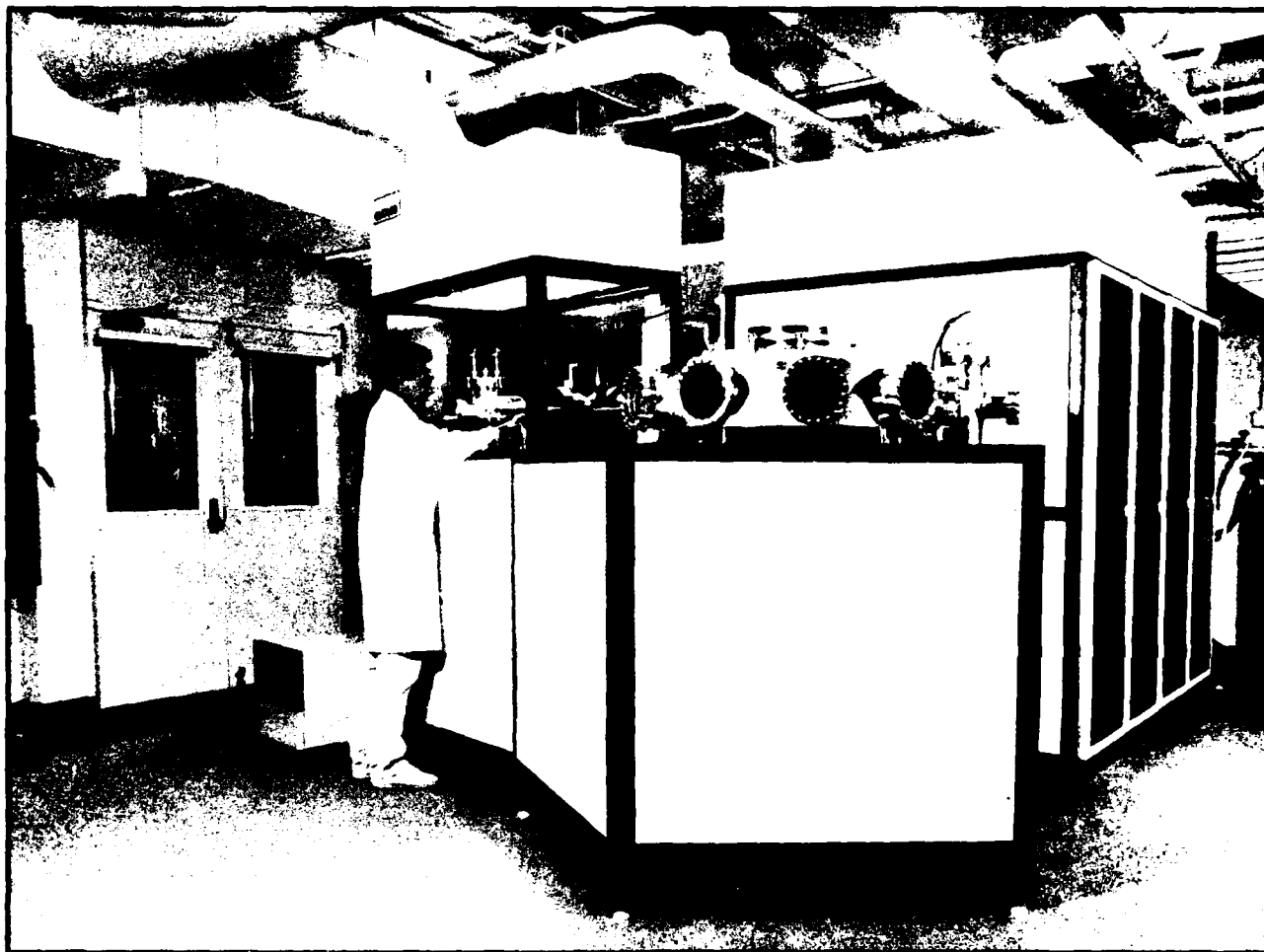
Nelson, K.A. "Impulsive Stimulated Raman Scattering with Single-pulse and Multiple-pulse Excitation." *Proceedings of the 12th International Conference on Raman Spectroscopy*. Forthcoming.

Nelson K.A., and E.P. Ippen. "Femtosecond coherent spectroscopy." *Adv. Chem. Phys.* 75: 1-35 (1989).

Weiner, A.M., D.E. Leaird, G.P. Wiederrecht, and K.A. Nelson. "Femtosecond Multiple Pulse Impulsive Stimulated Raman Scattering." *Optics News* 15(12): 29-31 (1989).

Weiner, A.M., D.E. Leaird, G.P. Wiederrecht, and K.A. Nelson. "Femtosecond Pulse Sequences Used for Optical Manipulation of Molecular Motion." *Science*. Forthcoming.

Weiner, A.M., D.E. Leaird, G.P. Wiederrecht, M.J. Banet, and K.A. Nelson. "Spectroscopy with Shaped Femtosecond Pulses: Styles for the 1990s." *Proceedings of the SPIE Conference on Optoelectronics and Lasers*. Forthcoming.



The system shown is a modular chemical beam epitaxy facility for the epitaxial growth of compound semiconductors. Research Specialist Steven C. Shepard places a sample into the ultra high vacuum introduction chamber, while Visiting Scientist Dr. Hidehito Nanto considers the layout of the growth reactor contained in the largest enclosure. The main circular chamber seen in the photo is the ultrahigh vacuum transfer chamber.

Chapter 6. Chemical Beam Epitaxy of Compound Semiconductors

Academic and Research Staff

Professor Leslie A. Kolodziejski, Stephen C. Shepard

Visiting Scientists and Research Affiliates

Dr. Hidehito Nanto¹

Graduate Student

Dana H. Lee

Technical and Support Staff

Angela R. Odoardi

6.1 Chemical Beam Epitaxy Facility

Sponsors

3M Company Faculty Development Grant

AT&T Research Foundation

Special Purpose Grant

Joint Services Electronics Program

Contract DAAL03-89-C-0001

National Science Foundation

Grants ECS 88-46919 and ECS 89-05909

Purdue University

Subcontract No. 530-0716-07

U.S. Navy - Office of Naval Research

Contract N00014-88-K-0564

We made substantial progress in 1989 toward establishing a chemical beam epitaxy (CBE) facility for the epitaxial growth of compound semiconductors. The major part of our effort was in the development and assembly of the CBE hardware including the growth, transfer, introduction, and bake chambers. By the end of 1989, the CBE system was approximately 85 percent complete. We expect delivery from the manufacturer by the middle of February 1990.

Figure 1 is a photograph of the CBE system showing its growth reactor module and some associated electronics. Within the black metal frame outlining the exhausted enclo-

sure are the gas manifold (upper left side), ultrahigh vacuum growth chamber (right side), and the pumping subsystem (bottom left). Figure 2 shows the transfer, introduction, and bake chamber modules. The black metal frame outlines a fully exhausted, filtered laminar flow enclosure.

The CBE growth reactor is equipped with four individual gas injectors for metalorganics of Zn, Ga and In, Se, and for the hydride arsine. The temperature of each gas injector can be varied between 0 to 1250 degrees Celsius so that the molecules can be "cracked" or thermally decomposed prior to impingement on the heated single crystalline substrate. Three typical effusion cells, such as those used in molecular beam epitaxy, can be used with dopant or alloying elements. In situ analysis facilities include reflection high energy electron diffraction, a residual gas analyzer, and a quartz crystal flux monitor. Four symmetrically placed heated sapphire viewports can be used to direct a laser beam at incident angles to the growing surface front and to collect the reflected laser beam.

The design of the original CBE system was expanded to include an additional ultrahigh vacuum analytical/metalization chamber, which will added in mid-1990. Attached to the transfer chamber, this new chamber will

¹ Professor, Department of Electronics, Kanazawa Institute of Technology, Kanazawa, Japan.

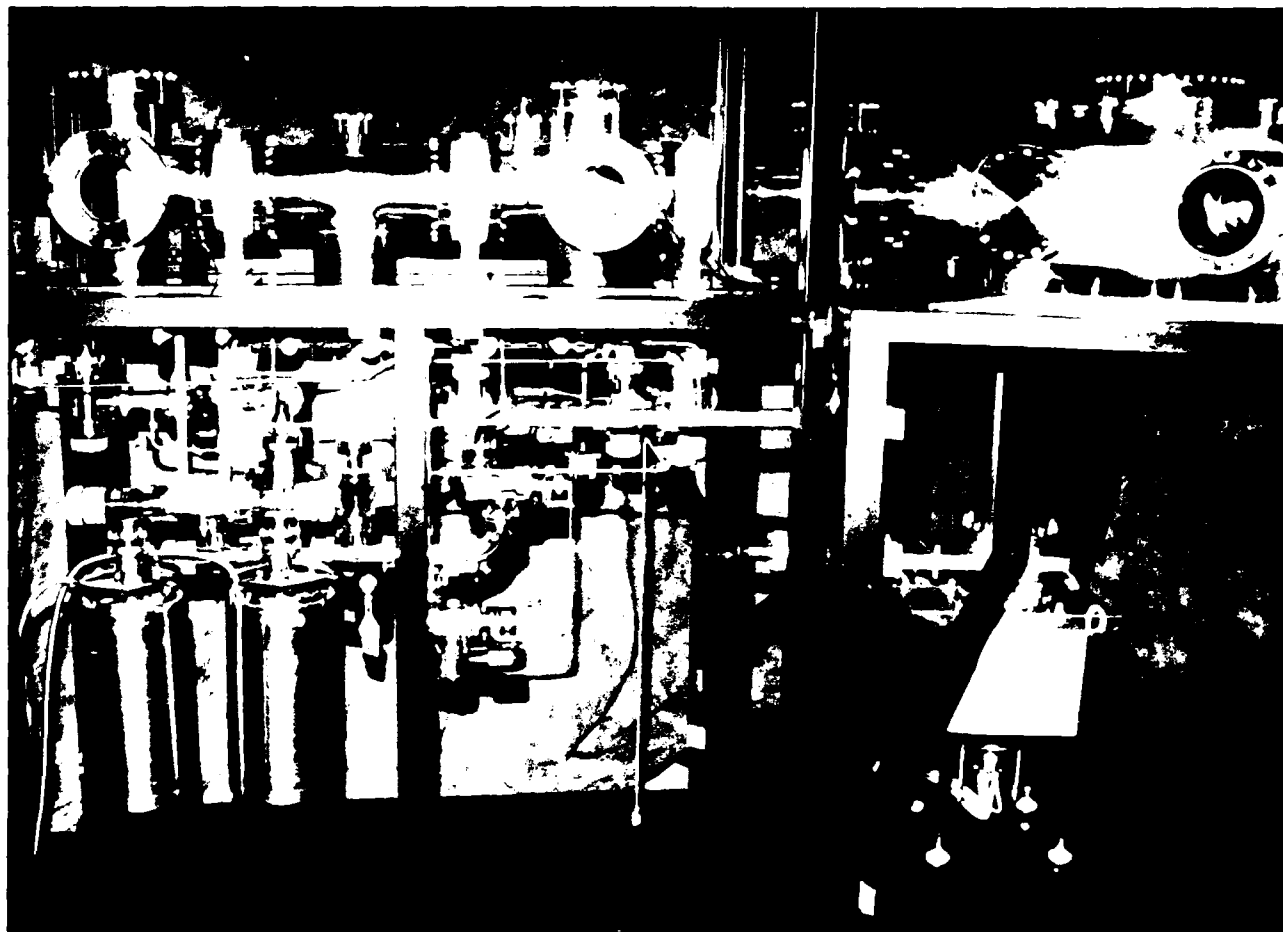


Figure 1. Growth reactor module and partially complete electronics rack of the chemical beam epitaxy system (as of November 1989).

allow samples to remain in the UHV environment before and after analysis or metalization. The additional chamber is subdivided to include both in situ analysis and metalization capabilities. Initially, the chamber will contain Auger electron spectroscopy (AES) and will be configured to have the associated ports, sample heater and manipulator, shutters, etc., necessary to add the electron beam evaporators to perform metalizations. Additional viewports will be provided to illuminate samples during Auger electron spectroscopic analysis and metalization with a coherent source of light. The source of photons will be provided by various lasers or lamps having a multitude of powers and wavelengths.

We envision that the laser-aided investigations carried out in the analytical/-metalization chamber will complement laser-assisted experiments planned during the

epitaxial growth of semiconductor layers. We anticipate that both types of experiments will provide clues to understanding the effect of photons on the physisorption, chemisorption and incorporation processes which occur during the chemical beam epitaxial growth process.

Funds for obtaining the analytical/-metalization chamber were provided by the National Science Foundation, Defense Advanced Research Projects Agency, and by a donation from Emcore Corporation.

The space which will house the new CBE system was completely remodeled. Renovation included: (1) major demolition of walls to create one large (1200 square foot) lab from three smaller labs; (2) an increase in the services available such as power, water, nitrogen, etc.; and (3) installation of a very sophisticated exhaust system, a design



Figure 2. Front view of the bake chamber (left), introduction chamber (center), and transfer chamber (right).

requirement for the custom CBE system. (Both the growth reactor module and the introduction chamber module are fully enclosed and exhausted.) The laboratory also includes a small entry room, typical for a clean room environment, and a substrate preparation area. The substrates can be chemically cleaned in dedicated solvent hoods followed by etching in dedicated acid hoods in adjacent laboratory space. The laboratory will also house a surface profilometer for studying film thickness and a Normarski interference microscope for studying surface morphology.

6.2 Controlled Substitutional Doping of ZnSe Grown by Chemical Beam Epitaxy

Sponsors

Joint Services Electronics Program
Contract DAAL03-89-C-0001
U.S. Navy - Office of Naval Research
Contract N00014-88-K-0564

The potential of the II-VI compound semiconductor family for optical device applications has been relatively underutilized. There are substantial difficulties in preparing them by any growth technique to be amphoterically doped in a controlled manner. In the past, because bulk, liquid phase, or vapor phase growth techniques required very high temperatures for fabrication of ZnSe, control of the carrier type could not be achieved. The resultant ZnSe exhibited n-type transport properties or the as-grown

material was so heavily compensated that the material was highly resistive. Newer growth technologies such as molecular beam epitaxy (MBE) and chemical beam epitaxy (CBE) provide promise for circumventing the doping problems of the II-VIs and ZnSe as one example, due to the non-equilibrium nature of the growth, and by their ability to affect the growth, with photon illumination. Once ZnSe is controllably doped as p-type and n-type material, many device applications could take advantage of the wide, direct bandgap (2.67 eV at room temperature) which provides for the emission of blue light. Blue light emitting diodes, blue semiconductor injection lasers, and flat panel electroluminescent display devices are representative of the many possible optical devices. The blue wavelength range will be useful in (1) underwater communication, (2) visible holography, (3) laser disc recording, where a shorter wavelength would allow for a ten-fold increase in the density of stored information, and (4) for short range communications where new polymer fibers can be utilized.

Studies of dopant incorporation reported in the literature for ZnSe were complicated by the presence of unintentional impurities found in both elemental and compound source material which is used in the MBE growth process. In most cases, undoped ZnSe grown by MBE, using commercially available source material, has been reported to be n-type with low resistivity ($\sim 1\Omega\text{-cm}$). The low resistivity of the "undoped" ZnSe material implied that the ZnSe was of correct stoichiometry because a relatively small deviation from a Zn-to-Se flux ratio of one-to-one toward either Zn-rich or Se-rich conditions was found to result in high resistivity material. (The defects generated during growth under non-stoichiometric conditions appeared to compensate for the non-intentionally incorporated impurities giving rise to the high resistivity.)

Although major progress was recently made in the molecular beam epitaxy of ZnSe, controlled substitutional n- and p-type doping is still significantly limited. The technique of chemical beam epitaxy (CBE), however, combines the many advantages of molecular beam epitaxy and metalorganic chemical vapor deposition (MOCVD) growth tech-

niques while eliminating their many disadvantages.

An ultrahigh vacuum environment, similar to that used in MBE, is utilized in CBE. Because in CBE the solid source material of MBE is replaced by gaseous source material, CBE is similar to MOCVD in that respect. The gas sources are controlled by precision mass flow controllers, permitting constant flux ratios at reasonable growth rates. By employing metalorganic gaseous sources for the Zn and Se species, we will obtain a greater degree of control of the flux intensities. The MBE technique of employing low temperature, high vapor pressure sources of Zn and Se cannot achieve this control. Because the elements originate from a gas bottle, long-term operation is possible since very little gaseous material is consumed. We will eliminate many hardware problems encountered during the growth of II-VI compounds by using CBE. We also anticipate that the use of the CBE technique will allow us to solve crystal growth problems. Scientists and device engineers will be able to capitalize on the many attractive material properties of the II-VI compound semiconductors.

With research support from the Office of Naval Research, we will explore the CBE of ZnSe. We will determine its optimum growth parameters following microstructural, optical, and electrical evaluation of the epitaxial layers. After we achieve high quality, ultrapure, undoped ZnSe, our objective under the program supported by the Joint Services Electronics Program will be to incorporate the impurity species in ZnSe.

6.3 Laser-Assisted Chemical Beam Epitaxy of Wide Bandgap Blue/Green II-VI Semiconductors

Sponsor

Purdue University
Subcontract No. 530-0716-07

In addition to the more typical growth experiments described above, chemical beam epitaxy (CBE) is naturally suited for experiments designed to modify or affect the

epitaxial growth process. For example, impingement of either coherent or incoherent light of various wavelengths can effect the "nature" of the incident atomic or molecular species; the actual bonding configuration of the molecules determines their sticking coefficient and their incorporation. We will investigate the effects of illuminating the growing surface front with a low power laser beam similar to that from a visible or ultraviolet argon ion laser. We will direct the optical illumination (1) parallel to the surface of the substrate to affect the impinging molecular species and (2) at various angles of incidence to the substrate surface to affect the surface of the semiconductor. Pulsed excimer lasers would provide a source of much higher power illumination to result in a thermal modification of the semiconductor surface. We will employ many different laser wavelengths and powers to explore the effects of photons on the nonequilibrium growth process of chemical beam epitaxy.

The use of gaseous sources to replace high vapor pressure solid sources will allow greater flexibility for use of the vacuum system for the fabrication of a variety of materials. Historically, the II-VI and III-V, or group IV, compounds have been grown in separate vacuum systems to eliminate problems associated with unintentional autodoping of each material. Since in CBE each element originates from a gas tank external to the vacuum, the source oven and material will not be contaminated with foreign elements. We envision that both ultrapure II-VI and III-V materials can be fabricated in the same vacuum system because II-VIs and III-Vs should not form a compound until the metalorganics interact with the heated single crystalline substrate. We will study the various II-VI/III-V heterostructures of complex design and dimensions that will now be feasible.

6.4 Publications

Glenn, J.L., O. Sungki, M. Kobayashi, R.L. Gunshor, L.A. Kolodziejski, D. Li, N. Otsuka, M. Haggerott, N. Pelekanos, and A.V. Nurmikko. "Multiple Quantum Wells of InSb/CdTe Grown by MBE." *J. Vacuum Sci. Tech.* B7: 249-252 (1989).

Gunshor, R.L., L.A. Kolodziejski, M.R. Melloch, N. Otsuka, and A.V. Nurmikko. "II-VI/III-V Heterointerfaces: Epilayer-on-Epilayer Structures." In *Growth and Optical Properties of Wide-Gap II-VI Low Dimensional Structures*. Eds. T.C. McGill, C.M. Sotomayor Torres, and W. Gebhardt. New York: Plenum Press, 1989.

Gunshor, R.L., L.A. Kolodziejski, A.V. Nurmikko, and N. Otsuka. "Molecular Beam Epitaxy of II-VI Semiconductor Microstructures." In *Semiconductors and Semimetals*. Ed. R. Pearsall. Boston: Academic Press, 1989.

Gunshor, R.L., L.A. Kolodziejski, M. Kobayashi, A.V. Nurmikko, and N. Otsuka. "Metastable Zincblende MnTe and MnSe: MBE Growth and Characterization." *Mat. Res. Soc. Symp. Proc.* 151:141-149 (1989).

Gunshor, R.L., and L.A. Kolodziejski, M. Kobayashi, A.V. Nurmikko, and N. Otsuka, "Wide Gap II-VI DMS Superlattices: MBE Growth and Characterization." Invited paper presented at the Spring Meeting of the Materials Research Society, San Diego, California, April 24-28, 1989.

Gunshor, R.L., M. Kobayashi, L.A. Kolodziejski, and A.V. Nurmikko, "Wide Gap II-VI Heterostructures." Invited Paper presented at the International Conference on II-VI Semiconductors, Berlin, West Germany, August 21-25, 1989.

Gunshor, R.L., M. Kobayashi, L.A. Kolodziejski, A.V. Nurmikko, and N. Otsuka, "MBE of Wide Bandgap II-VI Compounds." Invited Paper presented at the International Conference on Crystal Growth, Sendai, Japan, September 11-15, 1989.

Kolodziejski, L.A., R.L. Gunshor, A.V. Nurmikko, and N. Otsuka. "Exciton Self-Trapping in ZnSe/ZnTe Superlattice Structures." In *Growth and Optical Properties of Wide-Gap II-VI Low Dimensional Structures*. Eds. T.C. McGill, C.M. Sotomayor Torres, and W. Gebhardt. New York: Plenum Press, 1989.

Kolodziejski, L.A., R.L. Gunshor, and A.V. Nurmikko. "II-VI Compound Strained-Layer Superlattices." In *Strained Layer Superlattices*. Ed. R.B. Biefeld. Switzerland: Trans Tech Publications, 1989.

Qian, Q.-D., J. Qiu, M.R. Melloch, J.A. Cooper, L.A. Kolodziejski, M. Kobayashi, and R.L. Gunshor. "Low Interface State Density at an Epitaxial ZnSe/Epitaxial GaAs Heterointerface." *Appl. Phys. Lett.* 54: 1359-1361 (1989).

Vaziri, M., R.L. Gunshor, L.A. Kolodziejski, S. Venkatesan, R.F. Pierret, and R. Reifenberger. "Optical and Electrical Characterization of ZnSe Doped with Gallium." *J. Vacuum Sci. Tech.* B7: 253-258 (1989).

Venkatesan, S., R.F. Pierret, J. Qiu, M. Kobayashi, R.L. Gunshor, and L.A. Kolodziejski. "Deep Levels in Ga-Doped ZnSe Grown by Molecular Beam Epitaxy." *J. Appl. Phys.* 66: 3656-3660 (1989).

Chapter 7. High-Frequency InAlAs/InGaAs Metal-Insulator-Doped Semiconductor Field-Effect Transistors (MIDFETs) for Telecommunications

Academic and Research Staff

Professor Jesus A. del Alamo

Graduate Student

Sandeep Bahl

Undergraduate Student

Walid Azzam

Technical and Support Staff

Angela R. Odoardi

7.1 Introduction

Sponsors

Joint Services Electronics Program
Contract DAAL03-89-C-0001
Charles S. Draper Laboratory
Contract DL-H-404180

The goal of this project is to design, fabricate, test, and model submicron InAlAs/InGaAs Heterostructure Field-Effect Transistors (HFETs) on InP. These devices are of great interest for applications in long-wavelength optical communications and ultra-high frequency microwave telecommunications. We expect that extraordinary device performance will result from the unique combination of: (1) the large conduction bandgap discontinuity between InAlAs and InGaAs, (2) the large $\Gamma - L$ sep-

aration in InGaAs, and (3) the high velocity of electrons in InGaAs.

We have recently pioneered HFETs in which the InGaAs channel is heavily doped but the InAlAs insulator is undoped (MIDFETs for Metal-Insulator-Doped semiconductor FET).¹ We have found that these devices display a performance comparable to InAlAs/InGaAs Modulation-Doped FETs (MODFETs) of similar gate length. In addition, these devices offer a number of unique benefits not found in other device structures: reduced transconductance¹ and f_T collapse,² higher breakdown voltage,¹ and freedom to optimize gate insulator parameters.³ A new *modulation-doped channel* MIDFET also displays unprecedented microwave characteristics.⁴

During 1989, we obtained the first working InAlAs/InGaAs MIDFETs on InP fabricated

¹ J.A. del Alamo and T. Mizutani, "An $\text{In}_{0.52}\text{Al}_{0.48}\text{As}/\text{n}^+\text{In}_{0.53}\text{Ga}_{0.47}\text{As}$ MISFET with a Heavily-Doped Channel," *IEEE Electron Device Lett.* EDL-8 (11): 534-536 (1987).

² J.A. del Alamo and T. Mizutani, "Bias Dependence of f_T and f_{max} in an $\text{In}_{0.52}\text{Al}_{0.48}\text{As}/\text{n}^+\text{In}_{0.53}\text{Ga}_{0.47}\text{As}$ MISFET," *IEEE Electron Device Lett.* EDL-9 (12): 654-656 (1988).

³ J.A. del Alamo and T. Mizutani, "A Recessed-Gate $\text{In}_{0.52}\text{Al}_{0.48}\text{As}/\text{n}^+\text{In}_{0.53}\text{Ga}_{0.47}\text{As}$ MIS-type FET," *IEEE Trans. Electron Devices* ED-36 (4): 646-650 (1989).

⁴ J.A. del Alamo and T. Mizutani, "An $\text{In}_{0.52}\text{Al}_{0.48}\text{As}/\text{n}^+\text{In}_{0.53}\text{Ga}_{0.47}\text{As}$ MISFET with a Modulation-Doped Channel," *IEEE Electron Device Lett.* EDL-10 (8): 394-396 (1989).

at MIT.⁵ The performance and properties of these MIDFETs are similar to those fabricated elsewhere.³ More relevant to the problem, we fabricated, for the first time, strained-insulator InAlAs/InGaAs MIDFETs. This report gives a detailed description of our research on these devices.

We have exploited the inherent flexibility of gate insulator design of a MIDFET by increasing the AlAs content in the InAlAs insulator from the lattice-matching composition to InP ($\text{In}_{0.52}\text{Al}_{0.48}\text{As}$), straining it towards larger bandgaps. This rapidly effects an enhancement in the conduction band discontinuity (ΔE_c) between the InAlAs and the InGaAs channel (figure 1). We expect, in this manner, to obtain the following benefits:

- reduced gate leakage
- improved gate breakdown voltage
- reduced real-space transfer of hot electrons from the channel to the gate.

We have demonstrated all of these benefits experimentally while largely unaffected the rest of the device parameters (threshold voltage, transconductance, etc.).

7.2 Experiments

We grew four wafers by molecular-beam epitaxy in MIT's Riber 2300 system. Following standard procedures, we prepared the surface of the InP wafer. Figure 2 shows the cross section of the grown heterostructures. The layer structure is similar to those utilized previously,¹ except for:

1. The channel design is more aggressive: doping is higher, $4 \times 10^{18} \text{ cm}^{-3}$, and thickness is lower, 100 Å. This channel is expected to result in superior performance.
2. The Al composition in three of the wafers is increased over lattice matching conditions, i.e., wafers were grown in which x in the $\text{In}_{(1-x)}\text{Al}_x\text{As}$ layer is 0.48, 0.52, 0.60,

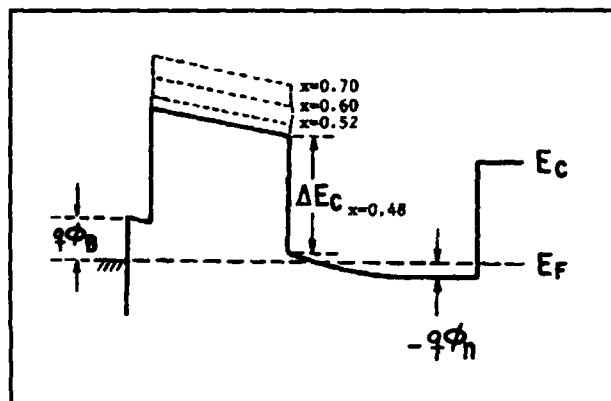


Figure 1. Cross-sectional equilibrium band diagram of device structure indicating the increase in ΔE_c with increase in Al composition.

and 0.70 (all insulator layers are 300 Å thick). This is the main purpose of the present experiment.

We continued fabrication after growth with mesa isolation utilizing a selective chemical etchant, AuGeNi ohmic contact formation, TiAu interconnect, and TiAu gate layer formation. Figure 2 shows the resulting device cross section.

We have integrated a number of devices of varying dimensions and a large set of test structures into a $2.9 \times 2.7 \text{ mm}^2$ chip. We present here DC I-V measurements on MIDFETs with a nominal gate length of 1.5 μm and a gate width of 30 μm .

7.3 Device Results

Figure 3 shows a plot of the transconductance versus gate to source voltage for four representative devices with varying $\text{In}_{(1-x)}\text{Al}_x\text{As}$ insulator compositions. As expected from simple theory, the threshold voltage is, to the first order, unaffected by the introduction of strain in the insulator. The lattice-matched device has a maximum transconductance of 220 mS/mm. This value is higher than for any of the InAlAs/InGaAs MIDFETs previously reported in the literature with a similar gate length and overall epitaxial structure (the best was 160

⁵ S. Bahl, W.J. Azzam, and J.A. del Alamo, "Fabrication of an InAlAs/n⁺-InGaAs MIDFET," unpublished paper presented at the Fourth New England MBE Workshop, Cambridge, Massachusetts, May 4, 1989.

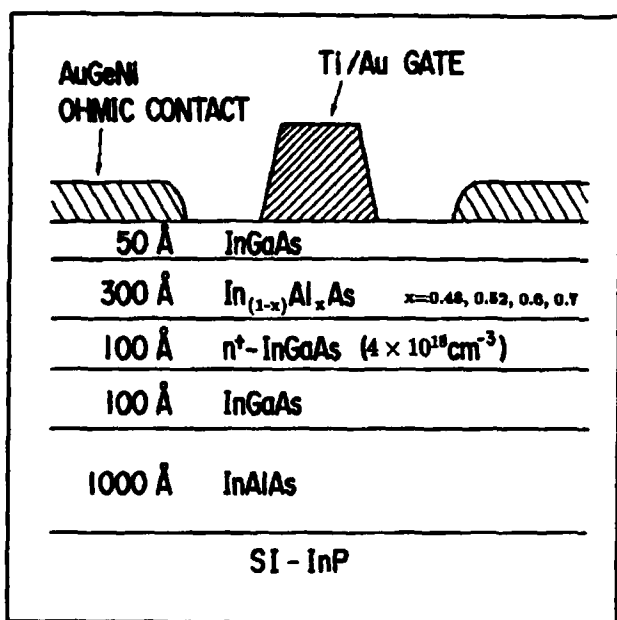


Figure 2. Cross section of device structure.

mS/mm).³ We believe that is due to the enhanced channel doping in this new device structure.

An increase of AlAs composition in the $\text{In}_{(1-x)}\text{Al}_x\text{As}$ gate insulator from the lattice-matched condition $x = 0.48$ to $x = 0.6$ brings about a slight reduction of peak g_m due to an enhanced contact resistance. First order theory predicts this result. A further increase of x to 0.7 results in a catastrophic reduction in g_m that cannot be explained by a larger source resistance. It appears that, from an electrical point of view, the critical layer thickness for the 300 Å $\text{In}_{(1-x)}\text{Al}_x\text{As}$ insulator has been exceeded in going from $x = 0.6$ to $x = 0.7$.

While there is a small reduction of g_m with AlAs composition, the g_m curve broadens in V_{gs} , as figure 3 indicates, because gate current is being suppressed due to the enhanced conduction band discontinuity (discussed below). Thus, the maximum current driving capability of the devices is not degraded. In fact, this capability improves with AlAs composition up to 0.6. The maximum drain current obtained is 300 mA/mm for the $x = 0.6$ device. This is better than that which had been reported previously in similar devices and is a very competitive value for any 1.5 μm gate length HFET.

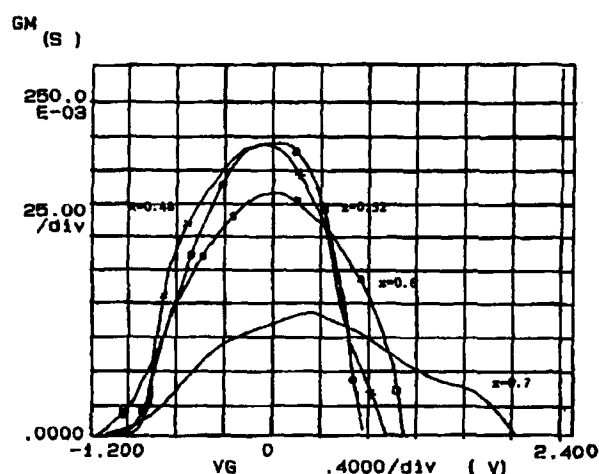


Figure 3. Transconductance versus gate to source voltage for $V_{ds} = 4$ V.

Increasing the AlAs composition results in a drastic reduction of forward gate current. Figure 4 illustrates gate current as a function of drain-source voltage for $V_{gs} = 1.2$ V. As the AlAs composition increases, gate current at all values of V_{ds} is drastically suppressed. This results in broader g_m versus V_{gs} characteristics (shown in figure 3) and higher $I_{D\text{max}}$, as mentioned above.

A more significant result, shown in figure 5, is the impact of AlAs composition on the real-space transfer of hot electrons from the channel to the gate. Such a phenomenon is very clearly observed in the devices with AlAs composition of 0.48 and 0.52. Its unique signature is an increase in the gate current as V_{ds} increases for a given V_{gs} . This increase is due to electrons that are heated by the high electric field prevalent inside the channel and then acquire sufficient energy to overcome the conduction band discontinuity between the channel and the gate insulator. The drain current saturates when the device itself enters saturation. An AlAs composition of 0.6 results in a sufficient conduction band discontinuity to completely suppress this phenomenon. This may be a major advantage of submicron strained-insulator MIDFETs in which the electric field in the channel can reach a very high value.

Figure 5 shows that real-space transfer of hot electrons to the gate causes a small negative differential output resistance. Because elec-

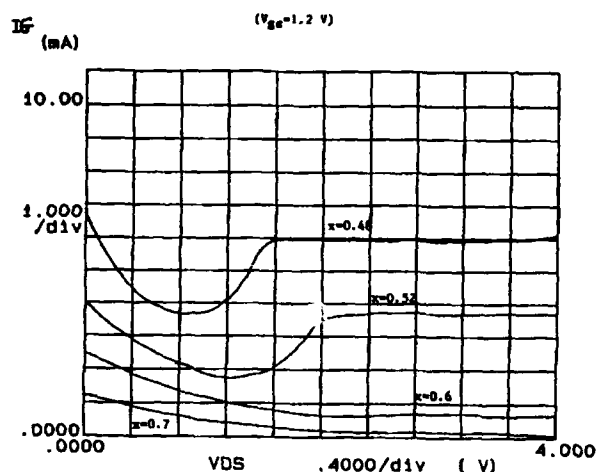


Figure 4. Gate current versus V_{ds} at $V_{gs} = 1.2$ V, as a function of AlAs composition.

trons are lost to the gate, this phenomenon results in drain current reduction. In addition, it may produce device instabilities and oscillations. For the $x = 0.6$ device, real-space transfer is completely suppressed and the drain current reaches higher values, as figure 5 indicates. Overall, the $x = 0.6$ device has ten times less gate current than the $x = 0.48$ device at practical operating points.

A final advantage of the strained-insulator MIDFETs is the enhanced reverse-bias gate breakdown voltage. Figure 6 shows the gate I-V characteristics measured with drain and source shorted. We obtain a rather hard breakdown for all devices. If we define breakdown at a reverse current of 1 mA, the breakdown voltage for the lattice matched device is 17 V. As the AlAs composition is increased in the insulator, the breakdown voltage increases very quickly, up to 28 V for $x = 0.7$.

The combination of the unique features investigated above makes strained-insulator $\text{InAlAs}/n^+-\text{InGaAs}$ MIDFETs very suitable

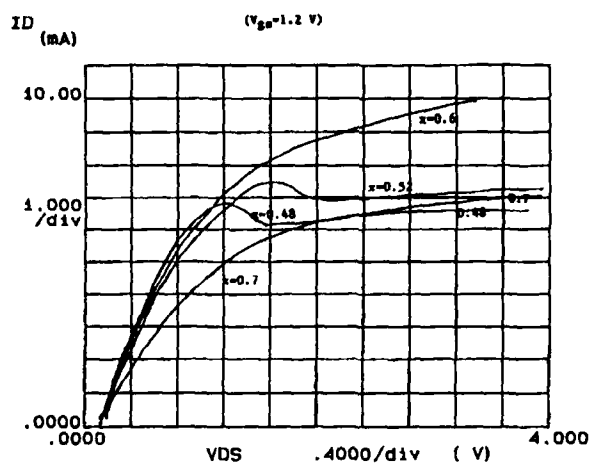


Figure 5. Drain current versus V_{ds} at $V_{gs} = 1.2$ V, as a function of AlAs composition.

candidates for high-power microwave applications. Figure 7, for example, shows that $\text{In}_{0.40}\text{Al}_{0.60}\text{As}/n^+-\text{In}_{0.53}\text{Ga}_{0.47}\text{As}$ MIDFETs displayed excellent I-V characteristics up to $V_{ds} = 10$ V.

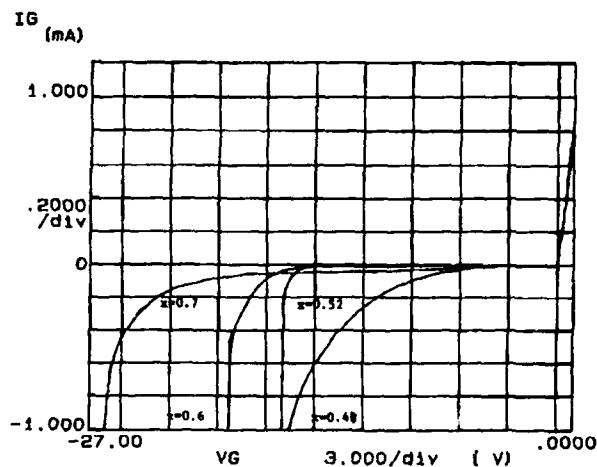


Figure 6. Reverse gate current characteristics of FETs as a function of AlAs composition $V_{ds} = 0$ V.

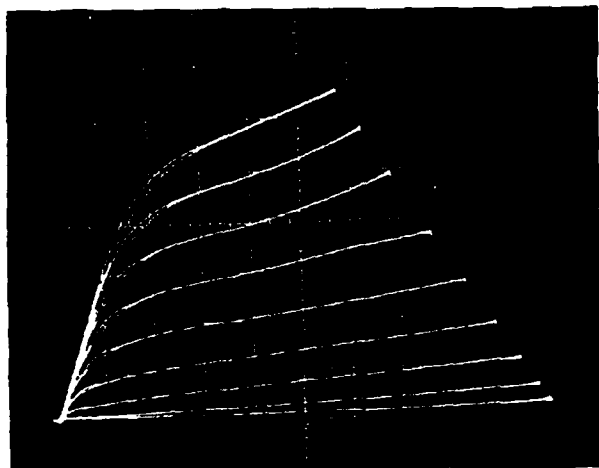


Figure 7. I-V characteristics of fabricated $\text{In}_{0.40}\text{Al}_{0.60}\text{As}/n^+-\text{In}_{0.53}\text{Ga}_{0.47}\text{As}$ MIFET. Scales: I_D : 1 mA/div, V_{ds} : 1 V/div, V_{gs} : 0.2 V/step, $V_{gs}(\text{max}) = 0$ V.

7.4 Publications

Bennett, B.R., and del Alamo, J.A. "Index of Refraction Anisotropy in Mismatched InGaAs/InP Heterostructures Measured by Ellipsometry." Paper presented at the Symposium on Layered Heterostructures - Heteroepitaxy, Superlattices, Strain and Metastability of the 1989 Fall Meeting

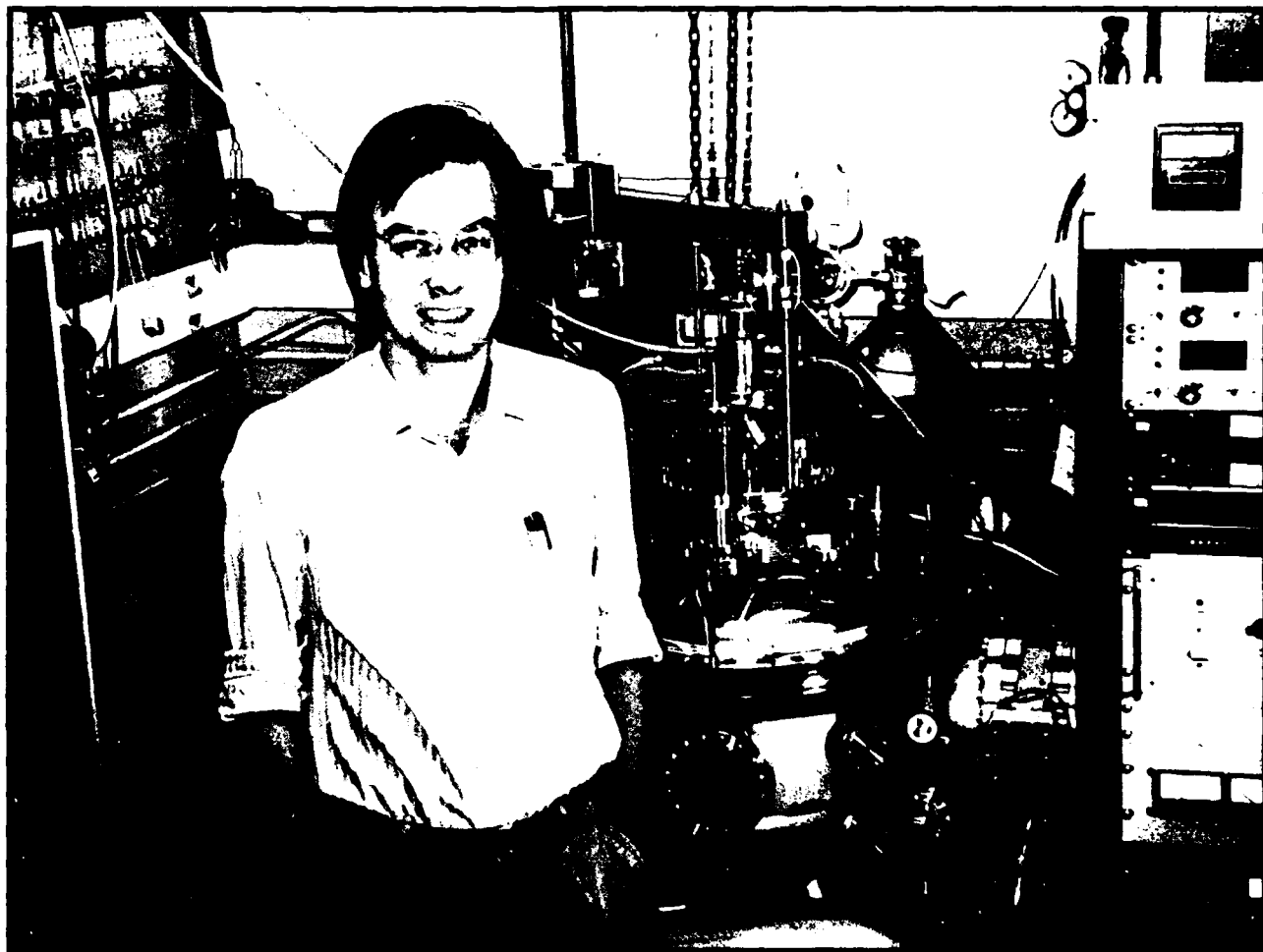
Materials Research Society, Boston, Massachusetts, November 27-December 2, 1989. Symposium *Proceedings*. Forthcoming.

del Alamo, J.A., and Azzam, W.J. "A Floating-Gate Transmission-Line Model (FGTLM) Technique for Accurate Measurement of Source Resistance in HFETs." Paper presented at 1989 Workshop on Compound Semiconductor Materials and Devices, Hilton Head, South Carolina, February 20-22, 1989.

del Alamo, J. A. and Mizutani, T. "A Recessed-Gate $\text{In}_{0.52}\text{Al}_{0.48}\text{As}/n^+-\text{In}_{0.53}\text{Ga}_{0.47}\text{As}$ MIS-type FET." *IEEE Trans. Electron Devices* ED-36 (4): 646-650 (1989).

del Alamo, J. A. and Mizutani T. "An $\text{In}_{0.52}\text{Al}_{0.48}\text{As}/n^+-\text{In}_{0.53}\text{Ga}_{0.47}\text{As}$ MISFET with a Modulation-Doped Channel." *IEEE Electron Device Lett.* EDL-10 (8): 394-396 (1989).

del Alamo, J.A., and Azzam, W.J. "A Floating-Gate Transmission-Line Model (FGTLM) Technique for Measuring Source Resistance in Heterostructure Field-Effect Transistors." *IEEE Trans. Electron Devices* 36 (11): 2386-2393 (1989).



Professor John M. Graybeal in his laboratory.

Chapter 8. Novel Superconducting Tunneling Structures

Academic and Research Staff

Professor John M. Graybeal

Graduate Student

George E. Rittenhouse

8.1 Project Description

Sponsor

Joint Services Electronics Program
Contract DAAL03-89-C-0001

In this program, we examine the behavior of the superconducting Josephson channel in electronically gated resonant tunneling structures. These hybrid superconducting/semiconducting structures represent the first attempt at Josephson coupling via resonant tunneling. A significant consequence of this approach is that the quantum confinement levels, not the semiconducting gap voltage, set the energy scale for modulating the Josephson coupling. Having made significant progress in the fabrication of such a device, we expect to have test devices available for initial measurements in coming months.

The envisioned device will use a thin silicon layer ($<1000 \text{ \AA}$) as a superconducting weak link between the superconducting source and drain electrodes. The superconducting counterelectrodes are separated from the silicon layer by a thin oxide layer. The weak link also defines a quantum well in which the superconducting Cooper pairs can interfere with each other (either constructively or destructively). This creates a resonant tunneling channel for Cooper pairs (i.e., the Josephson channel) between the source and drain in parallel with the normal quasiparticle (or single electron) channel. The applied gate voltage biases the levels within the

semiconducting well, modulating the Josephson current by varying the wavelength of the tunneling electrodes. In many ways, this structure is analogous to a Fabry-Perot interferometer. Previous efforts on similar hybrid Josephson devices have not utilized either resonant tunneling or quantum confinement. Thus, there is a mismatch between the semiconducting and superconducting gap energy scales.¹ The key motivation for our devices is that the energy scale is set by quantum confinement and can be tuned separately from either gap energy. For silicon well widths in the range of $500\text{--}1000 \text{ \AA}$, the energy levels separation in the well can be set more than ten times smaller than the semiconducting gap.

Current progress focuses on two areas. The first is the development of ultrathin uniform oxide tunneling barriers for the resonant quantum well. This tunnel barrier must be thin enough to enable a substantial number of Cooper pairs to tunnel through it, yet be thick enough to provide adequate isolation between the gate and the output. We have successfully fabricated ultrathin oxide layers of very high quality, grown at 800°C in a dilute (0.8 percent) oxygen atmosphere. Oxide layers have been fabricated with thicknesses of 15, 20, 25, 30 and 35 \AA , and all appear to have healthy barrier heights with no observable trap states (from C-V analysis).

The second area of progress is the examination of two different device structures. The first device structure has a vertical geometry

¹ A.W. Kleinsasser, T.N. Jackson, G.D. Pettit, H. Schmid, J.M. Woodall, and D.P. Kern, "Prospects for Proximity Affect Superconducting FETs," *IEEE Trans. Mag.* MAG-25 (2): 1274-1277 (1989) and references within.

and uses a silicon membrane as the weak link, a geometry that has been fabricated before albeit for much thicker silicon membrane thicknesses. The second structure is a novel new structure, done in collaboration with Professor Henry I. Smith. This structure has a lateral geometry with a silicon wall as the weak link. Both are shown in figure 1. The operational physics of the two structures is identical.

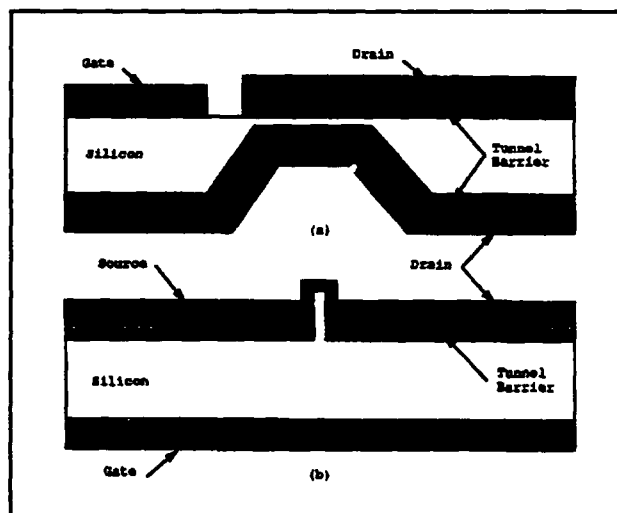


Figure 1. (a) Vertical device geometry, and (b) lateral device geometry. Note: drawings are not to scale.

In the vertical structure, the membrane is formed by an isotropic etch in ethylenediamine-pyrocatechol. This etch stops on a heavily boron-doped $1.75\ \mu\text{m}$ thick layer deposited at the surface of the wafer. After this etch, the membrane is thinned to the desired thickness. Two disadvantages of this structure are its extreme fragility and its process limitation, being only heavily boron-doped. The advantage of the structure is that its fabrication requires only one level of conventional VLSI optical lithography. However, we have found the fabrication of membranes much thinner than $1\ \mu\text{m}$ to be exceedingly difficult, primarily due to fabrication-induced mechanical stresses. We have therefore stopped work on this particular structure.

The second device structure has a lateral topology, as shown in figure 1(b). The

starting material for this device is (100) Si. The wall is formed by a strongly anisotropic potassium-hydroxide wet etch. As this weak link is defined by a mask layer, no etch stop is necessary. Therefore, this fabrication route places no constraints on the dopant type or level in the wafer, which is very desirable. Also, the mechanical integrity of this device is substantially more robust. In addition, the lateral structure allows it to be more easily integrated into circuits.

The primary difficulty in fabricating this lateral device is the production of the mask and the alignment of the mask pattern to the crystalline axes of the underlying wafer. We believe that both of these problems are surmountable, and our work is progressing on both fronts. Indeed, although we need to make some refinements, we have successfully produced thin silicon walls on test chips (figure 2). After finalizing the fabrication route, we will then begin careful measurement and analysis of the device behavior.



Figure 2. Nanow (500Å) wall structure (on right) etched into Si<110> wafer. Note scale at bottom of figure.

Chapter 9. Heterostructures for High Performance Devices

Academic and Research Staff

Professor Clifton G. Fonstad, Jr., Dr. Elias D. Towe, Richard R. Perilli

Visiting Scientists and Research Affiliates

Dr. Herve Blanck,¹ Dr. Sheila Prasad²

Graduate Students

Thomas P.E. Broekaert, Geoffrey Burns, Woo-Young Choi, Isako Hoshino, Lung-Han Peng, Yakov Royter, Richard Singer, James Vlcek

Undergraduate Students

Eric Monson, Melissa Frank, Debra Miller

Technical and Support Staff

Angela R. Odoardi

9.1 Introduction

The broad objective of our research effort is to develop III-V quantum heterostructures for high performance electronic, optoelectronic, and photonic devices for high speed optical communications and signal processing. To this end, we are developing (1) new, higher performance materials systems including InP-based InGaAlAs heterostructures and <111> oriented strained layer superlattices; (2) a new family of quantum-well-base, tunnel-barrier n-n-n transistors and near- and far-infrared optoelectrical devices; and (3) new damage-free in situ processing techniques for fabricating advanced quantum structures and embedded heterostructures.

The following sections describe our progress during the past year in the research areas listed above. Our group works closely with Professors Hermann Haus, Erich Ippen and James Fujimoto to develop the optical device application, characterization and modeling aspects of this program and with Professor

Sylvia Ceyer to develop new in situ processing techniques.

9.2 Computer Controlled Growth of Lattice-Matched InGaAlAs Heterostructures on InP

Sponsors

Charles S. Draper Laboratory
Contract DL-H-315251
Joint Services Electronics Program
Contract DAAL03-89-C-0001
National Science Foundation Grant
Grant EET 87-03404

Project Staff

James Vlcek, Professor Clifton G. Fonstad

The InGaAlAs material system, lattice-matched to InP substrates, includes alloy compositions with bandgaps that match the low-loss windows of silica-based optical

¹ Thomson CSF.

² Northeastern University, Boston.

fibers at 1.3 and 1.55 microns. Since the constituent "elements" of the pseudo-ternary alloy InGaAlAs (InAs, GaAs, and AlAs) each have the same anion, this compound is better suited to traditional molecular beam epitaxial (MBE) growth techniques than the more commonly used InGaAsP alloy system.

In electronic and optical semiconductor devices, the need for both graded-composition and hyper-abrupt metallurgical junctions frequently arises, but it is difficult to build these structures with solid-source Molecular Beam Epitaxy. In the case of graded junctions, the fluxes of the constituent elements must be precisely controlled during the growth process to maintain lattice matching of the epitaxial layer to the substrate, while varying the ratios of two or more beam fluxes to each other. This control is accomplished by ramping the setpoint temperature of the effusion cells for the constituent elements of the growing crystal. Achieving hyper-abrupt junctions, on the other hand, is complicated by use of mechanical shutters to block the beam fluxes during the growth process. Opening and closing of these shutters changes the thermal characteristics of the effusion cell, leading to transients in the emitted flux which must be removed to achieve truly abrupt metallurgical junctions.

Complications encountered in the growth of both graded layers and hyper-abrupt junctions can be addressed by a common solution: construction of a model for the effusion cell which takes into account not only the nonlinear relationship between flux and temperature, but also the temporal response of the cell to setpoint changes. This model is then used to construct the proper setpoint temperature profiles to achieve either a time-varying flux profile for a graded layer, or a flat flux profile to remove a shutter transient. These temperature profiles are executed by a digital computer which communicates with the feedback-loop (or PID, for Proportional Integral Derivative controllers which stabilize the effusion cells).

With this scheme, we have grown compositionally graded layers with maximum deviation from the desired flux profile maintained below one percent, reducing flux transients from values in the range of 10 to 25 percent

to less than 1.5 percent. Current research on this topic includes extending models of the effusion cell and eliminating overlapping shutter transients similar to those that would occur in superlattice structures (multiple, closely-spaced abrupt heterojunctions).

9.3 InGaAlAs Multiple Quantum Well Heterostructures for Guided Wave Optics

Sponsors

National Science Foundation Grant
Grant EET 87-03404

Project Staff

James Vlcek, Professor Clifton G. Fonstad, Jr., in collaboration with Mary R. Phillips and Professor Hermann A. Haus

Through the use of quantum confinement at InGaAs/InAlAs heterojunctions, emission and absorption edges of epitaxial grown structures can be continuously varied over the wavelength range of 1.3 to 1.6 microns, making them compatible with silica fiber communications. In addition to use in semiconductor lasers for optical emission and photodetectors for signal detection, these heterostructures can be employed for all-optical devices such as waveguides and modulators. The dynamics of optical nonlinearities in the transparent region of these structures will be an important factor in the speed of refractive, all-optical switches.

To measure subpicosecond optical nonlinearities just below the superlattice bandgap, we have fabricated InGaAs/InAlAs multiple quantum well heterostructures. In a pump-probe experiment, we collaborated with Mary R. Phillips and Professor Hermann A. Haus of RLE to measure the refractive and absorptive nonlinearities of these samples.

A typical heterostructure consisted of 72 periods of an InGaAs/InAlAs superlattice, each with periods of 70 Å. This structure was grown using the computer-automated MBE system described in Section 9.2. Room temperature infrared absorption measurements of our best sample showed clear, strong excitonic absorption lines for both $n=1$ and $n=2$ transitions. Both the $n=1$ light and

heavy hole transitions were within 1 meV of the projected value, while the $n=2$ heavy hole transition was within 11 meV of the projected value. Single crystal x-ray diffraction measurements clearly showed the first-order superlattice satellite peaks, and photoluminescence measurements at 23.1 K showed a strong peak at 1.357 micron with a linewidth of 5.0 meV, demonstrating the excellent period-to-period control of the superlattice barrier and well widths.

We made degenerate pump-probe measurements of optical nonlinearities 25 meV below the band edge of the superlattice with 150 fsec pulses at a power density on the sample of 100 MW/cm² from an additive-pulse-modelocked color center laser. The non-collinear pump and probe beams propagated normally to the quantum well layers. We measured the synchronous differential transmission and reflection of the probe as a function of delay between the two pulses.

We discovered three time constants characteristic of the superlattice from these measurements. An extremely short time constant, faster than the resolution of the pulse, is due to a blue shift of the exciton line caused by the optical Stark effect. A 250 fsec and a long time constant (on the order of tens of nanoseconds) are probably caused by bleaching of the exciton line by the presence of photo-generated excitons and free carriers.

These simultaneous measurements of reflection and transmission dynamics proved a means of quantifying index of refraction changes relative to those in absorption without making an interferometric phase measurement. Further measurements made at different temperatures will help us to determine the relative contribution of the fast and slow components as functions of detuning from the band-edge. This information will help us optimize the performance of nonlinear optical devices which are based on MQW materials.

9.4 MBE-Grown InGaAlAs/InP Long-Wavelength Laser Diodes for Narrow Linewidth Applications

Sponsors

Charles S. Draper Laboratory
Contract DL-H-315251

Project Staff

Woo-Young Choi, James Vlcek, Yakov Royter, Isako Hoshino, Professor Clifton G. Fonstad, Jr.

Semiconductor lasers emitting at wavelengths of 1.3 to 1.5 μm are a key element of low-loss optical fiber communication systems. A quaternary alloy InGaAsP lattice-matched to InP substrates is the material system most often used for these laser diodes. Liquid phase epitaxy (LPE) and metal-organic chemical vapor epitaxy (MOCVD) are the usual growth techniques for this material system.

The InGaAlAs material system, grown by conventional solid-source molecular beam epitaxy (MBE) techniques, is another promising candidate for laser diodes emitting in the 1.3 to 1.5 μm range. The InGaAs/InAlAs heterojunction has a larger conduction band discontinuity than the InGaAs/InP heterojunction. This enhances the quantum confinement of electrons, giving the device designer greater latitude in choosing layer structures for optimal electrical and optical confinement profiles. This enhanced design latitude, in turn, can be used to achieve lower threshold currents and temperature variation (T_0), and narrower spectral linewidth.

Our goal is to fabricate InGaAs/InAlAs quantum well laser diodes which achieve the above-mentioned performance improvements. Initially, we focused our efforts on development of basic laser diode technology. We grew MBE double heterostructure laser materials; fabricated broad-area and stripe laser diodes; and characterized their threshold currents, emission spectrum, far-field pattern, and temperature dependence of threshold currents. Initial data indicate that our devices are comparable to other laser diodes of the same material system reported

in the literature. Now, we are in the process of optimizing our layer structure, growth conditions, and device fabrication technology which should greatly enhance device performance.

In addition to multiple quantum well laser diodes, we are investigating the use of graded-index optical confinement structures for (1) an optimal gain profile with minimal angular dispersion of the emitted beam and (2) structures utilizing controlled amounts of lattice mismatch strain in the active layer to further enhance the quantum size effects of the confined carriers. To achieve our long range goal of producing ultra-narrow linewidth devices, we are extensively analyzing various theoretical techniques for reducing laser linewidth. Our ultimate goal is to produce room temperature laser diodes with emission linewidths below 100 kHz.

9.5 InGaAlAs Strained-Layer Heterostructures on 111 GaAs and InP for Optical for Modulator Applications

Sponsors

Joint Services Electronics Program
Contract DAAL03-89-C-0001
National Science Foundation Grant
Grant EET 87-03404

Project Staff

Richard Singer, Professor Clifton G. Fonstad, Jr., in collaboration with Stuart D. Brorson, Daryl Smith,³ B. Laurich,³ Christian Mailhoit,⁴ Bruce D. McCombe,⁵ and Bernie A. Weinstein⁵

When epitaxial layers with a slight lattice mismatch are deposited upon (111)-oriented GaAs or InP substrates, piezoelectric fields are generated. Whether a field points $\langle 111 \rangle_A$ or $\langle 111 \rangle_B$ is a function of whether a given epilayer is under tensile or compressive strain. Our group was the first

to produce these structures and to demonstrate experimentally the existence of piezoelectric fields. We are now applying this effect to optoelectronic devices.

If a quantum well structure is grown through appropriate choice of ternary composition and layering, the strain-induced field will red-shift the excitonic resonance of the well. This is the familiar Quantum Confined Stark Effect (QCSE). In the present structures, the internal strain-induced field provides a bias on the order of 105 V/cm. An applied voltage will either enhance or counteract the strain-induced field around a bias point in a highly sloped, nearly linear region of the field verses index and/or absorption characteristics of these structures. Thus, the external bias is expected to dramatically affect the transmittance or reflectance of the multiple quantum well structure at a given wavelength. Practical, low voltage modulation of optical signals should be possible.

Presently, we are seeking to grow, fabricate, and characterize window and waveguide p-i-n modulators in both the GaAs and InP material systems. Material of good surface morphology has been successfully grown by molecular beam epitaxy on (111) GaAs, and samples of (111)-oriented strained layer heterostructures have been distributed to a number of researchers interested in studying them. Recently, reflection modulators consisting of a mirror region of quarter wave plates and an active region of strained multiple quantum wells have been grown and tested with no applied bias. Work is currently underway to process these devices so that we can study their response to applied voltages.

MBE growth on InP is more difficult because of the conflicting requirements of a low substrate temperature and high As overpressure to stabilize the volatile (111) surface, on the one hand, and the opposite growth conditions needed to enhance surface mobility of Al on the other. To overcome this diffi-

³ Los Alamos National Laboratory.

⁴ Lawrence Livermore National Laboratory.

⁵ State University of New York at Buffalo.

culty, we will attempt a variation of migration enhanced epitaxy in which we will keep both the substrate temperature and As overpressure low.

9.6 Molecular Beam Epitaxial Growth on (h11) Vicinal Surfaces

Sponsor

MIT Funds

Project Staff

Dr. Elias D. Towe, Professor Clifton G. Fonstad, Jr., in collaboration with H.Q. Le,⁶ and J.V. Hryniewicz⁶

Traditionally, III-V compound semiconductors have been synthesized on (100) substrate surfaces. Because it is desirable to fabricate devices on chemically etched (100) surfaces, an understanding of molecular beam epitaxial growth on high-index planes vicinal to the (100) surface is important. Understanding the properties of material grown on such surfaces is also necessary. The particular planes of interest are those denoted by (h11).

We have continued our work on the growth of epi-layers on (h11) vicinal surfaces of GaAs. In particular, the growth conditions and characteristics on the (111)B, (211)B and (511)B surfaces for acceptable quality layers are fairly well understood. GaAs and (Al, Ga)As layers with luminescence superior to that of layers on the (100) surface have been grown on these surfaces.

Our interest in the epi-layers on the (h11) surfaces is due to the potential for improved performance and for their use in novel optical devices. We are currently studying some laser devices with strained-layer active regions on (111)-GaAs substrates. The devices have been fabricated, and we will test them soon. Some waveguide structures on (211) substrates have also been fabricated so that an undergraduate thesis student

can evaluate them with a tunable Ti:sapphire laser.

We expect that the threshold current densities of the lasers on the (111)-GaAs substrates will be lower than those on the conventional (100) substrates. This expectation is based on the fact that the relative photoluminescence emission of the layers on these substrates is higher than that on the (100) substrates.

9.7 Pseudomorphic AlAs/InAs/InGaAs Resonant Tunneling Structures

Sponsor

Joint Services Electronics Program
Contract DAAL03-89-C-0001

Project Staff

Thomas P.E. Broekaert, Professor Clifton G. Fonstad, Jr.

A fundamental objective in the design of resonant tunneling diodes (RTDs) for microwave oscillators and digital switching is achievement of the highest possible peak current density at the lowest possible peak voltage, while maintaining a high peak-to-valley current ratio and wide valley region. The InGaAlAs material system, lattice matched to InP, has the design flexibility to optimize the RTD for microwave performance and switching applications in terms of peak current density and peak voltage of the RTD.

Thus far, by using very thin, three monolayer AlAs barriers and InGaAs wells, within bounding regions of InGaAs lattice-matched to InP, we have achieved room temperature peak current densities in excess of 1 MA/cm², the highest reported value for RTDs to date, at peak voltages as low as 0.55 V. The peak-to-valley current ratio of these devices is approximately 2 to 4.

For the diode structure, a turn-on threshold voltage is apparent in the I-V characteristics. This threshold characteristic can be removed

⁶ MIT Lincoln Laboratory.

by widening the well or by including a low bandgap material, i.e., InAs, in the well. Diode structures of this type have been fabricated and display linear initial I-V characteristics with no turn-on threshold and a low peak voltage.

The combination of thin AlAs barriers and InAs containing wells should allow us to further optimize the RTDs.

9.8 Three-Terminal Quantum Well Base/Tunnel Barrier Devices

Sponsors

Joint Services Electronics Program
Contract DAAL03-89-C-0001

Project Staff

Thomas P.E. Broekaert, Lung-Han Peng, Professor
Clifton G. Fonstad, Jr.

We have gained our objective of making direct electrical contact to a populated conduction band quantum well in a resonant tunneling configuration. Recently, in a significant breakthrough, we succeeded in etching away the layers above the InAs quantum well layer in an AlAs/InAs/InGaAs resonant tunneling diode and making electrical contact directly to this 2 to 5 nm thick layer. This major advance in this technique opens the door to development of a new class of ultra-high performance electronic, optoelectronic, and photonic devices. We are currently beginning an aggressive program of research utilizing this advance to investigate quantum-well base, tunnel-barrier n-n-n transistors; tunnel injection, quantum-well-level laser diodes for the 2 to 5 micron region; sub-picosecond quantum-well-level, tunnel-barrier infrared photodiodes; and ultrafast quantum-well-level, tunnel-barrier optoelectronic modulators and non-linear optical components.

The basis for all these devices is the AlAs/InAs/InGaAs double barrier resonant tunneling structure discussed in the previous section. There are at least three unique features of this structure which make it ideally suited for these structures. First, the AlAs

tunnel barriers are unusually high relative to the InGaAs injectors and the InAs well, which yields multiple confined well states and sharp quantum structure at room temperature. Second, the InAs well lies below the band edges of the InGaAs injectors so that when it is suitably wide and doped, the first well level will be populated. This provides all-important lateral conduction in the plane of the well and the necessary ground-state population for detector and optical modulator applications. Third, the very wide range of materials in these structures has allowed us to develop a selective etch which, in turn, makes it possible to make electrical contact to the very thin quantum well layer.

9.9 Design and Fabrication of GaAlAs Heterostructure Laser Diodes for Monolithic Integration with Si Circuits

Sponsors

International Business Machines Corporation
National Science Foundation
Grant ECS 84-13178

Project Staff

Geoffrey Burns, Dr. Herve Blanck, Professor Clifton G. Fonstad, Jr., in collaboration with Professor Carl V. Thompson

Prospects for monolithic integration of III-V electrical and optical devices with Si circuits have focused vigorous research efforts in direct heteroepitaxial growth of these compounds on Si substrates. Developing III-V optical sources useful for VLSI optical interconnects is one goal which has been pursued by several groups. Along these lines, we have focused upon the laser diode due to its capacity for high speed modulation and large power output. During previous years, we have developed processes for direct epitaxial growth of GaAs on Si using molecular beam epitaxy. With particular attention to details of Si surface preparation, GaAs growth initiation, and in situ annealing, we have been able to repeatably produce GaAs layers with smooth growth fronts and reduced defect density. This growth sequence has been extended to produce AlGaAs/GaAs heterostructures for laser fabri-

cation, and working devices are now routinely fabricated and characterized.

Unfortunately, active optical devices such as the laser exhibit degraded luminescent efficiency and reliability when fabricated in heteroepitaxial GaAs on Si; threshold currents and lifetimes presently obtained are insufficient for Si integration. These shortcomings are imposed primarily by limitations in the quality of heteroepitaxial GaAs on Si currently produced, including dislocation densities above 10^6 per square cm and residual strains above 10^9 dynes per square cm, resulting from the 4.2 percent lattice mismatch and ~ 40 percent thermal expansion mismatch between GaAs and Si.

We have been exploring MBE growth and laser design alternatives to address these problems. Recently, we discovered that lasers can be grown selectively on window openings on Si substrates with minimal kerf regions. In addition to providing a convenient method for monolithic integration, growth patterning can reduce thermal stress on laser devices. Another advantage is its tendency for reduced growth rates near the stripe edges, providing optical and current confinement without using complicated techniques such as buried heterostructures. Devices prepared in this way have realized laser threshold currents as low as 75 mA, a two-fold improvement over lasers fabricated using etched ridge waveguide techniques. Further design optimizations, including narrower stripe widths, offer opportunity for continuing improvement.

We are also evaluating heteroepitaxial GaAs chemically removed from the Si substrate to study the effects of residual thermal strain on laser performance. Using photoluminescence to measure donor-valence band transition energies, which can be correlated with strain, we have observed partial relaxation of thermal strain upon removal of the epitaxial GaAs. Using methods which we have developed to handle and process thin (~ 4 micron) layers, rapid thermal annealing will be employed in an attempt to remove the remaining strain. Following these initial experiments, laser epitaxial layers will also be lifted off, processed, and characterized to provide the first data to evaluate separately the effect of strain on laser performance.

9.10 Microbridge Suspension of Monolithic GaAlAs Heterostructures Grown on Si by MBE

Sponsors

International Business Machines Corporation
National Science Foundation
Grant ECS 84-13178

Project Staff

Geoffrey Burns, Dr. Herve Blanck, Professor Clifton G. Fonstad, Jr.

As discussed in the preceding section, the tensile stress caused by the thermal expansion coefficient difference between GaAs and Si is a crucial problem facing GaAs-on-Si devices. We have made preliminary studies of a unique technique to overcome this problem. In this technique, we physically separate the GaAs device layers from the Si, except for preformed metal microbridges that hold it in place on the substrate. Recent work by Yablonovitch et al. of Bellcore, who used an AlAs sacrificial layer to remove GaAlAs heterostructures from GaAs substrates for hybridizing, provided the basis for this technique.

Using mesa, drain and source pad masks from an existing MESFET mask set, with GaAs-on-Si layers grown with 50-nm thick AlAs "sacrificial" layers, we have demonstrated the possibility of using the Yablonovitch technique to physically separate AlGaAs device regions from the initial, high defect density nucleation layers and the Si substrate, leaving them in position on the Si wafer held by thin gold leads.

Photoluminescence measurements on GaAs pieces etched free of their Si substrates show a peak shift in the direction of reduced strain, but do show full relaxation of the stress. We are currently studying the effects of post-separation annealing (see preceding section).

In addition to laser diodes, we are applying the microbridge suspension concept to a number of devices. The etalon formed by removing the AlAs sub-layer should be ideal for forming optical modulator cavities and

surface emitting laser cavities. Furthermore, the dielectric isolation provided by the thin air layer will greatly diminish the substrate parasitics experienced by high speed GaAs electronic circuitry fabricated in the GaAs-on-Si epilayers.

9.11 Damage-Free In-Situ UHV Etching and Cleaning of III-V Heterostructures Using Molecular Beams

Project Staff

Professor Clifton G. Fonstad, Jr., in collaboration with Professor Sylvia T. Ceyer and Professor Herbert H. Sawin

The development of damage-free ultra-high vacuum etching, cleaning, and regrowth techniques compatible with molecular beam epitaxy and ex situ processing of III-V heterostructures is a major challenge facing device researchers. The ability to selectively pattern, etch, and overgrow quantum heterostructures is crucial to the effective realization of integrated optical circuitry and quantum effect electronic structures. Present techniques involve relatively high energy (100 eV and above) ion beams which cause substantial sub-surface damage, much of which is impossible to remove.

As a solution to the problem of process-induced damage, we have begun investigating the use of UHV kinetic molecular beam techniques (widely used to study atomic interactions on surfaces) to etch and clean III-V substrates and heterostructures so that there is a minimum of surface damage and a maximum of flexibility. Depending on the etchant gas mixture established, we anticipate that low energy (0.5 to 2 eV) kinetic beams can be used to (1) anisotropically etch-pattern III-V heterostructure wafers with no damage; (2) clean surfaces allowing epitaxial growth on wafers which have been removed from the UHV environment for external processing; and (3) selectively remove masking materials and clean surfaces suitably for subsequent overgrowth.

This program is based on the work of Professor Sylvia Ceyer, an expert on using supersonic beams to probe surface reactions

and to etch silicon, and that of Professor Herbert Sawin, an expert on the design of molecular beam and rf plasma sources and reactors, as well as plasma reaction dynamics. We have obtained funding to assemble a UHV chamber for kinetic beam processing, which will be connected through a specially-designed transfer mechanism to the present Riber 2300 solid source molecular beam epitaxy system. Presently, we are seeking additional funding for a major collaborative research effort in this area.

9.12 Publications

Bagwell, P.F., T.P.E. Broekaert, T.P. Orlando, and C.G. Fonstad. "Resonant Tunneling Diodes and Transistors with a One, Two, and Three Dimensional Electron Emitter." *J. Appl. Phys.* Forthcoming.

Beery, J.G., B.K. Laurich, K. Elcess, C.G. Fonstad, C.G. Maggiore, C. Mailhoit, and D.L. Smith. "Growth and Characterization of (111) Oriented GaInAs/GaAs Strained-Layer Superlattices." *Appl. Phys. Lett.* 54: 233-235 (1989).

Broekaert, T.P.E., and C.G. Fonstad. "Extremely High Current Density, Low Peak Voltage Pseudomorphic InGaAs/AlAs/InAs Resonant Tunneling Diodes." In *Technical Digest of the 1989 International Electron Devices Meeting*. Piscataway, New Jersey: IEEE, 1989, pp. 559-562.

Broekaert, T.P.E., W. Lee, and C.G. Fonstad. "InGaAs/AlAs/InAs Resonant Tunneling Diodes with Peak-to-valley Current Ratios of 30 at Room Temperature." Submitted to *Appl. Phys. Lett.*

Broekaert, T.P.E. *The Growth and Characterization of Resonant Tunneling Diodes*. S.M. thesis. Dept. of Electr. Eng. and Comput. Sci., MIT, 1989.

Burns, G. *Growth of (Ga,Al)As on Silicon Substrates by Molecular Beam Epitaxy*. S.M. thesis. Dept. of Electr. Eng. and Comput. Sci., MIT, 1989.

Burns, G.F., H. Blanck, and C.G. Fonstad. "Low-threshold GaAs/AlGaAs Graded-

- index Separate-confinement Heterostructure Lasers Grown by Molecular Beam Epitaxy on Oxide-masked Si Substrates." Submitted to *Appl. Phys. Lett.*
- Chong, T.C., and C.G. Fonstad. "Theoretical Gain of Strain Layer Semiconductor Lasers." *IEEE J. Quantum Electron.* 25: 171-178 (1989).
- Frank, M. *Characterization of the Pulsed Behavior of InGaAlAs Laser Diodes*. S.B. thesis. Dept. of Electr. Eng. and Comput. Sci., MIT, 1989.
- Kim, H.M., C.R. Wie, and C.G. Fonstad. "Strain and Lattice-Mismatch in (001) and (111) GaInAs/GaAs Strained Layer Superlattices." Paper presented at the Materials Research Society Meeting, Boston, Massachusetts, November 27-December 2, 1989.
- Laurich, B. K., K. Elcess, C.G. Fonstad, C. Mailhoit, and D. Smith. "Optical Properties of (100) and (111) Oriented GaInAs/GaAs Strained Layer Superlattices." *Phys. Rev. Lett.* 62: 649-652 (1989).
- Liu, X., A. Petrou, K. Elcess, C. Fonstad, and C. Mailhoit. "Observation of Parity-breaking Interband Transitions in [111]-grown InGaAs/AlGaAs Strained-Layer Superlattices." Paper presented at the Meeting of the American Physical Society, San Diego, March 1989.
- McCann, P.J. and C.G. Fonstad. "Observation of an Interfacial Reaction Between Selenium Vapor and the Barium Fluoride Surface: Implications for Heteroepitaxy of PbSe on BaF₂." Paper presented at the Electronic Materials Conference, Cambridge, Massachusetts, June 21-23, 1989.
- Miller, D. *Microbridge Suspension of Heteroepitaxial Gallium Arsenide on Silicon*. S.B. thesis. Dept. of Mater. Sci. and Eng., MIT, 1989.
- Palmer, J.E., G. Burns, C.G. Fonstad, and C.V. Thompson. "Effect of As₄ Overpressure on Initial Stages of MBE Growth of Ga on Si." Paper presented at the Electronic Materials Conference, Cambridge, Massachusetts, June 21-23, 1989.
- Sato, H., J.C. Vitek, C.G. Fonstad, B. Meskoob, and S. Prasad. "InGaAs/-InAlAs/InP Collector-Up Microwave Heterojunction Bipolar Transistors." Submitted to *Electron Device Lett.*
- Sato, H., J.C. Vitek, C.G. Fonstad, B. Meskoob, and S. Prasad, "High Current Density Emitter-Down InGaAlAs Heterojunction Bipolar Transistors." Paper presented at the Device Research Conference, Cambridge, Massachusetts, June 18-21, 1989.
- Towe, E., C.G. Fonstad, H.Q. Le, and J.V. Hryniewicz. "Luminescence of (Al,Ga)As and GaAs Grown on the Vicinal (511) B-GaAs Surface by Molecular Beam Epitaxy." *J. Vac. Sci. Technol.* B7: 395-398 (1989).
- Towe, E., and C.G. Fonstad. "Synthesis of GaAs and (Al,Ga)As on (511)-GaAs Surfaces by Molecular Beam Epitaxy." *Proceedings of the Symposium on Heteroepitaxial Approaches in Semiconductors: Lattice Mismatch and its Consequences*. Eds. A.T. Macrander and T.J. Drummond, 347-357. Pennington, New Jersey: Electrochemical Society, 1989.
- Venkateswaran, V.D., L.J. Cui, M. Li, B.A. Weinstein, K. Elcess, C.G. Fonstad, and C. Mailhoit. "Strain Mapping in (111)- and (100)-InGaAs/GaAs Superlattices." *Appl. Phys. Lett.* 56: 276-288 (1990).
- Venkateswaran, V.D., T. Burnett, L.J. Cui, M. Li, B.A. Weinstein, H.M. Kim, C.R. Wie, K. Elcess, C.G. Fonstad, and C. Mailhoit. "Comparison and Spatial Profiling of Strain in [001] and [111] Oriented InGaAs/GaAs Superlattices from Raman and X-ray Experiments." Submitted to *Phys. Rev. B*.
- Venkateswaran, V., L. Cui, M. Li, B.A. Weinstein, H.M. Kim, C.R. Wie, C. Mailhoit, K. Elcess, and C.G. Fonstad. "Mapping of Internal Strain in InGaAs-GaAs Superlattices." Paper pre-

sented at the Meeting of the American Physical Society, San Diego, March 1989.

Yoo, B.S., J.-P. Cheng, A.A. Reeder, R. Ranganathan, Y.J. Wang, B.D. McCombe, K. Elcess, C.G. Fonstad, B. Lin, and F.

Kuchar. "Far Infrared Studies of [111] InGaAs/AlGaAs Strained-Layer Superlattices." Paper presented at the Meeting of the American Physical Society, San Diego, March 1989.

Section 2 Optics and Devices

Chapter 1 Optics and Quantum Electronics

**Chapter 2 Novel Processes and Materials for Infrared
Nonlinear Optics**

Chapter 1. Optics and Quantum Electronics

Academic and Research Staff

Professor Hermann A. Haus, Professor Erich P. Ippen, Professor James G. Fujimoto, Professor Peter L. Hagelstein, Dr. Santanu Basu, Dr. Jyhpyng Wang, Dr. Beat Zysset

Visiting Scientists and Research Affiliates

Dr. Hiroyuki Yokoyama¹

Graduate Students

Kristen K. Anderson, Keren Bergman, John Paul Braud, Stuart D. Brorson, Tak K. Cheng, James G. Goodberlet, Cris Eugster, Katherine L. Hall, Wei-Ping Huang, Charles T. Hultgren, Janice M. Huxley, Joseph M. Jacobson, Sumanth Kaushik, Michael J. LaGasse, Yinchieh Lai, Ling-Yi Liu, Martin H. Muendel, John D. Moores, Ann W. Morganthaler, Robert W. Schoenlein, Morrison Ulman

Undergraduate Students

Daniel Tauber

Technical and Support Staff

Mary C. Aldridge, Mary Ellen Butts, Donna L. Gale, Cynthia Y. Kopf

1.1 The Nonlinear Waveguide Interferometer

Sponsors

Charles S. Draper Laboratory
Contract DL-H-404179
Joint Services Electronics Program
Contract DAALO3-89-C-0001
National Sciences Foundation
Grant EET 87-00474

Project Staff

Professor James G. Fujimoto, Professor Hermann A. Haus, Professor Erich P. Ippen, Michael J. LaGasse, John D. Moores, Keren Bergman

Section 1.2 describes a single-arm interferometer invented in our laboratory that has been used for low power all-optical switching. We are currently investigating a switch very similar to the single arm interferometer, which is based on a fiber (waveguide) ring reflector, similar to, yet different from, the ring reflector demonstrated by the group at British Telecom.² In our research, we have shown that the fiber ring reflector is an excellent candidate for soliton switching and for producing squeezed light.³ Consequently, since any experiments limited by quantum noise (i.e., detector shot noise) must take into account the quantum properties of light, we have become interested in developing a self-consistent quantum theory

¹ NEC, Japan.

² N.J. Doran, K.J. Blow, and D. Wood, *Proc. SPIE* 836:238-243 (1987).

³ J.D. Moores, K. Bergman, H.A. Haus, and E.P. Ippen, "Optical Switching Using Fiber Ring Reflectors," submitted for publication; H.A. Haus, K. Watanabe, and Y. Yamamoto, "Quantum-Nondemolition Measurement of Optical Solitons," *J. Opt. Soc. Am. B* 6:1138-1148 (1989); Y. Lai and H.A. Haus, "Characteristic Functions and Quantum Measurements of Optical Observables," *J. Quant. Opt.*, forthcoming; M. Shirasaki and H.A. Haus, "Squeezing of Pulses in a Nonlinear Interferometer," *J. Opt. Soc. Am. B* 7(1): 30-34 (1990).

for optical solitons.⁴ The promise of a simple squeezing mechanism using optical pulses in fibers has also kindled our interest in developing a fiber gyro that would operate at a noise level below the standard quantum limit shot noise.

The fiber ring is one realization of a fiber ring gyro utilizing the Sagnac effect. Unfortunately, the ring cannot be used directly as a gyro with squeezed noise, because the noise that is in phase with the Sagnac signal is not reduced below the vacuum level. However, our theory predicts that a cascade of two rings, one as a squeezer and one as a gyro, can be made to perform at a level below the standard quantum limit. Ongoing experiments should determine whether squeezing is achieved in the ring. The squeezing process is broadband so that pulses can be used in the experiments. Nonlinearity is enhanced because the duty cycle enhances peak power. Through our experiments, we need to identify the several classical sources of noise that could prevent squeezing.

1.2 Picosecond Optical Signal Sampling

Sponsor

National Science Foundation
Grant EET 87-00474

Project Staff

Professor James G. Fujimoto, Professor Hermann A. Haus, Wei-Ping Huang, Michael J. LaGasse

The goal of our work is to develop optical waveguide devices for high rate all-optical switching. This objective involves development of (1) analytical and computer tools for the characterization of optical waveguide properties and (2) computer programs for describing optical pulse interactions and for experimentally verifying their predicted performance.

Through our pioneering work, we have achieved a better understanding of coupling modes theory and prediction of crosstalk in waveguide couplers.⁵ Our paper on this subject was selected for publication in an IEEE volume of reprints on optical couplers.

Along with our work on coupled mode theory, we have clarified the theory of transfer of power in grating assisted couplers⁶ and have developed a self-consistent theory for tapered couplers.⁷ In addition, we have developed simple computer programs for the IBM PC that characterize optical waveguide modes.⁸ In cooperation with Dr. Donnelly of MIT Lincoln Laboratory, we continued the work by Dr. L. Molter Orr, who was supported by the preceding National Science Foundation grant while working on her Ph.D. at MIT. This research has led to an improved understanding of the crosstalk problem in waveguide couplers.⁹

⁴ Y. Lai and H.A. Haus, "Quantum Theory of Solitons in Optical Fibers. I. Time-Dependent Hartree Approximations," *Phys. Rev. A* 40:844-853 (1989); Y. Lai and H.A. Haus, "Quantum Theory of Solitons in Optical Fibers. II. Exact Solution," *Phys. Rev. A* 40:854-866 (1989); H.A. Haus and Y. Lai, "Quantum Theory of Soliton Squeezing - A Linearized Approach," *J. Opt. Soc. Am. B* 7(3): 386-392 (1990).

⁵ H.A. Haus, W.P. Huang, S. Kawakami, and N.A. Whitaker, "Coupled-Mode Theory of Optical Waveguides," *J. Lightwave Tech.* LT-5:16-23 (1987).

⁶ W.P. Huang and H.A. Haus, "Power Exchange in Grating-assisted Couplers," *J. Lightwave Tech.* 7:920-924 (1989).

⁷ H.A. Haus and W.P. Huang, "Mode Coupling in Tapered Structures," *J. Lightwave Tech.* 7:729-730 (1989); W.P. Huang and H.A. Haus, "Selfconsistent Vector Coupled-Mode Theory for Tapered Optical Waveguides," *J. Lightwave Tech.*, forthcoming.

⁸ H.A. Haus, W.P. Huang, and N.M. Whitaker, "Optical Waveguide Dispersion Characteristics from the Scalar Wave Equation," *J. Lightwave Tech.* LT-5:1748-1754 (1987).

⁹ J.P. Donnelly, L.A. Molter, and H.A. Haus, "The Extinction Ratio in Optical Two-Guide Coupler $\Delta\beta$ switches," *J.*

All-optical switching and all-optical logic gates require that the output of gates and switches are reasonably undistorted versions of input pulses. We have demonstrated an all-optical switch with a record low switching intensity of 0.5 W and with a very low distortion of the switched out pulse.¹⁰ We achieved the low switchout power by using a long propagation distance through an optical fiber. The switch, invented in our laboratory by a visiting Japanese researcher, is interferometric, using a single fiber and two orthogonally polarized versions of the pulse that interfere with each other. One of the two pulses is acted upon by a control pulse. Because only a single fiber is used, the interferometer is stable even when considerably long (i.e., 100 m). Modifications of the switch into integrable form will be feasible, when sufficient nonlinearities have been realized in semiconductor waveguides.

1.3 Nonlinear Dynamics in Active Semiconductor Waveguides

Sponsors

Joint Services Electronics Program
Contract DAAL03-89-C-0001
National Science Foundation
Grant EET 88-15834
U.S. Air Force - Office of Scientific Research
Contract F49620-88-C-0089

Project Staff

Katherine L. Hall, Charles T. Hultgren, Professor
Erich P. Ippen

We have continued our study of carrier dynamics and nonlinear optical interactions in active semiconductor waveguide devices. Using 100-fs-duration pulses in the 800–900 nm regime obtained by fiber com-

pression of synch-pumped dye laser pulses and similar pulses in the 1.45–1.65- μm band from APM F-center lasers, we are investigating nonlinear dynamic behavior in both GaAlAs and InGaAsP devices under various excitation conditions. Varying the wavelength of the pump and probe beams, as well as injection current in our diode waveguide structures, we are studying interactions in the presence of gain, loss, or nonlinear transparency. In all of these cases, an injected carrier density on the order of $10^{18}/\text{cm}^3$ makes the nonlinear optical behavior considerably different from that observed in passive devices.

In both GaAlAs and InGaAsP devices, we have discovered a strong nonlinearity due to nonequilibrium carrier heating. Heating of the carrier gas with respect to the lattice has a recovery time on the order of 1 ps in GaAlAs and 650 fs in InGaAsP. Since heating occurs via free electron absorption without a change in carrier number, recovery is complete. During the past year, we have documented gain and loss dynamics, which include two-photon absorption and hole-burning effects in addition to heating in a variety of different devices. In our present experiments, we are observing the index of refraction changes associated with these nonlinearities and evaluating their potential for use in all-optical switching.

During 1989, we have also demonstrated a novel means for detecting nonlinear optical interactions in the active regions of diodes by monitoring changes in diode voltage. The forward bias voltage is measured as a function of time delay between two pulses passing through the active region. The result is a nonlinear autocorrelation measurement that, when compared with optical pump-probe data, allows us to distinguish between those interactions involving carriers in the active region and other interactions.

Quant. Electron. 25:924-932 (1989); J.P. Donnelly, H.A. Haus, and L.A. Molter, "Cross Power and Crosstalk in Waveguide Couplers," *J. Lightwave Tech.* 6:257-268 (1988).

¹⁰ M.J. LaGasse, D. Liu-Wong, J.G. Fujimoto, and H.A. Haus, "Ultrafast Switching with a Single-Fiber Interferometer," *Opt. Lett.* 14:311-313 (1989).

1.4 Saturation Characteristics of Semiconductor Optical Amplifiers

Sponsors

Joint Services Electronics Program
Contract DAAL03-89-C-0001
National Science Foundation
Grant EET 88-15834
U.S. Air Force - Office of Scientific Research
Contract F49620-88-C-0089

Project Staff

Katherine L. Hall, Yinchieh Lai, Professor Erich P. Ippen

Although in the future optical amplifiers will be essential components of optical communication networks and integrated photonic circuits, very little is known about their nonlinear behavior. We need to improve our understanding of this behavior to properly evaluate the gain saturation and intermodulation distortion effects limiting device performance. In our laboratory, we have studied amplifier characteristics as a function of pulse duration and energy in the nonlinear regime. We have also developed an analytical model to describe the observed behavior.

In our experiments, we have been the first to observe pulsewidth-dependent gain in diode laser amplifiers. We have obtained data by measuring amplifier gain (output pulse energy/input pulse energy) as a function of input pulse energy. At low input energies, the amplification of ultrashort (100 fs) pulses is the same as that for longer (20 ps) pulses. As energy increases, however, the gain for the 100-fs pulses decreases more rapidly than that for the 20-ps pulses. This effect, observed at 1.5 μm in both conventional and quantum-well quaternary devices, results in a 3-db roll-off for the 100-fs pulses at an output energy that is about a factor of ten lower than that for the longer pulses.

We have modeled this behavior with a system of coupled differential equations that includes changes in gain due to nonequilibrium carrier distributions. The standard set of two equations describing the coupling between photon density and excited state carrier density is supplemented by a third, and in some cases a fourth, equation that

represents the faster nonequilibrium dynamic. The time constant of this dynamic determines the pulsewidth at which gain roll-off occurs. The parameters of the model are consistent with results from time-resolved pump-probe experiments performed on the same devices. We have obtained excellent agreement with the observed saturation data. This model predicts that a more rapid sequence of femtosecond pulses should be able to extract full energy. Although individual ultrashort pulses are restricted to lower gains, gain recovery between them is faster.

1.5 Femtosecond Studies of Metallic and High T_c Superconductors

Sponsors

Joint Services Electronics Program
Contract DAAL03-89-C-0001
U.S. Air Force - Office of Scientific Research
Contract F49620-88-C-0089

Project Staff

Stuart D. Brorson, Tak K. Cheng, Professor Erich P. Ippen

Femtosecond pump-probe observations of reflectivity dynamics on metal surfaces provide a unique measure of nonequilibrium electron dynamics. Because of the high electron density, incident optical energy is absorbed directly by the electron gas. The resulting rise in electron temperature produces a dynamic change in reflectivity. Relaxation of this change occurs as the electrons lose energy to the lattice via phonon emission. The rate is governed by the electron-phonon coupling strength.

We have begun to systematically study the strength of electron-phonon coupling, an important component in BCS theory of superconductivity, in collaboration with Professor M. Dresselhaus' group. In a series of experiments, we measured $\lambda\{\omega^2\}$ for ten different metals (four of them superconducting). The agreement between the values obtained with those described in the literature was excellent. In addition, our method for measuring $\lambda\{\omega^2\}$, the temperature relaxation rate, has several advantages over other techniques such as tunneling or heat

capacity measurements because it: (1) is a direct measurement, (2) works at room temperature, and (3) can be applied to non-superconducting as well as superconducting samples. We have also demonstrated that thin overlayers of Cu, which has d-band transitions in the visible, can enhance the experimental reflectivity changes on metals which are otherwise too small to detect. This enhancement extends the method for use with any metal film.

We have also performed a series of pump-probe and transmission experiments on three high- T_c thin films: $\text{YBa}_2\text{Cu}_3\text{O}_{7-\delta}$, $\text{Bi}_2\text{Sr}_2\text{CaCu}_2\text{O}_{8+x}$, and $\text{Bi}_2\text{Sr}_2\text{Ca}_2\text{Cu}_3\text{O}_{10+y}$. In these materials, too, we have observed a strong correlation between observed relaxation rates and T_c . At present, there is no clear theoretical explanation for these results. We are performing additional experiments to improve our understanding of the observed correlation.

1.6 Suppressed and Enhanced Spontaneous Emission from Microcavities

Sponsor

Joint Services Electronics Program
Contract DAAL03-89-C-0001

Project Staff

Hiroyuki Yokoyama, Stuart D. Brorson, Professor
Erich P. Ippen

Optical microcavities could prove useful in the construction of efficient, high speed semiconductor lasers. One particularly interesting possibility is using a cavity to alter the spontaneous emission rate of the device. This alteration has been observed with atoms and molecules. However, altering the emission rate in a semiconductor device is more difficult because the broad spontaneous emission bandwidth requires cavity dimensions on the order of a wavelength. To determine its potential application in semiconductor devices, we have analyzed the radiation modes of oscillating dipoles in planar (one-dimensional confinement) and

optical-wire (two-dimensional confinement) structures. When we used a mode counting method equivalent to, but less complex than, traditional classical and quantum electrodynamical approaches, we found that an idealized planar metallic mirror cavity could suppress the spontaneous emission with respect to free space by no more than a factor of two. Emission was suppressed to a lesser degree with use of a real dielectric stack. Theory shows, however, that we could achieve greater suppression by restricting the dimensionality to that of the optical wire. Then, enhanced spontaneous emission should be easier to observe. With GaAs quantum-well cavities fabricated at NEC, Dr. Yokoyama observed reductions in the luminescence times by factors of two due to cavity effect. We have recently achieved femtosecond up-conversion detection of spontaneous emission from these structures and we are now attempting to observe more dramatic reductions with multiple-quantum-well structures grown at MIT by Professor Clifton G. Fonstad's group.

1.6.1 JSEP Publications

Ippen, E.P., H.A. Haus, and L.Y. Liu. "Additive Pulse Mode Locking." *J. Opt. Soc. Amer. B* 6(9): 1736-1745.

Ippen, E.P., L.Y. Liu, and H.A. Haus. "Self-starting Condition for Additive-pulse Mode-locked Lasers." *Opt. Lett.* 15(3): 183-185 (1990).

Kesler, M.P. and E.P. Ippen. "Femtosecond Time-Domain Measurements of Group Velocity Dispersion in AlGaAs Diode Lasers." *Electron. Lett.* 25(10): 640-641 (1989).

Nelson, K.A. and E.P. Ippen, "Femtosecond Coherent Spectroscopy." *Advances in Chemical Physics*. Vol. 75 (1989).

Mark, J., L.Y. Liu, K.L. Hall, H.A. Haus, E.P. Ippen. "Femtosecond Pulse Generation in a Laser with a Nonlinear External Resonator." *Opt. Lett.* 14(1): 48-50 (1989).

1.7 New Ultrashort Pulse Laser Technology

Sponsors

Joint Services Electronics Program

Contract DAAL03-89-C-0001

National Science Foundation

Grant ECS 85-52701

U.S. Air Force - Office of Scientific Research

Contract F49620-88-C-0089

Project Staff

Professor James G. Fujimoto, Dr. Jyhpyng Wang,
James G. Goodberlet, Joseph M. Jacobson,
Robert W. Schoenlein, Morrison Ulman

1.7.1 Introduction

Development of new ultrashort pulse laser technology is the cornerstone for studies of ultrafast phenomena and high speed optical measurement and communication techniques. In the area of ultrashort pulse generation and measurement technology, we are developing new techniques to extend the range of applications and resolution of ultrafast studies. In particular, development of tunable wavelength femtosecond sources is important for a wide range of spectroscopic as well as optoelectronic device studies. High repetition rate femtosecond amplifier technology permits the generation of high peak intensities for the study of nonlinear optical effects. Finally, our research places special emphasis on developing new solid state laser materials and diode pumping techniques. These developments could represent next generation technology, ultimately replacing existing dye laser systems to yield more compact and viable short pulse sources suitable for a wider variety of engineering applications.

1.7.2 Tunable Femtosecond Ti:Al₂O₃ Laser

Solid state lasers provide an attractive alternative to existing ultrashort pulse dye laser technology. Working in collaboration with researchers at MIT Lincoln Laboratory, we have developed a novel ultrashort pulse generation modelocking technique in the Ti:Al₂O₃ laser.¹¹ Ti:Al₂O₃ is a promising new solid state laser material which features room temperature operation, high energy storage, and a broad tuning range of 670 nm to 1000 nm. The broad gain bandwidth of this material make it ideal for femtosecond pulse generation and amplification. In addition, the tuning range is especially useful for the study of GaAs-based electronic and optoelectronic materials and devices.

Our ultrashort pulse generation technique is an extension of a pulse shortening technique developed in color center lasers known as additive pulse modelocking (APM).¹² However, in the Ti:Al₂O₃ laser, modelocking is achieved without the need for active gain or loss modulation. This self-starting additive pulse modelocking results in a significant reduction in the system cost and complexity since high frequency active modulation is not required for the laser system. Extending this technique to other laser materials holds the promise of developing a compact and low cost ultrashort pulse laser technology suitable for commercial application.

The self-starting additive pulse modelocking technique uses an external cavity which contains an optically nonlinear medium (a length of optical fiber). The nonlinear external cavity functions resemble a nonlinear Fabry Perot. The reflectivity of the Fabry Perot is a function of the relative cavity lengths or phase of the optical field. Since the optical fiber has a nonlinear index of refraction, the reflectivity of the Fabry Perot is intensity

¹¹ J. Goodberlet, J. Wang, J.G. Fujimoto, and P.A. Schulz, "Femtosecond Passively Mode-locked Ti:Al₂O₃ Laser with a Nonlinear External Cavity," *Opt. Lett.* 14:1125-1127 (1989).

¹² P.N. Kean, X. Zhu, D.W. Crust, R.S. Grant, N. Langford, and W. Sibbett, "Enhanced Mode Locking of Color-Center Lasers," *Opt. Lett.* 14:39-41 (1989); K.J. Blow and D. Wood, "Mode-Locked Lasers with Nonlinear External Cavities," *J. Opt. Soc. Am. B* 5:629-632 (1988); J. Mark, L.Y. Liu, K.L. Hall, H.A. Haus, and E.P. Ippen, "Femtosecond Pulse Generation in a Laser with a Nonlinear External Resonator," *Opt. Lett.* 14:48-50 (1989); E.P. Ippen, H.A. Haus, and L.Y. Liu, "Additive Pulse Mode Locking," *J. Opt. Soc. Am. B* 6:1736-1745 (1989).

dependent. If the relative cavity lengths are controlled appropriately, the nonlinear cavity will function like a fast saturable absorber to enhance intensity fluctuations in the laser. This produces the pulse formation process.

The additive pulse modelocked laser incorporates an all-optical switch in the form of a nonlinear Fabry Perot which produces pulse shortening. Alternatively, this system can be viewed as the analog of an RF or microwave feedback system, except that the feedback is nonlinear, operating at optical frequencies. Figure 1 shows a schematic diagram of the Ti:Al₂O₃ laser. In Ti:Al₂O₃, pulses as short as 1.4 ps have been generated directly from the laser with pulse durations of 200 fs obtained by externally compensating for chirp.

During the past year, we have studied the starting dynamics of the ultrashort pulse formation process and the scaling behavior of the laser system and performance. This research is relevant to extending the short pulse generation technique to other solid state laser materials at other wavelengths as well as to higher and lower power solid state lasers.

1.7.3 Diode Pumped Modelocked Nd:YAG Lasers

During preliminary studies in collaboration with investigators at MIT Lincoln Laboratory, we demonstrated the extension of this short pulse generation technique to a diode pumped Nd:YAG laser.¹³ Other studies at RLE by Professors Ippen and Haus have achieved short pulse generation in a lamp pumped Nd:YLF laser. Results suggest that self-starting additive pulse modelocking can be applied to a range of solid state laser materials.

The diode pumped Nd:YAG laser combines the advantages of diode pumping which

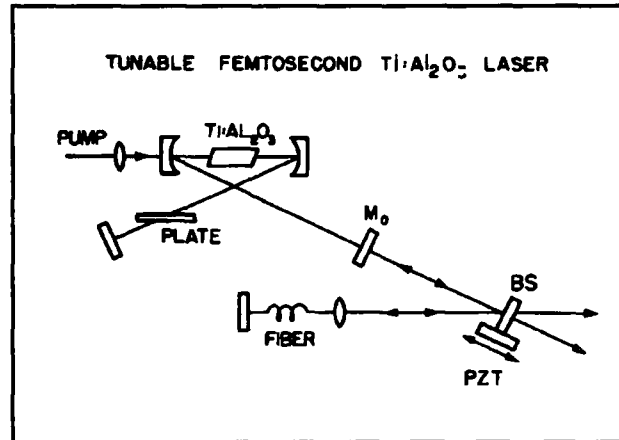


Figure 1.

offers high inherent stability, compactness, and low cost with the technique of additive pulse modelocking which has a simple design and especially short pulse generation. We have achieved a pulse width of 1.7 ps, which is the shortest pulse generated to date in a modelocked Nd laser. Preliminary measurements show that this system has excellent interpulse arrival time or phase stability, making it a suitable source for optoelectronic diagnostic studies that require synchronization of optical and electronic signals.

One of the key features of this technology is that the laser power and repetition rate can be scaled up or down. The extension of diode pumped self-starting additive pulse modelocking to lower output powers would permit development of extremely compact short pulse sources. Since the cavity length can be varied, this approach provides a method for obtaining variable pulse repetition rates. The development of compact short pulse sources could prove useful for a number of commercial applications including high speed optoelectronic sampling measurements and device diagnostics as well as possible applications for high speed signal processing using optical techniques.

¹³ J. Goodberlet, J. Jacobson, J.G. Fujimoto, P.A. Schulz, and T.Y. Fan, "Self Starting Additive Pulse Modelocked Diode Pumped Nd:YAG Laser," *Opt. Lett.*, forthcoming.

1.7.4 Multistage Femtosecond Dye Amplifier

While solid state laser systems are an important area of investigation for the next generation of ultrashort pulse laser technology, current measurement technology is based on dye laser systems and amplifiers. We are investigating new laser generation and high repetition rate amplification techniques for studying ultrafast phenomena, placing special emphasis on development of a multistage, high repetition rate, dye amplifier. The amplifier has a modular construction and may be easily configured for a variety of tasks.

The ultrashort pulse source for our system is a colliding pulse modelocked ring dye laser (CPM).¹⁴ This laser produces 50 fs pulses at 620 nm wavelength. The wavelength is not tunable because the laser is passively modelocked. The output of the CPM is amplified using a copper vapor laser pumped dye amplifier.¹⁵ The copper vapor laser operates at a repetition rate of 8 kHz which facilitates the use of signal averaging and lock-in detection techniques for high sensitivity measurements.

We have developed a new multistage copper vapor laser pumped dye cell amplifier system.¹⁶ The compact, multistage design allows the amplifier to be easily configured for advanced short pulse generation techniques. In comparison with earlier designs, we have improved its efficiency and experimental convenience while keeping the overall system complexity within manageable limits.

The high pulse intensity available from just one stage of amplification (2–3 microjoules) permits use of nonlinear optical techniques to generate wavelength tunable pulses in the near infrared. After the first amplification

stage, the femtosecond beam is focused in a cell of flowing water to generate a broadband continuum. A single wavelength may be selected from this continuum and amplified using an infrared dye in the second stage.

We are also currently investigating a third configuration which will produce compressed amplified pulses with pulse durations shorter than 20 fs. In this arrangement, a short single mode optical fiber is placed after the first stage of amplification. This increases bandwidth of the pulses because of self-phase modulation. After a second stage of amplification, the pulses can be compressed with a dispersive delay line or phase filter.

Thus, the high repetition rate amplifier forms the basis for a wide range of studies of ultrafast phenomena. Using nonlinear continuum generation techniques, the system provides a wavelength tunable source. For very high time resolutions, we can apply pulse compression techniques, achieving 20 fs measurement resolutions.

1.8 Ultrafast Processes in Waveguide Devices

Sponsors

International Business Machines Corporation
Joint Services Electronics Program
Contract DAAL3-89-C-0001
National Science Foundation
Grant ECS 85-52701
U.S. Air Force - Office of Scientific Research
Contract F49620-88-C-0089

Project Staff

Professor Hermann A. Haus, Professor James G. Fujimoto, Kristen K. Anderson, Claudio Chamon, Michael J. LaGasse

¹⁴ J.A. Valdmanis, R.L. Fork, and J.P. Gordon, "Generation of Optical Pulses as Short as 27 Femtoseconds Directly from a Laser Balancing Self-Phase Modulation, Group-Velocity Dispersion, Saturable Absorption, and Saturable Gain," *Opt. Lett.* 10: 131-133 (1985).

¹⁵ W.H. Knox, M.C. Downer, R.L. Fork, and C.V. Shank, "Amplified Femtosecond Optical Pulses and Continuum Generation at 5 kHz Repetition Rate," *Opt. Lett.* 9: 552-554 (1984).

¹⁶ M. Ulman, R.W. Schoenlein, and J. G. Fujimoto, "Cascade High Repetition Rate Femtosecond Amplifier," Paper FR3, presented at the Annual Meeting of the Optical Society of America, Orlando, Florida, October 15-20, 1989.

1.8.1 Optical Switching and Nonlinear Index in GaAs and MQW Waveguides

Femtosecond investigations of bandedge nonlinear dynamics in guided wave devices are directly relevant to the development of high-speed all-optical switches. Our group has recently developed a novel technique for nonlinear index measurements. This technique uses time division multiplexing to perform high resolution transient interferometric measurements on a nonlinear index. This approach reduces contributions from thermal and acoustic artifacts which traditionally limit interferometric measurements. The system can detect phase shifts as small as $\lambda/1000$.¹⁷

For studies in semiconductor devices, we took measurements using a synchronously-pumped, tunable femtosecond dye laser system. Using the dye Styryl 9, we obtained 430 fs pulses in the wavelength range 780 nm to 880 nm. We performed systematic studies to characterize the nonlinear response in AlGaAs ridge waveguide devices.¹⁸ We took the first direct measurement of the wavelength dependence of the instantaneous nonlinear index in this semiconductor. The results show values of n_2 in the range of 10^{-12} cm/W. Femtosecond time-resolved studies permit us to separate the real from the virtual contributions to the nonlinear index.

In one area of our investigation, we study new materials for all-optical switching. Other materials we are currently investigating include multiple quantum well (MQW) GaAs waveguides. After performing preliminary measurements of femtosecond nonlinear effects, we are now in the process of systematically characterizing the wavelength dependence of the nonlinear index as well as its linear optical properties.

A second material system of interest to us is nonlinear optical polymers. We have recently

begun studies in collaboration with investigators at Bell Communications Research to characterize the nonlinear index and absorption behavior in polydiacetylene waveguides. Nonlinear optical polymers are a rapidly emerging research area, and the combination of Bellcore's unique materials growth and fabrication capabilities with our capabilities in femtosecond optics will permit state-of-the-art studies to be performed.

1.8.2 Time Domain Optoelectronic Diagnostics

Femtosecond dye laser systems as well as future generation $\text{Ti:Al}_2\text{O}_3$ solid state laser systems can provide a tunable source of femtosecond pulses in the near IR wavelength range. This technology can form the basis for a wide range of diagnostics in optoelectronic devices. Diagnostics of optical waveguide devices can be divided roughly into two categories, measurement of nonlinear and linear properties.

As discussed in the previous section, high peak intensities associated with short pulses can be applied to study nonlinear index or n_2 effects in waveguide devices. In addition, other nonlinear effects such as two photon absorption can also be important in waveguide devices. We have measured the two-photon absorption coefficient β in GaAs waveguide devices. Since two-photon absorption produces excited carrier populations, this is an important limiting process for almost any application requiring high intensities in a waveguide.

In addition to nonlinear properties, we can also develop time domain techniques to measure linear absorption, group velocity, and dispersion. Since femtosecond pulse durations have a spatial extent which is less than the cavity round-trip of most waveguide devices, the transient linear response can be measured. For example, if a short pulse is

¹⁷ M.J. LaGasse, K.K. Anderson, H.A. Haus, and J.G. Fujimoto, "Femtosecond All-Optical Switching in AlGaAs Waveguides Using a Single Arm Interferometer," *Opt. Lett.* 14:314 (1989).

¹⁸ M.J. LaGasse, K.K. Anderson, C.A. Wang, H.A. Haus, and J.G. Fujimoto, "Femtosecond Measurements of the Nonresonant Nonlinear Index in AlGaAs," *Appl. Phys. Lett.* 56:417 (1990).

injected into the waveguide, the pulse will be reflected internally within the device and several echoes will be emitted corresponding to multiple round-trip paths through the device. Using a cross-correlation technique, the time resolved behavior of the echoes can be measured. The decay of the echoes contains information about the facet reflectivity and absorption of the device. The delay time or time of flight between the echoes gives the group velocity dispersion. Finally, measurements performed as a function of wavelength permit us to characterize absorption versus wavelength and group velocity dispersion. We have used GaAs passive waveguide devices to demonstrate these techniques.

By extending techniques further, we should be able to measure a wide range of optoelectronic device properties. With development of more compact and cost effective solid state tunable wavelength femtosecond lasers, a time domain optoelectronic diagnostic technology can become a viable alternative to continuous wave and other diagnostic approaches currently used for device characterization.

1.9 Image Potential and Electron Dynamics in Metals

Sponsors

Joint Services Electronics Program

Contract DAAL03-89-C-0001

National Science Foundation

Grant ECS-85-52701

U.S. Air Force - Office of Scientific Research

Contract F49620-88-C-0089

Project Staff

Professor James G. Fujimoto, Robert W. Schoenlein, Morrison Ulman

An improved understanding of electron dynamics in metals and at metal-semiconductor interfaces is necessary for the

development of high speed electronic devices. Semiconductors and metals are the major constituents of devices. As device speeds increase with the advent of new high electron mobility and quantum transport effects in semiconductors, dynamic processes in metals will also become an important factor in affecting device performances. Since the density of electrons in metals is high, nonequilibrium processes and excited state dynamics occur extremely rapidly. Femtosecond optical measurement, with its high sensitivity and ultrafast temporal resolution, provide one of the few techniques for directly measuring dynamical processes in metals.

We have continued our investigation of the transient dynamics of image potential states in metals. The image potential state has been a topic of recent active investigation in surface science. Image potential occurs when an electron, excited from the surface of a metal, is bound to its image charge in the bulk.¹⁹ The electronic states form a Rydberg-like series somewhat analogous to a two-dimensional electron gas in semiconductor quantum wells. Because the electronic wavefunction is maximized outside the metal surface, scattering processes are reduced, and the electron relaxes by tunneling from the image potential state to bulk states. Thus, the image potential state provides an important model system for investigating electron dynamics in metals.

Working in collaboration with researchers from General Motors Research Laboratories, our previous investigations combined femtosecond pump-probe spectroscopy with photoemission techniques to directly measure, for the first time, the lifetime of an image potential state in a metal.²⁰ In our studies, ultraviolet femtosecond pulses are used to populate the image potential states. The image potential dynamics are probed by photoemitting electrons out of these levels with a visible femtosecond pulse delayed in

¹⁹ D. Straub and F.J. Himpsel, "Identification of Image-Potential Surface States on Metals," *Phys. Rev. Lett.* 52:1922-1924 (1984).

²⁰ R.W. Schoenlein, J.G. Fujimoto, G.L. Easley, and T.W. Capehart, "Femtosecond Studies of Image-Potential Dynamics in Metals," *Phys. Rev. Lett.* 61:2596 (1988).

time. The energy spectrum of the photoemitted electrons is measured with a cylindrical mirror analyzer. This approach has allowed us to map the population of image potential states as a function of both time and electron energy. Studies performed on the surface of Ag(100) revealed an $n = 1$ image potential lifetime of 15–35 fs, representing one of the highest time resolution transient photoemission measurements ever made.

To test theoretical models for image potential electron dynamics, it is important to systematically study different states in the Rydberg series using different metal surfaces. For the image potential state to be long-lived, the image potential energy must occur in a range where there is a gap of bulk states. The image potential electron must be confined in the potential barrier outside the metal from the crystal lattice by Bragg reflection. In this case, the image potential state relaxes by inelastic scattering. Conversely, if a different metal surface is examined where the image potential is resonant with allowed bulk states, then the dominant relaxation channel is elastic scattering with electronic states in the bulk.

We have continued our earlier measuring efforts to examine the $n = 1$ and $n = 2$ image potential dynamics in Ag(100) and Ag(111).²¹ These experimental results can help explain differences in theoretical models based on simple single particle wavefunction analysis versus many-body effects. The image potential state has well defined quantum properties, providing an attractive model system for studying electronic quantum effects in metals.

1.10 Laser Medicine

Sponsors

Massachusetts General Hospital
Contract N00014-86K-0117
National Institutes of Health
Grant 2-RO1-GM35459

Project Staff

Dr. Jyhpyng Wang, David Huang, Professor James G. Fujimoto, Professor Erich P. Ippen

1.10.1 Heterodyne Ranging for Ophthalmic Diagnostics

The ability of excimer lasers to remove corneal tissue in submicron increments has led to interest in lasers in keratorefractive surgery. In this technique, the curvature or refractive power of the cornea is altered surgically to achieve refractive correction of a person's vision without glasses. To exploit the potential for micron-precision ablation control available with laser surgery requires a precise method for monitoring the incision depth. Previously, we had developed a femtosecond optical ranging technique for measurement of corneal incision depth.²² This technique is analogous to those used in radar or ultrasound except that short pulses of light are used to perform precise measurements of distance. Using this technique in corneal and intra-ocular surgery, distances in the eye can be measured noninvasively, i.e., without contact with the eye. Although this technique has achieved high sensitivity measurement performance, it required use of ultrashort pulse femtosecond lasers, and thus has limited potential for clinical applications.

Our recent research has focused on development of an alternate technique employing a short coherent length light source (AR-coated laser diode) and optical heterodyne detection to perform optical ranging. This method achieves measurement with longitudinal and transverse resolutions (10 μm

²¹ R.W. Schoenlein, J.G. Fujimoto, G.L. Eesley, and T.W. Capehart, "Femtosecond Image-Potential Dynamics in Metals: $n = 2$," *Phys. Rev. B* 41:5436-5439 (1990).

²² D. Stern, W.Z. Lin, C.A. Puliafito, and J.G. Fujimoto, "Femtosecond Optical Ranging of Corneal Incision Depth," *Inv. Ophthalm. Vis. Sci.* 30:99-104 (1989).

and 7 μm) and sensitivity to reflected signals as small as 1 part in 10^{10} (100 dB SNR). The technique uses a Michelson interferometer that gives interferometric signals only when the two arms of interferometer are matched within the coherence length of the light source.²³ The compactness and low power (7 μW incident power) of the light source greatly enhances the practicality and safety of the device for clinical applications. Measurements of corneal thickness, corneal incision depth, and corneal-lens distance were demonstrated. The technique was sufficiently sensitive to detection of scattered light from within the cornea and the detection of fluid-cornea boundaries in fluid-filled incisions. Other potential diagnostic applications include measuring retinal thickness and monitoring of intraocular laser ablations.

1.10.2 Ultrashort Pulse Laser Tissue Interactions

Laser induced optical breakdown using ultrashort laser pulse has recently achieved widespread clinical use in ophthalmic laser surgery for the incision of transparent eye structures.²⁴ Current clinical systems employ either Q-switched nanosecond pulses or modelocked picosecond pulse trains. The use of single picosecond or femtosecond pulses can result in more precise incisions with reduced collateral damage. Allowing for the use of less energetic pulses, shorter pulse duration lowers the threshold energy for optical breakdown.

We have performed optical breakdown studies with single 40 ps Nd:YAG laser pulses. Using time resolved measurement

techniques, we made a comprehensive study of the temporal and spatial dynamics of the plasma formation, shock wave, and cavitation processes that accompany optical breakdown.²⁵ Tissue effects were investigated using the corneal endothelium in vitro.²⁶ Comparison of tissue effects with physical measurements suggests that endothelial cell damage is mediated by shock wave and cavitation processes, while incisions confined to the focal region of the laser beam are produced by the laser-induced plasma. Systematic studies were performed to determine the energy scaling behavior of the tissue effects and to quantify the minimum "safe" distance for clinical photodisruption near sensitive structures. Tissue damage range was found to vary with the cube root of the pulse energy. Picosecond and nanosecond optical breakdown results in comparable damage if the same amount of energy is involved. The minimum damage range of 100/ μm was achieved with 8/ μJ picosecond pulses.

We have also studied laser-tissue interactions in the femtosecond regime using an amplifier, colliding pulse modelocked ring dye laser. We used retinal injury studies to investigate laser-tissue interaction mechanisms. The retina, a highly sensitive structure in which laser induced injury can be evaluated ophthalmoscopically as well as histologically, provides a valuable system for our studies.

Our earlier studies using 80 fs pulses demonstrated that retinal injury depended on energy density and not on peak intensities. However, these results also showed evidence of a nonlinear damage limiting mechanism. Only minimal retinal effects were detected for peak intensities higher than $10^{11}\text{W}/\text{cm}^2$. In

²³ R.C. Youngquist, S. Carr, and D.E.N. Davies, "Optical Coherence-Domain Reflectometry: a New Optical Evaluation Technique," *Opt. Lett.* 12:158 (1987).

²⁴ F. Fankhauser, P. Roussel, J. Steffen, E. Van der Zypen, and A. Cherenkova, "Clinical Studies on the Efficiency of High Power Laser Radiation Upon Some Structures of the Anterior Segment of the Eye," *Int. Ophthalmol.* 3:129-139 (1981); J.J. Aron-Rosa, J. Griesemann, and R. Thyzel, "Use of the Neodymium YAG Laser to Open the Posterior Capsule after Lens Implant Surgery: a Preliminary Report," *J. Am. Intraocul. Implant Soc.* 6:352-354 (1980).

²⁵ B. Zysset, J.G. Fujimoto, and T.F. Deutsch, "Time-resolved Measurements of Picosecond Optical Breakdown," *Appl. Phys. B* 48:139-147 (1989).

²⁶ B. Zysset, J.G. Fujimoto, C.A. Puliafito, R. Birngruber, and F.F. Deutsch, "Picosecond Optical Breakdown: Tissue Effects and Reduction of Collateral Damage," *Laser in Surgery Med.* 9:193-204 (1989).

contrast to laser injuries produced by longer pulses, exposures of more than 100 times threshold did not produce a significant increase in lesions or hemorrhaging.²⁷ In the context of previous retinal injury studies, this result was very surprising.

Research showed that laser pulses with intensities greater than 10^{12} W/cm² cannot be transmitted through the transparent media of the eye because of the presence of nonlinear optical effects such as self-focusing and continuum generation. Since nonlinear damage limiting effects do not occur with propagation of laser pulses in gases, we performed lensectomy, vitrectomy, and total air-fluid exchange in eighteen rabbit eyes. In some eyes, fibrin membranes were created adjacent to the retinal surface so that we could study the ability of femtosecond pulses to cut these membranes. We made a total of 222 laser exposures using pulse energies between 0.6 μ J and 125 μ J and pulse durations of 100 fs and 1 ps. We used pulse energies of 1 μ J to 10 μ J to cut membranes; histology showed minimal damage to adjacent neuroretinal tissue.²⁸

Compared with nanosecond pulses or multiple pulse modelocked picosecond trains, single picosecond and femtosecond pulses permit reduction in breakdown energy threshold, thereby reducing the extent of undesirable collateral damage. These results suggest that picosecond and femtosecond pulses can be used to develop surgical techniques for highly localized incisions of intra-ocular structures.

1.10.3 Ultrashort Pulse Laser Scalpel

Lasers of different wavelengths, power, and pulse duration produce drastically different effects on biological tissue, providing surgeons with a wide range of options in laser surgery. Optical breakdown using single picosecond laser pulses is a promising approach for generating highly controlled incisions of corneal as well as intraocular structures.

As discussed in the previous section, the range of tissue damage caused by ultrashort pulse optical breakdown decreases with decreasing pulse energy, and shorter pulses permit initiation of optical breakdown with lower pulse energy. While the nanosecond Q-switched pulses currently employed for intraocular photodisruption produces tissue damage in the mm range, a 40 ps pulse can have a damage range as small as 100 μ m.²⁶

We have studied corneal excisions generated with nanosecond, picosecond, and femtosecond pulses.²⁹ Compared to nanosecond pulses, picosecond and femtosecond pulses produced much smoother excision edges and less damage to the adjacent tissue. Pulses shorter than 1 ps produced additional strand-like collateral damage that may be caused by nonlinear processes other than optical breakdown. Because nonlinear propagation effects compromise the use of femtosecond pulse, our studies suggest that pulse durations in the 1 ps to 100 ps range might be optimal for constructing a precision laser scalpel.

To study the optimal pulse duration for a laser scalpel, we have constructed a solid state laser system featuring high pulse energy and variable pulse duration. The system consists of a high power modelocked Nd:YLF laser, a pulse stretching/compression stage,

²⁷ R. Birngruber, C.A. Puliafito, A. Gawande, W.-Z. Lin, R.T. Schoenlein, and J.G. Fujimoto, "Femtosecond Laser-Tissue Interactions: Retinal Injury Studies," *IEEE J. Quantum Electron.* QE-23:1836-1844 (1987).

²⁸ R. Birngruber, V.P. Gabel, B. Zysset, C.A. Puliafito, J.G. Fujimoto, "Femtosecond Retinal Injury and Membrane Cutting," *Suppl. to Inv. Ophthalmol. and Vis. Sci.* 30:372 (1989).

²⁹ D. Stern, R.W. Schoenlein, C.A. Puliafito, E.T. Dobi, R. Birngruber, and J.G. Fujimoto, "Corneal Ablation by Nanosecond, Picosecond, and Femtosecond Lasers at 532 and 625 nm," *Arch. Ophthalmol.* 107:587-592 (1989).

and a Nd:Phosphate glass regenerative amplifier.³⁰ Optical pulse compression/stretching techniques produce variable pulse duration. A pulse train from the modelocked Nd:YLF laser is first sent through a long optical fiber. Frequency dispersion and self-phase modulation in the fiber produce a linear frequency chirp and stretch the laser pulse, which is subsequently amplified and compressed by a grating pair. Varying the distance between the grating pair changes pulse duration.

This system can produce pulse durations from 100 ps to 1 ps with energies up to 1 mJ. The laser generation techniques used for this laser medical system are similar to those employed for the generation of high brightness laser systems. These systems used chirped pulse amplification to achieve high peak intensities with modest pulse energies. In our program, the development of a variable pulse duration laser for laser medicine would permit a wide range of studies that explain the roles of energy versus intensity in laser tissue as well as photochemical and photobiological reactions.

1.11 Developmental Status of a Table-top XUV Laser at 194 Angstrom

Sponsor

U.S. Department of Energy
Grant DE-FG02-89-ER14012

Project Staff

Professor Peter L. Hagelstein, Dr. Santanu Basu, Martin H. Muendel, Sumanth Kaushik, Daniel Tauber, John Paul Braud, Ann W. Morganthaler

Since the first prediction of gain in Sn at 110.5 eV,³¹ the Ni-like scheme has been used to experimentally demonstrate gain at 44.8 Å in Ta.³² The requirement of high electron temperature for high-Z materials over a long length of plasma required large-scale laboratory facilities for laser development in this wavelength region. One other limitation of a high-energy laser system is that the repetition rate is severely limited by thermal time constants of large-scale optical amplifiers.

We have previously shown³³ that gain can be produced at low pump energy in a low Z medium such as Mo when the medium is pumped repetitively by a series of short pulses of nominal 100-ps pulsewidth. In this case, the electron temperature rapidly rises to near 300 eV required for populating the upper laser level. At the same time, Mo is ionized through the Ni-like stage relatively slowly. In this transient stage, $3 - 5 \text{ cm}^{-1}$ gain coefficient is theoretically predicted.

We are working towards demonstration of the Ni-like Mo laser with a 5-10 J Nd:YLF oscillator/Nd:phosphate glass amplifier

³⁰ L. Yan, J.-D. Lin, P.-T. Ho, C.H. Lee, and G.L. Burdge, "An Active Modelocked Continuous Wave Nd:Phosphate Glass Laser and Regenerative Amplifier," *IEEE J. Quant. Electron.* 24:418 (1988); T. Sizer and I.N. Duling, "Neodymium Lasers as a Source of Synchronized High-Power Optical Pulses," *IEEE J. Quant. Electron.* 24:404 (1988); P. Bado, M. Bouvier, and J.S. Coe, "Nd:YLF Mode-Locked Oscillator and Regenerative Amplifier," *Opt. Lett.* 12:319 (1987).

³¹ S. Maxon, P.L. Hagelstein et al., *Appl. Phys. Lett.*, 57:971 (1985).

³² S. Maxon et al., Paper MC.6, LASERS '89, New Orleans, 1989.

³³ P.L. Hagelstein, "Short Wavelength Lasers: Something Old Something New," *Proceedings of the OSA meeting on Short Wavelength Coherent Radiation: Generation and Applications*, eds. R.W. Falcone and J. Kirz, 1988.



Figure 2. Nd-YLF oscillator/preamplifier system for the table-top 194-Å laser.

system³⁴ which can be run at a high repetition rate. The pump laser consists of a mode-locked and Q-switched Nd:YLF laser producing 70–100 ps pulses at 3.5-ns pulse to pulse separation (shown in figure 2). Five pulses from this laser are selectively amplified in a Nd:glass pre-amplifier to a total energy of 100 mJ. Subsequent amplification is carried out in a four-pass Nd:glass slab amplifier to produce two beams, each delivering 5 J of total energy.

The width of the gain region is chosen to be 5–10 μm to reduce radiation trapping of the lower laser level. The high repetition rate of the XUV laser, which is expected to be 2 ppm, requires a source of multiple targets and computer controlled alignment. We are fabricating the gain medium by optical litho-

graphy on Si wafer and on quartz substrate. A 4-inch long Si strip can accommodate 200 Mo lines of 10 micron width. Five such gain strips will be installed on a holder which will be positioned by computer controlled stages inside the vacuum chamber. The stringent requirement on plasma uniformity requires a new gain medium to be positioned in the center of the line focus to within 5 μm .

A grazing incidence monochromator will be used for gain measurement. In addition, we will use a x-ray pin-hole camera to determine the plasma size and uniformity. We are in the process of building a high-resolution grating monochromator with a fast detector to investigate the temporal characteristics of the laser line. A 1-GHz transient digitizer

³⁴ S. Basu, M.H. Muendel et al., Paper QTuD2, "Development of the Tabletop 194 Å Laser in Ni-like Mo," International Quantum Electronics Conference, Anaheim, California, 1990.

will be used to provide 350-ps time resolution.

We will also explore the major advantage of this repetitively pumped scheme which is the possibility of multipassing the gain medium for obtaining saturated XUV laser output.

1.12 Status of Zig-zag Slab Laser Development

Sponsor

U.S. Department of Energy
Grant DE-FG02-89-ER14012

Project Staff

Martin H. Muendel, Professor Peter L. Hagelstein,
Dr. Santanu Basu

We have designed a small Nd:glass MOPA system to use as a driver for an x-ray laser.³⁵ The system will consist of an oscillator and two-pass preamplifier supplying 100 mJ, which we have recently installed, and two zig-zag slab power amplifiers in parallel, each generating 5 J output. We describe our preliminary design for such a power amplifier in the 1990 U.S. Department of Energy Progress Report.³⁶

In most respects, our design follows those developed by the High Average Power Laser group at Lawrence Livermore National Laboratory (LLNL). It differs from them mainly in that the Livermore designs use long pulses (5–15 nsec), whereas our design is for short, mode-locked pulses (100 psec). The resulting higher intensities cause us considerable difficulty with potential damage by nonlinear self-focusing. Our slabs are forced to be proportionately shorter and wider than Livermore slabs, and apodizing, spatial filtering and image relaying must be done. For longer pulses, our design will be able to

handle considerably more energy than the 5 J specification. Also, since we are using a MOPA configuration rather than a regenerative amplifier, the successive passes must each go through different regions of the slabs. Finally, since for x-ray lasers and similar plasma experiments the target must be replaced and realigned on each shot, the repetition rate can be relatively low (once every ten seconds). This fact allows us to air cool the slabs, avoiding the problem of finding suitable water-resistant coatings for the slab faces.

An overview of the proposed system appears in figure 3. The zig-zag stands vertically, supported by its edges. It is pumped by four water-cooled linear flashlamps in a reflecting cavity and is cooled by air flowing down across its faces. The laser beam makes four passes lengthwise through the slab, using total internal reflection to zig-zag across the slab thickness.

The system can be divided logically into a number of subsystems, including electronics (triggering and firing circuitry), flashlamps and reflectors, glass slabs, air-cooling system, mechanical support, and optics for multiple passes. The triggering and firing circuitry has been built and tested successfully. The glass slabs have been cut (Schott APG-1), polished (Wild Leitz AG of Switzerland), delivered, and tested optically. The flashlamps are in and the reflectors have been cut and silver-coated. The mechanical support structure has been machined and the air-cooling system has been delivered.

We will shortly be in a position to test the first laser head to see whether the design specifications have been met, and begin work on the multiple pass optics. Our goal is to complete the system and return student and laser system from LLNL to MIT to begin laser-plasma experiments.

³⁵ M.H. Muendel and P.L. Hagelstein, "High Repetition Rate, Tabletop X-ray Lasers," *Proc. OE-Laser 90: Optics, Electro-optics and Laser Applications in Science and Engineering*, January 1990.

³⁶ M.H. Muendel and P.L. Hagelstein, "Design Notes for a Short-Pulse Nd:Glass Slab Amplifier," DOE Progress Report, January 1990.

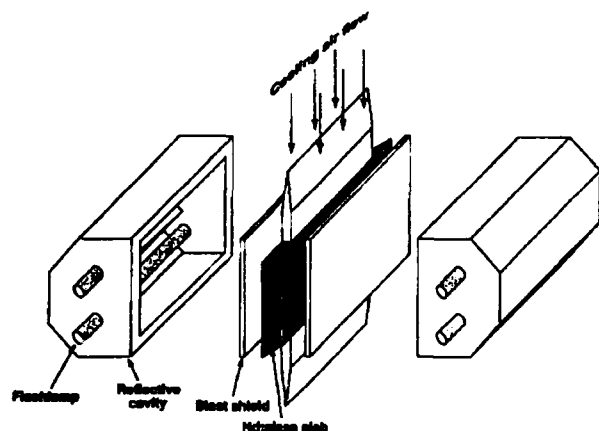


Figure 3. Zig-zag amplifier system.

1.13 Whisper Gallery Mirror Design

Sponsor

U.S. Department of Energy
Grant DE-FG02-89-ER14012

Project Staff

John Paul Braud, Professor Peter L. Hagelstein,

In the event that we are able to obtain amplification during the coming year, we would install a laser cavity and take advantage of feedback. Currently, the state of the art in any laser cavities is relatively primitive by optical laser standards; this is primarily due to the short lifetime of gain the EUV and soft x-ray regimes and the difficulty of fielding high quality optics in a "dirty" laser plasma environment. Our solution to this is to use a burst of driver-laser pulses to power our amplifier, such that gain would be available every few nanoseconds and the short wavelength radiation would have time to travel to relatively distant mirrors and return.

We are studying cavities based on both multilayer mirrors and whisper gallery mirrors. The efficient use of whisper gallery mirrors in the EUV is challenging due to the unusual nature of the radial cavity modes. The simplest possible design of a stable spherical

whisper gallery cavity leads to a radial mode that is poorly matched to the laser amplifier (it is too small). Modifications in geometry promise to improve the coupling, and we have explored several ideas on how to do this. Ultimately we hope to obtain a single mode laser, and from our studies to date, we feel that this will be difficult, but not impossible.

The problem of whisper gallery mirror design using geometries other than spherical or cylindrical is challenging, primarily because there seems to be little guidance from previous efforts as reported in the literature. The problem is that in order to match the mode size to the amplifier, very elongated mirrors must be employed. The modes need a substantial segment of relatively low curvature mirror to expand before reaching the plasma amplifier, and then a second elongated structure to compress before turning a corner. A schematic of this type of mirror is given in figure 4.

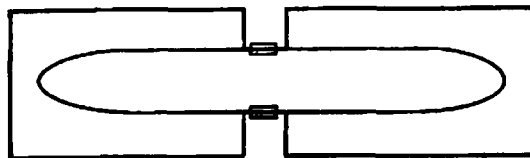


Figure 4. Cavity having an elongated geometry in order to increase size of low-order modes.

The design of this type of mirror requires obtaining solutions to the Helmholtz equation

$$[\nabla^2 + k^2]\vec{E}(r) = 0$$

subject to the boundary conditions appropriate to the mirror surface. The modes can apparently be studied using perfectly conducting boundary. The surface for an interesting whisper gallery mirror has transverse and longitudinal radii of curvature which vary around the perimeter, which is to say that the geometry is highly nontrivial and not describable in terms of elementary coordinate systems.

We have obtained a paraxial model which is applicable near the mirror surface.³⁷ The modes are found to evolve according to

$$2i\kappa \frac{\partial}{\partial s} u(\xi_1, \xi_2, s) = \left[-\frac{\partial^2}{\partial \xi_1^2} - \frac{\partial^2}{\partial \xi_2^2} + w(\xi_1, \xi_2, s) \right] u(\xi_1, \xi_2, s)$$

where the field is related to the mode through

$$E(r) = \hat{i}_\perp E_0 u(\xi_1, \xi_2, s) e^{iks}$$

and where ξ_1 and ξ_2 are coordinates normal and transverse relative to the surface, respectively. The variable s measures the pathlength along a geodesic. The potential $w(\xi_1, \xi_2, s)$ is found to be

$$w(\xi_1, \xi_2, s) = \kappa^2 - k^2 + \frac{2k^2}{R(s)} \xi_1 + \frac{k^2}{R(s)R_T(s)} \xi_2^2$$

valid above the surface ($\xi_1 > 0$). Below the surface $w(\xi_1, \xi_2, s)$ is infinite. The parameters $R(s)$ and $R_T(s)$ are the normal and transverse radii of curvature, respectively.

In the limit that the mirror surface has constant curvature, this model is solvable analytically in terms of Airy functions in ξ_1 and Hermite Gaussians in ξ_2 , which corresponds to known limits for exact solutions in simple geometries.

Due to the analogy to quantum mechanics, it is possible to view the mode evolution as the time evolution of a wavefunction in a two-dimensional potential well, where the well is parabolic in ξ_2 and linear for positive ξ_1 above zero. In essence, the average motion is like a pendulum transversely and like a basketball bouncing on pavement horizontally. The average height of the mode above

the surface satisfies approximately the non-linear equation

$$\frac{d^2}{ds^2} \langle \xi_1 \rangle = \frac{\lambda^2}{\langle \xi_1 \rangle^3} - \frac{C}{R(s)}$$

where C evaluates to 8.986. The mirror is adiabatic when the inertial term can be neglected, in which case

$$\langle \xi_1 \rangle_{\text{adiabatic}} = 0.481 [\lambda^2 R(s)]^{1/3}$$

which corresponds to the known limit for the lowest whisper gallery mode.

The mirror geometry for a design which is optimized to have the greatest rate of change of normal surface curvature, but remains adiabatic has been found to be a spiral.³⁸ The use of spiral segments to construct an elongated mirror is currently being considered for our short wavelength laser project. Further effort is underway to consider non-adiabatic mirror designs.

1.14 Polarizing Cavities for the Extreme Ultraviolet

Sponsor

U.S. Department of Energy
Grant DE-FG02-89-ER14012

Project Staff

John Paul Braud

One of the interesting features of whisper gallery mirrors in the EUV is their ability to polarize radiation. The effect is weak and amounts to about 10 percent discrimination per pass between TE and TM radiation. Motivated by this observation, we have examined the more general question of how to obtain a higher degree of polarization in an EUV laser cavity.

³⁷ J.P. Braud and P.L. Hagelstein, "Whisper Gallery Mirror Modes," to be submitted to *IEEE J. Quantum Electron.*

³⁸ J.P. Braud, "Adiabatic Whisper-Gallery Mirrors for EUV and Soft X-ray Laser Cavities," *Proceedings of Lasers '89*, New Orleans, December, 1989.

Improved polarization can be obtained using a multilayer polarization as suggested by Lee³⁹ and demonstrated by Khandar and Dhez.⁴⁰ A design of such a reflector can provide TE polarization at about 97 percent

at 45 degrees as shown in figure 5. Based on this effect, a wide range of polarizing EUV laser cavities are possible; a number of cavity geometries are shown in figure 6.⁴¹

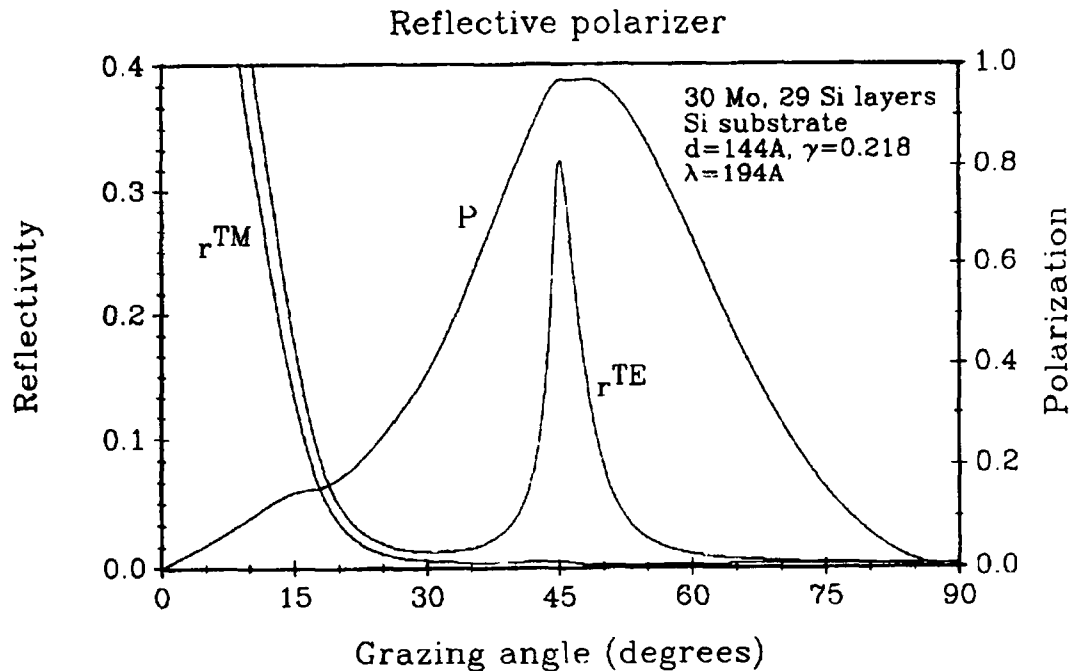


Figure 5. Reflection and polarization predicted from an EUV reflective polarizer.

³⁹ P. Lee, *Opt. Comm.* 43(4): 237-241 (1982); P. Lee, R. Bartlett, and D.R. Kania, *Opt. Eng.* 24(1): 197-201 (1985).

⁴⁰ A. Khandar and P. Dhez, "Applications of Thin-film Multilayered Structures to Focused X-ray Optics," Gerald F. Marshall, ed., *Proc. SPIE* 563:158-163 (1985); A. Khandar, P. Dhez, and M. Berland, "Multilayer Structures and Laboratory X-ray Laser Research," Natale M. Ceglie, Pierre Dhez, ed., *Proc. SPIE* 688: 176-183 (1986).

⁴¹ J.P. Braud, "Laser Cavities and Polarization Optics for Soft X-rays and the Extreme Ultraviolet," *Appl. Phys. B*, in press.

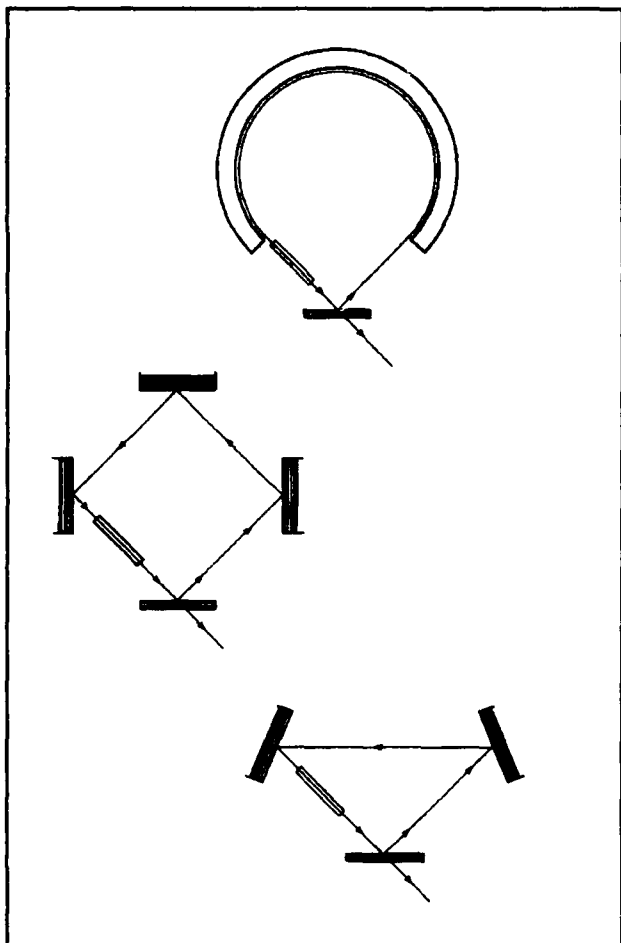


Figure 6. Geometries for polarizing cavities.

1.15 Unstable Resonators for XUV Lasers

Sponsor

U.S. Department of Energy
Grant DE-FG02-89-ER14012

Project Staff

Dr. Santanu Basu, Professor Peter L. Hagelstein

Stable resonators with multilayer optics have been used with XUV laser systems at 131 Å

and at 206.3 Å in Ne-like Mo and in Ne-like Se lasers respectively.⁴² We investigate possible applications of unstable resonators as efficient means of generating collimated output from XUV laser systems.⁴³ The study is motivated by the possibility that unstable resonator geometry can produce diffraction limited laser output and it can overcome the limit of low output coupling of multi-layer optics which are used in stable resonators in this wavelength region.

The resonator design is suited for an 194 Å Ni-like Mo laser which has been described separately in this report and is illustrated in figure 7. A confocal negative branch unstable resonator is chosen to match the 50–100 micron diameter gain region of 1-cm length. The resonator consists of two multi-layer mirrors⁴² deposited on concave substrates having radii of curvature of 42 cm and 63 cm. The cavity length of 52.5 cm provides a round trip time of 3.5 ns to match the pulse to pulse separation of the pump laser. The repetitively pumped Ni-like Mo laser allows flexibility in resonator design and reduces the possibility of mirror damage by the plasma debris. The resonator is designed with a magnification of 1.5 which corresponds to an output coupling of 55.5 percent.⁴³ The output coupling in an unstable resonator is large and adjustable as compared to a multi-layer beam splitter output coupler which has typically low transmission.⁴² In a high gain laser system such as in a XUV laser, large output coupling should give better extraction efficiency. The output mirror of 42-cm radius of curvature is designed to be of 1-mm diameter which gives an equivalent Fresnel number of 31 and a diffraction angle of 20 μrad. One beneficial effect of using a negative branch unstable resonator for this laser is the large angular tolerance of the output mirrors which is calculated to be 0.8 mrad, which is greater than a positive branch output coupler for the same output coupling and cavity length.

⁴² N. Ceglio, *J. X-ray Sci. Tech.* 1(1):7 (1989).

⁴³ S. Basu and P.L. Hagelstein, "Unstable resonators for XUV lasers," Paper CThO6, Conference on Lasers and Electro-Optics, Anaheim, California, 1990.

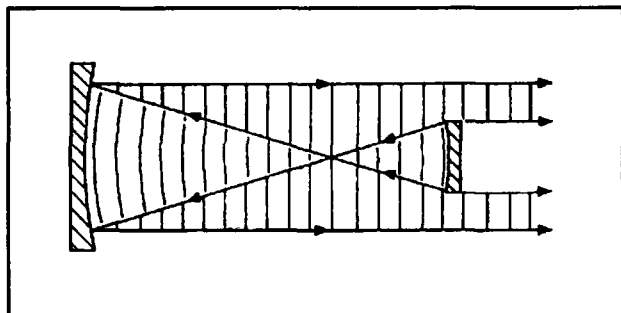


Figure 7. Schematic of a negative branch confocal unstable resonator for 194-Å laser.

The fabrication procedure for an unstable resonator will involve growing a multi-layer mirror on a 42-cm radius of curvature concave mirror substrate and cutting out a 1-mm diameter section. The 1-mm diameter mirror is to be mounted on a 1-mm diameter rod to form the output coupler of the unstable resonator. The gain medium will be placed at the common focal point of the end mirrors.

1.16 Advances in Conjugate Gradient Algorithm Development

Sponsor

Lawrence Livermore National Laboratory
Subcontract B048704

Project Staff

Sumanth Kaushik, Professor Peter L. Hagelstein

We described a new algorithm for the computation of level populations in x-ray laser simulations in last year's *RLE Progress Report*, and during the twelve months since that time we have improved the algorithm as we shall outline here.

Although our immediate application is x-ray laser simulations, the algorithm is applicable

to the rather generic stiff and conservative rate equation problem described by

$$\frac{d}{dt} x(t) = R(x, t) \cdot x(t)$$

where $x(t)$ is an N -component vector containing the level populations and $R(x, t)$ is the corresponding rate matrix. Straightforward linearization and application of the backward Euler discretization leads to

$$[I - \Delta t R^n] x^{n+1} = x^n$$

When the coupled equations are stiff (when the relaxation times are short), the linear matrix problem has been found to be difficult to solve efficiently. The application of relaxation techniques and conjugate gradient methods to this problem has yielded little or no advantage over direct Gaussian elimination previous to our efforts.

As reported in last year's *Progress Report*, we succeeded in applying the preconditioned biconjugate gradient algorithm⁴⁴ to a reduced version of the linear system (if the system is conservative, then one level is superfluous since it can always be found by subtracting the sum of the other level populations from the total). The resulting problem is of the form

$$A \cdot x = b$$

where A is an $(N - 1) \times (N - 1)$ nonsymmetric matrix and where x contains level populations for all the levels except the one that was eliminated.

We have improved upon the preconditioned conjugate gradient algorithm for this reduced problem through the application of a modified and preconditioned version of the generalized conjugate residuals algorithm.⁴⁵ This algorithm is given by

⁴⁴ S. Kaushik and P.L. Hagelstein, "The Application of the Preconditioned Conjugate Gradient Algorithm to Rate Matrix Equations," *J. Comp. Phys.*, forthcoming.

⁴⁵ S. Kaushik and P.L. Hagelstein, "The Application of Conjugate Gradient Methods to NLTE Rate Matrix Equations," *Applied Physics B*, forthcoming; S. Kaushik, and P.L. Hagelstein, "The Application of the Method of Generalized Conjugate Residuals to NLTE Rate Matrix Equations," submitted to *J. Comp. Phys.*

$$\alpha_0 = \frac{r_0 \cdot U^{-1} \cdot L^{-1} \cdot r_0}{p_0 \cdot A \cdot p_0} \quad k = 0$$

$$\alpha_k = \frac{p_k^T \cdot (A(LU)^{-1})^T \cdot r_k}{y_k^T \cdot y_k} \quad \text{for } k = (1, 2, \dots, k)$$

$$x_{k+1} = x_k + \alpha_k p_k$$

$$r_{k+1} = r_k - \alpha_k y_k$$

$$p_{k+1} = (L \cdot U)^{-1} \cdot r_{k+1}$$

$$y_{k+1} = A \cdot p_{k+1}$$

$$\beta_l = \frac{(y_l^T \cdot y_{k+1})}{y_l^T \cdot y_l} \quad \text{for } l = (0, 1, \dots, k)$$

$$p_{k+1} = p_{k+1} - \beta_l p_l$$

$$y_{k+1} = y_{k+1} - \beta_l y_l$$

The number of floating point operations (including additions and multiplications) required to solve a linear system by this new algorithm is

$$N_{\text{PGCR}} \approx (4N + 2fN^2 + 2mN^2) \cdot k + 2Nk(k + 1)$$

where f is the fill factor, k is the number of iterations, and m is the number of nonzero off-diagonal components in the preconditioning matrix. This is to be compared with the preconditioned biconjugate gradient algorithm, which requires

$$N_{\text{PBCG}} \approx (9N + 4fN^2 + 4mN^2)k$$

operations and with Gaussian elimination, which requires

$$N_{\text{Gauss}} \approx \frac{fN^3}{3} + \frac{N^2}{2}$$

The operation count estimates are in good agreement with our implementations, and

this new algorithm is currently the most efficient one proposed to date for this type of problem.

1.17 Frequency Upconversion of Extreme UV Radiation

Sponsor

U.S. Department of Energy
Grant DE-FG02-89-ER14012

Project Staff

Martin H. Muendel, Professor Peter L. Hagelstein

With the advent of laser sources in the EUV and soft x-ray regimes, it becomes of interest to consider the extension of optical laser techniques and applications to shorter wavelengths. In general, nonlinear optical phenomena have been of great interest and importance to laser physicists; the prospect of frequency mixing in the EUV is of special interest to our group, both for the eventual production of a bright tunable coherent source for applications, and for the prospect of achieving shorter wavelength radiation through doubling.

Unionized matter is highly absorbing in the EUV. Efficient frequency conversion in the EUV requires low loss, and we have concluded that a low density plasma will probably be most conducive to the mixing process. This conclusion immediately rules out frequency doubling since parity selection rules cannot be satisfied in isolated ions which are found in such plasmas.

Our approach is therefore to study four-wave mixing, in which two EUV beams are combined with an intense third optical beam to generate harder EUV radiation at roughly double the frequency of the initial EUV beams. Since it is unlikely that ions can be found with two connected transitions at the same energy (to within a few linewidths), it may not be practical to carry out four-wave mixing experiments with only one EUV laser and one optical laser. Our choice of ion was initially motivated by the hope of developing a scheme in which only a single EUV laser frequency would be required.

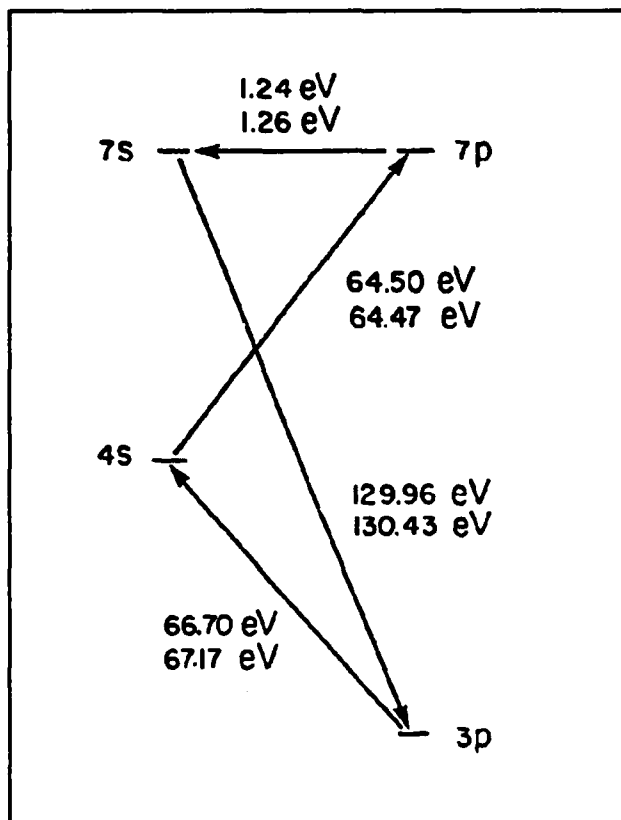


Figure 8. Schematic of K IX energy levels and the four-wave mixing.

The process which we have studied⁴⁶ is the four-wave mixing which produces ω_4 generated from

$$\omega_4 = \omega_1 + \omega_2 - \omega_3,$$

where ω_1 and ω_2 are x-ray laser photons with roughly equal energies, or possibly the same energy, and ω_3 is an optical laser photon. This difference process is used rather than the straight sum process because in positively dispersive media such as plasmas, only difference processes can be noncollinearly phasematched. As we shall demonstrate, the conversion rates are sufficiently low to regime phasematching, unless very high x-ray laser intensities are achieved; and of the various phasematching schemes only the

noncollinear type appears feasible in a plasma medium. Like the sum process, tripling processes also appear difficult to phasematch.

As an example, we have studied conversion in a plasma of Na-like K, as shown in figure 8.

The multiphoton transition rates can be calculated straightforwardly using Feynman diagrams, and the results are well known.⁴⁷ The nonlinear susceptibility is

$$\begin{aligned} \chi^{(3)}(-\omega_4; \omega_1, \omega_2, -\omega_3) \\ = \frac{1}{6\hbar^3} \sum \mu_{12} \mu_{23} \mu_{34} \mu_{41} \rho_{11} \\ \times \left(\frac{1}{\omega_{21} - \omega_1 - i\Gamma_{21}} + \frac{1}{\omega_{21} - \omega_2 - i\Gamma_{21}} \right) \\ \times \left(\frac{1}{\omega_{31} - (\omega_1 + \omega_2) - i\Gamma_{31}} \right) \\ \times \left(\frac{1}{\omega_{41} - (\omega_1 + \omega_2 - \omega_3) - i\Gamma_{41}} \right) \end{aligned}$$

where only the resonance denominators relevant for $\omega_1 \approx \omega_2 \gg \omega_3$ have been retained. Here ω_{ji} is the transition frequency from level i to level j .

For the case of just one x-ray laser, with $\omega_1 = \omega_2$, the nonlinear susceptibility $\chi^{(3)}$ is shown in figure 9.

The results of the study indicate that frequency upconversion is somewhat more difficult in the EUV range than in the optical regime since $\chi^{(3)} \sim 1/\omega^4$ off-resonance. The difficulty translates practically into a more stringent requirement on the degree of resonance than needed at longer wavelengths. Nevertheless, if resonances can be found,

⁴⁶ M.H. Muendel and P.L. Hagelstein, "Four-Wave Frequency Conversion of Coherent Soft X-rays," to appear in *Phys. Rev. A*; M.H. Muendel and P.L. Hagelstein, "Analysis of a Soft X-ray Frequency Doubler," *Proceedings of Lasers 89*, New Orleans, Louisiana, December 1989.

⁴⁷ J.F. Reintjes, *Nonlinear Optical Parametric Processes in Liquids and Gases* (Orlando: Academic Press, 1984).

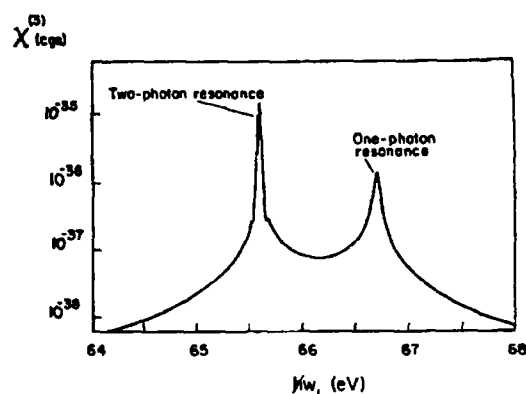


Figure 9. Nonlinear susceptibility for $\omega_4 = 2\omega_1 - \omega_3$ conversion as a function of $\hbar\omega_1$, assuming that $2\hbar\omega_1 - \hbar\omega_3 = 136.40\text{eV}$. The ion temperature is taken to be $2 \times 10^5\text{K}$.

then efficient frequency conversion should be possible.

1.18 X-ray Detectors Based on the Quantum Well Nonlinearity

Sponsor

Lawrence Livermore National Laboratory
Subcontract B048704

Project Staff

Dr. Santanu Basu, Sumanth Kaushik, Cris Eugster,
Professor Peter L. Hagelstein

A design for a novel quantum well based x-ray detector with good spatial and temporal resolutions is being investigated. Potential applications for such a detector are in areas such as x-ray microscopy, x-ray holography and diagnostics for laser produced plasmas.

A modest change in the optical susceptibility in the vicinity of the exciton absorption lines

in GaAs quantum wells is predicted⁴⁸ following the absorption of a single x-ray photon, which is potentially observable in the case of a multi-keV photon. At lower energy, the absorption of many low energy x-rays within a small area is expected to produce a sufficiently large number of carriers to produce a detectable modulation of an optical probe signal. Although this point is relatively straightforward, it has an important implication: it allows us now to consider an experiment which will give a reproducible result exhibiting the x-ray/optical nonlinearity with certainty. Previous to this observation, the detectability of the effect itself was a matter of doubt due to the marginal signal to noise ratio expected.

Our initial study is focused on the demonstration of the x-ray/optical nonlinearity in a quantum well device, characterization of the effect, and evaluation of its potential for use in a number of detection schemes.

The study is continuing with funding from Lawrence Livermore National Laboratory.

1.19 A Simple Line Shape Model for GaAs Multiple Quantum Wells

Sponsor

Lawrence Livermore National Laboratory
Subcontract B048704

Project Staff

Sumanth Kaushik, Professor Peter L. Hagelstein

We have recently proposed a simple model to numerically calculate the experimentally observed line shapes in GaAs multiple quantum well (MQW) structures.⁴⁹ The motivation for developing such a model is due in part to our interest in the design and con-

⁴⁸ C. Eugster and P.L. Hagelstein, "X-ray Detection Using the Quantum Well Exciton Nonlinearity," *IEEE J. Quantum Electron.* 26(1): 75 (1990); C. Eugster, "X-ray Detection Using the Quantum Well Exciton Nonlinearity," M.S. thesis, Dept. of Elec. Eng. and Comput. Sci., MIT, 1989; S. Kaushik and P.L. Hagelstein, "A Simple Lineshape Model for GaAs Multiple Quantum Wells," Paper CTuH62, Conference on Lasers and Electro-Optics, Anaheim, California, 1990.

⁴⁹ S. Kaushik and P.L. Hagelstein, "A Simple Lineshape Model for GaAs Multiple Quantum Wells," Paper CTuH62,

struction of an x-ray detector based on measuring the nonlinear absorption changes in GaAs quantum wells due to the presence of the excess carriers created by the absorbed x-ray photon.⁵⁰ A quantitative understanding of the line shape, especially as a function of carrier density and temperature, is very useful for the design of such a device.

In our model, we cast the absorption in the form

$$\alpha(E) = \sum_{j=l, h} \alpha_o^{(j)} \left[\sum_i \frac{1}{(i+1/2)^3} \frac{2B^{(j)}}{(\Gamma_i^{(j)})} \Phi\left(\frac{2(E - E_{ni}^{(j)})}{(\Gamma_i^{(j)})}, \gamma_i\right) + \int_{-\infty}^{x_{\max}^{(j)}} dx \frac{2\Phi(x, \gamma)}{\exp\left(-2\pi\sqrt{(E - E_c^{(j)} - \Gamma_L x/2)/R_{2D}}\right)} \right]$$

where the summation is extended over the light hole (l) and heavy hole (h) bands. The first term is the excitonic contribution to the absorption and the second term is the continuum contribution. The function Φ is a

nondimensional line shape function which is the convolution of a Lorentzian line shape (from homogeneous broadening) and a Gaussian line shape (from inhomogeneous broadening). R_{2D} is the two-dimensional Rydberg constant. The non-dimensional parameter γ is the ratio of the inhomogeneous linewidth Γ_G to the homogeneous linewidth $\Gamma_L \cdot \gamma = 2\Gamma_G/\Gamma_L$. The parameter α_o is given by

$$\alpha_o^{h, l} = \frac{2\pi\alpha_{\text{fine}}}{nL_z} \frac{\mu^{h, l}}{m_0} \cdot \frac{1}{E} \frac{|\langle c | \varepsilon \cdot p | v^{l, h} \rangle|^2}{m_0}$$

where L_z is the length of the QW, μ is the transverse reduced mass, $\alpha_{\text{fine}} (= e^2/\hbar c)$ is the fine structure constant m_0 is the free electron mass, n is the index of refraction and $|\langle \dots \rangle|^2$ is the momentum matrix element from the valence band to the conduction band.

Using available experimental theoretical values for the exciton binding energies, linewidths and matrix elements, we have in figure 10 shown the best fit of our model

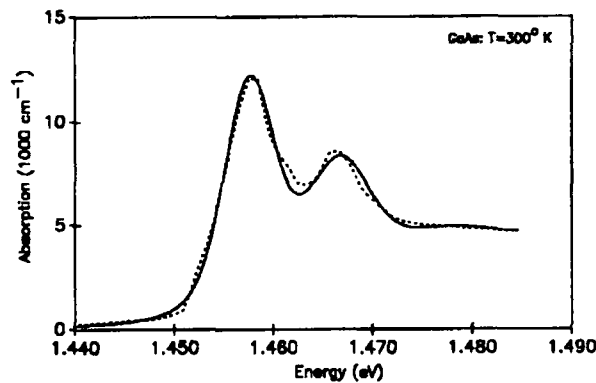


Figure 10. Plot of absorption vs. energy for the MQW structure as described by Kaushik and Hagelstein.⁴⁹ The solid line corresponds to the theoretical fit and the dotted line corresponds to the experimental data.

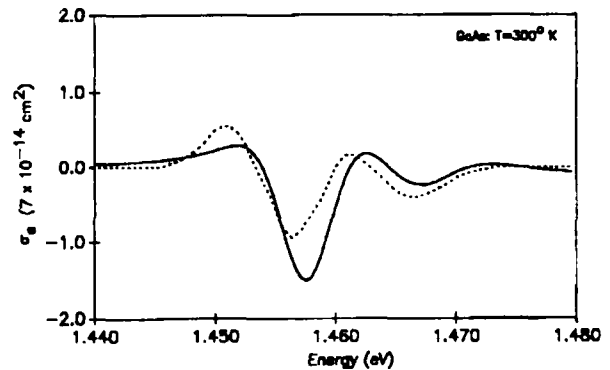


Figure 11. Plot of nonlinear coefficient vs. energy for MQW structure as described by Kaushik and Hagelstein.⁴⁹ The solid line corresponds to the theoretical result and the dotted line corresponds to the experimental data.

Conference on Lasers and Electro-Optics, Anaheim, California, 1990; S. Kaushik and P.L. Hagelstein, "A Semi-Empirical Model for Excitonic Absorption in GaAs Quantum Wells," to be submitted to *IEEE J. Quantum Electron.*

⁵⁰ C. Eugster and P.L. Hagelstein, "X-ray Detection Using the Quantum Well Exciton Nonlinearity," *IEEE J. Quantum Electron.* 26(1): 75 (1990).

against available experimental absorption spectrum.

We have extended this simple model to provide a quantitative description of absorption as a function of free-carrier density. In particular, we are interested in determining the nonlinear coefficient $\sigma_a = \partial\alpha/\partial n$.

Density dependence of absorption is introduced by assuming the linewidth and band gap are functions of density. We use the binary encounter model from atomic physics to describe the former and a RPA based many-body formula for the latter. In figure 11, we plot the results of our calculation. As can be seen, there is generally good agreement between theory and experiment.

Although the general features of the absorption spectra of GaAs MQWs has been reasonably well documented in the literature,⁵¹ to our knowledge, there has been hitherto no easily accessible model that can quantitatively predict the absorption line shape, especially as a function of carrier density. We have developed a semi-empirical model that can quantitatively describe the observed line shape. The attractive feature of this model is that it has virtually no free parameters, and more importantly, it can be useful for predicting the line shape as a function of carrier density and temperature approximately where no experimental data is available.

1.20 Coherent Fusion Theory

Sponsor

U.S. Department of Energy
Grant DE-FG02-89-ER14012

Project Staff

Professor Peter L. Hagelstein

During the year which has elapsed since the initial announcement of Pons and Fleischmann⁵² claiming the observation of fusion in an electrolysis cell, there has been some progress made in clarifying the technical situation. Those of the scientific community who remain active in the field can largely be divided into two groups: skeptics and proponents.

The skeptics' position is in essence that there is no anomalous effects observed under conditions described by Pons and Fleischmann, and that this is supported by several hundred experiments showing no effect whatsoever.⁵³ Any positive results can be accounted for either in poor signal to noise ratio, systematic experimental errors, or through incompetence, fraud or maliciousness. Cold fusion is considered in this school of thought to be "pathological science," similar to the polywater and N-ray affairs of previous years.

The proponents have clarified their position during the past year. The current claims include the observation of very substantial excess heat (reproducible but unpredictable) with no quantitative observations of fuel depletion or generation of byproducts, generation of tritium, and the production of neutrons. The claims of excess heat are

⁵¹ D.S. Chemla, D.A.B. Miller, P.W. Smith, A.C. Gossard and W. Wiegmann, *IEEE J. of Quantum Electron.* 20: 265 (1984).

⁵² M. Fleischmann and S. Pons, *J. Electroan. Chem.* 261:301 (1989).

⁵³ J.F. Ziegler, T.H. Zabel, J.J. Cuomo, V.A. Brusic, G.S. Cargill, E.J. O'Sullivan and A.D. Marwick, *Phys. Rev. Lett.* 62:2929 (1989); M. Gai, S.L. Rugari, R.H. France, B.J. Lund, Z. Zhao, A.J. Davenport, H.S. Isaacs, and K.G. Lynn, *Nature* 340:29 (1989); N.S. Lewis, C.A. Barnes, M.J. Heben, A. Kumar, S.R. Lunt, G.E. McManis, G.M. Miskelly, R.M. Penner, M.J. Sailor, P.G. Santangelo, G.A. Shreve, B.J. Tufts, M.G. Youngquist, R.W. Kavanagh, S.E. Kellogg, R.B. Vogelaar, T.R. Wang, R. Kondrat, and R. New, *Nature* 340:525 (1989); D. Albagli, R. Ballinger, V. Cammarata, X. Chen, R.M. Crooks, C. Fiore, M.J.P. Gaudreau, I. Hwang, C. K. Li, P. Linsay, S. Luckhardt, R.R. Parker, R.D. Petrasso, M.O. Schloh, K.W. Wentzel, and M.S. Wrighton, submitted to *J. Fusion Energy* (1989); M.H. Salamon, M.E. Wrenn, H.E. Bergeson, K.C. Crawford, W.H. Delaney, C.L. Henerson, Y.Q. Li, J.A. Rusho, G.M. Sandquist, and S.M. Seltzer, "Limits on the Emission of Neutrons, Gammas, Electrons and Protons from Cold Fusion Cells," submitted to *Nature* (1989).

supported by high precision closed cell calorimetry at Stanford,⁵⁴ SRI,⁵⁵ ORNL⁵⁶ and Texas A&M,⁵⁷ by corrected open cell calorimetry at Utah,⁵⁸ and by numerous positive observations elsewhere. The claims of excess tritium are supported by experiments at Texas A&M,⁵⁹ LANL⁶⁰ and BARC,⁶¹ and by a lesser number of positive results at other laboratories. The claim of neutron generation is supported most strongly by results from LANL,⁶² and by a number of other laboratories as well.

What is responsible for the anomalies is unclear. The hypothesis of the proponents that DD fusion is somehow occurring seems unlikely for a number of reasons: no primary DD fusion reaction products (n , T , γ) are seen quantitatively consistent with the excess heat; the tritium production is accompanied by very little neutron production which is inconsistent with the known tritium/neutron branching ratio, and is inconsistent with the secondary yield of neutrons expected from MeV tritons in deuterium; finally, there has been no mechanism known to cause DD fusion under anything remotely like the conditions claimed.

Although a moderate number of explanations have been proposed to account for the

effects, there is no credible model which can account even qualitatively to within fifty orders of magnitude of the effects claimed to have been observed. The experimentalists have been attempting to make progress in the nearly complete absence of any theoretical guidance.

Although we do not yet know with complete certainty whether the effects are actually real, the positive evidence seems relatively strong. Stanford's isoperibolic calorimeter has an accuracy of better than 1 percent and has seen bursts of heat at levels of 20 to 45 percent. The total closed cell energy generation is in excess of 20 MJ/mole Pd in a closed cell system, and it is hard to account for the results of such careful and relatively clean experiments through conventional arguments given to date. That a number of laboratories report positive heat effects provides motivation for pursuing a theoretical model.

The theoretical problem is terribly constrained. The observation of heat without accompanying radiation is unprecedented, and is almost as difficult to explain as the effect occurring at all. Tritium production without secondary neutrons (implying slow tritons, with a kinetic energy below about 10

⁵⁴ R. Huggins et al., paper presented at the Technology and Society Division of the ASME Winter Meeting, San Francisco, December 12, 1989. Huggins described recent experiments that employ closed cell calorimetry, and reported the production of 1.15 MJ in 260 hours in one experiment. He mentioned that in another cell he was able to sustain 8.5 Watts for 27 hours.

⁵⁵ M. McKubre et al., paper presented at the First Annual Cold Fusion Conference, March 1990.

⁵⁶ C.D. Scott, J.E. Mrochek, E. Newman, T.C. Scott, G.E. Michaels, and M. Petek, *A Preliminary Investigation of Cold Fusion by Electrolysis of Heavy Water*. ORNL report TM-11322, November 1989.

⁵⁷ O.J. Murphy et al., paper presented at the First Annual Cold Fusion Conference, March 1990.

⁵⁸ S. Pons and M. Fleischmann, *J. Fusion Tech.*, forthcoming.

⁵⁹ N.J.C. Packham, K.L. Wolf, J.C. Wass, R.C. Kainthla and J. O'M. Bockris, *J. Electroanal. Chem.* 270:451 (1989).

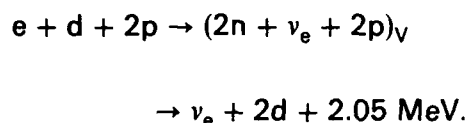
⁶⁰ T.N. Claytor, P.A. Seeger, R.K. Rohwer, D.G. Tuggle and W.R. Doty, *Tritium and Neutron Measurements of a Solid State Cell*. LANL report LA-UR-89-39-46, October 1989. Presented at the NSF/EPRI workshop on anomalous effects in deuterated materials, October 16-18, 1989; E. Storms and C. Talcott, *Electrolytic Tritium Production*, LANL report LAUR: 89-4138. This work was paper presented at a DOE contractors' meeting in Germantown on December 6, 1989. Enhancements in the vicinity of a factor of two in tritium levels were observed repeatedly.

⁶¹ *BARC Studies in Cold Fusion*, ed. Srinivasan (Bombay, India: Bhaba Atomic Research Centre, 1989.) The production of 190 and 375 μ Curies of tritium in two experiments is reported.

⁶² H. Menlove, paper presented at the First Annual Cold Fusion Conference, March 1990.

keV) eliminates essentially all conventional binary fusion reactions, and fission reactions fare no better. The conclusion which can be drawn from this type of consideration is that even if the coulomb barrier could somehow be overcome, the profile of expected reaction products would be inconsistent with observation on the heat and tritium. It can be concluded from arguments of this type that, if it is real, it is not conventional fusion.

Our present approach to developing a scenario is based on multi-step reactions initiated by electron capture.⁶³ For example, the candidate reaction for heat production in our current scenario



As an incoherent reaction it is easily shown that this reaction has an utterly negligible reaction rate. As a coherent reaction, it presents a number of interesting features. The electrons in a lattice are described by extended Bloch wavefunctions, and as such the electron capture process in a lattice properly involves the overlap of one electron orbital with a large number of nuclei. This provides an initial basis for looking for collective effects.⁶⁴

Usually electron capture results in the emission of an energetic neutrino, and it destroys any possible coherence between neighboring nuclei. If the neutrino has a very low energy, and if the neutrino momentum is equal to the Bloch wave momentum of the electron, then it can be shown that many nuclei can participate coherently in the electron capture process, through a superradiant neutrino emission process which is the analog of Dicke superradiance for photons.

But in order for this to occur, the virtual (off-shell) neutrons must find their way to protons (or in general other nuclei) to be

captured, and the excess energy must be radiated coherently (as opposed to incoherent gamma emission). In our scenario, the neutron wavelengths of interest are very large, extending over many lattice sites. S-wave neutron capture on protons would occur through coherent superradiant magnetic dipole transitions. The magnetic moment for this process is highly favored over magnetic dipole capture to the ground state of any other nucleus which we have found.

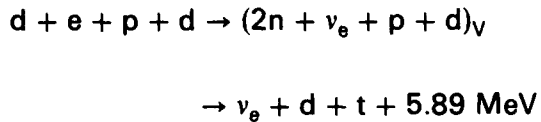
We are considering an interesting mechanism through which the energy is coupled from the microscopic (nuclear) to the macroscopic. The magnetic dipole interaction can couple a spin-flip transition to a near-field magnetic field produced by a nearby current. It may be remarked that nearly all successful heat-producing experiments have involved current and a coil around the palladium, which is an inductive coupling. Due to the mismatch in energy, it is not possible for a nuclear quantum to be coupled inductively to a near-linear electrical circuit. But if the circuit includes a very high order nonlinearity, such as may be provided by the electrochemical process itself, then it may be possible to couple out nuclear energy on a soft-photon by soft-photon basis. That the electrochemical process must involve a very high order nonlinearity can be seen easily: each gas molecule which is evolved from the electrochemical dissociation of D₂O was generated through the conversion of a very large number of electrical quanta to a chemical quantum. The conjecture in this is that the coupling of an electrical system to a quantum system occurs through a large number of paths, and each path has a dependence on voltage which is step-like. This mechanism would result in inverse power law coupling in energy mismatch, rather than exponential coupling characteristic of other multi-quanta emission rates.

The overall mechanism can be tested through monitoring for proton loss in heat-producing

⁶³ P.L. Hagelstein, "Status of Coherent Fusion Theory," Paper TS-4, ASME Winter Meeting, December 1989.

⁶⁴ P.L. Hagelstein, "Status of Coherent Fusion Theory," Proceedings of the the First Annual Cold Fusion Conference, March 1990.

cells. The basic mechanism can also account for tritium production through



The basic mechanism is in agreement with many of the qualitative features of the experiments reported to date. Numerous basic

physics issues remain to be clarified in regard to the mechanism, and we recognize that it may not be correct (the work is speculative, and we have considered nearly twenty models total in this effort). If correct, it implies a number of effects which ought to follow, including the potential of activating ^{31}P to ^{32}P , which is radioactive with a 15-day half-life (virtual neutron capture to the ground state would occur through a magnetic dipole transition, similar to protons and deuterons).



From left: Sponsored Research Technical Staff Dr. Sunny Y. Auyang and Research Assistant David B. Walrod.

Chapter 2. Novel Processes and Materials for Infrared Nonlinear Optics

Academic and Research Staff

Professor Peter. A. Wolff, Dr. Sunny Y. Auyang

Graduate Student

David B. Walrod

2.1 Project Description

Sponsor

National Science Foundation
Grant EET 87-18417

Optical systems such as signal processors, limiters, spatial light modulators, and optical computers require large and fast optical nonlinearities. Although free carrier-induced nonlinearities in semiconductors have the picosecond speeds required for use in many applications, they were considered too weak to be practical for optical systems applications. In our work, we have demonstrated that these nonlinearities can be substantially enhanced in certain materials and in structures such as superlattices. We have recently observed the first optical nonlinearity caused by subband effects in InSb/AlInSb and HgTe/CdTe superlattices.

Superlattices have the potential for generating large optical nonlinearities because their band structures can be tailored to optimize particular nonlinear effects. Several novel nonlinear optical processes that utilize either the large subband nonparabolicity in the growth direction¹ or intersubband transitions in various configurations² specific to superlattices have been proposed. To our knowledge, these processes have not been observed.

With support from the National Science Foundation, we have observed optical nonlinearities caused by subband nonparabolicity in InSb/InAlSb and HgTe/HgCdTe superlattices by using four-wave mixing techniques with CO₂ lasers. We have observed an enhancement in the third-order susceptibility, $\chi^{(3)}$, when the laser light was polarized along the growth direction instead of in-plane. This experiment demonstrated that the superlattice subband structure induced larger optical nonlinearity than that of its bulk counterpart.³

The coupling between light and electrons is given by $\mathbf{p} \cdot \mathbf{E}$, where \mathbf{E} is the electric field of the light and \mathbf{p} the momentum of the n^{th} energy subband $\epsilon_n(\vec{p})$. Therefore, to observe nonlinear optical effects caused by subband structures peculiar to superlattices, the electric field of the light must be polarized in the superlattice growth direction. We designated the direction perpendicular to the plane of the superlattice as \hat{z} and the in-plane direction as \hat{x} . Light polarized along \hat{x} probes only subband structures parallel to the superlattice plane, $\epsilon_n(p_x)$, which is not different from their bulk counterparts. The interesting superlattice effects are contained in $\epsilon_n(p_z)$; large enhancement of p_z -nonparabolicity has been predicted. Furthermore, intersubband transitions are induced by E_z but not E_x .

¹ W.L. Bloss and L. Friedman, *Appl. Phys. Lett.* 41:1023 (1982); S.Y. Yuen, *Appl. Phys. Lett.* 43:813 (1983); G. Cooperman, L. Friedman, and W.L. Bloss, *Appl. Phys. Lett.* 44:977 (1984); Y. Chang, *J. Appl. Phys.* 58:499 (1985).

² S.Y. Yuen, *Appl. Phys. Lett.* 43:813 (1983); D.J. Newson and A. Kurobe, *Appl. Phys. Lett.* 51:1670 (1987).

³ D. Walrod, S.Y. Auyang, and P.A. Wolff, *Appl. Phys. Lett.* 56:218 (1989).

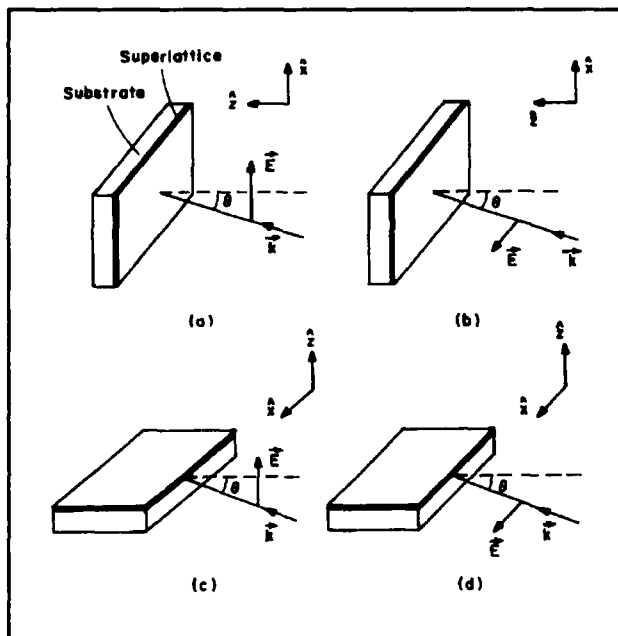


Figure 1.

The coupling to $\epsilon_n(p_z)$ is difficult to achieve in conventional nonlinear optical experiments in which light impinges upon the surface of the sample (figure 1). Because of the large indices of refraction of semiconductors E_z inside the sample, there was never more than a small fraction of the total field. Even at Brewster angle incidence, less than ten percent of the light intensity was polarized along \hat{z} since the nonlinear signal is proportional to the cube of the input intensity. Therefore, the third-order nonlinear susceptibility $\chi^{(3)}$ due to $\epsilon_n(p_z)$ must be at least fifty times larger than the bulk susceptibility to be distinguished in this geometry. We predicted these large susceptibilities for intersubband transitions when the subband gap was exactly matched to the photon energy.⁴ Intersubband transition was a resonant effect, however, and the predicted $\epsilon^{(3)}$ might not be achievable if the actual subband separation failed to match the photon energy. Optical nonlinearities generated by the non-

parabolicity of the lowest subband $\epsilon_0(p_z)$, were nonresonant, not placing as severe a demand on the specification of the sample. However, the enhancement over the bulk was smaller.⁵

We observed optical nonlinearities caused by subband structures in the growth direction in an AlInSb/InSb superlattice by using an end-firing technique. The AlInSb/InSb superlattice we studied consisted of 50 periods, each with 45 Å of InSb and 60 Å of $\text{Al}_{0.08}\text{In}_{0.92}\text{Sb}$. This superlattice was separated from the 350 μm Cr-doped GaAs substrate by a 200 Å AlSb buffer layer. The samples were undoped. We used a 50 μm InSb epilayer grown under the same conditions on the same kind of substrate for a control sample.

For the end-firing experiments, we cleaved off a strip about 1 mm in width. The cleaved edge provided good transmission. We observed about 50 percent transmission through the 1-mm sample; almost all loss was due to reflection. To ensure that the GaAs substrate did not contribute to the nonlinear optical signal, we cut off small sections of the samples and polished off the superlattice. Then we compared the substrate with a sample in which the superlattice was left intact. In all cases, the nonlinear signal vanished when we removed the superlattice.

The end-firing configuration enabled us to probe the \hat{z} -direction dispersion relation by changing the polarization direction. The four-wave signal from the InSb epilayer does not change as the light polarization is rotated 90 degrees. This result suggests that the material is isotropic. The four-wave signal from the superlattice was comparable to that of the InSb epilayer when the light was polarized along \hat{x} . However, as the polarization was rotated to the \hat{z} direction, the four-wave signal increases by twenty-two times, as depicted in figure 2.

⁴ S.Y. Yuen, *Appl. Phys. Lett.* 43:813 (1983); D.J. Newson and A. Kurobe, *Appl. Phys. Lett.* 51:1670 (1987).

⁵ W.L. Bloss and L. Friedman, *Appl. Phys. Lett.* 41:1023 (1982); S.Y. Yuen, *Appl. Phys. Lett.* 43:813 (1983); G. Cooperman, L. Friedman, and W.L. Bloss, *Appl. Phys. Lett.* 44:977 (1984); Y. Chang, *J. Appl. Phys.* 58:499 (1985).

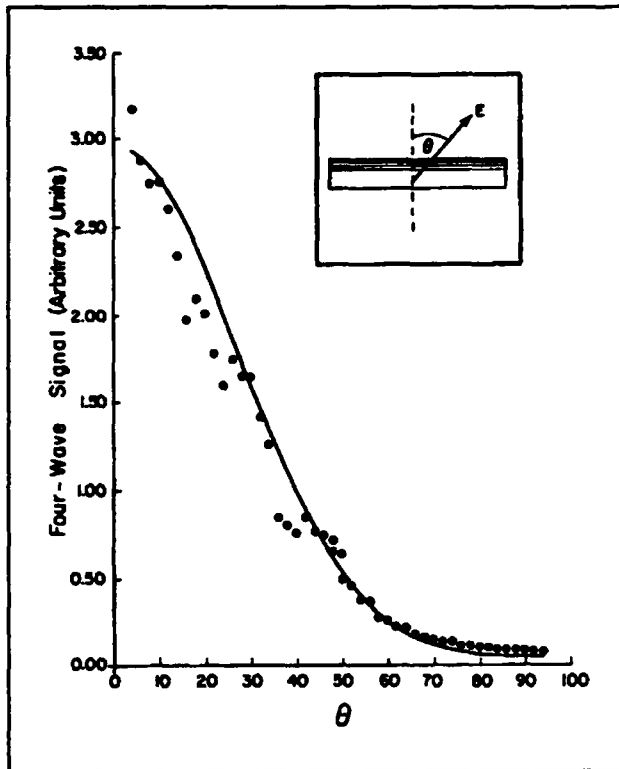


Figure 2.

By comparing the optical nonlinearities generated by different light polarizations, we ascertained that the \hat{z} -direction subband structure gave an enhancement of $\chi^{(3)}$ over the bulk value. There are several possible explanations for the enhancement, but we were unable to distinguish them quantitatively. Our research is continuing in this direction.

Publications

Auyang, S.Y., and P.A. Wolff. "Free-Carrier-Induced Third Order Optical Nonlinearities in Semiconductors." *J. Opt. Soc. Am. A* 6:2696 (1989).

Walrod, D., S.Y. Yuen, P.A. Wolff, and W. Tsang. "Optical Nonlinearities due to Subband Structures in $\text{Al}_{0.08}\text{In}_{0.92}\text{Sb}/\text{InSb}$ Superlattices." *Appl. Phys. Lett.* 56 (3):218-220 (1989).

Section 3 Surfaces and Interfaces

**Chapter 1 Statistical Mechanics of Surface Systems and
Quantum-Correlated Systems**

Chapter 2 X-Ray Diffuse Scattering

Chapter 3 Semiconductor Surface Studies

**Chapter 4 Ultralow Temperature Studies of Nanometer
Size Semiconductor Devices**

Chapter 5 The Quantum Hall Effect in Narrow MOSFETs

**Chapter 6 Epitaxy and Step Structures on Semiconductor
Surfaces**

Chapter 1. Statistical Mechanics of Surface Systems and Quantum-Correlated Systems

Academic and Research Staff

Professor A. Nihat Berker, Dr. Joseph O. Indekeu

Graduate Students

William Hoston, Kenneth Hui, John F. Marko, Roland Netz

Undergraduate Students

Joseph E. Hilliard, Galen T. Pickett

Technical and Support Staff

Imadiel Ariel

1.1 Introduction

Sponsor

Joint Services Electronics Program
Contract DAAL03-89-C-0001

Correlated fluctuations play an important role in systems with electronic and structural degrees of freedom. This role is most ubiquitous at phase transitions, but is also considerable away from phase transitions, extending down to the lowest temperatures due to quantum mechanics. The renormalization-group method is a new calculational method that can systematically deal with correlated fluctuations at each successive scale length. Since we can include even the consequences of defects, for the first time we can obtain predictive microscopic theories for realistic systems.

1.2 Finite-Temperature Phase Diagram of Vicinal Si(100) Surfaces

Project Staff

Professor A. Nihat Berker

With the collaboration of Professor John D. Joannopoulos and Dr. Oscar L. Alerhand, we have combined electronic energy calculations and such statistical mechanics to obtain ab initio descriptions of finite-temperature semi-

conductor surfaces and interfaces. The entropy, free energy, and other properties have been evaluated for the silicon (100) surface. The single-step/double-step phase diagram in the variables of crystal cut angle and temperature, as well as other observable properties such as step profiles, are predicted in very good agreement with ongoing experiments. Contrary to previous suggestions that only double-layer steps should appear on the equilibrium surface, it is predicted that the single-layer stepped surface is at equilibrium for small misorientation angles. This structure is stabilized by strain relaxation and by the thermal roughening of the steps. For annealed surfaces, the critical angle at which the transition between the single- and double-layered stepped surface occurs is calculated to be $\theta_c \approx 2^\circ$.

1.3 Absence of First-Order Phase Transitions in Physical Surface Systems

Project Staff

Professor A. Nihat Berker, Kenneth Hui

Most recently, we made a theoretical prediction using the renormalization-group method that appears to have general and far-reaching consequences: we discovered that even an infinitesimal amount of randomness in interactions (e.g., distribution of defects) in

surface systems, converts first-order phase transitions, characterized by discontinuities, to second-order phase transitions, characterized by infinite response functions. In bulk systems, as (calculable) threshold randomness is needed for this conversion to occur. This general prediction appears to be supported by experiments on doped KMnF_3 .

1.4 New Orderings in Systems with Competing Interactions

Project Staff

Professor A. Nihat Berker, William Hoston, Roland Netz

Our studies of realistic, complex systems with competing interactions have led to several new results. We have recently developed a new method that blends Monte Carlo simulation and mean-field theory. We are able to distinguish, for the first time, the effect of dimensionality on frustrated magnetic systems. We have obtained two ordered phases that nevertheless have considerable entropy. Also, we have recently obtained novel phases and multicritical points in systems with competing dipolar and quadrupolar interactions.

Publications

Alerhand, O.L., A.N. Berker, J.D. Joannopoulos, D. Vanderbilt, R.J. Hamers, and J.E. Demuth. "Finite-Temperature Phase Diagram of Vicinal Si(100) Surfaces." Submitted to *Phys. Rev. Lett.* (1989).

Berker, A.N. "Harris Criterion for Direct and Orthogonal Quenched Randomness." Submitted to *Phys. Rev. B* (1990).

Hilliard, J.E. *Monte Carlo Simulation of a One-Dimensional Ising System with Competing Interactions Using Domain Walls*. S.B. thesis, Dept. of Physics, MIT, 1989.

Hui, K., and A.N. Berker. "Random Field Mechanism in Random-Bond Multicritical Systems." *Phys. Rev. Lett.* 62:2507 (1989).

Hui, K. "Domain Wall Study of the Stacked Frustrated Triangular Lattice." Submitted to *Phys. Rev. Lett.* (1989).

Hui, K. *Quenched Disorder and Competing Interactions in Spin Systems*. Ph.D. diss. Dept. of Physics, MIT, 1989.

Marko, J.F. *On Structure and Scaling at First- and Second-Order Phase Transitions*. Ph.D. diss. Dept. of Physics, MIT, 1989.

Marko, J.F. "Exact Pair Correlations in a One-Dimensional Fluid of Hard Cores with Orientational and Translational Degrees of Freedom." *Phys. Rev. Lett.* 62:543 (1989).

Marko, J.F. "First-Order Phase Transitions in the Hard-Ellipsoid Fluid from Variationally Optimized Direct Pair Correlations." *Phys. Rev. A* 39:2050 (1989).

McKay, S.R., and A.N. Berker. "Magnetization of the d-Dimensional Random-Field Ising Model: An Intermediate Critical Dimension." In *New Trends in Magnetism*. Ed. S.M. Rezende. Teaneck, New Jersey: World Scientific, 1989.

Pickett, G.T. *Asymptotic Behavior of the Spectrum of Generalized Dimensions in Multifractal Tree Growth*. S.B. thesis. Dept. of Physics, MIT, 1989.

Chapter 2. X-Ray Diffuse Scattering

Academic and Research Staff

Professor Robert J. Birgeneau, Dr. Kenneth Blum, Dr. Joel Brock

Graduate Students

Kenneth Evans-Lutterodt, Hawoong Hong, Alan Mak, Do-Young Noh, William Nuttall

Technical and Support Staff

Elizabeth M. Salvucci

2.1 Introduction

Sponsor

Joint Services Electronics Program
DAAL03-89-C-0001

In this research program, we use modern x-ray scattering techniques to study structures and phase transitions in thin films and on surfaces. We have two principal experimental facilities, one at MIT and the other at the National Synchrotron Light Source at Brookhaven National Laboratory. At MIT, we have four high-resolution computer-controlled x-ray spectrometers using high intensity rotating anode x-ray generators. The angular resolution can be made as fine as 1.8 seconds of arc, which enables us to probe the development of order from distances of the order of the x-ray wavelength, $\sim 1\text{\AA}$, up to 30,000 \AA . The sample temperature can be varied between 2 K and 500 K with a relative accuracy of 2×10^{-3} K. At the National Synchrotron Light Source at Brookhaven National Laboratory, we have, in collaboration with IBM, three fully instrumented beam lines. Two of these beam lines allow studies with photons varying in energy between 3 and 12 keV; the third has a fixed energy of 18 keV. These facilities make possible high resolution scattering experiments with a flux more than three orders of magnitude larger than that from a rotating anode x-ray generator, opening up a new generation of experiments.

As part of this JSEP program, we have built an x-ray compatible high vacuum single crystal apparatus. This enables us to use synchrotron radiation to study the structures

and transitions occurring at a single surface, and, indeed, such experiments are now becoming routine. Our current experiments in this program are concentrated on the phases and phase transitions of metal and semiconductor surfaces and surface over-layers.

2.2 Metal Surface Studies

We have carried out detailed studies of the reconstruction of the (110) surface of gold: Au(110). Many noble metal facets are known to favor reconstructed structures at low temperatures. Further, at some temperature T_c , a reconstructed surface will typically undergo a reversible "deconstruction" to a high temperature structure which is no longer reconstructed. One such transition which has been studied theoretically as well as with electron diffraction is the Au(110) 1×2 to 1×1 deconstruction. While the "missing row" model of the reconstructed 1×2 surface is well established, the nature of the deconstruction transition itself remains controversial.

Previous work by our group has demonstrated that x-ray scattering is an effective means of studying surface phase transitions. Specifically, the lineshapes of bulk-forbidden surface peaks provide information about the surface height-height (or step-step) correlation functions and are thus a sensitive probe of the surface roughening transition. This transition is characterized by a proliferation of atomic steps which results in logarithmically divergent height fluctuations of the crystalline surface. We have carried out

glancing angle synchrotron x-ray scattering experiments as a means of studying the Au(110) structures and deconstruction transition. The results have been quite remarkable. The so-called 2×1 "missing row" model discussed above is a special case of a more general model in which one has (111) microfacets on the Au(110) surface. More extended microfacets can lead to reconstructions with longer periods: 1×3 , 1×4 , 1×5 , etc., and these are very close in energy to the 1×2 .

In our first set of experiments, the stable phase of the specific Au(110) surface turned out to be 1×3 rather than 1×2 . The basic structure and the possible step excitations are shown in figure 1. For this structure superlattice peaks occur at $(0\ 0\ \ell/3)$ positions. We find that at 485°C the surface undergoes a continuous, reversible transition. At this transition the 1×3 long range order is lost and the local period becomes incommensurate. This behavior results from the proliferation of atomic steps (such as those shown in figure 1b and 1c), which act as domain walls between coherent regions of the reconstructed surface. In fact, by further studies we can determine that both types of steps are present. This means that the 1×3 surface both deconstructs and roughens simultaneously.

After further treatment of this same Au crystal, we were able to obtain a stable 1×2 phase on the (110) surface. This latter structure is the one most commonly observed in previous experiments. The deconstructive transition of this surface appears to be fundamentally different from that of the 1×3 phase. First, the structure remains commensurate even in the disordered phase. Second, there is no evidence of roughening. Third, we have some indication of 2D Ising critical behavior. Further analysis and measurements are required to elucidate the 1×2 deconstruction fully.

2.3 Semiconductor Surface Studies

We have investigated the surface disordering transition of Ge (111) near the bulk melting point. The experiment was performed at the National Synchrotron Light Source beamline X20A during the summer of 1989. Our observation was made on Ge wafers resistively heated inside a surface chamber which has a base pressure of 1.3×10^{-10} torr. The sample surface was prepared by sputtering for 30 minutes and subsequent annealing at the same temperature for one hour. Auger-electron spectroscopy was done in situ to check the surface cleanliness. The sample and surface chamber were oriented such that the in-plane (i.e., grazing incidence) (10) and (20) surface peaks, as well as the (11) bulk peak, were observable.

We have studied the evolution of the (10) and (20) surface peaks between 700 K and 1170 K, finding radical changes in intensity. The surface peaks remain resolution limited

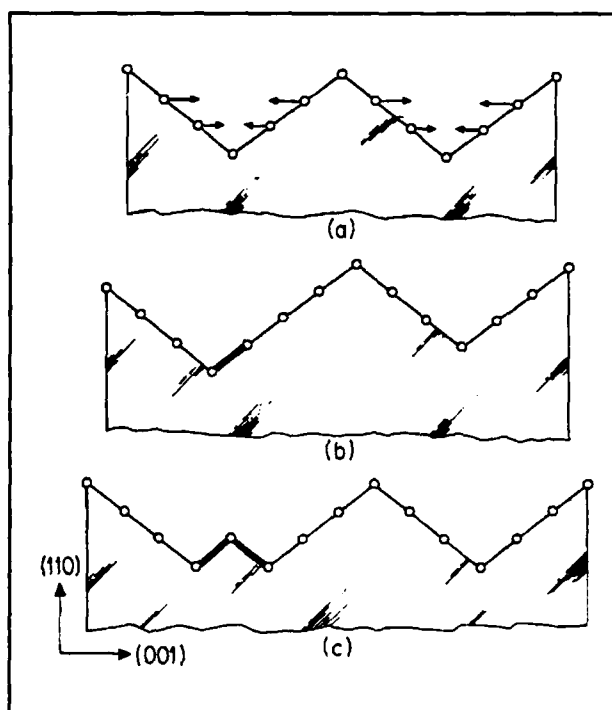


Figure 1. (a) Schematic representation of the Au(110) 1×3 missing-row reconstruction. The arrows indicate the southward atomic distortions observed in the second and third rows from the surface. (b) A single atomic step thermal excitation of the 1×3 surface. (c) A paired-step thermal excitation of the 1×3 surface.

in the radial direction and the transverse widths stay the same throughout the entire temperature range. As the temperature goes up from 700 K, the intensity of the (10) surface peak decreases exponentially with a Debye-Waller factor of 0.001 K^{-1} . At about 1000 K the rate of decrease of the (10) peak intensity per degree K intensifies. The peak intensity goes through a minimum at about 1100 K and then recovers partially. The transition shown here is reversible with temperature, indicating that it is indeed an equilibrium phase transition. Similar behavior is observed for the (20) surface peak. We have also looked for signs of a surface fluid layer which should manifest itself as a broad ring in reciprocal space, but found no indication of such a layer. Subsequent to the x-ray scattering experiment, we have performed mass spectroscopy measurement on some Ge(111) samples. Each sample was placed one inch away from and with the normal pointing towards the probe. Our data show that there is an exodus of Ge atoms from the surface starting at about 1050 K.

None of the existing models of surface disordering — surface roughening and surface melting — can explain the data. The partial recovery of the surface peak intensity at about 100 K below bulk melting is particularly intriguing. We propose a model which would give a surface peak intensity that is consistent with our observation. A Ge crystal with an ideally terminated (111) surface consists of bilayers of atoms, stacked in an ..ABCABC.. sequence. The structure factor is identically zero at the surface peak position in reciprocal space because the scattering from every three bilayers of atoms exactly cancel. However, the penetration depth of x-rays in the direction normal to the surface is drastically reduced at grazing incidence, due to absorption and total internal reflection. The magnitude of the wave amplitude caused by a layer is maximum at the surface, dropping quickly as one moves into the bulk. As a result the sum of wave amplitudes from every three bilayers is nonzero: the amplitude from the top layers dominates that from below. Suppose that at 1000 K atoms on the sample surface pop-out randomly, leaving vacant sites behind. This reduces the amplitude from the top layer of

atoms. The net scattering intensity from the top three bilayers of Ge atoms reduces due to more effective cancellation. At 1100 K, the cancellation is optimized. At higher temperature, the random vacancy at the surface layer may be so large that the amplitude from the bottom layers now dominates. Since intensity is proportional to the modulus squared of the total wave amplitude from every layer, the intensity starts to increase once the random vacancy exceeds some critical value. In this model there is no broadening of the surface peaks, which is consistent with our observation. The mass spectroscopy measurement also supports this picture. Of course, this model is by no means unique. Further studies are required.

2.4 Rare Gases in Graphite

We have studied the phases and the phase transitions for a xenon solid layer on graphite in the monolayer coverage regime. The incommensurate solid undergoes the sequence of transitions: aligned \rightarrow rotated \rightarrow reentrant aligned, before the solid transforms into the commensurate solid. The current theory of orientational epitaxy correctly predicts only the point at which the rotation to the reentrant aligned phases occurs. None of the current theories can explain the whole picture of orientational epitaxy. Neither the high temperature aligned solid nor the reduction of the rotation angle from that of the static prediction are explained.

The reentrant aligned phase at low temperatures is an incommensurate solid with a network of superlight domain walls. The observed first-order phase transition can be explained within the domain-wall theory. The incommensurability at constant coverage decreases approximately as $[(T - T_0)/T_0]^{1/3}$ until the first order C-IC transition point is hit. This one-third power law is close to the behavior seen for Kr on graphite following a similar thermodynamic pathway.

We estimated the potential corrugation of the surface adsorption from the intensity ratios between the main and satellite peaks in the domain-wall incommensurate phase. The corrugation of the potential estimated was near the one predicted by Steele. Along with the estimation from the onset of the rotated

phase, we set the limits for the dimensionless wall width, $36 < \ell_0 < 42$.

At low temperatures the xenon layer on vermicular graphite did not transform into the commensurate phase as on the single-crystal substrate. Instead, the xenon layer seems to have a pinned domain-wall network due to defects.

2.5 Publications

Evans-Lutterodt K., R.J. Birgeneau, E.D. Specht, J.W. Chung, J.D. Brock, M.S. Altman, P.J. Estrup, I.K. Robinson, and A.A. MacDowell. "X-Ray Study of W (001) With and Without Hydrogen." *J. Vac. Sci. Technol. A* 7:2209 (1989).

Evans-Lutterodt, K.W. *Synchrotron X-ray Diffraction Studies of Surface Phase Transitions*. Ph.D. diss. Dept. of Physics, MIT, 1989.

Held G. A., J.L. Jordan-Sweet, P.M. Horn, A. Mak, and R.J. Birgeneau. "X-ray Scat-

tering of the Deconstruction and Thermal Roughening of the Au(110) 1×3 Reconstructed Surface." *Solid State Comm.* 72:37 (1989).

Held G. A., J.L. Jordan-Sweet, P.M. Horn, A. Mak, and R.J. Birgeneau. "Disordering Transitions of Metal Surfaces." *J. de Physique Colloque* C7(50):245 (1989).

Hong, H., and R.J. Birgeneau. "X-ray Diffraction Study of the Structure of Xenon Multilayers on Single Crystal Graphite." *Z. Phys. B* 77:413 (1989).

Hong, H., C.J. Peters, Mak A., R.J. Birgeneau, P.M. Horn, and H. Suematsu. "Synchrotron X-ray Study of the Structures and Phase Transitions of Monolayer Xenon on Single-Crystal Graphite." *Phys. Rev. B* 40:4797 (1989).

Robinson I.K., A.A. MacDowell, M.S. Altman, P.J. Estrup, Evans-Lutterodt K., J.D. Brock, and R.J. Birgeneau. "Order-Disorder Transition of the W (001) Surface." *Phys. Rev. Lett.* 62:1294 (1989).

Chapter 3. Semiconductor Surface Studies

Academic and Research Staff

Professor John D. Joannopoulos, Dr. Efthimios Kaxiras, Dr. Oscar L. Alerhand

Graduate Students

Tomas A. Arias, Mark Needels, Andrew M. Rappe, Eugen G. Tarnow, Jing Wang

3.1 Introduction

Sponsor

Joint Services Electronics Program
Contract DAAL03-89-C-0001

Understanding the properties of surfaces of solids and the interactions of atoms and molecules with surfaces is extremely important from both a technological and academic point of view. The recent advent of ultrahigh vacuum technology has made microscopic studies of well-characterized surface systems possible. The way atoms move to reduce surface energy, the number of layers of atoms involved in this reduction, the electronic and vibrational states that result from this movement, and the final symmetry of the surface layer are all important in achieving a fundamental and microscopic understanding of the nature of clean surfaces, chemisorption processes, and the initial stages of interface formation.

The theoretical problems associated with surface systems are quite complex. We are currently, however, beginning to solve for the properties of these real surfaces systems (rather than for simple mathematical models). In particular, we continue to pursue our goal of calculating the total ground-state energy of a surface system from "first principles," to provide accurate theoretical predictions of surface geometries. In this program, we are concentrating our efforts on the areas of surface growth, surface reconstruction geometries, structural phase transitions, and chemisorption.

3.2 Thermal Amplitudes of Surface Atoms

The vibrational excitations of semiconductor surfaces provide a direct probe of the structural and bonding properties that result from their reconstruction. Moreover, studies of the vibrational properties of surfaces are necessary to understand the dynamical processes that occur on these surfaces (such as kinetics of adsorbates, diffusion and desorption, epitaxial growth, and possibly surface melting). The thermal fluctuations of the surface atoms are directly related to these phenomena. Furthermore, the analysis of a number of experimental probes requires a detailed knowledge of the vibrational amplitudes and correlations of the surface atoms. The Debye-Waller factors, which appear in the expressions for the intensity of radiation scattered from a surface, and the displacement-displacement correlations of the surface atoms enter into the interpretation of ion scattering and other experiments.

New developments in a number of experimental techniques for studying vibrational properties of surfaces have generated further interest, the need for realistic calculations, and better theoretical understanding. These include He-atom scattering, high-resolution electron-energy-loss spectroscopy, surface infrared spectroscopy, medium- and high-energy ion scattering, and surface extended x-ray-absorption fine-structure experiments. From a theoretical point of view, an underlying formalism for surfaces exists within the general framework of the theory of lattice dynamics, but we have made a few realistic calculations for specific surfaces.

In this work, we have made calculations of the atomic displacement-displacement correlation functions for atoms on the Si(111)

2×1 and Si(001) 2×1 surfaces. Both of these surfaces have been the subject of intense research for many years, and even though we have made considerable progress, several questions regarding their structure and basic excitations remain unresolved. Using a semi-empirical tight-binding theory for structural energies in Si, we investigate the thermal fluctuations of the atoms on these surfaces. Specifically, we determine the anisotropy of the vibrational amplitudes of the surface atoms between vibrations parallel and normal to the surface plane, their temperature dependence, and the interatomic vibrational correlations.

The Si(111) 2×1 surface is currently understood in terms of a π -bonding chain model. According to this model, the surface reconstructs by forming zigzag chains of surface atoms that run parallel to each other. The bonding along the chain is provided by the π interaction between the surface electrons. Figure 1 shows a side view of the Si(111) 2×1 surface. The chain model also helps us understand the unique vibrational properties observed on this surface. Its lattice dynamics are dominated by the chain geometry and the strong coupling between the electronic surface states and the structural degrees of freedom of the zigzag chains. In fact, the most salient features in the surface phonon spectrum are related to modes that have the same form and elementary vibrational excitations of the surface zigzag chains.

The appearance of a small-wavelength surface phonon with an unusually low energy is particularly relevant to the thermal fluctuations of the surface atoms. Indeed, one of the main reasons for this study is to investigate the thermal effects of this mode. This intrinsic vibration of the surface is dispersionless across the surface Brillouin zone, having an energy of $\hbar\omega = 10$ meV. Near the zone edge, it is located well below the acoustic continuum. Because of the low energy of this phonon and its lack of dispersion (leading to a large contribution to the phonon density of states at that energy), this mode is thermally populated with a large probability. Thus, one might expect that the vibrational amplitudes of the surface atoms on Si(111) 2×1 would be greatly enhanced.

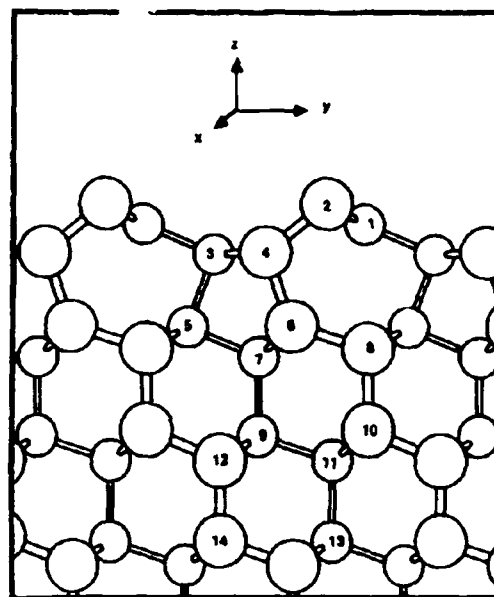


Figure 1. Side view of the π -bonded chain model of Si(111) 2×1 . The two surface atoms, numbered 1 and 2, form zigzag chains that run parallel to the $[112]$ direction (into the page); these chains are tilted with up (2) and down (1) atoms.

In contrast with the result for Si(111) 2×1 , this low-energy small-wavelength surface phonon does not appear in the phonon spectrum of Si(001) 2×1 . The basic building block in the reconstruction of Si(001) involves the formation of surface dimers between two neighboring surface atoms, halving the number of dangling bonds on the surface. Figure 2 shows a side view of the Si(001) 2×1 surface. The surface dimers do not remain symmetrical, tilting so that each dimer is formed by an up and down atom. With this model, we can understand the different periodicities observed on the surface [2×1 , $p(2 \times 2)$ and $c(4 \times 2)$] in terms of different ordered arrangements of the tilted surface dimers. We find that the normal modes of vibration of the higher-order reconstructions $p(2 \times 2)$ and $c(4 \times 2)$ are essentially the same as for the 2×1 reconstruction, since the surface phonons are essentially characterized by the vibrations of the nearly isolated surface dimers. Consequently, we concentrate only on the 2×1 reconstruction.

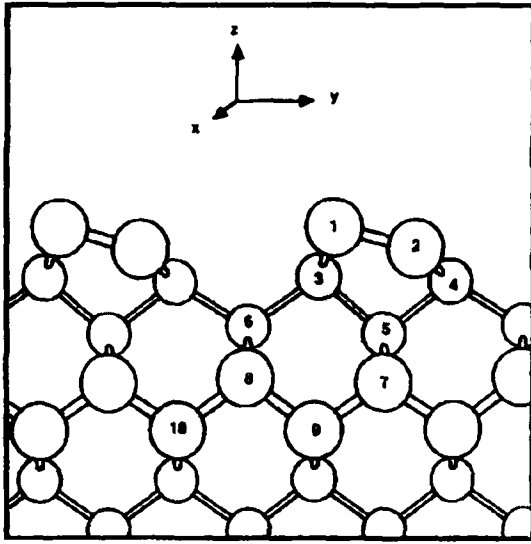


Figure 2. Side view of the tilted dimer model of Si(001) 2×1 .

In the harmonic approximation, the correlation function between the displacement $u_{i\mu}$ of atom i along the direction μ (from its equilibrium position), and the displacement of atom $u_{j\nu}$ of atom j along the direction ν , can be expressed in terms of the phonons or normal modes of the system:

$$\begin{aligned} \langle u_{i\mu} u_{j\nu} \rangle &= \frac{\hbar}{2N(M_i M_j)^{1/2}} \\ &\times \sum_{\mathbf{q}, \lambda} \frac{e_{i\mu}(\mathbf{q}, \lambda) e_{j\nu}^*(\mathbf{q}, \lambda)}{\omega_\lambda(\mathbf{q})} \\ &\times e^{i\mathbf{q}(\mathbf{R}_i - \mathbf{R}_j)} \{1 + 2n[\omega_\lambda(\mathbf{q})]\}, \end{aligned} \quad (1)$$

where the sum is over normal modes λ and wave vectors \mathbf{q} in the Brillouin zone, $\omega_\lambda(\mathbf{q})$ are the phonon frequencies and eigenvectors, respectively, \mathbf{R}_i denotes the two-dimensional lattice vector of the surface unit cell where atom i is located, M_i is its mass, and N is the number of unit cells within the periodic boundary conditions used in the calculations. The temperature T enters through the Bose-Einstein distribution function $n[\omega]$.

The main difficulty in evaluating eq. (1) is that it requires the knowledge of the phonon energies and eigenvectors of the system over the entire Brillouin zone. Therefore, the calculation of vibrational correlation functions is usually limited to simple systems where the normal modes are determined by symmetry. Also, eq. (1) is usually approximated by low- and high-temperature expansions using models for the dispersion of phonon energies and the density of states, like the Debye model.

To make reliable predictions and to extract microscopic information from the thermal vibrational amplitudes of the system, eq. (1) must accurately represent the system's phonon energies and eigenvectors. For semiconductor surfaces, this representation is further complicated because their reconstruction leads to bonding configurations that can be quite different from the bulk; thus, dynamical properties cannot be simply described using force constants calculated for the bulk and transferred to the surface.

A realistic theory must be used to calculate phonon energies and eigenvectors for each particular reconstructed surface. In this work, we use a formalism based on a semi-empirical tight-binding theory for structural energies in semiconductors. To explain the model briefly, the total energy of the system is expressed in terms of the band-structure energy, an empirical potential energy of interionic interactions, and the Coulomb energy of on-site electronic repulsions. The band-structure energy is calculated using an sp^3 tight binding representation of the valence electrons, and the interionic interactions are approximated with a sum of pairwise potentials. The on-site Coulomb repulsion term for the electrons is added to incorporate the effects of charge transfer. With this model, the dynamical matrix of a system can be calculated using perturbation theory, in which the bare ion-ion forces are renormalized by the electron polarizability; exponentially decaying interatomic forces are generated by the exchange of virtual electron-hole pairs between lattice distortions at different sites on the lattice. Because this approach incorporates the effects of reconstruction into the lattice dynamics of the surface, it successfully pro-

vides a description of the vibrational properties of Si surfaces.

The results of our calculations are presented in figures 3 and 4. Here we notice that for both Si(111) 2×1 and Si(001) 2×1 , the surface atoms have thermal vibrational amplitudes that are larger along the direction perpendicular to the surface plane than parallel to it. This is usually expected, since the surface atoms have reduced coordination normal to the surface. However, we find that the degree of anisotropy between normal and in-plane vibrations is very different for the two surfaces. Indeed, for Si(111) 2×1 we find that this anisotropy is quite large (1.8 in the mean-squared amplitudes of vibration), while on Si(001) 2×1 the fluctuations of the surface atoms are nearly isotropic. Furthermore, in the case of Si(111) 2×1 , the anisotropy increases rapidly with increasing temperature, a feature we attribute to the presence of a low-energy dispersionless surface phonon. This large temperature enhancement is not observed for the surface atoms of Si(001) 2×1 , which does not support a similar low-energy surface phonon. In comparing the atomic vibrational amplitudes on the two surfaces, the most salient feature is that, in the case of Si(111) 2×1 , the surface atoms have very large amplitudes of vibrations normal to the surface. The difference in the vibrational amplitudes of surface atoms on Si(111) 2×1 and Si(001) 2×1 shows that the specific microscopic properties of the surface must be considered in the calculation of the atomic vibrational correlation functions.

Specifically, we predict the degree of anisotropy between normal and in-plane vibrations and the difference in vibrational amplitudes between inequivalent surface atoms. Experimental techniques exist that can directly measure these variables. Perhaps the most important contribution of the calculations we have presented here is in their use in the analysis of experiments. Our calculated atomic vibrational amplitude and correlation function results might greatly reduce the uncertainties in the interpretation of scattering experiments that probe the structure of the surface; Debye-Waller factors might also be easily calculated with the information we have provided.

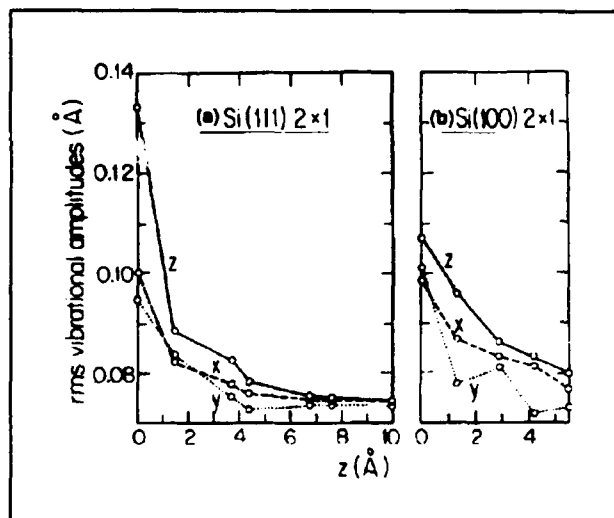


Figure 3. Atomic rms vibrational amplitudes at $T=270\text{K}$ as a function of penetration from the surface for (a) Si(111) 2×1 and (b) Si(100) 2×1 . The Cartesian directions are defined in figures 1 and 2, respectively.

3.3 Heteroepitaxial Growth

Heterostructures of semiconductors, elemental or compound, have recently been the subject of intense study as technologically promising artificial materials. GaAs on Si is a system of particular interest, not only from a technological but also from a theoretical point of view. Usually GaAs growth is initiated on Si substrates oriented along the (100) direction. The quality of the GaAs overlayers is far from ideal with a very high density of defects and dislocations present, presumably due to lattice mismatch and polarity differences. However, it is not known to what degree other interface factors, such as surface reactions or substrate morphology, play an important role in growth inhibition or initiation. These issues are at the core of current growth models of GaAs on Si(100).

In this work, we investigate, from an ab initio theoretical point of view, the possibility of layered growth of GaAs on atomically flat regions (terraces) of the Si surface. We shall focus on the initial stages of growth by considering very low coverages (one to two monolayers) where a number of important issues can be isolated and addressed in detail. For example, what is the structure of the initial monolayers? Are the Ga and As

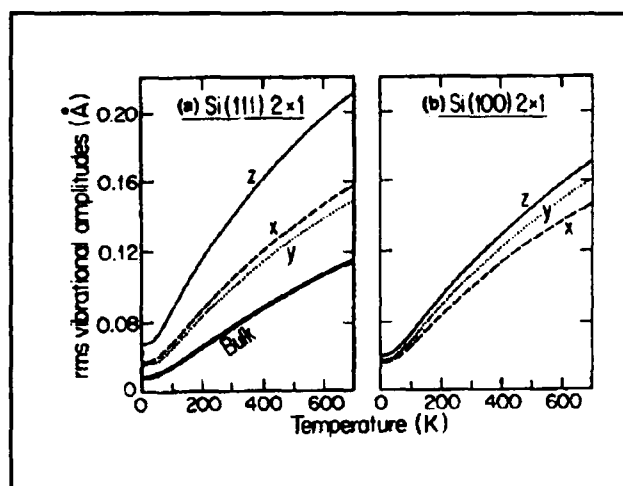


Figure 4. Atomic rms vibrational amplitudes of surface atoms on (a) Si(111) 2×1 (surface atom 2) and (b) Si(100) 2×1 (surface atom 1) as a function of temperature. The bold line is for a bulk atom.

atoms locally mixed or do they separate into domains of each species? Is the Si surface covered by Ga and As atoms to the largest possible extent at monolayers thickness or do these atoms form GaAs bilayer islands on part of the surface? What is the structure of the initial bilayer of GaAs? Does it resemble that of bulk GaAs with alternating planes of Ga and As or does it have a novel structure?

To address the possibility of two-dimensional growth on Si terraces, we consider a slab of Si bounded by (100) surfaces on which we place Ga and As atoms. The issue of interest is the lowest-energy local structure and its effects on prospects for growth. There are two possibilities: the lowest-energy local structure may be the same as the structure of bulk GaAs, so that two-dimensional growth can proceed, or the structure may be different, in which case layered growth of zincblende GaAs will be inhibited. The easiest way to envision formation of the lowest-energy structure is to consider a Si surface covered by a monolayer of one species (corresponding to pre-deposition, for example, of Ga or As) and to introduce some amount of the opposite species. One must then consider the possible local atomic con-

figurations and identify the lowest-energy structure. In this sense, the exact relative abundance (chemical potential) of Ga and As atoms is not important, but the presence of both species is crucial.

Each surface layer of the slab is taken to be reconstructed, for simplicity, in the standard (2×1) dimer pattern (this choice will be justified below). The Ga and As atoms are placed on the slab in five different ways as shown in figures 5(a)–5(e). The total energies resulting from ab initio calculations allowing these geometries to fully relax, are presented in table 1.

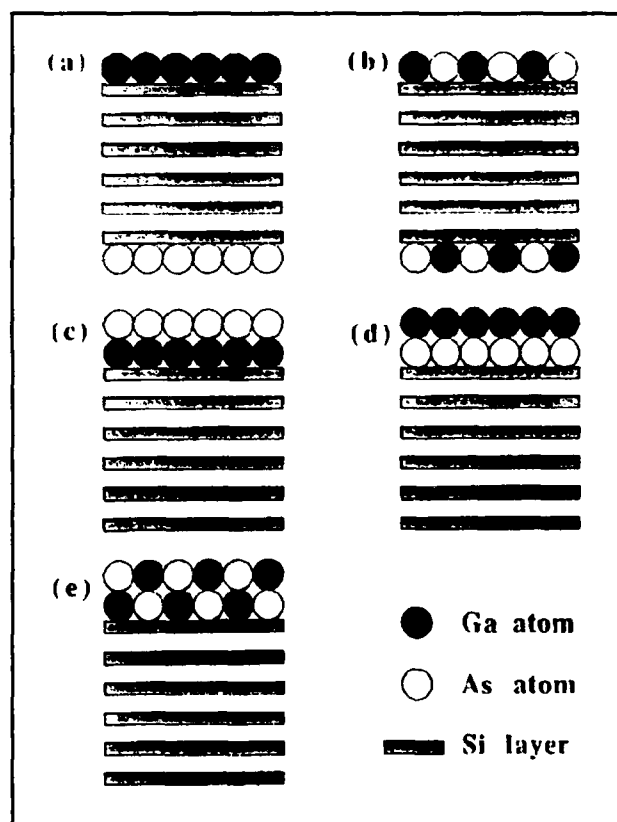


Figure 5. Schematic representation of overlayer arrangements. (a) Pure monolayer coverage, (Ga)[Si](As). (b) Mixed monolayer coverage, (GaAs)[Si](AsGa). (c) Bilayer coverage with pure layers and As-exposed surface, (As)(Ga)[Si]. (d) Same as (c) with Ga-exposed surface, (Ga)(As)[Si]. (e) Bilayer coverage with mixed layers, (GaAs)(AsGa)[Si].

Figure	Configuration	Relative Energy Difference
5(a)	(Ga)[Si](As)	0.8
5(b)	(GaAs)[Si](AsGa)	0.0
5(c)	(As)(Ga)[Si]	2.2
5(d)	(Ga)(As)[Si]	2.8
5(e)	(GaAs)(AsGa)[Si]	1.5

Table 1. Relative energy difference of the various overlayer configurations as depicted in figure 5 in eV/(2X1) SUC.

Based on the energies of the different configurations, a number of important conclusions can be drawn:

1. When the available amount of Ga and As atoms is less than a full monolayer, under equilibrium stoichiometric conditions, it wets the Si surface and formation of thicker GaAs islands is inhibited.
2. At monolayer coverage, the two species of atoms do not separate into pure Ga or pure As domains, but are locally mixed on the Si surface.
3. When GaAs is available in stoichiometric amounts sufficient for bilayer coverage, the equilibrium structure of the bilayers is not a succession of pure Ga and As layers as in bulk GaAs along the (100) direction. Rather, chemical and rehybrid-

ization reactions are energetically very favorable, leading to a passivating mixed overlayer configuration. Once this mixed layer is formed, it could persist in a disordered phase even under non-stoichiometric conditions because of its considerable stability. The mixed layer resembles locally a wurtzite structure under large uniaxial stress. A structural barrier (requiring creation of extensive defects at large energy cost) is encountered in reverting from the mixed layer structure to the zincblende structure of bulk GaAs.

This conclusion has important implications: Since the mixed layers have very different structure from the thermodynamically stable zincblende phase of bulk GaAs, the growth of mixed layers on terraces will be undermined by any surface topology which could lead to nucleation of zincblende GaAs. Thus, nucleation centers of zincblende GaAs at specific surface topologies will prevail in the growth process. It is possible to grow bulk GaAs experimentally on vicinal Si(100) surfaces, that is, surfaces with large density of steps. It is likely that surface steps are precisely the topology that nucleates zincblende GaAs, and growth occurs directly on the steps. Indeed, experimental evidence appears to support this view. Search for a possible microscopic mechanism for the initiation of this kind of growth, which involves formation of zincblende GaAs seeds at double-layer steps on the Si surface, is currently in progress.

Chapter 4. Ultralow Temperature Studies of Nanometer Size Semiconductor Devices

Academic and Research Staff

Professor Marc A. Kastner, Professor Dimitri A. Antoniadis, Dr. Stuart B. Field, Professor Henry I. Smith

Visiting Scientists and Research Affiliates

Mordehai Heiblum,¹ Shalom Wind¹

Graduate Students

Udi Meirav, Samuel L. Park, John H.F. Scott-Thomas

Technical and Support Staff

Angela R. Odoardi

4.1 Project Description

Sponsor

Joint Services Electronics Program
Contract DAAL03-89-C-0001

In the late 1970s, the rapidly improving theoretical description of disordered metals combined with the rapidly evolving technology of submicron lithography to create a new subfield of condensed-matter physics. The electronic properties of artificial structures — which are large compared with atomic size scales but comparable to quantum mechanical coherence lengths — have been shown to be fundamentally different from both those of larger and smaller structures. For this reason, the term "mesoscopic" was coined to differentiate them.

Almost from the start, the hallmark of mesoscopic structures has been the random, noise-like, but reproducible fluctuations in

their conductance. These fluctuations were first seen in the insulating regime of one-dimensional field-effect transistors when their Fermi energy was varied. The most dramatic discovery was that, in metallic samples, independent of their size and geometry, the fluctuations had magnitude of order e^2/h in the limit of zero temperature. These Universal Conductance Fluctuations were seen when the magnetic field, Fermi energy, or impurity configuration was varied, consistent with the theory of Altshuler, Lee and Stone.²

Recently, we reported the discovery of a new phenomenon in mesoscopic field effect structures. In the same regime where exponentially large random fluctuations had been seen in earlier devices,² we found fluctuations which, while still exponentially large, were accurately periodic in the density of the electron gas. We were the first to observe these oscillations in Si MOSFETs³ fabricated at MIT and in novel GaAs inverted semiconductor-insulator-semiconductor field

¹ IBM Thomas J. Watson Research Laboratories.

² For a review see M. A. Kastner, R. F. Kwasnick, J. C. Licini, and D. J. Bishop, "Conductance Fluctuations near the Localized-to-Extended Transition in Narrow Si MOSFETs," *Phys. Rev. B* 36: 8015 (1987).

³ J.F.H. Scott-Thomas, M.A. Kastner, D.A. Antoniadis, H.I. Smith, and S.B. Field, "Si Metal-Oxide Semiconductor Field Effect Transistor with 70-nm Slotted Gates for Study of Quasi-One-Dimensional Quantum Transport," *J. Vac. Sci. Technology B* 6: 1841 (1988); J.F.H. Scott-Thomas, S.B. Field, M.A. Kastner, H.I. Smith, and D.A.

effect transistors ISIS structures fabricated at IBM.⁴ An example of the latter is shown in figure 1.

A rich phenomenology is associated with this oscillatory behavior. The conductance is thermally activated between 1 K and about 0.3 K, and the activation energy oscillates with the number of electrons per unit length. At a lower temperature there is a tunneling component which also oscillates. The conductance is highly non-ohmic, showing dramatic threshold behavior with threshold voltage that oscillates out of phase with the conductance. Most surprising of all, the oscillations are independent of magnetic field. This is probably why the phenomenon was not observed earlier by other groups that typically study MODFETs in which the carrier density can not be varied over a wide range. For the quantum Hall effect, the variation of carrier density is equivalent to the variation of magnetic field. This is not the case for our new phenomenon.

The phenomenology suggests that the oscillations result from the opening of an energy gap whenever an integral number of electrons resides in a subsection of the one-dimensional channel. Several models have been proposed to explain the observations. It is probable that the electron-electron interactions are crucial. If so, this will be the first time that many-body effects will have been shown to dominate the behavior of mesoscopic systems.

The silicon device fabrication and part of the GaAs fabrication was sponsored by the National Science Foundation under Grant

ECS 88-13250. A portion of the ultralow temperature measurements was sponsored by the Joint Services Electronics Program under Contract DAAL03-89-C-0001.

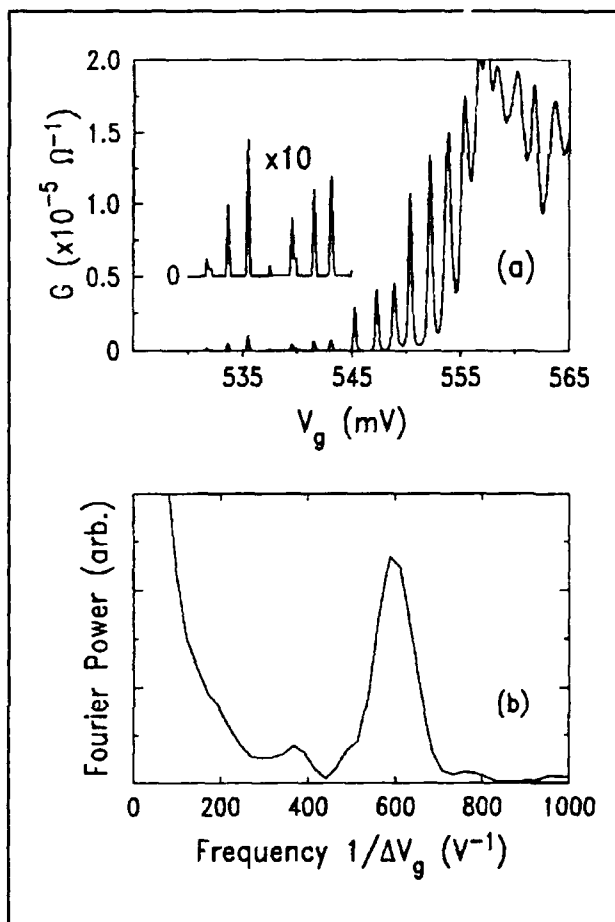


Figure 1. (a) Conductance vs. gate voltage of a narrow channel, $2 \mu\text{m}$ long, measured at $T = 50 \text{ mK}$. The inset shows an expansion of the first few oscillations. (b) Fourier power spectrum of the above. The peak corresponds to a period of $\Delta V \approx 1.7 \text{ mV}$.

Antoniadis, "Conductance Oscillations Periodic in the Density of a One-Dimensional Electron Gas," *Phys. Rev. Lett.* 62: 583 (1989).

⁴ U. Meirav, M.A. Kastner, M. Heiblum, and S.J. Wind, "A One-Dimensional Electron Gas in GaAs: Periodic Conductance Oscillations as a Function of Density," *Phys. Rev. (Rapid Comm.) B* 40: 5871 (1989); U. Meirav, M. Heiblum, and F. Stern, *Appl. Phys. Lett.* 52: 1268 (1988).

Chapter 5. The Quantum Hall Effect in Narrow MOSFETs

Academic and Research Staff

Professor Patrick A. Lee

Visiting Scientists and Research Affiliates

Dr. Alfred Gold¹

Graduate Students

Jari Kinaret

Technical and Support Staff

Imadiel Ariel

5.1 Project Description

Sponsor

Joint Services Electronics Program
Contract DAAL03-89-C-0001

We are investigating the conductance of narrow MOSFETs that are subject to a strong magnetic field. This investigation was motivated by an experiment conducted by Professor Marc A. Kastner's group two years ago,² in which the group studied the transport properties of narrow MOSFETs (width $\sim 500\text{\AA}$) subject to a large magnetic field of 5T to 10T. In these fields, only the lowest few Landau levels — in the quantum Hall regime — are occupied. At the same time, the cyclotron orbit is comparable to the sample width, making the finite size effect of the sample important. The experimentalists observed thresholds for large increases in conductance as a function of magnetic field, as well as ill-defined steps in the conductance of approximately $2e^2/h$. We tackled this problem using both computer simulation and analytic treatment of many-body effects.³

We use computer simulation to model disordered conductors subject to a large magnetic field. The model is defined on a tight binding lattice of finite width and length which is extended to infinity in both directions by connecting it to ideal lattices without randomness to simulate the source-drain leads. The novel feature of the model is that the leads are also subject to the same quantizing magnetic fields so that (1) the edge states in the leads consist of Landau level subject to a lateral boundary condition, and (2) the states at the Fermi level are edge states which are bound to the edge and propagate to the right along the upper edge and left along the lower edge. The conductance is then related to the transmission probability of these edge states using the Landauer formula. These transmission probabilities are computed numerically.

When the width of the wire is large compared with the cyclotron radius, the edge states are basically forward scattered in the disorder region so that the transmission probability is unity, leading to quantized Hall conductance of e^2/h . It is only when the width becomes comparable to the cyclotron

¹ Department of Physics, University of Munich, Germany.

² J. Scott-Thomas, S.B. Field, M.A. Kastner, H.I. Smith, and D.A. Antoniadis, *Phys. Rev. Lett.* 62:583 (1989).

³ J. Kinaret and P.A. Lee, to be published.

radius that the edge state can scatter across the width of the sample and is then reflected. The reduction in the transmission probability leads to ordinary metallic conduction. As the field is increased, the simulation shows a threshold for the appearance of quantized steps in the conductance in agreement with the experiment. The simulation also shows that in the step between plateaus, the system behaves as a metal in the sense that it exhibits conductance fluctuations in the order of e^2/h . The period of the fluctuation as given by the condition that the flux through the sample area is a flux quantum just as in universal conductance fluctuation.

The next puzzle to be resolved is understanding why the quantum Hall step is in units of $2e^2/h$. We believe that the $2e^2/h$ step is due to the presence of two degenerate valleys in the silicon interface, which is not

resolved. In ordinary two dimensional samples, the valley degeneracy is resolved due to the exchange effect. It is more energetically favorable to occupy one valley first, rather than occupying both valleys equally, because the exchange energy is nonlinear in the density. However, this mechanism will be weakened in narrow wires, because the Landau level is no longer completely flat and it costs kinetic energy to preferentially occupy one valley. We calculated the exchange energy for a model system confined by a parabolic potential demonstrating this competition between kinetic and exchange terms in quasi-one-dimensional MOSFETs. We conclude that the combination of numerical simulation and analytic work to account for the many-body effect gives a quite satisfactory account of the transport properties of a narrow MOSFET wire in a quantizing magnetic field.

Chapter 6. Epitaxy and Step Structures on Semiconductor Surfaces

Academic and Research Staff

Professor Simon G.J. Mochrie

Graduate Student

Douglas A. Abernathy

6.1 Project Description

Sponsor

Joint Services Electronics Program
Contract DAAL03-89-C-0001

Under the Joint Services Electronics Program, we have studied the Pt(001) surface as a model for the behavior of an incommensurate overlayer on a substrate.¹ This research will lead to a more complete understanding of what determines the orientation of a thin film on a substrate.

The (001) surface of platinum, like the (001) surfaces of gold and iridium, exhibits a radical reconstruction in which the topmost layer of atoms forms a hexagonal layer, in spite of the layers of square symmetry beneath. At $T = 300$ K, the hexagonal overlayer is rotated by 0.75 degrees away from a high symmetry direction of the cubic lattice (the substrate). Our recent synchrotron x-ray measurements have revealed, however, that the overlayer experiences a completely new class of rotational transition at high temperatures. For $T > 1670$ K, the hexagonal overlayer is aligned with the cubic substrate. The temperature $T_c = 1670$ K marks the onset of rotation, and as the temperature decreases further the rotation angle increases continuously, reaching 0.75° at $T = 1300$ K. Figure

1 shows typical experimental profiles. The two peaks are arranged symmetrically about the high symmetry $[1, 1, 0]$ direction and correspond to positive and negative rotation angles of the overlayer. The accompanying change in the overlayer lattice constant is on the order of one part in 1000.

Current theories of orientational epitaxy predict a definite relationship between the overlayer lattice constant and the rotation angle,² but our observations contradict this understanding. Nevertheless, the evolution of rotation angle with temperature follows a power-law behavior (see figure 2). In fact, the observed exponent is one-half, indicative of so-called mean-field behavior. An exponent of one-half is unusual for a two-dimensional phase transition because the effect of fluctuations are expected to be particularly severe in two-dimensions. However, an elegant interpretation is possible: If one supposes that the rotational transition occurs as a result of a rotational elastic constant becoming zero, then by considering the effect of such behavior on the low-energy modes (lattice vibrations) of the Pt overlayer, it emerges that there is no mode that becomes soft as the transition is approached. In other words, there simply are no fluctuations, and character of the transition must be mean-field.³ With this observation, we can

¹ D.L. Abernathy, S.G.J. Mochrie, D.M. Zehner, G. Grübel, and D. Gibbs, "Rotational Transitions of the Pt(001) Surface," unpublished.; D. Gibbs, G. Grübel, D.M. Zehner, D.L. Abernathy, and S.G.J. Mochrie, "Phase Behavior of the Pt(001) Surface: X-Ray Measurements," unpublished.

² J.P. McTague and A.D. Novaco, *Phys. Rev. B* 19: 5299 (1979); J. Villain, *Phys. Rev. Lett.* 41:36 (1978); H. Shiba, *J. Phys. Soc. Jap.* 46:1852 (1979), 48:211 (1980).

³ R.A. Cowley, *Phys. Rev. B* 13: 4877 (1976).

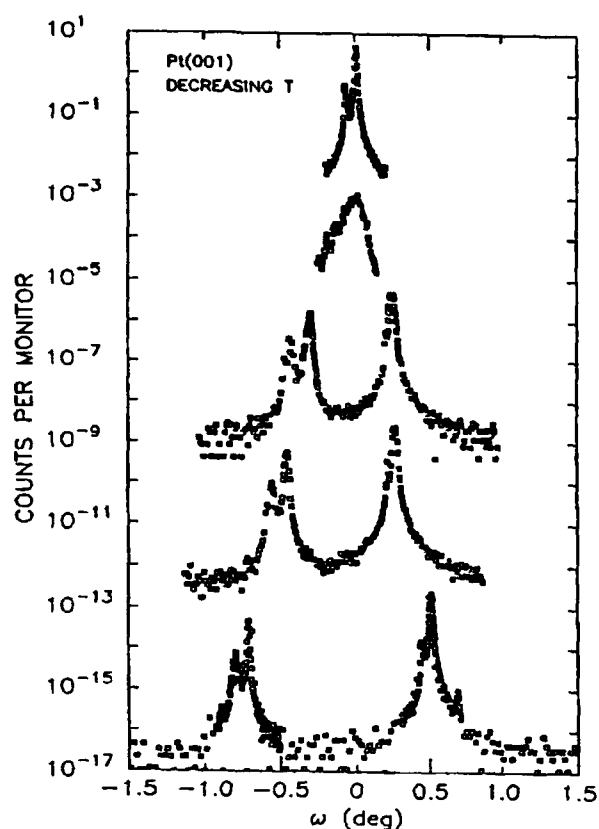


Figure 1. Transverse scans through a near hexagonal peak of the reconstructed Pt(001) surface for temperatures decreasing from the aligned phase (single peak) into the rotated phase (two peaks).

also understand the mean-field character of other high temperature rotational transitions.⁴

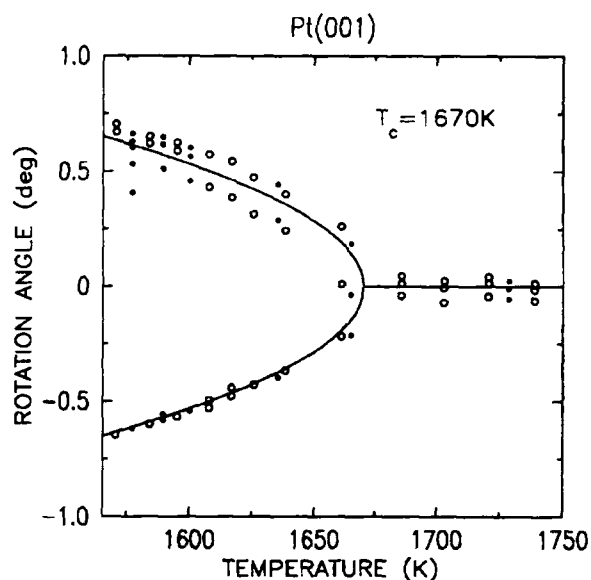


Figure 2. Evolution of the rotation angle vs. temperature for the Pt(001) surface.

⁴ K.L. D'Amico, D.E. Moncton, E.D. Specht, R.J. Birgeneau, S.E. Nagler and P.M. Horn, *Phys. Rev. Lett.* 53: 2250 (1984).

Part II Applied Physics

Section 1 Atomic, Molecular and Optical
 Physics

Section 2 Plasma Physics

Section 3 Electromagnetics

Section 4 Radio Astronomy

Section 1 Atomic, Molecular and Optical Physics

Chapter 1 Quantum Optics and Photonics

Chapter 2 Basic Atomic Physics

Chapter 3 Small Angle X-Ray and Neutron Scattering —
 Its Application to Supramolecular Solutions

Chapter 1. Quantum Optics and Photonics

Academic and Research Staff

Professor Shaoul Ezekiel, Dr. Mara G. Prentiss

Visiting Scientists and Research Affiliates

Dr. Philip R. Hemmer, John Kierstead, Dr. Elias Snitzer¹

Graduate Students

M. Selim Shahriar, Stephen P. Smith, Farhad Zarinetchi, John Donoghue

Technical and Support Staff

Margaret McCabe

1.1 Microwave Phase Dependent Optical Absorption

Sponsor

Rome Air Development Center

A laser excited resonant Raman interaction causes atoms to be optically pumped into a non-absorbing dressed state, called the trapped state.² We have shown how a microwave field can modify this non-absorbing state in a phase sensitive way to produce changes in the absorption of the optical Raman excitation fields.

Figure 1 shows a three-level atomic system in the lambda configuration, where ω_1 and ω_2 are the frequencies of the laser fields which excite the Raman transition, and ω_3 is the frequency of the microwave field. Here it is assumed that states 1 and 3 are long-lived, but state 2 is short-lived with a decay rate of γ_2 . The Raman trapped state has the form

$$[|1\rangle|\omega_1\rangle - |3\rangle|\omega_2\rangle]/\sqrt{2},$$

where equal Rabi frequencies have been assumed, and $|\omega_1\rangle$ and $|\omega_2\rangle$ are single photon states. In comparison, the high and

low energy dressed states of the single photon $1 \leftrightarrow 3$ microwave transition are

$$[|1\rangle|\omega_3\rangle - |3\rangle]/\sqrt{2}$$

and

$$[|1\rangle|\omega_3\rangle + |3\rangle]/\sqrt{2},$$

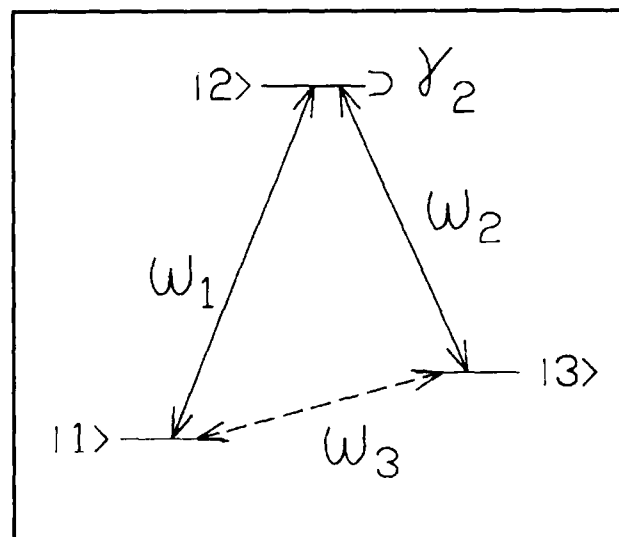


Figure 1. Three level atomic system showing resonance Raman excitation fields ω_1 and ω_2 and microwave field ω_3 .

¹ Rutgers University, New Jersey.

² H.R. Gray, R.M. Whitley, and C.R. Stroud, Jr., "Coherence Trapping of Atomic Populations," *Opt. Lett.* 3:218 (1978).

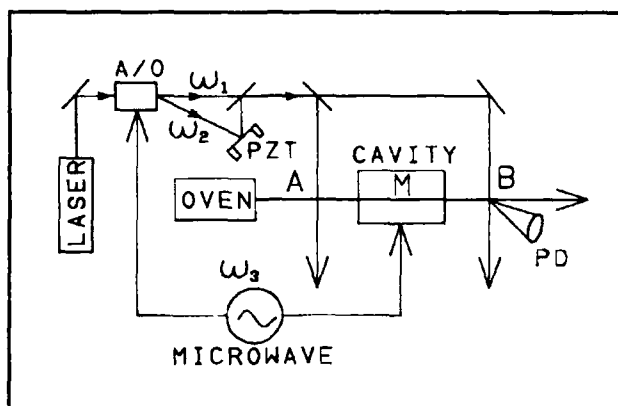


Figure 2. Schematic of experimental setup.

respectively.³

When the laser difference frequency $\omega_1 - \omega_2$ is exactly in (or out of) phase with the microwave frequency ω_2 , the Raman trapped state translates directly into the high (or low) energy microwave dressed state. For any other value of phase difference, a linear combination of microwave dressed states results. In this case, the microwave interaction partially destroys the Raman trapped state, resulting in increased optical absorption. Thus, the optical absorption is sensitive to microwave phase.

To observe this effect, we used a three-zone sodium atomic beam apparatus as illustrated schematically in figure 2. Here the interaction in zone A optically pumps the sodium atoms into the Raman trapped state. These prepared atoms then interact with a microwave field inside the cavity (zone M) and the changes in optical absorption are monitored in zone B via fluorescence induced with a Raman probing interaction. With no microwave field, the Raman-Ramsey fringe lineshape of figure 3a is observed.⁴ However, when microwave power corresponding to a π -pulse is present in zone M, the lineshape of figure 3b results. The oscillations shown

by this data are produced by a rapid scanning of the relative microwave and laser difference frequency phases via the PZT (figure 2). Large changes in optical absorption are produced by changing only the relative phase of the microwave field. Figure 3c shows the corresponding theoretical lineshape which includes the effect of velocity averaging in the atomic beam. The preliminary data shows qualitatively good agreement between theory and experiment.

There would be many applications for this technique if the microwave transition could be replaced by a mm-wave or FIR transition. For example, if a mm-wave or FIR beam and a double optical beam intersect at an angle, the resulting spatial dependence of the relative phase would produce a grating-like diffraction of both beams. This double diffraction effect may have applications in beam steering and, possibly, in converting real time holographic images.

1.2 A New Approach to Microwave Excitation of Atomic Beams

A beam of alkali atoms, e.g., sodium, initially state-prepared into one of the ground state hyperfine levels, undergoes Rabi flopping when passed through a microwave cavity excited by a resonant microwave frequency.⁵ Figure 4, plot I, shows how the amplitude of the oscillating B field is usually configured in the cavity. The population change is maximum when the microwave field strength corresponds to a π -pulse for the transit time. If the microwave frequency is scanned, the familiar Lorentzian lineshape (figure 5a, dashed line) is observed, its linewidth determined by transit time and power broadening. Figure 4, plot II, shows that, if the field

³ Y.S. Bai, A.G. Yodh, T.W. Mossberg, "Selective Excitation of Dressed Atomic States by Use of Phase-Controlled Optical Fields," *Phys. Rev. Lett.* 55:1277 (1985).

⁴ J.E. Thomas, P.R. Hemmer, S. Ezekiel, C.C. Leiby, Jr., R.H. Picard, and C.R. Willis, "Observation of Ramsey Fringes Using a Stimulated, Resonance Raman Transition in a Sodium Atomic Beam," *Phys. Rev. Lett.* 48:867 (1982).

⁵ N.F. Ramsey, *Molecular Beams*. (London: Oxford University Press, 1956).

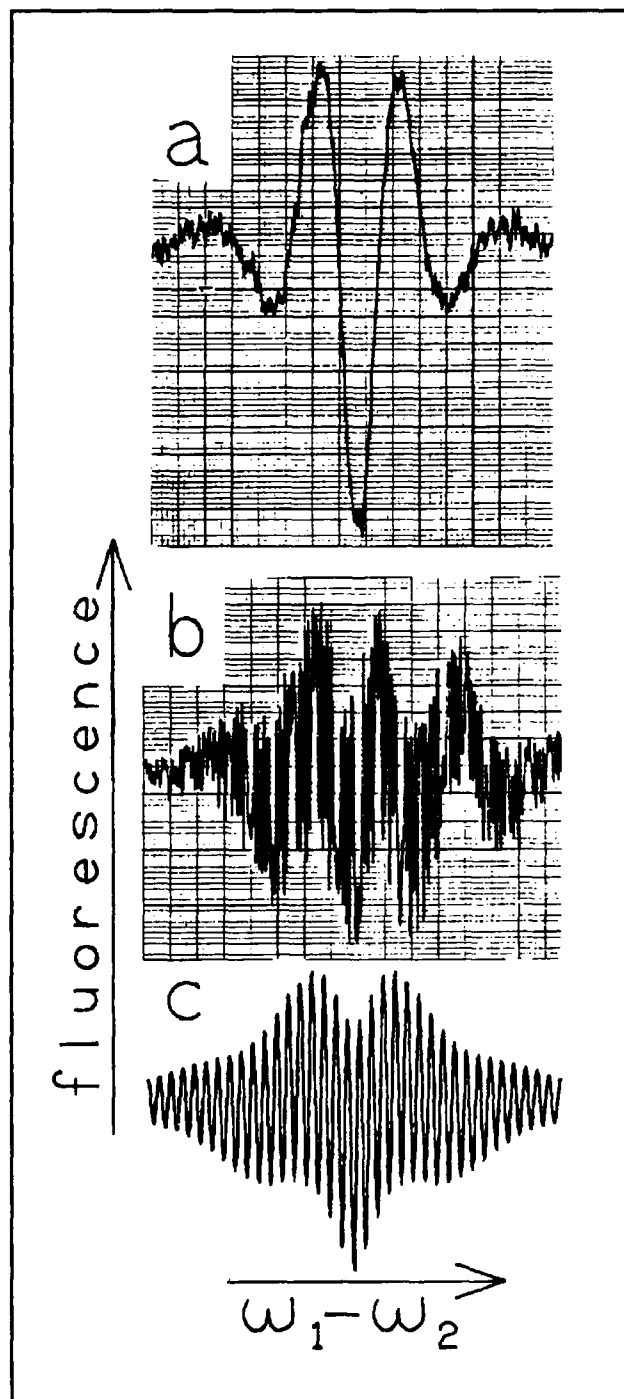


Figure 3. (a) Data showing Raman-Ramsey fringes with no microwave present. (b) Data showing modified fringes when a phase varying microwave field of π -pulse amplitude is introduced in zone M. (c) Theoretical plot corresponding to the data in (b) including the effect of velocity averaging.

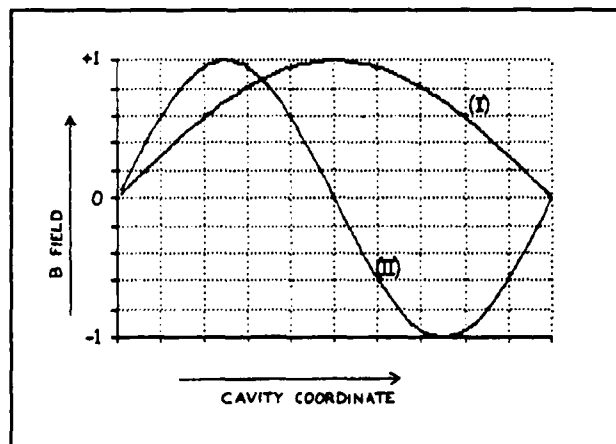


Figure 4. Cavity cross-section in a TE_{102} resonator in two different orientations. Plot I is the one usually used in microwave excitation, while Plot II is the one used here.

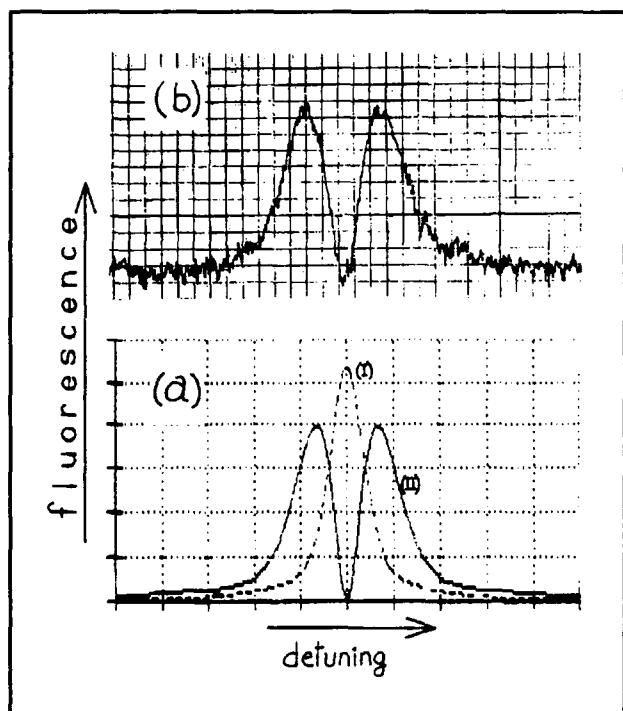


Figure 5. (a) Solid line shows the population change as a function of the microwave detuning, the dip corresponding to zero detuning. Dashed line shows the usual Lorentzian lineshape seen when there is no phase flip inside the cavity. (b) The experimental data corresponding to the solid line in (a).

profile has a node,⁶ then this Lorentzian lineshape develops a dip that goes to zero on resonance. The unique property of this dip is that it goes all the way to zero even for thermal beam with a wide velocity distribution. This is different from the usual dip (inverse of figure 5a, dashed line) observed in microwave resonance, which, due to velocity averaging, always remains well above zero. In addition, unlike the usual dip, this one remains zero at all powers. We can also extend the theory behind this effect to separated field excitations, suggesting that locking microwave oscillator to this lineshape might result in reduced shot noise.

We can more easily understand the physical aspects of this effect in terms of Bloch vectors.⁷ During the first half of the excitation, the vector rotates through an

angle (e.g., $\pi/2$ for a $\pi/2$ pulse) in the Rabi flop plane. Next, the vector rotates by an angle π in the phase plane, continuing to rotate in the same direction in the Rabi flop plane. If the pulse strength in the two lobes is equal, the rotation in the first lobe is undone. The initial amount of rotation must be arbitrary for total cancellation to occur. Thus, cancellation would occur for any pulse strength. In addition, this implies that different atoms with different velocities would be cancelled totally. The dip, therefore, would go to zero even for a thermal beam having a wide velocity distribution and inhomogeneous transit time broadening.

When the microwave is detuned, the vector no longer rotates in the Rabi-flopping plane. This negates total cancellation and generates maximum population inversion when the amplitude of the detuning is of the order of the Rabi frequency. Thus the spectrum, as a function of detuning, appears as two peaks; the separation between them increases as the microwave power increases. Figure 5b shows a lineshape with an average microwave power corresponding to approximately a π -pulse. Figure 5a, solid line, shows the corresponding theoretical plot, with good agreement. In comparison, the dashed line in figure 5a shows the corresponding lineshape for a conventional configuration.

By changing the level with an observable population, the peak of figure 5a, dashed line, can be converted into a dip. Figure 6a shows a set of these dips (corresponding to cavity cross-section I) as the microwave Rabi frequency varies. The dip moves up and down as microwave power changes, but never moves close to zero. In contrast, figure 6b shows the dips (corresponding to cavity cross-section II) as the microwave Rabi frequency varies by the same amounts as in figure 6a. The dip is always at zero, independent of changes in microwave power. Figure 6c also shows this, illustrating that the signal at the bottom of the dip varies as a function of Rabi frequency for these two sets of lineshapes.

⁶ J.A. Kong, *Electromagnetic Wave Theory*. (New York: John Wiley, 1988).

⁷ M. Sargent III, M.O. Scully, and W.E. Lamb, Jr., *Laser Physics*. (Reading, Massachusetts: Addison-Wesley, 1979).

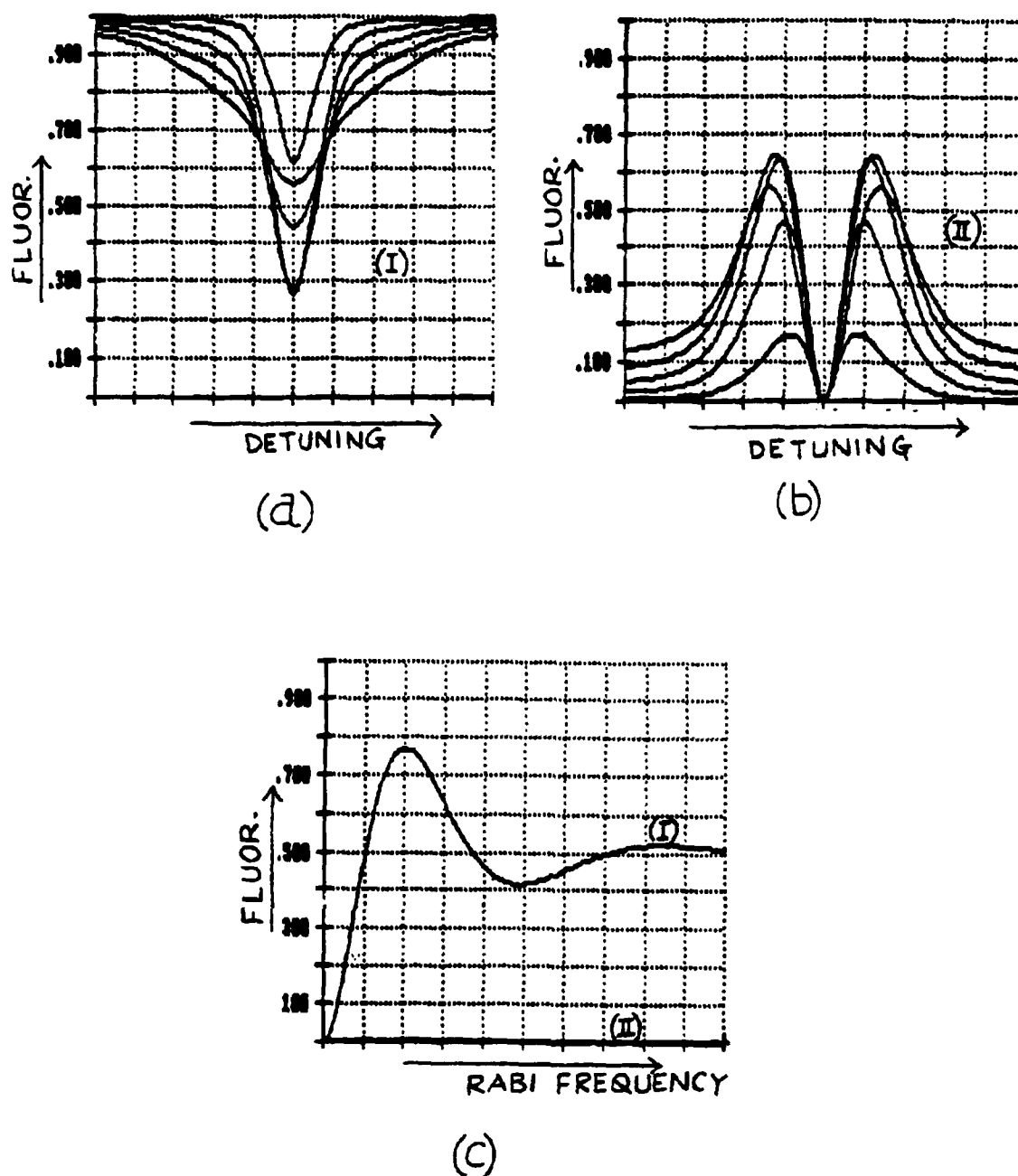


Figure 6. (a) Conventional dips for cross-section I, as the Rabi frequency is varied. (b) Corresponding set for new dips seen in cross-section II. (c) How the dips in sets I and II move as the Rabi frequency is varied continuously.

1.3 Stimulated Brillouin Fiberoptic Gyroscope

Sponsor

Charles S. Draper Laboratory

Fiberoptic inertial rotation sensors (or gyroscopes) have been based on the Sagnac effect in either a multiturn interferometer⁸ or a resonator.⁹ Both of these approaches constitute the fiberoptic implementation of previously demonstrated Sagnac interferometer¹⁰ gyroscopes and resonator¹¹ gyroscopes that employ bulk-optic components. However, we have recently begun to study a fiberoptic analog of the ring laser gyroscope,¹² which was a bulk-optic device. In the following figures, we are presenting preliminary data on a fiberoptic ring laser gyroscope with stimulated Brillouin¹³ scattering as the laser gain medium. To our knowledge, this is the first demonstration of a solid state ring laser gyroscope or RLG.

Figure 7 is a simplified diagram of a stimulated Brillouin fiberoptic gyroscope. A single frequency laser, He-Ne at $1.15 \mu\text{m}$, is coupled into the opposite direction from a non-polarization maintaining fiberoptic ring resonator (length $\approx 25\text{m}$; finesse ≈ 250 ; coil diameter $\approx 7.5\text{cm}$) and acts as the pump for the stimulated Brillouin laser. The frequency

of the Brillouin laser¹⁴ is downshifted from that of the pump by the acoustic frequency in the fiber (15 GHz at $1.15 \mu\text{m}$). The direction of the Brillouin laser is opposite from the pump's because it experiences the highest Brillouin gain. The clockwise pump in the resonator is denoted by P^- and the counter-clockwise pump by P^+ . The corresponding stimulated Brillouin lasers that are created by the pumps are denoted by B^- and B^+ .

To maintain the highest pump intensity in the resonator, the pump laser must be held at a cavity resonance by using a feedback loop. The threshold pump intensity for Brillouin lasing depends on the length and finesse of the resonator, as well as on the wavelength of the pump. In our case, we have achieved threshold intensities as low as $60 \mu\text{W}$ at the input of the resonator.

The counterpropagating Brillouin lasers, B^+ and B^- , coupled out of the resonator using fiber coupler C_1 , are brought together onto a detector via coupler C_2 . In the presence of inertial rotation, a beat note is generated between B^+ and B^- , proportional to the applied rotation component normal to the plane of the resonator, which is similar to the conventional RLG.

Figure 8a shows the Brillouin beat frequency (converted to an analog signal) as a function of a sinusoidal rotation (figure 8b) applied to the table supporting the gyro. The peak beat

⁸ V. Vali and L.W. Shorthill, "Fiber Ring Interferometer," *Appl. Opt.* 15, 1099 (1976).

⁹ R.E. Meyer, S. Ezekiel, D.W. Stowe and V.J. Tekippe, "Passive Fiber Optic Ring Resonator for Rotation Sensing," *Opt. Lett.* 8:644 (1983).

¹⁰ W.R. Carrington, R. Fredricks, and Lear Siegler, Inc., *Development of an Optical Sensor: Final Report to the U.S. Office of Naval Research on Contract N00014-73-C-0377*, November 1973.

¹¹ S. Ezekiel and S.R. Balsamo, "Passive Ring Resonator Laser Gyroscope," *Appl. Phys. Lett.* 30:478 (1977).

¹² A.H. Rosenthal, "Regenerative Circulatory Multiple-Beam Interferometry for the Study of Light-Propagation Effects," *J. Opt. Soc. Am.* 52:1143 (1962); W.M. Macek and D.T.M. Davis, Jr., "Rotation Rate Sensing with Traveling Wave Ring Laser," *Appl. Phys. Lett.* 2:67 (1963).

¹³ P.J. Thomas, H.M. van Driel, and G.I.A. Stegeman, "Possibility of Using an Optical Fiber Brillouin Ring Laser for Inertial Sensing," *Appl. Opt.* 19:1906 (1980).

¹⁴ K.O. Hill, B.S. Kawasaki, and D.C. Johnson, "Cw Brillouin Laser," *Appl. Phys. Lett.* 28:608 (1976); D.R. Ponikvar and S. Ezekiel, "Stabilized Single-Frequency Stimulated Brillouin Fiber Ring Laser," *Opt. Lett.* 6:398 (1981); L.F. Stokes, M. Chodorow, and H.J. Shaw, "All Fiber Stimulated Brillouin Ring Laser with Submilliwatt Pump Threshold," *Opt. Lett.* 7:509 (1982); P. Bayvel and I.P. Giles, "Evaluation of Performance Parameters of Single Mode All Fiber Brillouin Ring Lasers," *Opt. Lett.* 14:581 (1989).

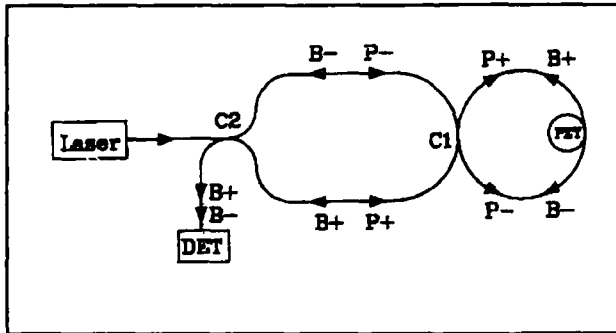


Figure 7.

frequency is about 3 kHz which is close to the 3.2 kHz value we calculated using the maximum applied rate of 3.8 deg/sec and the scale factor for the gyro. Figure 8a shows that a zero beat frequency appears whenever the rotation rate is low. This dead zone is the familiar "lock-in" phenomenon in RLGs that is caused by backscattering. The lock-in range is about 1 kHz or 1 deg/sec. Figure 7 shows that the beat frequency does not change sign with the rotation because the setup cannot detect the beat frequency phase.

In the bulk-optic RLG, use of mechanical dither overcomes the lock-in effect. In the case of the Brillouin RLG or B-RLG, we can also use mechanical dither to overcome lock-in. Other techniques, similar to those based on multiple frequency operation, can be implemented in the B-RLG, but not in the RLG.

Because the B-RLG does not require a measurement system for detecting the Sagnac effect, it has a major advantage over interferometers, which need to measure the Sagnac phase shift, and resonators that must measure frequency shift. In the B-RLG, similar to the RLG, the output is a beat frequency directly proportional to rotation rate.

We must study the preliminary data to resolve a number of issues that influence ultimate performance. At present, the B-RLG, which is basically simpler to implement and does not require highly specialized components, is a promising alternative to passive fiber interferometer and fiber resonator gyros.

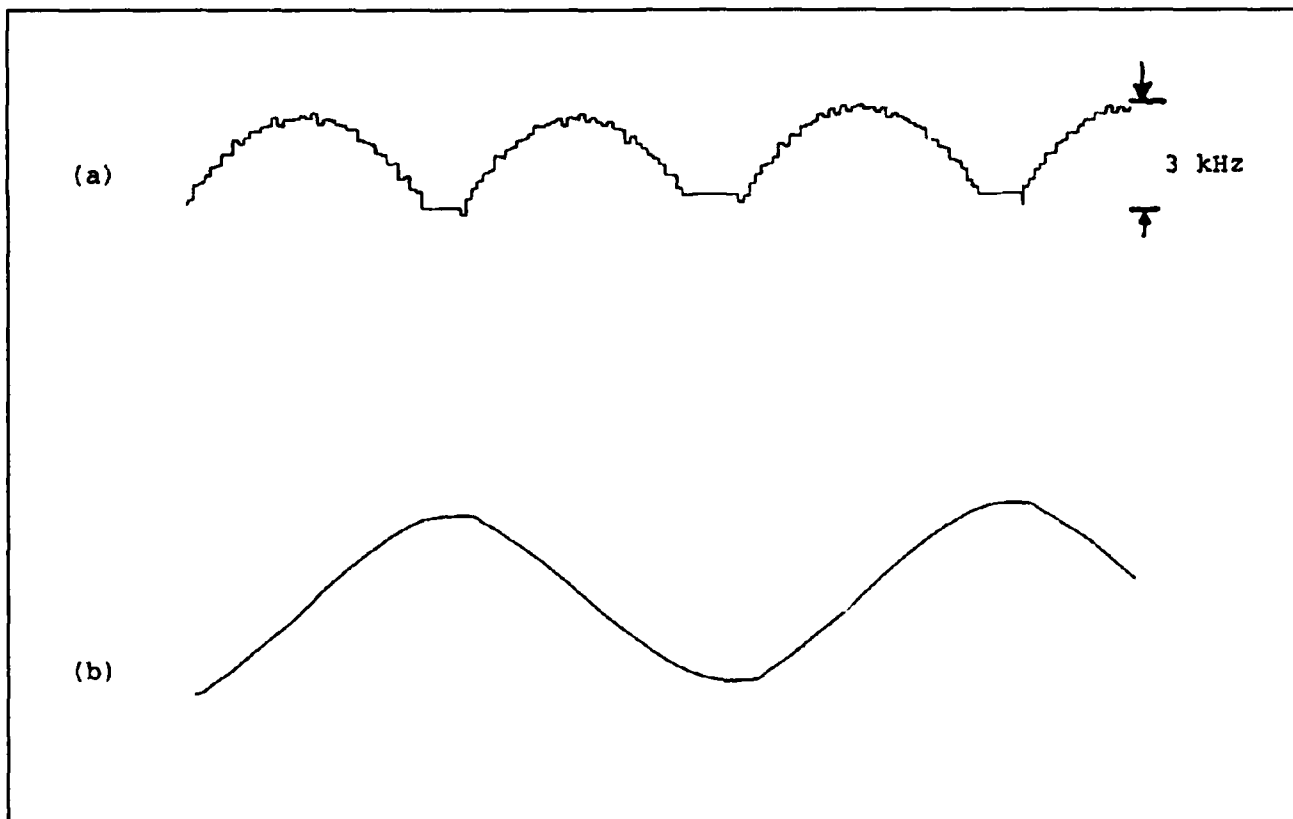


Figure 8.



Professor Daniel Kleppner, Associate Director, Research Laboratory of Electronics

Chapter 2. Basic Atomic Physics

Academic and Research Staff

Professor Daniel Kleppner, Professor David E. Pritchard, Dr. Min Xiao

Visiting Scientists and Research Affiliates

Dr. Theodore W. Ducas¹

Graduate Students

Kevin R. Boyce, Pin P. Chang, Eric A. Cornell, Michael W. Courtney, Chris R. Ekstrom, Thomas R. Gentile, Kristian Helmerson, Long Hsu, Barbara J. Hughey, Chun-Ho Lu, Michael A. Joffe, David W. Keith, Robert P. Lutwak, Bruce G. Oldaker, Scott Paine, Ke-Xun Sun, George R. Welch

Undergraduate Students

Deborah Kuchnir, James P. Schwonek, Quentin Turchette

Technical and Support Staff

Carol A. Costa

2.1 Experimental Study of Small Ensembles of Atoms in a Microwave Cavity

Sponsor

Joint Services Electronics Program
Contract DAAL03-89-C-0001

Project Staff

Barbara J. Hughey, Thomas R. Gentile, Dr. Theodore W. Ducas, Professor Daniel Kleppner

Cavity quantum electrodynamics — the study of interactions of individual atoms with quantum fields in cavities — has grown into an active area of quantum optics.² A seminal experiment in this area was the inhibition of

spontaneous emission of an excited atom, first demonstrated in our laboratory some years ago.³ During this past year, we have completed a study of the evolution of small ensembles of atoms in a microwave cavity. Our goal is to observe the dynamics of an atom-vacuum system in the quantum regime.

The states of our collective N-atom system are Dicke states.⁴ The total atom-field Hamiltonian for the system is⁵

$$\begin{aligned} H_{\text{tot}} &= H_A + H_F + H_{AF} \\ &= \hbar\omega_0 D^\circ + \hbar\omega(a^\dagger a + \tfrac{1}{2}) \\ &\quad + \tfrac{1}{2}\hbar\omega_a(aD^+ + a^\dagger D^-), \end{aligned} \quad (1)$$

¹ Department of Physics, Wellesley College, Wellesley, Massachusetts.

² S. Haroche and D. Kleppner, *Phys. Today* **B 42**(1): 24 (1989).

³ R.G. Hulet, E.S. Hilfer, and D. Kleppner, *Phys. Rev. Lett.* **55**: 2137 (1985).

⁴ R.H. Dicke, *Phys. Rev. B* **93**: 99 (1954).

⁵ S. Haroche, in *New Trends in Atomic Physics*, eds. G. Grynberg and R. Stora (Amsterdam: North Holland, 1984), 190.

where H_A and H_F are the atomic and field Hamiltonians, respectively, and H_{AF} describes the atom-field interaction. a and a^\dagger are the conventional destruction and creation operators for the electromagnetic field. D^+ and D^- are collective atomic raising and lowering operators, respectively, that act on the Dicke states like standard angular momentum raising and lowering operators. D^0 acts on the Dicke states like the z -component of the angular momentum operator.

The evolution of the system can be described by the density matrix equation

$$\frac{d\rho_{A+F}}{dt} = \frac{1}{i\hbar} [H_{\text{tot}}, \rho_{A+F}] + \Lambda_F \rho_{A+F}, \quad (2)$$

The last term in equation (2) accounts for dissipation. The probability that a member of the system is excited at time t is related to the expectation value of D^0 by

$$P_e(t, N) = \frac{1}{N} \langle D^0 \rangle + \frac{1}{2} \quad (3)$$

For more than fifty atoms, an alternative method based on the Bloch vector model becomes more practical than the above approach. The time derivatives of the quantum mechanical operators D^0 , D^+ , and a^\dagger are found in the Heisenberg picture. The atomic operators are related to the components (η, ρ) of the Bloch vector, a classical angular momentum vector with length $J = N/2$

$D^0 \rightarrow \eta \equiv \frac{1}{2}N \cos \theta$ and $D^+ \rightarrow \rho \equiv \frac{1}{2}N \sin \theta e^{i\phi}$, where θ and ϕ are the standard angles in spherical coordinates. The field operator a^\dagger is identified with ε , a classical electric field in the cavity. The evolution of the system is described by⁶

$$\frac{d\eta}{dt} = \frac{-i\omega_a}{2} (\varepsilon^* \rho - \varepsilon \rho^*), \quad (4a)$$

$$\frac{d\rho}{dt} = -i\omega_a \varepsilon \eta, \quad (4b)$$

$$\frac{d\varepsilon}{dt} = i\delta\varepsilon - \gamma\varepsilon + \frac{i\omega_a}{2} \rho + \tilde{F}^\dagger(t) \quad (4c)$$

where $\delta \equiv \omega - \omega_0$. Equation (4c) includes a damping term and a random force $\tilde{F}^\dagger(t)$ that account for the coupling of the radiation mode to the thermal reservoir of the cavity walls. It can be shown that the probability of excitation at time t is given by

$$P_e(t, N) = \frac{1}{N} \langle \eta(t, N, \theta(0)) \rangle_{\theta(0)} + \frac{1}{2} \quad (5)$$

where the average over $\theta(0)$ is carried out over an appropriate distribution of initial angles arising from thermal fluctuations.

There is no general way to parametrize the behavior of the atom-cavity system, but for underdamped motion one feature is particularly easy to observe experimentally: this is the time τ_{\min} at which $P_e(t, N)$ achieves its first minimum. We define the "collapse frequency" ν_{col} by

$$\nu_{\text{col}} \equiv (2\tau_{\min})^{-1} \quad (6)$$

Although $P_e(t, N)$ is a complicated function of the system parameters, Haroche⁵ has pointed out that the variation of ν_{col} with the number of atoms N can be accurately parameterized by

$$\nu_{\text{col}}(N) = \frac{a\sqrt{N}}{b + \ln N} \quad (7)$$

where a and b are adjustable parameters that depend on ω_a , γ , and β . The accuracy of this expression is illustrated by figure 1 which displays values of ν_{col} obtained from the exact solution [equation (3)] for $N \leq 50$ and from the Bloch method [equation (5)] for $N \geq 200$, along with the best fit of equation (7) to the calculations.

The experiments employ an atomic beam of calcium Rydberg atoms and a split superconducting cavity operated at 35 GHz. At the ambient temperature of 2 K, the mean blackbody photon number is 0.8. Selective

⁶ B.J. Hughey, *Cavity Modified Atom-Photon Interaction*, Ph.D. diss., Dept. of Physics, MIT, 1989.

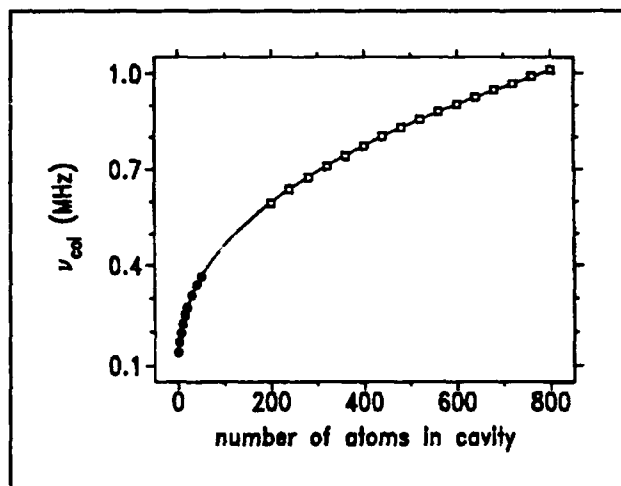


Figure 1. Dependence of the "collapse" frequency ν_{col} on number of atoms N for $Q = 1.2 \times 10^7$ and $T = 2.17\text{K}$. The filled circles are obtained from the exact method and the open squares from the Bloch method, as discussed in the text. The solid curve is a fit of the calculations to equation (7), which yields $a = 0.3187\text{MHz}$ and $b = 2.245$.

field ionization allows us to monitor simultaneously the populations of the initial and final states. The time evolution of the atomic system is probed by "Stark switching." The collective oscillations of energy between ensembles of atoms and a cavity with $Q > 10^7$ are being studied for one to several hundred atoms.

The experiment is carried out with the apparatus shown in figure 2. A calcium atomic beam is prepared in the $46p$ state (abbreviation for the $4s46p\ ^1P_1$ state) inside the cavity using a three-step pulsed dye laser system. The final laser beam is polarized along the cavity electric field so that the $46p(m=0)$ state is excited relative to this quantization axis. The two states involved in the atom-cavity oscillations are thus the $46p(m=0)$ (upper state) and $46s$ (lower state). The frequency of the $46p \rightarrow 46s$ transition in calcium is 35.332 GHz ; the atom-cavity coupling frequency $\omega_a/2\pi$ calculated for this transition and our cavity dimensions is 105 kHz . Observing underdamped behavior for a single atom in the cavity requires $Q > 2 \times 10^6$. To avoid undesirable effects of blackbody radiation, the one-atom experiments require temperatures $\lesssim 2\text{K}$, for which $\bar{n} \lesssim 0.8$.

The atoms are excited inside the cavity. The mean transit time to the cavity exit is 18

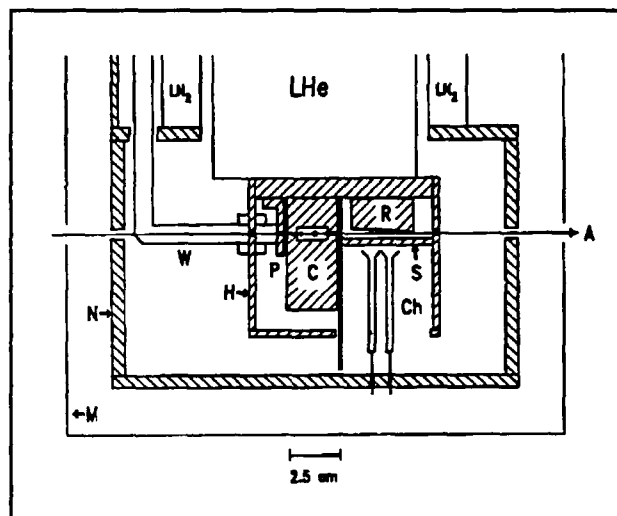


Figure 2. Diagram of the apparatus, side view. A: atomic beam, H: liquid helium temperature shield, N: liquid nitrogen temperature shield, M: single layer mu-metal shield, P: collimating plate of 2 channel field ionization detector, C: cavity, R: ramped plate, S: slotted plate, Ch: channel electron multipliers, W: waveguide, L: laser beams, B: waveguide holder, Co: coupler. The tuning mechanism is not shown for clarity.

μsec , which corresponds to two cycles of the single-atom-cavity oscillation. After the atoms exit the cavity, they enter the detector region where selective field ionization is used to detect and differentiate the two states. We measure $\bar{P}_e(t, N)$ for each value of N by scanning the time t when a 200 mV pulse is applied between the cavity halves. (N is the mean number of atoms in the cavity.) In this way, we count the number of atoms detected in the $46p$ and $46s$ states as a function of the atom-cavity interaction time. Sample data are shown in figure 3.

An important feature of the experiment is the use of a split superconducting cavity. By applying an electric field between the two halves, the atomic resonance can be shifted far from resonance with the cavity, thereby terminating the atom-cavity interaction. This effectively freezes the atomic population at the moment at which the voltage pulse is applied. By using a carefully designed choke groove structure, we suppress leakage from the cavity and achieve a quality factor $Q > 10^7$ in niobium and lead-plated copper cavities.

A series of time evolution curves for various values of \bar{N} was studied. Figures 4 and 5

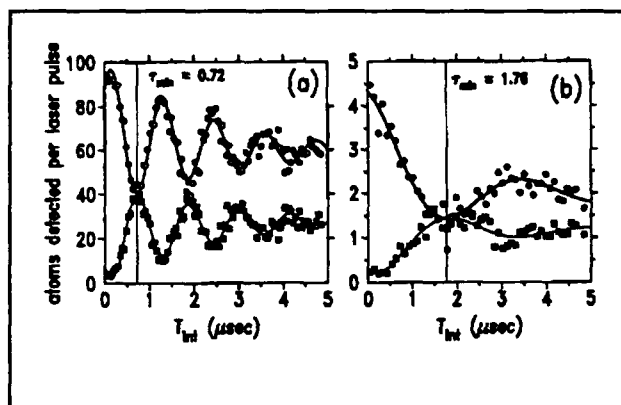


Figure 3. Observed atom-cavity oscillations for $Q = 1.18 \times 10^7$ and $T = 2.17\text{K}$ for two values of N_d . The solid curves are fits of the data to damped sinusoids, from which ν_{col} is extracted. The open circles are the atoms detected in the 46p state, and the filled squares are the atoms detected in the 46s state. T_{int} is the atom-cavity interaction time.

display some of the data along with the calculated time evolution curves.

We also compared our results with theory for a single atom in the cavity. Single atom experiments are of special significance because they represent the limit of small systems. Furthermore, they have the experimental advantage of being free of much of the uncertainty in detection efficiency, assuming that the mean number of atoms detected per pulse is small compared to unity. For these studies, we generally operated with an average of 0.04 atoms detected per laser pulse. The observed and calculated evolution of a single atom in the cavity with $Q = 1.5 \times 10^6$ and $T = 1.95\text{K}$ are shown in figure 6. We believe that the damping which is evident in the data is due to stray electric and magnetic fields, and possibly thermal effects.

In support of these studies, we also carried out a high resolution study of the microwave spectrum of calcium Rydberg states. The results are described in a thesis,⁷ and in the publications listed below.

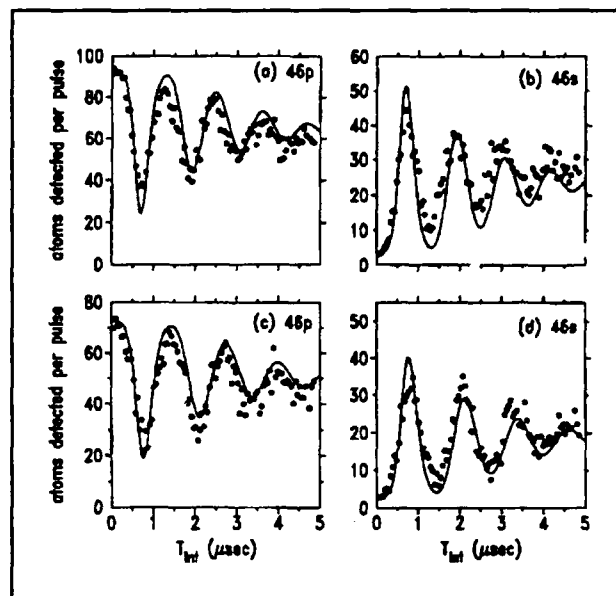


Figure 4. Comparison of calculated and observed evolution of the system for large ensembles of atoms in the cavity. The filled circles are the number of atoms detected in the 46p and 46s states as a function of atom-cavity interaction time T_{int} . The amplitudes of the theory curves are scaled to compare with data but there are no other adjustable parameters. (a) and (b): $N = 380$. (c) and (d): $N = 300$.

Publications

Gentile, T.R., B.J. Hughey, T.W. Ducas, and D. Kleppner. "Experimental Study of Two-Photon Rabi Oscillations." Paper presented at the Sixth Conference on Coherence & Quantum Optics, Rochester, New York, June 1989.

Gentile, T.R. *Microwave Spectroscopy and Atom-Photon Interactions in Rydberg States of Calcium*. Ph.D. diss. Dept. of Physics, MIT, 1989.

Gentile, T.R., B.J. Hughey, T.W. Ducas, and D. Kleppner. "Microwave Spectroscopy of Calcium Rydberg States." *Phys. Rev. A*. Accepted for publication.

Hughey, B.J., T.R. Gentile, T.W. Ducas, and D. Kleppner. "A Split High Q Superconducting Cavity." Submitted to *Rev. Sci. Instrum.*

⁷ T.R. Gentile, *Microwave Spectroscopy and Atom-Photon Interactions in Rydberg States of Calcium*, Ph.D. diss. Dept. of Physics, MIT, 1989.

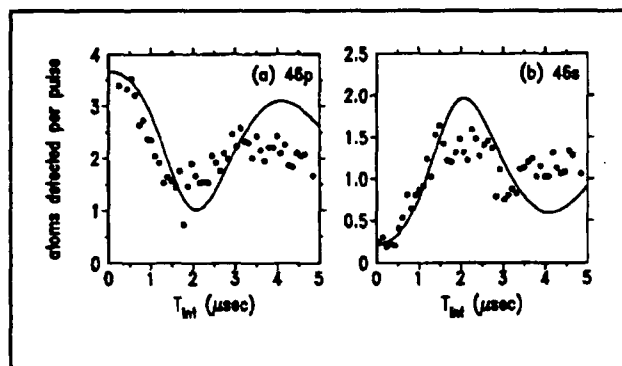


Figure 5. Similar to figure 4, but with $\bar{N} = 15$.

Hughey, B.J., T.R. Gentile, T.W. Ducas, and D. Kleppner. "Experimental Study of Small Ensembles of Atoms in a Microwave Cavity." Submitted to *Phys. Rev. A*.

Hughey, B.J., T.R. Gentile, T.W. Ducas, and D. Kleppner. "Atom-Photon Interaction Modified by a Microwave Cavity." Paper presented at the Sixth Conference on Coherence & Quantum Optics, Rochester, New York, June 1989.

Hughey, B.J., T.R. Gentile, D. Kleppner, and T.W. Ducas. "A Study of One- and Two-Photon Rabi Oscillations." *Phys. Rev. A* 40:5103 (1989).

Hughey, B.J. *Cavity Modified Atom-Photon Interaction*. Ph.D. diss. Dept. of Physics, MIT, 1989.

2.2 Rydberg Atoms in a Magnetic Field

Sponsor

National Science Foundation
Grant PHY 87-06560

Project Staff

George R. Welch, Chun-Ho Lu, Long Hsu, Michael W. Courtney, Professor Daniel Kleppner

A hydrogen atom in a strong magnetic field poses a fundamental challenge to atomic theory. The Hamiltonian looks almost trivial, but, in fact, no general solution yet exists and important aspects of the problem remain a mystery. If the atom is in a low-lying energy state, the magnetic effect can be

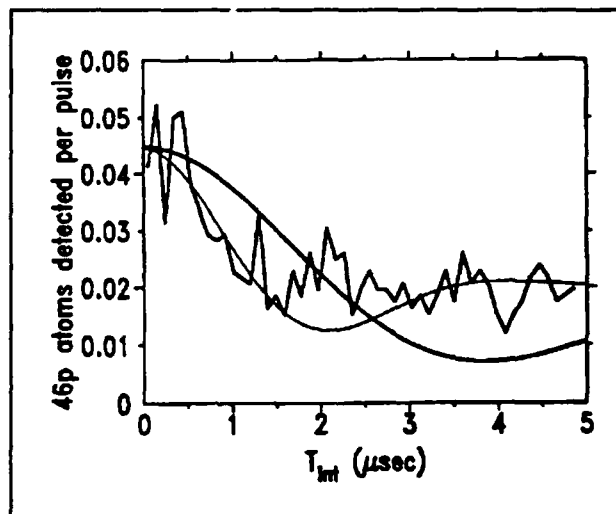


Figure 6. Observation of the time evolution with a single atom in the cavity. The solid curves are calculations for $Q = 1.5 \times 10^6$, $T = 1.95\text{K}$ (dark line) and $T = 9\text{K}$ (light line).

treated as a perturbation. However, for an atom in a Rydberg state, the magnetic interaction is comparable to the Coulomb interaction and perturbation theory fails completely. Although calculations based on diagonalizing as many as 200,000 basis states were carried out, theorists cannot yet predict energy levels for high-lying Rydberg states and for positive energy (continuum) states. Experiments are essential for guiding new theoretical approaches.

Our research centers on high resolution spectroscopy of Rydberg atoms in a magnetic field. Recent results include the study of: (1) anticrossings between energy levels, which provide information on mixing between levels in a regime of "approximate symmetry"; (2) quantum behavior in the regime where the classical system exhibits strong chaotic motion; and (3) energy level structure and ionization mechanisms when the energy is above the ionization limit.

The experiment employs two c.w. dye lasers to excite an atomic beam of lithium inside of a superconducting solenoid. (Lithium is essentially hydrogen-like, but with small differences which are of some interest in their own right.) The first laser excites the atom from the 2S to the 3S state by a two-photon transition; the second laser excites the atom to a Rydberg state with a single photon. Atoms which are excited to Rydberg states

are detected by electric field ionization in a region outside of the excitation region. The wavelength of the second laser is measured by using an etalon as a transfer standard between the Rydberg lines and iodine absorption lines. (The iodine lines and the free spectral range of the etalon are themselves calibrated relative to the zero-magnetic field lithium Rydberg spectrum.) The resolution and absolute energy accuracy are $\sim 10^{-3}\text{cm}^{-1}$. The magnetic field is determined by exciting $|\Delta m| = 1$ transitions and measuring the paramagnetic splitting of the $n=21$ manifold.⁸ The accuracy in field is $\sim 10^{-4}\text{T}$.

"Level repulsion," the tendency for energy levels to avoid crossing each other as the magnetic field is changed, provides information on the coupling between levels. We studied level repulsion effects due to the presence of lithium core electrons. In addition, we studied the level repulsion that occurs due to the inherent nature of the diamagnetic interaction. Figure 7 shows the first experimental study of level repulsion due to the diamagnetic interaction. The disappearance of the *lower* state is a characteristic feature which distinguishes this anticrossing

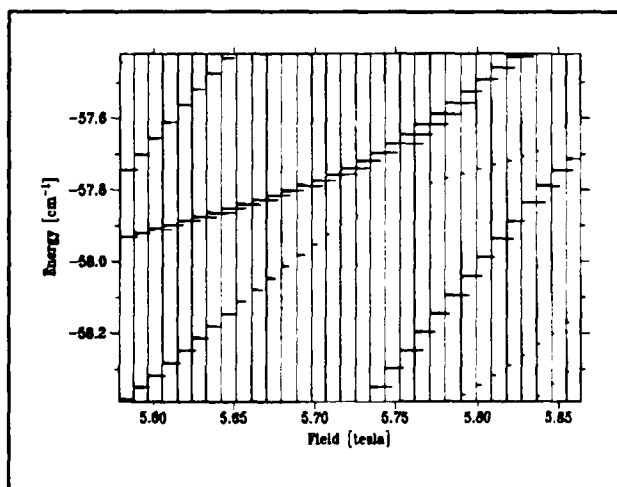


Figure 7. An example of a diamagnetic anticrossing induced by the breakdown of an approximate symmetry.

from a lithium core-induced anticrossing. The diamagnetic anticrossing is a result of a breakdown of an approximate symmetry of the system. The theory for this anticrossing, which is close to the region of complete chaos, is still not complete.⁹

When the energy is above the zero point energy of the free electron-magnetic field system, the atom can spontaneously ionize. We observed the first high resolution spectra near and above the ionization limit.¹⁰ Figure 8 shows some of these spectra. We discovered many narrow resonances in this regime. The lifetimes of the narrow resonances are greater than a few thousand cyclotron periods. Such long lifetimes are unexpected on the basis of classical studies.

We also found that states which approach the ionization limit form a series similar to the Rydberg series of the unperturbed atoms. Moreover, we discovered additional Rydberg-like series that each converge to one of a sequence of Landau levels. The system behaves as if the motion were separable. Because the atom-magnetic field system is confined in the direction perpendicular to the magnetic field, the quantum states extend along the magnetic field direction and behave like a one-dimensional hydrogen atom. As a result, traverse Landau energy is simply added to the longitudinal Rydberg energy. The discovery of orderly structure in a regime that is believed to be chaotic suggests that either the connection between quantum mechanics and chaos is not well understood, or that a good deal of order is possible in a region of chaos. Systematic study is continuing on the structure and linewidth of the positive energy resonances and the mechanisms of ionization.

During this past year, we have also carried out the first high resolution study of the atom-magnetic field system in the regime where classical motion undergoes a transition from regular to chaotic motion. The com-

⁸ M.M. Kash, G.R. Welch, C. Iu, and D. Kleppner, *Spectrochimica Acta A* 45: 57 (1989).

⁹ D. Delande and J.C. Gay, *Phys. Rev. Lett.* 57: 2006 (1986).

¹⁰ G.R. Welch, M.M. Kash, C. Iu, L. Hsu, and D. Kleppner, *Phys. Rev. Lett.* 62: 1975 (1989); C. Iu, G.R. Welch, M.M. Kash, L. Hsu, and D. Kleppner, *Phys. Rev. Lett.* 63: 1133 (1989).

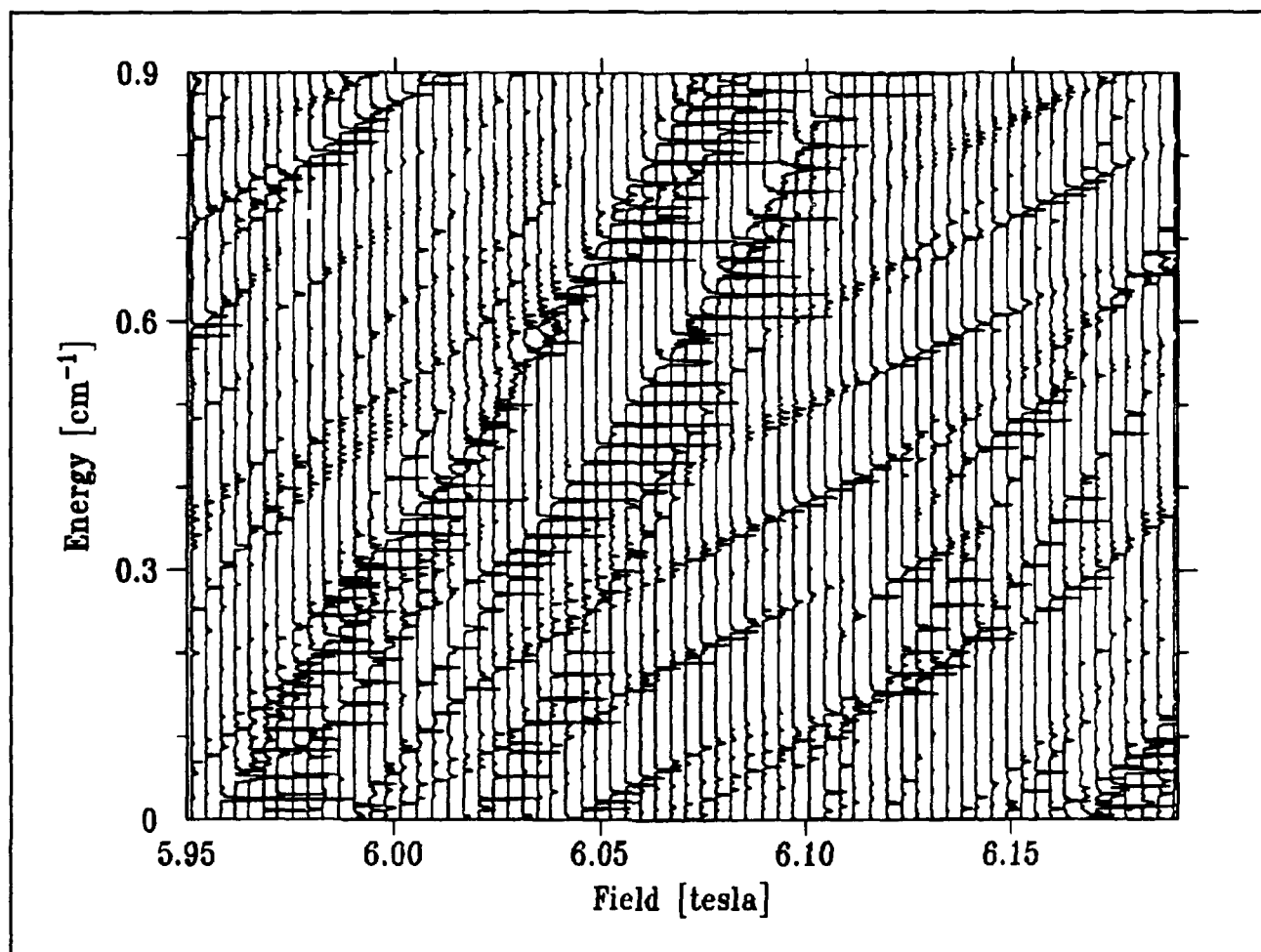


Figure 8. Positive energy spectra with magnetic field increments 50 gauss. The Rydberg series converging to the second Landau level can be seen as parallel and equal spaced levels with a slope of $1.7 \text{ cm}^{-1}/\text{T}$.

monly used tool for the study of quantum chaos is energy level statistics. Such studies require locating and resolving each level in a pure sequence, for example odd parity, $m=0$ states. The task becomes experimentally difficult when the system approaches chaos because small electric fields can cause mixing with states of opposite parity, and a small misalignment of the polarization can introduce states of $m = \pm 1$. Consequently, theoretical guidance is required to identify the states in the particular sequence under study. Figure 9 shows our recent progress in calculating levels for high Rydberg states in a magnetic field. The calculation is done by diagonalizing about 2,700 states of lithium using an IBM RT computer.

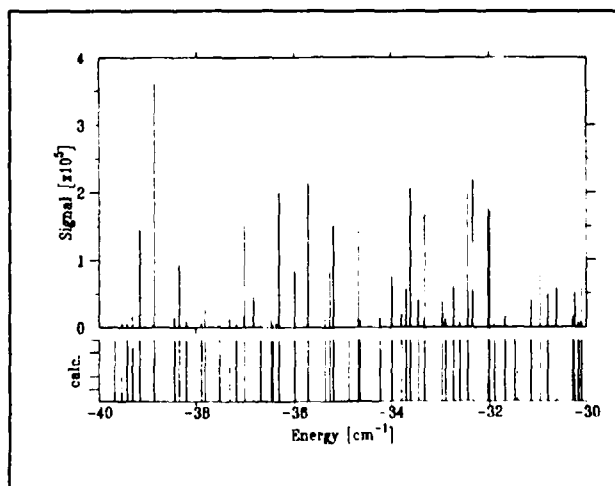


Figure 9. Spectrum of lithium atom in magnetic field of 6.1 T. Above: Experimental spectrum. Below: Calculated spectrum. The difference between experiment and calculation is less than 10^{-2} cm^{-1} .

Publications

Iu, C-H., G.R. Welch, M.M. Kash, L. Hsu, and D. Kleppner. "Orderly Structure in the Positive Energy Spectrum of a Diamagnetic Rydberg Atom." *Phys. Rev. Lett.* 63: 1133 (1989).

Kash, M.M., G.R. Welch, C-H. Iu, and D. Kleppner. "Diamagnetic Structure of Lithium $n \approx 21$," *Spectrochimica Acta* 45A: 57 (1989).

Welch, G.R., M.M. Kash, M. Michael., C-H. Iu, L. Hsu, and D. Kleppner. "Positive Energy Structure of the Rydberg Diamagnetic Spectrum." *Phys. Rev. Lett.* 62: 1975 (1989).

Welch, G.R., M.M. Kash, C-H. Iu, L. Hsu, and D. Kleppner. "Experimental Study of Energy Level Statistics in a Regime of Regular Classical Motion." *Phys. Rev. Lett.* 62: 893 (1989).

Welch, G.R. *High Resolution Spectroscopy of Rydberg Atoms in a Magnetic Field*. Ph.D. diss. Dept. of Physics, MIT, 1989.

2.3 Millimeter-Wave Measurement of the Rydberg Constant

Sponsor

National Science Foundation
Grant PHY 87-06560

Project Staff

Pin P. Chang, Scott Paine, Robert P. Lutwak, James P. Schwonek, Professor Daniel Kleppner

The Rydberg constant R is prominent among the fundamental constants as the primary atomic standard of length. Recent experiments determined R to an accuracy of nearly one part in 10^{10} , using optical spectroscopy.¹¹ The limitation to these measurements is not the inherent precision of the experiment but

the accuracy of the wavelength standard. It is now generally accepted that optical wavelengths cannot be compared to a precision greater than 1 part in 10^{10} . One consequence of this limitation is that length is now defined in terms of the distance traveled by light in a fixed time interval, rather than in terms of a certain number of optical wavelengths. Thus, wavelength measurements of R appear to have reached a natural barrier.

We are attempting to advance the precision of R by measuring it in frequency units. (The specific quantity we shall measure is cR). We shall accomplish this by measuring millimeter wave transitions between Rydberg states of hydrogen. Because the frequency of millimeter radiation can be measured to the full precision of modern atomic clocks, the experiment is not limited by metrological standards.

The goal of our experiment is three-fold: First is the reevaluation of R itself. Second is the measurement of the Lamb shift. Because our measurements involve high angular momentum states for which the Lamb shift is extremely small, a comparison of our results with optical measurements can yield an improved value of the Lamb shift. Third is the precise frequency calibration of the spectrum of hydrogen to allow an independent check of optical frequency metrology as it starts to advance.

We are determining the Rydberg constant by measuring the frequency of the $|n = 29 \rightarrow n = 30|$ "circular" transition in atomic hydrogen, using the Ramsey separated oscillatory field method. The experiment is designed to achieve an accuracy of 1 part in 10^{11} , an order of magnitude improvement over the present state of the art.¹¹ The transition frequency, 256 GHz, is low enough to allow us to use established techniques to phase lock our millimeter-wave source directly to a cesium primary frequency standard.

At the time of our last progress report, we had completed construction of an atomic

¹¹ F. Biraben et al., *Phys. Rev. Lett.* 62: 621 (1989); Zhao et al., *Phys. Rev. Lett.* 58: 1293 (1987); M.G. Boshier et al., *Nature* 330: 463 (1971).

beam apparatus with a cold (10K–80K) atomic hydrogen source and had demonstrated the population of the $n=29$ state by two-photon absorption via the 2p state, and the adiabatic transfer of the atoms to the high angular momentum state via the crossed fields method of Delande and Gay.¹²

During the past year, we experimented with an alternative excitation scheme for the Rydberg state, using three-step excitation to $n=29$ through the 2p and 3s states. This

effort included the development of a single-mode tunable pulsed YAG-pumped titanium sapphire laser. For the present, however, we have returned to our original method. Also, we developed a flexible, CAMAC-MAC-based data acquisition system. Using this, we studied the hydrogen intensity and dissociation within the discharge (see figure 10). The system is also being applied to numerous tasks in the diagnosis and control of the apparatus.

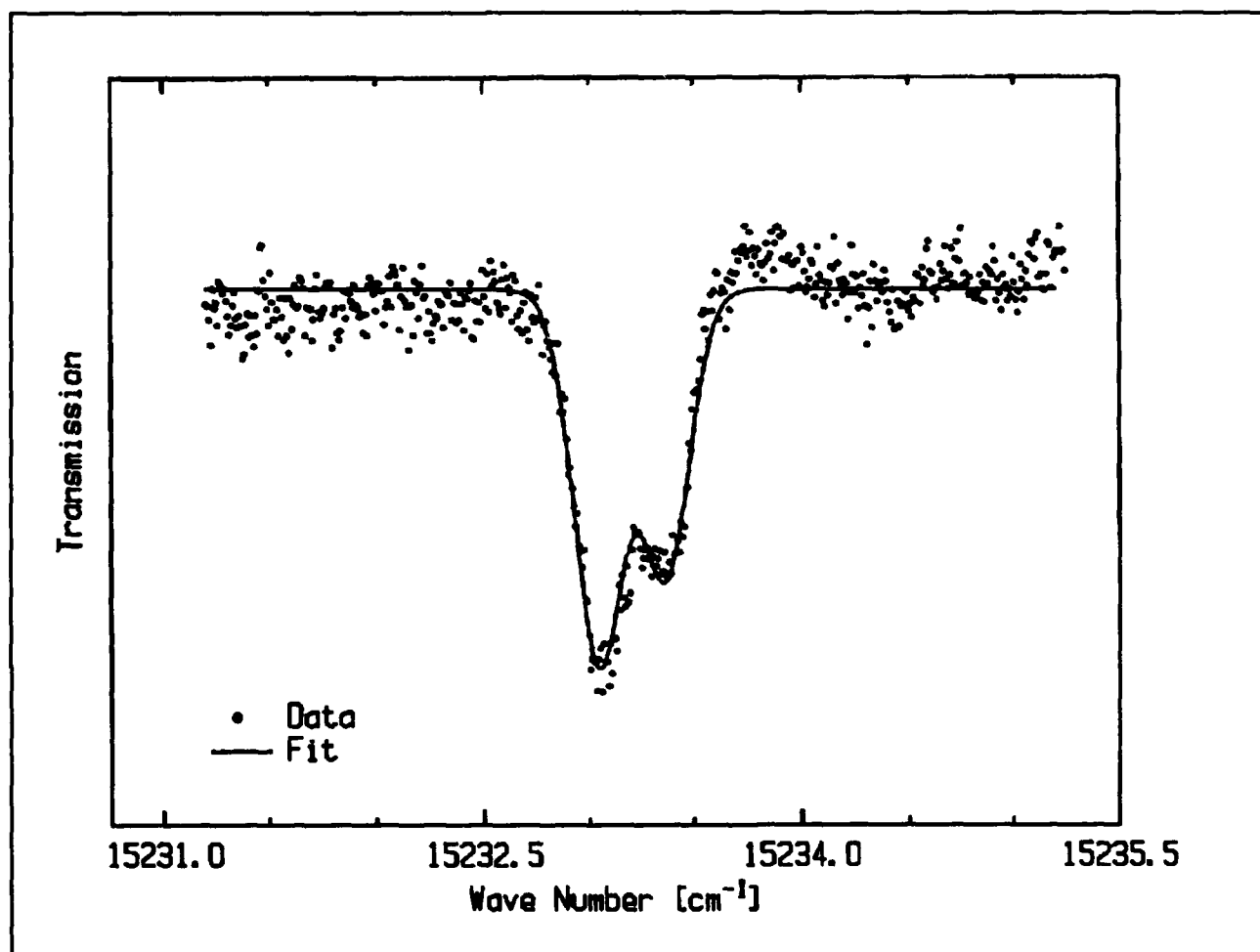


Figure 10. Transmission of pulsed dye laser through the rf discharge in the atomic beam source. The theoretical fit to the doppler-broadened spectrum indicates a discharge temperature of approximately 400 K. The hydrogen is subsequently cooled to produce a 10-80 K atomic beam.

The millimeter wave system is a critical element in the experiment. We have continued the development of quasi-optical

components for the manipulation and detection of the millimeter wave radiation, including lenses, beamsplitters, and

¹² D. Delande and J. C. Gay, *Europhys. Lett.* 5:303 (1988).

polarizers. A scanned antenna-coupled pyroelectric detector system has been developed for mapping the millimeter wave beam profiles. A map of the radiation profile at the atomic beam is shown in figure 11.

We have begun designing the controlled field region in which the actual measurement will take place and hope to complete construction of the apparatus in the coming year. Efforts are also continuing to optimize the hydrogen beam source and the efficiency of the circular state production.

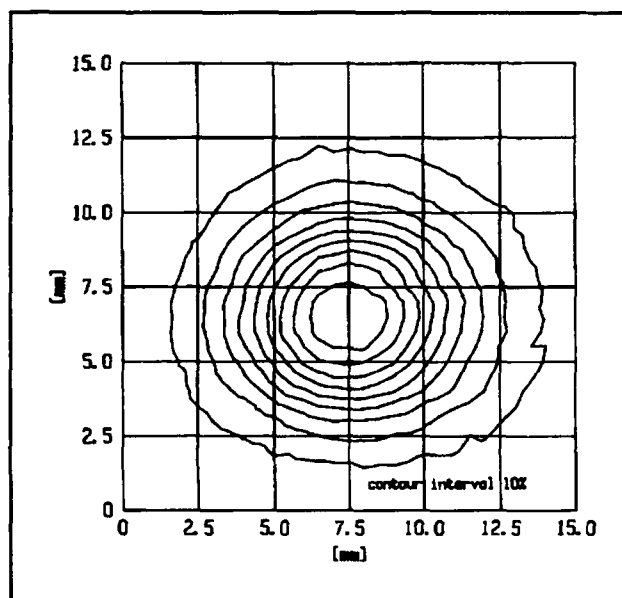


Figure 11. Intensity profile of the 256 GHz radiation used to drive the $n = 29 \rightarrow n = 30$ circular transition.

2.4 Precision Mass Spectroscopy of Ions

Sponsors

Joint Services Electronics Program
Contract DAAL03-89-C-0001
National Science Foundation
Contract PHY 86-05893

Project Staff

Kevin R. Boyce, Eric A. Cornell, Deborah Kuchnir,
Professor David E. Pritchard

In 1989, we made the first mass comparison of single trapped ions, raising the state of the

art for fractional precision in mass measurement to 4×10^{-10} . This is a first step toward our ultimate goal of determining the mass of individual atomic and molecular ions with precisions of 10^{-11} or better. This precision will give us the capability of making experiments that address issues in both fundamental and applied physics:

- The $^3\text{H}^+ - ^3\text{He}^+$ mass difference is important in ongoing experiments to measure the electron neutrino rest mass.
- Excitation and binding energies of typical atomic and molecular ions can be determined by weighing the small decrease in energy: $\Delta m = E_{\text{bind}}/c^2$.
- Experiments that weigh γ -rays can be used in a new method to determine Avogadro's number, N_A , a key fundamental constant whose accurate determination would permit the replacement of the artifact mass standard by an atomic mass standard.
- Traditional applications of mass spectroscopy should benefit from the several orders of magnitude improvement in both accuracy and sensitivity which our approach offers over conventional techniques.

In our experimental approach, we measure ion cyclotron resonance on a single molecular or atomic ion in a Penning trap, a highly uniform magnetic field with axial confinement provided by weaker electric fields. We monitor ions, oscillating along magnetic field lines, by the currents induced in the trap electrodes. Working with only a single ion is essential because space charge from other ions leads to undesired frequency shifts. This work in trapping and precision resonance draws on techniques developed by Hans Dehmelt at the University of Washington and Norman Ramsey at Harvard University, for which they shared the 1989 Nobel Prize.

Our most notable accomplishment this year was determining the carbon monoxide-molecular nitrogen mass ratio to an accuracy

of 4×10^{-10} .¹³ The ratio of the cyclotron frequencies of the two ions is the inverse of the ratio of the masses as long as the magnetic field remains constant. By trapping first a single N_2^+ ion and measuring its frequency, and then swapping to a single CO^+ ion, and then back again to N_2^+ , we are able to correct for drifts in the magnetic field to about 0.5 parts per billion (see figure 12).

We have developed techniques for driving, cooling, and measuring the frequencies of all three normal modes of Penning trap motion. Thus, we can manipulate the ion position reproducibly to within 30 microns of the center of the trap, correcting for electrostatic shifts in the cyclotron frequency to great accuracy. We use a π -pulse method to coherently swap the phase and action of the cyclotron with the axial modes.¹⁴ Therefore, although we detect only the axial motion directly, we can determine cyclotron frequency by measuring how much phase accumulates in the cyclotron motion in a known time interval (see figure 13).

Currently, precision is limited by magnetic field imperfections and temporal instabilities. Achieving our long range goal of 10^{-11} precision requires either dramatic improvements in field stability or simultaneous comparison of two different ions. With two ions of equal charge, the ion-ion perturbations are very similar for each ion and, hence, do not introduce significant uncertainty in the mass ratio. Our group has succeeded in trapping a single CO^+ ion and a single N_2^+ ion simultaneously.¹⁵ In the coming year, we plan to develop techniques for making precision resonance measurements on two ions simultaneously.

Publications

Cornell, E.A., R.M. Weisskoff, K.R. Boyce, R.W. Flanagan, G.P. Lafyatis, and D.E. Pritchard. "Single-Ion Cyclotron Resonance Measurements of $M(CO^+)/M(N_2^+)$." *Phys. Rev. Lett.* 63:1674 (1989).

Cornell, E.A., R.M. Weisskoff, K.R. Boyce, and D.E. Pritchard. "Mode Coupling in a Penning Trap: π Pulses and a Classical Avoided Crossing." *Phys. Rev. A* 41:312 (1990).

Kuchnir, D.L. *Trapping and Detecting Two Different Single Ions at Once: A Step Towards Ultra-High-Precision Mass Comparison Measurements*. B.S. thesis. Dept. of Physics, MIT, 1989.

2.4.1 Atom Interferometry

Sponsors

Joint Services Electronics Program
Contract DAAL03-89-C-0001
U.S. Army Research Office
Contract DAAL03-89-K-0082
U.S. Navy - Office of Naval Research
Contract N00014-89-J-1207

Project Staff

Chris R. Ekstrom, David W. Keith, Bruce G. Oldaker, Quentin Turchette, Professor David E. Pritchard

Using fabricated transmission gratings as optical elements for the matter waves, we are constructing an atom interferometer to physically separate atom waves before recombining them. This interferometer will be useful in studies of atomic properties, tests of basic quantum physics, for metrology, as rotation sensors, and, perhaps, ultimately as devices to make ultra-small structures using atom holograms.

¹³ E.A. Cornell, R.M. Weisskoff et al., *Phys. Rev. Lett.* 63:1674 (1989).

¹⁴ E.A. Cornell, R.M. Weisskoff et al., *Phys. Rev. A* 41:312 (1990).

¹⁵ D.L. Kuchnir, *Trapping and Detecting Two Different Single Ions at Once: A Step Towards Ultra-High-Precision Mass Comparison Measurements*, B.S. thesis, Dept. of Physics, MIT, 1989.

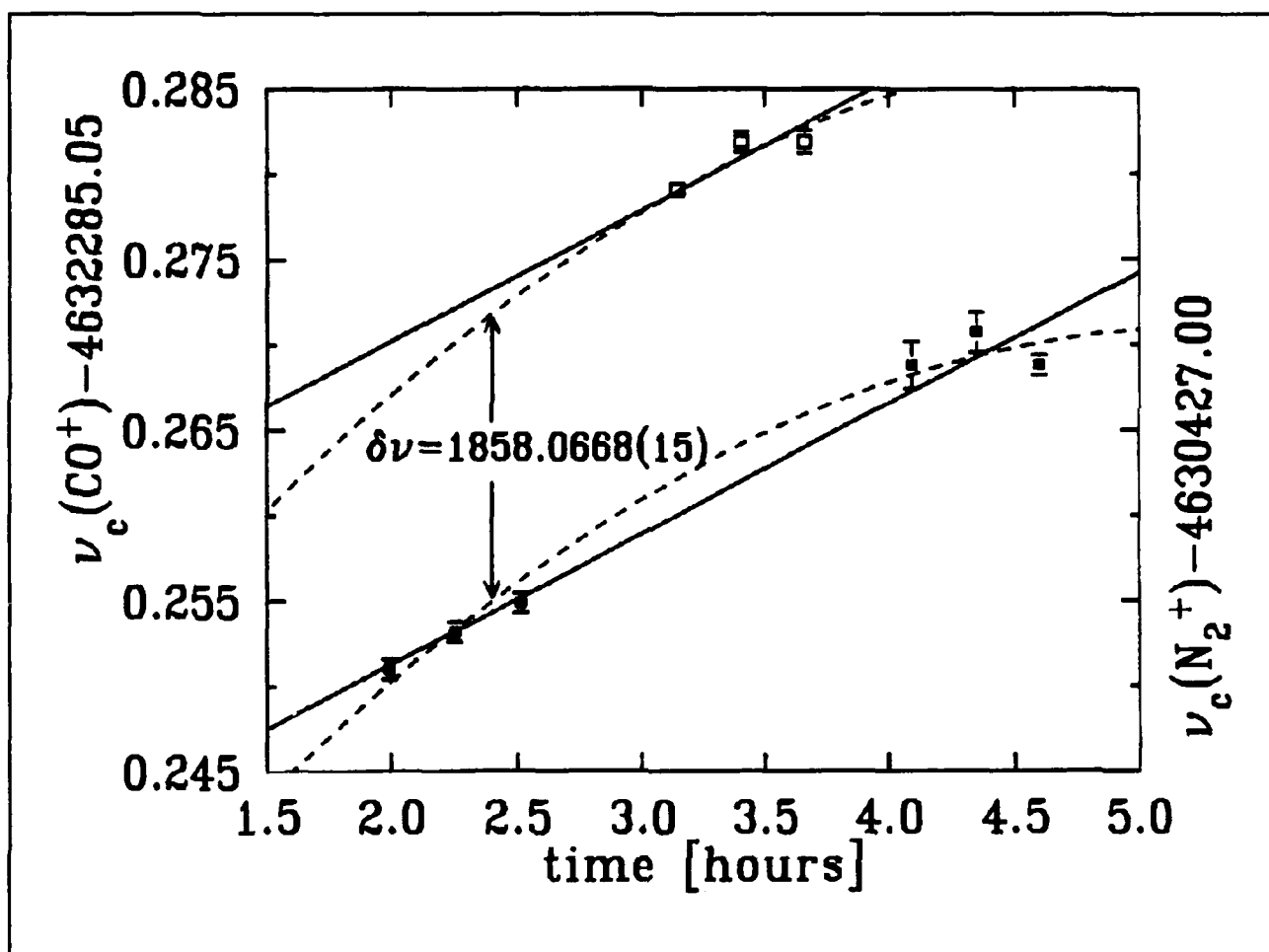


Figure 12. The data from a mass comparison run are shown. The solid squares (open squares) are the cyclotron frequency of $N_2^+(CO^+)$. A total of three ions were loaded in the order $N_2^+ - CO^+ - N_2^+$. The solid lines are a fit to the two frequencies assuming a field drift that is linear in time. The dotted-line assumes a quadratic field drift. The indicated value for the difference frequency results from the latter assumption, and corresponds to $M(CO^+)/M(N_2^+) = 0.9995988876(3)$.

During the last year, our atom interferometer evolved from a rough plan to an essentially complete device. At present, we have tested all its major components at least once. We will test the complete system during the coming year.

Our interferometer consists of three $0.2\ \mu\text{m}$ -period diffraction gratings equally spaced $\sim 0.65\ \text{m}$ apart in our atomic beam machine. The maximum separation of the beams will be $\sim 60\ \mu\text{m}$. The first two gratings separate and redirect the atomic beam forming a standing wave interference pattern in the atomic flux at the third grating, which acts like a mask to sample this pattern.

We can estimate our anticipated final signal strength from the properties of the individual

gratings. Attenuation caused by the primary grating and the grating support structure gives an intensity in the 0^{th} order of \sim one-eighth of the incident intensity and one-sixteenth in each of the ± 1 orders. The final intensity detected at the maximum of a fringe after transmission through all three gratings can be calculated by summing the amplitudes for the two sides of the interferometer and will be 0.005 of the incident intensity. The fringe constant will be 4 to 1, so the interference signal will be 0.004 of the incident intensity. We are anticipating that the final interference signal through the interferometer will be $\sim 4 \times 10^3$ counts per second. This should generously exceed the noise of the detector ($\leq 100\ \text{sec}^{-1}$).

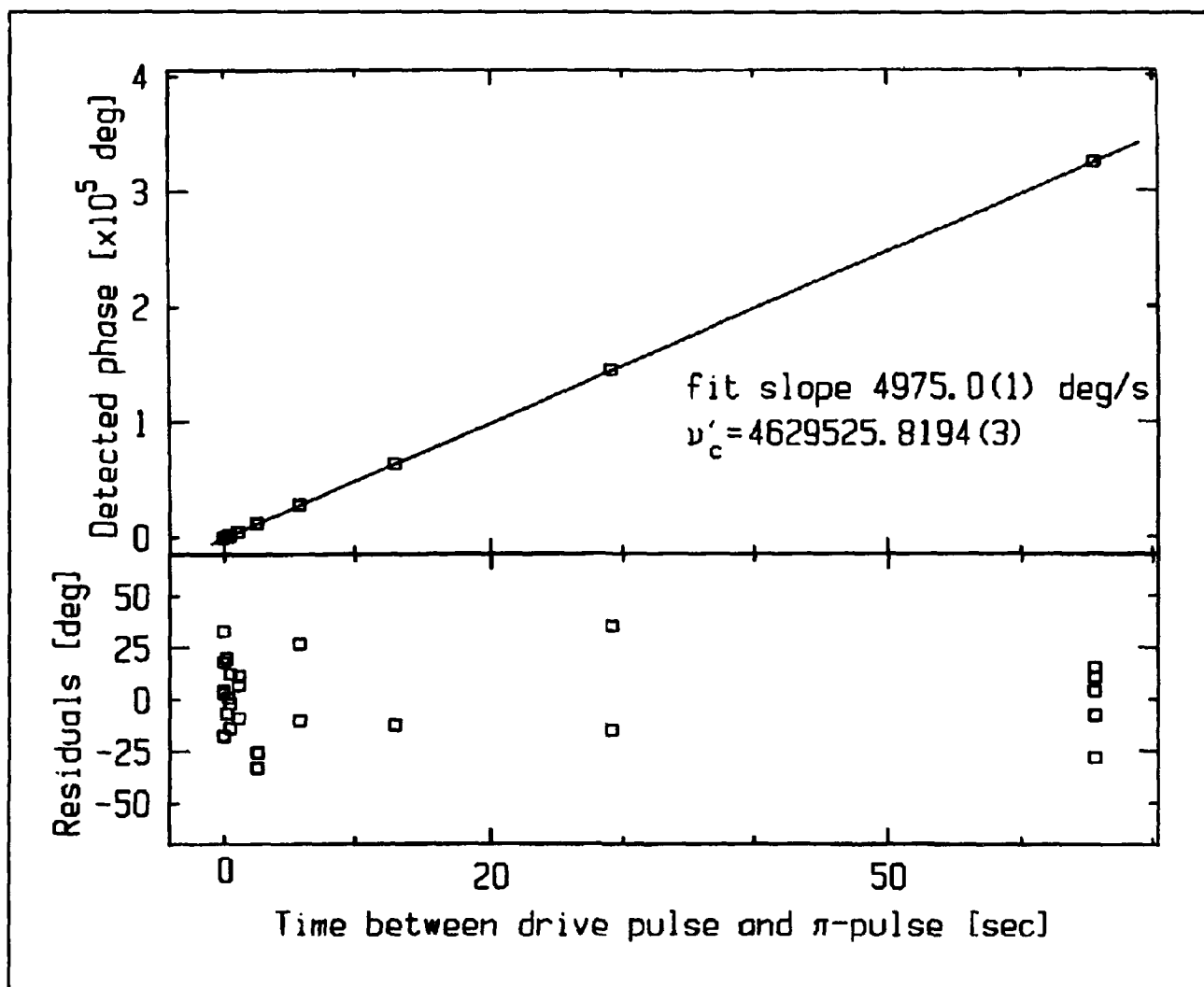


Figure 13. For each plotted point, we perform the following experiment: The initially cold ion is pulsed into a cyclotron orbit of known initial phase and then allowed to evolve "in the dark" for an indicated amount of time, t . Then a pulse is applied which exchanges cyclotron and axial motions, bringing the ion's cyclotron action and phase into the axial mode. As the ion's axial motion rings down, its phase is detected. The appropriate multiple of 360° is added, and a line is fitted to the points. The slope of the line is the frequency difference between the frequency generator and the trap cyclotron frequency.

The mechanical vibrations of our machine are a principal technical obstacle because they could blur the interference pattern. There are two types of required limits on vibrations. First, the three gratings must move relative to each other by less than $\sim 1/4$ period (50 nm) during the time the final grating samples the intensity at a given position. Thus, the rms amplitude of relative vibrations integrated over all frequencies greater than the reciprocal of the integration time must be less than ~ 50 nm. The second requirement is related to the motion of the gratings due to acceleration of, or rotation about, the center of mass of the grating system during the 1.3

ms time it takes for the atoms to traverse the interferometer. This means that below ~ 900 Hz the rms acceleration must be less than 10^{-2} ms^{-2} , and the rms angular velocity must be less than 10^{-5} radians per second.

We have solved our vibration problem by using a combination of passive isolation and active feedback. The passive isolation system consists of small pneumatic feet which act like damped springs to support the machine and give it a 3-Hz resonant frequency. This isolates the machine from building noise at higher frequencies. We have used the active feedback system to stabilize the relative posi-

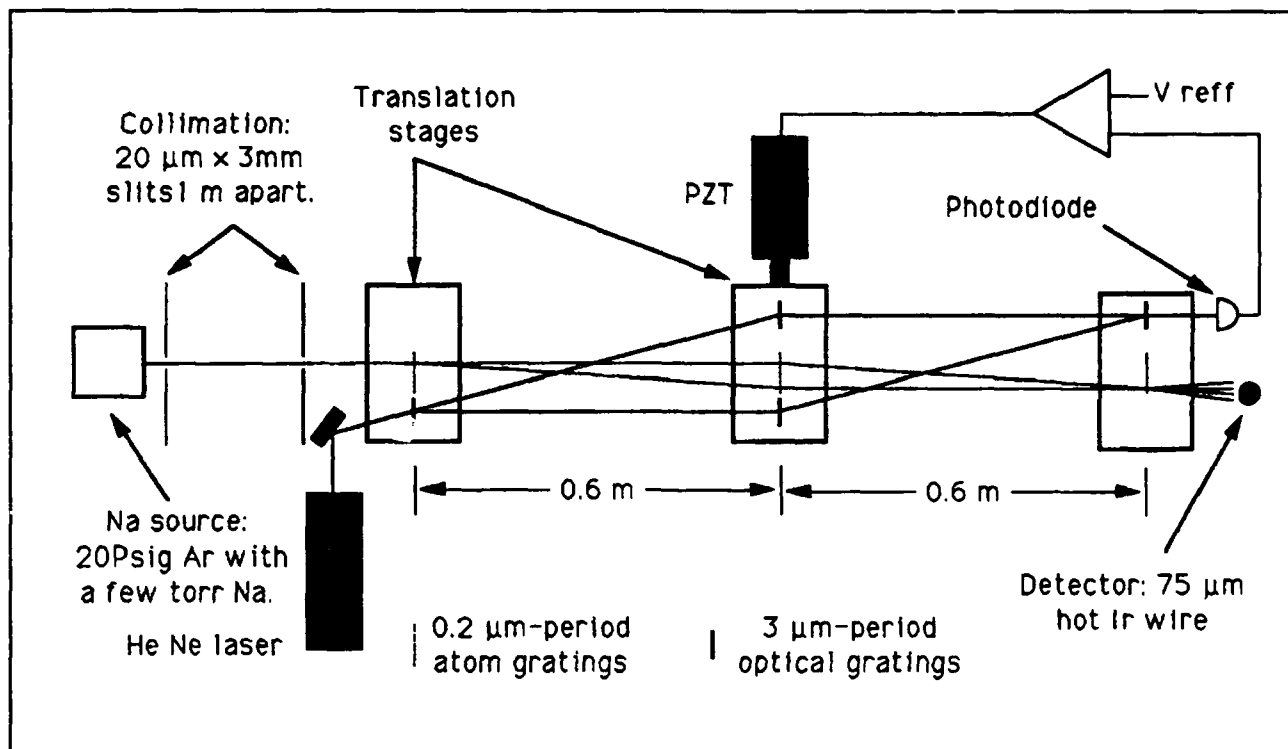


Figure 14. Our current atom interferometer with laser interferometer vibration isolation system is shown. (Not to scale.)

tions of the three gratings at frequencies below ~ 150 Hz. This system works best at low frequencies (< 10 Hz) where the passive system is least effective. The reduction of relative motion provided by the active system will allow us to use much longer integration times when we are looking for the interference signal. The active feedback system uses a laser interferometer which has the same transmission grating geometry as the atom interferometer. We mounted the gratings for the optical interferometer on the same three translation stages as the matter wave gratings to record the exact relative orientation of the matter wave interferometer. We apply the signal from the optical interferometer to provide a measure of the relative alignment of the three grating platforms to a Piezoelectric translator (PZT) through a feedback network to stabilize the platforms (figure 14). With this system, we have adequately reduced the relative rms motion (at frequencies less than 0.3 Hz) of the gratings from ~ 1500 to 40 nm. We also reduced the rms acceleration in a frequency range to which the interferometer is sensitive from 1.1×10^{-2} to $2.3 \times 10^{-3} \text{ ms}^{-2}$, which is safe by a factor

~ 5 , ensuring sufficiently low angular velocities of the apparatus.

We have also made significant progress in overcoming another technical obstacle, the relative alignment of the atom gratings. For all points along the height (3 mm) of our ribbon shaped beam to have the same phase of interference signal, the gratings must be aligned to an angle of $\sim 10^{-5}$ rads. with respect to rotations about the beam axis. We accomplished this by using a technique based on the optical polarizing properties of the gratings.

In addition to the work on vibrations and alignment mentioned above, our main progress during 1989 was construction of the various mechanical components that position the gratings inside the vacuum envelope. Also, we have written computer software and built electronic hardware to control the position of the three grating platforms and the detector, and the height, angle and position of the second collimating slit. Instead of directly varying the voltage of the PZT that controls the position of the last grating, now we will use the computer to vary the null point of the active feedback

system when we are searching for interference fringes.

When we have successfully demonstrated this interferometer, our first experimental objective will be a demonstration of Berry's phase with bosons. Another experiment could be an improved measurement of the Aharonov-Casher effect.

Publications

Keith, D.W., and D.E. Pritchard. "Atom Optics." In *New Frontiers in QED and Quantumoptics*. New York: Plenum Press. Forthcoming.

Keith, D.W., M.L. Schattenburg, H.I. Smith, and D.E. Pritchard. "Diffraction Gratings from Atoms." *QELS Conference*, Baltimore, Maryland, April 1989.

Oldaker, B.G., P.J. Martin, P.L. Gould, M. Xiao, and D.E. Pritchard. "Experimental Study of Sub-Poissonian Statistics in the Transfer of Momentum from Light to Atoms." Submitted to *Phys. Rev. Lett.*

Pritchard, D.E., and B.G. Oldaker. "Light Forces and Atom Diffraction: An Illustrated Summary." Paper presented at the *Sixth Conference on Coherence*, Rochester, New York, 1989.

Pritchard, D.E. Experimental Studies of Atom Diffraction and the Mechanical Forces of Light on Atoms, *NICOLS Conference*. Bretton Woods, New Hampshire: Academic Press, 1989.

2.5 Neutral Atom Trap

Sponsors

U.S. Navy - Office of Naval Research
Contracts N00014-83-K-0695 and
N00014-89-J-1207

Project Staff

Kristian Helmerson, Michael A. Joffe, Dr. Min Xiao, Ke-Xun Sun, Professor David E. Pritchard

We have trapped large numbers of neutral atoms, and cooled them to millikelvin temperatures. Our next objective is to cool them to microkelvin temperatures. Dense samples of atoms cooled to microkelvin temperatures promise to open up new and exciting areas of physics. The lack of interaction of the low velocity atoms due to their reduced thermal motion, together with the possibility of indefinitely long interaction times, make samples of trapped atoms ideal for high resolution spectroscopy and for use as atomic frequency standards. High density samples of ultra-cold atoms will also make possible new studies of interatomic collisions and collective effects, such as Bose condensation. We have made progress using our existing magnetic trap. In addition, we started a new project to develop a continuous source of slow atoms to load into future magnetic traps.

2.5.1 Magnetic Trap for Neutral Atoms

Now that techniques for trapping neutral atoms are well established,¹⁶ the field of neutral atom trapping has moved from infancy to adolescence and the emphasis is now on doing experiments with the trapped atoms.

Currently, our main effort in neutral atom trapping is cooling trapped atoms to low temperatures. While this remains a difficult and elusive goal (to date, we have only achieved microkelvin temperatures with untrapped atoms), the rewards for supercooling trapped atoms are significant. The long confinement times, together with the reduced thermal motion of cold atoms, could result in a new era of ultra-high resolution spectroscopy and precise frequency standards. Potentially more exciting is the possibility of combining the high densities achievable in traps and the long deBroglie

¹⁶ D.E. Pritchard, K. Helmerson, and A.G. Martin, "Atom Traps," in *Atomic Physics*, 11, eds. S. Haroche, J.C. Gay, and G. Grynberg (Singapore: World Scientific, 1989), pp. 179-97.

wavelength of ultra-cold atoms to observe novel quantum collective phenomena.

At present, we are trying to demonstrate cyclic cooling of magnetically trapped neutral atoms.¹⁷ A combined laser and radio frequency cooling scheme should allow us to cool our atoms to microkelvin temperatures. During the past year, we tried a newly designed cyclic cooling scheme that operates in a magnetic field of less than 300 gauss. (We currently trap atoms at a minimum field of 1500 gauss.) We have modified our superconducting magnets so that our trap operates at low magnetic fields. This modification, resulting in improved decoupling of the trapped atoms from the powerful slowing laser, could allow us to load more atoms into the trap than was previously possible. In addition, we have made many other modifications to the magnetic trap to optimize detection of cooled atoms and to extend the lifetime of the trapped atoms. We plan to test this trap during 1990.

As the only group in the world capable of doing both rf and laser spectroscopy of trapped atoms, we have performed laser fluorescence and absorption spectroscopy of magnetically trapped sodium atoms. Currently, we are analyzing the data from this research. Studying the theory of the radiative decay of densely confined atoms, we have found a substantial modification of the spontaneous decay rate of trapped atoms due to their quantum statistics. Finally, we completed a study of the Zeeman-tuned laser slowing process in the magnetic trap.¹⁸

2.5.2 Slow Atom Source

During 1989, we began building a simple, intensive and continuous source of slow atoms which can also separate the atoms from the laser light used to slow them. Separating the atoms is a crucial requirement, permitting additional low intensity laser light to collimate, focus and cool the slow beam further. This source of slow atoms is useful for loading traps or for atomic beam experiments because we do not have to introduce intense slowing laser light.

The technique we developed uses a continuous "zeeman slower,"¹⁹ a spatially varying magnetic field, to compensate the changing Doppler shift of the atoms in the slowing process and a second orthogonal laser beam to deflect and extract the slowed atoms. This simple, compact system has a 25-cm long zeeman slower and ignores atoms which start with thermal velocities greater than 600 meters/second. Since it slows only the low velocity portion of the Maxwell-Boltzman distribution, a low oven temperature (about 180 centigrade) is desirable. With this low temperature, the slower needs a large orifice to provide the requisite flux.

The major difficulty in making a continuous and intense slow atomic beam is in effectively extracting slowed atoms from the strong, slowing laser beam. We will extract the slowed atoms in a region of low magnetic field by using light pressure from a beam with two frequencies to circumvent optical pumping to hyperfine levels not excited by the laser. Figure 15 shows the configuration of the experimental arrangement.

In the zeeman slower, the slowing laser slows atoms with velocities smaller than 600 meters/second at position a to about 150 meters/second at position b where the magnetic field is held near zero. The deflection

¹⁷ D.E. Pritchard, "Cooling Neutral Atoms in a Magnetic Trap for Precision Spectroscopy," *Phys. Rev. Lett.* 51:1336-39 (1983).

¹⁸ V.S. Bagnato, G.P. Lafyatis, A. Martin, K. Helmerson, J. Landry, and D.E. Pritchard, "Laser Deceleration and Velocity Bunching of a Neutral Sodium Beam," *J. Opt. Soc. Am. B* 6: 2171-77 (1989).

¹⁹ J.V. Prodan, W.D. Phillips, and H. Metcalf, *Phys. Rev. Lett.* 49:1148 (1982).

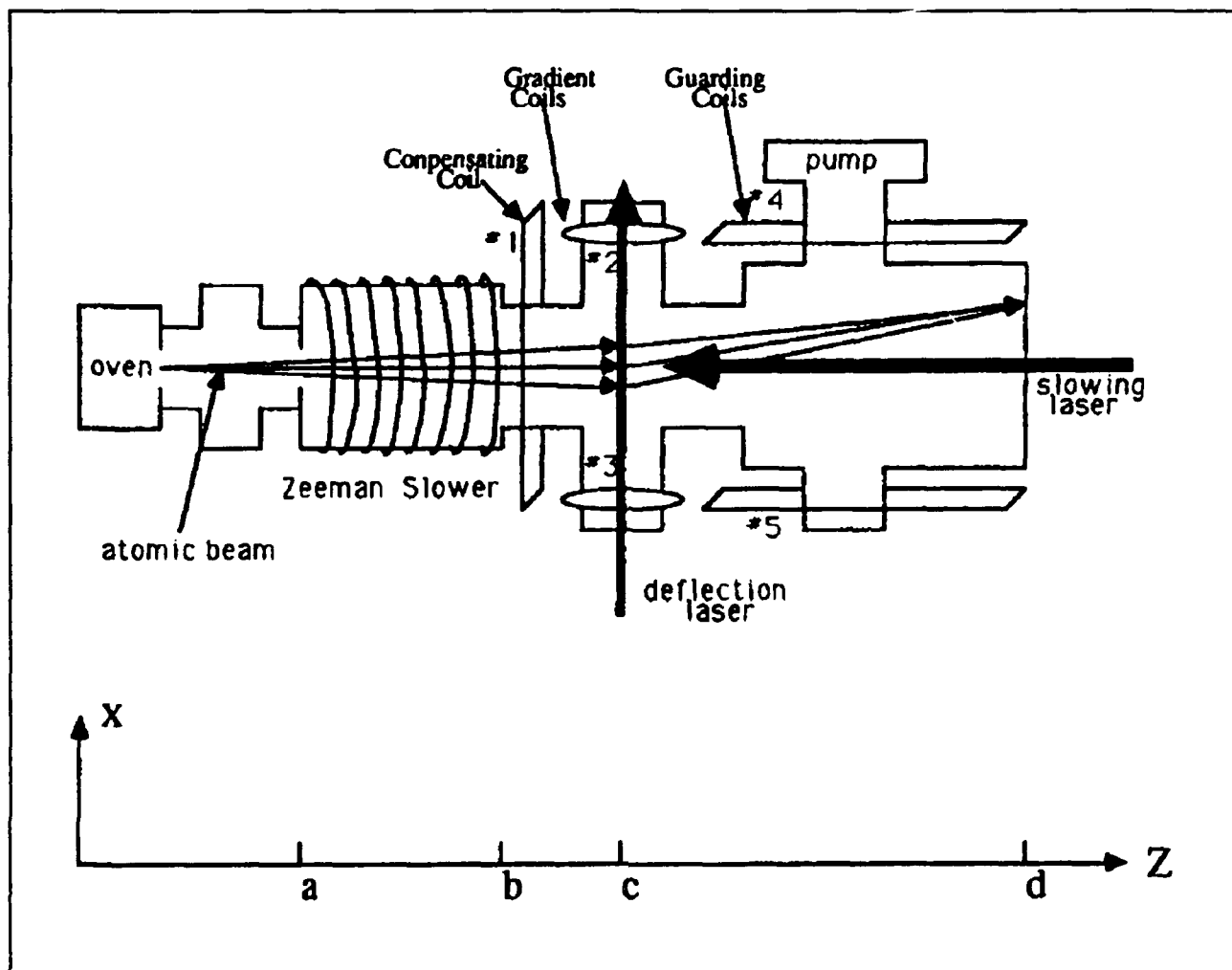


Figure 15. Schematic diagram of the slow-atom source.

laser deflects atoms slowed further by the intense slowing laser beam to velocities below 100 meters/second at c. c is right circular polarized with a strong sideband spaced at 1.77 GHz to repump the $F=1$ ground state atoms. So far, we have observed slowing of nearly 10^{10} atoms per second with photodetectors mounted inside the zeeman slower.

Publications

Bagnato, V.S., G.P. Lafyatis, A. Martin, K. Helmerson, J. Landry, and D.E. Pritchard. "Laser Deceleration and Velocity Bunching of a Neutral Sodium Beam." *J. Opt. Soc. Am. B*: 2171 (1989).

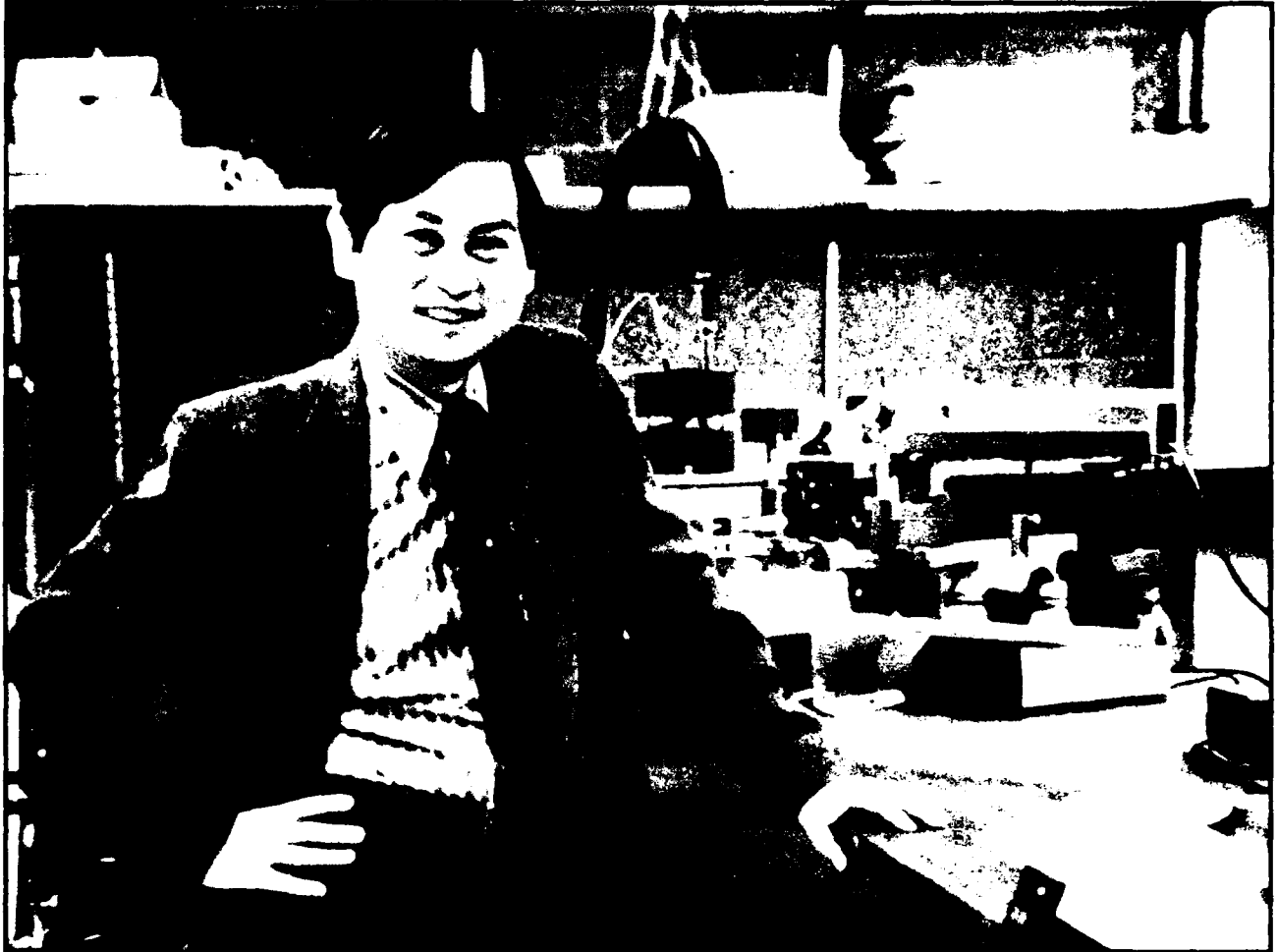
Gallagher, A., and D.E. Pritchard. "Exoergic

Collisions of Cold Na^+-Na ." *Phys. Rev. Lett.* 63:957 (1989).

Gould, P.L., P.J. Martin, G.A. Ruff, R.E. Stoner, J.-L. Picque, and D.E. Pritchard. "Momentum Transfer to Atoms By a Standing Light Wave; Transition From Diffraction to Diffusion." Submitted to *Phys. Rev. Lett.*

Pritchard, D.E. "Atom Optics." In *McGraw-Hill Yearbook of Science and Technology*. Forthcoming.

Pritchard, D.E., K. Helmerson, and A.G. Martin. "Atom Traps." In *Proceedings of the 11th International Conference on Atomic Physics*. Paris, 1988.



Professor Sow-Hsin Chen

Chapter 3. Small Angle X-Ray and Neutron Scattering — Its Application to Supramolecular Solutions

Academic and Research Staff

Professor Sow-Hsin Chen

Visiting Scientists and Research Affiliates

Pierandrea Lo Nostro,¹ Dr. Jacque Rouch,² Dr. Piero Tartaglia,³ Dr. Xiu-Bing Wei

Graduate Students

Bruce L. Carvalho, Szu-Li Chang, Xuan-Hui Guo, Vivian Leung

Undergraduate Student

John Chen

3.1 Interlayer Diffusion in Langmuir-Blodgett Films

Project Staff

Bruce L. Carvalho, Professor Sow-Hsin Chen

The Langmuir-Blodgett film deposition technique has recently been used to fabricate a variety of dense electronic and nonlinear optics devices on a single crystal silicon surface. An important technological problem arises from the use of this technique: the interdiffusion of polymer and surfactant molecules between multilayers in Langmuir-Blodgett films directly affects the stability of these films (as a function of temperature and age).

We have recently used the neutron surface specular reflection technique to study the dynamics of interdiffusion of polymer and surfactant molecules in Langmuir-Blodgett films. With this new technique, we can obtain the normal surface density profile at a spatial resolution of 10 Å. By varying the time-temperature annealing history, we observed the interdiffusion in a stepwise

fashion, also with a spatial resolution of 10 Å.

Figures 1a and 1b illustrate examples of our measurements. The system shown consists of 5.5 repeat units of deuterated surfactant/protonated optically active polymer, each component having approximately 25 Å thick layers. The first three peaks of the reflectivity curve come from an interference pattern of the total film thickness (about 270 Å); the fourth peak is a Bragg reflection from a lattice spacing of 53 Å. We measured this sample twice: immediately after we made it (figure 1a), and after it was annealed at 60°C for 10 minutes (figure 1b). A significant finding was that the interdiffusion of polymer and surfactant molecules during the annealing process completely destroyed the Bragg peak. This is a striking example of mutual diffusion at a length scale of about 10 Å, a distance scale which is difficult to measure by any other means in a hydrocarbon system.

In future experiments, we plan to increase the number of repeat units in the film,

¹ Department of Physical Chemistry, University of Florence, Italy.

² Physics Department, University of Bordeaux, France.

³ Physics Department, University of Rome, Italy.

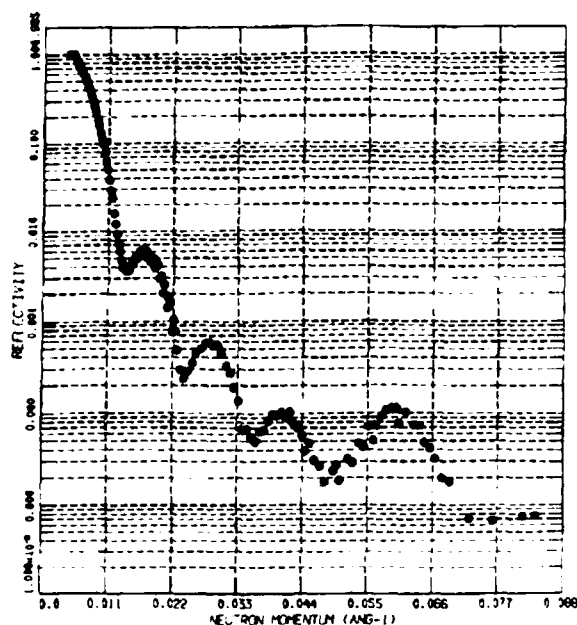


Figure 1a. Reflectivity vs. momentum transfer for the system 5 (deuterated cadmium arachidate - PECH polymer) - deuterated cadmium arachidate - silicon substrate, before annealing.

enhance the Bragg peak, and possibly observe intermediate intensities before the Bragg peak is destroyed. We then plan to extract the interdiffusion coefficient directly from the decay of the Bragg peak in time, as has been done in artificially modulated metallic thin film systems. In addition, we plan to perform a series of experiments on bilayer samples in which layers of deuterated surfactant are stacked on top of a layer of protonated polymer. We will anneal these samples, extracting the interdiffusion coefficient from the concentration profile of deuterium across the surfactant-polymer interface.

3.2 Thermodynamics of Protein/Surfactant Complex in Aqueous Solution and Reptation Mechanism for Protein/SDS Polyacrylamide Gel Electrophoresis

Project Staff

Xuan-Hui Guo, Professor Sow-Hsin Chen

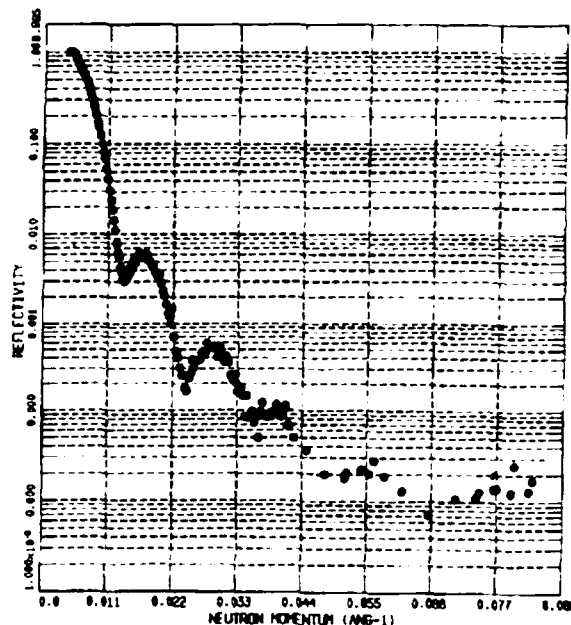


Figure 1b. Reflectivity vs. momentum transfer for the same system as figure 1a but after annealing, 10 minutes at 60°C.

During the past few years, we have studied the structure of bovine serum albumin (BSA)/sodium dodecylsulfate (SDS) complexes in solutions by small angle neutron scattering (SANS). From the quantitative interpretation of SANS intensity distributions, we concluded that BSA/SDS complexes in high ionic strength solution were most likely flexible polymer-like objects. Currently, we are exploring the consequences of our SANS studies. We recently discovered two significant phenomena: (1) polymer-like phase separation of the BSA/SDS complexes in solution; and (2) reptation behavior of the complexes migrating through a gel during electrophoresis.

Pertaining to the first phenomenon, we successfully discovered the specific conditions ($\text{pH} \leq 5.0$, ionic strength = 0.6M) under which the complexes undergo polymer-like phase separation in an accessible temperature range. We determined the cloud-point curve (CPC) of the complexes in solution. Then, we carried out the light scattering along an isotherm above CPC in the one-phase region to approximately determine the critical volume fraction, which we found to

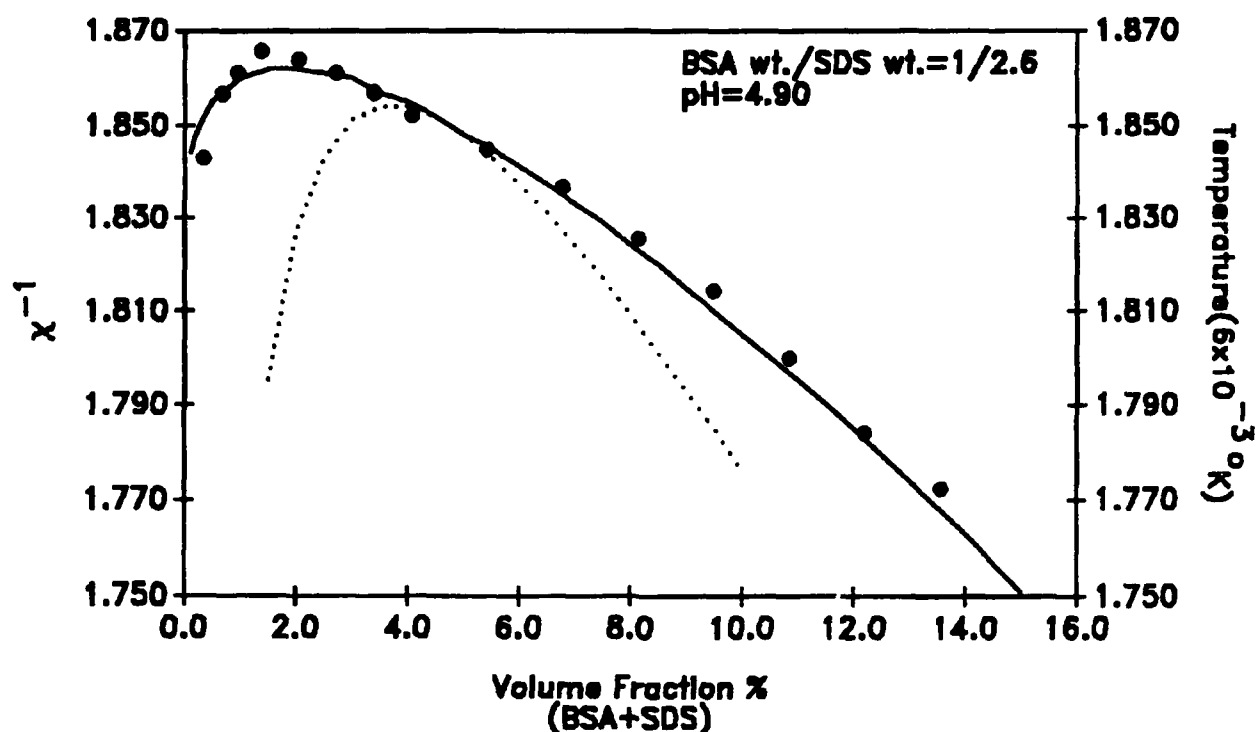


Figure 2. Comparison of the experimental cloud-point curve (CPC) with the theoretical CPC calculated using the generalized Flory-Huggins theory for polydisperse polymers in solution. The filled circles are the experimental cloud-point temperature scaled by the factor 6×10^{-3} and vs. ϕ_s curve. The solid line is the theoretical χ^{-1} calculated using a polydispersity index $Z = 1$ and an average effective chain length $\lambda_1 = 676$. The dashed line is the spinodal line corresponding to the CPC.

be about 4.5 percent. The critical point was located on the right branch of the CPC similar to synthetic polydisperse polymers.

To calculate the theoretical CPC, we applied the generalized Flory-Huggins (F.-H.) theory for polydisperse polymers. This theory was in strikingly good agreement with our experiment. Thus, our thermodynamic analyses also establish that the BSA/SDS complexes in solution are polymer-like objects. We are particularly interested in further exploring the complete ternary phase diagram of the protein/SDS/H₂O system and in more precisely locating the critical point.

Evidence accumulated from our SANS studies and phase separation study strongly supports the view that protein/SDS complexes in solution are polymer-like objects. We propose a reptation mechanism for the explanation of the migration of the pro-

tein/SDS complexes in polyacrylamide gel during electrophoresis. According to our model, the polymer-like object undergoes one-dimensional worm-like motions in a tube formed by the consecutive pores housing the molecule in the three-dimensional mesh of the gel. Electrophoretic data taken from four independent experiments confirms our conjecture. We discovered a power-law, namely mobility, that is inversely proportional to protein molecular weight within a broad range of molecular weights. The exact physical mechanism underlying this technique is not clearly understood, even though it is popular in protein chemistry and engineering. Further investigation of the influence of various parameters, such as electric field, ionic strength, temperature and gel concentration on mobility would increase our fundamental understanding of, and possibly improve, this popular biochemical technique.

3.3 Phase Separation in a Lipid/Water/Urea Micellar System

Project Staff

Bruce L. Carvalho, John Chen, Professor Sow-Hsin Chen

We have found that the upper consolute temperature of the dioctanoylphosphatidylcholine-water micellar system can be dramatically lowered by adding a small amount of urea. We found the lowering of the consolute temperature to be a linear function of urea concentration. After determining the cloud point curves for this micellar system at several urea concentrations in both water and heavy water, we analyzed the system in terms of a recent thermodynamic theory of micellar phase separation proposed by Blankschtein, Thurston and Benedek. This theory connects the phase separation phenomena to the micellar growth and polydispersity and the monomer-monomer interaction in the single phase region.

We performed three separate measurements on the dioctanoylphosphatidylcholine-heavy water [urea] = 1 Molar micellar system in the single phase region. We measured: (1) the temperature dependence of the critical micellar concentration; (2) small angle neutron scattering intensity distributions at dilute concentrations; and (3) static light scattering over a wide range of concentrations. We also measured the cloud point curve for this particular system. We made consistent analysis of these four measurements using the ladder model of micellar growth and this recent theory of micellar phase separation. We can explain the experimental data from these four measurements with the same set of model parameters.

3.4 Ion Distribution and Solubilization in Reverse Micelles

Project Staff

Bruce L. Carvalho, Vivian Leung, Professor Sow-Hsin Chen

This project concerns the thermodynamics of the preferential solubilization of multivalent cations into the interior of reverse microemulsions. We will use the results of this project to understand the removal of metal ions from a waste stream by microemulsions. The thermodynamics of ion solubilization depend on the distribution of ions in the water core of the reverse microemulsion.

We recently established a procedure for determining the ion distribution. We assume that a fraction of the counterions in the water core are localized at the surfactant head groups. The concentration of the remaining free ions varies with the electrostatic potential in the water core which can be expressed as solution of the Poisson-Boltzmann (P-B) equation. We have used this theoretical ion distribution to calculate the angular distribution of scattered x-ray intensities, comparing them with the experimental small angle x-ray scattering data. The preliminary results indicate that only a small fraction (30 percent) of the counterions are free in the water core of the microemulsion.

3.5 Ion Distribution around DNA Molecules

Project Staff

Szu-Li Chang, Professor Sow-Hsin Chen

Nucleic acids are highly charged molecules, and electrostatic interactions play an important role in many aspects of their structure and function. Electrical force is an important component of protein-DNA and drug-DNA interactions. For this reason, the study of the distribution of ions around DNA has received considerable attention in recent years.

In our project, we used small angle x-ray scattering (SAXS) to measure counterion distribution around the persistence length DNA molecules in aqueous solutions both with and without salts. We chose heavy metal counterions such as Tl^+ and Ba^{++} to enhance the counterion contribution to the scattering intensity (by a factor of Z^2), resulting in a measurable effect. Figure 3a shows the SAXS intensity distribution $I(Q)$ vs. Q in a semilog plot. This sample contains 2.5 mg/ml of thallium-DNA without added

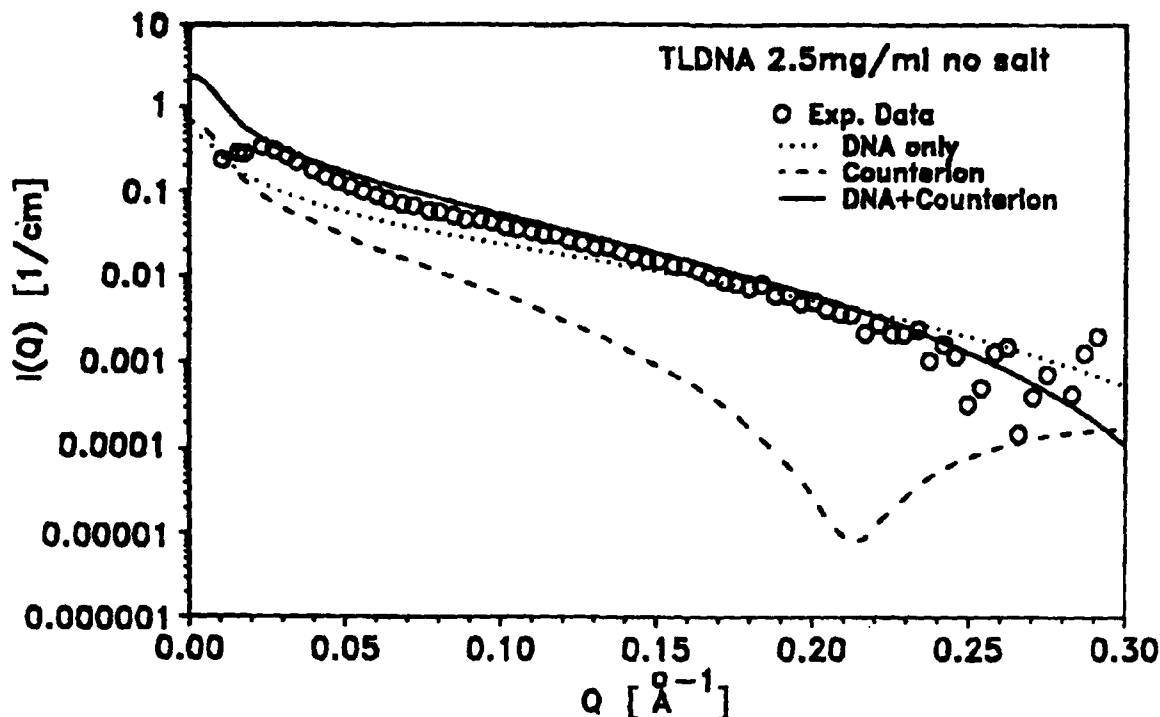


Figure 3a. SAXS intensity distribution $I(Q)$ vs. Q in a semilog plot. The sample contains 2.5 mg/ml of persistence length DNA. The counterion has been exchanged to Tl^+ by an extensive dialysis. There is a residual $TlCl$ on the order of 0.1 mM in the solution. The dotted line represents the contribution from the DNA core only, while the dashed line that from the counterions. The solid line represents the total calculated scattering intensity. Note, the solid line is not the sum of the dotted line and the dashed line because contribution from the DNA core and from the counterions do not add incoherently.

salt. The open circles represent the experimental data, the solid line represents the theoretical calculation. The dotted line represents the partial contribution of the DNA only, and the dashed line those of the counterions. The figure shows that, without taking into account the contribution of counterions, there would be poor agreement between the experiment and the theory. Figure 3b depicts the scattering length densities used to calculate the intensity. We calculated the intensities shown in figure 3a by assuming that 10 percent of the counterions are inside the DNA core, neutralizing 10 percent of the phosphate groups. If we exclude the counterions from the DNA core completely, the computation would not agree as well quantitatively with the experiment. We found similar agreement for the case of 4.2 mg/ml of thallium-DNA in a solution containing 10 mM of $TlCl$ and 3.7 mg/ml of

barium-DNA in a solution containing 5 mM of Ba_2Cl . The slight discrepancy between the experiment and the calculation in the region $Q \leq 0.03 \text{ \AA}^{-1}$ is due to the small DNA-DNA correlation effect at finite concentrations.

3.6 Structural Study of Vesicles Formed from a New Bolaamphiphile

Project Staff

Pierandrea Lo Nostro, Professor Sow-Hsin Chen

Amphiphilic molecules with one polar head group and two aliphatic chains can form vesicles (or liposomes) in water. Vesicles are sealed structures formed by one bilayer of amphiphiles that separate an inner aqueous compartment from the external medium. The

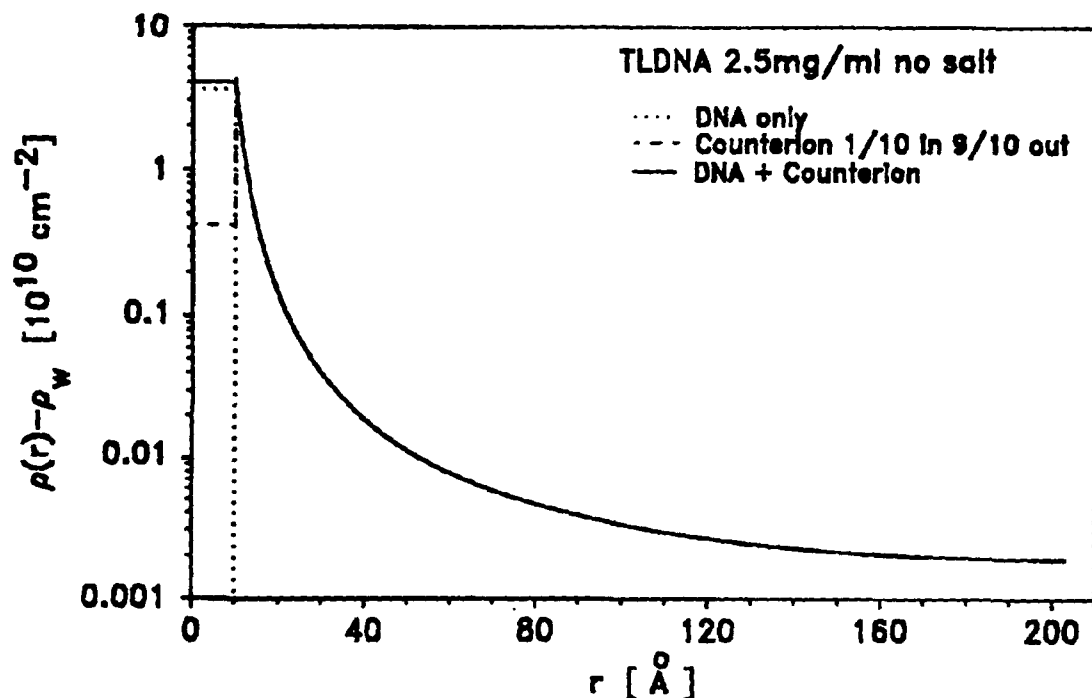


Figure 3b. The three net scattering length densities used to compute the corresponding three curves in figure 3a.

thickness of this bilayer is usually 4–5 nm. For this reason, vesicles constitute a very realistic model for biological membranes and an interesting system for entrapping and releasing large molecules (pollutants, nucleic acids or drugs), and for stereochemical centers of reactions.

We investigated aggregation properties of a new bolaform amphiphile, the (R,S)3,25,(26)-bis(β -D-glucopyranosylthio)-1,6,23,28-tetraoxacyclotetracontan-2,5,24,27-tetrone, which has never been studied. The Department of Chemistry at the University of Florence, Italy, first synthesized this amphiphile. A "bolaamphiphile" (or "bipolar lipid") is an amphiphilic compound containing two hydrophilic head groups connected by the hydrocarbon core and forming monolayered lipid membranes (MLM). Every molecule provides the two requested head groups facing the outer and the inner aqueous compartments. These bolaamphiphilic vesicles show some different and interesting properties from the usual bilayered membranes. For instance, the vesicles are thinner (2.5 nm) and do not fuse. If the two

polar head groups are different in charge, chemical composition or size, we can produce asymmetric vesicles, an interesting model for vectorial membranes. Bolaamphiphiles exist in nature, forming monolayered membranes in Archaeobacteria, the primordial microorganisms living in volcanoes and oceans in very drastic environmental conditions ($T > 90$ degrees C, high pressure, high salt concentration).

We sonicated and ultracentrifugated this bolaform compound in aqueous dispersions to investigate vesicular properties through scanning electron microscopy (SEM) and dynamic light-scattering. Observing the formation of vesicles with a diameter between 200 and 400 nm, we found the same value for the diameter both with SEM and with light-scattering (within experimental errors).

We also investigated the stability of the vesicles over time, temperature and addition of a co-surfactant, dioctanoylphosphatidylcholine (diC₈-PC). Vesicles were very stable even several weeks after the preparation. We found that their

hydrodynamic diameter increases with temperature (from 18 to 50 degrees C), probably because of the increased softness of vesicles at higher temperatures. The addition of different amounts of diC₈-PC (2.5 percent, 20 percent, and 40 percent) did not affect the stability or size of vesicles.

Calculations according to Nagarajan's theory show that this bolaform compound spontaneously aggregates in planar monolayers or in very large structures, but produces vesicles only upon sonication.

3.7 Photon Correlation Spectroscopy and Its Applications: Dynamic Transition at the Percolation Threshold of a Three-Component Microemulsion

Project Staff

Professor Sow-Hsin Chen, Jacques Rouch, Piero Tartaglia

We have performed an extensive series of dynamic light scattering experiments on a three-component water-in-oil microemulsion consisting of AOT(surfactant)/water/decane, in the isotropic one-phase region of the phase diagram (covering a range of volume fractions ϕ of the dispersed phase from 0.1 to 0.7 and temperatures T from 15 to 50°C). Previous studies have established a well-defined electrical percolation locus, extending from the cloud-point curve near $T = 40^\circ\text{C}$ and $\phi = 0.098$, down to 22°C and $\phi = 0.70$. The microemulsion droplet density time correlation function has a stretched exponential form for $\phi > 0.30$. The exponent β changes continuously as a function of temperature at a given volume fraction and shows a maximum close to unity at the percolation temperature. The relaxation time, as a function of temperature, also shows an abrupt change of slope at the percolation threshold. A physical interpretation of the results involves a theoretical model for the dynamics of percolated cluster of microemulsion droplets.

Publications

- Bellissent, M.C., J. Teixeira, S.H. Chen, B. Dorner, H.D. Middendorf, and H.L. Crespi. "Low Frequency Collective Modes in Dry and Hydrated Proteins." *Biophys. J.* 56:713 (1989).
- Cametti, C., P. Codastefano, A. Diasio, P. Tartaglia, and S.H. Chen. "Dynamic Scaling of Dielectric Relaxation in AOT/Water/decane Microemulsions Near the Percolation Threshold." *Phys. Rev. A* 40:1962 (1989).
- Carvalho, B., G. Briganti, and S.H. Chen. "Lowering of the Miscibility Gap in the Dioctanoylphosphatidylcholine-Water System by Addition of Urea." *J. Phys. Chem.* 93:4282 (1989).
- Chen, S.H., E.Y. Sheu, and J.S. Huang. "Non-Exponential Decay of Density Correlation Function in Dense Microemulsion." In *Dynamics of Disordered Materials*. Eds. D. Richter, W. Petry, J. Dianoux, and J. Teixeira. New York: Springer Verlag, 1989.
- Guo, X.H., N.M. Zhao, S.H. Chen, and J. Teixeira. "Small Angle Neutron Scattering Study of the Structure of Protein-Detergent Complexes." *Biopolymers* 29:335 (1990).
- Kalus, J., H. Hoffmann, S.H. Chen, and P. Lindner. "Correlations in Micellar Solutions Under Shear: A SANS Study of the Chain Surfactant N-Hexadecyloctyldimethylammonium Bromide." *J. Phys. Chem.* 93: 4267 (1989).
- Lin, T.L., S.H. Chen, N.E. Gabriel and M.F. Roberts. "SANS Study of Triglyceride Solubilization by Lecithin Micelles: A Direct Observation of Rod-to-Sphere Transition." *J. Phys. Chem.* 94: 855 (1990).
- Rouch, J., A. Safouane, P. Tartaglia, and S.H. Chen. "The Critical Region of Water-in-Oil Microemulsions: New Light Scattering Results." *Progr. Colloid Polym. Sci.* 79:279-286(1989).

Rouch, J., A. Safouane, P. Tartaglia, and S.H. Chen. "Experimental Evidence of a Crossover in Critical Behavior of Water-in-Oil Microemulsions." *J. Phys.: Condens. Matter* 1:1773-1778 (1989).

Rouch, J., A. Safouane, P. Tartaglia, and S.H. Chen. "Static and Dynamic Light Scattering Studies of Water-in-Oil Microemulsions in the Critical Region: Evidence of a Crossover Effect." *J. Chem. Phys.* 90:3756 (1989).

Rouch, J., P. Tartaglia, A. Safouane, and S.H. Chen. "Reexamination of the Static and Dynamic Critical Phenomena in Water-amphiphile Micellar Solutions." *Phys. Rev. A* 40:2013 (1989).

Sheu, E.Y., S.H. Chen, J.S. Huang, and J.C. Sung. "Non-Exponential Relaxations in Dense Microemulsions Near the Glass Transition." *Phys. Rev. A* 39:5867 (1989).

Section 2 Plasma Physics

Chapter 1 Plasma Dynamics

Chapter 1. Plasma Dynamics

Academic and Research Staff

Professor George Bekefi, Professor Abraham Bers, Professor Bruno Coppi, Professor Miklos Porkolab, Professor Jonathan S. Wurtele, Dr. Kuo-in Chen, Dr. Shien-Chi Chen, Dr. Thomas Dupree, Dr. Ronald C. Englade, Dr. Stanley C. Luckhardt, Dr. Stefano Migliuolo, Dr. Abhay K. Ram, Dr. Linda E. Sugiyama, Edward W. Fitzgerald, Ivan Mastovsky

Visiting Scientists and Research Affiliates

Jean-Loup Delcroix,¹ Paolo Detragiache,² Lazar Friedland,³ Vladimir Fuchs,⁴ Dr. Eli Jerby,⁵ Dr. Chaim Leibovitch,⁷ Dr. Marco Nassi⁶ Dr. Kongyi Xu⁸

Graduate Students

Riccardo Betti, Carson Chow, Stefano Coda, Jeffrey A. Colborn, Manoel E. Conde, Christian E. de Graff, Anthony C. DiRienzo, Darin Ehrnst, Mark Jablonski, Robert J. Kirkwood, Kenneth C. Kupfer, Alberto Leon, Jared P. Squire, Richard E. Stoner, Jesus N.S. Villasenor

Undergraduate Students

Daniel P. Aalberts, George Chen, Salvatore DiCecca, Weng-Yew Ko, John A. Marroquin, Kurt A. Schroder, Peter Woo

Technical and Support Staff

Ann Dix, Laura B. Dougherty, Toni Fischer, Catherine Lorusso

1.1 Relativistic Electron Beams

Contract DAAL02-86-C-0050
U.S. Navy - Office of Naval Research
Contract N00014-87-K-2001

Sponsors

Lawrence Livermore National Laboratory
Subcontract 6264005
National Science Foundation
Grants ECS 84-13173 and ECS 85-14517
U.S. Air Force - Office of Scientific Research
Contract AFOSR 84-0026
U.S. Army - Harry Diamond Laboratories

Project Staff

Professor George Bekefi, Professor Jonathan S. Wurtele, Manoel E. Conde, Christian E. de Graff, Richard E. Stoner, Anthony C. DiRienzo, Daniel P. Aalberts, Salvatore DiCecca, Dr. Kongyi Xu, Dr. Chaim Leibovitch, Dr. Eli Jerby, Ivan Mastovsky, Dr. Shien-Chi Chen

¹ University of Paris, Orsay, and Ecole Superieure d'Electricite, France.

² University of Turin, Torino, Italy.

³ Hebrew University of Jerusalem, Israel.

⁴ IREQ, Quebec, Canada.

⁵ Tel Aviv University, Tel Aviv, Israel.

⁶ Politecnico di Milano, Milan, Italy.

⁷ Rafael Laboratory, Haifa, Israel.

⁸ China University of Electronic Science and Technology, Chengdu, People's Republic of China.

1.1.1 Coherent Free-Electron Radiation Sources

The possibility of developing lasers and masers in which the active medium is a stream of free electrons has evoked much interest in recent years. The potential advantages are numerous, including continuous frequency tuning through variation of the electron energy and very high-power operation. In comparison with solid, liquid and gas lasers, little damage can occur to this lasing medium.

Interestingly, these novel sources and the underlying physical mechanisms have much more in common with the earliest sources of coherent electromagnetic radiation (namely the various microwave devices) than they have with the more recent atomic and molecular lasers. Indeed, the klystron, the magnetron, and the traveling wave tube conceived and developed in the 1940s and 50s are examples of free-electron sources capable of generating coherent microwave radiation. In the decimeter and centimeter wavelength ranges, these devices can emit at power levels as high as tens of megawatts with good efficiencies exceeding 60 percent. Today, these systems and their variations have become indispensable instruments of

modern science, technology and communication.

With the new generation of free-electron sources, we and others aim to extend the electromagnetic spectrum from the microwave to the millimeter, infrared, visible, and ultraviolet regimes with previously unattainable intensities and efficiencies. Potential applications include spectroscopy in condensed matter physics and in atoms and molecules, isotope separation, development of novel accelerators, millimeter and submillimeter wavelength radar and communication, heating of thermonuclear fusion plasma, biomedicine, and lithography.

Free electron lasers are large and expensive because their size and cost increase as the radiation wavelength decreases. Therefore, facilities are now limited to a few large laboratories. However, a number of novel concepts to reduce their size and cost are being explored at various institutions. One is the design and construction of novel, compact accelerators such as the high-gradient rf linacs powered by intense millimeter wavelength rf drivers. Acceleration gradients in excess of several hundred MeV per meter length may be possible. At present we are studying the performance of such structures operating at a frequency of 35 GHz (see figure 1).

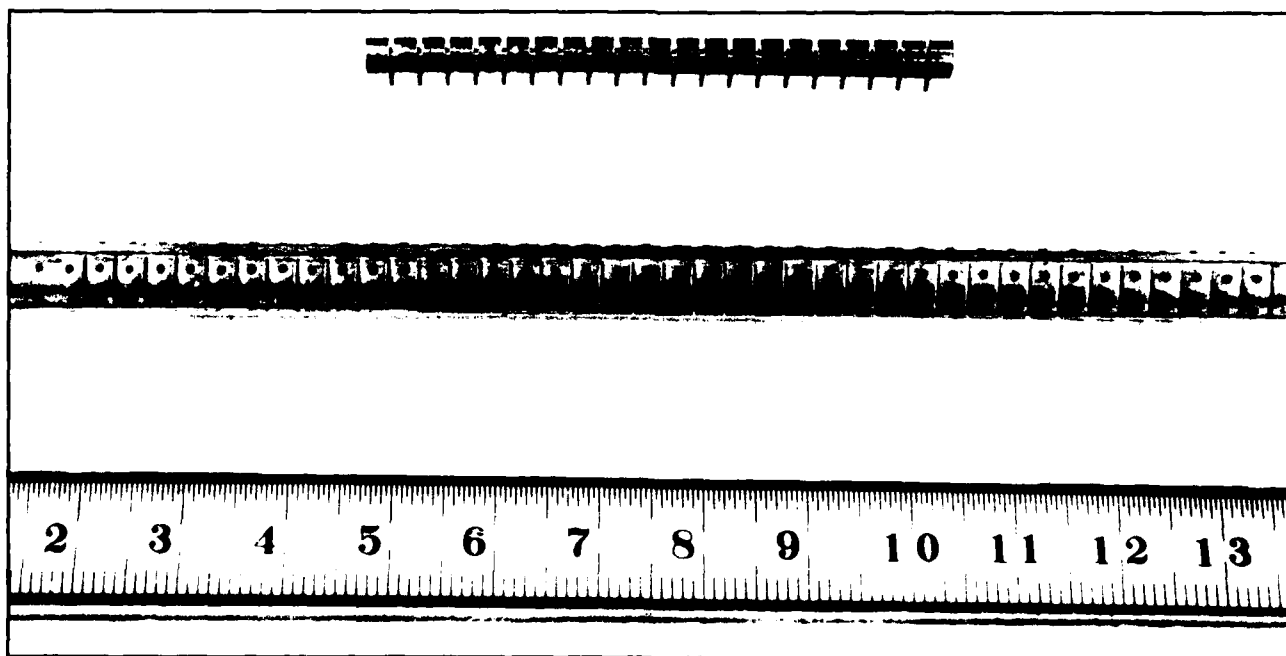


Figure 1.

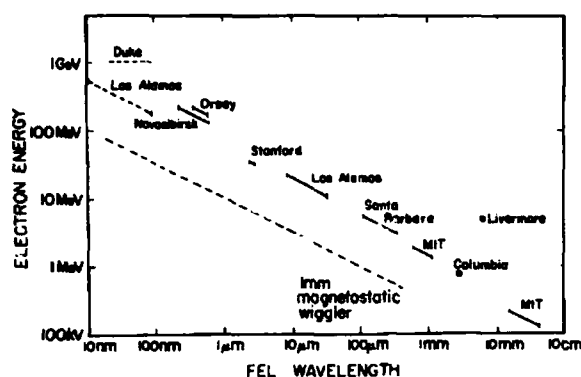


Figure 2.

The design and construction of novel, short-period wigglers is being examined at a number of research centers. Figure 2 illustrates which facilities are presently using conventional wigglers. The fact that all the existing FELs lie, for the most part, on a single straight line of the voltage versus wavelength graph implies that they all use wigglers with roughly the same periodicity, l_w . This is indeed the case with l_w ranging between ~ 3 and ~ 5 cm. A reduction of l_w by a factor of ten, for instance, leads to a reduction in wiggler length by 10 and a reduction in accelerator voltage by $\sqrt{10}$. The overall effect is a smaller accelerator, a shorter wiggler, and less stringent requirements on radiation shielding.

Many different designs are under scrutiny at present, as indicated in figure 3. Plotted along the vertical axis of figure 3 is the wiggler strength expressed in terms of the normalized vector potential defined as

$$a_w = \frac{eB_w}{m_0 k_w c} \simeq 0.1 B_w (\text{kG}) l_w (\text{cm}).$$

Since the FEL gain increases with increasing a_w , large a_w (≥ 1) is desirable, but difficult to achieve. Figure 3 shows that if the wiggler periodicity, l_w , is shorter, a_w tends to be smaller.

At MIT, we have tested prototype microwigglers with a period of 2.4 mm and 10 mm. A 70-period version is now under construction. When completed, it will be used in a collaborative effort on the 50-MeV rf linac at Brookhaven National Laboratory to

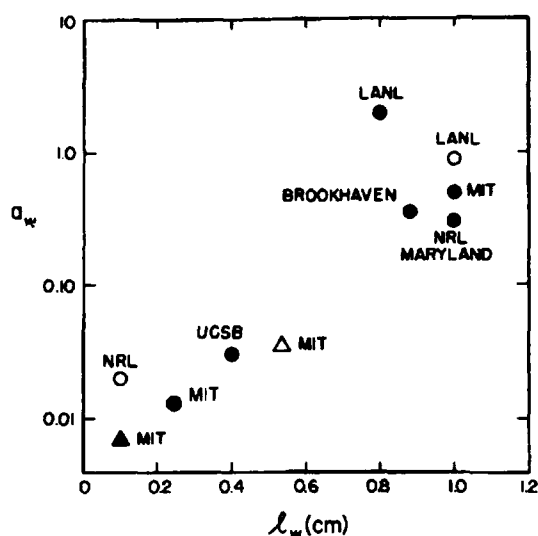


Figure 3.

produce coherent light at $0.47 \mu\text{m}$ wavelength.

1.2 Plasma Wave Interactions — RF Heating and Current Generation

Sponsors

National Science Foundation
Grants ECS 85-15032 and ECS 88-22475
U.S. Department of Energy
Contract DE-AC02-ET-51013

Project Staff

Professor Abraham Bers, Dr. Abhay K. Ram, Carson Chow, Mark Jablonski, Kenneth C. Kupfer, Jean-Loup Delcroix, Vladimir Fuchs, Lazar Friedland

1.2.1 Introduction

The research work of this group is concerned with studies on the electrodynamics of plasmas. Particular attention is directed toward understanding wave propagation and the nonlinear dynamics of plasmas driven by high frequency electromagnetic fields for plasma heating and/or current generation within the plasma.

In the following sections, we report on our progress on the following topics:

1. Particle and energy diffusion induced by intense RF fields. This entails a new description of such transport using non-linear dynamics techniques of induced stochasticity and chaos, and is reported in Section 1.2.2, "Transport in Intense RF Fields."
2. Wave propagation and mode conversion in ion-cyclotron heating for high-temperature, magnetically confined plasmas. We report on an analytic description of the reflection coefficient in mode conversion (Section 1.2.3, "The Reflection Coefficient in Ion-Cyclotron Heating" on page 171), on optimizing the energy deposition on ions in the mode conversion region (Section 1.2.4, "Optimizing the Absorption in Ion-Cyclotron Heating" on page 173), and on kinetic ray tracing of the mode converted waves (IBW) and their energy deposition on electrons (Section 1.2.5, "Propagation of Mode Converted Ion-Bernstein Waves in Toroidal Plasmas" on page 174).
3. Frequency locking and chaos in self-oscillating (linearly unstable) dynamics — a generic study of the combined van der Pol and Duffing oscillator nonlinearities (Section 1.2.6, "Dynamics of a Forced van der Pol-Duffing Oscillator" on page 176).

1.2.2 Transport in Intense RF Fields

We are studying the guiding center motion of charged particles interacting with electrostatic waves in a tokamak. This motion is described by a time dependent Hamiltonian in a four-dimensional phase space composed of the guiding center's three position coordinates and its parallel velocity (along the magnetic field). This is a generalization of previous studies in which either the drift motion⁹ or the parallel wave fields have been ignored.¹⁰ In our approach, we obtain diffusion of the guiding center parallel velocity and its radial position when the wave amplitudes exceed a threshold value for the onset of stochastic motion.¹¹

Using the guiding center Lagrangian¹² to describe the motion in an axisymmetric, time-independent equilibrium, the Hamiltonian describing the motion is given by:

$$H = \frac{m}{2} u^2 + MB(\psi, \theta) + e\Phi(\psi, \theta, \phi, t), \quad (1)$$

where M is the magnetic moment of a particle of mass m and charge e , Φ is the scalar potential of the imposed wave field, u is the parallel velocity of the guiding center and $B = |\mathbf{B}|$ is the magnetic field. The tokamak geometry is described by (ψ, θ, ϕ) , where ψ is the usual poloidal flux function and ϕ is the toroidal angle. The coordinate θ is chosen so that $\nabla\theta$ is perpendicular to both $\nabla\psi$ and $\nabla\phi$. In order to analyze the dynamics of the charged particles, it is convenient to transform the above coordinates to action-angle coordinates of the unperturbed Hamiltonian. Then the Hamiltonian can be written as:

$$H = H_0(I_\phi, I_\theta) + \Phi(I_\phi, I_\theta, \zeta_\phi, \zeta_\theta, t) \quad (2)$$

⁹ V. Fuchs, V. Krapchev, A.K. Ram, and A. Bers, "Diffusion of Electrons by Coherent Wavepackets," *Physica* 14D: 141-160 (1985); A.K. Ram, K. Hizanidis, and A. Bers, "Trapped-Electron Stochasticity Induced by Frequency-Modulated Waves," *Phys. Rev. Lett.* 56 (2):147-150 (1986).

¹⁰ R.G. Kleva and J.F. Drake, "Stochastic $\mathbf{E} \times \mathbf{B}$ Particle Transport," *Phys. Fluids* 27 (7): 1686-1698 (1984); W. Horton and D.I. Choi, "Electron Diffusion in Tokamaks Due to Electromagnetic Fluctuations," *Plasma Phys. Contr. Fusion* 29 (7): 901-918 (1987).

¹¹ K. Kupfer, A. Bers, and A.K. Ram, "Guiding Center Stochasticity by Electrostatic Waves in Toroidal Geometry," (abstract) *Bull. Am. Phys. Soc.* 34: 1927 (1989).

¹² R.G. Littlejohn, "Variational Principles of Guiding Centre Motion," *J. Plasma Phys.* 29: 111-125 (1983).

where I_ϕ is the toroidal action, I_θ is the poloidal action and ζ_ϕ and ζ_θ are the canonical angles, respectively. We have used this approach to study the stochasticity, including radial diffusion, of super-thermal electrons during lower-hybrid current drive (LHCD). A majority of the electrons interacting with the waves are not trapped by the toroidal magnetic field so we have explicitly evaluated the action-angle transformation for circulating electrons in a low β , circular equilibrium. The transformed potential is a periodic function of the angles ζ_ϕ and ζ_θ , so we write it as a Fourier series with respect to these coordinates:

$$\Phi = \text{Re}\{\sum C_{n,\ell}(\mathbf{I}) e^{i(n\zeta_\phi + \ell\zeta_\theta - \omega t)}\} \quad (3)$$

where the sum is over all n and ℓ , ω is the frequency of the source, and $\mathbf{I} = (I_\phi, I_\theta)$. We consider an ensemble of randomly phased waves in the plasma. The spectrum is assumed to be finite for $n_1 \leq n \leq n_2$. Typically LHCD experiments have broad spectra where n_2 is approximately twice n_1 , and n_1 is about 10^2 . The amplitude of the RF field is large enough that the trapping widths of the resonances in action space satisfy the overlap criterion, creating a broad region of connected stochasticity. The quasi-linear diffusion tensor in action space is¹³

$$D_{ij}(\mathbf{I}) = \sum \frac{\pi}{2} |C_{n,\ell}(\mathbf{I})|^2 \delta(R_{n,\ell}(\mathbf{I})) \Pi_{ij}(n,\ell) \quad (4)$$

where $R_{n,\ell}(\mathbf{I}) = n\Omega_\phi + \ell\Omega_\theta - \omega = 0$ is the resonance curve in action space and Ω_ϕ and Ω_θ are the linear frequencies determined by differentiating $H_0(\mathbf{I})$ with respect to each component of the action, I_ϕ and I_θ . The components of the Π_{ij} tensor are: $\Pi_{\phi,\phi} = n^2$, $\Pi_{\phi,\theta} = \Pi_{\theta,\phi} = \ell n$, and $\Pi_{\theta,\theta} = \ell^2$. Although $D_{ij}(\mathbf{I})$ is a singular tensor field it should be smoothed out by coarse graining action space because the resonances are broadened by small nonlinearities (i.e., they have finite trapping widths). We have computed the

coarse-grained $D_{ij}(\mathbf{I})$ numerically, with the spectrum, $C_{n,\ell}$, obtained by transforming the assumed RF field into action-angle coordinates. The results of this calculation have been compared to numerical computations of the non-linear equations of motion obtained directly from the Hamiltonian in (1). Agreement is achieved when the amplitude of the RF field is small enough so that the trapping width of each resonance in action space is small compared to the width of the stochastic region. In this case, the basic scaling for the radial diffusion is $D_{\text{RF}}/\omega_{ce}^2$, where D_{RF} is the average RF quasi-linear diffusion coefficient in parallel velocity and ω_{ce} is the electron cyclotron frequency. In typical LHCD experiments, D_{RF} is large enough so that the associated RF radial diffusion dominates classical collisional diffusion for the super-thermal electrons. The quasi-linear approximation overestimates the diffusion at larger amplitudes.

1.2.3 The Reflection Coefficient in Ion-Cyclotron Heating

The ICRH problem in a tokamak plasma, which can be formulated in general as an integro-differential equation, has usually been approximated by a fourth- or sixth-order differential equation and solved numerically. However, in order to make predictions and to better understand the scaling laws (see Section 1.2.4, following), it is important to have closed form solutions of the scattering coefficients for the mode-conversion region. Over the past two to three years, we have worked toward an approximate analytic description of the RF power transmission (T), reflection (R), mode-conversion (C), and kinetic dissipation (D) coefficients for ICRH. To achieve our goal, we have used the technique of "order reduction" whereby the fourth or higher order differential equations are reduced to combinations of lower order equations that retain the essential physics of the complete problem. So far, we have obtained a first-order differential equation for

¹³ A.N. Kaufman, "Quasilinear Diffusion of an Axisymmetric Toroidal Plasma," *Phys. Fluids* 15 (6): 1063-1069 (1972).

T ,¹⁴ and a set of coupled equations, which include the effects of kinetic dissipation, for C and T .¹⁵ These equations can be solved analytically to obtain C and T . A second order equation has also been found for R and T .¹⁶ Until recently, this equation, known as the "fast wave approximation," was solved numerically to find R . We have now found a closed form solution for R . Thus, for all heating scenarios of current interest,¹⁷ [$D - (H)$, $D - (^3\text{He})$], we have closed form solutions for all of the scattering coefficients using this order reduction technique.

The following is a summary of our new result for R . The approximate fast wave equation¹⁸ is a second-order, ordinary differential equation with a complex potential and, in general, has no closed-form, analytic solution. However, we noted that the real part of the potential looks like a resonance broadened "Budden" potential. The imaginary part has two peaks: one peak corresponds to the "Budden" like potential, the other to the ion-cyclotron resonance. The "Budden" part includes the effects of mode conversion to the ion-Bernstein wave and any dissipation that may be present in that particular process. To solve for R and T , we approximate the complex potential by the Budden potential,

for which analytic solutions exist.¹⁹ The ion cyclotron part is then treated as a perturbation which affects a slowly varying amplitude on the asymptotic Budden solutions. We obtain

$$T = e^{-\pi s_0} e^{-2\mu},$$

$$R = e^{-4\mu} e^{-4\nu} (1 - T^2)^2,$$

$$\mu = \left| \int_0^\infty \frac{g(s)}{2} ds \right| \quad (1)$$

where $\nu = \sqrt{\pi} N_c \gamma \varepsilon_r / \tau^2$, $g(s)$ is the imaginary part of the complex potential, $s_0 = N_c^3 \gamma / (2\tau + \lambda_N)^2$, and all the other quantities are given in Chow et al.²⁰ T in (1) checks with our previous, independent derivations for T . R in (1) has been compared with the numerical results generated by the codes of D. Smithe (PPPL) and E.F. Jaeger (ORNL). The results agree very well over a wide range of parallel wavenumbers for heating scenarios of current interest for Alcator C-mod and CIT. A detailed derivation and comparison of the results has been recently submitted to *Phys. Fluids B*.²¹

¹⁴ G. Francis, *Coupled-Mode Propagation and Instability in Inhomogeneous Plasmas*, Ph.D. diss., Dept. of Physics, MIT, 1987; G. Francis, A. Bers, and A.K. Ram, "Non-Resonant Mode-Coupling Model of ICRF Heating," in *Proceedings of the 7th Topical Conference on Applications of RF Power to Plasmas*, A.I.P. Conf. Proc. 159, eds. S. Bernabei and R.W. Motley, 370-373, (New York: 1987).

¹⁵ V. Fuchs and A. Bers, "Dissipative Mode Coupling in Ion-Cyclotron Resonance Minority Heating," *Phys. Fluids* 31 (12): 3702-3708 (1988). Note the following misprints: On line before (17a), $K_1 \sim \varepsilon$ should read $K'_1 \sim \varepsilon$; in second expression of (20) replace K_0 with $-K_0$; r.h.s. of (25) should have been multiplied by a factor of 2.

¹⁶ C. Lashmore-Davies, V. Fuchs, G. Francis, A.K. Ram, A. Bers, and L. Gauthier, "A Theory of Fast-Wave Absorption, Transmission, and Reflection in the Ion-Cyclotron Range of Frequencies," *Phys. Fluids* 31 (6): 1641-1622 (1988).

¹⁷ C. Chow, A. Bers, and V. Fuchs, "Analytic Studies of ICRF Heating," in *Radio Frequency Power in Plasmas*, A.I.P. Conf. Proc. 190, ed. R. McWilliams, 234-237, (New York: American Institute of Physics, 1989). Note the following misprints: In Section III, the expression for K_0 is missing a term $-N_f^2$; in Section IV, in the expression for ν replace $-N_f^2$ by $+N_f^2$.

¹⁸ C. Lashmore-Davies et al., *Phys. Fluids* 31 (6): 1641-1622 (1988).

¹⁹ R.B. White and F.F. Chen, "Amplification and Absorption of Electromagnetic Waves in Overdense Plasmas," *Plasma Phys.* 16: 565-587 (1974).

²⁰ C. Chow et al. A.I.P. Conf. Proc. 190: 234-237 (1989).

²¹ C. Chow, V. Fuchs, and A. Bers, *Reflection at the Resonance Layer of the Fast Alfvén Wave in Ion Cyclotron Heating*, Plasma Fusion Center Report PFC/JA-90-2 (Cambridge: MIT, 1989).

1.2.4 Optimizing the Absorption in Ion-Cyclotron Heating

In view of the results described in Section 1.2.3, we can now use a global power conservation (i.e., integrating over a volume of the plasma extending into the asymptotic regions away from the mode-conversion region) to determine the power dissipated (D):

- For a fast Alfvén wave (FAW) incident from the low- B_0 side,

$$T + R + C_L + D_L = 1 \quad (1)$$

- For a FAW incident from the high- B_0 side,

$$T + C_H + D_H = 1 \quad (2)$$

where the subscripts L and H stand for, respectively, low- and high- B_0 incidence. (Note that T is the same, and $R_L = R$, while $R_H = 0$). With these results, we can then find the plasma and RF heating parameter space for optimizing ion-cyclotron heating in tokamak plasmas. We summarize this in the following, with notation that we have used before.²²

Consider incidence of a FAW from the low- B_0 side of the tokamak. Note that the conversion coefficient²³ can be written as

$$C_L = \frac{1}{2\pi} f(\Lambda) T^{1/2} R e^{-2D_c} \quad (3)$$

where $f(\Lambda) \equiv |\Lambda| |\Gamma(-i\Lambda)|^2$. Now consider small N_i (Alfvén parallel index, $c_A k_{\parallel}/\omega$) so that the Z-functions that enter into (3) can be taken in their asymptotic limits. Then Λ is approximately real and (3) becomes

$$C_L \approx \frac{e^{-\pi\Lambda}}{2\sinh\pi\Lambda} R e^{-2D_c} \quad (4)$$

We now choose $\Lambda > 1$ so that both $T \approx 0$ and $C_L \approx 0$ in the range of small N_i of interest. This

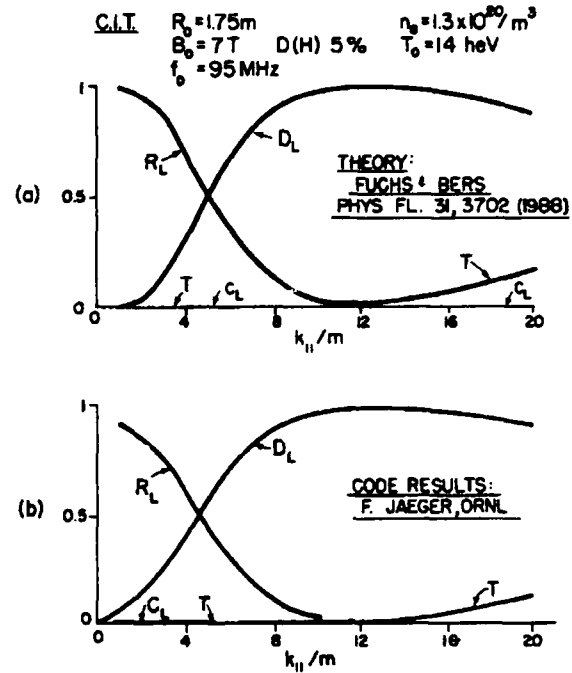


Figure 4. Power scattering coefficients for low- B_0 incidence of a FAW for CIT-type plasma. (a) Theory. (b) Numerical code results.

choice gives us a relation between η (the minority species concentration), R_A (the plasma major radius in units of Alfvén wavelengths), and β_i (the plasma ion beta). Then from (1) we have

$$R + D_L \approx 1 \quad (5)$$

It can readily be shown (see Section 1.2.3, preceding) that R decreases exponentially with $R_A N_i^2$ so that, according to (5), as N_i increases, the dissipation coefficient D_L increases to unity. We can thus establish a relationship between N_i^2 , R_A and β_i so that $D_L \approx 1$ and $R \approx 0$. This achieves the goal of single-pass absorption. Note that by these means one can approximately determine the optimum η and N_i for a given set of β_i and R_A .

²² C. Chow et al. A.I.P. Conf. Proc. 190: 234-237 (1989).

²³ V. Fuchs and A. Bers, *Phys. Fluids* 31(12): 3702-3708 (1988).

Figure 4 shows a computation (for CIT-type parameters) based upon the approximate analytic formulas obtained for T , R , and C_L . The results are in excellent agreement with the T , R , and C_L obtained from a numerical solution of the fourth-order differential equation (numerical results: courtesy of F. Jaeger, ORNL). Note that in this case, for low- B_0 incidence of a FAW, we have indeed a situation in which at low N_i 's $T \approx 0$, $C_L \approx 0$, and the interplay between reflection and dissipation is as given by (5).

Finally, note that for high- B_0 incidence of a FAW, there is a similar interplay between C_H and D_H , but at higher N_i 's. This can be understood from the fact that, approximately²⁴

$$C_H \approx 2 \sinh \pi \Lambda e^{-\pi \Lambda} e^{-2D_c} \quad (6)$$

so that for $\Lambda > 1$ we have again $T \approx 0$, and from (6), $C_H \approx \exp(-2D_c)$. Thus, equation (2) becomes

$$C_H + D_H \approx 1 \quad (7)$$

The kinetic dissipation in mode conversion D_c increases with N_i , and hence $C_H \rightarrow 0$ and, by (7), $D_H \rightarrow 1$. Thus, we have complete dissipation, although at a higher N_i than before, also for high- B_0 incidence. Figure 5 shows a computation (also for CIT-type parameters), based upon the approximate analytic formulas obtained for T and C_H , and compares them with the numerical results obtained from the fourth-order o.d.e. code mentioned above. Again the results are in excellent agreement, exhibiting the interplay between C_H and D_H as described in (7).

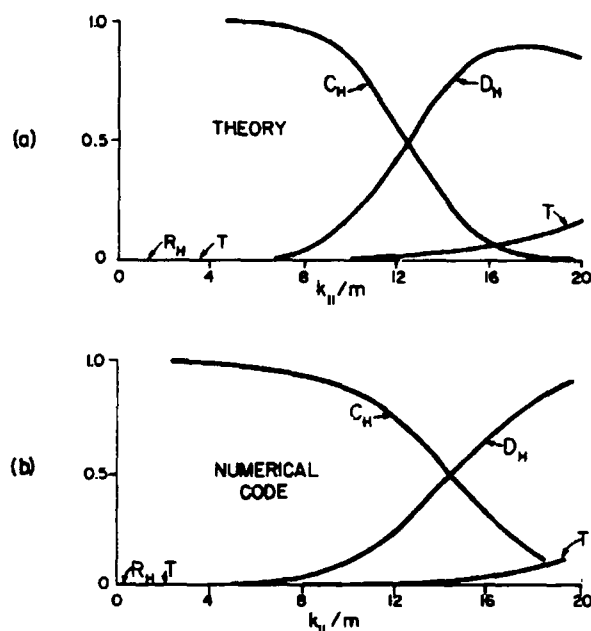


Figure 5. Power scattering coefficients for high- B_0 incidence of a FAW. Plasma parameters are the same as in figure 4. (a) Theory. (b) Numerical code results.

1.2.5 Propagation of Mode Converted Ion-Bernstein Waves in Toroidal Plasmas

For small values of k_{\parallel} (the component of the wave number parallel to the magnetic field in a tokamak), the fast Alfvén wave can effectively excite the ion-Bernstein wave (IBW) during ICRF heating of tokamak plasmas. This occurs near the ion-ion hybrid resonance layer in a plasma consisting of two ion species. The amount of power coupled to low values of k_{\parallel} is significant for single antennas at the edge of the plasma which excite fast Alfvén waves that propagate into the plasmas. We have been studying the propagation characteristics of this IBW in a toroidal plasma. Toward this end, we have developed a numerical code which solves for the propagation characteristics of rays in

²⁴ Ibid.

three-dimensional toroidal equilibria.²⁵ The local dispersion function, $D(\vec{k}, \omega, \vec{r})$, used for following the rays is obtained from the fully electromagnetic *hermitian* dielectric tensor²⁶ describing a kinetic, hot Maxwellian plasma. Here $\vec{r} = (r, \theta, \phi)$ is the position vector where r is the radius measured from the magnetic axis of the torus, θ is the poloidal angle, and ϕ is the toroidal angle; $\vec{k} = (k_r, m, n)$ is the wave vector with components k_r , m and n in the radial, poloidal and toroidal directions, respectively; and ω is the frequency. The spatial profiles of the density, temperature, and the magnetic field components are included, in a WKB sense, explicitly in D . Besides the usual ray trajectory equations:

$$\frac{d\vec{k}}{dt} = \frac{(\partial D / \partial \vec{r})}{(\partial D / \partial \omega)}, \quad \frac{d\vec{r}}{dt} = - \frac{(\partial D / \partial \vec{k})}{(\partial D / \partial \omega)} \quad (1)$$

the numerical code also solves for the variation of the wave energy density, U , along the rays:²⁷

$$\frac{\partial U}{\partial t} + \nabla \cdot \left(\frac{\partial \omega}{\partial \vec{k}} U \right) + \frac{1}{2} \bar{\sigma}^H : \vec{a} \vec{a}^* = 0 \quad (2)$$

where $\bar{\sigma}^H$ is the hermitian part of the conductivity tensor and \vec{a} is the slowly varying (complex) part of the electric field of the wave. The relation between U and \vec{a} is given by:

$$U = \frac{1}{16\pi} \frac{\partial(\omega \bar{D})}{\partial \omega} : \vec{a} \vec{a}^* ; \quad (3)$$

$$\bar{D} = (1 - \frac{c^2 k^2}{\omega^2}) \bar{I} + \frac{c^2 \vec{k} \vec{k}}{\omega^2} + \frac{4\pi i \bar{\sigma}^A}{\omega}$$

where $\bar{\sigma}^A$ is the anti-hermitian part of the conductivity tensor, $k^2 = \vec{k} \cdot \vec{k}$, c is the speed of light, \bar{I} is the unit tensor, and

$\det(\bar{D}) = D(\vec{k}, \omega, \vec{r})$. The second term in equation (2) describes changes associated with the convergence and divergence of a bundle of rays, and the third term describes changes in U due to damping of the wave energy on the particles.

A numerical analysis of the propagation of ion-Bernstein waves shows that they can effectively damp onto the electrons. The rate of damping, and the spatial location where the damping takes place, is determined primarily by, \bar{B} , the ratio of the poloidal magnetic field to the total magnetic field. For large values of \bar{B} the IBW damp onto the electrons close to the ion-ion hybrid resonance layer. As \bar{B} is decreased, the IBW damp out closer to the edge of the tokamak in the high toroidal magnetic field and low density and temperature regimes. The damping is a consequence of an upshift in $|m|$ leading to a subsequent enhancement in $|k_r|$. The change in m over a radial distance of propagation Δr in a hydrogen-deuterium plasma (with hydrogen as a minority species) is approximately given by²⁸

$$\Delta m \approx \frac{2}{3} \frac{\omega_{cd}^2}{k_r v_{td}^2} \left(2 + 11 \frac{v_{td}^2}{c^2} \frac{\omega_{pd}^2}{\omega_{cd}^2} \right) \frac{r \sin \theta}{(R + r \cos \theta)} \Delta r \quad (4)$$

where $\omega_{cd}(\omega_{pd})$ is the local deuterium cyclotron (plasma) frequency, and v_{td} is the deuterium thermal velocity. This formula shows that the enhancement in m is not unidirectional. The direction of the upshift is determined by the horizontal axis of symmetry of the plasma. Above this axis the

²⁵ A.K. Ram and A. Bers, "Kinetic Ray Tracing in Toroidal Geometry with Applications to Mode-Converted Ion-Bernstein Waves," in *Proceedings of the 1989 Conference on Plasma Physics*, New Delhi, India, 57-60, eds. A. Sen and P.K. Kaw (1989).

²⁶ A. Bers, "Linear Waves and Instabilities," in *Plasma Physics — Les Houches 1972*, eds. C. DeWitt and J. Peyraud (New York: Gordon and Breach, 1972); I.B. Bernstein and L. Friedland, "Geometric Optics in Space and Time Varying Plasmas," in *Handbook of Plasma Physics*, Vol. 1, eds. M.N. Rosenbluth and R.Z. Sagdeev (New York: North Holland Pub. Co., 1983).

²⁷ Ibid.

²⁸ A.K. Ram and A. Bers, *Proceedings of the 1989 Conference on Plasma Physics*, New Delhi, India (1989).

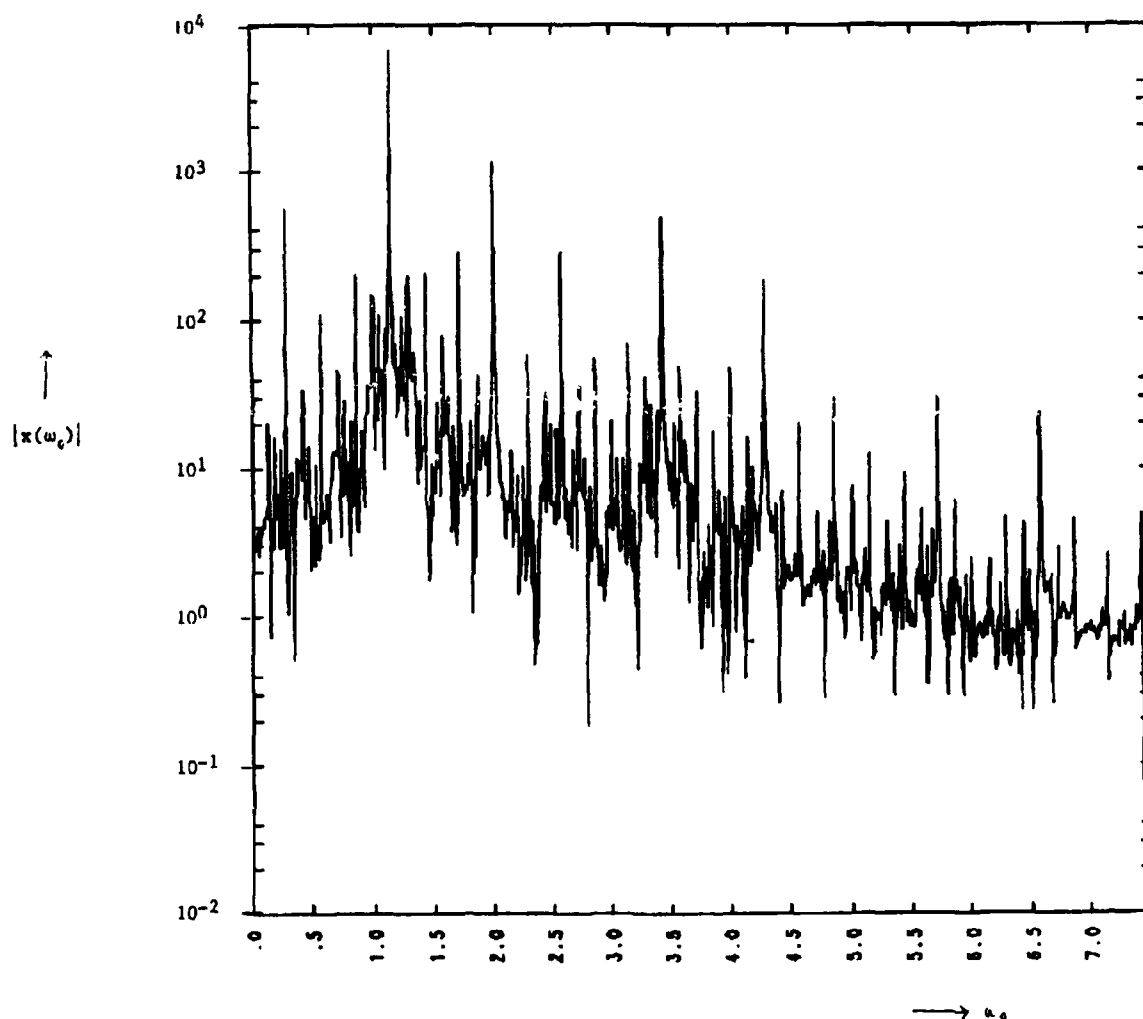


Figure 6. The frequency spectrum of x for the quasi-periodic case ($\varepsilon = 0.51$).

upshift is towards larger negative values and below the axis the upshift is towards larger positive values. Consequently, ion-Bernstein waves are not good candidates for driving plasma currents.

1.2.6 Dynamics of a Forced van der Pol-Duffing Oscillator

The phenomena of frequency locking and quasi-periodic behavior in physical systems, which are described by nonlinear ordinary differential equations in time and exhibit nonlinear oscillations, is well-known.²⁹ Study of the occurrence of chaos in physical systems, on the other hand, is more recent. Frequency locking occurs in self-oscillatory systems (i.e., systems that oscillate in the

²⁹ See for example: C. Hayashi, *Nonlinear Oscillations in Physical Systems* (New York: McGraw Hill Book Co., 1964).

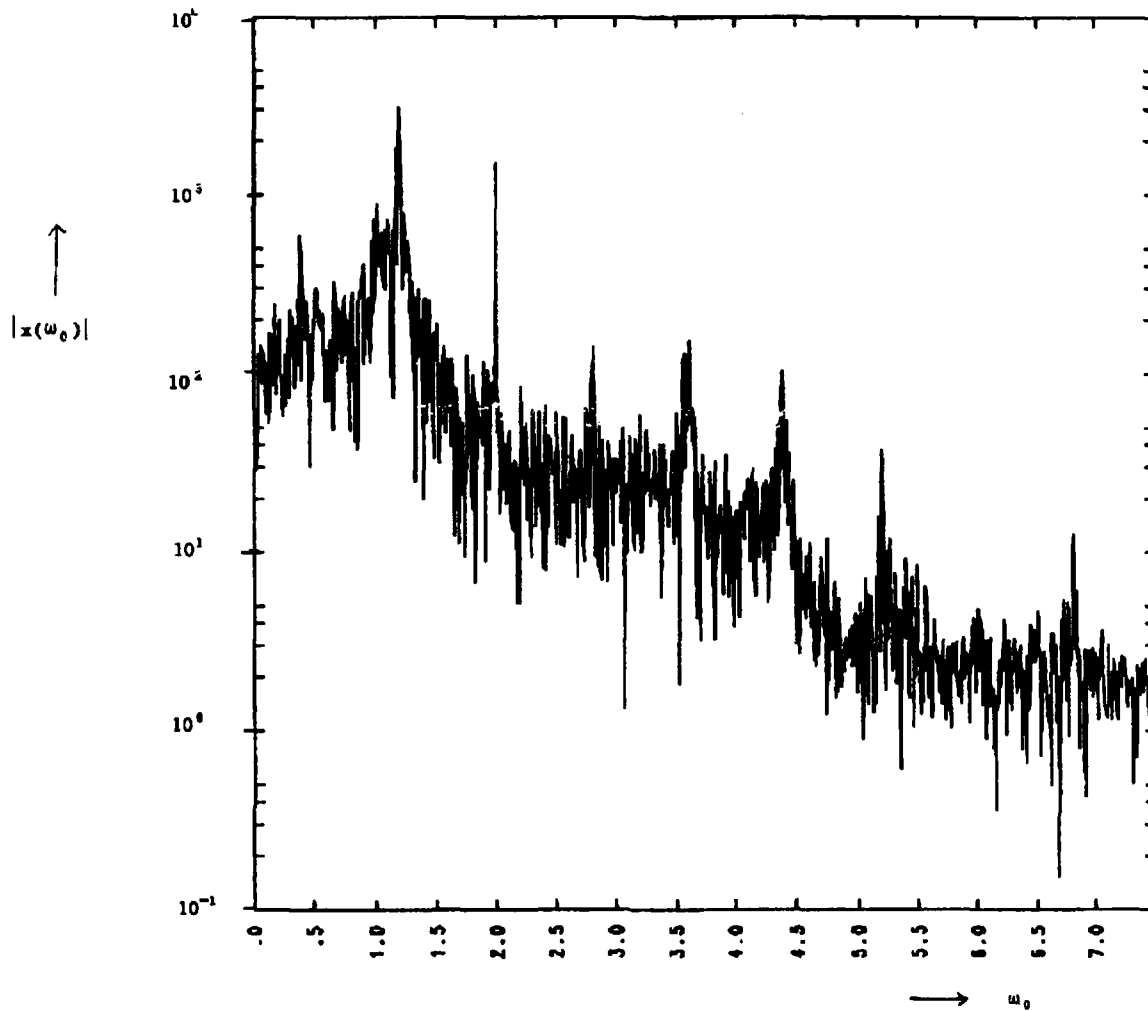


Figure 7. The frequency spectrum of x for the chaotic case ($\varepsilon = 0.79$).

force-free state) when, under certain conditions, they oscillate at the frequency of the drive. Self-oscillatory systems are linearly unstable so that the initial amplitude of the oscillations grows in time. The amplitude eventually saturates due to nonlinearities, leading to the self-oscillation steady-state.³⁰

We have been studying the behavior of a self-oscillating system when acted upon by a temporally oscillating force. The model we are studying combines a van der Pol-type of self-oscillating nonlinearity with a Duffing-

type of nonlinear potential. The governing equation of motion is of the form:

$$\frac{d^2x}{dt^2} - \mu(1 - \gamma x^2) \frac{dx}{dt} + \alpha x + \beta x^3 = \varepsilon \cos \omega t \quad (1)$$

where the right-hand side is the external drive. For $\mu < 0$, $\gamma = 0$, $\alpha < 0$, and $\beta > 0$, the left-hand side describes the Duffing oscillator, while for $\mu > 0$, $\gamma > 0$, $\alpha > 0$, and $\beta = 0$, it describes the van der Pol oscillator. The van der Pol oscillator is self-oscillatory

³⁰ Ibid.

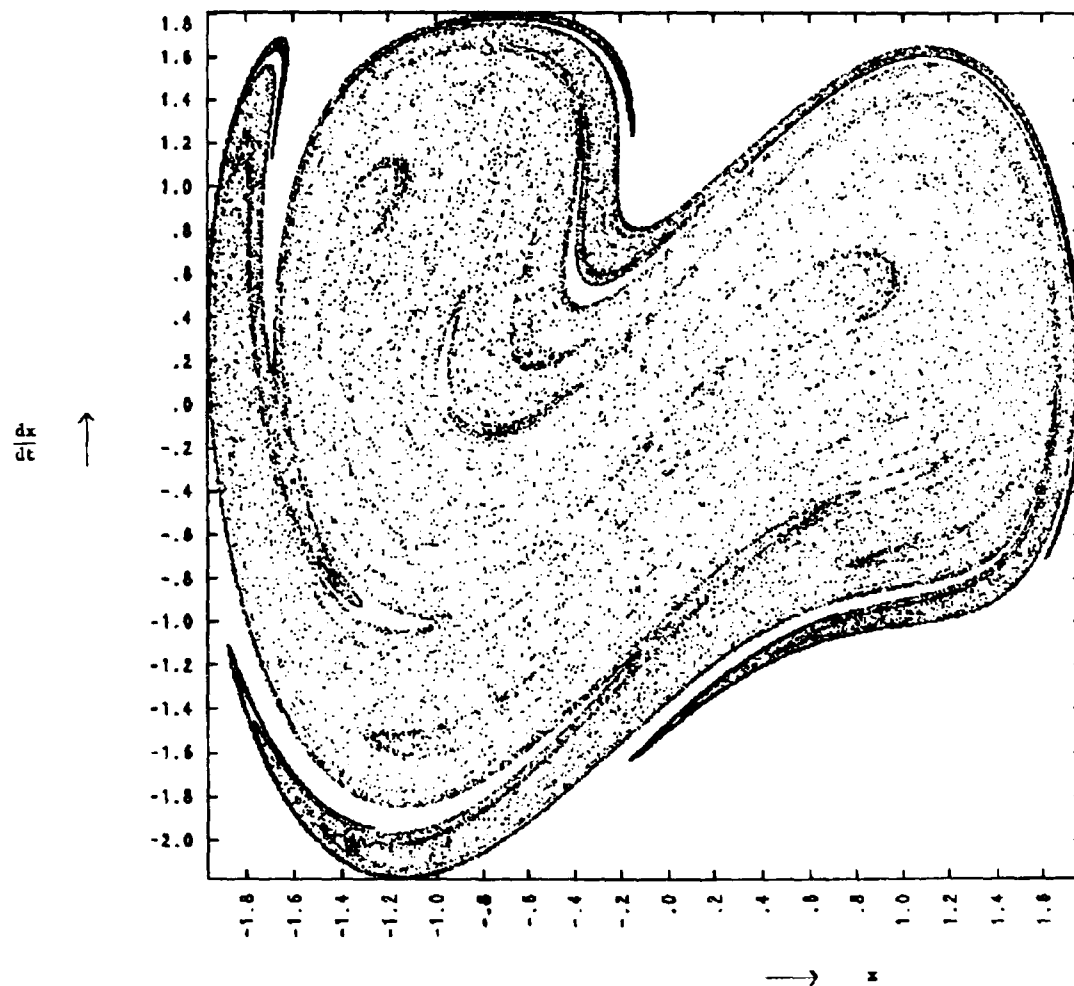


Figure 8. The Poincaré surface of section showing the strange attractor for the chaotic case ($\varepsilon = 0.79$).

(unlike the Duffing oscillator) and exhibits frequency locking as well as quasiperiodicity under the influence of an external drive.³¹ However, we found, through our numerical investigations, that the van der Pol oscillator, within the range of parameters we investigated, does not behave chaotically.³² After investigating the case in which $\alpha = 0$, $\beta > 0$,

corresponding to a van der Pol oscillator with a nonlinear restoring force, we found that it leads to chaos for very large values of ε and for ω much larger than the natural frequency of self-oscillations of the system.³³ Meanwhile, it is well-known that the Duffing oscillator exhibits chaotic motion when

³¹ Ibid.

³² Y. Ueda and N. Adamatsu, "Chaotically Transitional Phenomena in the Forced Negative-Resistance Oscillator," *IEEE Trans. Circuits Syst. CAS-28*: 217-224 (1981).

³³ C. Hayashi, *Nonlinear Oscillations in Physical Systems* (New York: McGraw Hill Book Co., 1964); Y. Ueda and N. Adamatsu, *IEEE Trans. Circuits Syst. CAS-28*: 217-224 (1981).

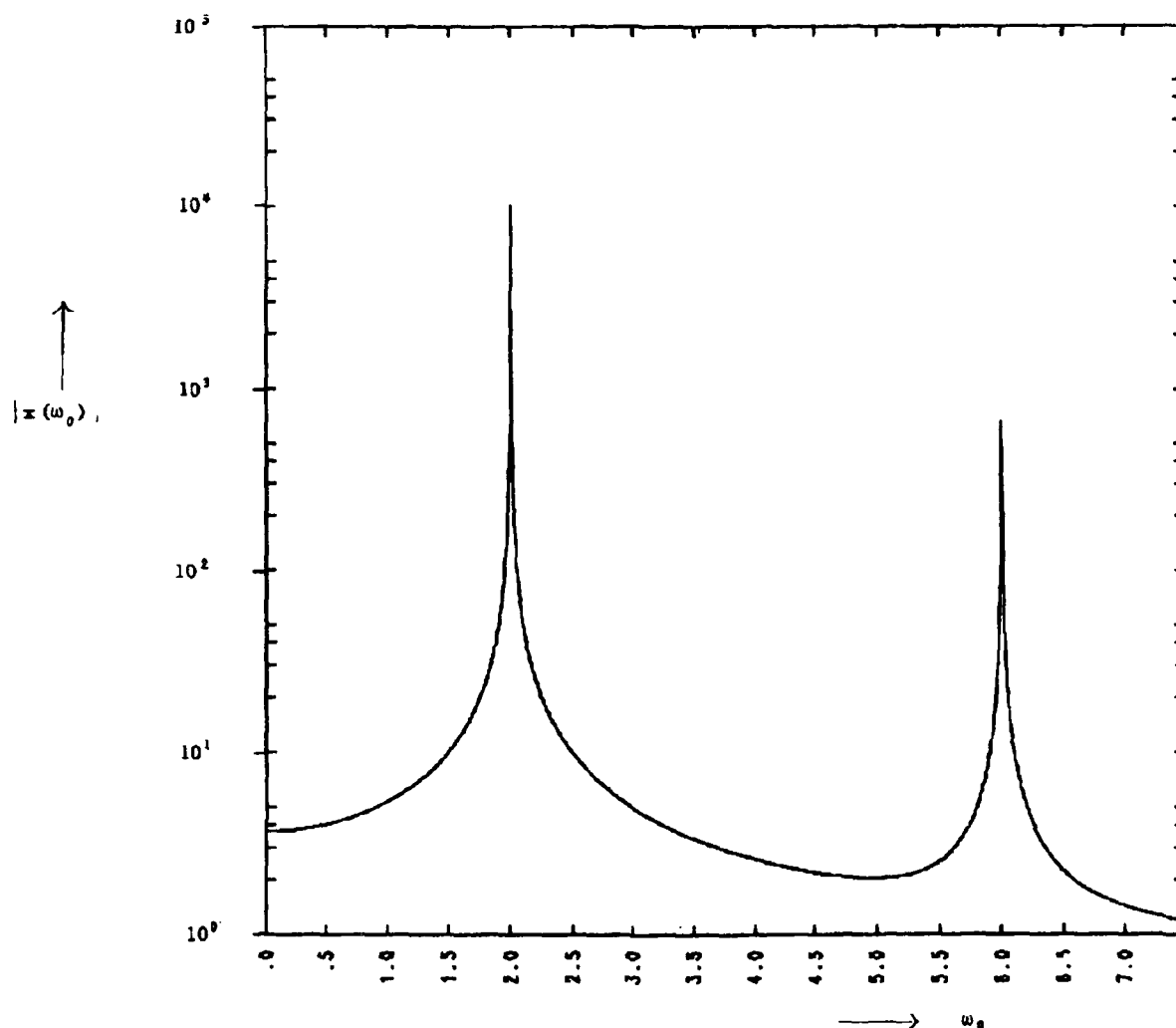


Figure 9. The frequency spectrum of x for the frequency locked case ($\varepsilon = 1.94$).

driven by external periodic force.³⁴ Upon combining the van der Pol self-oscillating nonlinearity with the Duffing potential equation (1), we found that the system became chaotic for small values of ε and for ω close to the natural frequency of self-oscillations.

The system which we studied was with $\mu > 0$, $\gamma > 0$, $\alpha < 0$, and $\beta > 0$. The frequency of self-oscillations, Ω , of the (stable) limit cycle of the system is (to leading order in μ)

given by $\Omega^2 = |\alpha| + (3\beta/\gamma)$. The amplitude, A of the limit cycle (to the same order in μ) is: $A^2 = 4/\gamma$. With an imposed external force this system exhibits a very rich dynamical behavior encompassing a variety of nonlinear dynamics phenomena. As a function of ε and ω , the system demonstrates periodic, quasiperiodic, frequency locked, and chaotic states.

We have numerically solved equation (1) for $\mu = 0.4$, $\alpha = -1$, $\beta = 1$, $\gamma = 1$, $\omega = 2$ and as

³⁴ Y. Ueda, "Steady Motions Exhibited by Duffing's Equation: A Picture Book of Regular and Chaotic Motions," in *New Approaches to Nonlinear Problems in Dynamics*, ed. P.J. Holmes (Philadelphia: SIAM, 1980).

a function of ε . For those parameters, the frequency of the limit cycle ($\varepsilon = 0$) is $\Omega \approx 1.13$. As ε is increased, the system has quasiperiodic solutions, shown in figure 6. The transition to chaos occurs around $\varepsilon \sim 0.785$. Figures 7 and 8, respectively, show the frequency spectrum and the strange attractor for $\varepsilon = .79$, where the system is chaotic. The transition to frequency locking, where the system (1) oscillates at the driving frequency (ω), occurs around $\varepsilon \sim 1.93$ (see figure 9). The transition to locking is abrupt (e.g., at $\varepsilon = 1.9322$ the system is chaotic, while at $\varepsilon = 1.9323$ the system is locked). Before reaching this frequency locked state, the system goes through other regions of locking where the ratio of the frequency of the system to ω is a rational number.

The system behaves similarly for fixed ε and as a function of ω . For $\varepsilon = 1$ and $\omega \sim \Omega$, there is frequency locking. As ω is increased, there is a transition to chaos around $\omega \sim 1.8$. The transition to quasi-periodicity occurs around $\omega \sim 2.3$.

Publications

- Batchelor, D.B., E.F. Jaeger, B.A. Carreras, H. Weitzner, K. Imre, D.C. Stevens, V. Fuchs, and A. Bers. "Full-Wave Modeling of Ion-Cyclotron Heating in Tokamaks." Proceedings of the 12th International Atomic Energy Agency Conference on Plasma Physics and Controlled Nuclear Fusion, Nice, France, October 12-19, 1988, Vol. 1, 611-620, IAEA-CN-50/E-II-5. Vienna: International Atomic Energy Agency, 1989.
- Bers, A., G.S. Triantafyllou, and A.K. Ram. "Absolute Instabilities in Inhomogeneous Flows." *Bull. Am. Phys. Soc.* 34: 2263 (1989).
- Chow, C., A. Bers, and V. Fuchs. "Analytic Studies of ICRF Heating." In *Radio Frequency Power in Plasmas*. A.I.P. Conf. Proc. 190. Ed. R. McWilliams, 234-237. New York: American Institute for Physics, 1989.
- Chow, C., V. Fuchs, and A. Bers. "Reflection at the Resonance Layer of the Fast Alfvén Wave in Ion Cyclotron Heating." Submitted to *Phys. Fluids B*.
- Chow, C., V. Fuchs, and A. Bers. "The Dispersion Relation for D(³He) Ion-Cyclotron Resonance Heating." *Phys. Fluids B*. Forthcoming.
- Chow, C., V. Fuchs, and A. Bers. *Reflection at the Resonance Layer of the Fast Alfvén Wave in Ion Cyclotron Heating*. MIT Plasma Fusion Center Report PFC/JA-90-2. Cambridge: MIT, 1990.
- Chow, C., V. Fuchs, and A. Bers. *The ICRF Dispersion Relation for D(³He)*. MIT Plasma Fusion Center Report PFC/JA-89-42. Cambridge: MIT, 1989.
- Chow, C., V. Fuchs, and A. Bers. "An Analytic Theory of ICRF Heating." (Abstract) *Bull. Am. Phys. Soc.* 34: 2094 (1989).
- Chow, C., V. Fuchs, and A. Bers. "Analytic Studies of ICRF Heating." Paper presented at the Sherwood Theory Conference, San Antonio, Texas, April 3-5, 1989.
- Chow, C., A. K. Ram, and A. Bers. "Damping of the Fast Alfvén Wave in Ion-Cyclotron Resonance Heating." *Phys. Fluids B* 1(10):2018-2026 (1989).
- Chow, C., A.K. Ram, and A. Bers. *Damping of the Fast Alfvén Wave in Ion-Cyclotron Resonance Heating*. MIT Plasma Fusion Center Report PFC/JA-89-19. Cambridge: MIT, 1989.
- Kupfer, K., A. Bers, and A.K. Ram. "Guiding Center Stochasticity by Electrostatic Waves in Toroidal Geometry." (Abstract) *Bull. Am. Phys. Soc.* 34: 1927 (1989).
- Kupfer, K., A. Bers, and A.K. Ram. "RF Induced Transport in Tokamak Plasmas." In *Radio Frequency Power in Plasmas*. A.I.P. Conf. Proc. 190, ed. R. McWilliams, 434-437. New York: American Institute for Physics, 1989.
- Kupfer, K., A. Bers, and A.K. Ram. "Transport of Charged Particles Interacting with Coherent Wave-Fields in a Tokamak

Plasma." Paper presented at the Sherwood Theory Conference, San Antonio, Texas, April 3-5, 1989.

Kupfer, K., A. Bers, and A.K. Ram. "Transport of Charged Particles Interacting with Coherent Wave-Fields in a Tokamak." Abstract presented at the Transport Task Force Meeting, Institute for Fusion Studies, Austin, Texas, January 11-13 1989.

Ram, A.K., and A. Bers. "Ray Tracing of Mode-Converted Ion-Bernstein Waves in Toroidal Plasmas." Paper presented at the Sherwood Theory Conference, San Antonio, Texas, April 3-5, 1989.

Ram, A.K., and A. Bers. "Kinetic Ray Tracing in Toroidal Geometry with Application to Mode-Converted Ion-Bernstein Waves." In *Proceedings of the 1989 International Conference on Plasma Physics*, New Delhi, India, 57-60. Eds. A. Sen and P.K. Kaw, 1989.

Ram, A.K., and A. Bers. "Kinetic Ray Tracing in Toroidal Plasmas." (Abstract) *Bull. Am. Phys. Soc.* 34: 2094 (1989).

Ram, A.K., and A. Bers. *Kinetic Ray Tracing in Toroidal Geometry with Application to Mode-Converted Ion-Bernstein Waves.* MIT Plasma Fusion Center Report PFC/JA-89-37. Cambridge: MIT, 1989.

Ram, A.K., A. Bers, and K. Kupfer. "Periodic Interactions of Charged Particles with Spatially Localized Fields." *Phys. Lett. A* 138: 288-294 (1989).

Shoucri, M., I. Shkarofsky, V. Fuchs, K. Kupfer, A. Bers, and S. Luckhardt. "A Quasilinear Fokker-Planck Code for the Numerical Solution of the Lower-Hybrid Current Drive Problem in the Presence of Electron Cyclotron Heating." *Comp. Phys. Comm.* 55: 253-268 (1989).

Shoucri, M., I. Shkarofsky, V. Fuchs, K. Kupfer, A. Bers, and S. Luckhardt. *A Quasilinear Fokker-Planck Code for the Numerical Solution of the Lower-Hybrid Current Drive Problem in the Presence of Electron Cyclotron Heating.* Report No.

CCFM-RI-298e. Varennes, Canada: Centre Canadien de Fusion Magnetique, Tokamak de Varennes, 1989.

1.3 Physics of Thermonuclear Plasmas

Sponsor

U.S. Department of Energy
Contract DE-AC02-ET-51013

Project Staff

Professor Bruno Coppi, Dr. Ronald C. Englade, Dr. Stefano Migliuolo, Dr. Linda E. Sugiyama, Sergio Angelini, Riccardo Betti, Paolo Detragiache, Darin Ehrnst, Marco Nassi

The main theme of our research program is the theoretical study of magnetically confined plasmas in regimes of thermonuclear interest. A variety of physical regimes that fall in this category characterize both present-day experiments on toroidal plasmas (e.g., Alcator, TFTR, JET) as well as future experiments that will contain ignited plasmas. These will either involve first generation fuels, namely a deuterium-tritium mixture (Ignitor, CIT), or more advanced fuels such as deuterium-deuterium or deuterium-helium mixtures (Candor).

We are participating in a collaborative effort involving the U.S. design group for the compact ignition experiment (CIT) and that for the European experiment, Ignitor. At MIT, the Alcator C-MOD experiment, combining the favorable features of elongated plasma cross section with high magnetic field, is under construction. These features, which are also being planned for CIT and Ignitor, were originally proposed for a machine called Megator, which we designed in the early 1970s.

Presently, our research program follows two major avenues. First, we are studying the basic physical processes of thermonuclear plasmas (equilibrium, stability, transport, etc.) as applied to existing or near-term future systems. In this effort, we are collaborating closely with our experimental colleagues, as well as with theorists from other research groups (e.g., JET, Princeton, Columbia). This work also involves time-

dependent simulations of plasma discharges in the planned D-T burning Ignitor experiment, with particular attention being focused on the evolution of spatial profiles of plasma current and temperature. Collaboration with our colleagues at the Italian laboratories of E.N.E.A., as well as in-house code development by a young scientist "on loan" from Italy plays a major role in this endeavor. Second, we are exploring advanced regimes of thermonuclear burning, including those employing low neutron yield fuels (D-³He, and "catalyzed" D-D). We are considering the design of machines that will contain these very high temperature plasmas as well as the physics that govern their behavior.

In the following section, we present some of the salient results of work which members of our research group have completed or are presently involved with.

1.3.1 Symmetries and Global Transport Equations

Understanding the time evolution of the current density profile and of the electron temperature is necessary in order to assess the effectiveness of the ohmic heating and, in general, to predict the stability of the plasma against global (resistive) MHD modes whose excitation depends on the current density distribution.

We formulate³⁵ constraints that apply to the current density profile in a high temperature toroidal plasma and introduce an effective thermal force and electron viscosity term in the current density equation. Correspondingly, the electron thermal energy equation acquires new terms. A matrix equation that relates the electron thermal energy transport to that of the current density is derived. The symmetry properties of this matrix are identi-

fied and used to prescribe realistic conditions on the electron temperature and current density profiles.³⁶

These profiles are relevant to high temperature regimes where: (a) the presence of a population of magnetically trapped electrons affects the plasma resistivity in such a way as to cause a current density distribution with a cusp-like profile³⁷ at the magnetic axis for the observed (canonical)³⁸ electron temperature profiles, when a simple Ohm's law is adopted to relate the current to the electric field, (b) the "ballooning" character of the $m=1$, $n=1$ instability which is driven by the plasma pressure gradient and can be expected to lead mainly to a pressure profile relaxation, leaving the current density profile mostly unchanged.

Furthermore, as the plasma temperature is increased, the contribution to the stability of this mode by terms related to microscopic plasma properties becomes important. In an ignited plasma, the presence of a population of energetic particles may lead to regimes where the $m=1$, $n=1$ relaxation is suppressed. These effects are not expected to account for the $m=1$, $n=2$ instability so that one half can be taken as a "hard" lower bound for the (inverse) helicity parameter, i.e., $q_0 > 1/2$.

1.3.2 Stabilization of Drift-Tearing Modes

A region of stability, in $\omega_* \tau_H - \Delta'$ parameter space (where $\omega_* = (mc/eBrn)(dp_e/dr)$ = electron diamagnetic frequency, m = poloidal mode number, τ_H = characteristic hydrodynamic time, Δ' = stability parameter for tearing modes) is discussed.³⁹ The growth rate of the drift-tearing mode is found to be a non-monotonic function of Δ' . As Δ'

³⁵ B. Coppi and F. Pegoraro, MIT/RLE Report PTP-90/2, MIT, 1990.

³⁶ Ibid.

³⁷ B. Coppi and L. Sugiyama, *Comm. Plasma Phys. Cont. Fusion* 10:43 (1986).

³⁸ B. Coppi, *Comm. Plasma Phys. Cont. Fusion* 5:261 (1980).

³⁹ S. Migliuolo, F. Pegoraro, and F. Porcelli, submitted to *Phys. Fluids* (1990).

increases from zero, the growth rate first reaches a maximum for $\Delta' \approx 0.5\Delta'_1$ and becomes negative for

$\Delta' \geq \Delta'_1 \approx 2m/\sqrt{\tau_H \omega_{*e}(\omega_{*e} - \omega_{*i})}$. Here ω_{*i} is the corresponding ion diamagnetic frequency. As this threshold for restabilization is approached, the mode eigenfrequency, ω , moves further and further away from ω_{*e} , and the mode eigenfunction acquires a strongly varying form within the singular layer. This is recognized as the breakdown of the constant- Ψ approximation, which occurs⁴⁰ in conjunction with large parallel electron currents within the layer, shielding of the perturbation from the ideal region and inhibiting reconnection.

As Δ' is increased further past a second threshold value $\Delta'_2 \approx \sqrt{2\tau_H \omega_{*e}/\epsilon_\eta}$ (where $\epsilon_\eta = \eta c^2 \tau_H / 4\pi r_0^2$ is a measure of the collisional resistivity at the singular surface, $q(r=r_0)=1$), a second root becomes unstable. This root corresponds to the diamagnetic modification of the $\epsilon_\eta^{1/3}$ version of the resistive tearing mode. For the $m=1$ case this mode is known as the resistive internal kink. Its stabilization for $\Delta' \leq \Delta'_2$, is understood to arise from the lessening in the free energy available to the mode from the plasma pressure gradient.

This window of stability had been identified previously,⁴¹ but its large width had been hitherto unrecognized. Its primary dependence is on ω_{*e} , with a weak dependence on the electron-ion temperature ratio: it disappears entirely for $\omega_{*e} \tau_H \leq 0.83\epsilon_\eta^{1/3}$. In figure 10, we show the stability diagram in the $\omega_{*e} - \Delta'$ space. The heavy continuous line denotes marginal stability, $\text{Im}(\omega) = 0$, while regimes are shown in which various modes appear with characteristic growth rates: $\gamma_R = m^{2/3}\epsilon_\eta^{1/3}\tau_H$ is the basic resistive mode growth rate, $\gamma_R = m^2\epsilon_\eta/|\omega_{*e}\omega_{*i}|\tau_H^2$ is the growth rate modified by finite diamagnetic

frequency, $\gamma_T \approx 0.5m^{2/5}\epsilon_\eta^{3/5}(\Delta')^{4/5}/\tau_H$ is that of the tearing mode, and $\gamma_{DT} \approx 0.2m^{2/3}\epsilon_\eta(\Delta')^{4/3}[\omega_{*e}(\omega_{*e} - \omega_{*i})]^{-1/3}\tau_H^{5/3}$ is that of the drift-tearing mode. There exists a branch cut for the problem, arising from the dispersion relation which can be written as:⁴²

$$\Delta'\delta = \frac{-m\pi}{8} Q \frac{\Gamma[(Q-1)/4]}{\Gamma[(Q+5)/4]}$$

where $\delta^4 \equiv -im^2\epsilon_\eta\tau_H\omega(\omega - \omega_{*i})/(\omega - \omega_{*e})$, and $Q \equiv -i\delta^2(\omega - \omega_{*e})/\tau_H m^2\epsilon_\eta$. Following one root of the dispersion relation along a closed path that encircles this point will cause us to return to the point of departure with a different eigenfrequency than that with which we started.

This theory applies directly to resistive $m=1$, $n=1$ modes with the substitution $\Delta' \rightarrow -m\pi/\lambda_H$. Values of parameters that correspond to the stable domain in figure 10 are relevant to $m=1$ modes in magnetically confined toroidal plasmas with low values of the poloidal beta parameter. For these modes, the stable region can be accessed when the magnetic shear, \hat{s} , is reduced near the $q=1$ surface even if q at center is significantly less than unity. This is because $\tau_H\omega_{*e}/\epsilon_\eta^{1/3} \propto \hat{s}^{-2/3}$, while $\hat{\lambda}_H = -\pi m^{1/3}/(\Delta'\epsilon_\eta^{1/3}) \propto (q_0 - 1)/\hat{s}^{5/3}$.⁴³ Thus, lowering the shear takes us toward the upper left corner of figure 10, i.e., deep into the stable region.

1.3.3 $M^0 = 1$ Internal Modes in High Temperature Regimes

As present experiments (e.g., JET) reach the multi-keV regime of plasma temperatures, models for the stability of $m^0 = 1$ internal modes must be improved to account for kinetic effects due to the ions and electrons. In these regimes, as well as in those relevant

⁴⁰ J.F. Drake, T.M. Antonsen, Jr., A.B. Hassam, and N.T. Gladd, *Phys. Fluids* 26:2509 (1983).

⁴¹ M.N. Bussac, R. Pellat, D. Edery, and J.L. Soule, in *Plasma Physics and Controlled Nuclear Fusion Research 1976* (Vienna:IAEA, 1977), Vol. 1, p. 607; B. Coppi, R. Englade, S. Migliuolo, F. Porcelli, and L. Sugiyama, in *Plasma Physics and Controlled Nuclear Fusion Research 1986* (Vienna:IAEA, 1987), Vol. 3, p. 397.

⁴² S. Migliuolo, F. Pegoraro, and F. Porcelli, submitted to *Phys. Fluids* (1990).

⁴³ F. Porcelli, W. Han, F. Pegoraro, and A. Taroni, *JET Report JET-IR(88)16*.

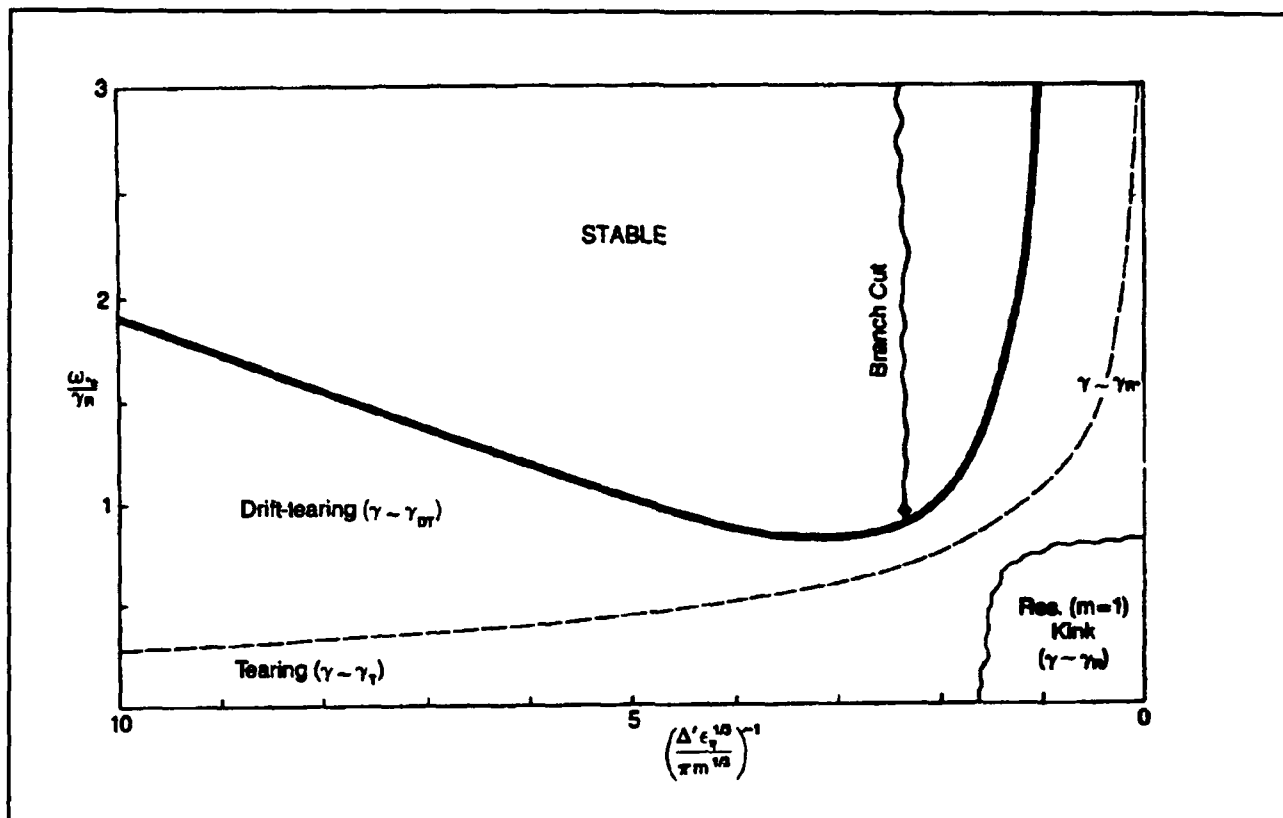


Figure 10. Stability diagram for resistive internal modes and drift-tearing modes. For $m^0 = 1$, $\Delta'/m\pi \rightarrow -1/\lambda_H$.

to planned ignition experiments such as Ignitor, standard two-fluid theory⁴⁴ is inadequate: the gyral radius of the plasma ions, ρ_i , becomes a finite fraction of the scaled radius of the singular surface, $\epsilon_\eta^{1/3} r_0$. Here r_0 is the radius where $q(r) = rB_z/RB_\theta = 1$ and $\epsilon_\eta = \eta c^2 \tau_H / 4\pi r_0^2$ is a measure of the electrical resistivity. As a consequence finite Larmor radius (FLR) effects must be taken into account. These effects are known⁴⁵ to be destabilizing because they establish a minimum value for the thickness of the singular layer about $r = r_0$, where reconnection can occur: $\delta/r_0 = \max(\rho_i/r_0, \lambda_H)$ where λ_H is the ideal MHD stability parameter. Also, in regimes where $\lambda_H < \rho_i/r_0$, FLR acts to raise the mode frequency thereby lessening the

stabilizing effect of finite diamagnetic ion frequency (ω_i).

We have generalized the kinetic model described in Pegoraro et al.,⁴⁶ including the stabilizing effects of ion viscosity through a particle and momentum conserving Krook collision operator. For low values of FLR and ion viscosity effects (i.e., compared to λ_H and in the regime where the ideal mode is stable, $\lambda_H < \omega_i \tau_H / 2$), the normalized eigenfrequency of the internal $m^0 = 1$ resistive kink, $\lambda = -i\omega \tau_H$ becomes:

$$\lambda = i \frac{\lambda_H^2}{\lambda_i} + \frac{5\epsilon_\eta}{2\lambda_i^2} - \frac{\rho_i^2 \lambda_v}{4\lambda_H^2}$$

⁴⁴ G. Ara, B. Basu, B. Coppi, G. Laval, M.N. Rosenbluth, and B.V. Waddell, *Ann. Phys. (N.Y.)* 112:443 (1978).

⁴⁵ F. Pegoraro, F. Porcelli, and J.J. Schep, *Phys. Fluids* B1:364 (1989).

⁴⁶ Ibid.

$$\left[\frac{\lambda_i^2 \lambda_v^2 + 2\lambda_H^4}{\lambda_i^2 \lambda_v^2 + \lambda_H^4 - \frac{3}{4}} \right] + \frac{i\rho_i^2}{4\lambda_i} \left[\frac{3}{4} - \frac{\lambda_i^2 \lambda_v^2}{\lambda_i^2 \lambda_v^2 + \lambda_H^4} \right]$$

which clearly shows the stabilization of the FLR enhanced resistive mode when $\lambda_v \equiv v_i \tau_H$ is large enough to overcome the effect of finite electrical resistivity, e.g., $\lambda_v \geq 40\epsilon_\eta(\lambda_H/\rho_i \lambda_i)^2$ when $\lambda_H^4 \ll \lambda_i^2 \lambda_v^2$.

We are continuing this study by numerically exploring regions in parameter space (e.g., $\lambda_H \rightarrow 0$ and/or $\rho_i/\epsilon_\eta^{1/3}\tau_0 > 1$) where analytic perturbation techniques are inappropriate. In this manner, we are able to rather accurately predict regimes where ignition experiments (e.g., Ignitor) will be able to operate without incurring sawtooth crashes.

1.3.4 Nonlinear Ballooning Modes

Ballooning modes⁴⁷ play a very important role in the dynamics of high β equilibrium configuration. A two dimensional Rayleigh-Taylor-ballooning-like model has been developed to simulate their nonlinear behavior. In this model the equilibrium magnetic field lines are at an angle ψ with the two-dimensional domain. Two forces act on the plasma: the buoyancy force which drives the dense fluid to the bottom and the less dense fluid to the top; and the line bending force, which resists any movement of the fluid and vanishes at $\psi = 90$ deg.

A set of reduced MHD equations,⁴⁸ is numerically solved using a novel magnetic stress-tensor formulation,⁴⁹ which allows energy conservation with an explicit time advance, and a finite difference scheme in both directions.

An equilibrium configuration with a steep density gradient has been studied extensively in both the ideal and resistive regimes, and for different initial perturbations.

In the ideal case with random initial conditions, the dominant mode chooses a wavelength that is the maximum between the grid size and $\hat{K}y^2d^2 = (1/v_A^2)(gd/r_\rho)/\sin^2\Phi - \pi/2$ where d is the vertical dimension, v_A is the Alfvén speed, g is the gravity, r_ρ is the density gradient scale length, and $\Phi = \pi/2 - \phi$. The saturation mechanism is provided by the bending of the magnetic field lines. Single wavelength initial perturbations have shown a non-linear growth of a bubble-like structure in the limit of a very steep density gradient and large value of the angle ψ .

The inclusion of resistivity⁵⁰ drives unstable modes with wavelengths of the size of the physical domain in the presence of perfect conducting walls and incompressible flow.

The numerical solution is in good agreement with the finite amplitude analytic results obtained with a multiple time scale analysis of the equations for a sharp boundary configuration and an angle $\psi = 0$.⁵¹

In order to include the effect of magnetic field curvature as the driving mechanism, a three-dimensional code is being developed. A preliminary simplified version of the code has been completed using finite difference in all three dimensions and the first results were

⁴⁷ B. Coppi, J. Filreis, and F. Pegoraro, *Ann. Phys.* 121:1 (1979).

⁴⁸ H.R. Strauss, *Phys. Fluids* 8:1354 (1977).

⁴⁹ R. Betti, J.U. Brackbill, B. Coppi, and J.P. Freidberg, *Proceedings of the 13th Plasma Simulation Conference*, Santa Fe, New Mexico, 1989.

⁵⁰ H.P. Furth, J. Killeen, M.N. Rosenbluth, and B. Coppi, in *Plasma Physics and Controlled Nuclear Fusion Research 1966* (Vienna: IAEA, 1967), Vol. 1, p. 103; B. Coppi, *Phys. Rev. Lett.* 39:939 (1977).

⁵¹ R. Betti, J.U. Brackbill, B. Coppi, and J.P. Freidberg, *Bull. Am. Phys. Soc.* 34:2046 (1989).

reported at the 1989 APS meeting.⁵² However, the final version of the three-dimensional mode will adopt spectral method in θ and ϕ ,⁵³ finite difference in r , and a Semi-Implicit time advance algorithm.⁵⁴

1.3.5 SOL Plasma Behavior in a Compact High Field Torus

Recent data for large and small limiter tokamaks in the ohmic phase have been analyzed. These experimental results have been correlated⁵⁵ to important properties of the plasma scrape-off layer (SOL), namely: $\nabla_{\perp} T_e \neq 0$, plasma recycling, shielding of impurities, and radiative cooling. The basic behavior of the SOL plasma in the Ignitor device may be anticipated on the basis of simple physical considerations.⁵⁶ Recent experimental data has confirmed that the higher the average density is, the lower are the edge temperature and edge density.⁵⁷ A high edge density means a high probability of interaction between ions and neutrals as well as impurities. Taking into account that the average density predicted in the Ignitor device is an order of magnitude larger than that in present large tokamaks, the following phenomena may be expected:

- High ionization rate of neutrals, hence a high level of recycling.
- Ability to screen the main plasma from impurities and, thus, the opportunity to reduce Z_{eff} .

- High level of impurities in the SOL plasma and its strong radiative cooling.

The main numerical results⁵⁸ have been obtained for plasma edge density $= 2.4 \times 10^{20} \text{ m}^{-3}$ (with $\bar{n} = 6 \times 10^{20} \text{ m}^{-3}$), edge temperature $= 10 \text{ eV}$, and scrape-off decay length $= 7.5 \times 10^{-3} \text{ m}$. These results confirm that the SOL in the Ignitor device has a complex behavior and that some distributed processes ($\nabla_{\perp} T_e$, recycling, impurity shielding, radiative cooling) are occurring. The consequences of this situation for the power balance and for the thermal wall loading can be summarized as follows:

- The radiative cooling becomes dominant.
- The mean kinetic energy of the ions impinging on the first wall is low (4.8 eV) and might be lower than that required to cause sputtering.
- The thermal wall loading is of the order of 1.2 MW/m^2 .

1.3.6 Plasma Dynamics Simulation by the TSC Code

We have begun an investigation of the plasma dynamics of the flat top of the plasma current, as well as of the ramp-up phase, of the discharge in a deuterium-tritium ignition experiment, using the TSC⁵⁹ code. This Tokamak Simulation Code, developed at PPPL, models the axisymmetric transport time evolution, positional stability, and control properties of non-circular, free

⁵² Ibid.

⁵³ H.C. Ku, R.S. Hirsh, and T.D. Taylor, *J. Comp. Phys.* 70 (1987).

⁵⁴ D.D. Schnack, D.C. Barnes, and Z. Mikic, *J. Comp. Phys.* 70 (1987).

⁵⁵ P.C. Strangeby, *J. Nucl. Mat.* 105:145-147 (1987).

⁵⁶ P.C. Strangeby, in *Physics of Plasma Wall Interactions in Controlled Fusion*, eds. D.E. Post and R. Behrisch (New York: Plenum Press, 1986); J. Roth, *ibid.*; P.C. Strangeby, *Phys. Fluids* 28:55 (1985).

⁵⁷ S.K. Erents et al., *Nucl. Fusion* 28:1209 (1988).

⁵⁸ M. Nassi, in *Tritium and Advanced Fuels in Fusion Reactors*, ISPP-5, eds. G. Bonizzoni and E. Sindoni (Bologna, Italy: SIF, 1989), p. 289.

⁵⁹ S.C. Jardin, N. Pomphrey, and J. DeLucia, *J. Comp. Phys.* 66: 481 (1986).

boundary tokamaks.⁶⁰ It provides a time dependent, nonlinear description of the axisymmetric MHD and transport behavior of the plasma in two spatial dimensions. This problem is very complex, due to the disparate time scales of diffusion-like and wave-like phenomena, and to the anisotropy introduced by the magnetic field. A self-consistent solution is obtained by solving the plasma momentum and field evolution equations on a two-dimensional X-Z grid, and the plasma energy and particle evolution equations in a one dimensional coordinate system which evolves with the plasma magnetic surfaces.⁶¹ The TSC code takes into account the plasma interaction with a set of poloidal conductors that model the passive structure of the plasma chamber as well as with the active poloidal field coils. These conductors obey electromagnetic circuit equations with active feedback systems included.

An extensive numerical simulation is being performed in order to determine the characteristic time scale for vertical instability of the plasma column and to design a feedback system to control it. The axisymmetric vertical instability occurs when the plasma column shifts rapidly due to a loss of vertical control. As soon as the plasma moves slightly off the equilibrium position at the midplane, its current interacts with the radial component of the external poloidal magnetic field, giving rise to a force that increases its vertical displacement. This motion, if not controlled, leads to a disruption. The rapid plasma displacement from the midplane induces toroidal currents in the upper and lower halves of the vacuum vessel, which flow in opposite directions. These currents interact with the plasma and produce a force that

attempts to return the column back to its equilibrium position. This stabilizing effect is very important because it increases the time scale for the vertical instability from an ideal MHD time measured in microseconds to the L/R time scale (milliseconds). On this slower time scale, it is possible to design an active feedback system which can control the plasma vertical position. Preliminary results have been presented⁶² on the growth rate of the plasma vertical instability with and without an external stabilizing structure and on the plasma vertical position control by an external feedback system.

Preliminary results⁶³ on the ignition plasma performance using the Coppi-Tang transport model⁶⁴ as well as a study on the Volt-second requirements throughout the discharge have been presented.⁶⁵ We have modified the transport model by assuming that the anomalous electron heat flux can be described by a modified form of the Coppi-Mazzucato-Gruber thermal diffusivity, which can reproduce ohmic and L- or H-mode experimental results in the auxiliary heating regimes. We are presently engaged in studying the problem of the plasma current penetration during the current ramp phase of the discharge in which the magnetic field, current, and plasma density are simultaneously ramped.

1.3.7 Thermal Transport in the Transition Regime

We have used a transport code to investigate semi-empirical forms for anomalous electron and ion heat transport in the transition regime linking "cool" ohmic plasmas and "hot" discharges sustained predominantly by

⁶⁰ S.C. Jardin et al., *Nucl. Fusion* 27: 569 (1987); B.J. Merrill and S.C. Jardin, *J. Nucl. Mat.* 881: 145-147 (1987).

⁶¹ S.C. Jardin, in *Multiple Time Scale*, eds. J.U. Brackbill and B.I. Cohen (New York: Academic Press, 1985).

⁶² M. Nassi, in *Tritium and Advanced Fuels in Fusion Reactors*, ISPP-5, eds. G. Bonizzoni and E. Sindoni (Bologna, Italy: SIF, 1989), p. 289.

⁶³ M. Nassi, S.C. Jardin, and N. Pomphrey, *Bull. Am. Phys. Soc.* 34: 1974 (1989).

⁶⁴ W.M. Tang, *Nucl. Fusion* 26: 1605 (1986).

⁶⁵ M. Nassi, in *Tritium and Advanced Fuels in Fusion Reactors*, ISPP-5, eds. G. Bonizzoni and E. Sindoni (Bologna, Italy: SIF, 1989), p. 289.

external auxiliary heating or fusion heating.⁶⁶ Knowledge of the thermal transport appropriate to this regime is particularly relevant to the expected performance of compact ignition devices such as Ignitor and CIT.

We have represented the electron heat diffusivity with a modified form of the well-known Coppi-Mazzucato-Gruber coefficient, written as:

$$\chi^e = \frac{7.9 \times 10^{15}}{\bar{A}_i^{0.4} n_e} \frac{I(r)}{T_e(r)} \frac{a}{r^2} \left[1 + \gamma_0 \left(1 - \frac{P_{OH}}{P_{TOT}} \right)^2 <\beta_p> \right]$$

where I is the total plasma current in kA within the radius r , n_e is the electron density in cm^{-3} , T_e is the electron temperature in keV, a is the radius of the outermost flux surface in cm, \bar{A}_i is the mean ion atomic weight, P_{OH} and P_{TOT} are the Ohmic and total heating powers, and $<\beta_p>$ is the volume average total poloidal beta parameter.

This transport accounts reasonably well for the temperature behavior of a wide variety of ohmically heated toroidal devices when the effects of ion heat conductivity are small. The term proportional to $<\beta_p>$ is intended to reflect an enhanced level of microinstabilities that accompanies the increase of the thermal energy content above a threshold value assumed close to that of a steady state ohmic discharge.⁶⁷ The ion heat transport is modelled with a combination of neoclassical and

anomalous thermal diffusivity. For operational purposes, we assume the latter to have the same outwardly increasing spatial behavior as the χ_e discussed above but with a magnitude that is allowed to vary from simulation to simulation.

We have applied this model to a series of ohmic and L-mode neutral beam heated discharges performed at 1.4 MA and 2.2 MA on the TFTR device in which the individual temperature behavior of the electrons and ions could be resolved.⁶⁸ Comparing simulation results with the observations and directly testing the effects of model variation, we find that $\gamma_0 \approx 9.0$ in combination with a ratio of $(\chi_i/\chi_e)^{ANOM}$ that increases with auxiliary power from 0.2 at $P_{AUX} = 0$ ($T_i \sim 2.5$ keV) to a value between 1.1 and 1.8 at $P_{AUX} = 15$ MW ($T_i \sim 8$ keV) yields a good fit for the complete data set. The inferred temperature dependence of χ_i^{ANOM} is not inconsistent with that associated with either the ion mixing mode⁶⁹ or the trapped particle ubiquitous mode.⁷⁰ We note that the value of γ_0 reported above can also be applied to L-mode discharges on ASDEX.⁷¹

1.3.8 Electron Thermal Transport in Ohmic Experiments

The investigation of the electron thermal diffusion coefficient in ohmic toroidal experiments carried out in the past year has included the numerical simulation of the steady states of a number of ohmic toroidal experiments with circular cross section.⁷² These included Alcators A and C, FT, ASDEX, TEXT, T-10, and TFTR. The ASDEX

⁶⁶ R. Englade, submitted to *Nucl. Fusion* (1990).

⁶⁷ R. Englade, *Nucl. Fusion* 29: 999 (1989).

⁶⁸ R. Hawryluk, V. Arunasalam, M. Bell et al., in *Plasma Physics and Controlled Nuclear Fusion Research: Proceedings of the 11th International Conference*, Kyoto, 1986 (Vienna: IAEA, 1987), Vol. 1, p. 51; R. Goldston, V. Arunasalam, M. Bell et al., p. 75.

⁶⁹ T. Antonsen, B. Coppi, and R. Englade, *Nucl. Fusion* 19: 641 (1979).

⁷⁰ B. Coppi, MIT/RLE Report PTP-89/1 (Cambridge: MIT, 1989).

⁷¹ M. Keilhacker, G. Gierke, E. Müller et al, *Plasma Phys. Controlled Fusion* 28: 19 (1986).

⁷² L. Sugiyama, MIT/RLE Report PTP-89/3 (Cambridge: MIT, 1989).

cases included pellet-injected and improved ohmic confinement (IOC) phases as well as the corresponding "saturated" ohmic (SOC) phases. Similarly, Alcator C cases included pellet-injected and saturated ohmic phases, although here the pellet injected phase was not in steady state. The transport model assumed a Coppi-Mazzucato-Gruber electron thermal diffusion and neoclassical ion thermal diffusion. It correctly identified the cases where the ion thermal transport exceeded neoclassical (Alcator C and ASDEX saturated states).

In cases where the energy balance was dominated by the ohmic heating and the electron thermal diffusion, the CMG model gave a good fit to the experimental data. These included Alcator A at low q , FT, lower radiation TFTR cases, and one of the ASDEX pellet cases. The model predicted excess transport loss for cases where other losses were large — in particular, to some degree for all the ASDEX pellet and IOC cases, where radiation loss was large and centrally peaked (60 percent P_{OH}). Alcator A at high q , with higher radiation loss than the low q cases (~ 50 percent P_{OH}), was also poorly fit, although the experimental uncertainties in this case were relatively large. The single TEXT case could not be matched because a large particle inflow at the plasma edge and the corresponding density profile near the edge was difficult to fit with the simple model. The T-10 case behaved differently from the others and could not be fit; it has been suggested that charge exchange cause large thermal losses through the ions, consistent with the very low ion temperatures observed but not reproduced by the model.

In all cases except TFTR, only the purely ohmic form of the χ_e diffusion coefficient was used. Since it was derived by balancing the ohmic heating and the thermal diffusion, it is not surprising that it fits these cases best and that it overestimates the electron thermal transport when other losses, such as radiation, are important. One important result of the simulation is that the scaling adopted for the plasma voltage, V_p , is shown to fit a wide

range of different experiments, particularly in the plasma dimensions, where the voltage ranges from less than unity to 2.6.

The results are consistent with the results from the analysis of the TFTR ohmic discharges, that the electron energy confinement time

$$\tau_{Ee} = W_e / P_{He} \equiv W_e / (P_{OH} - P_{RAD} - P_{ie})$$

does not have a good power law scaling with the plasma parameters except in the case when $P_{RAD} + P_{ie}$ is small, because the net heating P_{He} does not. In contrast, the total energy confinement $\tau_E = (W_e + W_i) / P_{OH}$ possesses a good power law scaling, for example, neo-Alcator $\bar{n}_e q R^2 a$, although the exact powers cannot be determined too accurately. This state of affairs is consistent with the fundamental role of the loop voltage, and the existence of a good global scaling for it, in determining τ_E , but not τ_{Ee} . The loop voltage scaling, like the τ_E scaling, holds even for cases where radiation losses are large, but would be expected to break down when the ion thermal transport becomes large enough to affect the electron temperature and, therefore, the voltage. These conjectures, as well as an improved form for the CMG thermal diffusion, are being investigated. A test of the implications for the electron thermal transport of auxiliary heated discharges will also be made.

1.3.9 Combined Transport and Ray Tracing Studies of ECRF Heating in CIT

We have continued our fruitful collaboration with Dr. Miklos Porkolab, task leader for the assessment of electron cyclotron radio frequency (ECRF) heating prospects in the proposed Compact Ignition Tokamak (CIT). A 1 1/2 D equilibrium and transport code⁷³ in which thermal fluxes are expressed as the sum of an outward conduction term and an inward heat pinch and which models power deposition results obtained from a stand-alone ray tracing package has been used to

⁷³ M. Porkolab, P. Bonoli, R. Englade et al., 16th European Conference on Controlled Fusion and Plasma Physics, Venice, 1989.

study ECRF-assisted ignition scenarios for the most recent design parameters. These simulations take into account realistic start-up conditions in which current, magnetic field, and density are simultaneously ramped and the rays launched appropriately to maintain efficient plasma heating. Recently, we have made excellent progress in developing a large combined code in which the ECRF ray propagation and absorption, the MHD equilibrium calculation, and the plasma heat transport are treated self-consistently.⁷⁴ The ECRF package is a variation of the TORAY⁷⁵ toroidal ray tracing code, valid in both the Doppler and relativistic regimes. The values along a ray trajectory of the temperature, density, magnetic field components, and the derivatives of these quantities in a Cartesian coordinate system that are required inputs to TORAY have been obtained by a modification of the BALDUR 1 1/2 D equilibrium package utilized in⁷⁶ This modification makes extensive use of a procedure originally developed to track a chord through the nested flux surface geometry of a toroidal device.⁷⁷ Much work remains to be done on optimizing the combined code, reducing its use of computer resources, and installing necessary diagnostics. Based on the few trials performed so far, however, it is performing its basic functions as expected and has the potential to become a useful physics tool.

1.3.10 Studies of Advanced Fuel Fusion

Magnetic confinement geometries employing tight aspect ratios, high current densities, and high magnetic fields have long been proposed for the study of the ignition of deuterium-tritium plasmas and α -particle heating.⁷⁸ Recent work⁷⁹ on the Ignitor project in Europe has demonstrated in detail the feasibility of constructing such devices and suggested means of further increasing their operating pulse lengths and flexibility. Simultaneously, studies of the physics of the ignition process suggest that D-T ignition may be relatively easy to achieve.⁸⁰ These considerations have brought renewed interest (since 1980)⁸¹ in the possibility of burning the so-called advanced fuels with significantly lower neutron yields than D-T, i.e., D - ^3He or D-D with an initial fueling of ^3He , where 6-10 percent of the energy is produced in energetic neutrons for a 30 percent mixture of ^3He , compared to 80 percent for D-T.

We have developed⁸² a 1D transport model that includes two ion species, the important D - ^3He and D-D cycle fusion reactions, and the synchrotron and bremsstrahlung radiation losses and applied it to the ignition problem. We have further investigated the character-

⁷⁴ P. Bonoli, R. Englade, M. Porkolab et al., *Bull. Am. Phys. Soc.* 34:2133 (1989).

⁷⁵ A. Kritz et al., *Proceedings of the Third International Symposium on Heating in Toroidal Plasmas*, Brussels, 1982, Vol. II, p. 707.

⁷⁶ M. Porkolab, P. Bonoli, R. Englade et al., Sixteenth European Conference on Controlled Fusion and Plasma Physics, Venice (1989).

⁷⁷ S. Attenburger, W. Houlberg, and S. Hirshman, *J. Comput. Phys.* 72:435 (1987).

⁷⁸ B. Coppi, MIT/RLE Report PRR-75/18, MIT, 1975, and *Comm. Plasma Phys. Cont. Fusion* 3:2 (1977).

⁷⁹ B. Coppi and L. Lanzavecchia, *Comm. Plasma Phys. Cont. Fusion* 11:47 (1987).

⁸⁰ L. Sugiyama, MIT/RLE Report PTP-84/2 (Cambridge: MIT, 1984); R.C. Englade, *Nucl. Fusion* 29:999 (1989).

⁸¹ S. Atzeni and B. Coppi, *Comm. Plasma Phys. Cont. Fusion* 6:77 (1980); B. Coppi and G. Vlad, MIT/RLE Report PTP-82/16 (Cambridge: MIT, 1982); and G. Vlad, *Il Nuovo Cimento* 84B:141 (1984).

⁸² B. Coppi and L. Sugiyama, MIT/RLE Report PTP-88/6 (Cambridge: MIT, 1988), submitted to *Nucl. Fusion*.

istics of an experiment of the Candor⁸³ type and shown⁸⁴ that it may be possible to ignite in D-³He, under "favorable" although still degraded conditions on the plasma thermal transport, with either an initial deuterium and tritium plasma and a moderate amount of auxiliary heating, or with no tritium and a much larger amount of auxiliary heating. Some of the major problems uncovered were the need to rapidly heat a fairly dense plasma from a few keV to some 70 keV and $\bar{n}_e \approx 1.5 - 2 \times 10^{15} \text{ cm}^{-3}$, and central control of the concentrations of the various nuclei, so that fuel nuclei can be added and the inert fusion products removed after they have slowed down in the plasma. The neutron production and the α -particle buildup may be significant if D-T burning is used to start the sequence, even with small amounts of initial tritium (10-15 percent). The plasma β may reach or exceed the first limit of stability to ideal MHD modes and means to control the transition to the second stability region may be necessary.

In the past year, work has focused on extending the analysis to include the effects of plasma geometry and finite beta,⁸⁵ by modifying a 1 1/2D transport simulation code, BALDUR, as developed by G. Bateman at PPPL. Concurrent work done on low beta DT ignition in a similar configuration suggests a number of areas to investigate, but we have not developed a consistent set of models valid for high beta yet. This work is continuing.

1.4 Investigation of Electron Cyclotron Resonance Plasma Production in the Versator II Tokamak

Sponsor

U.S. Department of Energy
Contract DE-AC02-ET-51013

Project Staff

Professor Miklos Porkolab, Dr. Kuo-In Chen, Dr. Stanley C. Luckhardt, Stefano Coda, Jeffrey A. Colborn, Edward W. Fitzgerald, Robert J. Kirkwood, Alberto Leon, Kurt A. Schroder, Jared P. Squire, Jesus N.S. Villasenor

During 1989, we investigated the characteristics of plasmas generated by RF and electron cyclotron resonance (ECR) in the Versator II device. These RF produced and sustained plasmas have important applications in the start-up phase of proposed large scale fusion power producing tokamaks such as ITER and CIT. These plasmas have potential use in applications as diverse as laboratory simulation of space and ionospheric plasmas, basic plasma turbulence studies, and plasma processing of materials. The principle distinction between RF sustained plasmas and standard tokamak plasmas is that the RF sustained plasmas have little or no net toroidal plasma current. The plasma confinement in the tokamak relies on a magnetic field configuration produced by a large current flowing in the plasma and a toroidal field supplied by external coils. In the case of the ECR sustained plasmas, little or no net plasma current flows, instead the plasma is confined by a combination of a toroidal field, a weak externally applied vertical field, and radial electric fields generated by plasma transport processes. Plasma theory suggests that these electric fields, in combination with the external magnetic fields, provide the surprisingly good plasma confinement observed in our experiments.

⁸³ Ibid.; B. Coppi, *Nucl. Instr. Methods Phys. Res.* A271:2 (1988).

⁸⁴ B. Coppi and L. Sugiyama, MIT/RLE Report PTP-88/6, MIT, 1988, submitted to *Nucl. Fusion*.

⁸⁵ L.E. Sugiyama, *Bull. Am. Phys. Soc.* 34:2171 (1989).

The aim of the present electron cyclotron heating experiments on Versator II is to (1) develop an understanding of the particle and energy transport, ionization processes, and single particle orbital confinement; (2) determine the characteristics of EC-ionized plasmas and their dependence on RF power levels and other parameters; (3) measure internal electric fields; and (4) investigate plasma currents that can be initiated by launching lower-hybrid waves into such plasmas.

Last year, we performed EC-ionization experiments on Versator-II using the NRL/MIT gyrotron, which produces 35.07 GHz microwaves in the circular TE_{10} mode. These microwaves are subsequently converted to the TE_{11} and then the HE_{11} mode.⁸⁶ In the present configuration, these linearly-polarized waves are launched perpendicularly to B_0 in the X-mode polarization from the high magnetic field side (inside) of the torus via a mirror. By rotating the mirror, we can vary the toroidal launch angle from -60 degrees to $+60$ degrees. The gyrotron is quite compact, requiring extensive modification of several of its components in a nearly-completed program to increase the pulse length and power level to 10–20 ms and 75–100 kW. For the data presented here, we achieved pulse lengths and power levels of 1–2 ms and 40–50 kW, and $B_0 = 1.25T$, placing the electron-cyclotron layer at the center of the vacuum chamber, which has $R_0 = 0.40m$ and $a = 0.13m$. In the experiments described below, a vertical field $B_v < 0.017T$ was applied, the vacuum chamber was prefilled with H_2 gas, and no gas was puffed in during the discharges. We measured density profiles along vertical chords using a radially-movable microwave interferometer, but measured the H_α light emission profiles vertically and horizontally by a movable detector that we placed on the bottom or side of the tokamak.

We found several phenomena in these initial experiments that were consistent with our

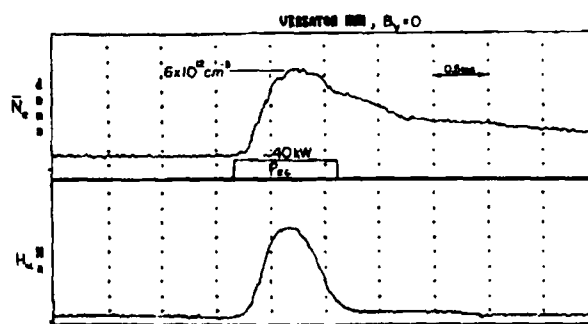


Figure 11. Time evolution of typical ECRH ionization plasma density and H_α light emission signals. The externally applied magnetic field is purely toroidal in this case.

theoretical interpretation. In the following, we summarize the results briefly. Figure 11 shows the time evolution of a typical EC-ionized discharge. The long decay-time of the electron density in these experiments, also shown in figure 11, in the absence of a measurable poloidal magnetic field is indicative of good plasma confinement. We believe this long delay time can be explained if there are internally generated radial electric fields in the plasma. We believe that a combination of the external magnetic field and internally generated electric fields and currents provides confinement of the plasma on a time scale much greater than the single particle drift time scale ~ 10 microseconds. As indicated by the H_α light emission (proportional to the hydrogen ionization rate), the ionization rate reaches a maximum about 0.5 ms into the EC pulse. Both of these features are roughly independent of applied B_v .

The electron density as a function of time and radius (vertically chord-averaged) is shown in figure 12. The most notable feature is that, starting from very early in the discharge, the density peaks at a point between the cyclotron layer (at $r=0$) and the upper-hybrid layer. This is consistent with the

⁸⁶ S.C. Luckhardt et al., "Applications of Radio Frequency Power to Plasmas," in *Proceedings of the Seventh Topical Conference*, Kissimmee, Florida, 1987, p. 29.

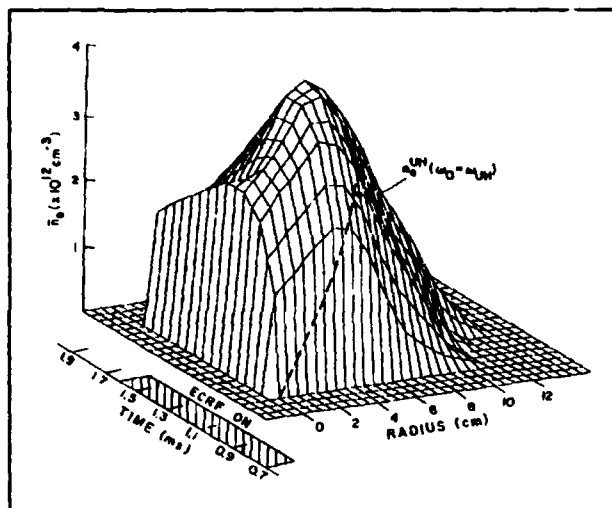


Figure 12. Time evolution of plasma density profiles during ECRH ionization.

findings of others.⁸⁷ Figure 13 shows the analogous plot for the H_α light emission. Note that the plot peaks sharply, shifting outward to a position near the upper-hybrid layer ($\omega = \omega_{UH}$) as the discharge progresses. These radial dependencies of the plasma

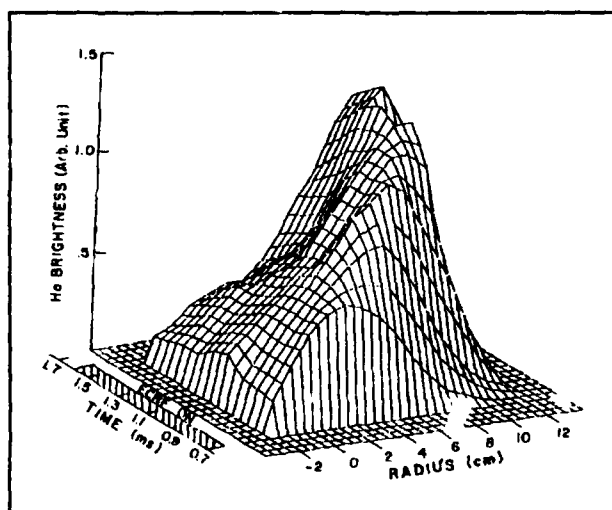


Figure 13. H_α light emission profiles during ECRH ionization.

density and H_α light emission are consistent with the currently accepted understanding of the plasma heating/ionization processes going on near the cyclotron resonance layer. That is, after a very low density plasma is formed at the cyclotron layer, the incident electromagnetic wave in the extraordinary mode is mode-converted at the upper-hybrid layer to electron Bernstein waves. These waves are locally damped and build up the plasma density and temperature near and on the inside of the upper-hybrid layer.⁸⁷

The dependence of plasma density versus prefill Hydrogen pressure is shown in figure 14. The sharp absence of breakdown below fill pressures of $3-4 \times 10^5$ torr confirms the results of Anisimov et al., who worked on a very small device.⁸⁸ This feature can be explained by (1) equating the drift-confinement time of energetic electrons created by ECRH to the average time required for them to ionize neutrals, and (2) solving for the gas pressure below which the energetic electrons are lost before ionizing a significant number of neutrals. This minimum pressure is a function of ECRH power.

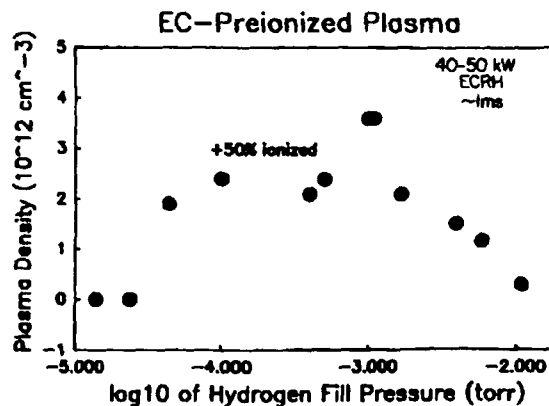


Figure 14. Dependence of peak plasma density on gas fill pressure, $P_{ECRH} = 50\text{ kW}$.

⁸⁷ A.I. Anisimov et al., *Sov. Phys. Tech. Phys.* 16:546 (1971); R.M. Gilgenbach et al., *Nucl. Fus.* 12:319 (1981); T. Cho et al., *Nucl. Fus.* 26:349 (1986).

⁸⁸ A.I. Anisimov et al., *Sov. Phys. Tech. Phys.* 18:459 (1973).

Figure 15 shows the electron density during ECRH and 2 ms after ECRH turn-off as a function of applied vertical magnetic field. This data seems to indicate that confinement of the bulk plasma electrons is best when only a very small vertical field (<0.001 T) is present, and that the degradation in confinement that accompanies increased vertical field saturates near $B_v = 0.008$ T.

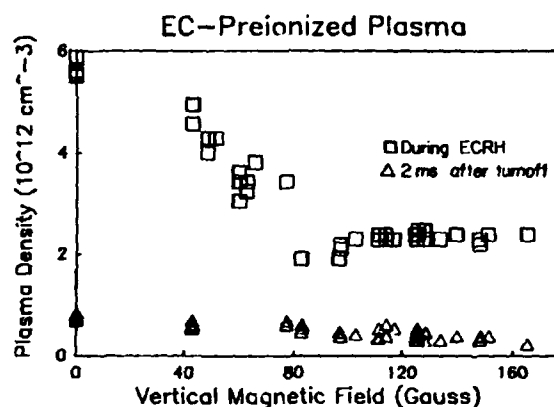


Figure 15. Dependence of plasma density on externally applied vertical magnetic field strength.

Section 3 Electromagnetics

Chapter 1 Electromagnetic Wave Theory and Applications

Chapter 1. Electromagnetic Wave Theory and Applications

Academic and Research Staff

Professor Jin Au Kong, Dr. Sami M. Ali, Dr. Robert T. Shin, Dr. Ying-Ching E. Yang

Visiting Scientists and Research Affiliates

Dr. Pinchas D. Einziger,¹ Qizheng Gu,² Dr. Tarek M. Habashy,³ Dr. Arthur K. Jordan,⁴ Dr. Kevin O'Neill,⁵ Dr. Soon Y. Poh,⁶ Dr. Tsuneki Yamasaki,⁷ Dr. Harold R. Raemer⁸

Graduate Students

Khurram K. Afridi, Jerome J. Akerson, David V. Arnold, Robert G. Atkins, Maurice Borgeaud, Ike Chang, Judy Chen, Nelson C. Chu, Hsiu C. Han, Yoshihisa Hara, Jean-Fu Kiang, Cheung-Wei Lam, Gloria W. Lau, Check-Fu Lee, Kevin Li, Victor Liao, Harold H. Lim, Son V. Nghiem, Kelly Savage, David M. Sheen, Mohammad A. Tassoudji, Michael J. Tsuk, Ann N. Tulintseff, Murat E. Veysoglu, Li-Fang Wang, Jiging Xia, Herng A. Yueh

Undergraduate Students

Daniel Chung, Laura Marmorstein

Technical and Support Staff

Margery Brothers, Kit-Wah Lai, Anh Lieu, Wei Ming-yu Lin

1.1 Electromagnetic Waves in Multilayer Media

U.S. Army Research Office
Contract DAAL03 88-K-0057

Sponsors

Joint Services Electronics Program
Contract DAAL03-89-C-0001
National Science Foundation
Contract ECS 86-20029
Schlumberger-Doll Research

Project Staff

Professor Jin Au Kong, Dr. Sami M. Ali, Dr. Tarek M. Habashy, Dr. Soon Y. Poh, Dr. Ying-Ching E. Yang, Robert G. Atkins, Ike Chang, Qizheng Gu, Check-Fu Lee, Kevin Li, David M. Sheen, Michael J. Tsuk, Ann N. Tulintseff, Jiging Xia

¹ Department of Electrical Engineering, Technion-Israel Institute, Haifa, Israel.

² Shanghai Research Institute of Mechanical and Electrical Engineering, Shanghai, China.

³ Schlumberger-Doll Research, Ridgefield, Connecticut.

⁴ Office of Naval Research, U.S. Navy, Arlington, Virginia.

⁵ Civil and Geotechnical Engineering, Department of the Army, Hanover, New Hampshire.

⁶ Digital Equipment Corporation, Andover, Massachusetts.

⁷ Department of Electrical Engineering, College of Science and Technology, Nihon University, Tokyo, Japan.

⁸ Electrical and Computer Engineering Department, Northeastern University, Boston.

We are developing a generalized formulation for the electromagnetic fields in multilayered uniaxially anisotropic media containing arbitrary distribution of current sources. A spectral domain dyadic Green's function for multilayered uniaxially anisotropic media containing three-dimensional sources is derived. Tractable forms are shown to be easily deduced from the physical picture of the waves radiated by the primary sources and the multiple reflections from the stratified medium. The formulation decomposes the dyadic Green's function into TE and TM waves. The dyadic Green's function in the source region is properly represented by extracting the delta function singularity. A simple procedure to obtain the fields in any arbitrary layer is described. Recursion relations for appropriately defined reflection and upward and downward propagating transmission coefficients are presented. Forms suitable for transmission line applications in multilayered media are derived.

Finite difference time domain (FDTD) techniques show great promise in their ability to solve three-dimensional problems with arbitrary geometry. Advantages of this method include the ability to model spatially or temporally varying media. These advantages are due to the complete discretization of both space and time. Considering the volume of information being calculated, these techniques are very efficient and well suited to calculation on future parallel processing computers. This method was first formulated by Yee in 1966, and his basic algorithm is still in use.

Recent work has demonstrated the applicability of the FDTD technique to microstrip problems. The centered finite difference approximations used are second order accurate in both space and time yielding good results for reasonable mesh sizes. Numerical techniques used to solve electromagnetic problems must limit the domain over which the fields are calculated. This mandates the use of an absorbing boundary condition to simulate the outward propagation of waves incident on the walls of the mesh. An absorbing boundary condition, developed by Mur and based on the work of Enquist and Majda, is used in this work.

Our work in this area includes development of the algorithms mentioned above into a general purpose computer code which can be used to solve for the transient response of electromagnetic problems having arbitrary geometries. In addition to the transient response, frequency domain parameters can be obtained by Fourier transform of the time domain results. Since the fields are calculated throughout space and time all other desired parameters can be calculated from the field quantities.

Specifically, we are analyzing rectangular microstrip structures with as many as two or more ports. Such structures can be used in MMIC filters or antennas. This problem is of interest for several reasons. First, there are existing frequency domain solutions to the resonance problem of a rectangular microstrip patch, which we compare with the FDTD solution. Secondly, the FDTD technique can be used to analyze coupling of microstrip lines to the rectangular structure. This coupling can be either a direct connection or a gap coupled connection. Advantages of the FDTD solution to this problem are that (1) the full wave solution allows for radiation or surface wave loss, (2) no empirical values such as "effective" dimensions are needed for the analysis, and (3) the geometry can be altered easily to allow for various connections or coupling to the patch. This method is a significant improvement over those that rely on a planar circuit approach in which the substrate thickness must be small compared to wavelength and inherently three-dimensional coupling problems are not easily handled. We will compare our results with various planar circuit approaches.

The leakage phenomenon is important in the area of millimeter-wave integrated circuits and integrated optics. We have performed theoretical analyses and experiments to investigate this phenomenon. The leakage is due to the TE-TM coupling occurring at the geometrical discontinuities, and the leaky power in the form of surface wave propagates in the background medium.

We are using various methods to analyze the dielectric strip waveguides including the approximate field matching, effective dielectric constant (EDC), and mode matching. Because the first two methods are approxi-

mate, they can not be used to predict the imaginary part of the propagation constant. When using the third method, we must place ground planes at some distance from the guiding structure and omit the effect of radiation loss.

To solve for the dispersion relation of single and coupled dielectric strip waveguides, we derive an integral equation formulation using dyadic Green's function. We also present a method for predicting the leakage. Three different dielectric strip waveguides are investigated: optical rib waveguide, strip dielectric guide, and insulated image guide. Both single and coupled strip waveguides are studied. The cross section of the dielectric strips are assumed to have rectangular shape. Applying the Galerkin's method, the field distribution on the cross section is represented by a set of unit pulse basis functions. By substituting these basis functions into the integral equations and choosing the same set of basis functions as the testing functions, we can obtain a determinant equation from which the propagation constant can be solved.

For single dielectric strip waveguide, we have observed that the leakage occurs when the effective refractive index is smaller than that of a surface wave mode in the background medium. We also observed that if the lowest TE-like (TM-like) mode is leaky, the lowest TM-like (TE-like) mode is non-leaky. When the lowest order mode leaks, the surface wave mode of opposite polarization is excited. When the higher order mode leaks, the surface wave modes of both polarizations can be excited.

For two symmetrical dielectric strip waveguides, we investigated both the even and odd modes. In the leaky mode, the total leakage is due to the leakage from each individual strip waveguide. At the separation where the even mode has a maximum leakage, it is implied that the surface wave modes excited by each waveguide add in phase. For the odd mode at about the same separation, these surface wave modes add out of phase; hence, a null in the leakage is observed.

We are analyzing the propagation properties of single and coupled inhomogeneous slab

waveguides and propose an integral equation formulation using the dyadic Green's function which covers both the TE and TM modes. The dispersion relations are obtained by applying Galerkin's method to solve the integral equation. We also investigate the coupling between two symmetrical inhomogeneous slab waveguides. This method is applicable to arbitrary dielectric constant profiles.

Full modal analysis is used to study the dispersion characteristics of microstrip lines periodically loaded with crossing strips in a stratified uniaxially anisotropic medium. Dyadic Green's functions in the spectral domain for the multilayered medium in conjunction with the vector Fourier transform (VFT) are used to formulate a coupled set of vector integral equations for the current distribution on the signal line and the crossing strips. Galerkin's procedure is applied to derive the eigenvalue equation for the propagation constant. We investigate the effect of anisotropy for both open and shielded structures on the stopband properties.

We are analyzing the quasistatic fields generated by an electrode mounted on a perfectly conducting pad of finite extent buried in a planar stratified medium. An integral equation in the spectral domain is derived for the outflowing current density distribution on the pad-electrode surface. The method of moments is then applied to solve the integral equation. We are investigating the effects of the electric properties of the stratified medium and the standoff thickness on the total electrode current. Several conductivity profiles modelling different practical measurement environments are also considered. Numerical results reveal that the total electrode current is insensitive to the standoff thickness, and can be used to prospect for the conductivity of rock formation.

Based on a hybrid transmission lines-lumped element circuit model, we analyze the transient propagation characteristics of VLSI interconnects with discrete capacitive loads at various locations. Exact expressions of the Laplace transform of unit step responses are first obtained through the ABCD matrix formulation. We then apply the equivalent dominant pole approximation to the transfer function with the propagation delays fac-

tored out. The approximated transfer function can be inverted in closed form and quickly evaluated. These results provide efficient ways of finding approximately the effects on delays and rise time brought by VLSI off-chip interconnects.

Because of the dramatic increase in device densities on microelectronic chips, the propagation delay for off-chip interconnects has become the factor limiting the speed of VLSI packages. Typical scales of these interconnects will be comparable or larger than the characteristic wavelength of the high frequency components of the signal. Therefore, to calculate the delays caused by these interconnects properly, a hybrid circuit model containing transmission line sections as well as lumped elements must be used in place of the all-lumped elements. Nevertheless, most circuit simulation packages are based on the latter and have to resort to subsection approximation when dealing with transmission lines. This scheme will undoubtedly lead to lengthy computation — which is not desirable when a quick, heuristic estimate of bounds is needed for the initial phase of the design cycle.

We have developed two approaches for obtaining the approximate transient response without lengthy simulation. The first emphasizes the calculation of bounds to voltage responses from the differential equations either by direct integration or by using the optimal control theory. The second analyzes the properties of Laplace transform domain solution. Thus far, their applications are limited to all lumped-element and distributed RC networks, which can only handle on-chip interconnects. For off-chip delay estimation, we took the second approach by incorporating transmission line elements.

Extensive work has been published on radiation by a microstrip patch excited by a probe. Most of the published work did not rigorously model the correct current distribution on the probe. In the case of electrically thin substrates, the probe current is usually approximated as uniform along the probe. This leads to acceptable numerical results for the computation of the radiation pattern by the patch and the mutual impedance between the probe and the patch. However, this approximation is not sufficiently accurate

to solve for the current distribution on the patch or for the computation of the self impedance across the terminals of the probe. Furthermore, this approximation is not appropriate in the case of electrically thick substrates.

We rigorously analyzed the radiation problem of a circular patch which is center fed by a coaxial-line driven probe over a ground plane and situated in an arbitrary layered medium. The current distribution on both the patch and the probe is rigorously formulated using a planar stratified medium approach. A set of three coupled integral equations is derived which governs the axial current distribution on the probe, the radial current distribution on the patch and the azimuthal magnetic current sheet across the aperture of the driving coaxial line. This set of equations is then solved using the method of moments. The resulting matrix equation is obtained in terms of Sommerfeld-type integrals that take into account the effect of the layered medium. These integrals are efficiently computed by a simple deformation in the complex wavenumber domain. The probe current distribution, input impedance and radiation pattern are presented and compared to the case of an uniform probe current distribution.

The analysis of microstrip antennas with electrically thick substrates has many applications pertaining to millimeter wave systems and to achieving wide bandwidth. Most of the published work on the input impedance and other parameters of a probe-fed microstrip antenna employ an approximation to the probe feed where it is replaced by a uniform current ribbon of equivalent dimensions. This approximation fails to give sufficiently accurate results for the input impedance of the probe especially for thick substrates. Recently, we have made some progress in this area — we obtained the current distribution on the metallic probe in a closed magnetic wall cavity. Then, we accounted for the radiation losses by lumping them artificially into an effective loss tangent.

We have formulated the problem of a center fed circular microstrip antenna in terms of a Weber transform, which allowed us to develop the Green's function of the layered medium with the probe and the microstrip

patch as part of the medium. Using the Weber transform automatically enforces the boundary conditions on the probe and the patch. This allows us to cast the problem as the solution of a set of two coupled integral equations governing the tangential component of the electric field across the aperture of the coaxial line feed and that aperture across the interface where the patch lies. Next, we solve this set of equations using the method of moments. We then compute the current distribution on both the probe and the patch from the component of the magnetic field tangential to their surfaces. Furthermore, from the computed electric field across the aperture of the coaxial line feed, we obtain the reflection coefficient for the TEM mode which allows us to compute the input impedance across the terminals of the probe. The probe current distribution, input impedance and radiation pattern are presented, and the obtained results compared with those using the stratified medium formulation.

The transient fields of a current source on a layered medium are calculated using the double deformation technique, in which complex integrals are deformed in the transverse wavenumber and frequency planes. Singularities from these complex planes correspond to physical modes of the structure, such as guided and leaky waves, and the relative importance of each to the overall response can be discovered. Unlike the Cagniard-de Hoop method, double deformation can be applied to dispersive and dissipative media. Also, the causality of the electromagnetic signal can be shown analytically.

We developed a modification to the double deformation technique, which splits the Fourier transform of the source current into two halves, one for times before the arrival at the observation point, and one after. This greatly increases the range of sources to which the double deformation technique can be applied. Another advantage of the modification is the individual causality and continuity of each mode.

We have computed results for both line and strip currents on the surface of a coated perfect conductor for cases where the dielectric coating is both lossless and dissipative.

In most cases, only a small number of modes suffices to reproduce the important features of the response, including the arrivals of reflected and lateral rays. The importance of each type of arrival depends on certain features of the time function, especially the initial slope. The response due to a strip current resembles that of a line current although there is some smoothing of the sharper features.

The complex resonant frequencies of the open structure of a microstrip antenna consisting of two circular microstrip disks in a stacked configuration have been rigorously calculated as a function of the layered parameters and the ratio of the radii of the two disks. Using a dyadic Green's function formulation for horizontally stratified media and the vector Hankel transform, the mixed boundary value problem is reduced to a set of coupled vector integral equations. Employing Galerkin's method in the spectral domain, we calculated the complex resonant frequencies and demonstrated convergence of the results. We show that for each mode, the stacked circular microstrip structure has dual resonant frequencies which are associated with the two coupled constitutive resonators of the structure and a function of the mutual coupling between the two disk resonators. This mutual coupling is a function of the geometrical configuration of the stacked structure; the layered parameters, permittivities, permeabilities, and heights; and the ratio of the radii of the two disks. The dual frequency behavior of the stacked microstrip structure can be used to broaden the bandwidth or to provide for dual frequency use of the antenna.

Publications

Ali, S.M., T.M. Habashy, and J.A. Kong. "Dyadic Green's Functions for Multilayered Uniaxially Anisotropic Media." Submitted to *J. Electromag. Waves Appl.*

Ali, S.M., T.M. Habashy, and J.A. Kong. "Probe Excitation of a Center-Fed Circular Microstrip Antenna Employing a Stratified Medium Formulation." In *IEEE AP-S International Symposium and URSI Radio Science Meeting*, San Jose, California, June 26-30, 1989.

Habashy, T.M., S.M. Ali, and J.A. Kong. "Probe Excitation of a Center-Fed Circular Microstrip Antenna Employing the Weber Transform." In *IEEE AP-S International Symposium and URSI Radio Science Meeting*, San Jose, California, June 26-30, 1989.

Kiang, J.F., S.M. Ali, and J.A. Kong. "Integral Equation Formulation of Inhomogeneous Slab Waveguides." Submitted to *IEEE J. Quantum Electron.*

Kiang, J.F., S.M. Ali, and J.A. Kong. "Integral Equation Solution to the Guidance and Leakage Properties of Coupled Dielectric Strip Waveguides." In *IEEE Trans. Microwave Theory Tech.* Forthcoming.

Kiang, J.F., T.M. Habashy, and J.A. Kong. "Electrostatic Fields Due to an Electrode Mounted on a Conducting Pad of Finite Extent in a Planar Stratified Medium." *IEEE Trans. Antennas Propag.* 37 (9):1140-1149 (1989).

Kiang, J.F., S.M. Ali, and J.A. Kong. "Analysis of Dielectric Strip Waveguides Using Integral Equation Formulation." *Progress in Electromagnetics Research Symposium*, Boston, Massachusetts, July 25-26, 1989.

Lam, C.W., S.M. Ali, and J.A. Kong. "The Propagation Characteristics of Signal Lines with Crossing Strips in Multilayered Anisotropic Media." *J. Electromag. Waves Appl.* Forthcoming.

Poh, S.Y., M.J. Tsuk, and J.A. Kong. "Transient Response of Sources Over Layered Media Using the Double Deformation Method." *IEEE AP-S International Symposium and URSI Radio Science Meeting*, San Jose, California, June 26-30, 1989.

Sheen, D.M., S.M. Ali, M.D. Abouzahra, and J.A. Kong. "Application of the Three Dimensional Finite Difference Time Domain Method to the Analysis of Planar Microstrip Circuits." Submitted to *IEEE Trans. Microwave Theory Tech.*

Sheen, D.M., S.M. Ali, M.D. Abouzahra, and J.A. Kong. "Analysis of Multiport Rectangular Microstrip Structures Using a Three Dimensional Finite Difference Time Domain Technique." In *Progress in Electromagnetics Research Symposium*, Boston, Massachusetts, July 25-26, 1989.

Tulintseff, A.N., S.M. Ali, and J.A. Kong. "Resonant Frequencies of Stacked Circular Microstrip Antennas." In *IEEE AP-S International Symposium and URSI Radio Science Meeting*, San Jose, California, June 26-30, 1989.

Tulintseff, A.N., S.M. Ali, and J.A. Kong. "Resonant Frequencies of Stacked Circular Microstrip Antennas." Submitted to *IEEE Trans. Antennas Propagat.*

Yang, Y.E., and J.A. Kong. "Transient Analysis of Capacitively Loaded VLSI Off-Chip Interconnections." In *Progress in Electromagnetics Research Symposium*, Boston, Massachusetts, July 25-26, 1989.

1.2 Remote Sensing of Earth Terrain

Sponsor

National Aeronautics and Space Administration
Contract NAGW-1617

Project Staff

Professor Jin Au Kong, Dr. Pinchas D. Einziger, Dr. Robert T. Shin, David V. Arnold, Robert G. Atkins, Nelson C. Chu, Harold H. Lim, Son V. Nghiem, Heng A. Yueh

We are developing models of various kinds of earth terrain using a two-layer configuration to investigate the polarimetric scattering properties of remotely sensed media. The scattering layer is an anisotropic random medium characterized by a three-dimensional correlation function with lateral and vertical correlation lengths and variances. Based on the wave theory under Born approximations, we applied this model to derive the fully polarimetric backscattering coefficients of the Mueller and covariance matrices. We considered a single scattering process, taking into account all the multiple reflections at the boundaries. For an anisotropic random

medium with optic axis tilted off the vertical axis, the corresponding Mueller and covariance matrices do not contain any zero elements. To account for the azimuthal randomness in the growth direction of leaves in tree and grass fields, an averaging scheme is applied to obtain the backscattering coefficients. In this case, the Mueller matrix contains eight zero elements, the covariance matrix has four zero elements, and the cross-polarization term σ_{vh} does not vanish. Theoretical predictions are matched with experimental data for sea ice and vegetation fields.

During the transionospheric propagation of a high power radio wave beam, the nonuniform electromagnetic field interacts with the background plasma, leading to a ponderomotive force and a thermal pressure force. Both of the two nonlinear forces mainly act on the electrons, but eventually will have an effect on the ions through the ambipolar diffusion process. The spatial redistribution of the plasma density caused by the actions of these forces will change the local plasma permittivity along the beam path and consequently lead to the focusing of the radio wave beam.

We examine the self-focusing phenomena by taking into account both the ponderomotive force and the thermal pressure force as the two primary mechanisms. The threshold power intensity is determined by balancing the natural diffraction and the nonlinear focusing effects of the wave beam. The focal length for the concerned process is then estimated after solving the nonlinear wave equation.

To illustrate the self-focusing process, we carried out a series of numerical simulations for high frequency beams with various initial beam widths propagating in the ionospheric plasmas. The peak field intensity and the electron temperature along the beam path were calculated numerically. We showed that the thermal pressure force is predominant over the ponderomotive force in large incident beam width cases; however, the ponderomotive force is more significant if the beam width is small.

Earth terrains are modeled by a two-layer configuration to investigate the polarimetric

scattering properties of the remotely sensed media. The scattering layer is a random medium characterized by a three-dimensional correlation function with correlation lengths and variances respectively related to the scatter sizes and the permittivity fluctuation strengths. Based on the wave theory with Born approximations carried to the second order, this model is applied to derive the Mueller and the covariance matrices which fully describe the polarimetric scattering characteristics of the media. Physically, the first- and second-order Born approximations account for the single and double scattering processes.

For an isotropic scattering layer, the five depolarization elements of the covariance matrix are zero under the first-order Born approximation. For the uniaxial tilted permittivity case, the covariance matrix does not contain any zero elements. To account for the randomness in the azimuthal growth direction of leaves in vegetation, the backscattering coefficients are azimuthally averaged. In this case, the covariance matrix contains four zero elements although the tilt angle is not zero. Under the second-order Born approximation, the covariance matrix is derived for the isotropic and the uniaxial untilted random permittivity configurations. The results show that the covariance matrix has four zero elements and a depolarization factor is obtained even for the isotropic case.

To describe the effect of the random medium on electromagnetic waves, the strong permittivity fluctuation theory, which accounts for the losses due to both of the absorption and the scattering, is used to compute the effective permittivity of the medium. For a mixture of two components, the frequency, the correlation lengths, the fractional volume, and the permittivities of the two constituents are needed to obtain the polarimetric backscattering coefficients. Theoretical predictions are illustrated by comparing the results with experimental data for vegetation fields and sea ice.

The phase fluctuations of electromagnetic waves propagating through a scattering medium, such as a forest, is studied with the random medium model. It is of practical reasons interest to determine the effectiveness of the synthetic aperture radar (SAR) in

detecting and imaging objects within the scattering medium. As an electromagnetic wave propagates through the scattering medium, its energy is attenuated and a random phase fluctuation is introduced. The magnitude of this random phase fluctuation is important in estimating the effectiveness of SAR imaging techniques for objects within the scattering medium. We are investigating the phase degradation of the one-way problem, i.e., transmitter outside the scattering medium and receiver inside the scattering medium.

We use the two-layer random medium model, which consists of a scattering layer between free space and ground, to calculate the phase fluctuations introduced between a transmitter located above the random medium and a receiver located within the random medium. The scattering property of the random medium is characterized by a correlation function of the random permittivity fluctuations. The effective permittivity of the random medium is first calculated using the strong fluctuation theory, which accounts for the large permittivity fluctuations of the scatterers. The distorted Born approximation is then used in the past to calculate the backscattering coefficients. In calculating the phase fluctuations of the received field, we introduced a perturbation series for the phase of the received field and solved to first order in permittivity fluctuations.

Phase fluctuations are first calculated for the case of the transmitter located directly over the receiver, which corresponds to the normal incidence case. The first-order scattered field normalized to the zeroth-order transmitted field is calculated using the Green's function for the unbounded medium (thereby neglecting boundary effects). We compute the variance of the normalized scattered field at the receiver, which can be directly related to the magnitude of the phase fluctuations. We then compare the results obtained under these approximations to the results obtained using the paraxial approximation. The results are then extended to account for the effects of boundaries by using the two-layer Dyadic Green's function. We also consider the extension of the results to oblique angles of incidence and multi-layer random media. The theoretical results

are illustrated by comparing the calculated phase fluctuations and attenuation of the electromagnetic waves propagating through the random medium to the available experimental data over forested areas.

We present a finite difference time domain technique for two dimensional time domain scattering of electromagnetic waves. The triangular grids and the control region approximation are employed to discretize Maxwell's equations. The finite difference time domain techniques with uniform rectangular grids have been used in the past. The scatterers are modeled using staircases and, recently, we have investigated the accuracy of this approximation. We have proposed several types of other grids to improve the staircase approximation. Generalized nonorthogonal grid can model scatterer without staircasing. It has been applied to spherical systems, yet they appear to be cumbersome for general scatterers. The "distorted rectangular grid" model approximates the computational domain using rectangular grids and distorts the boundary grids to fit the interfaces. The triangular grid is used, which is very flexible in dealing with arbitrary scatterers and absorbing boundaries.

The control region approximation, which calls for Delaunay and Dirichlet tessellation, has been successfully applied to the frequency domain problems in the past. Two double integral terms are obtained by integrating the Helmholtz equation about the Delaunay tessellation. The term involving the Laplace operator can be converted to a closed loop integral of normal derivatives, which can easily be approximated in finite difference manner by utilizing the orthogonal property of Delaunay and Dirichlet tessellation. The remaining term can be approximated by multiplying the field at the node with the area. In the time domain problem, the same approximation is applied to the wave equation, except the term involving time derivatives is used in time marching scheme. Alternatively, as in Yee's algorithm, the first order Maxwell's equations are solved by spatially and temporally separating the electric and magnetic fields. In the case of electric polarization, the electric fields are placed at the nodes and the magnetic fields are placed at the center of triangular edges. The curl H equation is integrated by

applying Stoke's theorem and converting it to a closed loop integral of tangential magnetic fields. This equation can be used to advance electric fields in time. To update magnetic fields, the second curl equation is used. This equation is approximated in the finite difference manner by utilizing the orthogonality property of the tessellation. The equations for the magnetic polarization case can also be derived following the similar procedure.

In order to limit the computation domain, the scatterers are enclosed with artificial outer boundaries. Continuous smooth outer boundaries, such as circles and ellipses, are chosen. The second-order time domain absorbing boundary conditions derived from the pseudo-differential operator approach is imposed at the outer boundaries. These boundary conditions are implemented with the control region approximation to determine necessary field quantities at the boundary. The results of the time domain control region approach are presented for simple scatterer geometries, such as conducting and coated cylinders and strips, by calculating both the transient and time-harmonic responses.

The finite element and finite difference methods are increasingly popular in the computational electromagnetics community. A major issue in applying the methods to electromagnetic wave scattering problems is confining the computation domain. This is accomplished by selecting an outer boundary and imposing absorbing boundary conditions to simulate the free space. The absorbing boundary conditions used can be exact or approximate conditions. In general, exact absorbing boundary conditions are computationally inefficient, so approximate absorbing boundary conditions, which are efficient and have sufficient accuracy, are widely used. Two distinct approximate absorbing boundary conditions have been used in the past. For the circular outer boundary, Engquist and Majda obtained the absorbing boundary conditions via the pseudo-differential operator approach. Bayliss and Turkel derived a circular boundary operator by assuming the Wilcox type expansion for the scattered fields and developing a series of operators to eliminate the inverse power series. The most widely used operator, the

second-order operator, has higher absorbability than the corresponding Engquist and Majda condition.

The pseudo-differential operator approach provides a systematic way to obtain absorbing boundary conditions in orthogonal coordinate systems. Furthermore, following careful observation, we can improve the absorbability of the boundary conditions derived by Engquist and Majda. The first-order condition contains the normal propagation term and a portion of tangential variation term. The decay term along the normal direction appears in the second-order condition only. Since Sommerfeld's radiation condition contains both normal propagation and decay terms, the first-order condition alone cannot be reduced to the Sommerfeld's condition. In the case of cylindrical coordinate, the Laplace operator contains both first and second order normal derivative terms. These two terms can be grouped together by completing the square. A factorization scheme is then proposed which yields a first-order absorbing boundary condition that contains the Sommerfeld's radiation condition and a second-order condition.

The pseudo-differential operator approach is then extended to the elliptic boundary case. For scattering by elongated scatterers, the elliptic outer boundary can be used to reduce the computational domain. The elliptic coordinate system is employed which has two dimensionless parameters. In the circular boundary case, the normal parameter has the dimension of length and the decay term comes from the first order derivative. Thus, a new normal parameter, which is the arc length along a constant tangential parameter, is defined in the elliptic coordinate. The Helmholtz equation is then converted to include first-order derivative of the new normal parameter. The absorbing boundary conditions for the elliptic boundary is obtained following a similar procedure as in the circular boundary case. It is shown that in the limit of vanishing interfocal distance, the boundary conditions for the elliptic boundary reduces to the results of the circular boundary case.

The effectiveness of the second-order absorbing boundary condition on the elliptic outer boundary is illustrated by calculating

scattered fields from various objects. The results obtained with elliptic boundaries are compared with those obtained using circular boundaries. The advantage of using the elliptic outer boundary in reducing the computational domain is illustrated by calculating scattering from elongated objects, such as strip. Furthermore, the choices for the ellipticity of the outer boundary for a given scatterer dimension are discussed.

The correlation function plays the important role in relating the electrical response of the geophysical medium to its physical properties. In the past, the volume scattering effect of electromagnetic waves from geophysical media such as vegetation canopies and snow-ice fields has been studied by using random medium models. Even though theoretical treatments were rigorous within certain constraints, the correlation functions were chosen according to researchers' knowledge and experience on physical properties of scatterers. Correlation functions have been extracted from digitized photographs of cross-sectional samples for snow and lake ice, and artificially grown saline ice. It was shown that the extracted correlation lengths corresponded to the physical sizes of ice grains, air bubbles, and brine inclusions. Also the functional forms of the extracted correlation functions were shown to be dependent on the shape and orientation of embedded inhomogeneities. To illustrate the importance of the correlation function study, the extracted correlation lengths for saline ice sample were then used to derive the effective permittivity and compared with in situ dielectric measurements of the sample. However, without any mathematical model, it is very difficult to relate the distribution, size, shape, and orientation of the scatterers to the variances, correlation lengths, and functional dependence of the correlation function.

The first analytical survey of correlation functions for randomly distributed inhomogeneities with arbitrary shape can be traced back to the work by Debye and his co-workers. In order to explain the fourth-power law of the intensity distribution of x-rays scattered by porous materials (hole structures) at larger angles, Debye et al., derived the correlation function for two-phase isotropic random medium. Debye showed that materials with holes of perfectly random shape, size and

distribution can be characterized by a spherically symmetric correlation function of exponential form. The correlation length was related to the fractional volume and the specific surface which are among the important factors in determining the catalytic activity.

To demonstrate the feasibility of the method, we first derive in detail the correlation function and the correlation length for isotropic random medium with spherical inclusions. Then, we extend the correlation function study to consider randomly distributed prolate spheroids with preferred alignment in the vertical direction for the anisotropic random medium. We employ a scaling scheme to transform the surface equation of prolate spheroids to spheres so that we can utilize the same approach in the isotropic case to derive the correlation function. Since most geophysical media are complex materials such as wet snow — which is a mixture of air, ice grains, and water content — and multiyear sea ice — which consists of pure ice, air bubbles, and brine inclusions — we also establish the correlation function study for three-phase mixtures. We considered two different kinds of inclusions with spherical and spheroidal shapes. We found that there is a close relationship between the form of the correlation function and the distribution, geometrical shape, and orientation of the scatterers. Also, the calculated correlation lengths are related to the fractional volumes and total common surface areas. These results can be utilized to identify the feature signature and characteristics through its microscopic structure. For instance, dry or slush snow can be distinguished from grain sizes, water contents, and density via the comparison of the variances and correlation lengths. The form of the correlation function provides information about the physical shape and alignment of brine inclusions, in addition to the concentration of brine inclusions versus air bubbles for the tracing of the sea-ice signatures (such as thick first-year sea ice and multiyear sea ice).

As radio waves propagate through the ionosphere, wave scattering can occur as a result of ionospheric density irregularities which give rise to fluctuations in Faraday rotation angles, known as Faraday Polarization Fluctuations (FPF). FPF have been observed with low-orbit satellite beacon

signals transmitted at frequencies 20, 40, and 54 MHz, and also with geostationary satellite signals at 136 MHz. Experimentally, it has been shown that when the linearly polarized waves, decomposed into two characteristic wave modes, were measured separately after transionospheric propagation, there was a loss of correlation between the two characteristic wave modes. It has been suggested that diffractive scattering of radio waves by ionospheric density irregularities is responsible for this phenomenon. The density irregularities have been considered to be isotropic and modeled by correlation functions having the same correlation length in all directions. Ionospheric plasma, however, is magnetized by the geomagnetic field, and ionospheric density irregularities tend to elongate along the magnetic field. The elongation results in the formation of field-aligned rod-like irregularities. Sheet-like irregularities have also been predicted theoretically and measured recently. The geomagnetized ionosphere with density irregularities is modeled as a gyrotropic random medium and the effects of both rod-like and sheet-like random density irregularities in causing FPF of VHF radio signals are studied by means of three-dimensional correlation functions.

The model is used to explain the intense FPF observed in polarimetric records of 136-MHz satellite signals received at Ascension Island in 1980 and 1981. The VHF signals were transmitted from the geostationary satellite SIRIO and propagated through the ionosphere near the Appleton equatorial anomaly crest where the ambient plasma density was high especially during the 1980 solar-maximum period. For rod-like irregularities, the theoretical results predict the field-aligned enhancement of FPF. The enhancement is shown to be stronger for longer rod-like irregularities. Furthermore, the results also demonstrate an inverse relation between the strength of FPF and the wave frequency. For sheet-like irregularities, the results also exhibit the field-aligned enhancement of FPF and the decreasing FPF strength with increasing propagation angle. The difference, however, is that the FPF strength due to the sheet-like irregularities have slower decreasing rates at small propagation angle and have larger values at large propagation angle than the FPF due to the

rod-like irregularities. For VHF waves, the RMS FPF due to the rod-like and the sheet-like irregularities are quite distinctive. This suggests that the RMS FPF data with multi-frequencies and multipropagation angles can be used to infer the size and shape of ionospheric irregularities.

A multivariate K-distribution is proposed to model the statistics of fully polarimetric radar data from earth terrain with polarizations HH, HV, VH, and VV. In this approach, correlated polarizations of radar signals, as characterized by a covariance matrix, are treated as the sum of N n -dimensional random vectors; N obeys the negative binomial distribution with a parameter α and mean N . Subsequently, an n -dimensional K-distribution, with either zero or nonzero mean, is developed in the limit of infinite N or illuminated area. The probability density function (PDF) of the K-distributed vector, normalized by its Euclidean norm, is independent of the parameter α and is the same as that derived from a zero-mean Gaussian-distributed random vector. The above model is well supported by experimental data provided by MIT Lincoln Laboratory and the Jet Propulsion Laboratory in the form of polarimetric measurements.

Publications

- Borgeaud, M., S.V. Nghiem, R.T. Shin, and J.A. Kong. "Theoretical Models for Polarimetric Microwave Remote Sensing of Earth Terrain." *J. Electromag. Waves Appl.* 3 (1):61-81 (1989).
- Borgeaud, M., J.A. Kong, R.T. Shin, and S.V. Nghiem. "Polarimetric Remote Sensing of Earth Terrain with Two-Layer Random Medium Model." *Progress in Electromagnetics Research Symposium*, Boston, Massachusetts, July 25-26, 1989.
- Chu, N.C., S.V. Nghiem, R.T. Shin, and J.A. Kong. "Phase Fluctuations of Waves Propagating Through a Random Medium." *Progress in Electromagnetics Research Symposium*, Boston, Massachusetts, July 25-26, 1989.
- Han, H.C., and J.A. Kong. "Self-focusing of a Radio Wave Beam During the Trans-ionospheric Propagation." *International*

Union of Radio Science Commission H Meeting, Boulder, Colorado, January 4-7, 1989.

Lee, C.F., R.T. Shin, J.A. Kong, and B.J. McCartin. "Finite Difference Time Domain Techniques for Two Dimensional Triangular Grids." *Progress in Electromagnetics Research Symposium*, Boston, Massachusetts, July 25-26, 1989.

Lee, C.F., R.T. Shin, J.A. Kong, and B.J. McCartin. "Absorbing Boundary Conditions on Circular and Elliptic Boundaries." *Progress in Electromagnetics Research Symposium*, Boston, Massachusetts, July 25-26, 1989.

Lee, C.F., R.T. Shin, J.A. Kong, and B.J. McCartin. "Absorbing Boundary Conditions on Circular and Elliptic Boundaries." *J. Electromag. Waves Appl.* Forthcoming.

Lin, F.C., H.A. Yueh, J.A. Kong, and R.T. Shin. "Correlation Function Study for Random Media with Multiphase Mixtures." *Progress in Electromagnetics Research Symposium*, Boston, Massachusetts, July 25-26, 1989.

Yueh, H.A., R.T. Shin, and J.A. Kong. "Scattering from Randomly Perturbed Periodic and Quasiperiodic Surfaces." In *Progress in Electromagnetics Research*. New York: Elsevier, 1989, Vol. 1, Chapter 4, pp. 297-358.

Yueh, H.A., J.A. Kong, J.K. Jao, R.T. Shin, and L.M. Novak. "K-distribution and Polarimetric Terrain Radar Clutter." *J. Electromag. Waves Appl.* 3 (8):747-768 (1989).

1.3 Remote Sensing of Sea Ice

Sponsor

U.S. Navy - Office of Naval Research
Contract N00014-89-J-1107

Project Staff

Professor Jin Au Kong, Dr. Robert T. Shin,
Maurice Borgeaud, Son V. Nghiem

We are studying fully polarimetric scattering of electromagnetic waves from snow and sea ice with a three-layer random medium model. This model can account for snow covered sea ice. The snow layer is modeled as an isotropic random medium characterized by a scalar permittivity. The sea ice is modeled as an anisotropic random medium with a symmetric permittivity tensor due to the elongated form of brine inclusions. The underlying sea water is considered as a homogeneous half-space. Volume scattering effects of both random media are described by three-dimensional correlation functions with variances and correlation lengths corresponding to the strengths of the permittivity fluctuations and the physical sizes of the inhomogeneities, respectively. We use the strong fluctuation theory to derive the mean fields in the random media under the bilocal approximation, taking into account the singularities of the dyadic Green's functions and calculating the effective permittivities of the random media with two-phase mixing formulas. We then apply the distorted Born approximation to obtain the covariance matrix which describes the fully polarimetric scattering properties of the remotely sensed media.

The three-layer configuration is first reduced to two-layer to observe polarimetric scattering directly from snow, first-year sea ice, and multiyear sea ice. We investigate the distinctive characteristics of the media with the conventional backscattering coefficients and the complex correlation coefficient ρ between σ_{hh} and σ_{vv} . The correlation coefficient ρ is shown to be important for identifying the characteristics of snow and sea ice. We then use the three-layer configuration to investigate the effects on polarimetric radar returns from snow covered sea ice.

Using a 14-GHz scatterometer and a collocated IR wave gauge, we made tower-based measurements of sea-state bias. The measured bias was found to be an increasing fraction of the significant wave height (SWH) with increasing wind speed. Theoretical modeling of the scattering from a two-dimensional two-scale model of the sea surface leads to a prediction of sea-state bias based on the wave height-dependent scattering cross section in the physical optics approximation. We are examining the impli-

cations of the measurements and modeling for sea-state bias algorithms.

EM bias is an error in the altitude measurement of an ocean altimeter caused because the troughs of ocean waves are better reflectors of electromagnetic waves than the crests. In the past, other researchers have attempted to predict the EM bias using a geometric optics solution based on a knowledge of the joint height-slope probability density function of the ocean surface. This solution does not predict any frequency dependence of the EM bias contrary to experiment, because it assumes that the curvature of the ocean surface is negligible compared to its slope (which might not be correct).

The EM bias can be solved more accurately by modeling the ocean surface with a two-scale model and solving for the EM bias using the physical optics solution. Using the saddle point method, we can solve a gaussian height probability density, (for normal incidence) and the physical optics integral (for small slopes of the large-scale ocean waves) for the backscattered power. The solution is a superposition of two terms: (1) the geometric optics solution, and (2) a correction term added due to the curvature of the ocean surface.

The ocean can be divided into large and small scales by choosing a separation wavenumber k_0 . The small-scale height variance can be measured from experimental data and the small-scale slope and curvature variances can be estimated by using a suitable wavenumber spectrum. Assuming a one-dimensional wavenumber spectrum of the k^{-3} form with an upper cutoff wavenumber k_s , the slope and curvature variances are obtained.

By using the experimental results of Cox and Munk, we can find an approximate upper cutoff wavenumber. Consequently, when we know the wind speed and small-scale height variance, we can estimate the EM bias by calculating the centroid of the backscattered power. Finally, the results are compared with experimental data.

In the research on the satellite-borne antennas, the study of electromagnetic radiation from sources in the ionospheric

plasmas has received much attention. For many years, special attention has been given to the radiation in very low frequency (VLF) bands due to its applications in down-link communication systems and local ionospheric plasma diagnostics. Many authors have published results of both theoretical and experimental investigations on single element radiations. However, limited by low radiation efficiency, the utility of a practically-sized single VLF radiator could highly depend upon the focusing effects, which are characterized by inflection points on the k -surface associated with the medium. In recent years, the construction of a large space-based antenna array has been made feasible through the progress of spacecraft technology. With a properly phased large VLF linear or planar array, a narrow beam width and, consequently, high directivity can be achieved.

We analytically examined the far field pattern of a two-dimensional VLF phased array located in the ionosphere. We presented several designs of a phasing scheme which allows the planar array to be physically rotated 360 degrees with respect to an axis perpendicular to the plane of the array. The main beam stays in the same direction as that of the geomagnetic field line at the same time. We discussed the tradeoffs between the beamwidth, the operating frequency and the size of the array and compared the performances of the array of different designs.

We also discussed the applicability of the principle of pattern multiplication. More specifically, when there is more than one stationary phase point during the process of evaluating the radiation integral, or, in other words, when the k -surface of the medium possesses inflection points, the simple multiplication of the array factor and the element pattern will not result in the correct overall far field pattern of the array. For these cases, we took into account the type (e.g., electric dipole or magnetic dipole) and the orientation (e.g., parallel or perpendicular to the geomagnetic field line) of the radiating elements as well as the array configuration in calculating the far field pattern.

The scattering of electromagnetic waves from a two-dimensional slot in a ground plane is solved using the method of moments. The

contribution of the surface features, such as slots and other discontinuities, to the total radar cross section (RCS) of objects is of practical interest in the RCS community. In formulating the integral equation for the transverse magnetic field case, the problem is separated into two regions: the region below and above the ground plane. The region below the ground plane is treated as a parallel plate waveguide. In the region above the ground plane, the slot aperture is replaced with a magnetic surface current sheet and the ground plane is removed by adding the necessary image sources. The integral equation for the magnetic surface current sheet over the slot aperture is then obtained by matching the boundary conditions over the aperture. The resulting integral equation is then solved with the method of moments using Galerkin's method with the pulse basis function.

Then, we extend the solution to the case when the slot is terminated and/or filled with dielectric/magnetic materials. This is a straightforward extension, since we can express simply the waveguide modes for the parallel plate waveguide filled with materials. We illustrated the scattering characteristics of surface slots by plotting the two-dimensional RCS as functions of incidence angle and frequency and presented the effects of filling the slots with conducting materials. We also discussed other useful techniques for studying the electromagnetic wave scattering characteristics of various two-dimensional surface features.

We developed the random medium model with three-layer configuration to study fully polarimetric scattering of electromagnetic waves from geophysical media. This model can account for the effects on wave scattering due to weather, diurnal and seasonal variations, and atmospheric conditions such as ice under snow, meadow under fog, and forest under mist. The top scattering layer is modeled as an isotropic random medium which is characterized by a scalar permittivity. The middle scattering layer is modeled as an anisotropic random medium with a symmetric permittivity tensor whose optic axis can be tilted due to the preferred alignment of the embedded scatterers. The bottom layer is considered as a homogeneous half-space. Volume scattering effects

of both random media are described by three-dimensional correlation functions with variances and correlation lengths corresponding to the strengths of the permittivity fluctuations and the physical sizes of the inhomogeneities, respectively. We used the strong fluctuation theory to derive the mean fields in the random media under the bilocal approximation, properly taking singularities of the dyadic Green's functions account, and to calculate effective permittivities of the random media with two-phase mixing formulas. We then applied the distorted Born approximation to obtain the covariance matrix, which describes the fully polarimetric scattering properties of the remotely sensed media.

First, the three-layer configuration is reduced to two-layers to observe fully polarimetric scattering directly from geophysical media such as snow, ice, and vegetation. Such media exhibit reciprocity as experimentally manifested in the close proximity of the measured backscattering radar cross sections σ_{vh} and σ_{hv} , and as theoretically established in the random medium model with symmetric permittivity tensors. The theory is used to investigate the signatures of isotropic and anisotropic random media on the complex correlation coefficient ρ between σ_{hh} and σ_{vv} as a function of incident angle. For the isotropic random medium, ρ has the value of approximately 1.0. For the untilted anisotropic random medium, ρ has complex values with both the real and imaginary parts decreased as the incident angle is increased. The correlation coefficient ρ is shown to contain information about the tilt of the optic axis in the anisotropic random medium. As the tilted angle becomes larger, the magnitude of ρ is maximized at a larger incident angle, where the phase of ρ changes its sign. It should be noted that the tilt of the optic axis is also related to the nonzero depolarization terms in the covariance matrix (which will also be considered).

We identified the effects on polarimetric wave scattering due to the top layer by comparing the three-layer results with those obtained from the two-layer configuration. We used the theory to investigate the effects on polarimetric radar returns due to a low-loss and a lossy dry-snow layer covering a sheet of thick first-year sea ice. For the low-

loss snow cover, both σ_{hh} and σ_{vv} are enhanced compared to those observed from bare sea ice. Furthermore, the boundary effect is manifested in the form of the oscillation on σ_{hh} and σ_{vv} . The oscillation can also be seen on the real and imaginary parts of the correlation coefficient ρ . The magnitude of ρ , however, does not exhibit the oscillation while clearly retaining the same characteristics as observed directly from the uncovered sea ice. In contrast to the low-loss case, the lossy top layer can diminish both σ_{hh} and σ_{vv} and depress the boundary-effect oscillation. When the thickness of the lossy top layer increases, the behavior of the correlation coefficient ρ becomes more and more similar to the isotropic case, signifying that the information from the lower anisotropic layer is masked. At appropriate frequency, the fully polarimetric volume scattering effects can reveal the information attributed to the lower layer even if it is covered under another scattering layer. Due to the physical base, the random medium model renders the polarimetric scattering information useful in the identification, classification, and radar image simulation of geophysical media.

The three-layer random medium model is developed for microwave remote sensing of snow-covered sea ice. The electromagnetic wave theory and strong fluctuation theory are employed to study the propagation and volume scattering of electromagnetic waves in the medium. With the application of the Feynman diagrammatic technique and the renormalization method, mean fields for the isotropic and anisotropic random media are derived under the bilocal approximation. Then, the effective permittivities for both random media are obtained from the dispersion relations of the mean fields. Further, with the discrete-scatterer concept for two-phase mixtures, the scattering parts of effective permittivities are computed, in the low-frequency limit, for both isotropic and anisotropic random media with specified correlation functions. The distorted Born approximation is then used to compute the co-polarized and cross-polarized backscattering coefficients which are compared with scatterometer data at 9 GHz and 13 GHz for bare and dry-snow covered thick first year (TFY) sea ice taken at Point Barrow, N.W.T.

Publications

- Arnold, D.V., J.A. Kong, W.K. Melville, and R.W. Stewart. "Theoretical Prediction of EM Bias." *Progress in Electromagnetics Research Symposium*, Boston, Massachusetts, July 25-26, 1989.
- Han, H.C., J.A. Kong, and T.M. Habashy. "Far Field Pattern of a VLF Antenna Array in the Ionospheric Plasmas." *Progress in Electromagnetics Research Symposium*, Boston, Massachusetts, July 25-26, 1989.
- Han, H.C., J.A. Kong, T.M. Habashy, and M.D. Grossi. "Principles of VLF Antenna Array Design in Magnetized Plasmas." *URS National Radio Science Meeting*, Boulder, Colorado, January 3-5, 1990.
- Li, K., R.T. Shin, and J.A. Kong. "Radar Cross Section Prediction of Slots in Ground Planes Using Method of Moments." *Progress in Electromagnetics Research Symposium*, Boston, Massachusetts, July 25-26, 1989.
- Lin, F.C., J.A. Kong, and R.T. Shin. "Application of Three-Layer Random Medium Model for Microwave Remote Sensing of Snow-covered Sea Ice." Submitted to *J. Geophys. Res.*
- Melville, W.K., J.A. Kong, R.H. Stewart, W.C. Keller, A. Jessup, D. Arnold, and A. Slinn. "The Measurement and Modelling of Sea-State Bias in SAXON." *IGARSS '89 and 12th Canadian Symposium on Remote Sensing*, Vancouver, Canada, July 10-14, 1989.
- Nghiem, S.V., F.C. Lin, J.A. Kong, R.T. Shin, and H.A. Yueh. "Three-Layer Random Medium Model for Fully Polarimetric Remote Sensing of Geophysical Media." *Progress in Electromagnetics Research Symposium*, Boston, Massachusetts, July 25-26, 1989.
- Nghiem, S.V., J.A. Kong, R.T. Shin, and H.A. Yueh. "Application of Three-Layer Random Medium Model to Polarimetric Remote Sensing of Snow and Sea Ice." *North American Sea Ice Workshop*,

Amherst, Massachusetts, June 26-28, 1989.

1.4 SAR Image Interpretation and Simulation

Sponsors

National Aeronautics and Space Administration
Contracts NAGW-1272 and 958461
Simulation Technologies
Contract DAAH01-87-C-0679
U.S. Army Corp of Engineers
Contract DACA39-87-K-0022
WaveTracer, Inc.

Project Staff

Professor Jin Au Kong, Dr. Robert T. Shin, Dr. Ying-Ching E. Yang, Hsiu C. Han, Heng A. Yueh, Mohammad A. Tassoudji

Supervised and unsupervised classification procedures are developed and applied to synthetic aperture radar (SAR) polarimetric images in order to identify their various earth terrain components. For supervised classification processing, we used the Bayes technique to classify fully polarimetric and normalized polarimetric SAR data. We also considered simpler polarimetric discriminates, such as the absolute and normalized magnitude response of the individual receiver channel returns, in addition to the phase difference between the receiver channels. In addition, we discussed another processing algorithm, based on comparing general properties of the Stokes parameters of the scattered wave to that of simple scattering models. This algorithm, which is an unsupervised technique, classifies terrain elements based on the relationship between the orientation angle and handedness of the transmitting and receiving polarization states. These classification procedures have been applied to San Francisco Bay and Traverse City SAR images (supplied by the Jet Propulsion Laboratory). We showed that supervised classification yields the best overall performance when accurate classifier training data is used, whereas unsupervised classification is applicable when training data is not available.

Polarimetric radar backscatter data observed with satellite and airborne synthetic aperture radars (SAR) have demonstrated potential

applications in geologic mapping and terrain cover classification. Accurate calibration of such polarimetric radar systems is essential for polarimetric remote sensing of earth terrain. A polarimetric calibration algorithm using three in-scene reflectors is developed which will be a useful tool in the radar image interpretation.

The transmitting and receiving ports of the polarimetric radar are modeled by two unknown polarization transfer matrices. The measured scattering matrix is equal to the product of the transfer matrix of the receiving port, scattering matrix of the illuminated target, the transfer matrix of the transmitting port, and a common phase factor. The objective of polarimetric radar calibration is to determine these two unknown polarization transfer matrices using measurements from targets with known scattering matrices.

The transfer matrices for the transmitting and receiving ports are solved in terms of measurements from three in-scene reflectors with arbitrary known scattering matrices. The solutions for several sets of calibration targets with simple scattering matrices are first presented. Then, the polarimetric calibration using three targets with general arbitrary scattering matrices is derived using the method of simultaneous diagonalization of two matrices. A transformation matrix is found to convert the general scattering matrices into the simple cases, and the problem is solved in the transformed domain. We can then express solutions to the original problem in terms of the solutions obtained for the simple scattering matrices. We discussed all possible combinations of calibration targets and presented the solutions of each case. Thus, if three scatterers with known scattering matrices are known to exist within a radar image, then the whole image can be calibrated using the exact solution presented. We also illustrated the effects of misalignment of calibration targets and of receiver noise for several sets of calibration targets.

Polarimetric terrain backscatter data observed with satellite and airborne synthetic aperture radars (SAR) demonstrate potential applications in geologic mapping and terrain cover classification. In previous publications on this subject, Gaussian statistics have fre-

quently been assumed for the radar return signals to build the Bayes terrain classifier. However, abundant experimental evidence shows that the terrain radar clutter is non-Gaussian, i.e., non-Rayleigh in amplitude distribution. Among many non-Gaussian statistics, the K-distribution has proven useful in characterizing the amplitude distribution of electromagnetic echoes from various objects, including diverse ground surfaces, sea surface and wave propagation through atmospheric turbulence.

There has been considerable interest in the use of additional information provided by the polarization in the remote sensing of earth terrain. By measuring the amplitudes and phases of the HH, HV, and VV returns in the backscattered direction, fully polarimetric scattering characteristics of the earth terrain can be obtained. Once the scattering matrix is known, then the scattered power for any receiving and transmitting polarizations can be synthesized. The variation of the synthetic aperture radar (SAR) images due to the changes in the polarization has motivated the study in terrain discrimination and classification using the fully polarimetric SAR images. First, we presented the problem of determining the optimal polarizations that maximizes contrast between two scattering classes. Then, we presented the more general problem of classifying the SAR images into multiple classes using the polarimetric information.

The problem of determining the optimal polarization that maximizes the contrast between two terrain classes in the polarimetric radar images has many practical application in terrain discrimination. A systematic approach is presented for obtaining the optimal polarimetric matched filter, i.e., that filter which produces maximum contrast between two scattering classes. The maximization procedure involves solving an eigenvalue problem where the eigenvector corresponding to the maximum contrast ratio is optimal polarimetric matched filter. To exhibit the physical significance of this filter, it is transformed into its associated transmitting and receiving polarization states and written in terms of horizontal and vertical vector components. For the special case where the transmitting polarization is fixed, the receiving polarization which maximizes

the contrast ratio is also obtained. Polarimetric filtering is then applied to synthetic aperture radar (SAR) images obtained from the Jet Propulsion Laboratory. We have shown, both numerically and through the use of radar imagery, that maximum image contrast can be realized when data is processed with the optimal polarimetric matched filter.

We developed a polarimetric radar calibration algorithm using three in-scene reflectors based on the exact solution for general target choices. The transmitting and receiving ports of the polarimetric radar are modeled by two unknown polarization transfer matrices. These transfer matrices are solved in terms of measurements from three independent calibration targets with known scattering matrices. First, we presented the solutions for several sets of calibration targets with simple scattering matrices. Then, when at least two of the target scattering matrices can be simultaneously diagonalized, polarimetric calibration is derived using the method of simultaneous diagonalization of two matrices. A transformation matrix is found to convert the general scattering matrices into the simple cases, and the problem is solved in the transformed domain. The solution to the original problem then can be expressed in terms of the solutions obtained for the simple scattering matrices. All possible combinations of calibration targets are discussed and the solutions are presented for the cases that at least two of the scattering matrices can be simultaneously diagonalized.

Conventional classification techniques for identification of vehicle types from their range profiles, or pulse responses, have been shown to be limited in their practical ability to distinguish targets of interest. These limitations arise from the need for large signature libraries and time consuming processing for profile matching algorithms, and from the assumptions made toward the statistics of extracted features for parametric methods. To overcome the practical constraints of existing techniques, we are examining a new method of target recognition which utilizes neural nets. The effectiveness of this neural net classifier is demonstrated with synthetically generated range profiles for two sets of geometries, as produced using RCS prediction techniques. The first set consists of three simple canonical geometries for which

RCS predictions can be done directly. For these targets, two neural net configurations are compared, and the effects of varied aspect sampling density for the training profiles and noise corruption in the test profiles are demonstrated. Comparisons are made between the neural net classifier and several conventional techniques to determine the relative performance and cost of each algorithm. A similar set of comparisons is performed for the second group of targets, consisting of more realistic air vehicle models, each composed from a collection of canonical shapes. In both cases, the neural net classifier is shown to match or exceed the performance of conventional algorithms while offering a more computationally efficient implementation.

We used strong permittivity fluctuation theory to solve the problem of scattering from a medium composed of completely randomly oriented scatterers under the low frequency limit. Based on Finkelberg's approach, Gaussian statistics is not assumed for the renormalized scattering sources. The effective permittivity is obtained under the low frequency limit and the result is shown to be isotropic due to no preferred direction in the orientation of the scatterers. Numerical results of the effective permittivity are illustrated for oblate and prolate spheroidal scatterers and compared with the results for spherical scatterers. The results derived are shown to be consistent with the discrete scatterer theory. The effective permittivity of random medium embedded with nonspherical scatterers shows a higher imaginary part than that of spherical scatterer case with equal correlation volume. Under the distorted Born approximation, the polarimetric covariance matrix for the backscattered electric field is calculated for the half-space randomly oriented scatterers. The nonspherical geometry of the scatterers shows significant effects on the cross-polarized backscattering returns σ_{hv} and the correlation coefficient ρ between HH and VV returns. The polarimetric backscattering scattering coefficients can provide useful information in distinguishing the geometry of scatterers.

Publications

- Atkins, R.G., R.T. Shin, and J.A. Kong. "A Neural Net Method for High Range Resolution Target Classification." *J. Electromag. Waves Appl.* Forthcoming.
- Kong, J.A., R.T. Shin, H.A. Yueh, H.H. Lim, and J.J. van Zyl. "Classification and Maximum Contrast of Earth Terrain Using Polarimetric Synthetic Aperture Radar Images." *Progress In Electromagnetics Research*. New York: Elsevier, 1990.
- Lim, H.H., A.A. Swartz, H.A. Yueh, J.A. Kong, R.T. Shin, and J.J. Van Zyl. "Classification of Earth Terrain Using Synthetic Aperture Radar Images." *J. Geophys. Res.* 94 (B6):7049-7057 (1989).
- Lim, H.H., H.A. Yueh, J.A. Kong, R.T. Shin, and J.J. van Zyl. "Contrast and Classification Studies of Polarimetric SAR Images for Remote Sensing of Earth Terrain." *Progress in Electromagnetics Research Symposium*, Boston, Massachusetts, July 25-27, 1989.
- Shin, R.T., and J.A. Kong. "Radiative Transfer Theory for Active Remote Sensing of Two-Layer Random Medium." In *Progress In Electromagnetics Research*. New York: Elsevier, 1989, Vol. 1, Chapter 5, pp. 359-417.
- Yueh, H.A., J.A. Kong, R.M. Barnes, and R.T. Shin. "Calibration of Polarimetric Radars Using In-Scene Reflectors." *Progress in Electromagnetics Research Symposium*, Boston, Massachusetts, July 25-26, 1989.
- Yueh, H.A., J.A. Kong, R.M. Barnes, and R.T. Shin. "Calibration of Polarimetric Radar Using In-Scene Reflectors." *J. Electromag. Waves Appl.* 4 (1):27-49 (1990).
- Yueh, H.A., R.T. Shin, and J.A. Kong. "Scattering from Randomly Oriented Scatterers with Strong Permittivity Fluctuations." *J. Electromag. Waves Appl.* Forthcoming.
- Yueh, H.A., J.A. Kong, R.T. Shin, H.A. Zebker, and T. Le Toan. "K-distribution and Multi-frequency Polarimetric Terrain

Radar Clutter." *J. Electromag. Waves Appl.* Forthcoming.

Yueh, H.A., J.A. Kong, and R.T. Shin. "Calibration of Polarimetric Radars Using In-scene Reflectors." In *Progress In Electromagnetics Research*. New York: Elsevier, 1990.

1.5 Microwave and Millimeter Wave Integrated Circuits

Sponsors

U.S. Navy - Office of Naval Research
Contract N00014-89-J-1019
U.S. Air Force Systems -
Electronic Systems Division
Contract F19628-88-K-0013

Project Staff

Professor Jin Au Kong, Dr. Sami M. Ali, Dr. Tarek M. Habashy, Dr. Soon Y. Poh, Dr. Ying-Ching E. Yang, Jean F. Kiang, Cheung-Wei Lam, Check-Fu Lee, David M. Sheen, Michael J. Tsuk, Ann N. Tulintseff, Jiging Xia

We have found many applications for cylindrical microstrip antennas which pertain to high speed aircrafts and space vehicles. This is due to their conformity with the aerodynamical structure of such vehicles. Recently, there has been some progress in the theoretical study of these antennas — where the radiation from various cylindrical microstrip elements was computed by assuming an electric surface current distribution on the microstrip patch. The excitation problem of realizing such a current distribution must still be addressed. Furthermore, the input impedance for the cylindrical microstrip antennas has not yet been reported.

We presented a rigorous analysis of the resonant frequency problem of both the cylindrical-rectangular and the wraparound microstrip structures using two different approaches: integral equation formulation and a perturbational approach. Using Galerkin's method in solving the integral equations, we studied the complex frequencies with sinusoidal basis functions and investigated the effect of the edge singularity of the patch current on the convergence. Numerical results show that the HE_{10} mode

for the wraparound patch and the cylindrical-rectangular patches have narrow bandwidth; thus, they are more appropriate for resonator applications. The TE_{01} and HE_{01} modes of the wraparound and cylindrical-rectangular patches, respectively, have wide bandwidth and are efficient radiating modes.

We investigated a more realistic problem of the radiation from a cylindrical microstrip antenna excited by a probe, discussing both the cylindrical-rectangular and the wraparound elements. Using a cylindrically stratified medium approach, we rigorously formulated the current distribution on the patch, deriving a set of vector integral equations that govern it. We then solved this set of equations using Galerkin's method, which expands the patch current in terms of a complete set of basis functions that can take into account the edge singularity condition. The input impedance, together with the radiation pattern, are derived both exactly and in the small substrate thickness limit where a single mode approximation is employed. For thick substrates, hybrid modes are excited. Only in the case of axially symmetric modes ($n = 0$), is the TE_{0m} decoupled from the TM_{0m} ; modes of different parity do not couple. The presence of the dielectric substrate widens the bandwidth and broadens the radiation pattern. The radiation pattern is insensitive to the substrate thickness (especially for high dielectrics). For wraparound antenna, all current modes with no axial variation tend to weakly radiate and consequently have narrow bandwidth. When the TE_{01} mode is excited, the wraparound antenna works as a good antenna. The rectangular-cylindrical patch is, generally, less radiating than the wraparound.

For microwave integrated circuit applications, the characteristics of interconnects have been investigated for the propagation modes, time response, crosstalk, coupling, delay, etc. For these analyses, we assumed that quasi-TEM modes are guided along the multiconductor transmission lines. The analysis was performed for two asymmetric transmission lines. Also, an arbitrary number of transmission lines was analyzed in which the load and the source conditions were presented in terms of the modal reflection and transmission coefficient matrices.

A quasi-TEM analysis for multiconductor transmission lines with finite strip thickness embedded in arbitrary layers of a lossy isotropic stratified medium is presented. A spectral domain scalar Green's function of a uniform line charge immersed in a lossy isotropic stratified medium is introduced. In the formulation, no side walls are introduced, the transmission structure is not truncated, and the analysis is valid for arbitrary number of dielectric layers.

Based on the scalar Green's function, a set of coupled integral equations is obtained for the charge distribution on the strip surfaces. We used Pulse basis functions and a point-matching scheme is used to numerically solve the set of integral equations for the charge distribution, and hence the capacitance matrix. The duality between electrostatic formulation and a magnetostatic one is applied to calculate the inductance matrix. The conductance matrix is obtained by using the duality between the electrostatic and current field problem. To calculate the resistance matrix, we used a perturbation method.

Finally, we derived a transmission line analysis to obtain the transfer matrix for multiconductor uniform lines, which significantly reduces the effort in treating the load and the source conditions. We obtained transient responses by using the Fourier transform and presented the results for two coupled lines.

Due to their many advantages (including low profile and light weight), conventional microstrip antennas consisting of a single perfectly conducting patch on a grounded dielectric slab have received much attention in recent years. However, due to their resonant behavior, their use is severely limited in that they radiate efficiently only over a narrow band of frequencies, with bandwidths typically only a few percent. Techniques for increasing the bandwidth have included stacking a number of microstrip patches in multilayer configurations, introducing additional resonances in the frequency range of interest, and achieving wider bandwidths.

We have considered using a microstrip antenna consisting of two microstrip disks in a stacked configuration. With the dyadic Green's function formulation, we performed a rigorous analysis of the two stacked circular

microstrip disks in a layered medium. We derived a set of coupled integral equations for the current distribution on the disks using the vector Hankel transform. This coupled set is then solved using Galerkin's method. The choice of the current basis functions is based on the currents of the magnetic wall cavity. Complex resonant frequencies are calculated as a function of the layered substrate, permittivities and thicknesses, and the ratio of the two disks radii. The resonant frequencies of two different stacked configurations are studied as function of the coupling interaction. Critical coupling between the two resonators occurs at the point where the real part of the resonance curves for the two isolated resonators intersect. The splitting of the complex resonance curves at this point is a function of the strength of the coupling between the two resonators. The dual frequency or wide band operation is shown to be achieved by changing the coupling coefficient.

We investigated the input impedance of a microstrip antenna consisting of two circular microstrip disks in a stacked configuration driven by a coaxial probe and performed a rigorous analysis using a dyadic Green's function formulation where the mixed boundary value problem is reduced to a set of coupled vector integral equations. Galerkin's method is employed in the spectral domain with an additional term used in the disk current expansion (1) to account for the singular nature of the current in the vicinity of the probe, (2) to ensure continuity of the current, and (3) to speed up convergence of the solution. To confirm the validity of the uniform probe current assumption with the use of the attachment mode, we compared the input impedance results of a single disk on both a thin and thick substrate with published data. The input impedance of the stacked microstrip antenna is calculated as a function of the layered parameters and the ratio of the two disks. We showed that the results of the stacked microstrip configuration are in good agreement with experimental data.

Many authors have studied microstrip discontinuities, such as open end, gap and step in width. There are different methods for analyzing microstrip discontinuities, such as quasi-static approach, planar waveguide

model, and integral equation formulation. As the frequency increases, the quasi-static assumption is not valid. In the planar waveguide model analyses, the thickness of the substrate is assumed to be much smaller than the wavelength, so that we can apply a two-dimensional model. In this case, the effect of radiation and surface waves are not considered. We applied the integral equation method to study the open end and gap discontinuities on isotropic substrates. In applying the integral equation method, we introduced various approximation in the computation procedure. More recently, we used finite element expansion currents to formulate a full-wave analysis of microstrip discontinuities on isotropic substrate.

We rigorously analyzed the open end, gap, and step in width discontinuities placed on anisotropic substrates. Both uniaxial and tilted uniaxial anisotropy are considered. The materials are assumed to be lossless and the metal strips to be infinitely thin. A dyadic Green's function for layered anisotropic media is used to formulate a set of vector integral equations for the current distribution. The fundamental hybrid mode is assumed to be propagating on the input and output of microstrip lines. In solving the set of vector integral equations, we employed the method of moment. The basis functions for the current on the metal strip consider the edge effect. Both longitudinal and transverse currents are considered in the calculation. First, the propagation constant for the infinitely long uniform microstrip line is calculated. Then, the propagation constant of the fundamental mode is used to formulate the excitation of the discontinuity problem. At the discontinuity, local basis functions are used to simulate the local currents near the discontinuity. The scattering matrix can then be obtained, and an equivalent circuit model can be proposed. We investigated the effect of the anisotropy and discussed the results.

We investigated wave propagation along microstrip lines on uniaxially anisotropic substrates, in which the width is periodically modulated, by dividing the structure into consecutive uniform sections. We derived a rigorous formulation for calculating the capacitance matrix of uniform lines. We then used a quasi-TEM approximation to obtain the circuit parameters for each section. To

obtain the dispersion relation of the periodic structures, the transfer matrix is applied. The effects of the anisotropy of substrate material and the strip line geometry on the stopband characteristics are exploited. We also investigated the properties of two coupled width-modulated lines.

Most of the published work on the input impedance and other parameters of a probe-fed microstrip antenna employ an approximation to the probe feed by assuming thin dielectric substrates; the probe current can be modeled by an idealized uniform current ribbon of the same dimensions as the probe. To ensure the proper variation of the patch current near the probe and to enforce the continuity of current at the probe-patch junction, an attachment current mode has been incorporated in the patch current expansion. This leads to acceptable numerical results for the computation of the radiation pattern by the patch and for the mutual impedance between the probe and the patch. However, this approximation is not sufficiently accurate to solve for the current distribution on the patch nor for the computation of the self impedance at the terminals of the probe. Furthermore, in millimeter wave applications and for wideband operation where thick substrates or stacked structures are used, the thin substrate approximation is not valid. Recently, an alternative approach for the computation of the input impedance was developed. In this formulation, an approximate solution satisfying the boundary condition on the metallic probe was obtained in the framework of the magnetic cavity model. The fringing of the field at the edges of the patch and the radiation and surface wave losses were artificially considered by using an edge extension formula and an effective loss tangent.

We rigorously analyzed the problem of a circular microstrip disk on a thick dielectric substrate, fed by an eccentric probe. We formulated the problem in terms of a Vector Weber Transform which allows us to develop the Green's function of the layered medium with the eccentric probe and the microstrip patch as part of the medium. Using the Vector Weber Transform automatically enforces the boundary conditions on the probe and the patch. This allows us to cast the problem as the solution of a set of two

coupled vector integral equations governing the tangential components of the electric field across the aperture of the coaxial line feed and those across the interface where the patch lies. This set is then solved using the method of moments where the magnetic frill current across the aperture of the coaxial line is represented by a Vector Weber Series expansion. From the computed electric field across the aperture of the coaxial line feed, the reflection coefficient for the TEM mode is obtained which allows us to compute the input impedance at the terminals of the probe. Numerical results for the input impedance are presented.

Publications

Ali, S.M., T.M. Habashy, J.F. Kiang, and J.A. Kong. "Resonance in Cylindrical-Rectangular and Wraparound Microstrip Structures." *IEEE Trans. Microwave Theory Tech.* 37 (11):1773-1783 (1989).

Ali, S.M., T.M. Habashy, and J.A. Kong. "Input Impedance of a Circular Microstrip Antenna Fed by an Eccentric Probe." *Progress in Electromagnetics Research Symposium*, Boston, Massachusetts, July 25-26, 1989.

Habashy, T.M., S.M. Ali, and J.A. Kong. "Impedance Parameters and Radiation Pattern of Cylindrical-Rectangular and Wraparound Microstrip Antennas." *IEEE Trans. Antennas Propag.* Forthcoming.

Kiang, J.F., S.M. Ali, and J.A. Kong. "Modeling of Lossy Microstrip Lines with Finite Thickness." *J. Electromag. Waves Appl.* Forthcoming.

Tulintseff, A.N., S.M. Ali, and J.A. Kong. "Input Impedance and Radiation Fields of a Probe-Fed Stacked Circular Microstrip Antenna." *Progress in Electromagnetics Research Symposium*, Boston, Massachusetts, July 25-26, 1989.

Xia, J., S.M. Ali, and J.A. Kong. "Analysis of Microstrip Discontinuities on Anisotropic Substrates." *Progress in Electromagnetics Research Symposium*, Boston, Massachusetts, July 25-26, 1989.

1.6 High-Speed Integrated Circuit Interconnects

Sponsor

Digital Equipment Corporation
International Business Machines Corporation

Project Staff

Professor Jin Au Kong, Dr. Sami M. Ali, Dr. Tarek M. Habashy, Dr. Soon Y. Poh, Dr. Ying-Ching E. Yang, Ann N. Tulintseff, Jean-F. Kiang, Check-Fu Lee, Michael J. Tsuk, Cheung-Wei Lam, David M. Sheen

We developed a new method for analyzing frequency-dependent transmission line systems with nonlinear terminations by using the generalized scattering matrix formulation for the time domain iteration scheme. Previous works have employed either the admittance matrix, which results in extended impulse responses, or introduced artificial matching networks, which could render the solution unstable. In contrast, the generalized scattering matrix approach is most closely tied to the concept of waves. Therefore, it can achieve a shorter impulse response that leads to smaller computer memory requirement and faster computation time.

We have carried out the detailed procedure for solving this kind of nonlinear transient problem for a microstrip transmission line with linear source resistance. The diode-like terminal characteristics has been considered, and the speed of convergence is quite satisfactory.

We have applied the Time-Domain Finite-Difference modeling to obtain propagation characteristics of microstrip structures. Maxwell equations are expressed in finite-difference form, and the substrates are considered to be anisotropic in general. By positioning the components of the electric and magnetic fields at different positions and evaluating them at alternate time steps, we obtain the components of Maxwell's equations. Boundary condition implementation in this method is an important issue. Electric and magnetic walls can be implemented simply by setting the appropriate field com-

ponents to zero. Open-end termination is simulated by using the open-circuit, short-circuit technique, to cancel out the reflected waves. We have used this method to illustrate graphically the field propagation along an open microstrip line. Field components are plotted in both space and time domains. The dispersive behavior of the wave propagation can be observed. It should be noted that this method can be conveniently applied to obtain frequency-dependent characteristics of various microstrip structures such as effective permittivity, characteristic impedance, scattering matrix elements, and equivalent circuit components. An improved source plane implementation using magnetic wall is applied for better modeling of the matched source. This method is very powerful in obtaining both the time-domain and the frequency-domain characteristics of microstrip lines, discontinuities and coupled lines.

We have developed general purpose finite difference time domain (FDTD) algorithms to solve electromagnetic wave propagation in integrated circuit problems, in particular the discontinuities such as bends and corners. The geometry is read from a file which assigns dielectric constants, permeability, and conductivity to each discrete mesh point. To limit the domain of computation, we have implemented an absorbing boundary condition which simulates an outward propagating wave at the faces of the mesh, thus eliminating reflection from these faces. Specific problems simulated so far include two-dimensional propagation from a point source to demonstrate the effectiveness of the absorbing boundary condition and three-dimensional propagation around a 90 degree microstrip corner.

We have developed a new perturbation series, coupled integral equation approach for calculating the frequency dependent circuit parameters for quasi-TEM transmission lines with lossy conductors. The method considers the addition of loss and dispersion to be perturbations on the lossless TEM case, and therefore the difference between the propagation constant and the wavenumber in free space is a small parameter. We obtain the lowest order term of the perturbation series by solving two quasistatic problems; the electrostatic problem to get the

capacitance, and the magnetoquasistatic problem, with the distribution of current inside the wire considered, which gives the frequency-dependent inductance and resistance. Both of these problems are solved using one-dimensional integral equations for quantities on the surface of the conductor; this represents a significant improvement in efficiency over previous methods. For most cases of practical interest, the lowest order term of the series will suffice. If, however, the change in the propagation constant from the lossless case, due to the altered inductance and the addition of resistance, is significant, additional terms in the perturbation series can be calculated.

The method has been applied to the case of one or more wires embedded in a uniform dielectric. In the original magnetoquasistatic problem, the current is directed entirely along the axis of propagation and satisfies the frequency-domain diffusion equation. Outside the wire, the magnetic vector potential is in the same direction, and obeys Laplace's equation. The boundary conditions are the continuity of tangential and normal magnetic field at the interface, which can be expressed in terms of the current density and vector potential and their derivatives. Since we can express the ratio of the frequency-dependent resistance to the DC resistance in terms of the values of the volume current and its normal derivative on the surface of the wire only, we can use a pair of coupled integral equations to solve for these quantities alone, which we can solve by Galerkin's method or other finite element methods.

In microelectronic packaging, a problem of practical interest is the study of propagation characteristics of a shielded microstrip line in the presence of crossing strips in a multilayered structure. We have investigated the dispersion characteristics of strip lines crossed by metallic strips and embedded in the same isotropic layer and bounded by two conducting planes. We used a rigorous dyadic Green's function formulation in the spectral domain and derived a set of coupled vector integral equations for the current distribution on the conductors. We then applied Galerkin's method to derive the matrix eigenvalue equation for the propagation constant. We studied the dispersion

properties of the signal lines for both cases of finite and infinite length crossing strips.

We analyzed the effects of the structure dimensions on the passband and stopband characteristics. For crossing strips of finite length, the stopband is mainly affected by the period, the crossing strip length, and the separation between the signal and the crossing strips. For crossing strips of infinite length carrying travelling waves, attenuation along the signal line exists over the whole frequency range of operation.

Publications

Gu, Q., Y.E. Yang, and J.A. Kong. "Transient Analysis of Frequency-Dependent Transmission Line Systems Terminated with Nonlinear Loads." *J. Electromag. Waves Appl.* 3 (3):183-197 (1989).

Kiang, J.F., S.M. Ali, and J.A. Kong. "Propagation Properties of Strip Lines Periodically Loaded with Crossing Strips." *IEEE Trans. Microwave Theory Tech.* 37 (4):776-786 (1989).

Lam, C.W., S.M. Ali, and J.A. Kong. "A New Finite-Difference Time-Domain Grid Model for Microstrip Problems in Anisotropic Media." *Progress in Electromagnetics Research Symposium*, Boston, Massachusetts, July 25-26, 1989.

Tsuk, M.J., and J.A. Kong. "The Frequency-Dependent Resistance of Conductors with Arbitrary Cross-Section." *Progress in Electromagnetics Research Symposium*, Boston, Massachusetts, July 25-26, 1989.

1.7 ILS/MLS Frequency Management Assessment

Sponsor

U.S. Department of Transportation
Contract DTRS-57-88-C-00078

Project Staff

Professor Jin Au Kong, Dr. Robert T. Shin, Dr. Ying-Ching E. Yang, Qizheng Gu, Mohammad A. Tassoudji, Murat A. Veysoglu, Khurram K. Afridi, Li-Fang Wang

Because of the rapid expansion of air traffic in the United States and around the world, precision landing systems play an important role in both increasing airport capacity and safety. Both the traditional instrument landing system (ILS) and the newer microwave landing system (MLS) have established international standards.

In this research project, we develop simulation tools for evaluating (from the spectrum management aspect) the growth potential of ILS and MLS in metropolitan areas. Suitable electromagnetic propagation models will be established with all possible electromagnetic radiation sources within the ILS/MLS operating bands considered in our study of electromagnetic interference level. We can then use this interference level to judge whether the capacity can be met by adding a certain type of precision landing system without causing any problems.

Our technical approach included the following tasks:

1. Identification of radiation sources,
2. Development of propagation models,
3. Development of receiver models,
4. Construction of computer simulation tool,
5. Verification and validation of the simulation software, and
6. Generation of metropolitan channel capacity projection database.

The major deliverable of this project is a simulation software named EMSALS (Electromagnetic Modeling and Simulation Applied to Landing Systems). It will be subdivided into EMSALS/I (for ILS) and EMSALS/M (for MLS). Because ILS has been in use for more than forty years and its operation characteristics and interference sources are better known, our initial emphasis will be on ILS assessment. The MLS assessment will build upon the experience with ILS simulation and be implemented in a more gradual manner.

For a greater degree of feedback on our research, we decided to carry out the project in a progressive manner by dividing it into five self-contained phases. Each phase is

marked by different combinations of theoretical models. An exhaustive analysis encompassing all six tasks listed above will be done during each phase. Thus, we can obtain intermediate results at any time, and can use existing data to check the degree of accuracy of the theoretical models.

The first two phases of ILS studies are devoted to automating FAA spectrum engineering procedure on 386-based PCs. We spent the past few months developing the computation model and user interface for such procedure, implementing the free-space and the IF-77 propagation models and a minimum performance standard (MOPS) compliant receiver model. At the conclusion of Phase 1, coding of the procedure is completed. Our software takes as much input as possible from site-specific information such as antenna type and radiated power, with runway headings achieving maximum degree of accuracy. We stored a digitized map of the United States, accurate to one hundredth of a degree, to be displayed with the assessment. Besides the menu feature, we also added the capability to zoom in and out at various magnification levels with a mouse or with keyboard control. Site-specific data such as antenna type and power are taken into the computation module. The next step,

verification of the simulation code, will involve examining and comparing the manual analysis results with the computer output. This verification will be done on a larger scale, including several metropolitan areas. Meanwhile, we continued with building modules for the cell display simulation. The modules, originally written in Turbo Pascal, have been converted to Turbo C codes. The user interface has also been improved. On the first screen, the user can specify the name of signal strength database, which has been precalculated. On the second screen, the user specifies the models and computational parameters, on the display screen, where assessment is being made. Here "cell" refers to an area of one nautical mile by one nautical mile at the designated altitude. The cells are color coded according to the seriousness of interference. The user will be able to zoom in and out, to inquire the signal and interference strength with the mouse, and to turn on and off, or change the power of the transmitting antenna. Thus, the cell display will provide abundant information and will be an invaluable tool for FAA Spectrum Engineering Division personnel to pinpoint where the problem is and to what extent the simulation tool is eventually released.

Section 4 Radio Astronomy

Chapter 1 Radio Astronomy

Chapter 1. Radio Astronomy

Academic and Research Staff

Professor Bernard F. Burke, Professor David H. Staelin, Professor Jacqueline N. Hewitt, Dr. Philip W. Rosenkranz, John W. Barrett

Visiting Scientists and Research Affiliates

Dr. Alfred P. DeFonzo,¹ Dr. Michael Shao²

Graduate Students

Ashraf Alkhairy, Pierino G. Bonanni, Christopher Carilli, William J. Chiarchiaro, Kevin G. Christian, Samuel R. Conner, John T. Delisle, Andre B. Fletcher, Mark Griffith, Jens-Ole Hansen, Michael B. Heflin, Edward J. Kim, Charlene C. Kuo, Joseph Lehar, Darren L. Leigh, Jerome M. Shapiro, Howard R. Stuart

Undergraduate Students

Alexander Angelus, Talal M. Bahrani, Nicholas P.T. Bateman, Shiufun Cheung, Jee Chung, Stephen S. Eikenberry, Muriel Medard, Michael C. Petro

Technical and Support Staff

Wendy E. Hunter, Clare F. Smith

1.1 Galactic and Extragalactic Research

Sponsor

National Science Foundation
Grant AST 88-19848

Project Staff

Professor Bernard F. Burke, John W. Barrett, Christopher Carilli, Nicholas P.T. Bateman, Jee Chung, Samuel R. Conner, Andre Fletcher, Mark Griffith, Jens-Ole Hansen, Michael Heflin, Joseph Lehar

1.2 Gravitational Lens Search

Two particularly interesting examples of the "Einstein ring" phenomenon were described in last year's *RLE Progress Report*. Both Einstein rings were discovered during the search program for gravitational lensed radio sources being carried out at MIT in collaboration with scientists at Princeton University and California Institute of Technology. We have established a data archive accessible to RLE students and visitors that includes the 4000 maps from this survey.

We have extended the MIT-Green Bank (MG) Survey, working with the National Radio Astronomy Observatory (NRAO) and using the Green Bank 300-foot telescope to cover a wider declination range beyond that of the original MG Survey. The results comprise Parts II, III and IV of the MG catalog. MG Part II has been published, Part III is in press, and Part IV has been submitted for

¹ University of Massachusetts, Amherst.

² Jet Propulsion Laboratory, California Institute of Technology.

publication. The survey had covered the entire band of sky between declinations 0.5 degrees and +3.9 degrees and approximately half of the band +37 degrees to +51 degrees when the Green Bank telescope collapsed in November 1988.

Currently, we are beginning a new survey, using the seven-feed NRAO cooled receiver at the Parkes 210-foot telescope in Australia. This new survey, known as the Parkes-MIT-Green Bank Survey (PMG Survey), will cover from 40 degrees declination to the South Celestial Pole.

Reduction of the 4000 VLA source maps, derived from MG I, is almost complete. The VLA has accepted our proposal to begin a program to search for more lenses, using the MG II and MG III survey results. We will map the first 1000 sources during the first six months of 1990.

1.2.1 Einstein Rings

We are continuing to study the two examples of the Einstein ring phenomenon that we discovered over the past two years: MG1131+0456 and MG1654+1346. The Einstein ring effect occurs when a distant object, usually a quasar, is aligned in a particular way with a foreground galaxy that acts as a gravitational lens. If the foreground object has spherical symmetry, the rays bend around it uniformly to form a ring-like image of a point source. Most lensing galaxies are ellipsoidal, so the result is an elliptical image that is not a perfect ring. The phenomenon is so striking that it can be recognized easily from radio data alone. Furthermore, optical data can provide complementary information on the redshifts of source and lens. This information can be used to define the total mass encircled by the ring and to deduce the degree of flattening of the ellipsoidal mass distribution.

The source MG1654+1346 is the first ring to be completely analyzed. Figure 1 gives a superposition of the radio and optical images. The distant quasar is labeled Q and the foreground galaxy is labeled G. The radio contours at A and C, on opposite sides of the quasar, are radio lobes driven by the

central engine at Q, but the contours at C are distorted into a ring.

Figure 2 shows the model and the effect of an ellipsoidal lens on a set of three objects, labeled 1, 2, and 3. These are imaged as shown, with source 1 becoming A1 and B1, source 2 becoming A2 and B2, etc. The redshift of the lensing galaxy is 0.254, and the quasar redshift is 1.74, leading one to calculate a mass of $(2.97 \pm 0.32) \times 10^{11} h^{-1}$ for the galaxy, where $h = 1$ if the Hubble constant H degrees = 100 km/sec/Mpc. The mass-to-light ratio is $15.9 \pm 2.3 h$, probably the best determination of this ratio ever made for any galaxy.

The success of our work on MG1654+1346 has led us to conclude that similar determinations can be made for other systems. In our new survey, we expect to find additional lenses, which would make possible a wider search for dark matter. Several theories suggest that substantial quantities of nonluminous matter, possibly of exotic character, is present in galaxies and in the universe as a whole. Locating and analyzing gravitational lenses, especially in well-defined systems such as Einstein rings, is one of the best methods for measuring this important constituent of the universe.

1.2.2 VLBI Studies of 2016+112

Part I of the MIT-Green Bank survey and the associated VLA survey led to discovery of the 2016+112 gravitational lens system. Subsequent optical and radio observations have revealed a surprising number of components. There are three radio sources called A, B, and C respectively. We have found optical counterparts for all three radio sources. Components A and B appear to be gravitationally-lensed images of a single source as indicated by spectra with the same unusually narrow emission lines and identical redshifts of 2.273 within a given error of measurement. The light from the C component region is believed to come from a weak third image, C, in addition to the radio galaxy, C. There is a radio quiet galaxy, D, located between A, B, and C, which has a redshift of 1.010 ± 0.005 . There are also two extended emission line objects to the west of A and B called A1 and B1, respec-

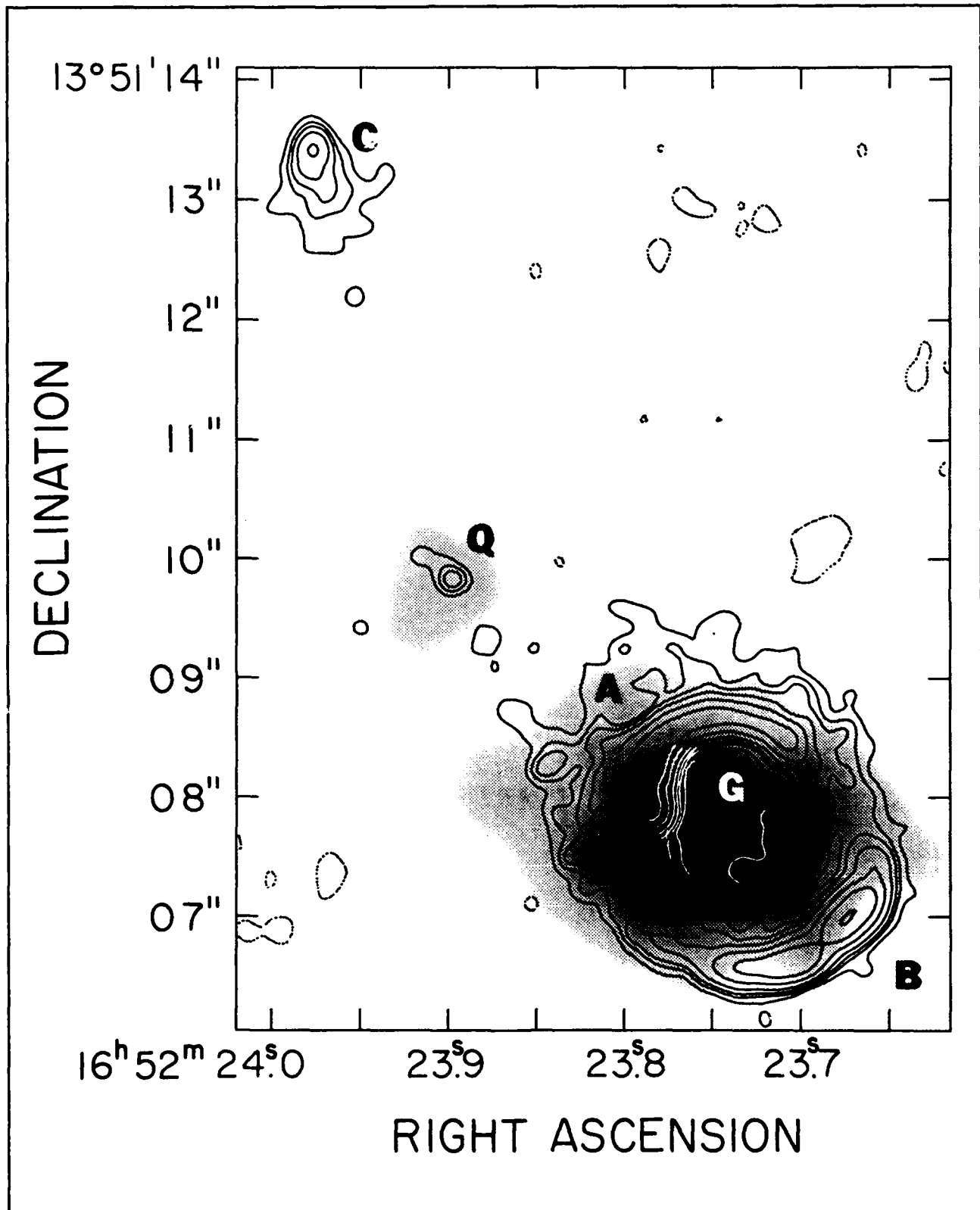


Figure 1. Superposition of optical image of MG1654+1346 on contours of VLA radio image.

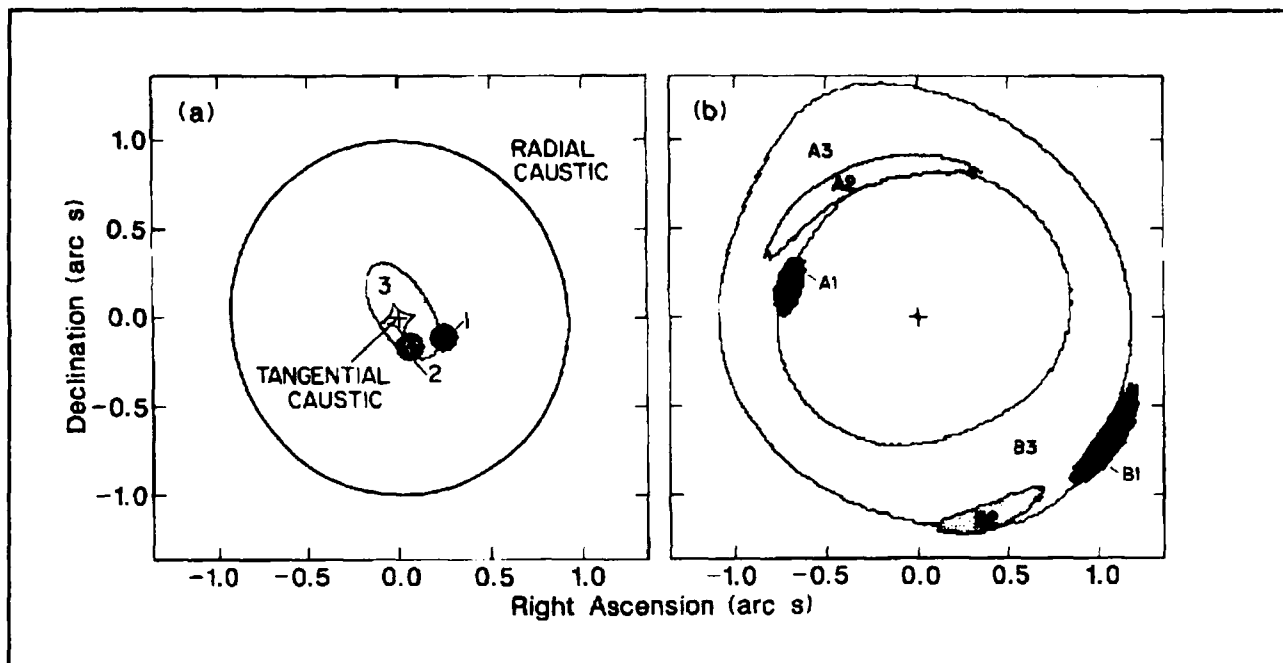


Figure 2. On the left, a 3-component source model with the model image shown on the right, to be compared with the radio image in figure 1.

tively, which may be two separate clouds of ionized gas that lie within a few kiloparsecs of the lensed source.

First epoch VLBI observations took place on June 1, 1984. Components A and B are both doubles at the milliarcsecond level. Models which allow A and B to be adjusted independently have a slightly better fit than those which constrain A and B to be related by a linear matrix, suggesting some source evolution on a time scale shorter than the unknown time delay. If a time delay of zero is assumed and the slightly degraded fit accepted, then the resulting model can be used for comparison with theoretical lens models by predictions of the magnification matrix. Three lens models by Narasimha, Subramanian, and Chitre (1987) and one by Narasimha and Chitre (1989) predict magnification matrices. None of the predictions agree, but the dark halo model by Narasimha and Chitre (1989) works best. Final results are currently being submitted for publication. Second epoch observations were carried on November 9, 1989. Analysis should be complete by August of 1990.

1.2.3 Time Variations

The double quasar 0957+561, discovered by Walsh, Carswell and Weymann in 1979, was the first gravitational lens to be recognized. It has two compact radio components, A and B, separated by 6 arcseconds, which have optical counterparts with nearly identical spectra at a redshift of 1.4. We have also observed the principal lensing galaxy, about 1 arcsecond away from the B image, with a redshift of 0.36. The A and B components were observed to be variable in radio brightness by our group in 1980. According to models of this gravitational lens, there should be a time delay of about one year between variations observed in the A and B components. Measurement of the time delay would provide a further constraint to the lens models. Finally, Falco et al. showed in 1988 that the time delay could be applied to the lens models to estimate Hubble's constant.

In order to observe this time delay, we have been monitoring the radio flux of the two images for the past ten years. Both images decreased steadily in brightness by about 20 percent over the first five years of observation, leaving us without any features for time delay measurement. In 1984, however, the decline flattened out in the A image, and

subsequently in the B component. The feature allowed us to roughly measure the time delay to be 500 ± 200 days (reported at the Cambridge Conference on Gravitational Lenses in 1988). Incidentally, applying the models of Falco et al., this measurement estimates Hubble's constant to lie between 50 and 100 km/s per Mpc.

Two factors prevented a more precise measurement: the feature was not very strong compared to our measurement error, and our time coverage was incomplete. The radio observations are made at the VLA roughly every month. The VLA alternates between four configurations, of which only the A and B arrays have sufficient angular resolution to clearly resolve the two images of 0957+561. Hence, for half of each year, we were unable to accurately measure the brightness of the two components. The annual 50 percent gaps made the measurement of a slight change in the light curves exceedingly difficult.

During the past year, we have been working on improving the quality of the time delay measurement by filling in the gaps in the light curves. We have applied a more complex reduction technique that enables us to extract the A and B image fluxes from the C array data that comprise about 80 percent of the missing time samples. We are also attempting to use the total source brightness of the D-array observations to fill the remaining gaps. With the C-array fluxes, the curve looks much better already.

We have also benefitted from a timely change in the radio source. During the spring of 1989, the A component increased sharply in flux, by a factor of about 15 percent. We have begun to observe the subsequent rise in the B component this spring. This much stronger feature, combined with our more complete time coverage, should allow us to improve the time delay measurement.

1.2.4 Lens Modeling

The derivation of cosmological information (such as H_0) from instances of gravitational lensing is dependent on accurate modeling of the mass of the lens. The model information is itself interesting since it gives the mass (and, with optical observations, the mass-to-light ratio) of the matter enclosed by the multiple images. In view of this, we are developing a ray-tracing/lens-modeling package.

The ray-tracing package is nearly complete. The package supports a wide variety of analytic mass profiles. In addition, arbitrary mass distributions on a grid are supported, permitting the use of optical images of the lens as mass models and the direct determination of M/L of the lens. The package permits the determination of image configuration for arbitrary source brightness distributions lensed by one or many galaxies at one or many redshifts. The modeling package permits the estimation of lens model parameters for a given configuration of images. At present, only point images are supported. The package will be upgraded to use arbitrary extended images (such as radio maps of the ring images).

In collaboration with an optical observer at MIT, the package in its present form will be used to model the gravitational lens system 1115+080 (for which the point image approximation is valid). The upgraded version (capable of dealing with extended images) will be used to model MG1654+1346 and extended image configurations which will be discovered in the upcoming VLA lens survey.

1.3 Orbiting VLBI

Sponsors

Jet Propulsion Laboratory
Contract 957687
National Aeronautics and Space Administration
Grant NAGW 1386

Project Staff

Professor Bernard F. Burke, John W. Barrett,
Samuel R. Conner, Michael B. Heflin

1.3.1 The Japanese VSOP Mission

The Japanese Institute for Science and Astronautics in Space (ISAS) has approved a mission to carry a VLBI radio telescope into space. The mission, which will have a 10-meter paraboloid with observing frequencies of 1.6, 6, and 22.3 GHz, will be launched in early 1995. The United States will participate by providing the ground radio telescopes and the correlator of the National Radio Astronomy Observatory's Very Long Baseline Array (VLBA), now scheduled for completion in 1993. The Deep Space Net (DSN) of NASA will provide data acquisition, tracking, and orbital determination, and will serve as a participant in the mission management. Professor Bernard F. Burke, active in the Japanese advisory group for VSOP, is also chairman of the Science Consulting Group set up by NASA to coordinate U.S. participation in foreign VLBI missions.

Our group has been active in the preliminary TDRSS experiment (described in last year's *RLE Progress Report*). During the past year, we have been investigating the scientific aspects of the mission. We have also studied possible approaches to ground tracking and acquisition of information if the NASA Deep Space Net Program cannot fulfill that role.

1.3.2 The Soviet RADIOASTRON Mission

The Institute for Space Research (IKI) of the U.S.S.R. has approved deployment of a VLBI mission, designated RADIOASTRON. Complementary to the Japanese VSOP mission, RADIOASTRON will orbit much farther from the earth, giving baselines an order of magnitude larger than any achieved so far.

Recently, Vice President Quayle announced that the U.S. will join the Soviet mission as a memorial to academician Sakharov, who supported this effort. The roles of the United States and MIT will be similar to those established for the VSOP mission.

1.4 Development of an Undergraduate Laboratory

Sponsor

National Science Foundation
Grant AST 88-19848

Project Staff

Professor Bernard F. Burke, John W. Barrett, Jee Chung

The classical way of introducing undergraduate students to astronomy has been through optical results, i.e., using optical telescopes as part of the laboratory experience. In recent years, some of the most startling developments in astronomy have come from studying the radio domain: pulsars, quasars, and cosmic "big bang" radio background are outstanding examples. Although previously radio techniques had been considered too complex and too expensive, the rapid development of inexpensive digital systems and computers has changed the circumstances dramatically. We have been developing a new experiment for the MIT Junior Physics Laboratory to introduce students to the new science of radio astronomy.

In the experiment, we use an 8-foot telescope on the roof of our building that has a modern low noise L band amplifier. The receiver chain converts the incoming signal to baseband where the spectrum is analyzed by an autocorrelator. The local oscillator and filter frequencies are chosen so that the 21 cm hydrogen line, coming from the interstellar medium, is in the middle of the analyzed band. The autocorrelator uses multichannel chips developed by the Netherlands Foundation for Radio Astronomy and incorporated into a working autocorrelator function to a spectrum by taking the Fourier transform. An IBM PC controls the telescope.

Not only does the experiment introduce the student to radio astronomy, it introduces modern techniques of noise analysis and the use of Fourier transform methods. Thus, there are practical benefits to the student's educational experience in addition to the exciting and intellectual adventure of directly measuring the large-scale motions of our galaxy.

1.5 Radio Interferometry of Nearby dMe Stars

Sponsor

Annie Jump Cannon Award

Project Staff

Jens-Ole Hansen, Professor Jacqueline N. Hewitt

dMe stars are dwarf M stars that show evidence of unusual surface activity. They have been known for some time to flare strongly at optical and radio wavelengths, and more recently it has been recognized that many dMe stars exhibit low level quiescent emission at centimeter wavelengths that is detectable with the Very Large Array radio telescope. In collaboration with colleagues at Haystack Observatory, Jet Propulsion Laboratory, and Bureau des Longitudes (France), we have shown that several nearby dMe stars are detectable with a Very Long Baseline Interferometry (VLBI) array. These measurements place limits on quantities of direct relevance to theories of the radio emission mechanism. In addition, detection of dMe stars on VLBI baselines makes possible measurement of the position of these stars with very high precision (≤ 0.5 milliseconds of arc). This high-precision astrometry would have several interesting applications, most notably in detecting planetary companions to the dMe stars. For example, the orbital motion of nearby dMe star about a companion of Jovian mass would be detectable in just a few years. We are currently working on more extensive VLBI measurements of the dMe star emission and undertaking a program aimed at identifying radio reference sources for use as positional standards in the astrometry.

1.6 Gravitational Lenses as Astrophysical Laboratories

Sponsor

Annie Jump Cannon Award

Project Staff

Alexandar Angelus, Professor Jacqueline N. Hewitt

Previous work (in collaboration with Professor Bernard F. Burke and colleagues at Princeton University and California Institute of Technology) has identified two gravitational lens systems, MG1131+0456 and MG0414+0534, that display a high degree of symmetry. As a consequence of this symmetry, these systems should be interesting astrophysical laboratories. They could provide new measurements of cosmological interest, such as Hubble's constant and the mass-to-light ratio of the matter forming the lens. After having carried out VLA observations of MG1131+0456, we are analyzing the data to determine whether the source is variable, a necessary condition to measure Hubble's constant. We have acquired VLBI and additional VLA data of the two lens systems so that we can model their gravitational fields.

1.7 Tiros-N Satellite Microwave Sounder

Sponsor

SM Systems and Research, Inc.

Project Staff

Professor David H. Staelin, Dr. Philip W. Rosenkranz, Charlene C. Kuo

This project scientifically supports the Advanced Microwave Sounding Unit (AMSU) scheduled for launch on polar-orbiting weather satellites in the mid-1990s. Support of this passive microwave spectrometer program emphasizes atmospheric transmittance spectra, retrieval methods, and instrumentation issues.

One issue we addressed this year concerned the strong nonlinearities in AMSU relative humidity retrievals; both the nature of the nonlinearities and the resulting limits to the altitude coverage and vertical resolution of AMSU were characterized. A manuscript describing the accuracy of such humidity retrievals is being prepared.

Studies of precipitation cell sizes observed in summer and winter aircraft flights of the MTS 118-GHz spectrometer suggest that AMSU-A will resolve perhaps one-third of such cells with 50-km resolution and that

AMSU-B should resolve perhaps two-thirds of these cells with its 15-km resolution; the implication is that AMSU-A and AMSU-B might have a useful role to play in estimation of global precipitation, which is an important parameter in understanding the global hydrological cycle and climate.

Further consideration of atmospheric transmittances in the 5-mm oxygen band resulted in improved expressions for the temperature dependence. In particular, the temperature dependence of the interference coefficient for each line was revised to be consistent with detailed balance and a tri-diagonal model for the relaxation matrix.

Study of AMSU has led to the conclusion that a simple circularly-polarized double-sideband spectrometer could be added to module A2, yielding temperature soundings to 75-km altitude using the 7+ and 9+ oxygen resonances. Polarization reversal between the sidebands and use of a 2-bit, 16-channel digital autocorrelator would efficiently yield approximately ten spectral channels with good altitude resolution for all magnetic field configurations.

1.8 Long-Baseline Astrometric Interferometer

Sponsor

U.S. Navy Office of Naval Research
Contract N00014-88-K-2016

Project Staff

Professor David H. Staelin, John W. Barrett,
Edward J. Kim, Howard R. Stuart

During 1989, our effort involved (1) completion of a study on dispersed-fringe, group-delay astrometry for the Mark-III optical interferometer and (2) initial development of infrared observing capabilities for the same instrument.

Fringe-tracking systems are typically limited to stars of ~ 9 th magnitude, but dispersing the white fringe into a continuum of colors for which the interference pattern can be separately estimated permits integration over longer time periods and improved signal-to-noise ratio.³ This technique was demonstrated using the Mark-III stellar interferometer at the Mount Wilson Observatory. For these tests the detectability limit (SNR ~ 1) was between 2 and 4 detected photons per 4-msec frame, using only 4000 frames. This represents an improvement of ~ 3 stellar magnitudes over the standard fringe-tracking mode which requires 40 photons per 4-msec interval. These results from four stars are believed to be the first stellar observations of dispersed-fringe group delays made with a visible-light stellar interferometer.

To facilitate infrared stellar diameter measurements, work began on modifying the interferometer to operate at ~ 2.2 microns. A preliminary system design was developed and work began on the electronics. Analyses predict that second magnitude stars could be observed with this system.

Previous progress in developing optical trusses for monitoring the positions of the siderostat mirrors was documented further.⁴

1.9 Nonthermal Radio Emission from the Jovian Planets

Sponsor

NASA/Goddard Space Flight Center
Grant NAG 5-537

Project Staff

Professor David H. Staelin, Stephen S. Eikenberry

The Planetary Radio Astronomy (PRA) experiment on the Voyager-2 spacecraft

³ E.J. Kim, *Dispersed Fringe Group Delay Astrometry Using the Mark III Stellar Interferometer*, S.M. thesis, Dept. of Electr. Eng. and Comput. Sci., MIT, 1989.

⁴ B. Hines, M. Shao, M.M. Colavita, and D.H. Staelin, "Use of Laser Metrology Optical Truss for Monitoring Baseline Motion," paper presented at SPIE Conference 1237: Amplitude and Spatial Interferometry, February 14-16, 1990.

observed radio emission from five planets in 198 channels distributed over the band from 1.2 kHz to 40.5 MHz. The characterization of the observed Uranian radio emission was extended and documented in a draft manuscript, which is being prepared for publication.

During August 1989, Voyager 2 encountered Neptune. The PRA instrument again measured varied strong radio emission from the planet.⁵ The types of emission observed included strong narrowband highly polarized bursts in the frequency range 0.1–1.3 MHz, episodes of smooth emission at 20–865 KHz, and excess emission during the ring plane crossing and the inbound crossing of the magnetospheric bowshock. Initial studies of the emission with high spectral resolution reveal frequency structures that evolve in a manner reminiscent of the emission seen on the other three Jovian planets. One unique feature is the presence of a very sharply defined and slowly drifting spectral region of no emission, bounded on both sides by emission that varies relatively smoothly with time and frequency. None of the other planets exhibited such a marked forbidden frequency band.

1.10 High-Resolution Passive Microwave Imaging of Atmospheric Structure

Sponsor

NASA/Goddard Space Flight Center
Grant NAG 5-10

Project Staff

Professor David H. Staelin, John W. Barrett, Pierino G. Bonanni, William J. Chiarchiaro, Dr. Philip W. Rosenkranz

The scientific results obtained from the passive microwave observations of clear air and storms by an imaging microwave spectrometer on the NASA ER-2 high-altitude aircraft were documented for publication. The first paper⁶ describes the instrument (MTS), which employed eight double-sideband channels centered around the 118.75-GHz O₂ resonance, in addition to describing the results from 32 aircraft flights during the Genesis of Atlantic Lows Experiment (GALE) and the Cooperative Huntsville Meteorological Experiment (COHMEX). Simultaneous observations were made with a single-beam 53.6-GHz radiometer and a video camera. It was shown that the response to clouds near 118.75 ± 1.47 GHz was ~ 1.7 times greater than that near 53.65 GHz, a modest ratio considering that both frequencies sound tropospheric temperatures with approximately the same weighting functions.

Also prepared for publication were studies of the utility of these same 118-GHz O₂ observations for estimating parameters of precipitation cells imaged by the instrument.⁷ It was shown that errors on the order of 1–2 km rms can be obtained for estimated altitudes

⁵ J.W. Warwick, D.R. Evans, G.R. Peltzer, R.G. Peltzer, J.H. Romig, C.B. Sawyer, A.C. Riddle, A.E. Schweitzer, M.D. Desch, M.L. Kaiser, W.M. Farrell, T.D. Carr, J. de Pater, D.H. Staelin, S. Gulkis, R.L. Poynter, A. Boischot, F. Genova, Y. Leblanc, A. Lecacheux, B.M. Pedersen, and P. Zarka, "Voyager Planetary Radio Astronomy at Neptune," *Science* 246:1498-1501 (1989).

⁶ A.J. Gasiewski, J. Barrett, P.G. Bonanni and D. Staelin, "Aircraft Based Radiometric Imaging of Tropospheric Profiles and Precipitation Using the 118.75 GHz Oxygen Resonance," accepted for publication *J. App. Meteor.* (1990).

⁷ A.J. Gasiewski and D.H. Staelin, "Statistical Precipitation Cell Parameter Estimation Using Passive 118-GHz O₂ Observations," *J. Geophys. Res.* 94:18367-18378 (1989).

of rain cell tops. The retrieval operator consisted of a Karhunen-Loeve transformation followed by a rank reduction, a nonlinear operator, and a linear mean-square-error estimator. Comparisons were made to celltop altitudes obtained by optical stereoscopy from the same high altitude aircraft flying near 65,000 feet.

Studies of the observability of temperatures in the upper stratosphere and mesosphere continued.⁸ It was shown that ground-based observations near the 27-oxygen line can yield weighted temperatures near the strato-pause (~ 1 mbar). Sensitivities would be ~ 1 K rms with 20 minutes of integration⁹ for receiver noise temperatures of ~ 1000 K. Observations from aircraft near 20 km altitude will be four times more sensitive since tropospheric attenuation will be eliminated.

In preparation for future experiments, improvements were made to the present MTS 53.6-GHz radiometer. Its local oscillator, calibration switch, and mixer preamplifier were replaced, and a 16-channel, 2-bit autocorrelation unit is being constructed for observations of oxygen lines.¹⁰ The varactor-tuned Gunn-diode local oscillator can be rapidly tuned over the 52.8–54.94 GHz frequency range, thus permitting emulation of the Advanced Microwave Sounding Unit (AMSU) channels 4–7, which sound the lower troposphere. These improvements will make possible ground-based and airborne measurements of mesospheric temperatures and atmospheric transmittance microwave properties.

1.11 Characterization of Dolphin Whistles

Sponsor

Woods Hole Oceanographic Institution
Contract SC-28860

Project Staff

Professor David H. Staelin, Kevin G. Christian

Dolphin communication is characterized by a combination of repetitive whistles, not unlike bird song, and high speed clicks generally used for echo location. This project involves substantially compressing these signals and developing methods for organizing them in a database for rapid identification of repetitious song elements. One anticipated result of this research is improved understanding of how various songs are created and evolve in dolphin communities. The results of this research should also lead to signal analysis tools useful for acoustic diagnosis of machinery and other devices.

1.12 Rapid Precision Net-Form Manufacturing

Sponsor

Leaders for Manufacturing Program

Project Staff

Professor David H. Staelin, Ashraf S. Alkhairy, John T. Delisle, Darren L. Leigh, Howard R. Stuart

This project has three interrelated elements which include the development of (1) methods and apparatus for measuring the shape of arbitrary three-dimensional objects with sub-mil accuracy; (2) methods and apparatus for forming such objects in metal, ceramics, or plastics rapidly with sub-mil pre-

⁸ P.W. Rosenkranz and D.H. Staelin, "Polarized Thermal Microwave Emission from Oxygen in the Mesosphere," *Radio Science* 23:721-729 (1990).

⁹ P.W. Rosenkranz, "Oxygen Line Emission as a Measure of Temperature in the Upper Stratosphere and Mesosphere," paper to be presented at the 1990 International Geoscience and Remote Sensing Symposium, University of Maryland, May 20-24, 1990.

¹⁰ M.C. Petro, *An Autocorrelator for Determining the Temperature of the Upper Atmosphere*, S.B. thesis, Dept. of Electr. Eng. and Comput. Sci., MIT, June 1989.

cision; and (3) new methods for adaptive experiment design that could facilitate process characterization and help achieve desired levels of precision by iteration of elements (1) and (2).

Most of the work involved development of a 4-axis stage with a scannable volume of ~ 20 cubic inches; its open loop accuracy is better than 25 microns. A 512^2 pixel CCD

camera was linked to a telescope with an adjustable field of view down to 1-mm^2 , and to a computer capable of receiving up to 30 frames per second. Holographically generated illumination patterns provide the signal which permits object shape to be measured at high data rates. Work on methods for adaptive experiment design and materials forming is still in the formative stages.

Part III Systems and Signals

Section 1 Digital Signal Processing

Section 1 Digital Signal Processing

Chapter 1 Signal Processing Research Program

Chapter 2 Speech Processing Research Program

Chapter 3 Advanced Television Research Program

Chapter 4 Computer-Aided Fabrication System Structure

Chapter 5 Optical Propagation and Communication

Chapter 6 Custom Integrated Circuits

Chapter 7 Neurophysiology and Neural Computation

Chapter 1. Signal Processing Research Program

Academic and Research Staff

Professor Alan V. Oppenheim, Professor Arthur B. Baggeroer, Professor Bruce R. Musicus, Dr. Charles S. Burrus,¹ Giovanni Aliberti, Giampiero Sciutto

Visiting Scientists and Research Affiliates

Dr. Meir Feder,² Dr. Jules Jaffe,³ Dr. Timothy Stanton,⁴ Makoto Tabei,⁵ Dr. Ehud Weinstein⁶

Graduate Students

Paul E. Beckmann, John R. Buck, Lawrence M. Candell, Daniel T. Cobra, Michele M. Covell, Dennis C. Fogg, Jacek Jachner, Tae H. Joo, G.N. Srinivasa Prasanna, James C. Preisig, Michael D. Richard, John M. Richardson, Andrew C. Singer, William S. Song,⁷ Gregory W. Wornell

Technical and Support Staff

Deborah A. Gage, Hassan Gharavy

1.1 Introduction

The Signal Processing Research Program develops new algorithms and their applications in a variety of areas including speech, image, and underwater acoustic signal processing. In addition, the program deals with issues related to algorithm implementation. We are following a new direction in signal processing, which we refer to as knowledge-based signal processing. While, historically, signal processing has principally emphasized numerical techniques, knowledge-based processing involves a combination of numerical and symbolic processing techniques.

In addition to working on specific on-campus projects, our group interacts closely

with MIT Lincoln Laboratory and Woods Hole Oceanographic Institution.

1.2 Algorithmic Fault Tolerance in Digital Signal Processing

Sponsors

Charles S. Draper Laboratory
Contract DL-H-404158
U.S. Navy - Office of Naval Research
Grant N00014-89-J-1489

Project Staff

Professor Bruce R. Musicus, William S. Song, Paul E. Beckmann

¹ Director, Department of Electrical Engineering, Rice University, Houston, Texas.

² Faculty of Engineering, Dept. of Electronic Systems, Tel Aviv University, Tel Aviv, Israel.

³ Marine Physical Laboratory, Scripps Institution of Oceanography, La Jolla, California.

⁴ Woods Hole Oceanographic Institution.

⁵ Tokyo Institute of Technology, Yokohama, Japan.

⁶ Faculty of Engineering, Director, Department of Electronic Systems, Tel Aviv University, Tel Aviv, Israel.

⁷ Charles S. Draper Laboratory Fellow.

Conventional methods for achieving fault tolerant computer architectures rely on triplicating computational resources and using voter circuitry to reject incorrectly computed results. From an information theory viewpoint, however, using coding techniques would achieve a high level of error recovery with minimal overhead. Essentially, a coder distributes information across a noisy channel bandwidth, so that individual noise spikes may destroy a portion of many bits, but not an entire bit. A decoder at the receiver could combine information from the full channel bandwidth to reconstruct the original message with a very high degree of reliability.

High-performance memory systems and communication networks use coding techniques heavily. These techniques work well to protect modules in which data enters at one end and is expected to arrive intact and unchanged at the other. However, coding techniques are not usually used to protect actual computation. Instead, high levels of fault tolerance within CPUs are traditionally achieved by duplicating or triplicating processor resources and voting on the results. Also, the coding and decoding procedure adds to the latency of the channel, slowing down any machine using the protected component.

We are developing a new approach to fault tolerance that protects certain types of linear computation against processor failure. In this approach, a small number of redundant processors protect each other and the "real" processors. One design employs a bank of analog-to-digital converters operating in round-robin fashion to achieve an overall sampling rate somewhat above the Nyquist rate for the signal. A dither system and digital low-pass filter combine to reduce quantization errors in the front end. We can use this same low-pass, however, to detect and correct temporary or permanent errors in any of the converters without substantially increasing the total amount of computation time. The system trades off additional hardware for greater accuracy and higher levels of fault protection. When converters fail, an

increase in the effective quantization error is the only result.

Another application of algorithmic fault tolerance is the FFT processor system used in range and velocity doppler sonar processing. In this processor system, we use a stack of processors to process multiple scans of sonar data from a phased-array antenna. Each processor does the same linear FFT processing, but on different sets of range cells. Adding extra processors working on linear combinations of the inputs to the other processors allows simple fault detection and correction. Regardless of the number of processors in the system, detecting K simultaneous failures requires only K extra processors; detecting and correcting K simultaneous failures requires only $2K$ extra processors. When conventional truncation or rounding arithmetic is used, however, then the error checking is only approximate.

In this case, adding more processors improves the accuracy of the fault checking and correction. We use generalized likelihood ratio tests to select the most likely failure hypothesis and to perform the most likely fault correction. Realistic systems result, using comparatively small computational overhead (<50 percent) to achieve 100 percent single fault detection and correction.

We are presently working with Draper Laboratories to design a prototype hardware system incorporating 16 DSP-32C processors and a 68000 controller for testing a sonar application of this theory. We are also currently trying to extend the idea to cover non-linear computation.

Publications

Beckmann, P., and B.R. Musicus. "Fault-Tolerant Round Robin A/D Converter System." *Proceedings of the IEEE International Conference on Acoustics, Speech, and Signal Processing*, April 1990.

Song, W.S. *A Fault-Tolerant Multiprocessor Architecture for Digital Signal Processing Applications*. Ph.D. diss. Dept. of Electr. Eng. and Comput. Sci., MIT, 1989.

1.3 Active Noise Cancellation Using the EM Algorithm

Sponsors

National Science Foundation
Grant MIP 87-14969
U.S. Navy - Office of Naval Research
Grant N00014-89-J-1489

Project Staff

Professor Alan V. Oppenheim, John R. Buck

Active noise cancellation seeks to eliminate or reduce unwanted noise by creating a signal which will destructively interfere with the noise. Active cancellation is especially attractive for low-frequency noise, which is particularly resistant to traditional passive methods. Problems in active noise cancellation fall into two categories: removing noise from a desired signal and cancelling noise in an environment. This work will focus primarily on the former problem, although it has applications to the latter as well.

Specifically, the research will further investigate an adaptive, recursive time-domain implementation of the EM (Estimate-Maximize) algorithm for removing additive noise from a corrupted signal. This research focuses primarily on the two-microphone case. One microphone receives primarily speech with some filtered noise component, while the other receives primarily noise with some filtered speech components. With each additional new sample of information, the algorithm attempts to refine its estimate of the speech and noise signals, and then uses this estimate to further estimate the filters through which the speech and noise are passed through before reaching the microphone. By repeating this process, the algorithm should converge to the original speech, the filter coefficients, and the variance of the noise.

After initial investigation of the algorithm, the research will pursue a streamlined version that removes much of the unnecessary matrix manipulation in the original description of the algorithm. We will utilize known structural properties of the matrices used by the algorithm in its successive estimations.

1.3.1 Iterative Algorithms for Stochastic Estimation

Sponsors

Battelle Laboratories
National Science Foundation
Grant MIP 87-14969
Tel-Aviv University, Department of Electronic Systems
U.S. Navy - Office of Naval Research
Grant N00014-89-J-1489

Project Staff

Professor Bruce R. Musicus, Dr. Meir Feder, Dr. Ehud Weinstein

Maximum Likelihood (ML) is a well-known technique for generating asymptotically efficient estimates of unknown system parameters using noisy and incomplete observations. Classic ML algorithms include Wiener and Kalman filtering for estimating signals from noisy observations and auto-regressive, moving-average algorithms for estimating pole-zero models from clean data.

Unfortunately, when the signal model has unknown parameters and the observations are corrupted by noise, the optimal ML algorithm is often difficult to compute. We have been working on a variety of iterative algorithms for solving these difficult ML problems, similar to the Estimate-Maximize (EM) algorithm. The key idea is to decouple the estimation of the unknown internal signal from the estimation of the unknown parameters. We iteratively estimate the signal, use the signal to estimate the parameters, and then use the parameters to build a better filter for estimating the signal. Each step is quite similar to a classical ML filter or parameter estimation calculation, and convergence can be guaranteed to a stationary point of the likelihood function.

We have explored in depth the time-delay estimation on an array of receivers and with a single source. Our algorithms iteratively estimate the time of arrival at each sensor, along with the attenuation of the signal at each sensor, the signal power spectrum, the noise gain at each sensor, and the signal itself. After developing a novel convergence rate analysis for this EM algorithm, we used it to develop hybrid EM-ML algorithms capable of achieving superlinear convergence in some or

all of the parameters with only a modest boost in computational effort. Extensive simulation has verified the performance of our algorithms. Future work will extend the technique to multiple signals and the convergence analysis to cover other EM algorithms, such as pole-zero estimation.

Publications

Liou, C.-Y., and B.R. Musicus. "A Separable Cross-Entropy Approach to Power Spectral Estimation." *IEEE Trans. Acoustics, Speech Signal Proc.* 38(1): 105-113 (1990).

Musicus, B., and E. Weinstein. *Iterative Maximum Likelihood Time Delay and Doppler Estimation Using Stationary Signals*. RLE Technical Report No. 545. MIT, 1989.

Segal, M., E. Weinstein, and B.R. Musicus. "Estimate-Maximize Algorithms for Multi-Channel Time Delay and Signal Estimation." *IEEE Trans. Acoustics, Speech Signal Proc.* (1989), forthcoming.

1.4 Iterative Maximum Likelihood Time Delay and Doppler Estimation Using Stationary Signals

Sponsors

Tel-Aviv University, Department of Electronic Systems

U.S. Army Research Office
Contract DAAL03-86-D-0001

U.S. Navy - Office of Naval Research
Grant N00014-89-J-1489

Project Staff

Professor Bruce R. Musicus, Dr. Ehud Weinstein

We develop computationally efficient iterative algorithms for the joint Maximum Likelihood (ML) estimation of the time delays, Doppler shifts, and spectral parameters of stationary Gaussian signals radiated from a stationary or moving point source and observed in the presence of uncorrelated additive noise at two or more spatially distributed receivers. A particularly important

feature of these algorithms is that they decompose the estimation of the signal spectral parameters from the estimation of the delay and Doppler parameters, leading to a considerable simplification in estimator structure and computation. The proposed algorithms converge to the set of stationary points of the likelihood function, and each iteration increases the likelihood. Because all algorithms are derived from a common iterative framework related to the Estimate-Maximize algorithm, we analyze their convergence rates both theoretically and via simulation.

Publication

Musicus, B., and E. Weinstein. *Iterative Maximum Likelihood Time Delay and Doppler Estimation Using Stationary Signals*. RLE Technical Report No. 545. MIT, 1989.

1.4.1 Research in Digital Signal Processing

Project Staff

Dr. Charles S. Burrus

This research has been in two areas: digital filter design and efficient DFT and convolution algorithms. In the first area, we have developed a new method for the least squared error design of linear phase FIR filters. This method introduces a spline transition band in the ideal frequency response so that we can derive an analytical design formula that is as simple as the Window method, yet which retains optimality and explicit control over the band edges. We have developed a numerical method that allows error weighting which analytical methods cannot achieve. In the area of algorithms, the use of tensor and Kronecker product formulation of the DFT shows some promise for implementation on parallel and vector computer architectures.

A paper on the FIR filter design method will be published in *IEEE Transactions on Acoustics, Speech and Signal Processing*, and another will be presented at the 1990 International Conference on Acoustics, Speech and Signal Processing (ICASSP). A paper

on tensor formulations of the FFT will also be presented at ICASSP '90.

1.5 Estimation and Correction of Geometric Distortions in Side-Scan Sonar Images

Sponsors

The Federative Republic of Brazil
Scholarship
National Science Foundation
Grant MIP 87-14969
U.S. Navy - Office of Naval Research
Grant N00014-89-J-1489

Project Staff

Professor Alan V. Oppenheim, Daniel T. Cobra

Since its introduction in the early 60s, side-scan sonar has proved to be an important tool for underwater exploration and, in particular, for marine geological research. Its applications include surveying the seafloor, searching for and locating objects on the bottom of the sea, and prospecting for deepsea mineral deposits.

The information contained in reflected sound waves is used by side-scan sonars to produce acoustic images, called sonographs. These sonographs constitute a composite representation of the topographic features and the relative reflectivity of the various materials on the seabed. However, sonographs do not precisely depict seafloor topology. The sonar image can suffer from radiometric interferences such as those caused by dense particle suspension in the water, shoals of fish, or ultrasonic waves generated by passing ships. Large-scale geometric distortions may be caused by deviations in the ship's trajectory from the ideal straight path. Small-scale distortions may be caused by motion instability of the towed body on which the transducers are mounted because of underwater currents or ship sway. As a result, the interpretation of sonographs often requires extensive practice and can be a tedious and time-consuming task.

We have successfully corrected radiometric distortions and large-scale geometric distortions through standard image-processing techniques. Using digital post-processing of

sonographs, our goal is to develop techniques for detecting and correcting small-scale geometric distortions due to sonar motion instabilities. Previously, there has been inadequate information available in the literature. We are exploiting the cross-correlation between segments of adjacent image lines as a measure of the local degree of geometric distortion in sonographs. With a mathematical model derived from the geometry of side-scan sonars, we then employ these measures of geometric distortion to estimate the attitude parameters of the sonar array. Finally, the geometric distortions are corrected by resampling the image to compensate for the estimated motion instabilities of the array.

This project is being conducted under MIT's Joint Program with the Woods Hole Oceanographic Institution and with the cooperation of the U.S. Geological Survey.

1.6 An Algorithm Design Environment for Signal Processing

Sponsors

National Science Foundation
Grant MIP 87-14969
Sanders Associates, Inc.
U.S. Navy - Office of Naval Research
Grant N00014-89-J-1489

Project Staff

Professor Alan V. Oppenheim, Michele M. Covell

Signal processing uses the computer primarily for numerical calculations. Recently, a number of signal-processing environments have evolved which simplify the initial creation of a signal-processing algorithm from a series of low-level signal-processing blocks. Despite this progress, the majority of the design process is generally completed without computer support: Analyses of the properties of the selected algorithm are generally completed by hand, as is the manipulation of the algorithm to find efficient, input/output equivalent implementations. This study explores some of the issues involved in providing software tools for the symbolic analysis and rearrangement of

signal-processing algorithms as well as for the initial algorithm selection.

We have developed a software environment that supports numeric signal-processing computations as well as the symbolic analysis and manipulation of signal-processing expressions. This study is primarily involved with the symbolic manipulation of signal-processing expressions. To allow for the efficient manipulation of a variety of "regular" algorithms such as polyphase and FFT structures, we introduce correspondence constraints and use them to guide the rearrangement of these structures. We develop detailed cost descriptors to allow the environment to accurately compare the costs of the various equivalent implementations. We then use these comparisons to reduce the number of implementations presented to the user by removing the uncomputable and computationally inefficient forms.

We have demonstrated the potential of constrained algorithm manipulation with two examples. First, we considered briefly the problem of noninteger sampling rate conversion. Second, we explored in detail the more complex problem of detecting and discriminating FSK codes in sonar returns. Thirdly, we used an example on the recovery of in-phase and quadrature samples of an RF signal to highlight some of the limitations of the design tools developed in this study, which was completed in December 1989.

1.7 Compiling Signal Processing Algorithms into Architectures

Sponsors

National Science Foundation
Grant MIP 87-14969
U.S. Navy - Office of Naval Research
Grant N00014-89-J-1489

Project Staff

Professor Bruce R. Musicus, G.N. Srinivasa Prasanna, Dennis C. Fogg

We are currently studying several important and difficult problems which arise when compiling signal processing algorithms into either prespecified architectures or into

custom hardware designs. In general, the problem of optimized high-level mapping of algorithms into flexibly defined architectures is extraordinarily difficult, requiring a search over an enormous algorithmic and architectural design space and matching arbitrarily structured algorithms onto arbitrary architectures. Focusing on signal processing has several advantages including: (1) a large literature on efficient algorithms for many signal processing problems is available, and (2) often there are clear strategies for converting a signal processing calculation into a variety of alternative forms that may be better suited for particular implementations. These algorithms also typically rely on a large amount of matrix algebra and are, therefore, composed of high-level modules with regular computation, data access, and control structure. Often, much of the branch control inside these high-level modules can be pre-compiled or otherwise anticipated, thus allowing for highly efficient pipelining and parallelism. Because we can rely on static analysis of the program, effective optimizing compilers and optimizing Computer-Aided Design packages can be developed. We can use special techniques which exploit knowledge of signal processing to reorganize the computation into appropriate large-scale modules and map the large regular computation modules onto specialized hardware. Finally, the real-time constraints and huge computational burden often associated with signal processing applications such as radar, sonar, speech or image processing, often justify investment in special purpose, parallel and pipelined systems.

Our efforts have focused on a small set of issues whose solution is critical to the development of high-level algorithm compilers. In one project, we are writing a parallel algorithm expert for doing matrix computations and Fast Fourier Transforms (FFT) on linear or general arrays of processors. Because these computations are highly-structured, we can prove theorems setting lower bounds on the computation time for a given architecture with fixed computation, communication, and memory bandwidths. Furthermore, we can derive optimal algorithmic transformations of these problems for a given ratio of computation speed to memory speed to communication speed. Systematic sweep strategies based on Critical Path Method (CPM)

scheduling can achieve execution times very close to the optimal bounds. We have written a compiler in Multi-LISP which incorporates our strategies, and are testing the code on an Encore Multimax processor and on a new computer architecture being developed by Professor Anant Agarwal.

Our second focus is on mapping a given dataflow graph into custom VLSI. We are attempting large numbers of possible designs for solving the given problem, rating each according to multiple performance objectives. The result is a scatter plot illustrating the achievable system design tradeoffs between speed and cost. The human designer can then choose a particular performance range for further exploration. The architectural exploration proceeds in two phases. In the first, the system proposes a variety of possible hardware block diagrams for solving the problem. In the second phase, we assign pipelining and instantiate the modules from a library of possible parts, combining decoupled design techniques with sample search methods and heuristics for pruning the search space to reduce the complexity of searching through the design space. We have also found a fast linear programming algorithm for solving approximately for the optimal system tradeoff of speed versus area. We have extended this algorithm into a mixed integer-linear programming technique that simultaneously chooses components and places pipeline registers. Our current efforts focus on enriching the user interface, allowing dynamic exploration of the design space, and developing good heuristically-limited enumeration techniques to restrict the search through the design space and guide the linear programming solution.

Graduate students Jim Olsen, Kevin Peterson and Tom Dennedy, who are not members of the Signal Processing Research Program, are also involved in this study, but are not funded by the above-listed sponsors.

1.8 Vector Quantization with Adaptive Structured Codebooks

Sponsors

Bell Northern Research, Ltd.
National Science Foundation
Grant MIP 87-14969
U.S. Navy - Office of Naval Research
Grant N00014-89-J-1489

Project Staff

Professor Alan V. Oppenheim, Jacek Jachner

In this research project, we investigate a class of adaptive structured codebooks for Vector Quantization (VQ), for which both codebook design and codeword matching are sufficiently fast to be performed on-line. Recent work in low bit rate speech coding has applied VQ to code the residual signal after both short-term linear prediction (LPC) and long-term (pitch) prediction. For example, in Code Excited Linear Prediction (CELP) coders, each block of residual signal is matched with one codeword vector from a codebook set to minimize a linearly weighted mean square error (WMSE) criterion. The noise weighing criterion is time-varying with the LPC model of short-term speech characteristics.

The performance of a codebook depends on its design, or the choice of codewords to populate it, and on the error criterion. Performance-optimal design requires complex clustering techniques not suitable for on-line computation. Since optimality depends on the error criterion, the CELP coder would require time-varying codebooks for optimal performance. As multiple codebook storage is not practical, a non-optimal fixed codebook is commonly used instead. The designs proposed here are also not optimal, but may be simply adapted to the time-varying criterion to enhance performance relative to fixed codebook systems.

Our proposed design approach is to optimize a structurally constrained codebook for each time-varying error criterion. A rotationally symmetrical distribution is assumed for the prediction residual. In the Karhunen-Loeve transform domain of the error criterion weighing matrix, we use adaptive bit allocation (ABA) to assign levels to sample-by-

sample quantizers for the high-energy coefficients, representing the remainder of the coefficients by two-level quantizers. The assignment of sign for each codeword coefficient is controlled by a binary error-correcting code. This design provides a continuous range of good performance from binary error-correcting codes suitable for unweighted MSE, to simple adaptive bit allocation when only a few coefficients are dominant.

The complexity of codeword matching depends on the structural properties of the codebook; the proposed design allows fast matching. Both optimal and random codebooks (which are designed by random selection), require a computationally intensive search to match the speech residual to one of the codewords. Known structured codebooks based on trees or lattices accelerate the computation, but do not simply adapt to time-varying error criteria. For the proposed codebook structure, we achieve efficient codeword search by a novel combination of fast methods for soft-decision decoding of binary error-correcting codes with the sample-by-sample independent property of the multi-level quantizers.

Computer simulation is currently being used to evaluate the performance of the proposed technique.

1.8.1 Detection Statistics for Multichannel Data

Sponsors

Amoco Foundation Fellowship
National Science Foundation
Grant MIP 87-14969
Sanders Associates, Inc.
U.S. Navy - Office of Naval Research
Grant N00014-89-J-1489

Project Staff

Professor Alan V. Oppenheim, Tae H. Joo

In our research, we have developed a new detection statistic for a class of multichannel detection problems for which, in the presence of an emitter, a narrowband signal exists in all channels in addition to wideband

noise. When an emitter is absent, the received data may contain narrowband noise components in some, but not all of the channels, as well as wideband noise. A detector which tests each channel separately for the existence of the narrowband component does not perform as well as the detectors which use all channels collectively.

To collectively use the data from different channels, the average has been previously used as a detection statistic. However, because the average only tests the total energy, its detection performance noticeably degrades when a narrowband component exists in many channels. As an alternative detection statistic, we considered the semblance, which measures the coherence between the channels. The receiver operating characteristic curves show that the average performs better than the semblance if more than half of the channels contain only wideband noise when the emitter is absent, while the semblance performs better if more than half of the channels contain narrowband components when the emitter is absent. Therefore, we could improve the detection performance of both the average and the semblance.

We developed an improved detection statistic by combining the average and the semblance, determining a combining function and satisfying a set of constraints which ensure that the average and the semblance contribute equally to the detection statistic. Before being combined, the average is transformed to make its probability density function match the probability density function of the semblance. The receiver operating characteristic curves show that the combined statistic performs better than other statistics including the average and the semblance.

We have applied this new detection statistic to the gravitational wave signal detection problem and developed a new algorithm which computes the Fourier transform magnitudes at the exact frequencies using the chirp z-transform. Examples of the gravitational wave signal detection demonstrate that the new algorithm performs better than the previously developed algorithm. This study was completed in December 1989.

1.9 The Application of Complex Approximation Algorithms to the Design of Robust Range-Dependent Beamformers

Sponsors

General Electric Fellowship
National Science Foundation Fellowship
National Science Foundation
Grant MIP 87-14969
U.S. Navy - Office of Naval Research
Grant N00014-89-J-1489

Project Staff

Professor Alan V. Oppenheim, James C. Preisig

Beamformers often operate in environments having characteristics that could not be specified at the time of design. These unknown environmental characteristics can relate to signals received, interfering signals, the environment in which the signal propagates, or the beamformer itself. Given a criterion that is a measure of beamformer performance under a given fixed set of conditions, the smaller the value of the criterion, the better the beamformer performs. Therefore, by minimizing the maximum value of the criterion evaluated over the range of possible environmental characteristics, we can design beamformers that cope with these uncertainties.

Mathematically, this type of design problem can be posed as a complex approximation problem. For some applications, such as far-field beamforming in a known homogeneous propagation environment, efficient algorithms already exist that can solve this design problem. The goal of our research is to develop efficient algorithms for range-dependent beamformers operating in non-homogeneous propagation environments.

We are performing this research under the auspices of the MIT-Woods Hole Oceanographic Institution Joint Program.

1.10 Analysis and Applications of an Adaptively Trained Recurrent Neural Network

Sponsors

National Science Foundation
Grant MIP 87-14969
U.S. Air Force - Office of Scientific Research
Fellowship
U.S. Navy - Office of Naval Research
Grant N00014-89-J-1489

Project Staff

Professor Alan V. Oppenheim, Michael D. Richard

Neural networks have proven useful in many signal processing applications, particularly in those involving pattern classification. In fact, nonparametric neural-network classifiers perform better than traditional ones, such as parametric Bayesian classifiers, on many problems. However, neural-network research has focused on the properties and uses of feedforward networks. Because these networks are only capable of performing memoryless input-output mappings, they are ineffective for problems requiring exploitation of temporal properties of the input data. One of these problems is the analysis of sequential speech patterns for performing speech recognition.

Several neural networks, collectively referred to as recurrent neural networks, have been proposed to deal with "temporal" problems. Most of these consist of traditional feedforward networks, which have feedback connections to transform the networks into nonlinear dynamical systems. Because they have feedback connections, recurrent neural networks are difficult to "train"; and because they are nonlinear dynamical systems, they are difficult to analyze. Therefore, until recently, recurrent neural networks have been primarily curiosity factors rather than practical, useful problem-solving tools.

This research investigates a novel recurrent neural network and its utility for speech recognition. The research is addressing unique methods for adaptively and continuously training this network as input data is received. In addition, we will explore various methods for analyzing recurrent networks to

improve the current, superficial understanding of the properties of these networks.

1.11 A Code-Division, Multiple Beam Sonar Imaging System

Sponsors

National Science Foundation
Grant MIP 87-14969
U.S. Navy - Office of Naval Research
Grant N00014-89-J-1489

Project Staff

Dr. Jules Jaffe, Professor Alan V. Oppenheim, Dr. Timothy Stanton, John M. Richardson

In this research project, we are exploring the development of a new active sonar imaging concept using the principle of code-division and the simultaneous transmission of multiple-coded signals. The signals are sixteen symbol, four-bit, non-linear, block Frequency-Shift Keyed (FSK) codes, each of which is projected into a different direction. Upon reception of the reflected waveform, each signal is separately detected and the results are inverted to yield an estimation of the spatial location of an object in three dimensions. The code-division sonar is particularly effective, operating in situations where the phase of the transmitted signal is perturbed by the propagation media and target.

Most imaging techniques presently used rely on preserving the phase of the received signal over the dimension of the receiving array. In code-division sonar, we use the combined effects of code-to-code rejection and the a priori knowledge of the direction from which each code was transmitted to obtain spatial resolution. We show that the coded signals are highly tolerable of phase distortion over the duration of the transmission. The result is a high-resolution, three-dimensional image that we can obtain in a highly perturbative environment. Additionally, the code-division sonar is capable of a high frame rate due to the simplicity of the processing required.

We have presented two algorithms to estimate the spatial coordinates of an object in the ensonified aperture of the system, com-

paring their performance for different signal to noise levels. Finally, employing the concept of code-division imaging in a series of experiments, we used code-division sonar image objects under a variety of conditions. We presented the results of the experiments, showing the resolution capabilities of the system.

This research was conducted under the auspices of the MIT-Woods Hole Oceanographic Institution Joint Program and completed in August 1989.

1.12 Back-projection with Fourier Series Expansion and FFT

Project Staff

Makoto Tabei

In this research, we are investigating a computationally efficient procedure for CT reconstruction. The reconstruction procedure that is most commonly used on CT scanners is based on the convolution back-projection (CBP) algorithm. The CBP algorithm consists of two steps: first, projection data is linearly convolved with filter function (convolution); then, the convolved projection is back-projected onto the image frame (back-projection). Although this algorithm is accurate and can be easily implemented, the back-projection is a very time-consuming process, especially when higher-order interpolation is employed for best accuracy. This computational complexity is due to the fact that the contribution of the convolved projection at each projection angle must be evaluated and summed at all pixels in the image frame.

We are proposing an alternative approach to interpolating and back-projecting the convolved projection onto the image frame. The technique is based on the synthesis of arbitrary frequency 2-D sinusoidal functions using the Gaussian function and a 2-D inverse FFT. The procedure is as follows: We transform the convolved projection using a 1-D FFT and replicate it at higher frequencies to perform upsampling (the interpolation generally requires upsampling before filtering out higher-frequency components). Then we

multiply the projection with the frequency response of the interpolation function. The resultant sequence provides the Fourier series coefficients of the filtered projections to be back-projected. We use the Gaussian function to project each of the coefficients given along the radial line in polar coordinates and onto rectangular grids. When the filtered projections for all projection angles are projected in the frequency domain, a 2-D IFFT is evoked, correcting its result by division with the reciprocal Gaussian function to produce the reconstructed image.

The computation required in this procedure is one-sixth of conventional back-projection with linear interpolation for the image of 512 x 512. The use of the modified cubic spline or any other higher-order interpolation functions does not affect the computational complexity, requiring only replacement of the tables representing the frequency response of the interpolation function. The proposed algorithm also produces images as accurate as those of any known algorithm.

The results of this study were presented at the IEEE International Conference on Acoustics, Speech, and Signal Processing, Albuquerque, New Mexico, April 3-6, 1990.

1.13 Iterative Algorithms for Parameter Estimation from Incomplete Data and Their Applications to Signal Processing

Sponsors

Tel-Aviv University, Department of Electronic Systems
Sanders Associates, Inc.
U.S. Navy - Office of Naval Research
Grants N00014-85-K-0272 and
N00014-89-J-1489

Project Staff

Dr. Ehud Weinstein

The Estimate-Maximize (EM) algorithm is an iterative method for finding the Maximum Likelihood (ML) or the Maximum-A-Posteriori (MAP) parameter estimates with incomplete data. The method has been

found useful in a variety of signal processing problems including medical imaging, parameter estimation of superimposed signals, speech enhancement in multiple microphone environments, and signal reconstruction from spatial information.

We have developed an extension of the EM algorithm, termed the Cascade EM (CEM) algorithm, that is useful in accelerating the rate of convergence of the algorithm and in simplifying the computations involved. This research was developed with Mordechai Segal of Tel-Aviv University.

Using the EM and the CEM algorithms, we have considered the problem of simultaneous state estimation and parameter identification in linear dynamical continuous/discrete systems. The main result is that we can use Kalman smoothing equations for ML identification of the system parameters. We also developed a new method for calculating the log-likelihood gradient (score), the Hessian, and the Fisher's Information Matrix (FIM), that we used for efficient implementation of gradient-search algorithms and for assessing the mean square accuracy of the ML parameter estimates. This research was developed with Mordechai Segal.

We have also developed a computationally efficient algorithm for estimating the spatial and spectral parameters of multiple source signals using radar/sonar arrays. The most attractive feature of the proposed algorithm is that it decouples the spatial parameter optimization from the spectral optimization, leading to a significant reduction in the computations involved.

This research was developed with Mordechai Segal of Tel-Aviv University and Professor Bruce R. Musicus.

1.14 Equalization (Identification) of Non-Minimum Phase Systems

Sponsors

Tel-Aviv University, Department of Electronic Systems
U.S. Navy - Office of Naval Research
Grants N00014-85-K-0272 and

N00014-89-J-1489

Project Staff

Dr. Ehud Weinstein

The problem considered in this study is the following: We observe the output of a discrete time-invariant linear possibly non-minimum phase system H with input being a realization (sample function) from a stochastic process. We want to recover the input signal or equivalently to identify the magnitude and phase of the inverse of H using a tap-delay line (Equalizer). This problem, referred to as self-recovering or blind equalization, is of prime interest in data communications and acoustical and geophysical signal processing.

We have developed necessary and sufficient conditions for equalization. Based on these conditions, we proposed several equalization criteria and proved that their solution corresponds to the desired response. These criteria are universal in the sense that they do not impose any restrictions on the probability law of the input (unobserved) process. The resulting algorithms only involve the computation of a few moments of the system output, implying a simple tap update procedure.

This research was developed with Mr. Ofir Shalvi of Tel-Aviv University.

1.15 Signal Processing with 1/f Processes using Wavelets

Sponsors

National Science Foundation
Grant MIP 87-14969

Natural Science and Engineering Research
Council of Canada - Science and
Technology Scholarship

U.S. Navy - Office of Naval Research
Grant N00014-89-J-1489

Project Staff

Professor Alan V. Oppenheim, Gregory W. Wornell

Recently, we have developed a wavelet-based Karhunen-Loeve expansion for a family of nearly-1/f processes. Our subsequent work focused on exploiting this expansion in the solution of some rather general signal processing problems involving these processes. Since 1/f models are applicable to a wide range of natural and man-made phenomena, there are many applications of this work.

In the area of 1/f signal modeling, we are investigating two problems. The first involves determining the wavelet which leads to a Karhunen-Loeve expansion for exactly-1/f processes. Secondly, we have defined a discrete-time counterpart to the continuous-time 1/f process. At present, we are developing useful characterizations of this process and studying its properties.

Some identification problems involving 1/f processes are also of interest. The first involves hypothesis testing, i.e., determining whether a process under investigation is a sample function of a 1/f process. In solving the second problem, we estimated the parameters of a 1/f process from possibly noisy observations. We have obtained a number of results for this problem using Maximum Likelihood theory.

In terms of detection problems, we are working on the development of likelihood-ratio tests for the detection of signals in additive 1/f-noise environments. Also of interest is the design of signals for low probability of detection in 1/f-noise backgrounds.

Finally, we are considering a variety of estimation problems for 1/f processes. In general, we are studying the problems of smoothing, filtering, and prediction of 1/f processes based on noisy observations.

In all of the above cases, we are finding not only computationally efficient solutions that exploit the self-similar structure of these processes, but intuitively satisfying interpretations as well.

Chapter 2. Speech Processing Research Program

Academic and Research Staff

Professor Jae S. Lim, Giovanni Aliberti, Giampiero Sciutto

Graduate Students

Michael S. Brandstein, Shiufun Cheung, Warren Chou, John C. Hardwick, Rosalind W. Picard, Paul Shen, Katherine S. Wang

Technical and Support Staff

Hassan Gharavy, Cynthia LeBlanc, Julia Sharp

2.1 Introduction

The objective of this research program is to develop methods for solving important speech communication problems. Current research topics in progress include (1) real-time implementation of a multiband excitation vocoder operating at bit rates ranging between 2.4 and 8.0 kbits/sec and (2) development of algorithms for enhancing speech degraded by background noise and for modifying the time scale of speech. We are also investigating methods for displaying spectrograms more efficiently.

2.2 Development of a 1.5 Kbps Speech Vocoder

Sponsors

National Science Foundation
Grant MIP 87-14969
National Science Foundation Fellowship
U.S. Air Force - Electronic Systems Division
Contract F19628-89-K-0041

Project Staff

Michael S. Brandstein, Professor Jae S. Lim

The recently developed Multi-Band Excitation Speech Model accurately reproduces a wide range of speech signals without many of the limitations inherent in existing speech model based systems.¹ The robustness of this model makes it particularly applicable to low bit rate, high quality speech vocoders. In Griffin and Lim,² a 9.6 Kbps speech coder based on this model was first described. Later work resulted in a 4.8 Kbps speech coding system.³ We have shown that both of these systems are capable of high quality speech reproduction in both low and high SNR conditions.

The purpose of this research is to explore methods of using the new speech model at the 1.5 Kbps rate. Results indicate that a substantial amount of redundancy exists between the model parameters. Current research is focused on exploiting these redundancies to quantize these parameters more efficiently. Attempts are also under way to simplify the existing model without significantly reducing speech quality.

¹ D.W. Griffin and J.S. Lim, "A New Model-Based Speech Analysis/Synthesis System," *IEEE International Conference on Acoustic, Speech and Signal Processing*, Tampa, Florida, March 26-29, 1985, pp. 513-516.

² D.W. Griffin and J.S. Lim, "A High Quality 9.6 kbps Speech Coding System," *IEEE International Conference on Acoustic, Speech and Signal Processing*, Tokyo, Japan, April 8-11, 1986.

³ J.C. Hardwick, *A 4.8 Kbps Multi-Band Excitation Speech Coder*, S.M. thesis, Dept. of Electr. Eng. and Comput. Sci., MIT, 1988.

2.3 A New Method for Representing Speech Spectrograms

Sponsors

National Science Foundation
Grant MIP 87-14969
U.S. Navy - Office of Naval Research
Contract N00014-89-J-1489

Project Staff

Shiufun Cheung, Professor Jae S. Lim

The spectrogram, which is a two-dimensional time-frequency display of a one-dimensional signal, is used extensively in speech research. Existing spectrograms are generally divided into two types, wide-band spectrograms and narrow-band spectrograms, according to the bandwidth of the filters used to generate them. Due to the different characteristics of the two types of spectrograms, they are employed for different purposes. The wide-band spectrogram is valued for its quick temporal response and is used for word boundary location and formant tracking. On the other hand, the narrow-band spectrogram, with its high frequency resolution, is primarily used for measuring pitch frequency.

Since each of the spectrograms has its own advantages and weaknesses, efforts are being made to incorporate the desirable aspects of the two spectrograms into one display. One approach is to mimic the human auditory system and use critical band filters to generate neural spectrograms. Another method is to construct an optimum window, which is the temporal equivalent of the filter.

In this research, we propose an entirely different view of the problem. Instead of viewing the spectrogram as a transformed speech signal, we consider it an image or digital picture. Given this type of approach, the whole gamut of image processing techniques is available for use, and the problem becomes theoretically much simpler. In fact, the most interesting aspect of this research is that we transform a problem in speech processing into an image-processing problem.

2.4 A Dual Excitation Speech Model

Sponsors

National Science Foundation
Grant MIP 87-14969
U.S. Air Force - Electronic Systems Division
Contract F19628-89-K-0041

Project Staff

John C. Hardwick, Professor Jae S. Lim

One class of speech analysis/synthesis systems (vocoders) which have been extensively studied and used in practice are based on an underlying model of speech. Even though traditional vocoders have been quite successful in synthesizing intelligible speech, they have not successfully synthesized high quality speech. The Multi-Band Excitation (MBE) speech model, introduced by Griffin, improves the quality of vocoder speech through the use of a series of frequency dependent voiced/unvoiced decisions. The MBE speech model, however, results in a loss of quality as compared to the original speech. This degradation is caused in part by the voiced/unvoiced decision process. A large number of frequency regions contain a substantial amount of both voiced and unvoiced energy. If a region of this type is declared voiced, then a tonal or hollow quality is added to the synthesized speech. Similarly, if the region is declared unvoiced, then additional noise occurs in the synthesized speech. As the signal-to-noise ratio decreases, the classification of speech as either voiced or unvoiced becomes more difficult, and, consequently, the degradation increases.

We have proposed a new speech model in response to the problems mentioned above. This model is referred to as the Dual Excitation (DE) speech model, because of its dual excitation and filter structure. The DE speech model is a generalization of most previous speech models which, with the proper selection of the model parameters, reduces to either the MBE speech model or to a variety of more traditional speech models.

Currently, our research is examining the use of this speech model for speech enhancement, time scale modification and bandwidth

compression. Additional areas of study include further refinements to the model and improvements in the estimation algorithms.

2.5 Image Texture Modeling

Sponsors

National Science Foundation
Grant MIP 87-14969
U.S. Navy - Office of Naval Research
Contract N00014-89-J-1489

Project Staff

Rosalind W. Picard, Professor Jae S. Lim

Textured regions are the nemesis of many image processing algorithms. For example, algorithms for image segmentation or image compression usually assume stationarity or high correlation of the image gray-level data, failing in textured regions. In this research, we are developing a model with only a small number of parameters which synthesizes the textures. This model would have applications for image enhancement, segmentation, scene synthesis, and low bit rate image coding.

The ability to synthesize syntactically regular "structural" textures, e.g., a tiled wall, as well as the more random "stochastic" textures, e.g., shrubbery, is desirable in a texture model. Most models assume only one of these cases and perform poorly when the data is not perfectly periodic or stochastic. Our goal is to develop a model which is capable of exhibiting a continuum of structural and stochastic behavior.

We have confirmed the fact that the Markov Random Field model, which is equivalent to the Gibbs Distribution of statistical mechanics, synthesizes a wide variety of stochastic textures. By using concepts from statistical mechanics, we have modified the Gibbs distribution so that it synthesizes a greater variety of textures. One modification,

imposing an "external field," allows discontinuities to appear in the texture. We have explored other modifications which simulate "physical" processes. Recently, by using dominant spectral coefficients, we have induced some structure in the random field. We are currently investigating the limitations of this mixed structural and stochastic model by estimating the structural and stochastic parameters of natural textures and trying to synthesize visually similar textures.

2.6 Speech Enhancement Techniques for the Dual Excitation Vocoder Model

Sponsors

National Science Foundation
Grant MIP 87-14969
National Science Foundation Fellowship
U.S. Navy - Office of Naval Research
Contract N00014-89-J-1489

Project Staff

Katherine S. Wang, Professor Jae S. Lim

We are exploring some conventional methods for speech enhancement in the presence of additive white noise,⁴ in a new framework where the voiced estimation provided by the MBE model⁵ allows us to perform noise reduction separately on voiced and unvoiced components. Conventional methods which take advantage of the periodic structure of voiced speech include comb filtering and adaptive noise cancellation. A technique based on short-time spectral amplitude estimation obtains the minimum mean-square-error, linear estimator of the speech signal by noncausal Wiener filtering, which we could approximate by an adaptive Wiener filtering technique. Speech enhancement can also be model based, such as using classical estimation theory applied to an all pole model of speech. We will draw from some of these conventional techniques to create a speech

⁴ J.S. Lim and A.V. Oppenheim, "Enhancement and Bandwidth Compression of Noisy Speech," *Proc. IEEE* 67 (12): (1979); ed. J.S. Lim, *Speech Enhancement*. (Englewood Cliffs, New Jersey: Prentice Hall, 1983).

⁵ D.W. Griffin and J.S. Lim, "A New Model-Based Speech Analysis/Synthesis System," *IEEE International Conference on Acoustics, Speech and Signal Processing*, Tampa, Florida, March 26-29, 1985, pp. 513-516.

enhancement system customized to the traits of the Multi-Band Excitation (MBE) Vocoder and, subsequently, to the Dual Excitation Model.⁶ The noise-like characteristics of unvoiced speech and the harmonic structure of voiced speech suggest that noise can most effectively be reduced in speech that has been separated into the two components,

rather than attempting to categorize the frequency band as purely voiced and unvoiced.

We have shown that the recently developed Multi-Band Excitation (MBE) Speech Model accurately reproduces a wide range of speech signals without many of the limitations inherent in existing speech model based systems.

⁶ John C. Hardwick, Ph.D. research, MIT.

Chapter 3. Advanced Television Research Program

Academic and Research Staff

Professor Jae S. Lim, Professor William F. Schreiber, Giovanni Aliberti, Giampiero Sciutto

Graduate Students

Matthew M. Bace, David M. Baylon, Ibrahim A. Hajjahmad, Steven H. Isabelle, David Kuo, Peter A. Monta, Julien Piot, Ashok C. Popat, Kambiz C. Zangi

Technical and Support Staff

Francis M. Dougherty, Hassan Gharavy, Cynthia LeBlanc, Julia Sharp

3.1 Advanced Television Research Program

The present television system was designed nearly 35 years ago. Since then, there have been significant technological developments highly relevant to the television industries. For example, advances in the very large scale integration (VLSI) technology and signal processing theories make it feasible to incorporate frame-store memory and sophisticated signal processing capabilities in a television receiver at a reasonable cost. To exploit this new technology in developing future television systems, Japan and Europe established large laboratories, funded by government or industry-wide consortia. The lack of this type of organization in the U.S. was considered detrimental to the broadcasting and equipment manufacturing industries, and, in 1983, a consortium of U.S. companies established the Advanced Television Research Program (ATRP) at MIT.

Currently, the consortium members include ABC, Ampex, General Instruments, Kodak, Motorola, NBC, NBC Affiliates, PBS, Tektronix and Zenith. The major objectives of ATRP are:

- To develop the theoretical and the empirical basis for the improvement of existing television systems, as well as the design of future television systems.
- To educate students through television-related research and development and to motivate them to enter careers in television-related industries.

- To facilitate continuing education of scientists and engineers already working in the industry.
- To establish a resource center for discussion and detailed study of problems and proposals
- To transfer the technology developed from this program to its industrial sponsors.

The research areas of the program include the development of transcoding methods and the design of (1) a channel-compatible advanced television (ATV) system, (2) a receiver-compatible ATV system, and (3) a digital ATV system. We have already made significant advances in some of these research areas. We have designed a channel-compatible ATV system, scheduled for testing in 1991 by the FCC for its possible adaption as the U.S. HDTV standard for terrestrial broadcasting.

3.1.1 ATRP Computer Facilities

The main ATRP computer facility currently is a VAX 11/785 minicomputer with approximately 2.4 GBytes of online disk space. Attached to the VAX is a DATARAM Wide Word Storage system which provides 320 MBytes of RAM. The high speed interface to the Wide Word system drives a three-dimensional interpolator that was constructed by graduate students in the lab. The three-dimensional interpolator can perform separable spatiotemporal interpolation. The

output of the interpolator feeds a custom built data concentrator which drives a Sony 2k by 2k monitor, running at 60 frames/sec.

In addition to displaying high resolution real time sequences, the ATRP facilities include a 512 by 512 Rastertek frame buffer and an NTSC encoder. The Rastertek frame buffer feeds static images to nearly a dozen monitors that are distributed throughout the lab. The NTSC encoder allows us to record the results of sequence processing onto either 3/4 inch or VHS tape. For hard copy output, the lab uses an Autokon 8400 graphics printer for generating high resolution black and white images directly onto photographic paper.

For preparing presentations, ATRP also employs a Macintosh SE30 microcomputer and a Mac IIX, feeding an Apple LaserWriter.

To support the growing computation needs of the group, three Sun-4 workstations will be installed in the near future. They will have 24-bit color displays, local disk storage, and DSP boards to assist with computation-intensive image processing.

A fast network (FDDI) is under consideration to link the machines and to display devices such as the Dataram. The workstations will also support Ethernet and will be connected to Internet through the building subnet.

3.1.2 Receiver-Compatible Adaptive Modulation for Television

Sponsors

National Science Foundation
Grant MIP 87-14969

National Science Foundation Fellowship

Project Staff

Matthew M. Bace, Professor Jae S. Lim

There have been numerous proposals for developing methods to improve the quality of the current NTSC television picture. Most of these proposals have concentrated on methods for increasing either the spatial or the temporal resolution of the television picture. While these proposals promise significant improvements in picture quality, until

an effective scheme to combat channel noise has been introduced, these improvements will never be fully realized. Degradations such as random noise ("snow"), echo, and intersymbol interference (channel crosstalk) are still the greatest barrier to high-quality television.

This research will attempt to develop a receiver-compatible scheme to reduce the effects of channel imperfections on the received television picture. In particular, the method of adaptive modulation will be employed to make more efficient use of the currently under-utilized bandwidth and dynamic range of the NTSC signal. By concentrating more power in the higher spatial frequencies and using digital modulation to send additional information in the vertical and horizontal blanking periods, we can make existing television signals more robust in the presence of high frequency disturbances. Furthermore, we can adjust the parameters of this scheme so that the modulated signal may be received intelligibly even on a standard receiver (although an improved receiver will be required to realize the full benefits of adaptive modulation).

Before we can conclude which adaptive modulation schemes are optimal, we must consider many details. Among the parameters which can be varied are: (1) the control over the adaptation and compression factors, (2) the form of the input low-pass filters, (3) the interpolation scheme to be used at both the transmitter and receiver, and (4) the encoding of the digital data. We will adjust these parameters to optimize the performance of the modulation scheme with respect to two fundamental performance criteria. These criteria are the degree to which (1) the channel degradations are removed when the signal is received on an improved receiver and (2) the signal is distorted when received on a standard receiver.

3.2 Adaptive Amplitude Modulation for Transform Coefficients

Sponsor

Advanced Television Research Program

Project Staff

David M. Baylon, Professor Jae S. Lim

In this project, we have shown that adaptive amplitude modulation/demodulation (AM/DM) is an effective noise reduction technique. However, this technique requires transmitting the adaptation factors as side information. It is important to minimize the required side information in systems that have limited transmission bandwidth. Our research will focus on representing the adaptation factors by a few parameters exploiting properties of the signal in the transform (frequency) domain.

Previous investigations of adaptive amplitude modulation have been based on time domain methods. Specifically, in two-dimensional subband filtering, an image is decomposed into a set of spatial frequency subbands that are adaptively modulated. Similarities among subbands are exploited by reducing the number of adaptation factors to about one-sixth the number of data points. Nevertheless, further reduction in the amount of side information is desirable.

This research will take a different approach to reducing the amount of side information by adaptively modulating the transform of the signal. Transform coefficients of typical images tend to decrease in energy away from DC. By exploiting this property, we can model the transform coefficients and the adaptation factors with a few parameters (for example, an exponential model). Consequently, we can significantly reduce the amount of side information compared with that required by previous methods.

Research will focus on determining the best way to model the adaptation factors with a few parameters in systems that are bandwidth and peak power constrained. Performance criteria of the various AM/DM schemes will include signal-to-noise ratios and overall image quality. Among the many ways of obtaining the coefficients (such as using

subband filtering or the lapped orthogonal transformation (LOT)), the discrete cosine transformation (DCT) will be used because of its many desirable properties, including coefficient uncorrelation, energy compaction, and efficient computation using the fast Fourier transform (FFT). Issues that we will address include choosing the appropriate block size and determining the best AM/DM method with an adaptive coefficient selection scheme (such as used in image coding systems). We will study both two-dimensional images and three-dimensional video.

3.3 Transform Coding for High Definition Television**Sponsor**

Advanced Television Research Program

Project Staff

Ibrahim A. Hajjahmad, Professor Jae S. Lim

Image coding has many useful applications. One important application is for compressing channel bandwidth for image transmission systems such as HDTV, video conferencing, and facsimile. Reducing storage requirements for tasks such as digital video recording is another important application of image coding.

Image coding can be divided into a number of classes, depending on which aspects of the image are being coded. One class is the transform image coder,¹ in which an image is transformed from the spatial domain to a different domain more suitable for coding. Then, the transform coefficients are quantized and coded. When received, the coded coefficients are decoded and then inverse transformed to obtain the reconstructed image.

To perform transform coding one must select an appropriate transform. In particular, the

¹ J.S. Lim, *Two-Dimensional Signal and Image Processing* (Englewood Cliffs, New Jersey: Prentice Hall, 1990); R.J. Clarke, *Transform Coding of Images* (London: Academic Press, 1985).

Discrete Cosine Transform (DCT)² is very useful because of two important properties. First, the energy compaction property states that a large amount of energy is concentrated in a small fraction of the transform coefficients (typically the low frequency components). Because of this property, only a small fraction of the transform coefficients need to be coded, while little is sacrificed in terms of the quality and intelligibility of the coded images. Second, the correlation reduction property reduces the high correlation among pixel intensities in the spatial domain. In effect, the redundant spatial information is not coded.

Currently, we are investigating the use of the DCT for bandwidth compression. In addition, we are studying new adaptive techniques for quantization and bit allocation to reduce further the bit rate without sacrificing image quality or intelligibility.

3.4 Filter Design for Multirate Filter Banks

Sponsors

Advanced Television Research Program
AT&T Bell Laboratories Doctoral Support Program
National Science Foundation
Grant MIP 87-14969

Project Staff

Steven H. Isabelle, Professor Jae S. Lim

Multirate filter banks have wide application in the areas of subband coding of speech and images. In this application, the signal is passed through a bank of bandpass filters. The resulting bandpass signals are decimated and then coded. At the receiver, the signals are interpolated and added to form the reconstructed signal. In this scheme, the coding technique can be adjusted on a frequency dependent basis to match the observer's perceptual characteristics. Clearly, the performance of this kind of analysis/synthesis system depends strongly on the properties of the filters in the analysis and synthesis filter banks. For example, there

are two desirable properties: (1) in the absence of coding, the reconstructed signal should be nearly identical to the original, and (2) there should be little interaction between the different subband signals. One goal of this research is to develop improved analysis and design tools for multirate filter banks. To this end, we have developed a design algorithm with improved convergence behavior over existing methods for the special case of a two-channel perfect reconstruction filter bank.

The subband decomposition of an image is typically performed using separable filters along its horizontal and vertical axis. The use of nonseparable filters allows for directional selectivity in the subband decomposition and a potential improvement in the subjective quality of encoded images. A second goal of this research is to develop design techniques for general multidimensional, multirate filter banks.

3.5 Adaptive Spatiotemporal Filtering

Sponsors

Advanced Television Research Program
Kodak Fellowship

Project Staff

David Kuo, Professor William F. Schreiber

The current NTSC television standard specifies a frame rate of 60 fields/sec throughout the transmission chain. The purpose of this frame rate is for minimizing the visibility of annoying flicker at the display. However, to eliminate flicker, only the display must operate at the high frame rate; the channel does not need to be constrained to operating at 60 frames/sec. Because there is a great deal of correlation between neighboring frames of an image sequence, a high frame rate through the channel seems bandwidth inefficient.

One way to take advantage of the correlation between neighboring frames is to transmit

² N. Ahmed, T. Natarajan, and K.R. Rao, "Discrete Cosine Transform," *IEEE Trans. Comput.* C-23:90-93 (1974).

only a temporally subsampled version of the original sequence, relying on the receiver to recover the inbetween frames. However, our prior work suggests that the receiver must have more information than simply the subsampled frames. This research focuses on using motion vectors as part of the image sequence representation.

There are three main areas of focus in this research. First, we consider the use of adaptive spatiotemporal prefiltering as a means of reducing the aliasing that arises from temporal subsampling. Secondly, we explore the characteristics of the motion vectors. Finally, we consider how to use multiple frames of data to improve the motion estimation process.

3.6 Signal Processing for Advanced Television Systems

Sponsors

Advanced Television Research Program
U.S. Air Force - Electronic Systems Division
Contract F19628-89-K-0041

Project Staff

Peter A. Monta, Professor Jae S. Lim

Digital signal processing will play a large role in future advanced television systems. Source coding to reduce the channel capacity necessary to transmit a television signal and display processing such as spatial and temporal interpolation are the major applications. Present-day television standards will also benefit significantly from signal processing designed to remove transmission and display artifacts. This research will focus on developing algorithms and signal models to (1) enhance current standards (both compatibly and with some degree of cooperative processing at both transmitter and receiver) and (2) improve proposed HDTV systems.

Using a receiver with a high-quality display and significant computation and memory, we can improve the American television standard, NTSC, in several ways. We can remove interlace artifacts, such as line visibility and flicker by converting the signal to a progressive format prior to display. We can

greatly reduce color cross-effects with accurate color demodulators implemented with digital signal processing techniques. We have tested and implemented an algorithm for an advanced receiver that can recover a much improved image by exploiting structure in the film-NTSC transcoding process if film is the original source material.

Similar ideas apply to HDTV systems. For example, film will be a major source material well into the next century, and HDTV source coders should recognize film as a special case, trading off the inherent reduced temporal bandwidth for better spatial resolution. The MIT-CC channel-compatible HDTV system will adapt to film in this way.

3.7 Adaptive Frequency Modulation for Satellite Television Systems

Sponsor

Advanced Television Research Program

Project Staff

Julien Piot, Professor William F. Schreiber

Frequency modulation is the first choice coding scheme in many existing applications such as satellite television transmission.

A simple model of image formation predicts large variations in the short-time bandwidth of the modulated signal. Based on this model, we adjust the frequency deviation in a small block of the picture to keep the bandwidth constant. We show that the resulting noise improvement is significant when we use a subjective measure of the transmission error. This measure, based on noise masking, has an average intensity related to the block statistics.

In some applications the modulated signal is bandlimited, resulting in envelope and phase distortion. Both terms generate artifacts in the recovered picture, mostly when noise is present in the link. We show through measurements that the peak short-time bandwidth is related to the severity of the distortion, hence justifying the prior approach to adaptation. We introduced improved algorithms

that minimize the transmission noise while maintaining negligible distortion.

When the information is transmitted in the form of multiple components, we present a technique based on a sequential transmission such as subbands. This technique can also be used to transmit some side information, such as the adaptation function of the modulator. By adjusting the rate of transmission of the various components, we can minimize the subjective impairment. For example, we show that a vertical subband decomposition is very effective in reducing transmission noise, with a larger improvement than preemphasis techniques. Alternatively, adaptive modulation can be combined with this technique.

Finally, we applied the principle of adaptive frequency modulation to broadcasting and distributing television signals by satellite. We demonstrated a dual-in-one system, where two NTSC video signals are transmitted through one transponder. Another system proposes direct broadcasting by satellite of high definition television using subband coding and adaptive frequency modulation. A simulation of the two systems demonstrates that high quality transmission is possible in noisy narrow-band channels, using analog modulation.

This study was completed in December 1989.

3.8 Subband Coding for Channel-Compatible Transmission of High-Definition Television

Sponsor

Advanced Television Research Program

Project Staff

Ashok C. Popat, Professor William F. Schreiber

In recent years, subband coding has received considerable attention from the image coding community as a simple and effective means of efficiently representing image and image-sequence data.³ We have proposed a three-dimensional (horizontal, vertical, and temporal) subband coding technique for application in a 6-MHz channel-compatible high-definition television (HDTV) distribution system.⁴ Although preliminary "proof-of-principle" tests have demonstrated that the technique is effective, the tests have also shown that there is considerable room for improvement. The technique can be improved by adjusting various parameters in the system; these parameters include the degree of data compression, the number of subbands in each dimension, the type and length of the subband analysis/synthesis filters, and the means of selecting subband pixels to be retained and transmitted. We have observed a high degree of interdependency among many of the system parameters which has complicated the process of identifying the particular combination of parameters that is best suited to the present application. In particular, the strong interdependency seems to eliminate the possibility of finding the best choice for each parameter separately. A major objective of the present research is to search through the vast parameter space by judicious choice of parameters for computer simulation, and by objective and subjective evaluation of the simulation results.

One critical set of system parameters is the set of coefficients used in the subband analysis/synthesis filter banks. We have developed a novel approach to designing such filters based on time-domain numerical search; the approach is fairly general and has resulted in critically-sampled filter banks that

³ J.W. Woods and S.D. Oneil, "Subband Coding of Images," *IEEE Trans. Acoustics, Speech, and Signal Processing*, 34:1278-1288 (1986); H. Gharavy and A. Tabatabai, "Subband Coding of Monochrome and Color Images," *IEEE Trans. Circuits Syst.* 35:207-214 (1988).

⁴ W.F. Schreiber, et al., *Channel-Compatible 6-MHzHDTV Distribution Systems*, CIPG Technical Report ATRP-T-79, MIT, January 1988.

are extremely well-suited to image coding applications.⁵

A seemingly basic principle of image subband/transform coding has emerged from the present study. In particular, the best choice for the length of the analysis/synthesis filters depends only weakly on the number of subbands, depending more strongly on the spatial extent over which the image can be well-modeled as stationary. Thus, the nonstationarity of images inevitably leads to an uncertainty-principle based tradeoff in the selection of the number of subbands and lengths of filters.

We also found that it is extremely important that the allocation of channel capacity is spatially varying. It is essential to be able to increase the number and/or fidelity of samples used in representing action regions of the image at the expense of more poorly representing inactive regions. Currently, we are devising a fixed-rate, practicable means of exploiting this principle.

3.9 Channel Equalization and Interference Reduction Using Adaptive Amplitude Modulation and Scrambling

Sponsor

Advanced Television Research Program

Project Staff

Adam S. Tom, Professor William F. Schreiber

Terrestrial broadcast channels and cable channels are imperfect. Random noise, multipath (ghosts), adjacent and co-channel interference, and an imperfect frequency response degrade these transmission channels so that the quality of the signal at the receiver is significantly below that at the transmitter. To appreciate the increased resolution of high definition images, degradation due to channel defects needs to be reduced. Conventional methods of channel

equalization, which use adaptive filters, are limited by convergence time, length of filters, and computational complexity. We are researching a new method of channel equalization and interference reduction based upon the ideas of adaptive amplitude modulation and pseudo-random scanning (scrambling). This new method is not bound by the above limitations; however, it is limited by the energy of the channel degradations produced.

Adaptive modulation is a noise reduction technique that is applied only to high frequency components of signals. Prior to transmission, a set of adaptation factors are multiplied with the input signal to raise the amplitude of the signal according to the strength of the signal. At the receiver, the signal is divided by these same adaptation factors. In this manner, the random noise added in the channel is reduced by a factor equal to the adaptation factor. The noise is reduced more in the blank areas relative to the busy areas.

Scrambling is a technique for reducing the effects of multipath, adjacent and co-channel interference and also imperfect frequency response. Prior to transmission, we pseudo-randomly scan the input signal, scrambling the signal so that it appears as random noise. Then we transmit this scrambled signal through the channel and perform the reverse of the scrambling at the receiver. Consequently, any degradations in the channel are themselves scrambled at the receiver and, thus, have the appearance of pseudo-random noise in the decoded signal, while the desired signal remains sharp and in full bandwidth.

Since the resultant signal in the receiver now has a noisy appearance, we apply the noise reduction technique of adaptive modulation to the input signal. In our scheme, we apply adaptive modulation to the input signal before scrambling. The coded signal is transmitted through the imperfect channel and decoded at the receiver. The decoding con-

⁵ A.C. Popat, "A Note of QMF Design," unpublished memo, Advanced Television Research Program, MIT, December 1988; A.C. Popat, "Time-Domain Numerical Design of Critically Sampled Filter Banks," presentation viewgraphs, Advanced Television Research Program, MIT, October 1988.

sists of doing the reverse of the scrambling and then the reverse of the adaptive modulation. Scrambling causes any channel degradations to have a noiselike appearance, and adaptive modulation reduces the appearance of this pseudo-random noise. In this manner, the degradations to a transmitted signal are reduced and the channel is equalized.

3.10 A Novel QMF Design Algorithm

Sponsor

Advanced Television Research Program

Project Staff

Kambiz C. Zangi, Professor William F. Schreiber

In this research, we presented a new algorithm for designing two-band quadrature mirror filter (QMF) banks. We show that this algorithm is computationally more efficient by a factor of eight than existing algorithms. Moreover, because this algorithm is not sensitive to the choice of the initial guess, by using it we can also design two-band QMF banks in which one of the filters is predescribed.

This work was completed in December 1989.



Professor William F. Schreiber shown with his graduate students. From the left: David Kuo, Adam S. Tom, Professor Schreiber, and Peter A. Monta.

Chapter 4. Computer-Aided Fabrication System Structure

Academic and Research Staff

Professor Donald E. Troxel

Visiting Scientists and Research Affiliates

Michael B. McIlrath

Graduate Students

Michael Heytens, Abbas Kashani

Undergraduate Students

Creighton Eldridge, Kenneth Ishii, Joseph Kalisewski

Technical and Support Staff

Francis M. Doughty

4.1 Introduction

Sponsor

Defense Advanced Research Projects Agency
Contract MDA 972 88-K-0008

The Computer-Aided Fabrication (CAF) system structure carried out within RLE is part of a larger project within the Microsystems Technology Laboratories (MTL). The overall goal of the CAF project is to integrate computers into the control, data collection, modeling, and scheduling of the integrated circuit fabrication process. The goal of Computer-Aided Fabrication (CAF) of integrated circuits is to provide effective management of information associated with the fabrication of integrated circuits to improve flexibility, portability, and quality and to minimize turn around time, development cost, confusion, error, and manufacturing cost.

4.2 Computer-Aided Fabrication Environment

CAFE (Computer Aided Fabrication Environment) is a software system being developed at MIT for use in the manufacture of integrated circuits. CAFE is intended to be used

in all phases of process design, development, planning, and manufacturing of integrated circuit wafers. While still under active development, CAFE presently provides day-to-day support to several research and production facilities at MIT with both standard and flexible product lines.

The MIT CAFE architecture is a framework provided for a wide variety of software modules including both development tools and on-line applications. The key components of the CAFE architecture are the data model and database schema, the process flow representation (PFR), the user interface, and the application programming and database interfaces.

Our database schema is based on GESTALT, an object-oriented, extensible data model which provides an extended set of intrinsic data types including various temporal types as well as inexact, interval, and null values. This powerful base allows us to design a schema which captures important aspects of plant and process management such as fabrication facilities and equipment, users, equipment reservations, lots, lot tracking, wafers, process flow descriptions, work in progress (wip) tracking, and lab activity information, in an especially natural and effective way.

We developed mechanisms to facilitate changes in the CAFE schema. Application programmers can experiment with new schema definitions and test them by using the new schema in their programs. This ability to create and modify new object types facilitated more rapid development of applications.

We developed an application interface to the database through the Common Lisp Object System (CLOS). The interface provides transparent access to persistent objects, which are described and manipulated via CLOS constructs. This transparency simplifies application programming because it frees the programmer from the task of translating between programming language structures and database structures, which is required in many systems. Application programmers may utilize the rich object modeling and generic functions of CLOS in the integrated environment of Common Lisp to aid in program development.

The use of a common, unified representation of the manufacturing process throughout the cycle of design, simulation, fabrication, and maintenance is central to CAFE. The Process Flow Representation (PFR) provides an extensible framework for knowledge about process steps, including instructions to operators and equipment, scheduling requirements, changes effected to the wafer product, and physical process model parameters. In particular, the PFR accommodates a two-stage process step model which relates the goal of a change in wafer state first to the physical treatment parameters and finally to the actual machine settings used to process the wafers. Its arbitrarily complex hierarchical structure makes it easy for the process designer to abstract away cumbersome details and to focus on the issues of particular interest. Applications are built from specialized "process flow interpreters" which execute a PFR as if it were a program. For example, one such application drives

wafer lots through the fabrication line. Other applications include various process simulators and production planning support.

Process flows are developed and maintained using a process flow editor which enables users to create process flows from basic, pre-defined steps. Using this editor, preparing new flows which are minor variations on existing flows is easy. During the creation of a new flow, the editor provides a number of syntactical and semantic checks, prompting the user concerning the availability of a library of subprocess flows. Starting with these process flows, a simulation interpreter prepares input data suitable for SUPREM III, invokes the SUPREM III simulation, transforms the processed output, and generates various graphical presentations of the simulated process flow. Users can then run SUPREM III simulations without having to know anything about the details of SUPREM III. A key feature of the simulation manager is the "validator," which checks the validity of previous simulation computations after the process flow representation has been modified and retains computations which are still valid. Thus, computation time is minimized while maintaining correctness of the final simulations. This software also allows the user to conveniently generate reports such as plots of impurity concentrations and calculations of sheet resistance, etc.

Ease of use requires a coherent user interface. At the same time, this user interface must be flexible enough to be suitable for a wide variety of applications, many of which remain to be defined. It also must support a wide variety of devices for user interaction, including ASCII terminals and bit-mapped graphic stations. It is quite important to require the provision of a programmatic interface to all application modules including user interfaces. Without this, it becomes virtually impossible to build on previously developed software modules and to integrate them into other systems.

Chapter 5. Optical Propagation and Communication

Academic and Research Staff

Professor Jeffrey H. Shapiro, Dr. Robert H. Rediker, Dr. Ngai C. Wong

Graduate Students

D. Shane Barwick, Bradley T. Binder, Donald E. Bossi, Christopher J. Corcoran, Thomas J. Green, Jr., Stephen M. Hannon, Seng-Tiong Ho, Kin-Wai Leong, Robert E. Mentle, Lily Y. Pang, Scott R. Shepard, Suzanne D. Lau-Shiple, Peter T. Yu, Naomi E. Zirkind

Undergraduate Students

Theresa A. Brennan, Bing Wang

Technical and Support Staff

Barbara A. King

5.1 Introduction

The central theme of our programs has been to advance the understanding of optical and quasi-optical communication, radar, and sensing systems. Broadly speaking, this has entailed: (1) developing system-analytic models for important optical propagation, detection, and communication scenarios; (2) using these models to derive the fundamental limits on system performance; and (3) identifying, and establishing through experimentation the feasibility of, techniques and devices which can be used to approach these performance limits.

5.2 Squeezed States of Light

Sponsors

Maryland Procurement Office
Contract MDA 904-87-C-4044
National Science Foundation
Grant ECS 87-18970

Project Staff

Professor Jeffrey H. Shapiro, Dr. Ngai C. Wong,
Seng-Tiong Ho, Kin-Wai Leong, Scott R. Shepard,
Theresa A. Brennan, Bing Wang

The squeezed states of light (also called the two-photon coherent states) are minimum uncertainty states for the quadrature components of the electromagnetic field which possess an asymmetric noise distribution between the two quadratures. The standard minimum uncertainty state that appears in quantum optics is the Glauber coherent state; it has an equal noise division between the two quadratures and is the quantum analog of the classical electromagnetic wave.

Squeezed states are nonclassical, and are of interest because their asymmetric noise division can lead to lower noise in photodetection measurements than that achievable with coherent states of the same energy. These noise reductions have been shown, theoretically, to afford significant benefits in interferometric precision measurements and novel guided-wave optical communication devices. We have pursued a vigorous program of experimental and theoretical research on squeezed-state and related nonclassical light.

5.2.1 Experiments

We have two principal experiments for the generation of nonclassical light: a forward four-wave mixer, and an optical parametric oscillator (OPO). The forward four-wave mixer is a simple, single-beam configuration using atomic sodium vapor. This experiment has its roots in our original suggestions for generating squeezed light via four-wave

mixing.¹ However, owing to the complications associated with the Doppler-broadened resonant atomic medium, correct selection of operating conditions for this system have required vastly more sophisticated theoretical considerations.² Our best results show approximately 60 percent inferred quadrature-noise squeezing, at our overall measurement efficiency of approximately 40 percent.³ The results of an extensive set of single-beam measurements are in reasonable agreement with our theory over a large range of experimental parameters. However, we have identified a hitherto unexpected effect — differential pump/probe self-focusing (DPS) — which limits the amount of squeezing obtainable with a Gaussian-beam pump source. Follow-on experiments will address circumvention of the DPS limit by use of high Fresnel number beams, and work with ytterbium vapor will begin, to reap the benefits of a simpler atomic level system than sodium.

In our OPO experiment, we are trying a different approach to nonclassical light. The parametric downconversion process which is involved automatically creates pairs of perfectly correlated photons, one at the signal wavelength and one at the idler wavelength, as a result of absorption of one pump photon. This correlation provides a directly detectable nonclassical signature — perfect intensity correlation between the photocurrents produced by detectors viewing the signal and idler beams separately — and can be adapted, through feedback or feedforward schemes, to produce squeezed light. We

have the first Type I phase-matched OPO to show this nonclassical correlation.⁴ Our MgO doped LiNbO₃ system has yielded approximately 50 percent observed noise reduction in the differenced photocurrent from the signal and idler detectors (see figure 1).

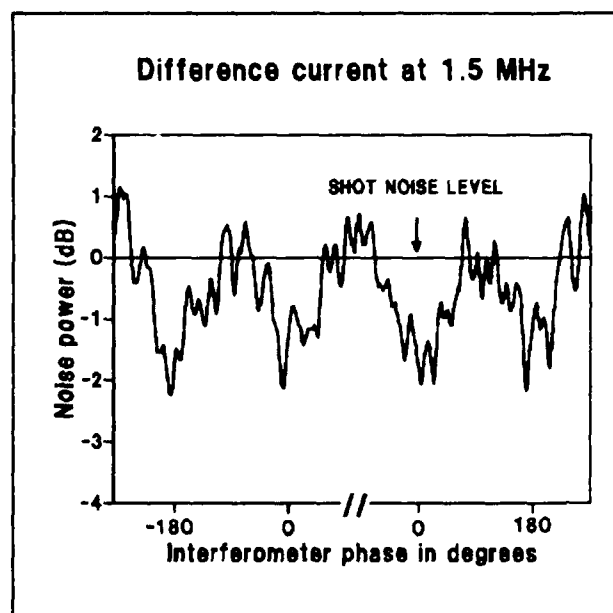


Figure 1. OPO differenced-photocurrent noise power at 1.5 MHz as a function of the relative phase between the arms of an interferometer used to separate the signal and idler beams. The shot noise level is normalized to 0 dB. Nonclassical correlation between the signal and idler is demonstrated by noise powers below 0 dB.

Work is continuing to improve this correlation and to perform feedback and feedforward squeezed-state generation with this setup.

- ¹ H.P. Yuen and J.H. Shapiro, "Generation and Detection of Two-Photon Coherent States in Degenerate Four-Wave Mixing," *Opt. Lett.* 4 (10): 334-336 (1979); P. Kumar and J.H. Shapiro, "Squeezed State Generation via Forward Degenerate Four-Wave Mixing," *Phys. Rev. A* 30 (3): 1568-1571 (1984).
- ² S.-T. Ho, P. Kumar, and J.H. Shapiro, "Quantum Theory of Nondegenerate Multiwave Mixing," *Phys. Rev. A* 35 (9): 3982-3985 (1987); S.-T. Ho, P. Kumar, and J.H. Shapiro, "Quantum Theory of Nondegenerate Multiwave Mixing: General Formulation," *Phys. Rev. A* 37 (6): 2017-2032 (1988); S.-T. Ho, *Theoretical and Experimental Aspects of Squeezed State Generation in Two-Level Media*, Ph.D. diss., Dept. of Electr. Eng. and Comput. Sci., MIT, 1989.
- ³ S.-T. Ho, *Theoretical and Experimental Aspects of Squeezed State Generation in Two-Level Media*, Ph.D. diss., Dept. of Electr. Eng. and Comput. Sci., MIT, 1989; S.-T. Ho, N.C. Wong, and J.H. Shapiro, "Self-Focusing Limitations on Squeezed State Generation in Two-Level Media," to appear in *Coherence and Quantum Optics VI*, eds. L. Mandel, E. Wolf, and J.H. Eberly (Plenum: New York, 1989).
- ⁴ K.-W. Leong, *Intensity Quantum Noise Reduction with an Above-Threshold Optical Parametric Oscillator*, Ph.D. diss. prop., Dept. of Electr. Eng. and Comput. Sci., MIT, 1990.

5.2.2 Theory

Our recent theoretical work on nonclassical light has addressed issues relevant to our experimental work with both the four-wave mixer⁵ and the optical parametric oscillator.⁶ In addition, we have begun a new fundamental investigation of the sensitivity of quantum phase measurements. This work, which is based on quantum estimation theory, has provided some fundamental justification for identifying the probability operator measure (POM) associated with the Susskind-Glogower phase measurement as the correct description of quantum phase. Using this measurement with an optimal choice of state, we have found that substantially lower phase-measurement errors can be obtained, at the same average photon number, than those predicted for optimized squeezed-state interferometers.⁷

This result has motivated our work to determine an explicit realization of the Susskind-Glogower POM. Toward that end we have established an analogy with the familiar optical heterodyne realization of the annihilation operator POM. This has led to a commuting observables picture of the Susskind-Glogower POM on a larger, signal cum apparatus, state space,⁸ as well as the definition and principal properties of two new classes of quantum states, the coherent

phase states and the squeezed phase states.⁹ Work on quantum phase is continuing through connections between digital signal processing theory that arise because of the Fourier transform relations that exist between the number and phase representations of an arbitrary ket.

5.3 Laser Radar System Theory

Sponsor

U.S. Army Research Office - Durham
Contract DAAL03-87-K-0117

Project Staff

Professor Jeffrey H. Shapiro, Stephen M. Hannon, Thomas J. Green, Jr., Naomi E. Zirkind, Robert E. Mentle

Coherent laser radars represent a true translation to the optical frequency band of conventional microwave radar concepts. Owing to the enormous wavelength disparity between microwaves and light, laser systems offer vastly superior space, angle, range, and velocity resolution as compared to their microwave counterparts. However, the resolution benefits associated with the shortness of laser wavelengths are accompanied by the penalties of this wavelength region: the ill-effects of atmospheric optical wave propagation in turbulent or turbid conditions, and

⁵ S.-T. Ho, P. Kumar, and J.H. Shapiro, "Quantum Theory of Nondegenerate Multiwave Mixing," *Phys. Rev. A* 35 (9): 3982-3985 (1987); S.-T. Ho, P. Kumar, and J.H. Shapiro, "Quantum Theory of Nondegenerate Multiwave Mixing: General Formulation," *Phys. Rev. A* 37 (6): 2017-2032 (1988); S.-T. Ho, *Theoretical and Experimental Aspects of Squeezed State Generation in Two-Level Media*, Ph.D. diss., Dept. of Electr. Eng. and Comput. Sci., MIT, 1989; S.-T. Ho, N.C. Wong, and J.H. Shapiro, "Self-Focusing Limitations on Squeezed State Generation in Two-Level Media," to appear in *Coherence and Quantum Optics VI*, eds. L. Mandel, E. Wolf, and J.H. Eberly (Plenum: New York, 1989).

⁶ K.-W. Leong, *Intensity Quantum Noise Reduction with an Above-Threshold Optical Parametric Oscillator*, Ph.D. diss. prop., Dept. of Electr. Eng. and Comput. Sci., MIT, 1990; K.-W. Leong, N.C. Wong, and J.H. Shapiro, "Pump Noise in an Optical Parametric Oscillator Operated Above Threshold," paper presented at the Annual Meeting of the Optical Society of America, Santa Clara, California, Oct. 30 - Nov. 4, 1988.

⁷ J.H. Shapiro, S.R. Shepard, and N.C. Wong, "Ultimate Quantum Limits on Phase Measurement," *Phys. Rev. Lett.* 62 (20): 2377-2380 (1989).

⁸ J.H. Shapiro, S.R. Shepard, and N.C. Wong, "A New Number-Phase Uncertainty Principle," to appear in *Coherence and Quantum Optics VI*, eds. L. Mandel, E. Wolf, and J.H. Eberly (Plenum: New York, 1989).

⁹ J.H. Shapiro, S.R. Shepard, and N.C. Wong, "Coherent Phase States and Squeezed Phase States," to appear in *Coherence and Quantum Optics VI*, eds. L. Mandel, E. Wolf, and J.H. Eberly (Plenum: New York, 1989); T.A. Brennan, *The Statistical Behavior of Coherent and Squeezed Phase States*, S.B. thesis, Dept. of Physics, MIT, 1989.

the speckle patterns resulting from target roughness on wavelength scales. The ensuing trade-off between resolution advantages and propagation/speckle disadvantages makes it likely that laser radars will fill new application niches, rather than supplant existing microwave systems.

We have been working to quantify the preceding issues through development and experimental validation of a laser radar system theory. Our work includes a collaboration arrangement with the Opto-Radar Systems Group of the MIT Lincoln Laboratory, whereby the experimental portions of the research are carried out with measurements from their CO₂ laser radar test beds.

5.3.1 Multipixel Detection Theory

We have been developing the appropriate target-detection theory for multipixel multidimensional laser radar imagers, including those systems which augment their active-sensor channels with a forward-looking infrared (FLIR) passive channel. Previously, we established the structure of quasi-optimum intensity-only, range-only, and joint range-intensity processors for deciding whether or not a speckle target is present within an image frame.¹⁰ This problem was solved for the realistic case in which the target, if it is present, has unknown azimuth, elevation, range, and reflectivity, and in which there is a spatially-extended speckle background of unknown reflectivity.

Recently, we have reported on the quasi-optimum processors that include the passive channel as well.¹¹ The great advance in all of our work — over alternative ad hoc treat-

ments — is its associated performance theory, which allows trade-off assessments to be made between radar-system parameters and target-detection performance. Our initial analytic performance results were limited to intensity-only and range-only processors.¹² They were later verified by a computer simulation, which also provided the first quantitative measure of the performance improvement afforded by joint range-intensity processing.¹³ The simulation has since been extended to include the full panoply of detection processors.¹¹ The simulations show that, in general, adding a sensor dimensionality significantly improves detection performance. These results have been confirmed, experimentally, using the MIT

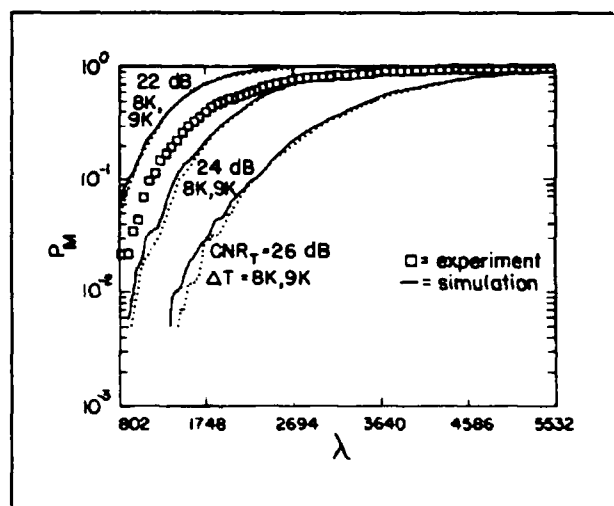


Figure 2. Experimental and computer-simulated miss probabilities (P_M) for a joint range-intensity-passive processor plotted vs. detection threshold λ . The experimental performance is well fit by simulation using a 23 dB target carrier-to-noise ratio (CNR_T) and at thermal contrast (ΔT) between 8 and 9 K. These parameter values are consistent with those inferred directly from the experimental data.

¹⁰ M.B. Mark and J.H. Shapiro, "Multipixel, Multidimensional Laser Radar System Performance," *Proc. SPIE* 783, 109-122 (1987); S.M. Hannon and J.H. Shapiro, "Laser Radar Target Detection with a Multipixel Joint Range-Intensity Processor," *Proc. SPIE* 999, 162-175 (1988).

¹¹ S.M. Hannon, *Detection Processing for Multidimensional Laser Radars*, Ph.D. diss., Dept. of Electr. Eng. and Comput. Sci., MIT, 1990; S.M. Hannon and J.H. Shapiro, "Active-Passive Detection of Multipixel Targets," *Proc. SPIE* 1222 (1990).

¹² M.B. Mark and J.H. Shapiro, "Multipixel, Multidimensional Laser Radar System Performance," *Proc. SPIE* 783, 109-122 (1987).

¹³ S.M. Hannon and J.H. Shapiro, "Laser Radar Target Detection with a Multipixel Joint Range-Intensity Processor," *Proc. SPIE* 999, 162-175 (1988).

Lincoln Laboratory multidimensional laser radar test bed (see figure 2).¹¹

5.3.2 Multipixel Laser Radar Target Tracking

The preceding target detection work is a multipixel multidimensional single-frame theory. Once a laser radar has detected a target, it will usually need to track that target. Here we have a multipixel multidimensional multiframe task. In recent work,¹⁴ we have established a basic theory for such tracking problems. The correct pixel-level statistics are used to develop the first and second moments of an observation equation for use in a Kalman-filter track-while-image linear least-squares algorithm. The preceding development assumed there were no background reflectors, i.e., an uplooking geometry was presumed. We have now recast the analysis¹⁵ to handle the downlooking geometry that is employed in our detection work.

5.4 Fiber-Coupled External-Cavity Semiconductor High Power Laser

Sponsor

U.S. Navy - Office of Naval Research
Grant N00014-89-J-1163

Project Staff

Dr. Robert H. Rediker, Lily Y. Pang, Christopher J. Corcoran, D. Shane Barwick

During this year, we have achieved the milestone of five semiconductor gain elements (lasers with one facet AR coated) fiber-coupled into the external cavity and acting as a coherent ensemble. The combined output from the external cavity is that of a coherent laser. We have *experimentally* verified the concept of this program. In this concept,

high average powers were obtained by fiber coupling of physically separated individual lasers and/or monolithic arrays into an external cavity. In this way, the density of power that has to be dissipated can be kept below the value at which it would cause excessive heating and/or would require complicated and space consuming coolers.

Preliminary experiments have been performed on the sensitivity of the ensemble external cavity operation to changes in the optical length of the fiber or to rotation of the output polarization of the fiber. To first order, there is no effect due to a change in the optical length of one of the fibers and thus there must be a compensating self-adjustment to keep the output phase constant. The operation of the ensemble external-cavity laser is more sensitive to rotation of the polarization from one fiber than is the operation of a single external-cavity laser.

Publications

Pang, L.Y. *Polarization Effects on an External Cavity Controlled Ensemble of Fiber-Coupled Semiconductor Diode Lasers*. S.M. thesis. Dept. of Electr. Eng. and Comput. Sci., MIT, 1989.

Rediker, R.H., C. Corcoran, L.Y. Pang and S.K. Liew. "Validation of Model of External-Cavity Semiconductor Laser and Extrapolation from 5-element to Multi-element Fiber-Coupled High-Power Laser." *IEEE J. Quantum Electron.* QE-25(6): 1547-1552 (1989).

Corcoran, C., and R.H. Rediker. "Operation of Five Discrete Diode Lasers as a Coherent Ensemble by Fiber-Coupling into an External Cavity." To be published in the *Technical Digest of Conference on Electoptics and Lasers CLEO 90*, Anaheim, California, May 1990. Washington, DC: Optical Society of America, 1990.

¹⁴ R.H. Enders and J.H. Shapiro, "Laser Radar Tracking Theory," *Proc. SPIE* 999, 192-207 (1988).

¹⁵ R.E. Mentle, *Laser Radar Performance Theory for Track-While-Image Operation*, S.M. thesis prop., Dept. of Electr. Eng. and Comput. Sci., MIT, 1989.

5.5 Analog Processing of Optical Wavefronts Using Integrated Guided-Wave Optics

Sponsor

U.S. Air Force - Office of Scientific Research
Contract F49620-87-C-0043

Project Staff

Dr. Robert H. Rediker, Donald E. Bossi, Suzanne D. Lau-Shiple

This program, initiated in March 1987, explores fundamental issues associated with optical wavefront corrections using integrated guided-wave optical devices in GaAlAs. Device fabrication and optimization are being performed at MIT Lincoln Laboratory while results are being evaluated at RLE.

Two tasks were emphasized during 1989. The first has been the development of an adiabatic antenna (an antenna that remains single-mode and loses no energy out of this mode) with an antenna pattern in which almost all of the energy is in a highly-directional central lobe. The second task that is being addressed is the measurement of the wavefront phase. This task includes the development of heterostructure waveguides, bends and Y-junctions, two- and three-guide couplers and phase modulators. These optical components must be consistent with the eventual goal of integration with electronic components on the same chip.

Reduced-confinement GaAlAs slab-waveguide antennas have been fabricated by using an improved MBE growth technique to produce longitudinal variations in the refractive index and thickness of a waveguide film. This technique utilizes the fact that for substrate surface temperatures above 650°C the sticking coefficient of Ga on GaAs decreases with increasing temperature, while below 650°C this sticking coefficient is essentially independent of temperature. By using both growth-temperature regimes and by applying graded heating to the substrate wafer throughout the growth process, the entire reduced-confinement antenna is now produced in a single MBE run without breaking vacuum. The experimentally determined beam divergences for both the guide

and the antennas are in excellent agreement with those predicted from the width and Al composition of both these structures. Up to a 37 percent reduction in the beam divergence due to the antenna has been measured.

Numerical simulations demonstrate that requirements on both the amplitude and phase profiles at the antenna output impose a stringent lower limit on the acceptable taper length for optimal device performance. However, by choosing an appropriate taper function, such as a parabolic index profile, the minimum necessary taper length is reduced. For example, a 69 percent reduction in transverse beam divergence, from 16 degrees to 5 degrees FWHM, is attainable from a 1 mm-long taper for which the cladding and film thicknesses total $> 9 \mu\text{m}$.

In wavefront sensing and correction, it is envisioned that 10^3 – 10^4 basic modules would be used. In integrated optics, as in integrated circuits, it is important to relax the requirements on individual components and require that the operation of the integrated optics (circuits) be independent of significant component variations. Therefore, two optical wavefront phase tilt measurement configurations have been developed theoretically to measure the wavefront phase tilt, regardless of input power non-uniformity. The first consists of a Y-junction interferometer with a phase dither applied to one of the input arms. The second consists of a three-guide coupler with inputs to the outer arms; a square-wave bias phase function, which switches between zero and $\pi/2$ radians, is applied to one of the input arms. Work is underway to build these two measurement configurations.

Publications

Bossi, D.E., W.D. Goodhue, and R.H. Rediker. *Integrated and Guided-Wave Optics*. 1989 Technical Digest Series Vol. 4. Washington, DC: Optical Society of America, 1989, pp. 80-83.

Bossi, D.E., W.D. Goodhue, M.C. Finn, K. Rauschenbach, J.W. Bales and R.H. Rediker. "Reduced-Confinement Antennas for GaAlAs Integrated Optical Wave-

guides." *Appl. Phys. Lett.* 56 (5): 420-422 (1990).

Bossi, D.E., W.D. Goodhue, M.C. Finn, K. Rauschenbach and R.H. Rediker. "Fabrication and Enhanced Performance of Reduced-Confinement GaAlAs Tapered-Waveguide Antennas." To be published in the *Technical Digest of the Topical*

Meeting on Integrated Photonics Research, Hilton Head, South Carolina, March 1990. Washington, DC: Optical Society of America.

Bossi, D.E. *Reduced-Confinement GaAlAs Tapered Waveguide Antennas*. Ph.D. diss. Dept. of Electr. Eng. and Comput. Sci., MIT, 1990.



Professor Jeffrey H. Shapiro, Associate Head, Department of Electrical Engineering and Computer Science



Professor Jonathan Allen, Director, Research Laboratory of Electronics

Chapter 6. Custom Integrated Circuits

Academic and Research Staff

Professor Jonathan Allen, Professor John L. Wyatt, Jr., Professor Srinivas Devadas, Professor Jacob White, Professor Dimitri A. Antoniadis, Professor Berthold K.P. Horn, Professor Hae-Seung Lee, Professor Bruce R. Musicus, Professor Tomaso Poggio, Professor Charles G. Sodini

Graduate Students

Robert C. Armstrong, Donald G. Baltus, Cyrus S. Bamji, Michael J. Bryan, Curtis S. Chen, Steven J. Decker, Ibrahim M. Elfadel, Mikko Hakkarainen, Craig Keast, Kevin Lam, Jennifer A. Lloyd, Andrew Lumsdaine, Steven P. McCormick, Ignacio McQuirk, Keith S. Nabors, Joel R. Phillips, Mark W. Reichelt, Mark N. Seidel, Luis M. Silveira, David L. Standley, Ricardo Telichevsky, Christopher B. Umminger, Filip Van Aelten, Woodward Yang

Technical and Support Staff

Dorothy A. Fleischer, Susan E. Nelson

6.1 Custom Integrated Circuits

Sponsors

Analog Devices, Inc.
International Business Machines Corporation
Joint Services Electronics Program
Contract DAAL03-89-C-0001
U.S. Air Force - Office of Scientific Research
Contract AFOSR 86-0164B

Project Staff

Professor Jonathan Allen, Robert C. Armstrong, Donald G. Baltus, Cyrus S. Bamji, Steven P. McCormick, Mark W. Reichelt, Filip Van Aelten

Through our VLSI CAD research, we seek the means to produce custom integrated circuits correctly, quickly, and economically. Traditionally, correctness has been checked at several representational levels such as layout (via design rule checking), circuit, and logic (both via simulation). The techniques for checking correctness are local to the particular representational level involved. While these techniques are important components of design testing, they do not attempt to provide alignment and consistency checks between the different levels of representation and an input behavioral specification. In addition, they do not characterize the set of possible designs at each representational

level corresponding to the initial functional specification, while ranging over a variety of performance levels. For this reason, there is an increasing need to provide CAD tools that can serve as the framework for design exploration, providing the desired performance together with consistently aligned representations at all levels.

In this research group, we are studying a variety of research topics with an emphasis on performance directed synthesis of custom VLSI designs. Professor Allen has recently provided an overview of these issues,¹ in which he emphasizes the need for coordinating the design optimization process over the several levels of representation.

Since there is so much to be gained by aggressive circuit design, our research group has placed considerable emphasis on this level. In addition, the group has focused on optimized architectures for digital signal processing (1) because of the highly parallel nature of the algorithms involved, and (2) because of the need for a very high level of real time performance. We have also increased our emphasis on developing means for formally specifying designs that facilitate performance directed design exploration, as well as efficient verification of correctness of the coordinated set of design level represent-

¹ J. Allen, "Performance Directed Synthesis of VLSI Systems," *Proc. IEEE* 78(2): 366-355 (1990).

ations. All of these studies are taking on an increasingly theoretical approach, signifying the transition of digital system design from an art to a science.

The circuit level of design representation is the most abstract level at which performance can be characterized explicitly in terms of delay, and also where performance can be substantially manipulated through changes in circuit style and device sizing. It is an important level of design because optimization techniques which manipulate circuit representation can have great impact on resulting performance. More abstract representations can be transformed into a circuit representation, but the need to transform a circuit into layout in a general yet efficient way is needed for the rapid design of custom circuits. Baltus² has developed a very general yet efficient technique for compiling circuits into layout. The algorithm converts both NMOS and CMOS circuits in any style, and provides special means for the efficient layout of circuits with highly varying transistor width-to-length ratios. While initially focused on implementation technologies with only one level of metal, it is now being generalized to multiple levels of metal. Recent comparisons of this program with other techniques at a benchmark competition have demonstrated the effectiveness of these procedures.

Now that there is assurance of the generation of a high quality layout from any circuit specification, we are turning our attention to design performance exploration at the architectural level. For this research, our goal is to study the performance of quasi-regular architectures through manipulations of an initial behavioral specification. A new language has been developed for algorithms which can be compiled into either regular systolic architectures, or structures with a limited degree of irregularity. From the input language specification, a prototype descriptor is generated which compactly and efficiently represents both the structural hierarchy and the degree

of replication of architectural elements. This descriptor can be readily expanded into a fully parallel data flow graph if necessary, but has the advantage that its complexity does not appreciably grow with circuit element replication.

After obtaining the prototype descriptor, we apply a series of three types of transformations in order to explore the architectural design space. First, various amounts of serialization can be instantiated, cutting down the amount of inherent parallelism in the input language specification, but also reducing the area of the resultant implementation. Next, we explore a variety of architectural transformations that map the index spaces associated with each array variable into a common global index space. Finally, we explore pipelining to localize communication between architectural elements. This approach is expected to lead to a flexible but powerful framework for architectural design exploration in the context of known capability for the conversion of the circuit form of the architectural elements into efficient layout. One important research issue is the degree of irregularity that is desirable in the resultant arrays due to non-local communication. It may be possible to make the distance of communication a designer-controlled parameter, thus providing a means to depart from regularity when the communication needs of the algorithm favor it, thereby expanding the class of designs that can be efficiently converted to layout.

Another example of the mapping of a high level specification to the circuit level representation has focused on the technology mapping process. Much research has focused on the conversion of a high-level functional specification to a highly optimized logic specification. This logic representation is usually then converted to the circuit form by means of a technology mapping in terms of a cell library. Heretofore the cell library was made up of typical restoring gates, such as

² D.G. Baltus and J. Allen, "SOLO: A Generator of Efficient Layouts from Optimized MOS Circuit Schematics," *Proceedings of the 25th Design Automation Conference*, June 1988.

NAND and NOR cells, but Kaplan³ has recently expanded this process to include pass transistor gates as well as restoring forms. By broadening the class of circuit forms, and hence basic library gate cells, new flexibility is introduced into the technology mapping process. New logic-level representations have been introduced to facilitate the optimization of these circuits. By coupling to the existing SOLO layout generator, savings in the area of approximately 20 percent have been demonstrated for a number of designs that take advantage of the use of pass transistor gates as well as restoring gates. This research exemplifies the need to coordinate design at several levels. Logic synthesis must contemplate the class of library cells that will be used in implementations, while increased circuit flexibility leads to new layout savings by means of a more powerful technology mapping.

Driven by the requirements of performance optimization, we have devoted a considerable amount of research to delay characterization associated with circuit waveform transitions. McCormick⁴ has developed an efficient scheme for computing these transitions accurately using a small number (four or less) of circuit transform moments. Interactions between interconnection lines, even as general as RLC lines, can be readily computed with these moments. In addition to passive interconnect, we have expanded these techniques to also include the efficient characterization of active circuits. Using these techniques, efficiency of delay calculation, together with accuracy, is obtained, thus avoiding the substantial numerical load of comprehensive circuit simulation. Moment calculations are thus part of an overall strategy of performance estimation that must be done quickly and accurately in order to

facilitate rapid exploration of design alternatives. It is also important to note that delay due to interconnect is now dominating the delay caused by active circuits in large systems. The ability to accurately characterize circuit delay in complex branching interconnect structures, including the effect of interconnect material together with driving and terminating impedances, is essential to the accurate exploration of circuit performance.

With the advent of very small devices operating at very high speeds, we need to revise device models for circuit simulation. Rather than use average value parameters, we must now solve the device equations directly to provide the accuracy required. Unfortunately, direct use of these equations implies very long simulation run times, making it important to find ways of obtaining required accuracy with reduced computational expenditure. Reichelt⁵ has applied waveform relaxation techniques to this problem in a way that readily allows for the use of parallel waveform relaxation simulators. Initial results have proved the effectiveness of this approach, which guarantees convergence of the simulation. Investigations of possible parallel architectures for this purpose are now under way.

Recently, our emphasis on verification techniques has grown as the complexity of designs, and the need for overall correctness, has increased. There are a variety of approaches to verification, including logical proofs that implementation structures correspond to behavior specifications, and symbolic simulation. Because the need for formal characterizations of design has grown, we are searching for representations that can compactly characterize the class of correct

³ J.T. Kaplan, *Pass and Restoring Logic Technology Mapping for the Efficient Automated Generation of Combinational Leaf Cells*, S.M. thesis, Dept. of Electr. Eng. and Comput. Sci., MIT, 1989.

⁴ S.P. McCormick and J. Allen, "Waveform Moment Methods for Improved Interconnection Analysis." *Proceedings of the 27th Design Automation Conference*, Orlando, Florida, June 1990.

⁵ M. Reichelt, J. White, and J. Allen, "Waveform Relaxation for Transient Simulation of Two-Dimensional MOS Devices." *Proceedings of the International Conference on Computer Aided Design*, November 1989.

designs. Bamji⁶ has applied context free formal grammars to the specifications for the class of MOS digital integrated circuits. Compact grammars can represent classes of infinite cardinality, so that, for example, the class of all CMOS static combinatorial circuits can be generated by only five grammatical rules. Many circuit styles can be characterized in this way, and the corresponding parsing procedures can deal with mixed styles in an efficient way. Bamji has represented the class of all layouts generated by a regular grammar by use of the Regular Structure Generator, and he has shown how to verify the correctness of the resulting layout by parsing techniques. Finally, both of these grammatical representations, one at the circuit level and the other at the layout level, have been combined into a coupled grammar that can be used to verify the proper correspondence between layout and circuit. Thus, not only can both layout and circuit structures be verified independently by similar grammatical techniques, but we can show that their alignment is correct so that they are both coordinated representations of the same underlying abstract circuit in a consistent fashion. Successful verification demonstrates that all circuit and layout structures have correspondents at related layout and circuit representations, respectively, so that no loose fragments at either level are isolated from those at other design levels. Since these grammatical techniques have been successful at the circuit and layout levels, we are now focusing on their application at higher levels of design.

Grammatical techniques are appropriate for characterizing correct structure of circuits, but they are not easily adapted to the verification of nonstructural circuit properties such as device sizing and allowable capacitance sizes that could lead to undesirable charge sharing. To deal with these attributes, Van

Aelten⁷ has developed an efficient technique for verification of circuit properties. This approach builds on the grammatical techniques of Bamji, parsing the circuit first to reveal its constituent structure. Semantic checks are then applied to the circuit to verify its specified performance. The circuit is effectively mapped into logic level representations by a process of recursive interpretation. Checks for electrical constraints are made at the level of the individual subcircuits, and the behavioral description of these elements is composed in order to provide a match with the user supplied specification. Extensions to this approach require more comprehensive circuit grammars that may have to be interleaved with the semantic interpretation process, thus breaking down the traditional separation of syntax and semantics.

To continually maintain a consistent set of design representations that are properly aligned, it is important to build a unified framework for all levels of representation. Armstrong⁸ has developed a technique for specifying design at all levels of abstraction with a uniform formalism. The way in which each of these abstractions is a consistent projection of one underlying abstract design entity is explicitly described, thus facilitating the automatic alignment of these representations. In this way, when one design projection at a specific level of representation (e.g., circuit level) is manipulated, all other levels are changed automatically to provide the correct alignment. In general, this is a one-many process, since there is usually an infinite number of less abstract design projections corresponding to a more abstract projection of the same overall design. All that is required, however, is that all levels are consistent, so that performance optimization algorithms can select the best design projection at a given level, subject to some

⁶ C.S. Bamji and J. Allen, "GRASP: A Grammar-based Schematic Parser." *Proceedings of the 26th Design Automation Conference*, June 1989.

⁷ F. Van Aelten and J. Allen, "Efficient Verification of VLSI Circuits Based on Syntax and Denotational Semantics," *Proceedings, IMEC/IFIP Workshop on Applied Formal Methods for Correct VLSI Design*, Houthalen, Belgium, 1989.

⁸ R.C. Armstrong, *A Formal Approach to Incremental Consistency Maintenance in Multirepresentation VLSI Databases*, Ph.D. diss. proposal, Dept. of Electr. Eng. and Comput. Sci., MIT, 1987.

overall optimization criterion. Upon completion, this new formal framework will provide a basis for interconnecting an entire suite of design tools and will easily contemplate the addition of new levels of representation without the need to provide an entirely new framework.

The above descriptions show how several aspects of performance-driven synthesis are being studied and adapted to new CAD tools. There is a clear trend toward adopting more formal notions of behavior, structure, and attributes, together with techniques for coordinating these several levels of description in one overall consistently maintained structure. In the future, we will emphasize completion of the theoretical framework and unification of optimization procedures across all levels of design.

6.2 The Vision Chip Project

Sponsors

DuPont Corporation
National Science Foundation
Grant MIP 88-14612

Project Staff

Professor John L. Wyatt, Jr., Professor Berthold K.P. Horn, Professor Hae-Seung Lee, Professor Tomaso Poggio, Professor Charles G. Sodini, Steven J. Decker, Ibrahim M. Elfadel, Mikko Hakkarainen, Craig Keast, Ignacio McQuirk, Mark N. Seidel, David L. Standley, Christopher B. Umminger, Woodward Yang

6.2.1 Overall Project Description

Problem Definition and Methods

Computational Demands of Vision and the Smart Sensor Paradigm: A major problem in machine vision is the extraordinary volume of input data that must be acquired, managed and processed. This large quantity of data in real-time grey-level images leads to communication bottlenecks between imager, memory and processors, while the computational demands remain high once data have reached the processors. The result is that

conventional machines are incapable of any but the most rudimentary forms of real-time vision processing.

The *smart sensor paradigm* shows great promise as a new approach to this problem. Although potentially applicable to a variety of sensor types, e.g., tactile and acoustic arrays, in this project we are restricting its application to vision. The key idea is to incorporate signal processing as early as possible into a system's signal flow path to reduce demands for transmission bandwidth and subsequent computation.

In this paradigm, the major themes are:

- sensors and processing circuitry integrated on a single chip,
- parallel computation,
- processing circuits distributed throughout the array for spatially local operations in situ with minimal wiring overhead,
- use of analog circuits for early processing tasks to avoid the speed and area costs of analog-to-digital conversion on high-bandwidth data streams,
- selection of tasks and algorithms requiring low to moderate precision, and
- special emphasis on computations that map naturally to physical processes in silicon, e.g., to relaxation processes or to resistive grids.

Analog Integrated Circuits: Both continuous-time and sampled-data analog integrated circuits play a key role in our research. Analog circuits offer substantial advantages in speed, functionality per unit silicon area, and ease of interfacing to inherently analog input data, while digital circuits are easier to design and can obtain unlimited precision through use of progressively longer wordlengths.

The Gilbert 2-quadrant multiplier is a dramatic example of analog capability. Requiring only four transistors, its similar, although slightly more complex circuits, achieve 0.02 percent precision multiplication in under 200 nanoseconds with a dynamic

range of about five orders of magnitude!⁹ More generally, analog circuits that perform basic operations such as addition, subtraction, multiplication, thresholding, absolute value, logarithm, exponentiation, time integration and simple linear filtering are much more compact and, in most instances, faster than corresponding digital implementations. These circuits can be fabricated in array form on the same chip as transducers and operate directly on transducer outputs.

The trade-off is in the inevitable drift and imprecision of analog integrated circuits, which require careful design. Although these problems make analog methods inappropriate for certain tasks, they are not major drawbacks in early vision applications, in which the input data (pixel intensities) are rarely accurate to much better than 1 percent (about 7 bits equivalent). In vision applications, the demand is for a *massive volume of computation*, rather than high precision.

In our research, we use the speed and area advantages of analog systems, as distinct from single components like multipliers. For example, the CCD 2-D *binomial convolver* we are building is conceptually an analog systolic array, capable of massively parallel computation at an estimated 10 MHz rate using minimal area. The *parallel spatial correlator* will achieve a similar level of parallelism in a small space using the special properties of resistive grids.

Advances in parallel computation and VLSI technology will also enable the continued growth of general purpose digital computer

capabilities. We expect that advanced digital machines will remain the tool of choice for high-level, i.e., *late*, vision tasks such as object recognition, while the analog implementation of the smart sensor paradigm will enable enormous further reductions in machine size, power consumption, speed and cost required for low-level or *early* vision processing.

Project Direction and Goals

The goal of this project is to develop novel, high-performance silicon systems for several real-time processing tasks in early vision. We are pursuing two parallel routes. The first leads to *single-chip sensor and processor systems*, while the second leads to a *modular early vision system*.

As used here, the term "single-chip sensor and processor system" refers to any chip that acquires image data through a photoreceptor array, has processors spatially distributed throughout the array, and performs a specialized form of parallel computation resulting in low-bandwidth output. Most systems designed in Carver Mead's Laboratory¹⁰ are of this form.¹¹ These systems are small in physical size, inexpensive to manufacture, and specialized in application. The term "modular early vision system" refers to a larger, much less specialized system that will require board-level implementation or, perhaps eventually, wafer-scale integration. Its primary output will consist of arrays of intensity, depth and velocity information, and it will be useful as a front-end processor for a variety of vision applications.

⁹ B. Gilbert, "Four Quadrant Analog Divider/Multiplier with 0.01 Percent Distortion," *ISSCC Digest of Technical Papers*, pp. 248-249, February 1983.

¹⁰ The silicon retina only partially fits this category as defined above. That system passes entire images off chips at a high data rate and may not be considered very specialized, within the vision domain.

¹¹ J. Tanner, and C. Mead, "An Integrated Optical Motion Sensor," *VLSI Signal Processing II*, paper presented at the ASSP Conference on VLSI Signal Processing, University of California, Los Angeles, November 5-17, 1986; S.Y. Kung, R.E. Owen, and J.G. Nash, eds., IEEE Press, 59-76, 1987; M.A. Sivilotti, M.A. Mahowald, and C.A. Mead, "Real Time Visual Computations Using Analog CMOS Processing Arrays," in *Advanced Research in VLSI: Proceedings of the 1987 Stanford Conference*, ed. P. Losleben (Cambridge: MIT Press, 1987), 295-312; C.A. Mead and M.A. Mahowald, "A Silicon Model of Early Visual Processing," *Neural Networks 1* (1):91-97 (1988); S. DeWeerth and C.A. Mead, "A Two-Dimensional Visual Tracking Array," in *Advanced Research in VLSI: Proceedings of the 1988 MIT Conference* (Cambridge: MIT Press, 1988); C.A. Mead, *Analog VLSI and Neural Systems* (Reading, Massachusetts: Addison-Wesley, 1989).

These two routes occupy complementary positions in our program. The former will yield a working system quickly, enabling us to evaluate our approach at an early stage. Although the latter allows for continued leverage from our past work for future system designs, it requires a major, time-consuming initial investment in developing the early vision modules.

This project has distinct goals that lie both within and beyond the three-year funding period of this project. Within three years, we will make components that are useful for a variety of early vision tasks. In five years, we will make a more general early vision system using these components and a more advanced specialized component useful for robot navigation. Our long-term goal is an advanced early vision system with highly processed, low-bandwidth output representing robustly segmented images.

Three-Year Goals: For the modular early vision system, we are building three components that will be useful for a wide range of image processing tasks: (1) an analog charged-coupled-device (CCD) restoring *image memory*, (2) a parallel pipelined CCD 2-D *binomial convolver*, and (3) a parallel *spatial correlator* using resistive grid averagers. These three systems are the foundation for our long-term plans outlined on the following pages.

MOSIS presently has no CCD capability. Therefore, we will develop a CCD enhancement to MIT's baseline CMOS process to fabricate the CCD binomial convolver and image memory. We are exploring both MOS and bipolar designs for the resistor circuits and arithmetic circuits used in the correlator. The fairly rapid turnaround CMOS process at MOSIS and the BiCMOS process on campus give us valuable flexibility in developing this system.

During the third year, we will complete design and simulation of the modular early vision system which will employ these components. Basing these simulations in part on experimental data from test circuits, we will modify circuit specifications as a function of simulated overall system performance.

For the single-chip sensor and processor part of the project, we will fabricate a working single-chip *image sensor and moment extractor* through MOSIS in the second year. Experimental data from testing and evaluating it will play a role in our development of a more general performance evaluation methodology for early vision systems.

Five-Year Goals: The work in this project is organized around two five-year goals. The first is development of a *single-chip motion sensor and analyzer* useful for robot navigation. Based on a new algorithm, it is a complex system using many of the circuits developed for the simpler image sensor and moment extractor.

The second goal is a *modular early vision system*: a relatively inexpensive, low-power, single-board system that will operate in real time. Its sensor arrays can be placed at the focal plane of a pair of lenses to acquire binocular image input directly from the environment. Its outputs will consist of the intensity field, velocity field, and depth map of the scene. Edge detector circuits will detect and enhance discontinuities in the individual fields.

The CCD imager, image memory, spatial correlator, and binomial convolver with edge detector circuits are key components in this system. Our current plans call for discrete- and continuous-time circuits with continuous voltage levels used to represent pixel values — only the edge detector outputs will be binary. This system will be of industrial value as a front-end processor for vision applications such as robot navigation and object recognition.

6.2.2 Progress in 1989

The National Science Foundation provided the initial funding for this project in September 1988; DuPont Corporation provided additional funding in December 1988.

The following describes our accomplishments in 1989:

- Mr. Craig Keast, working with Professor Charles Sodini, has designed, implemented and tested the additional process

steps that enable the MIT CMOS fabrication line to produce CMOS/CCD chips. We can now make 4-phase buried-channel CCDs.

- Mr. David Standley, working with Professors Berthold Horn and John Wyatt, has designed and tested a novel analog CMOS chip to determine the position and orientation of objects using linear and quadratic moments. The chip operates in continuous time on an optical image focused directly on its surface. A phototransistor array senses the image, processor cells transduce image intensity to current, and a uniform grid of resistors (connecting each processor to its four nearest neighbors) carries the currents to the edge of the array. The exciting feature of this design is that there is no need to address each processor separately — the resistive grid automatically conveys the required information to its periphery for further processing.
- Mr. Woodward Yang, working with Dr. Alice Chiang at Lincoln Laboratories and Professor Tomaso Poggio at MIT, has designed and begun testing a parallel, pipelined 2D CCD binomial convolver. This is a very high speed image bandpass filtering device useful in edge detection and a variety of vision applications.
- Resistive grid networks are frequently useful in parallel analog image processing operations on chips. Mr. Christopher Umminger, working with Professor Charles Sodini, has begun experimental work on switched capacitor networks as an alternative to resistor networks. The major advantages of switched capacitors are their smaller area and controllable effective resistance. Mr. Umminger has designed a switched-capacitor test chip to investigate this alternative method of fast image processing.
- Nonlinear resistors with incrementally active regions of operation are useful for image smoothing and segmentation tasks, but the design of small, accurate controllable circuits for this purpose remains a challenge. Mr. Steve Decker, working with Professors John Wyatt and

Charles Sodini, has created some promising designs for these circuits and will fabricate a test chip that requires custom processing available at MIT.

- As a person or robot moves through a fixed environment, most of the scene projected on the retina or focal plane appears to move as well. But the image of the point toward which the motion is directed, i.e., the eventual point of impact if the motion were to continue in a straight line, expands without moving. The image of this point in the focal plane is called the *focus of expansion*. The magnitude of the divergence of the velocity field at this point is known to be inversely related to the *time of impact*. Ignacio McQuirk, working with Professors Berthold Horn and John Wyatt, is simulating algorithms that will automatically locate the focus of expansion of a moving scene projected onto it. His simulation studies are aimed toward the design of an analog chip that will rapidly perform this computation.

Publications

- Harris, J., C. Koch, J. Luo, and J. Wyatt. "Resistive Fuses: Analog Hardware for Detecting Discontinuities in Early Vision." In *Analog VLSI Implementations of Neural Systems*, eds. C. Mead and M. Ismail, 27-56. New York: Kluwer, 1989.
- Hengeveld, J.A. *Smooth Surface Reconstruction in VLSI*. S.B. thesis. Dept. of Electr. Eng. and Comput. Sci., MIT, 1989.
- Horn, B.K.P., H.-S. Lee, T. Poggio, C. Sodini, and J. Wyatt. *The First Year of the MIT Vision Chip Project*. VLSI Memo No. 89-555. MIT, 1989.
- Keast C.L., P. Tedrow and C.G. Sodini. "A CCD/CMOS Process for Integrated Image Acquisition and Early Vision Signal Processing." Abstract presented at the VLSI Research Review, MIT, May 22, 1989.
- Keast, C.L. *A CCD/CMOS Process for Integrated Image Acquisition and Early Vision Signal Processing*. S.M. and E.E. thesis,

Dept. of Electr. Eng. and Comput. Sci., MIT, 1989.

Lumsdaine, A., J. Wyatt, Jr., and I. Elfadel. "Parallel Distributed Networks for Image Smoothing and Segmentation in Analog VLSI." Paper presented at the *Proceedings of the 28th IEEE Conference on Decision and Control*, Tampa, Florida, December 1989, pp. 272-279.

Lumsdaine, A., J. Wyatt, and I. Elfadel. "Parallel Distributed Networks for Image Smoothing and Segmentation in Analog VLSI." Abstract presented at the VLSI Research Review, MIT, December 18, 1989.

Standley, D.L., and J.L. Wyatt, Jr. "Stability Criterion for Lateral Inhibition and Related Networks that is Robust in the Presence of Integrated Circuit Parasitics." *IEEE Trans. Circuits Syst.* 36 (5):675-681 (1989).

Standley, D.L. "Design Criteria Extensions for Stable Lateral Inhibition Networks in the Presence of Circuit Parasitics." Paper presented at the *IEEE Symposium on Circuits and Systems*, Portland, Oregon, May 1989, pp. 837-840.

Standley, D.L. "Criteria for Robust Stability in a Class of Lateral Inhibition and Related Networks Coupled Through a Resistive Grid." *Proceedings of the 1989 Conference on Information Sciences and Systems*, Johns Hopkins University, Baltimore, Maryland, March 1989, pp.441-446.

Standley, D., and J.L. Wyatt, Jr. "Stability Criterion for Lateral Inhibition and Related Networks that is Robust in the Presence of Integrated Circuit Parasitics." Abstract presented at the VLSI Research Review, MIT, December 18, 1989.

Wyatt, J.L., Jr., and D.L. Standley. "Criteria for Robust Stability in a Class of Lateral Inhibition Networks Coupled Through Resistive Grids." *Neural Computation* 1 (1):58-67 (1989).

Yang, W. "A Charged-Coupled Device Architecture for On Focal Plane Image Signal Processing." *Proceedings of the International Symposium on VLSI Technology, Systems and Applications*. Taipei, Taiwan, R.O.C., May 1989, pp. 266-270.

Yang, W. "Method and Charge Coupled Apparatus for Algorithmic Computations." Patent application submitted to U.S. Patent Office on May 1, 1989, receipt number 07/352,765.

Yang, W., and A.M. Chiang. "VLSI Processor Architectures for Computer Vision," *Proceedings of the Image Understanding Workshop*. Palo Alto, CA, May 1989, pp. 193-199.

6.3 Techniques for Logic Synthesis, Testing and Design-for-Testability

Sponsors

U.S. Navy - Office of Naval Research
Contract N00014-87-K-0825

Project Staff

Professor Srinivas Devadas, Michael J. Bryan, Curtis S. Chen, Kevin Lam

This research focuses on the development of Computer-Aided Design (CAD) tools for integrated circuits with area, performance and reliability as design parameters.

To produce a highly reliable large-scale computer, it is vital for its hardware components to be individually reliable. It is essential to detect failures in VLSI components caused by defective manufacturing processes. Each component of a computer must be *tested* for correct functionality before assembly.

Test strategies must keep pace with increasing circuit complexity. Increased emphasis must be placed on finding a defect as early as possible in the manufacturing cycle, new algorithms must be devised to create tests for logic circuits, and more attention must be given to design-for-test techniques that require active participation by the logic designers.

Today's logic designer must work toward a multivariate objective — the designer must meet area, performance and technological constraints while also trying to ensure that the design is testable with a small set of patterns. Needless to say, it is almost impossible for the designer to find an optimal tradeoff of all these competing objectives for anything except the most simple circuits. For this reason, designers will often attempt to find a feasible design that meets performance and area goals and later modify the design to meet test requirements. Testing, even for combinational circuits, has been a post-design activity.

Current research focuses on automated logic synthesis and optimization strategies, targeting area and performance objectives. The logic restructuring steps used in the optimization of combinational and sequential circuits have a *very* profound affect on the testability of the eventual circuit. The purpose of our research is to *completely integrate reliability and testability considerations* into automated synthesis and optimization procedures instead of the "after-thought" post-design-for-test methodologies in vogue today. We believe that this integration can result in design of logic circuits which are not only optimal for area and performance, but also have *unprecedented levels of reliability, testability and diagnosability*.

Our work focuses on several critical areas which are elaborated on in the following sections.

6.3.1 Synthesis of Fault-Tolerant Designs

Use of static redundancy for system level fault-tolerance is an established practice. However, massive hardware redundancy introduced to mask faults can also prevent the detection of potential faults in the circuit

during manufacturing testing and system diagnostics. Therefore, a fault-tolerant circuit must be completely testable in terms of both original circuit function and fault masking capability.

For example, to ensure desired reliability, digital systems used in a deep-space probe must be tested for both correct functional operation as well as for the capability of the circuit to mask faults. If the fault masking capability allows the original circuit function to perform properly when faults are present, the fault-tolerant circuit may not be reliable during system operation. In other words, the next fault sustained by the system could exceed the threshold of the fault masking capability so that the circuit no longer performs the original logic function correctly. Therefore, complete testability of the original circuit function as well as the fault masking capability is necessary during manufacturing testing. We are currently developing synthesis techniques targeting circuit testability and diagnosability.¹²

6.3.2 Combinational Logic Synthesis for Testability

Combinational logic synthesis and optimization is a well-understood problem. The traditional cost functions used in synthesis are layout area and circuit performance. Researchers have only recently begun investigating the effect of logic transformations on single and multiple stuck-at fault testability of a circuit. This work concentrates on deriving algebraic and Boolean transformations for logic circuits to improve testability (and remove redundancy) with minimal or no impact on area and performance. Methods for *implicit* test generation, i.e., obtaining test vectors to detect stuck-at faults as a by-product of the optimization steps, are being investigated. These methods are potentially much more efficient than explicit test gener-

¹² S. Devadas, H-K.T. Ma, A.R. Newton, and A. Sangiovanni-Vincentelli, "Irredundant Sequential Machines Via Optimal Logic Synthesis," *IEEE Trans. Comput.-Aided Des.* 9 (1):8-18 (1990); S. Devadas and K. Keutzer, "Necessary and Sufficient Conditions for Robust Delay-Fault Testability of Logic Circuits," in the *Proceedings of the Sixth MIT Conference on Advanced Research on VLSI* (Cambridge: MIT Press, 1990).

ation algorithms, especially for multiple stuck-at faults and delay faults.¹³

6.3.3 Sequential Logic Synthesis for Testability

A digital computer can be viewed as a set of interacting finite state machine (FSM) controllers and datapath components. Test generation for large sequential circuits is recognized as a very difficult problem. We are studying this problem by using both synthesis-for-testability and explicit test generation techniques. We began preliminary investigations into the nature of the relationships between testability of interacting FSMs and the optimization steps used during FSM synthesis such as state minimization, decomposition, state assignment and combinational logic optimization.¹⁴

A "perfect" set of optimization steps can ensure that all stuck-at faults in the synthesized FSMs are testable. In reality, "perfect" optimization is difficult to attain. However, it appears feasible that highly testable control portions and test sequences that detect faults within these controllers can be obtained implicitly during synthesis with reasonable CPU time expenditure. We will use Register-Transfer (RT) level as well as State Transition Graph descriptions of sequential circuits as a starting point for these testability-driven synthesis approaches. We will also investigate

alternate representations that are more compact and/or easy to manipulate. This work can potentially reduce the area and performance overheads imposed by conventional design-for-testability schemes (e.g., LSSD) and dramatically reduce the time required to test the chip.

6.3.4 Test Generation for Sequential Circuits

Datapath components in a VLSI circuit have a large number of memory elements with a very regular structure. We are developing strategies based on our work¹⁵ that exploit the *specific topology* of a datapath component to efficiently generate tests for faults within the component. Exploiting design knowledge available in the register-transfer level specification of the component can dramatically speed up test generation.¹⁶

For example, one can use to advantage the knowledge that an arithmetic unit performing addition and subtraction is embedded in a datapath during the backward justification step in test generation. If one requires a set of binary values at the outputs of the adder, rather than justifying back across many logic gates in a gate-level description, one can simply find the different pairs of numbers that sum up to the given output of the adder (and justify the output at a higher level of abstraction).

¹³ S. Devadas and K. Keutzer, "Necessary and Sufficient Conditions for Robust Delay-Fault Testability of Logic Circuits," in the *Proceedings of the Sixth MIT Conference on Advanced Research on VLSI* (Cambridge: MIT Press, 1990).

¹⁴ S. Devadas, H-K.T. Ma, A.R. Newton, and A. Sangiovanni-Vincentelli, "Irredundant Sequential Machines Via Optimal Logic Synthesis," *IEEE Trans. Comput.-Aided Des.* 9 (1):8-18 (1990); S. Devadas and K. Keutzer, "A Unified Approach to the Synthesis of Fully Testable Sequential Machines," in the *Proceedings of the 23rd Hawaii Conference on System Sciences* (IEEE Computer Society Press, 1990); S. Devadas, "Delay Test Generation for Synchronous Sequential Circuits," in the *Proceedings of the International Test Conference* (Washington, DC: August 1989), 144-152.

¹⁵ A. Ghosh, S. Devadas, and A.R. Newton, "Test Generation for Highly Sequential Circuits," paper presented at the International Conference on Computer-Aided Design, Santa Clara, California, November 1989.

¹⁶ A. Ghosh, S. Devadas, and A.R. Newton, "Sequential Test Generation at the Register Transfer and Logic Levels," paper presented at the 27th Design Automation Conference, Orlando, Florida, June 1990.

6.3.5 Synthesis for Delay-Fault Testability

Physical defects in integrated circuits (ICs) can degrade performance without affecting logic functionality. It is important to ensure that a given IC satisfies its timing specifications — this requires that a *delay fault test* be performed. This is especially important for aggressive design methodologies that push processing technology to the utmost.

Unfortunately, most circuits being designed/synthesized today are typically difficult to test for delay faults. This is because the conditions for *robust* delay-fault testability are quite stringent, requiring the single sensitization of paths to ensure hazard-free error propagation. In this part of our research project, we concentrated on synthesis methodologies for completely and robustly delay-fault-testable combinational and sequential logic circuits, continuing our preliminary work.¹⁷ We found necessary and sufficient conditions for robust delay-fault testability of combinational circuits,¹³ and used these conditions as desirable requirements of synthesis procedures.¹⁸

6.3.6 Performance-Directed Logic Synthesis

To design high-performance computers, each of the processing elements constituting the computer is required to have minimal delay. Processing elements are comprised of combinational and sequential logic circuits. We are focusing on the automated, performance-directed optimization of logic functions with a view of synthesizing logic that is as fast as, if not faster than, implementations designed manually.

For purely combinational logic functions the Boolean and algebraic transformations in use today are mature and well-developed as far as minimizing for layout area is concerned. However, circuit delay, which depends on complex technological and topological considerations, proved to be a more difficult objective function. We recently proposed a form of logic optimization that we term four-level Boolean minimization.¹⁹ We are investigating a formal and elegant way of incorporating delay considerations into four-level Boolean minimization. This incorporation can result in a logic optimization strategy that exactly minimizes the delay of a logic function.

The optimization of interacting sequential circuits for area and performance has received very little attention. Optimizing for performance entails the redistribution or migration of logic across latch boundaries to minimize the required clock period. Classical retiming techniques cannot be used if the basic blocks forming the interconnection are finite state machines (FSMs), rather than being simply combinational. To address this problem, we developed automata-theoretic FSM decomposition strategies that *recompose* a set of interacting FSMs to minimize critical path delay.²⁰

Publications

Ashar, P., S. Devadas, and A.R. Newton. "Optimum and Heuristic Algorithms for Finite State Machine Decomposition and Partitioning." Paper presented at the International Conference on Computer-Aided Design, Santa Clara, California, November 1989.

¹⁷ S. Devadas, "Delay Test Generation for Synchronous Sequential Circuits," in *Proceedings of the International Test Conference* (Washington, DC: August 1989), 144-152.

¹⁸ S. Devadas and K. Keutzer, "Synthesis and Optimization Procedures for Delay-Fault Testable Combinational Logic," paper to be presented at the 27th Design Automation Conference, Orlando, Florida, June 1990.

¹⁹ S. Devadas and A.R. Newton, "Exact Algorithms for Output Encoding, State Assignment and Four-Level Boolean Minimization," *Proceedings of the 23rd Hawaii Conference on System Sciences*.

²⁰ K. Lam and S. Devadas, "Performance-Oriented Synthesis of Finite State Machines," paper presented at the International Conference on Circuits and Systems, New Orleans, May 1990.

- Ashar, P., S. Devadas, and A.R. Newton. "A Unified Approach to Decomposition and Re-Decomposition of Sequential Machines." Paper presented at the 27th Design Automation Conference, Orlando, Florida, June 1990.
- Ashar, P., S. Devadas, and A.R. Newton. "Multiple-Fault Testable Sequential Machines." Paper presented at the International Conference on Circuits and Systems, New Orleans, May 1990.
- Devadas, S. "Delay Test Generation for Synchronous Sequential Circuits." Paper presented at the International Test Conference, Washington, DC, August 1989.
- Devadas, S. "Minimization of Functions with Multiple-Valued Outputs: Theory and Applications." Paper presented at the 20th International Symposium on Multiple-Valued Logic, Charlotte, North Carolina, May 1990.
- Devadas, S. "Optimal Layout Via Boolean Satisfiability." Paper presented at the International Conference on Computer-Aided Design, Santa Clara, California, November 1989.
- Devadas, S. "Optimal Layout Via Boolean Satisfiability." *Int. J. Comput.-Aided VLSI Des.* Forthcoming.
- Devadas, S., and K. Keutzer. "A Unified Approach to the Synthesis of Fully Testable Sequential Machines." Paper presented at the 23rd International Conference on System Sciences, Hawaii, January 1990.
- Devadas, S., and K. Keutzer. "Synthesis and Optimization Procedures for Robust Delay-Fault Testability of Logic Circuits." Paper presented at the 27th Design Automation Conference, Orlando, Florida, June 1990.
- Devadas, S., K. Keutzer, and J. White. "Estimation of Power Dissipation in CMOS Combinational Circuits." Paper presented at the Custom Integrated Circuits Conference, Boston, May 1990.
- Devadas, S., H-K.T. Ma, A.R. Newton, and A. Sangiovanni-Vincentelli. "Irredundant Sequential Machines Via Optimal Logic Synthesis." Paper presented at the 23rd International Conference on System Sciences, Hawaii, January 1990.
- Devadas, S., H-K.T. Ma, A.R. Newton, and A. Sangiovanni-Vincentelli. "A Synthesis and Optimization Procedure for Fully and Easily Testable Sequential Machines." *IEEE Trans. Comput.-Aided Des.* 8 (10):1100-1107 (1989).
- Devadas, S., and A.R. Newton. "Exact Algorithms for Output Encoding, State Assignment and Four-Level Boolean Minimization." Paper presented at the 23rd International Conference on System Sciences, Hawaii, January 1990.
- Devadas, S., and K. Keutzer. "Logic Synthesis and Testability." *Proceedings of the International Conference on Circuits and Systems*, New Orleans, May 1990.
- Devadas, S., and K. Keutzer. "Validatable Nonrobust Delay-fault Testable Circuits Via Logic Synthesis." *Proceedings of the International Conference on Circuits and Systems*, New Orleans, May 1990.
- Devadas, S., H-K. T. Ma, and A.R. Newton. "Redundancies and Don't Cares in Sequential Logic Synthesis." Paper presented at the International Test Conference, Washington, DC, August 1989.
- Devadas, S., H-K. T. Ma, A.R. Newton, and A. Sangiovanni-Vincentelli. "The Relationship Between Logic Synthesis and Test." Paper presented at VLSI '89, Munich, August 1989.
- Devadas, S., and K. Keutzer. "Boolean Minimization and Algebraic Factorization Procedures for Fully Testable Sequential Machines." Paper presented at the International Conference on Computer-Aided Design, Santa Clara, California, November 1989.
- Devadas, S., and A.R. Newton. "Algorithms for Hardware Allocation in Datapath Syn-

thesis." *IEEE Trans. on Comput.-Aided Des.* 8(7):768-791 (1989).

Devadas, S., and A.R. Newton. "Decomposition and Factorization of Sequential Finite State Machines." *IEEE Trans. Comput.-Aided Des.* 8 (11):1206-1217 (1989).

Devadas, S., H-K.T. Ma, A.R. Newton, and A. Sangiovanni-Vincentelli. "Irredundant Sequential Machines Via Optimal Logic Synthesis." *IEEE Trans. Comput.-Aided Des.* 9 (1):8-18 (1990).

Devadas, S., and K. Keutzer. "Necessary and Sufficient Conditions for Robust Fault-Delay Testability of Combinational Logic Circuits." Paper presented at the *Sixth MIT Conference on Advanced Research in VLSI*, Cambridge, April 1990.

Devadas, S., and K. Keutzer. "A Unified Approach to the Synthesis of Fully Testable Sequential Machines." *IEEE Trans. Comput.-Aided Des.* Forthcoming.

Devadas, S., and A.R. Newton. "Exact Algorithms for Output Encoding, State Assignment and Four-Level Boolean Minimization." *IEEE Trans. Comput.-Aided Des.* Forthcoming.

Devadas, S., H-K.T. Ma and A.R. Newton. "Redundancies and Don't Cares in Sequential Logic Synthesis." *J. Electronic Testing: Theory and Appl.* 1:15-30 (1990).

Devadas, S., and H-K.T. Ma. "Easily Testable PLA-based Finite State Machines." *IEEE Trans. Comput.-Aided Des.* Forthcoming.

Ghosh, A., S. Devadas, and A.R. Newton. "Test Generation for Highly Sequential Circuits." Paper presented at the International Conference on Computer-Aided Design, Santa Clara, California, November 1989.

Ghosh, A., S. Devadas, and A.R. Newton. "Verification of Interacting Sequential Circuits." Paper presented at the 27th Design Automation Conference, Orlando, Florida, June 1990.

Ghosh, A., S. Devadas, and A.R. Newton. "Sequential Test Generation at the Register-Transfer and Logic Levels." Paper presented at the 27th Design Automation Conference, Orlando, Florida, June 1990.

Lam, K., and S. Devadas. "Performance-Oriented Synthesis of Finite State Machines." Paper presented at the International Conference on Circuits and Systems, New Orleans, May 1990.

6.4 Mixed Circuit/Device Simulation

Sponsors

International Business Machines Corporation
U.S. Navy - Office of Naval Research
Contract N00014-87-K-0825

Project Staff

Mark W. Reichelt, Professor Jacob White, Professor Jonathan Allen

For critical applications, the four-terminal lumped models for MOS devices used in programs such as SPICE are not sufficiently accurate. Also, using lumped models to relate circuit performance to process changes is difficult. We can perform sufficiently accurate transient simulations if instead of using a lumped model for each transistor, we compute some of the transistor terminal currents and charges by numerically solving the drift-diffusion based partial differential equation approximation for electron transport in the device. However, because accurate solution of the transport equations of an MOS device requires a two-dimensional mesh with more than a thousand points, simulating a circuit with even a few of the transistors treated by solving the drift-diffusion equations is very computationally expensive.

One way of accelerating mixed device and circuit simulation is with waveform relaxation, which performs the transient simulation, not only at the circuit level, but also inside the devices being simulated with a drift-diffusion description. In this investigation, we apply the waveform relaxation (WR) algorithm to the sparsely-connected system of algebraic and ordinary differential equations in time generated by standard spatial

discretization of the drift-diffusion equations that describe MOS devices. Two theoretical results indicate that the method will be effective. One result suggests that the WR algorithm will converge in a uniform manner independent of the time interval,²¹ and the other implies that the multirate integration will be stable.²²

In addition, in preliminary experiments, we have used waveform relaxation to perform transient two-dimensional simulation of MOS devices. Experiments demonstrate that WR converges in a uniform manner and that there is typically some multirate behavior in a device that the WR algorithm can exploit. Speed and accuracy comparisons between standard direct methods, red/black Gauss-Seidel WR and red/black overrelaxed WR, indicate that, for the experiments examined, calculated terminal currents match well between the methods and that overrelaxed WR was between two and five times faster than direct methods.²³ A recently implemented modification based on a waveform-Newton algorithm increased this from a factor of 5 to 11.²⁴

6.5 Circuit Simulation Algorithms for Specialized Applications

Sponsors

American Telephone and Telegraph
Analog Devices
Digital Equipment Corporation
International Business Machines Corporation
National Science Foundation

Grant MIP 88-58764
U.S. Navy - Office of Naval Research
Contract N00014-87-K-0825

Project Staff

Andrew Lumsdaine, Luis M. Silveira, Professor
Jacob White, Professor John L. Wyatt

For all practical purposes, the general circuit simulation problem has been solved. Given enough time, programs like SPICE or ASTAP are capable of simulating virtually any circuit. Unfortunately, for some types of circuits, "enough time" is too much time for simulation to be a practical part of a circuit design cycle. To obtain large performance increases over a program such as SPICE, one must exploit special properties of the specific problem to be solved. In particular, we are developing fast and accurate simulation algorithms for two application areas: (1) the simulation of clocked analog circuits like switching filters, switching power supplies, or phase-locked loops and (2) the simulation of analog signal processing circuits used for early vision.

The simulation of clocked analog circuits such as switching filters, switching power supplies, and phase-locked loops poses a challenging problem. These circuits are computationally expensive to simulate using conventional techniques because they are all clocked at a frequency with a period orders of magnitude smaller than the time interval of interest to the designer. To construct such a long time solution, a program such as SPICE or ASTAP must calculate the behavior of the circuit for many high frequency clock cycles. The basic approach to making simulation of

²¹ M. Reichelt, J. White, J. Allen and F. Odeh, "Waveform Relaxation Applied to Transient Device Simulation," paper presented at the International Symposium on Circuits and Systems, Espoo, Finland, June 1988.

²² M. Crow, J. White and M. Ilic, "Stability and Convergence Aspects of Waveform Relaxation Applied to Power System Simulation," in *Proceedings of the International Symposium on Circuits and Systems*, Portland, Oregon, May 1989.

²³ M. Reichelt and J. White, "Techniques for Switching Power Converter Simulation," invited paper presented at the NASECODE Conference, Dublin, Ireland, June 1989.

²⁴ M. Reichelt, J. White and J. Allen, "Waveform Relaxation for Transient Simulation of Two-Dimensional MOS Devices," paper published the *Proceedings of the International Conference Computer-Aided Design*, Santa Clara, California, October 1989; R. Saleh, J. White, A. S. Vincentelli, A. R. Newton, "Accelerating Relaxation Algorithms for Circuit Simulation Using Waveform-Newton and Step-Size Refinement," *IEEE Trans. Comput.-Aided Des.* (October 1990), forthcoming.

these circuits more efficient is to exploit only the property that the behavior of such a circuit in a given high frequency clock cycle is similar to, but not identical to, the behavior in the preceding and following cycles. Therefore, by accurately computing the solution over a few selected cycles, an accurate long time solution can be constructed.

Simulating clocked analog systems is an old problem, but this novel approach has led to a very efficient algorithm for the distortion analysis of switched-capacitor filters. The idea is based on simulating selected cycles of the high-frequency clock accurately with a standard discretization method and pasting together the selected cycles by computing the low frequency behavior with a truncated Fourier series. If carefully constructed, the nonlinear system that must be solved for the Fourier coefficients is almost linear, and can be solved rapidly with Newton's method.²⁵ Transient behavior, important for switching power supply designers, was also accelerated using similar techniques.²⁶ In particular, the "envelope" of the high-frequency clock can be followed by accurately computing the circuit behavior over occasional cycles.

The "vision circuits" form a class of circuits which, for the most part, cannot be simulated with traditional programs. These circuits are necessarily very large and must be simulated exactly at an analog level (i.e., one cannot perform simulations at a switch or gate level as is commonly done with very large digital circuits). Typical analog circuit simulators are not able to handle vision circuits simply because of their immense size — the computation time for these simulators grows super-linearly with the size of the circuit. However, because these circuits are somewhat similar

to certain discretized partial differential equations, one can exploit their special characteristics to obtain efficient simulation techniques.

During the past year, we completed the development of Simlab, an extensible circuit simulation program constructed to facilitate algorithm development for circuit simulation.²⁷ After adding vision simulation extensions to Simlab, we used the program to investigate the behavior of a class of nonlinear smoothing and segmentation networks. In addition, we added several conjugate-gradient based matrix solution algorithms to Simlab, testing their performance on resistive grid and vision circuits. Finally, we are investigating what we hope will be a novel and very general extension to the algebraic multigrid algorithm suitable for vision circuit simulation.

6.6 Numerical Simulation of Short Channel MOS Devices

Sponsors

Analog Devices
U.S. Navy - Office of Naval Research
Contract N00014-87-K-0825

Project Staff

Jennifer A. Lloyd, Joel R. Phillips, Khalid Rahmat, Professor Dimitri A. Antoniadis, Professor Jacob White

The model used in conventional device simulation programs is based on the drift-diffusion model of electron transport, but this model does not accurately predict the field distribution near the drain in small geometry

²⁵ K. Kundert, J. White, and A. Sangiovanni-Vincentelli, "A Mixed Frequency-Time Approach for Finding the Steady State Solution of Clocked Analog Circuits," paper presented at the Custom Integrated Circuits Conference, Rochester, New York, May 1988; K. Kundert and J. White, A. Sangiovanni-Vincentelli, "A Mixed Frequency-Time Approach for Distortion Analysis of Switched Capacitor Filters," *IEEE J. Solid State Circuits* 24 (2):? (1989).

²⁶ K. Kundert and J. White, A. Sangiovanni-Vincentelli, "An Envelope-Following Method for the Efficient Transient Simulation of Switching Power Converters," paper published in the *Proceedings of the International Conference on Computer-Aided Design*, Santa Clara, California, October 1988; M. Reichelt and J. White, "Techniques for Switching Power Converter Simulation," invited paper presented at the NASECODE Conference, Dublin, Ireland, June 1989.

²⁷ A. Lumsdaine, L. Silveira and J. White, "Simlab Users Guide," *MIT VLSI Memo*, September 1989; A. Lumsdaine, L. Silveira and J. White, "Simlab Programmers Guide," *MIT VLSI Memo*, September 1989.

devices. This is particularly important for predicting oxide breakdown due to penetration by "hot" electrons. There are two approaches for more accurately computing the electric fields in MOS devices: the first is based on adding an energy equation to the drift-diffusion model and the second on particle or Monte-Carlo simulations.

In the first approach, an energy balance equation is solved along with the drift-diffusion equations so that the electron temperatures are computed accurately. This combined system, which is numerically less tame than the standard approach, must be solved carefully. We have developed a 2-D simulator for MOS devices based on the drift-diffusion plus energy equations, uncovering a source of instability in the computation. The instability occurs when the semiconductor mobility is made a function of the inverse of carrier temperature. Using a very fine mesh removes this instability, but makes this method computationally expensive. Currently, we are trying to understand the cause of the instability so that we can use a coarse mesh and still produce accurate results.

In the area of Monte Carlo device simulation, we are focusing on transient calculations with self-consistent electric fields. Specifically, we are trying to apply the recently developed implicit particle methods to semiconductors by decomposing the field calculation into a part due to charged particles, a part due to dopant ions, and a part due to boundaries. This allows us to calculate the electric field acting on every charged particle in the system rapidly and accurately. Specifically, we are able to use the fast multipole algorithm for the particle-particle interactions. After rewriting (with J. Phillips) a Silicon Monte Carlo code from the National Center for Computational Electronics for use with ensemble Monte Carlo methods, we are now including the electric field calculations.

6.7 Efficient Capacitance Extraction Algorithms

Sponsors

International Business Machines Corporation
U.S. Navy - Office of Naval Research
Contract N00014-87-K-0825

Project Staff

Keith S. Nabors, Professor Jacob White

To achieve the dense packing of processors and memory required for high performance parallel computers, we must design interconnection aggressively. It is not possible to achieve high interconnect wire density by following commonly used conservative design rules for avoiding unintended coupling between wires. However, to assure some degree of reliable data transfer, we must examine signal corruption due to interconnect coupling. Extracting an equivalent resistor-capacitor-inductor (RLC) circuit for the interconnect is an effective approach that lends insight into the effects of coupling. However, this parasitic extraction calculation is computationally expensive because it implies solving electrostatic and magneto-static equations in three space dimensions.

We developed and tested a fast algorithm for computing the capacitance of a complicated 3-D geometry of ideal conductors in a uniform dielectric.²⁸ The method is an acceleration of the standard integral equation approach for multiconductor capacitance extraction. These integral equation methods are slow because they lead to dense matrix problems typically solved with some form of Gaussian elimination. This implies the computation grows like n^3 , where n is the number of tiles needed to accurately discretize the conductor surface charges. We developed a preconditioned conjugate-gradient iterative algorithm with a multipole approximation to compute the iterates. This reduces the complexity of the multiconductor capacitance calculations to grow as nm where m is the number of conductors. Recently, we began to improve the imple-

²⁸ K. Nabors and J. White, "A Fast Multipole Algorithm for Capacitance Extraction of Complex 3-D Geometries," in *Proceedings of the Custom Integrated Circuits Conference*, San Diego, California, May 1989.

mentation of the capacitance calculation algorithm. Specifically, we developed a faster code which includes a novel adaptive multipole algorithm. In the future, our work in this area will be to include dielectric interfaces in the development of a multipole algorithm to accelerate the calculation of inductances.

6.8 Parallel Numerical Algorithms

Sponsors

U.S. Navy - Office of Naval Research
Contract N00014-87-K-0825

Project Staff

Andrew Lumsdaine, Mark W. Reichelt, Luis M. Silveira, Ricardo Telichevsky, Professor Jacob White

We are trying to develop parallel algorithms for circuit and device simulation that are effective on either massively parallel machines similar to the Connection Machine, or on hypercube machines like the Intel hypercube. In addition, we are also trying to understand the fundamental problem involved in developing these algorithms by investigating the interaction between architecture and certain numerical algorithms (with Professor William J. Dally).

The key problem in parallelizing many of the numerical algorithms used in circuit and device simulators is finding efficient techniques for solving large sparse linear systems in parallel. Most parallel matrix solution algorithms fall into one of two general categories: the direct (Gaussian-elimination based) and the iterative; each algorithm presents different problems. The computation in the direct approach is not very structured, and is, therefore, difficult to parallelize. Iterative methods are easily parallelized, but are not as numerically robust.

The direct solution of circuit simulation matrices is particularly difficult to parallelize. Methods such as parallel nested dissection are ineffective because finding good separators is difficult. For that reason, we are studying general sparse matrix techniques and, specifically, the interaction between sparse matrix data structures, computer memory structure, and multiprocessor communication (with Professor Dally). The most interesting results from simulations so far is that communication throughput, and not latency, is more crucial to final performance.

As mentioned above, relaxation algorithms for solving matrices are easily parallelized. It is also possible to apply relaxation directly to the differential equations, a method referred to as waveform relaxation (WR), to develop a parallel algorithm in which different differential equations are solved on different processors. A recently developed variant of the WR algorithm, referred to as waveform-relaxation Newton (WRN), allows for additional parallelism. Much of the computation for each of the discretization timepoints for a single differential equation can be computed in parallel. This method may be appropriate for massively parallel computers. In recent theoretical work, we proved that WRN converges globally even when applied to circuits with nonlinear capacitors.²⁹ We also successfully applied WRN to device simulation. Currently, we are implementing a WR-based device simulation program on an Intel hypercube.

6.9 Integrated Circuit Reliability

Sponsors

Digital Equipment Corporation
U.S. Navy - Office of Naval Research
Contract N00014-87-K-0825

Project Staff

Professor Srinivas Devadas, Professor Jacob White

²⁹ R. Saleh, J. White, A. S. Vincentelli, A. R. Newton, "Accelerating Relaxation Algorithms for Circuit Simulation Using Waveform-Newton and Step-Size Refinement," *IEEE Trans. Comput.-Aided Des. (October 1990)*, forthcoming.

The high transistor density now possible with CMOS integrated circuits makes peak power dissipation and peak current density important design considerations. However, because peak quantities in a logic circuit are usually a function of the input vector or vector sequence applied, accurate estimation of peak quantities is extremely difficult. The number of input sequences that must be simulated to find the sequence that produces the peak is *exponential* in the number of inputs to the circuit. By using simplified models of power and current dissipation, we can relate peak quantities such as power or current density to maximizing gate output activity, weighted to account for differing load capacitances or transistor sizes. Then, we can

derive transformations that convert a logic description of a circuit into a multiple-output Boolean function of the input vector or vector sequence in which each output of the Boolean function is associated with a logic gate output transition. Next, we must solve a *weighted max-satisfiability* problem to find the input or input sequence that maximizes the quantity of interest. For solving the problem of estimating peak power dissipation, we derived algorithms for constructing the Boolean function for dynamic CMOS circuits, as well as for static CMOS, which take into account dissipation due to glitching. Lastly, we developed exact and approximate algorithms for solving the associated weighted max-satisfiability problem.³⁰

³⁰ S. Devadas, K. Keutzer, J. White, "Estimation of Power Dissipation in CMOS Combinational Circuits," in *Proceedings of the Custom Integrated Circuits Conference*, Boston, 1990.

Chapter 7. Neurophysiology and Neural Computation

Academic and Research Staff

Professor Jerome Y. Lettvin

Graduate Students

Arthur C. Grant, Gill A. Pratt, Robert J. Webster, Jr.

7.1 Abstracts of Doctoral Dissertations

The following are abstracts of dissertations submitted to the Department of Applied Biological Sciences in partial fulfillment of the requirements for the Degree of Doctor of Philosophy in Applied Biological Sciences.

7.1.1 The Nature of Electrical Transients Recorded in the Neuropil of the Frog's Optic Tectum

Arthur C. Grant

Abstract

An investigation was made of those transients evoked in the neuropil of the frog, *Rana pipiens*, by excitation of retinal ganglion cell types 1 and 2. Both visual stimulation, and electrical stimulation in the optic nerve and nucleus isthmi, were used to generate responses in the tectal neuropil. These responses were recorded with low impedance, metal-filled, extracellular micro-electrodes.

Unlike their component single unit receptive fields, which are circular or slightly oval, multiunit receptive fields (MURFs) recorded in the tectal neuropil have a definite anisotropy. The MURFs are oval and often tapered, the long axis being typically about three times the length of the short axis. Each MURF has an internal tripartite structure. This structure is defined by the shape of electrical transient, evoked in the neuropil, by visual stimulation within each of the MURFs three adjacent "unit type" receptive fields. The three transient shapes can be described as follows. One is of relatively low ampli-

tude. It has a small initial positive phase followed by a markedly asymmetric negative phase, whose rise is more rapid than its fall. The second unit type is diphasic with a large initial positive phase followed by a large negative phase. In addition to their tripartite structure, MURFs are oriented in space so as to define a "visual pole," the type C unit RF farthest away.

Only the type A units are thought to be generated by the afferent fiber terminal arborizations. Type B and C transients are shown to be generated postsynaptically by active dendritic structures, presumed to be the dendritic appendages of large pear-shaped tectal neurons, as described by Székely and Lázár (1976). The type B units are presumed to be recorded by an electrode within the appendage, while the type C units are presumed recorded from an active segment of apical dendrite at the level where the appendage branches off. These dendritic appendages, under stereo viewing of Rapid-Gogi impregnations, appear to have a local anisotropy, which is consonant with MURF structure and orientation as found physiologically.

There is a many many connection between the terminal bushes of the unmyelinated fibers, and the dendritic appendage bead structures postsynaptic to them. This many many connectivity between terminal twigs and receiving structures is responsible for the high synaptic efficiency of the unmyelinated fibers, which successfully excite the postsynaptic structures at rates up to 90/sec.

The appendages of adjacent apical dendrites are synaptically connected among themselves. This synaptic interconnectivity of the dendritic clusters is mirrored in the complex but repeatable waveforms termed "patterned

units." Finally, the large single triphasic spikes most commonly used by physiologists as representing optic nerve activity are often demonstrably composite of several smaller synchronously firing transients.

Our conclusions are that a significant amount of processing occurs in the tectal neuropil before any cellular action is invoked, and that this processing has several important possible uses.

7.1.2 Pulse Computation

Gill A. Pratt

Abstract

This thesis considers the design of a computer that represents information with impulses instead of the usual binary signals. In such a machine, computation is effected through the fine grained interaction of continuously timed impulses arriving at the inputs of simple elements with finite life memory. The impulses themselves are atomic events, individually indistinguishable from one another. Thus, unlike binary symbols, the "meaning" of any impulse is given entirely by its context in place and time.

We begin with a look at pulse computation in animal nervous systems, demonstrating how fine grained impulse computation can, and most likely is, put to use by nature. Some compelling evidence in conflict with the traditional activity based (frequency modulated) view of nerve cell coding will be presented, and the important role of conduction block as a computational process explored.

Because of the brain's incredible connectivity and the microscopic scale of its circuitry, modern neuroscience enjoys no lack of conflicting, non-disprovable theories about neural coding and computation. To elevate the theory of fine grained pulse computation from this morass, the evidence presented from nature will be followed by the constructive approach of demonstrative design. Given hard constraints on the characteristics of a basic device, we will address the task of

designing efficient pulse circuits that implement useful functions. Methods for simulating, programming, and evaluating the performance of pulse circuits will be described.

The encoding of large dimensional input spaces into single fiber temporal rhythms is a major conjecture of the natural pulse computation theory, and we conclude with an automatic method for teaching artificial pulse systems to solve specific problems in single fiber rhythmic feature classification.

7.2 Abstract of Masters Thesis

The following is an abstract of a thesis submitted to the Department of Electrical Engineering and Computer Science in partial fulfillment of the requirements for the Degree of Master of Science in Electrical Engineering.

7.2.1 An Interactive Environment for the Investigation of Pulsed Neural Networks

Robert C. Webster, Jr.

Abstract

Pulsed neural networks provide the opportunity for a man-made system to perform computation using circuit elements that are only sensitive to the time intervals between pulses rather than the occurrence of the pulses as events. A software system is described that allows easy manipulation of simulated neurons in order to understand the patterns that evolve. Time series of pulses are applied at the input and the processing results in time series of pulses along "axons" between nodes. The user is able to monitor the travel of pulses from node to node, and to note visually the patterns that develop from the processing. All of the system parameters, such as the weight of connection and the delay of transmission along the axon, can be changed and monitored from within the environment. Full control over placement of the nodes and connections on the graphics field is also provided.

Part IV Language, Speech and Hearing

Section 1 Speech Communication

Section 2 Sensory Communication

Section 3 Auditory Physiology

Section 4 Linguistics

Section 1 Speech Communication

Chapter 1 Speech Communication

Chapter 1. Speech Communication

Academic and Research Staff

Professor Kenneth N. Stevens, Professor Jonathan Allen, Professor Morris Halle, Professor Samuel J. Keyser, Dr. Corine A. Bickley, Dr. Suzanne E. Boyce, Dr. Carol Y. Espy-Wilson, Seth M. Hall, Dr. Marie K. Huffman, Dr. Sharon Y. Manuel, Dr. Melanie L. Matthies, Dr. Joseph S. Perkell, Dr. Mark A. Randolph, Dr. Carol Chapin Ringo, Dr. Stefanie R. Shattuck-Hufnagel, Dr. Mario A. Svirsky, Dr. Victor W. Zue

Visiting Scientists and Research Affiliates

Giulia Arman-Nassi,¹ Dr. Harvey R. Gilbert,² Dr. Richard S. Goldhor,³ Dr. Robert E. Hillman,⁴ Dr. Jeannette D. Hoit,⁵ Eva B. Holmberg,⁶ Jacques Koreman,⁷ Dr. Harlan L. Lane,⁸ Dr. John L. Locke,⁹ Dr. John I. Makhoul,¹⁰ Aniruddha Sen,¹¹ Dr. Victor N. Sorokin,¹² Dr. Arend Sulter,¹³ Dr. Noriko Suzuki,¹⁴ Jane W. Webster¹⁵

Graduate Students

Abeer A. Alwan, Marilyn Y. Chen, A. William Howitt, Caroline B. Huang, Lorin F. Wilde

Undergraduate Students

Anita Rajan, Lorraine Sandford, Veena Trehan

Technical and Support Staff

Ann F. Forestell, Laura B. Glicksman, Sandra I. Lugo, D. Keith North

¹ Milan Research Consortium, Milan, Italy.

² Pennsylvania State University.

³ Sensimetrics Corporation.

⁴ Boston University.

⁵ Department of Speech and Hearing Sciences, University of Arizona.

⁶ MIT and Department of Speech Disorders, Boston University.

⁷ University of Nijmegen, The Netherlands.

⁸ Department of Psychology, Northeastern University.

⁹ Massachusetts General Hospital.

¹⁰ Bolt Beranek and Newman, Inc.

¹¹ Tata Institute of Fundamental Research, Bombay.

¹² Institute of Information Transmission Problems, Moscow.

¹³ University of Groningen, The Netherlands.

¹⁴ First Department of Oral Surgery, School of Dentistry, Showa University, Tokyo.

¹⁵ Massachusetts Eye and Ear Infirmary.

1.1 Introduction

Sponsors

C.J. Lebel Fellowship
Dennis Klatt Memorial Fund
Digital Equipment Corporation
National Institutes of Health
Grants T32 DC00005, R01 DC00075, F32
DC00015, S15 NS28048, R01 NS21183,¹⁶ P01
NS23734¹⁷, T32 NS 07040
National Science Foundation
Grant IRI 88-05680¹⁸

The overall objective of our research in speech communication is to gain an understanding of the processes whereby (1) a speaker transforms a discrete linguistic representation of an utterance into an acoustic signal, and (2) a listener decodes the acoustic signal to retrieve the linguistic representation. The research includes development of models for speech production, speech perception, and lexical access, as well as studies of impaired speech communication.

1.2 Studies of the Acoustics, Production and Perception of Speech Sounds

1.2.1 Vowels

Although vowels often show a great deal of variability, humans can identify them well enough to be able to communicate through speech. The present study continues work (performed here and at other laboratories) to improve the understanding of (1) factors that cause the variability of vowels and (2) the perceptual effects of this variability.

The effects of consonant context, lexical stress, and speech style (e.g., carrier phrase, continuous read, or spontaneous) on vowels have been investigated in a number of pre-

vious acoustic studies. However, those studies of consonant context and lexical stress involved only isolated words or words in a carrier phrase, and the studies of continuous speech did not consider each consonant context separately. In the present study, formant frequencies are measured in vowels taken from a read story which is well-controlled with respect to consonant context and lexical stress. The vowel set was chosen to illustrate the feature distinctions high/non-high (/i/-/e/, /I/-/ε/), front-back (/ε/-/Λ/), and tense-lax (/i/-/I/, /e/-/ε/). The consonant contexts were chosen to include liquids and glides (/w/, /r/, and /l/) and stops (/b/, /d/, /g/). Liquids and glides have been found to have a stronger effect on adjacent vowels than stops, presumably because liquids and glides constrain the tongue body more than stops (with the possible exception of /g/). The vowels in the corpus carry primary or secondary lexical stress. The same vowels and contexts are elicited in spontaneous speech and in non-sense words spoken in a carrier phrase. In total, the database consists of approximately 1700 vowel tokens from four speakers. Vowels from each speaker are analyzed separately.

Preliminary results indicate that consonant context has a greater effect on vowel formant frequencies at the midpoint than lexical stress or speech style. For example, the tokens /I/ from the syllables /bIt/ and /wIt/, both taken from a carrier phrase, tend to differ more than two tokens of /wIt/, one taken from a carrier phrase and one from spontaneous speech. Of the factors considered in this study, consonant context is the most important for understanding the variation found in non-reduced vowels. This result is especially relevant now for speech synthesis and speech recognition systems, which are moving from read speech to more spontaneous styles.

Future work will follow several directions. The interaction of the factors consonant

¹⁶ Under subcontract to Boston University.

¹⁷ Under subcontract to Massachusetts Eye and Ear Infirmary.

context, lexical stress, and speech style will be quantified. The formant trajectory throughout the duration of the vowel, not only the midpoint value, will be examined. Also, the vowels will be presented to listeners for identification to determine if the measured differences in the vowel tokens are perceptually relevant. The listeners' ability to identify these tokens will be compared to the performance of statistical classifiers on the same tokens.

1.2.2 Nasal Consonants and Vowel Nasalization

A nasal sound is produced when the nasal cavities are coupled to the oral cavity by movement of the velum (soft palate). For some speech sounds (e.g., /m/, /n/), this coupling is a requirement; for others, coupling occurs due to phonetic context — the vowel in *bean* is nasalized because nasal coupling occurs on the vowel in anticipation of the nasal sound *n*. We are carrying out a detailed analysis of this contextual, anticipatory nasalization.

In one study, the central task involves tracking changes in nasalization over time, by comparing spectral properties of nasalized vowels with those of oral counterparts (e.g., the vowels in *bean* and *bead*). Spectral analysis is used to identify differences in harmonic amplitudes between the nasalized vowels and the oral vowels. Additional poles due to nasal coupling will increase harmonic amplitudes of nasal vowels relative to oral vowels; additional zeroes have the opposite effect.

Our results indicate that in such nasalized vowels, additional energy appears fairly consistently in the range of 600–1000 Hz; the additional pole which is thus indicated moves up through this frequency range as the velopharyngeal port opens and the mouth closes for the approaching nasal consonant. Since acoustic theory predicts addition of a pole-zero pair(s) to the spectrum of the vowel, we also want to identify the presence and behavior of the zero. Because this is not easily done with spectral data, analysis-by-synthesis is used to clarify the contribution of the nasal zero to the spectral characteristics of the nasalized vowels.

One goal of this work is to provide measures of nasalization which give reliable information about changes in velopharyngeal opening, without the invasiveness characteristic of physiological studies. The methods used here are particularly useful for determining changes in nasalization over time. Understanding when velum movement begins for production of nasal speech sounds, and the time course it follows, is an essential part of characterizing motor planning for speech. An important additional benefit of this work should be improved synthesis of contextually nasalized vowels. Studies in progress will use synthesized speech to investigate the role of various acoustic factors in the perception of nasalization.

A second study of nasalization has examined the acoustics, synthesis and perception of vowels in a nasal consonant context (e.g., /mam/) and in a nonnasal context (e.g., /bab/), with emphasis being placed on the acoustic attributes around the midpoints of the vowels. There was considerable variability in the acoustic data, but one reasonably consistent result was that the spectrum amplitude of the first formant for the vowel in relation to the amplitude of the first harmonic was less for the nasal context than for the nonnasal context. This property is presumably due, at least in part, to the increased acoustic losses with nasal coupling, causing a widening of F1. In one of the perception experiments, judgments of nasality were obtained with synthetic vowels whose spectra were manipulated to match those of naturally spoken vowels. The data showed that use of a pole-zero pair to synthesize a matching vowel yielded reasonably consistent nasality judgments, but that attempts to match vowel spectra without using a pole-zero pair failed to produce vowels that were judged to be nasal.

In addition to the experimental studies of vowel nasalization in the context of nasal consonants in English, we have attempted to refine existing theoretical treatments of the acoustics of vowels produced with coupling to the nasal cavity. Particular attention was given to the effect of the combined output from the nose and the mouth on the locations of the principal low-frequency

pole-zero pair that is contributed by the nasal coupling. For reasonable areas of the velopharyngeal opening, the predicted frequency of the additional pole is in the range of 750–900 Hz, and of this pole causes a peak with an amplitude that is up to 13 dB above the spectrum amplitude for the corresponding nonnasal vowel.

1.2.3 Analysis, Modeling, and Synthesis of Fricative Consonants

Data on airflow and intraoral and subglottal pressure have been collected for voiced and voiceless fricatives in intervocalic position. From these data, estimates have been made of the time course of the turbulence noise sources at the supraglottal and glottal constrictions. Reasonable agreement was obtained between the time-varying acoustic spectra of the fricatives calculated from these sources and the spectra actually observed in the sound. Based on these analyses, new strategies for the synthesis of fricative consonants are being developed. These strategies are focusing particularly on the time variation of the frication, aspiration, and voicing sources at the boundaries between the fricative consonant and the adjacent vowels.

1.2.4 Influence of Selected Acoustic Cues on the Perception of /l/ and /w/

Although the sounds /l/ and /w/ are articulated quite differently, they are acoustically quite similar. In a recognition system we have developed, /l/ and /w/ were frequently confused, especially when they occurred intervocalically. In the present study, we are attempting to refine some of the acoustic properties used to distinguish between these sounds by investigating the perceptual importance of some of the cues used in the recognition system, as well as some others which appear to be salient.

An [ala]-[awa] continuum was synthesized. The starting point was an easily identifiable [ala] stimulus. Three factors were varied

orthogonally to shift the percept towards [awa]. First, the rate of change in the formant transitions between the semivowel and following vowel was varied in five steps from 20 msec to 60 msec. Second, the rate of change in the amplitudes of F3, F4 and F5 between the semivowel and following vowel was varied in five steps so that the amplitude of the spectral peaks in the higher frequencies could change as slowly as 10 dB in 60 ms or as fast as 10 dB in 20 ms. Finally, the spectral shape of the consonant could contain either prominent peaks above F2 (coronal shape) or little energy in the higher frequencies (labial shape). All combinations of the parameters were synthesized, yielding a total of 50 stimuli, and stimuli were presented in a test to listeners who gave a forced choice response of /l/ or /w/.

Results of the identification tests show that the rate of change of the formant transitions is an important cue. Stimuli with formant transitions of 30 ms or less are heard as [ala]. As the durations of formant transitions are increased above 30 ms, the perception moves towards [awa]. Spectral shape also greatly influences which consonant is heard. In general, for each formant transition duration, more of the stimuli synthesized with a labial spectral shape are heard as [awa]. However, there were two types of responses. Regardless of the rate of formant transitions between the consonant and following vowel, one set of listeners could not hear [awa] unless the consonant was synthesized with a labial spectral shape. On the other hand, regardless of the spectral shape, the response of another set of listeners moved from [ala] to [awa] as the formant transitions became more gradual.

The effect on the listeners' responses of the rate of change in the amplitude of F3, F4 and F5 between the consonant and following vowel was negligible. However, since this abrupt change in amplitude of some high frequency spectral prominence between an /l/ and a following vowel (as much as 20 dB in 10 ms) has been observed systematically in natural speech, we plan to investigate the perceptual importance of this cue more carefully.

1.2.5 Acoustic Theory of Liquid Consonants

As a part of our systematic study of different classes of speech sounds, we have been attempting to develop a theory of sound production for the liquid consonants /r/ and /l/. A distinguishing attribute of these consonants appears to be that the acoustic path from the glottis to the mouth opening consists of at least two channels of different lengths, and possibly includes a side branch. The side branch is under the tongue blade for /r/ and between the tongue blade and the palate for /l/. A consequence of these configurations is a transfer function that includes a zero and an additional pole in the frequency range below about 4 kHz. When the consonant is released into a vowel, the zero and the pole ultimately cancel. Acoustic data appear to support this analysis.

1.2.6 The Consonant /h/ and Aspiration Noise

The consonant /h/ in English is unique in that its primary articulation is at the glottis, and it apparently lacks an invariant configuration (the oral gestures accompanying /h/ seem to be due almost entirely to surrounding phones). We have been studying acoustic phenomena related to /h/ to get a better understanding of how it behaves and to improve synthesis of it. We have used a common measure of breathy voice, that is, the difference in amplitudes of the first two harmonics (H1-H2), to characterize changes in the glottal spectrum as speakers move into and out of an /h/. Across speakers, we find consistent H1-H2 changes associated with /h/ of about 10 dB, in spite of large individual differences in absolute H1-H2. We have also examined the characteristics of the turbulence noise that is generated during /h/. In addition to a source of noise near the glottis, we find evidence for noise generation at points in the upper vocal tract, particularly adjacent to high vowels when the oral tract is relatively constricted. The measured spectrum of the radiated sound for /h/ is in reasonable agreement with the spectrum calculated from theories of turbulence noise generation.

1.2.7 Modeling of Vocal-Fold Vibration

A computer model of the interaction between vocal-fold vibration and vocal-tract configuration has been implemented; this model is useful in analyzing interactions between the vocal tract and the glottal source. The model includes two-mass representations of the vocal folds and an open or closed vocal tract. In many ways, the behavior of the model is consistent with measurements of vocal-fold vibration and inferences of vibratory characteristics which are based on acoustic observations. The model generates periodic glottal pulses when the vocal tract is unconstricted, if a sufficient pressure drop across the glottis exists, and if the vocal folds are appropriately positioned. For the cases of modal and "breathy" voicing, there is good agreement between many characteristics of the behavior of the model and measurements of speech. The results of the model also seem reasonable in cases in which voicing is inhibited, such as a reduction in the transglottal pressure and changes in the glottal configuration. When the vocal-tract load is changed, the model also produces the expected behavior. In the case of a closed vocal tract, the model shows a decay in vocal-fold vibration within a time interval of 2-3 glottal pulses, and the vocal folds come to rest with the upper fold more abducted than the lower.

1.2.8 Perception of Some Constant Contrasts in Noise

The goals of this study are: first, to examine perceptual confusions of place of articulation of some consonants when these consonants are heard in noise; and second, to use the results of the masking theory of the human auditory system in predicting when these confusions occur.

In order to determine whether the results of masking theory (which were established primarily for simple tones) could be applied to formant frequencies of vowels, two psycho-physical experiments were conducted. In the first one, a 1-kHz tone was used; in the second, a synthetic vowel with only one formant frequency. The formant frequency of

the vowel was the same as that of the tone, i.e., 1 kHz. The levels of both the tone and the one-formant sound were the same, as was the duration of both the tone and the vowel. The masker in these experiments was white noise. Results of the experiment show that both the tone and the synthetic vowel were masked at about the same noise level.

The second series of experiments consisted of perceptual experiments using natural /Ca/ syllables spoken by one male speaker where the consonant C was one of the four consonants /b/, /d/, /m/, or /n/. The utterances were then degraded by adding various levels of white noise and presented to subjects in identification experiments. Preliminary results show that the thresholds where confusions in place of articulation occur can, indeed, be estimated with a high degree of accuracy from masking theory. Future work includes conducting more psychophysical experiments using different vowels and extending the stimuli to include synthetic consonant-vowel syllables for better control of the different parameters of the speech signal.

1.3 Studies and Models of the Perception and Production of Syllables, Words, and Sentences

1.3.1 Distinctive Features and Lexical Access

A model of lexical access has been proposed in which acoustic correlates of distinctive features are identified in the speech signal prior to lexical access. These acoustic properties are identified by a two-stage process: first, the locations of acoustic landmarks or events are determined; and second, additional acoustic properties are extracted by examining the signal in the vicinity of these landmarks. As a first step in implementing automatic procedures for extracting these properties, we are hand-labeling some speech data according to a specified inventory of landmarks and properties that bear a rather direct relation to distinctive features. A system for facilitating this hand-labeling

has been developed to permit the observer to examine, with any degree of detail, the waveform and successive spectra in the vicinity of specified landmarks in the signal. These labeled data will be used as a basis for evaluating automatic algorithms for extracting the relevant properties.

1.3.2 Syllable-Based Constraints on Properties of English Sounds

The objective of this research is to develop a phonological representation and corresponding rule framework for modeling constraints on an utterance's acoustic-phonetic pattern. The primitives of our descriptive framework are distinctive features, which characterize an utterance's underlying surface-phonemic representation. An associated set of acoustic properties comprise an utterance's acoustic description. At present, rules for relating these two domains of representation are based on the syllable. Specifically, constraints on patterns that comprise the acoustic representation of an utterance are stated as conditions on the realization of well-formed syllables; an immediate constituent grammar is assumed for representing syllable structure at the surface-phonemic level. Thus far, our efforts have been directed towards two lines of investigation: (1) providing empirical justification for the use of the syllable in the current feature-based representational framework, and (2) developing a formal model of lexical representation and lexical access incorporating syllable-based constraints.

It has been argued by linguists that the syllable provides the basis for effectively describing the phonotactics of English. The syllable is also viewed as providing an appropriate domain of application for a wide range of rules of segmental phonology. We have developed statistical methods for testing these two claims. In addition, we have performed experiments for evaluating the possible role of syllabic constraints during word recognition. For example, binary regression trees have been used to quantify the extent to which knowledge of a segment's position within the syllable, in conjunction with other contextual factors, aids in the prediction of its acoustic realization. The principle of Maximum Mutual Information is used in con-

structuring trees. The principle of mutual information is also used in quantifying collocational constraints within the syllable. We have performed a hierarchical cluster analysis in order to determine an appropriate immediate constituent structure for describing syllable internal organization. Finally, a model of lexical access has been proposed based on the notion of constraint satisfaction. Constraints, stated primarily in terms of the syllable, are applied to an utterance's acoustic description in order to derive a partial phonemic specification of an utterance in which features are arranged in columns and assigned to the terminal positions of the syllable's internal structure. In this partial phonemic specification, selected constituents of the syllable are left unspecified for their feature content. Partitions of a 5500-syllable lexicon have been constructed and evaluated to determine which constituents within the syllable are most informative in identifying word candidates.

In the study examining the role of syllable structure in predicting allophonic variation, we evaluated a database of approximately 12,000 stop consonants obtained from the TIMIT database. We found that a stop's syllable position is the single most important factor in explaining the variation in its acoustic realization. Furthermore, we have found interesting interactions between acoustic-phonetic constraints and constraints on an utterance's phonemic representation. For example, a stop consonant is almost certain to be released when placed in the syllable-onset position, whereas in the syllable coda, a stop tends to be unreleased. A syllable-coda stop may also exhibit a number of other phonetic variants (e.g., released, glottalized, deleted, etc.). Given that place-of-articulation and voicing features are well represented for released stops, the latter result suggests the syllable coda to be a less reliable source of phonetic information than the syllable onset. In agreement with this finding, results from lexical partitioning experiments suggest that the coda is the least informative of the syllable's constituents in terms of providing information regarding the lexical identity of the syllable.

The results of our experiments suggest that linguistic information is conveyed in the signal in a highly constrained and redundant

manner. We are currently developing a formal model of lexical representation capable of exploiting this redundancy. Concurrent with the development of this model, we are also extending the above experiments, as well as exploring parsing methods capable of implementing the emerging framework for word recognition.

1.3.3 Temporal Spreading of the Feature Retroflex

We are investigating some of the domains in which we expect a significant influence of /r/ on neighboring sounds. In particular, we are looking at the effects of speaker, speaking rate and phonetic context on the spreading of the feature retroflex.

In an earlier acoustic study, we observed that postvocalic /r/s are often merged with preceding vowels, especially in words where the /r/ is followed by a syllable-final consonants such as in "cartwheel." In comparison with spectrograms of the word "car" where there are two distinct time periods for the /a/ and /r/, spectrograms of "cartwheel" show one vocalic region for these sounds which appears to be an r-colored /a/. In addition, we observed that in words like "everyday" ([ɛvrɪdeɪ]), retroflexion from the /r/ often spreads across the preceding labial consonant (/v/) to the end of the vowel (/ɛ/). The spreading of retroflexion is evidenced by the lowering of the third formant F3.

In the present study, we recorded several speakers saying the minimal pair words "car," "cart," "card," "carve," and "carp" at a slow and a more casual speaking rate. We also recorded the speakers saying minimal pair sentences which contained various combinations of a vowel, one or more /r/s, and one or more labial consonants.

Preliminary results suggest that spreading of the feature retroflex occurs mainly when the talkers are speaking casually. Merging of postvocalic /r/s and preceding vowels does not always occur when the /r/ is followed by a syllable-final consonant, even when the utterance is spoken at a casual speaking rate. The feature retroflex can spread across one or two labial consonants into the preceding

vowel, although most of the vowel is unaffected, and F3 is lowered only in the last two or three pitch periods. The labial consonants, on the other hand, can be considerably affected by retroflexion. For example, in a sentence which contains the sequence /vwɜ/, the /v/ and /w/ are merged into one consonant and they have a lower F3 than the following /ɜ/.

1.3.4 Speech Production Planning

Work has continued on experiments eliciting error evidence to evaluate a frame-and-insert model of serial ordering for speech production. A task involving sentence generation from target words is being used to extend results from read-aloud tongue twisters, showing that (1) word onsets are more susceptible to segmental interaction errors than are stressed-syllable onsets located in word-medial position, suggesting a word-based representation at the point where such errors occur; and (2) word-final segments are protected against interaction errors in phrases but not in lists of words, suggesting a different planning framework for grammatically- and prosodically-structured utterances.

1.3.5 Prosodic Prominence and Stress Shift

Work has continued on acoustic and perceptual measures of the change in prosodic prominence called "stress shift" (e.g., in the word "thirteen," the syllable "thir-" is perceived as more prominent than the main-stress syllable "-teen" when the word is combined in the phrase "thirteen men"). Perceptual judgments by both phonetically sophisticated and unsophisticated listeners show that stress is perceived to shift; acoustic measures suggest little or no increase in fundamental frequency (F0) or in duration. Both of these results are consistent with a model in which perceived stress shift results from the disappearance of the pitch accent from the main stress syllable of the target word.

1.3.6 Analysis and Synthesis of Prosody

During the first year of this new project we have collected most of our speech database, and have demonstrated that prosodic patterns are effective at disambiguating certain types of structural ambiguity.

Prosody Database

We have collected an extensive database of speech from six speakers using the FM radio newscaster style, with the cooperation of WBUR radio at Boston University. Both in-studio newscasts and laboratory recordings of experimental utterances have been obtained. Several hours of speech have been transcribed orthographically, and much of it digitized. A prosodic transcription system has been developed for labeling the parts of speech, word stress patterns, and intonation units of the utterances; we are working on a labeling system for phrase-level prominences.

Prosodic Disambiguation

Many pairs of sentences in English consisting of the same string of words and segments differ strikingly in their structure and, thus, in their interpretation. For example, "The men won over their enemies" might mean that the men persuaded their opponents to their point of view, or that the men vanquished their foes. By providing contrasting preceding contexts, we obtained two spoken versions for each of 30 such sentences, ascertained by listening that the prosody of each was appropriate to the preceding context, and then asked listeners which preceding context was the appropriate one for each version. Results demonstrate conclusively that prosodic differences can lead to appropriate structural interpretations of phonologically identical sentences. We are currently developing a transformation algorithm that will allow us to impose the durations and F0 patterns of one version onto the phonetic shape of the other, providing a stronger test of the hypothesis that prosodic differences alone are responsible for the difference in interpretation by listeners.

1.4 Basic Speech Physiology

1.4.1 Timing of Upper Lip Protrusion Gestures for the Vowel /u/

Timing of upper lip protrusion gestures and accompanying acoustic events was examined for multiple repetitions of word pairs such as "lee coot" and "leaked coot" for four speakers of American English. The duration of the intervocalic consonant string was manipulated by using various combinations of /s,t,k,h,#/. Data from one of the speakers formed a bimodal distribution which made them difficult to analyze. For the other three subjects, pairwise comparisons and other analyses were made of times of: acoustic /i/ offset to acoustic /u/ onset (consonant string duration), protrusion onset to acoustic /u/ onset (onset interval), maximum acceleration to acoustic /u/ onset (acceleration interval), and acoustic /u/ onset to protrusion offset (offset interval). In spite of considerable token-to-token and cross-speaker variation, several general observations were made: There were some consonant-specific effects, primarily for /s/. The non-s subset evidenced two patterns: (1) The lip protrusion gesture for /u/ had a relatively invariant duration, but its timing varied with respect to the oral consonant gesture complex: the longer the consonant string, the earlier the lip protrusion gesture, or (2) The protrusion gesture duration correlated positively with consonant duration. In the predominating pattern 1, the slope of the timing relationship between oral and labial gestures differed across subjects.

1.4.2 Kinematics of Upper Lip Protrusion Gestures for the Vowel /u/ at Normal and Fast Speaking Rates

Acoustic events were identified manually and kinematic events were identified algorithmically on the lip-protrusion versus time signal for one of the above four subjects, using a program developed for this purpose. In addition to the parameters examined in the

previous analysis, peak velocity and peak acceleration for the lip protrusion gestures were included in pairwise correlations and comparisons. As anticipated, peak velocity and peak acceleration of the lip protrusion gesture for /u/ correlated with one another and with movement distance. Consistent with the timing results (above), peak velocity and acceleration were not correlated with duration of the consonant string preceding the /u/. This result, in combination with overall gesture timing that correlated with consonant string duration (pattern 1 from the previous analysis), was found in the fast speech of this subject as well as in his normal rate speech. Most parameters differed significantly between the two rate conditions in expected ways. Higher average values of peak velocity and peak acceleration in the fast condition agreed with results of others which suggest that movement kinematics are adjusted as part of the mechanism for speaking at different rates.

1.4.3 Articulatory Movement Transduction: Hardware and Software Development

Our alternating magnetic field system for transducing articulatory movements has been recalibrated after making several changes in the electronics to reduce field strength and improve electrical safety. The performance of the system with the revised electronics was initially somewhat degraded; considerable effort was expended in restoring performance to an acceptable level. New single-axis transducers have been received, and tests are being conducted on the system's performance in simultaneously tracking multiple receivers while recording an acoustic signal. An interactive, menu-driven computer program has been implemented for the display and initial analysis of data from the movement transducer. The program simultaneously displays time-synchronized acoustic and multi-channel displacement data, and generates x-y plots of the displacement data over selected time intervals. It also allows for audition of the acoustic signal and a number of other useful data-analysis functions.

1.5 Speech Production of Cochlear Implant Patients

1.5.1 Speech Breathing in Cochlear Implant Patients

A study has been completed of the effects on speech breathing of postlingual profound-to-total deafness and of the reintroduction of auditory stimulation, including some self-hearing. Three postlingually deafened adults read passages before and after receiving stimulation from a cochlear prosthesis while changes in their respiratory volumes were transduced and recorded. (The schedule of eight to ten recordings of each subject covers a period two years; it is complete for two of the three subjects.) All subjects read initially with abnormal average airflow and volume of air expended per syllable. These two parameters changed significantly in the direction of normalcy following the onset of stimulation.

1.5.2 Work in Progress

We have begun an experiment on the short-term changes in speech breathing and speech acoustics caused by brief periods of auditory stimulation and its interruption within a single session. The subjects are two of the three from the previous experiment.

A program has been completed for the efficient measurement of fundamental frequency, vowel formants and harmonic amplitudes from the acoustic signal, and open quotient from the electroglottographic signal. The resulting data will allow us to explore several areas of potential acoustic phonetic abnormalities and to correlate those data with the associated changes in speech breathing.

Longitudinal recordings of speech samples pre- and post-implant and signal processing of those recordings continue. In a later stage, measures from a pneumotachometer and from a nasal accelerometer will be integrated with the respiratory and acoustic measures with the aim of clarifying the role of audition and the effects of its loss on adult speech elaboration.

1.6 Phonatory Function Associated with Misuse of the Vocal Mechanism

1.6.1 Studies in Progress

Complete sets of subject recordings have been obtained, and data extraction is nearly complete for the following studies:

(a) Intra-subject variation in glottal airflow, transglottal pressure, and acoustic and electroglottographic measurements for normal male and female speakers. We have made three recordings each of three normal male and female speakers (with at least one week between each repeated recording). Results from this study will begin to provide important information concerning the reliability of our measurements. Such information is critical to evaluating the utility (sensitivity) of these measurements for the clinical assessment of vocal pathology.

(b) Relationships between glottal airflow and electroglottographic measurements for female speakers in soft, normal and loud voice. Recordings have been obtained for twelve normal females. Results from this study will represent the first group-based information concerning relationships between glottal airflow and electroglottographic measures of vocal function.

(c) Phonatory function associated with vocal nodules in females. Recordings have been obtained for a group of twelve females with vocal nodules, and for twelve sex- and age-matched normal subjects serving as a control group. These data will enable the first group-based statistical tests for significant differences in our measures between normal vocal function and hyperfunctionally-related vocal pathology. The results of this study will be used to identify those measures which differentiate hyperfunctional (adducted) from normal voice. Five of these subjects have also been recorded following therapy. Comparisons of their pre- versus post-therapy data will provide information about the efficacy of the therapeutic techniques.

(d) Changes in phonatory function associated with spontaneous recovery from functional dysphonia: A case study. We have

obtained repeated recordings of a female subject who initially displayed functional dysphonia and then (approximately one year later) appeared to spontaneously recover normal voice. Results of this study will enable us to identify those measures which differentiate hyperfunctional (non-adducted) from normal voice.

1.6.2 Development of Facilities and Methodological Refinements

Signal processing has been refined, and an interactive, menu-driven analysis program has been developed for extraction of aerodynamic, electroglottographic and acoustic measures on a new engineering workstation that was installed last year. With the new software, we can measure additional parameters (relative harmonic amplitudes, adduction quotients from electroglottographic and flow waveforms). Extensive use of command procedures and algorithmic data extraction has greatly increased the ease and efficiency with which signals are processed and analyzed.

We have decided to eliminate the measure of vocal-fold adduction that is obtained from the first derivative of the electroglottographic (EGG) waveform. The first derivative of the EGG is often too weak and noisy (particularly for female voices and for males in the soft voice condition) to reliably locate the

points on the signal that are needed to obtain the adduction measure. We still obtain two more reliable estimates of vocal-fold adduction, one from the undifferentiated EGG signal and another from the inverse filtered flow signal (i.e., the glottal airflow waveform).

1.7 Computer Facilities

Our Vax 11/750, which was used for analysis and synthesis of acoustic signals, has been replaced with a Local Area VaxCluster consisting of five engineering workstations received through a grant from the Digital Equipment Corporation. Four of the workstations have hardware for real-time A/D and D/A; the analysis and synthesis software developed by Dennis Klatt has been ported to run on these machines (with the help of colleagues in the Linguistics Department, University of Texas). The new "speech" cluster is on the same DECNet network as our previously-described physiology cluster, allowing for the effortless interchange of data and shared printing and backup functions. An 8-mm tape backup system has been added, with dual porting for access by both clusters. An erasable optical disk subsystem has been added to the physiology cluster, providing for storage and rapid access of large signal files.

Section 2 Sensory Communication

Chapter 1 Auditory Psychophysics and Aids for the Deaf

Chapter 1. Auditory Psychophysics and Aids for the Deaf

Academic and Research Staff

Dr. Joan Besing, Professor Louis D. Braida, Dr. Rachel K. Clifton, Dr. H. Steven Colburn, Lorraine A. Delhorne, Nathaniel I. Durlach, Richard Freyman, Dr. Kenneth W. Grant, Seth M. Hall, Dr. Janet D. Koehnke, Dr. Neil A. Macmillan, Dr. Xiao Dong Pang, Dr. Karen Payton, Dr. Patrick M. Peterson, Dr. William M. Rabinowitz, Christine Rankovic, Dr. Charlotte M. Reed, Dr. Bruce Schneider, Dr. Mandayam A. Srinivasan, Dr. Rosalie M. Uchanski, Dr. Victor W. Zue, Dr. Patrick M. Zurek

Graduate Students

Paul Duchnowski, Ellen M. Eide, Joseph A. Frisbie, Julie Greenberg, Douglas H. Henderson, Yoshiko Ito, Wolfgang G. Knecht, J. William Maney, Matthew H. Power, Rebecca J. Renn, Barbara Shinn-Cunningham, Tali J. Tamir, Derrick Yim, Jenny S. Yu, Hong Z. Tan, Marc A. Zissman

Technical and Support Staff

Eleanora M. Luongo

1.1 Introduction

Research is being conducted on a variety of topics concerned with the auditory and tactile senses, particularly with a view to the development of improved aids for the deaf. Supporting grants are listed below. Detailed progress reports are available from principal investigators listed and granting agencies. Publications and talks reporting this work follow the project listing.

1.2 Binaural Hearing

Sponsor

National Institutes of Health
Grant 2 R01 NS10916

Principal Investigator

Dr. H. Steven Colburn

1.3 Hearing Aid Research

Sponsor

National Institutes of Health
Grant 5 R01 NS12846

Principal Investigator

Professor Louis D. Braida

1.4 Tactile Communication of Speech

Sponsor

National Institutes of Health
Grant 5 R01 NS14092

Principal Investigator

Dr. Charlotte M. Reed

1.5 Multimicrophone Hearing Aids

Sponsor

National Institutes of Health
Grant 2 R01 NS21322

Principal Investigator

Dr. Patrick M. Zurek

1.6 Cochlear Prostheses

Sponsor

National Institutes of Health
Grant 1 P01 NS23734

Principal Investigator

Dr. William M. Rabinowitz

1.7 Hand Function

Sponsor

National Science Foundation
Grant DMC 83-32460

Principal Investigator

Nathaniel I. Durlach

Publications

- Clifton, R.K., P.M. Zurek, B.G. Shinn-Cunningham, and N.I. Durlach. "Cross-Frequency Interactions in the Precedence Effect." *J. Acoust. Soc. Am.* 85:S83 (1989).
- Duchnowski, P., and P.M. Zurek. "Simulation of Sensorineural Hearing Loss." *J. Acoust. Soc. Am.* 85:S26 (1989).
- Duchnowski, P. *Simulation of Sensorineural Hearing Impairment*. S.M. thesis. Dept. of Electr. Eng. and Comput. Sci., MIT, 1989.
- Durlach, N.I., L.A. Delhorne, A. Wong, W.Y. Ko, W.M. Rabinowitz, and J. Hollerbach. "Manual Discrimination and Identification of Length by the Finger-Span Method." *Percept. Psychophys.* 46:29-38 (1989).
- Durlach, N.I., C.E. Sherrick, and J.D. Miller. "Sensory Substitution: Visual and Tactual Methods." in *Speech Communication Aids for the Hearing Impaired: Current Status and Needed Research*. Report of CHABA Working Group 95. Eds. C.S. Watson, R.A. Dobie, N.I. Durlach, H. Levitt, J.D. Miller, C.E. Sherrick, F.B. Simmons, G.A. Studebaker, R.S. Tyler, and Widin, forthcoming.
- Durlach, N.I., H.Z. Tan, N.A. Macmillan, W.M. Rabinowitz, and L.D. Braida. "Resolution in One Dimension with Random Variations in Background Dimensions." *Percept. Psychophys.* 46:293-296 (1989).
- Eide, E.M. *Extracting Stimulus and Response Center Locations from Confusion Matrices*. S.M. thesis. Dept. of Electr. Eng. and Comput. Sci., MIT, 1989.
- Greenberg, J.E. *A Real-Time Adaptive Beamforming Hearing Aid*. S.M. thesis. Dept. of Electr. Eng. and Comput. Sci., MIT, 1989.
- Greenberg, J.E., and P.M. Zurek. "Evaluation of a Real-Time Adaptive Beamforming Hearing Aid." *J. Acoust. Soc. Am.* 86:S87 (1989).
- Greenberg, J.E., P.M. Zurek, and P.M. Peterson. "Reducing the Effects of Target Misalignment in an Adaptive Beamformer for Hearing Aids." *J. Acoust. Soc. Am.* 85:S26 (1989).
- Henderson, D.R. *Tactile Speech Reception: Development and Evaluation of an Improved Synthetic Tadoma System*. S.M. thesis. Dept. of Electr. Eng. and Comput. Sci., MIT, 1989.
- Maney, J.W. *Token Variability of Intra-Speaker Speech*. S.B. thesis. Dept. of Electr. Eng. and Comput. Sci., MIT, 1989.
- Payton, K., R. Uchanski, and L.D. Braida. "Speech Intelligibility as a Function of Environment and Speaking Style." *J. Acoust. Soc. Am.* 85:S55 (1989).
- Picheny, M.A., N.I. Durlach, and L.D. Braida. "Speaking Clearly for the Hard of Hearing III: An Attempt to Determine the Contribution of Speaking Rate to Differences in Intelligibility between Clear and Conversational Speech." *J. Speech Hear. Res.* 32:600-603 (1989).
- Reed, C.M., N.I. Durlach, and L.D. Braida. "Analytic Study of the Tadoma Method: Effects of Hand Position on Segmental

- Speech Perception." *J. Speech Hear. Res.* 32:921-929 (1989).
- Reed, C.M., N.I. Durlach, L.D. Delhorne, W.M. Rabinowitz, and K.W. Grant. "Research on Tactual Communication of Speech: Ideas, Issues, and Findings." *The Volta Rev.* 91:65-78 (1989). (Special Monograph on Sensory Aids for Hearing-Impaired People. Ed. N.S. McGarr.)
- Schneider, B.A., and P.M. Zurek. "Lateralization of Coherent and Incoherent Targets Added to a Diotic Background." *J. Acoust. Soc. Am.* 85:1756-1763 (1989).
- Shinn-Cunningham, B.G. *Understanding the Precedence Effect: An Examination of Parameters Affecting Its Strength*. S.M. thesis. Dept. of Electr. Eng. and Comput. Sci., MIT, 1989.
- Tamir, T.J. *Characterization of the Speech of Tadoma Users*. S.B. thesis. Dept. of Electr. Eng. and Comput. Sci., MIT, 1989.
- Tan, H.Z., W.M. Rabinowitz, and N.I. Durlach. "Analysis of a Synthetic Tadoma System as a Multidimensional Tactile Display." *J. Acoust. Soc. Am.* 86:981-988 (1989).
- Zissman, M.A. *Co-channel Talker Interference Suppression*. Ph.D. diss. Dept. of Electr. Eng. and Comput. Sci., MIT, 1989.
- Zissman, M.A., C.J. Weinstein, L.D. Braida, R.M. Uchanski, and W.M. Rabinowitz. "Speech State Adaptive Simulation of Co-channel Talker Interference Suppression." ICASSP '89, pp. 361-364.
- Zurek, P.M. "Binaural Advantages and Directional Effects in Speech Intelligibility," In *Acoustical Factors Affecting Hearing Aid Performance II*, eds. G.A. Studebaker and I. Hochberg. Boston: College-Hill Press, forthcoming.

Section 3 Auditory Physiology

Chapter 1 Signal Transmission in the Auditory System

Chapter 1. Signal Transmission in the Auditory System

Academic and Research Staff

Professor Lawrence S. Frishkopf, Professor Nelson Y.S. Kiang, Professor William T. Peake, Professor William M. Siebert, Professor Thomas F. Weiss, Dr. Robin L. Davis, Dr. Bertrand Delgutte, Dr. Donald K. Eddington, Dr. Dennis M. Freeman, Dr. Barbara Fullerton, Dr. Miriam Furst, Dr. Jill C. Gardner, Dr. John J. Guinan, Jr., Dr. James B. Kobler, Dr. Robert A. Levine, Dr. Xiao Dong Pang, Dr. William M. Rabinowitz, Dr. John J. Rosowski, Dr. Sylvette R. Vacher, Patricia A. Cuneo

Visiting Scientists and Research Affiliates

Dr. Jay T. Rubenstein, Debra S. Louison, Frank J. Stefanov-Wagner, David A. Steffens

Graduate Students

Kathleen M. Donahue, Farzad Ehsani, Donna K. Hendrix, Michael P. McCue, Jennifer R. Melcher, Michael E. Ravicz, Jenny S. Yu

Technical and Support Staff

Susan M. Ross

1.1 Introduction

Sponsors

National Institutes of Health

Grants 5 T32 NS07047, 5 P01 NS13126, 8 R01 DC00194, 5 R01 NS25995, 8 R01 DC00238, 5 R01 NS20322, 5 R01 DC00235, 5 R01 NS20269, 1 P01 NS23734

Johnson and Johnson Foundation

Unisys Corporation Doctoral Fellowship

Research on the auditory system is carried out in cooperation with two laboratories at the Massachusetts Eye and Ear Infirmary (MEEI). Investigations of signal transmission in the auditory system involve the Eaton-Peabody Laboratory for Auditory Physiology. Our long-term objective is to determine the anatomical structures and physiological mechanisms that underlie vertebrate hearing and to apply that knowledge to clinical problems. Studies of cochlear implants in humans are carried out at the MEEI Cochlear Implant Laboratory. The ultimate goal of

these devices is to provide speech communication for the deaf through electric stimulation of intracochlear electrodes to elicit patterns of auditory nerve fiber activity that the brain can learn to interpret.

1.2 Signal Transmission in the External- and Middle-Ear

1.2.1 Structure-Function Relationships in Middle Ears

Project Staff

Professor William T. Peake, Dr. John J. Rosowski, Michael E. Ravicz

In cooperation with scientists at the Harvard Museum of Comparative Zoology, we have written two manuscripts which analyze the ear structures of a 200 million year old fossil, *Morganucodon*, considered by some to be the earliest known mammal. The first manu-

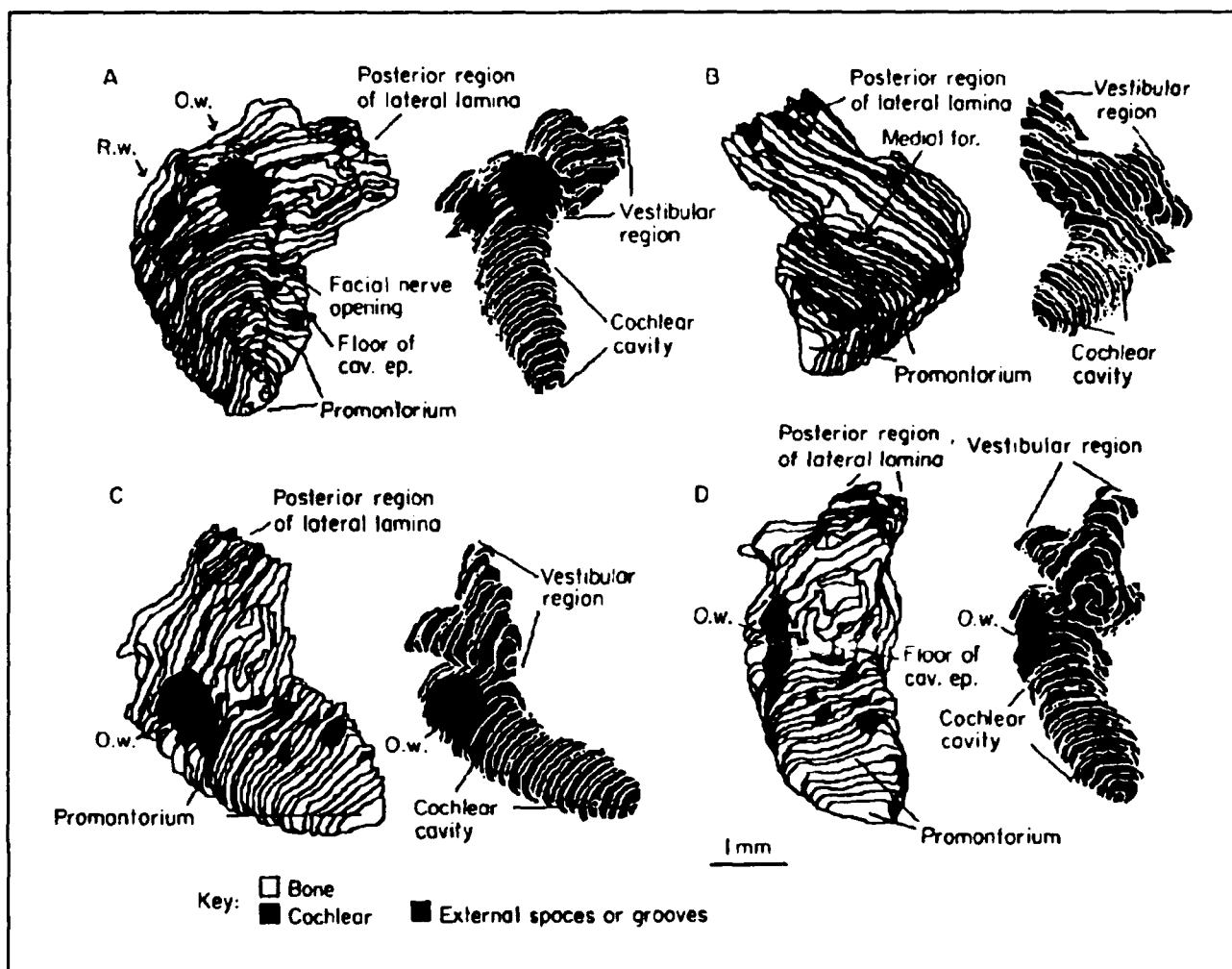


Figure 1. Reconstructions of the right inner ear of *Morganucodon* in four views. A, ventrolateral; B, anteromedial; C, lateral, and D, dorsoanterior. Each quadrant A-D shows two reconstructions: the left is a simultaneous reconstruction of the bone, cochlear cavity and the external spaces or grooves; the right is a reconstruction of the cochlear cavity. The side-by-side representation of the two types of reconstructions shows how the cochlear cavity is oriented within the bone. (Abbreviations: o.w. = oval window; r.w. = round window; cav. ep. = cavum epiptericum) After Graybeal et al., 1989.

script¹ describes the boney structure of the auditory inner-ear in this beast (see figure 1). The second manuscript² analyzes the middle-ear structures in this early mammal and suggests that its hearing was similar to that observed in modern mice and shrews.

This year, Michael Ravicz submitted his master's thesis to the Boston University Department of Bio-Medical Engineering describing the measurements of the impedance of the middle and external ears of gerbils.³ The results indicate that the size of the gerbil auditory structures plays a role in defining

¹ A. Graybeal, J.J. Rosowski, D.R. Ketten, and A.W. Crompton, "The Inner-Ear Structure of *Morganucodon*, An Early Jurassic Mammal," *Zool. J. Linn. Soc.* 96: 107-117 (1989).

² J.J. Rosowski and A. Graybeal, "What Did *Morganucodon* Hear?" submitted to *Zool. J. Linn. Soc.*

³ M.E. Ravicz, *The Acoustic Impedance of the Gerbil Ear*, S.M. thesis, Dept. of Bio-Med. Eng., Boston University, 1990.

these impedances; smaller ear dimensions result in larger acoustic impedances. Another significant finding is that small diameter ear canals place large restrictions on the power available to the ear.

We also participated in several scientific conferences. Talks detailing the action of the middle-ear cavities in cat and human⁴ along with a simple model for auditory nonlinearities observed in the alligator lizard⁵ were presented at the conference celebrating the sixtieth birthday of Professor Nelson Kiang. Manuscripts of these talks are being prepared for publication. Dr. Rosowski was also invited to address the November Symposium on Noise-Induced Hearing Loss organized by the Committee on Hearing, Bioacoustics and Biomechanics of the National Research Council. This presentation reviewed work on the flow of sound power through the external and middle ear and argued that the external and middle ear play a large role in defining the strength of noxious acoustic stimuli. A manuscript describing this work has been submitted for publication.⁶

1.2.2 External and Middle Ears

Project Staff

Professor William T. Peake, Dr. John J. Rosowski, Kathleen M. Donahue

Our work on development of a cadaver model for study of the human middle ear was presented to the American Otological Society (San Francisco, April 4, 1989), and a companion manuscript accepted for publication.⁷ This paper noted that measurements of the

middle-ear input impedance in cadaver ears are indistinguishable from similar measurements made in living subjects. The cadaver-ear preparation was used in a series of experiments by Kathleen Donahue to describe the motion of the human malleus.⁸ The results indicate that at frequencies below the middle-ear "resonant" frequency, the malleus rotates about a fixed axis. At higher frequencies, the measurements suggest that the malleus motion is more complex and perhaps dependent on the load of the ossicular chain.

Publications

Donahue, K.M. *Human Middle-Ear Malleal Motion: Models and Measurements*. S.M. thesis. Dept. of Elec. Eng. and Comput. Sci., MIT, 1989.

Graybeal, A., J.J. Rosowski, D.R. Ketten, and A.W. Crompton. "The Inner-Ear Structure of *Morganucodon*, an Early Jurassic Mammal." *Zool. J. Linn. Soc.* 96: 107-117 (1989).

Peake, W.T., J.J. Rosowski and T.J. Lynch III. "The Cat's Middle Ear: Measurements, Models and Predictions." Paper presented at the Symposium in Honor of N.Y.S. Kiang, Dedham, Massachusetts, July 5-7, 1989.

Ravicz, M.E. *The Acoustic Impedance of the Gerbil Ear*. S.M. thesis. Dept. of Bio-Med. Eng., Boston University, 1990.

Rosowski, J.J. "The Effects of External- and Middle-Ear Filtering on Auditory Thres-

⁴ W.T. Peake, J.J. Rosowski, and T.J. Lynch III, "The Cat's Middle Ear: Measurements, Models and Predictions," paper presented at the Symposium in Honor of N.Y.S. Kiang, Dedham, Massachusetts, July 5-7, 1989.

⁵ J.J. Rosowski, W.T. Peake and N. Yang, "A Simple Model for Level-dependent Growth Rates of Auditory Distortion," paper presented at the Symposium in Honor of N.Y.S. Kiang, Dedham, Massachusetts, July 5-7, 1989.

⁶ J.J. Rosowski, "The Effects of External- and Middle-Ear Filtering on Auditory Threshold and Noise-induced Hearing Loss," submitted to *J. Acoust. Soc. Am.*

⁷ J.J. Rosowski, P.J. Davis, S.N. Merchant, K.M. Donahue, and M.D. Coltrera, "Cadaver Middle-Ears as Models for Living Ears: Comparisons of Middle-Ear Input Immittance," *Ann. Otol., Rhinol., Laryngol.*, forthcoming.

⁸ K.M. Donahue, *Human Middle-Ear Malleal Motion: Models and Measurements*, S.M. thesis, Dept. of Electr. Eng. and Comput. Sci., MIT, 1989.

hold and Noise-induced Hearing Loss." Submitted to *J. Acoust. Soc. Am.*

Rosowski, J.J., P.J. Davis, S.N. Merchant, K.M. Donahue, and M.D. Coltrera. "Cadaver Middle-Ears as Models for Living Ears: Comparisons of Middle-Ear Input Immittance." *Ann. Otol., Rhinol., Laryngol.* Forthcoming.

Rosowski, J.J., and A. Graybeal. "What Did *Morganucodon* Hear?" Submitted to *Zool. J. Linn. Soc.*

Rosowski, J.J., W.T. Peake, and N. Yang. "A Simple Model for Level-dependent Growth Rates of Auditory Distortion." Paper presented at the Symposium in Honor of N.Y.S. Kiang, Dedham, Massachusetts, July 5-7, 1989.

1.3 Cochlear Mechanisms

Project Staff

Professor Thomas F. Weiss, Professor Lawrence S. Frishkopf, Dr. Dennis M. Freeman, Farzad Ehsani, Donna K. Hendrix

We completed a paper⁹ that describes a theoretical study of the degradation of timing information in the cochlea. Results of this study suggest that three hair-cell processes, each acting as a first-order lowpass filter process, contribute to the degradation of timing information in the cochlea. These are: (1) the charging of the membrane capacitance; (2) the kinetics of opening of calcium channels; and (3) the time course of accumulation of calcium in intracellular compartments.

We have submitted for publication a manuscript¹⁰ that describes methods used to construct an accurate, three-dimensional, plastic model of the cochlea of the alligator lizard. The model, which consists of three pieces (representing the otic capsule, the cochlear duct, and the posterior branch of the VIIIth nerve), is based directly on histological sections of the cochlea.

We have submitted for publication¹¹ the results of theoretical studies of the mechanical stimulation of the hair bundles of hair cells.

We have completed a study¹² whose goals were to develop an *in vitro* preparation of the cochlear duct of the alligator lizard and to evaluate the effects of placing the duct in different solutions. The technique is to dissect the duct and place it in an artificial lymph solution. The vestibular membrane is opened, and a cement (derived from mussels) is used to attach the duct to a glass slide at the bottom of a chamber. Microspheres (1 μm and 3 μm diameter polystyrene) are added and allowed to settle onto the duct. The chamber is perfused with an artificial lymph solution, and the duct is observed through a compound microscope with interference contrast (Nomarski) optics. Three different types of iso-osmotic lymph solutions have been tested: an artificial perilymph (AP), artificial endolymph (AE), and a tissue culture medium (L-15). Results show that the microspheres on the endolymphatic surface of the duct move in characteristically different ways in the three iso-osmotic lymphs, suggesting that the tissue swells in AE and changes rather little in AP and in L-15. Most of the measure-

⁹ R.C. Kidd and T.F. Weiss, "Mechanisms That Degrade Timing Information in the Cochlea," *Hear. Res.*, forthcoming.

¹⁰ D.M. Freeman, "Anatomical Model of the Cochlea of the Alligator Lizard," *Hear. Res.*, forthcoming.

¹¹ D.M. Freeman and T.F. Weiss, "Superposition of Hydrodynamic Forces on a Hair Bundle," *Hear. Res.*, forthcoming; D.M. Freeman and T.F. Weiss, "Hydrodynamic Forces on Hair Bundles at Low Frequencies," *Hear. Res.*, forthcoming; D.M. Freeman and T.F. Weiss, "Hydrodynamic Forces on Hair Bundles at High Frequencies," *Hear. Res.*, forthcoming; D.M. Freeman and T.F. Weiss, "Hydrodynamic Analysis of a Two-dimensional Model for Micromechanical Resonance of Free-standing Hair Bundles," *Hear. Res.*, forthcoming.

¹² D.K. Hendrix, *Development of an in vitro Preparation of the Alligator Lizard Cochlear Duct*, S.M. thesis, Dept. of Electr. Eng. and Comput. Sci., MIT, 1990.

ments of microsphere displacement versus time could be fit acceptably with exponential time functions. The time constants were of the order of 10^2 minutes. Comparison of the motion of microspheres at different locations in the duct does not reveal any systematic dependence of motion on location. We conclude that the methods we have developed provide a simple tool for determining the artificial lymph compositions that result in osmotic stability of the cochlear duct. Based on our present results, on the physical appearance of the cochlear duct, and on the work of other investigators, we believe that a medium consisting of L-15 of appropriate osmolarity will prove to be superior to either AE or AP in maintaining the viability of an *in vitro* preparation of the alligator-lizard cochlea.

Publications

- Freeman, D.M. "Anatomical Model of the Cochlea of the Alligator Lizard." *Hear. Res.* Forthcoming.
- Freeman, D.M., and T.F. Weiss. "Superposition of Hydrodynamic Forces on a Hair Bundle." *Hear. Res.* Forthcoming.
- Freeman, D.M., and T.F. Weiss. "Hydrodynamic Forces on Hair Bundles at Low Frequencies." *Hear. Res.* Forthcoming.
- Freeman, D.M., and T.F. Weiss. "Hydrodynamic Forces on Hair Bundles at High Frequencies." *Hear. Res.* Forthcoming.
- Freeman, D.M., and T.F. Weiss. "Hydrodynamic Analysis of a Two-dimensional

Model for Micromechanical Resonance of Free-standing Hair Bundles." *Hear. Res.* Forthcoming.

Hendrix, D.K. *Development of an in vitro Preparation of the Alligator Lizard Cochlear Duct.* S.M. thesis. Dept. of Electr. Eng. and Comput. Sci., MIT, 1990.

Kidd, R.C., and T.F. Weiss. "Mechanisms That Degrade Timing Information in the Cochlea." *Hear. Res.* Forthcoming.

1.4 Regeneration of Primary-Auditory Neurons in vitro

Project Staff

Dr. Robin L. Davis

The regenerative capacity of primary-auditory neurons was studied in a tissue culture system that permits single goldfish primary-auditory neurons to be maintained *in vitro* for up to one or two months.¹³ Following placement in tissue culture, only very few of these neurons regenerate their processes. These cells are, however, physiologically active as evaluated with intracellular and single-channel recordings.¹⁴ Focal crush lesions made to the goldfish primary-auditory nerve one and two days prior to removal for tissue culture increased the amount of neurite outgrowth observed *in vitro*.¹⁵ The rate, extent and pattern of this growth response is being characterized for individual neurons and will be compared to the effects of known neurotropic factors added to the medium.

¹³ R.L. Davis, E.A. Mroz, and W.F. Sewell, "Isolated Auditory Neurons in Culture," *Abstr. Assoc. Res. Otol.* 11: 240 (1988).

¹⁴ R.L. Davis, E.A. Mroz, and W.F. Sewell, "Single Channel Properties of Goldfish (*Carassius auratus*) Auditory Neurons *in vitro*," *Society for Neuroscience Abstr.* 14 (Part 2): 798 (1988).

¹⁵ R.L. Davis, "Conditioning Lesions Promote Primary-Auditory Neurite Regeneration *in vitro*," submitted to the Association of Research for Otolaryngology, St. Petersburg, Florida, February 4-8, 1990.

Publications

Davis, R.L. "Conditioning Lesions Promote Primary-auditory Neurite Regeneration *in vitro*." Submitted to the Association of Research for Otolaryngology, St. Petersburg, Florida, February 4-8, 1990.

Davis, R.L., E.A. Mroz, and W.F. Sewell. "Isolated Auditory Neurons in Culture." *Abstr. Assoc. Res. Otol.* 11: 240 (1988).

Davis, R.L., E.A. Mroz, and W.F. Sewell. "Single Channel Properties of Goldfish (*Carassius auratus*) Auditory Neurons *in vitro*." *Soc. Neurosci. Abstr.* 14 (Part 2): 798 (1988).

1.5 Stimulus Coding in the Auditory Nerve

Project Staff

Dr. Bertrand Delgutte, Jenny S. Yu

During the past year, a report of earlier experiments on physiological mechanisms of psychophysical masking was submitted for publication and accepted.¹⁶ In these experiments, masked thresholds of auditory-nerve fibers were measured for tone signals of different frequencies in the presence of 1-kHz tone maskers. Physiological masking patterns were obtained by selecting the lowest masked threshold for each signal frequency among many fibers with different characteristic frequencies (CF) and spontaneous rates of discharge. These physiological masking patterns resemble psychophysical masking patterns in that they show rapid growth of masking with masker level for signal frequencies above the masker. A correlate of the psychophysical phenomenon of off-frequency listening was found in that fibers

with the lowest masked thresholds were not tuned to the signal frequency in quiet, but had their CF's slightly on the opposite side of the masker frequency with respect to the signal frequency. Comparison of simultaneous and nonsimultaneous masked thresholds showed that two-tone rate suppression plays an important role in masking, particularly for signal frequencies well above the masker.

In order to study physiological mechanisms of masking for a broader range of stimulus conditions than would be practical in physiological experiments, a phenomenological model of responses of auditory-nerve fibers was developed. This model simulates discharge rate responses of an array of auditory-nerve fibers for arbitrary steady-state stimuli defined by their frequency spectrum. The model produces two-tone rate suppression by having the output of a suppression filter modify the tuning of an excitation filter resembling tuning curves of auditory-nerve fibers. The model qualitatively predicts responses of auditory-nerve fibers to many stimuli, including single tones, two tones, broadband noise, and synthetic vowels, and produces masking patterns resembling those measured in auditory-nerve fibers. With the model, simulations of masking experiments show that suppression plays a complex role in masking, depending on stimulus conditions. Specifically, suppression among different frequency components of a complex masker can result in the unmasking of a tone signal in nonsimultaneous masking. Under certain conditions, tone signals can be detected because they suppress the response to broadband maskers. This effect was not found for narrowband maskers. Off-frequency listening plays a significant role in signal detection for intense signals, but not for low-level signals. These modeling results have been presented at several conferences.¹⁷

¹⁶ B. Delgutte, "Physiological Mechanisms of Psychophysical Masking: Observations from Auditory-Nerve Fibers," *J. Acoust. Soc. Am.*, forthcoming.

¹⁷ B. Delgutte, "Physiological Mechanisms of Masking and Intensity Discrimination," paper presented at the 117th Meeting of Acoustical Society of America, Syracuse, New York, May 22-26, 1989; B. Delgutte, "Does Suppression Result in Masking or Unmasking?" paper presented at the Symposium for Basic Research in a Clinical Environment, Dedham, Massachusetts, July 5-7, 1989; B. Delgutte, "Two-tone Suppression in Auditory-nerve Fibers: a Model and its Psychophysical Implications," paper presented at the 13th Meeting of the Association for Research in Otolaryngology, St. Petersburg Beach, Florida, February 4-8, 1990.

In fitting model parameters to physiological data, we made use of earlier data on the two-tone rate suppression in auditory-nerve fibers. A new analysis of these data showed that the rate of growth of suppression with the level of the suppressor tone depends on both the CF of auditory-nerve fibers and the frequency separation between the suppressor and the CF. For suppressors in the vicinity of the CF, the rate of growth decreases markedly with increasing suppressor frequency. However, the rate of growth reaches a plateau for suppressor frequencies well below the CF. The rate of growth in this plateau region increases slowly with increasing CF. These results pose difficulties for existing models of two-tone suppression. A report of these findings has been submitted for publication.¹⁸

Publications

Delgutte, B. "Physiological Mechanisms of Psychophysical Masking: Observations from Auditory-nerve Fibers." *J. Acoust. Soc. Am.* Forthcoming.

Delgutte, B. "Two-tone Rate Suppression in Auditory-nerve Fibers." Submitted to *Hear. Res.*

Delgutte, B. "Physiological Mechanisms of Masking and Intensity Discrimination." Paper presented at the 117th Meeting of Acoustical Society of America, Syracuse, New York, May 22-26, 1989.

Delgutte, B. "Does Suppression Result in Masking or Unmasking?" Paper presented at the Symposium for Basic Research in a Clinical Environment, Dedham, Massachusetts, July 5-7, 1989.

Delgutte, B. "Two-tone Suppression in Auditory-nerve Fibers: a Model and its Psychophysical Implications." Paper pre-

sented at the 13th Meeting of the Association for Research in Otolaryngology, St. Petersburg Beach, Florida, February 4-8, 1990.

1.6 Middle-Ear Muscle Reflex

Project Staff

Dr. John J. Guinan, Jr., Dr. James B. Kobler, Dr. Sylvette Vacher, Michael P. McCue

We aim to determine the structural and functional basis of the middle-ear reflexes. During the past year, we have published papers describing the course of stapedius motor axons within the brainstem,¹⁹ and the correlation between the locations of stapedius-motoneuron cell bodies and their responses to sound.²⁰ These results are consistent with the idea that the stapedius motoneuron pool is divided into subgroups that are spatially segregated in the brainstem in terms of their patterns of input from the two ears. Continuing this work, we have traced to their endings in the muscle five physiologically-identified stapedius motor axons which were labeled with horseradish peroxidase (from the cells labeled in Vacher et al., 1989). The results are interesting in that one axon innervated only one muscle fiber (in most muscles, each axon innervates tens or hundreds of muscle fibers), but in two cases, one axon innervated muscle fibers spread throughout the stapedius muscle (this demonstrates that the innervation of the stapedius is not restricted to several non-overlapping zones, as had been thought). Thus, although stapedius motoneurons appear to be functionally segregated in the brainstem, the available evidence suggests that there is not a corresponding segregation in the muscle.

We have recently published a commentary on the function of muscle and reflex partitioning

¹⁸ B. Delgutte, "Two-tone Rate Suppression in Auditory-nerve Fibers," submitted to *Hear. Res.*

¹⁹ J.J. Guinan Jr., M.P. Joseph, and B.E. Norris, "Brainstem Facial-Motor Pathways from Two Distinct Groups of Stapedius Motoneurons in the Cat," *J. Comput. Neurol.* 289: 134-144 (1989).

²⁰ S.R. Vacher, J.J. Guinan Jr., and J.B. Kobler, "Intracellularly Labeled Stapedius-Motoneuron Cell Bodies in the Cat are Spatially Organized According to Their Physiologic Responses," *J. Comput. Neurol.* 289: 401-415 (1989).

in the stapedius.²¹ In this commentary, we point out ways in which the organization of the stapedius motor system does not fit with a leading current theory on the organization of mammalian neuromuscular systems.

During the past year, work has been done to prepare for publication results in two areas: (1) data which demonstrate "unmasking" produced by stapedius contractions, and (2) data on the responses to sound and axon conduction velocities of stapedius motoneurons (these data provide the basis for the division of stapedius motoneurons into response-type groups).

This past year we have made progress on our project to determine whether there are systematic differences in motor-unit strengths and time courses across the different functional groups of stapedius motoneurons. To facilitate the work of this project, we have upgraded our experimental facility with a new data acquisition system centered around a MacIntosh II computer and National-Instruments input, output and direct-memory-access boards. Progress has also been made on many experimental issues, such as finding a location at which stapedius motor axons can be intracellularly recorded and stimulated without the electrode being dislodged by muscle motion, and developing a reliable paradigm for stimulating impaled stapedius motor axons and determining that the axon has responded. We plan to obtain measurements of the effects of individual stapedius motor units as monitored by the changes produced in middle-ear transmission and middle-ear input impedance.

Publications

Guinan, J.J., Jr., M.P. Joseph, and B.E. Norris. "Brainstem Facial-Motor Pathways from Two Distinct Groups of Stapedius Motoneurons in the Cat." *J. Comput. Neurol.* 289: 134-144 (1989).

McCue, M.P., J.J. Guinan Jr., J.B. Kobler, and S.R. Vacher. "Acoustic-Reflex Parti-

tioning in the Stapedius." *Behav. Brain Sci.* 12: 663-665 (1989).

Vacher, S.R., J.J. Guinan Jr., and J.B. Kobler. "Intracellularly Labeled Stapedius-Motoneuron Cell Bodies in the Cat are Spatially Organized According to Their Physiologic Responses." *J. Comput. Neurol.* 289: 401-415 (1989).

1.7 Cochlear Efferent System

Project Staff

Dr. John J. Guinan, Jr.

In this project, we aim to understand the physiological effects produced by medial olivocochlear (MOC) efferents which terminate on outer hair cells. To test the hypothesis that efferent activity and two-tone suppression might affect the cochlear amplifier at different sites but produce similar effects, we compared effects of these agents on stimulus-frequency otoacoustic emissions (SFOAEs) in cats. Measurements were made of ΔP , the vector change in ear-canal sound pressure relative to the pressure with a probe tone alone. As a first approximation, ΔP is the removal of part of the probe SFOAE. Changes due to two-tone suppression (ΔP_s) or efferent stimulation (ΔP_{oc}) could be measured over a very wide range of probe frequencies (0.2–30 kHz). As the level of a suppressor tone was increased, ΔP_s often had a constant phase and a monotonically increasing magnitude, but under certain conditions the relationship was strongly non-monotonic (e.g. showed a sharp dip and an abrupt phase change). With efferent stimulation, we did not find similar abrupt changes in ΔP_{oc} . With both efferent stimulation and a suppressor tone, the resulting ΔP_{oc} 's ranged from vector addition of the separate effects to a result which was more like a mean than an addition. The results suggest that efferent and suppressive effects are not identical and that at least two different mechanisms produce suppressive effects.

²¹ M.P. McCue, J.J. Guinan Jr., J.B. Kobler, and S.R. Vacher, "Acoustic-Reflex Partitioning in the Stapedius," *Behav. Brain Sci.* 12: 663-665 (1989).

During the past year, we have prepared a manuscript on previously unpublished experimental results on the physiology of the medial nucleus of the trapezoid body (MNTB).²² There has been a renewed interest in MNTB principal neurons as possible sources of inputs to olivocochlear neurons and as sources of inputs to neurons of the lateral superior olivary nucleus. By orthodromic and antidromic stimulation of MNTB principal neurons, we have shown that there is usually one-to-one transmission from each calyx of Held (a very large presynaptic ending) to the contacted MNTB principal neuron. In addition, we demonstrated that the smaller, non-calyceal, synapses can also excite MNTB principal neurons. Finally, we found some evidence of inhibition, possibly recurrent inhibition, in MNTB principal neurons. Our data firmly establish that there is fast, secure spike transmission from calyces of Held to MNTB principal neurons and suggest that under some circumstances there is additional signal processing in MNTB principal neurons.

Publications

Guinan, J.J., Jr., and R.Y.S. Li. "Signal Processing in Brainstem Auditory Neurons which Receive Giant Endings (calyces of Held) in the Medial Nucleus of the Trapezoid Body of the Cat." *Hear. Res.* Forthcoming.

1.8 The Generators of the Brainstem Auditory Evoked Potential

Project Staff

Professor Nelson Y.S. Kiang, Jennifer R. Melcher

When a punctate sound is presented to the ear, a time-varying potential can be recorded from electrode pairs on the surface of the head. The potential waveform at short

latencies (<10 msec following the stimulus) is distinguished from the potential at longer latencies by a characteristic series of deflections, each about one msec in duration. Similar waveforms have been measured in every mammalian species in which recordings have been attempted. It is believed that the short-latency potential is generated by cells in the auditory nerve and brainstem. Thus, it is called the brainstem auditory evoked potential (BAEP).

The goal of Jennifer Melcher's thesis²³ is to gain a better understanding of which cells generate the different components of the BAEP. In previous years, progress has been made along two lines: (1) a model for BAEP generation was developed, and (2) a series of lesion experiments were begun. The model relates the activity of individual cells in the auditory pathway to the BAEP and has served as a guide for designing and interpreting the experiments. The lesion experiments involve injecting a neurotoxin into different parts of the cat brainstem and correlating the resulting cell loss with changes in the BAEP. Preliminary experimental results suggested that different cell populations generate different components of the BAEP.

Further results of the past year are qualitatively consistent with the preliminary data and also support the hypothesis that one particular BAEP component is generated by a particular population of cells. In order to stabilize that interpretation, we have begun comparing data from many experiments to look for a quantitative relationship between the amplitude of the BAEP component and the number of cells eliminated from the population. To do this, we have developed a method for quantifying lesions that involves counting and characterizing individual cells. A quantitative description of a lesion is obtained by comparing the number of cells with particular characteristics in the experimental (lesioned) brainstems with the number in a normal brainstem. We plan to

²² J.J. Guinan Jr. and R.Y.S. Li, "Signal Processing in Brainstem Auditory Neurons which Receive Giant Endings (calyces of Held) in the Medial Nucleus of the Trapezoid Body of the Cat," *Hear. Res.*, forthcoming.

²³ J. Melcher, *Generators of the Brainstem Auditory Evoked Potentials*, Ph.D. diss., work in progress, Dept. of Electr. Eng. and Comput. Sci., MIT.

complete the experiments and quantitative lesion analysis during the next year.

1.9 Cochlear Implants

1.9.1 Models of Current Spread and Nerve Excitation During Intracochlear Stimulation

Project Staff

Dr. Donald K. Eddington, Dr. Jay T. Rubenstein

The basic function of a cochlear prosthesis is to elicit patterns of activity on the array of surviving auditory nerve fibers by stimulating electrodes that are placed in and/or around the cochlea. By modulating these patterns of neural activity, these devices attempt to present information that the implanted subject can learn to interpret. The spike activity patterns elicited by electrical stimulation depend on several factors: the complex, electrically heterogeneous structure of the cochlea, the geometry and placement of the stimulating electrodes, the stimulus waveform, and the distribution of excitable auditory nerve fibers. An understanding of how these factors interact to determine the activity patterns is fundamental (1) to the design of better devices and (2) to the interpretation of the results of experiments involving intracochlear stimulation of animal and human subjects. As a first step towards this understanding, the goal of this project is to construct a software model of the cochlea that predicts the distribution of potential produced by the stimulation of arbitrarily placed, intracochlear electrodes and use these potential distributions as inputs that drive models of auditory nerve fibers.

As reported over the last two years, a three-dimensional, finite element model of the human cochlea has been developed that predicts the potential distribution produced in this structure by electrical stimulation of model electrodes of arbitrary position and geometry. For a scala tympani/far-field electrode pair, the model predicts that potential along the scala tympani falls monotonically from the electrode toward the base while, from the electrode to the apex, the potential falls initially and then plateaus.

These potential distributions indicate that current spreads more toward the base than it does toward the apex. Measurements of potential at unstimulated electrodes made in five human subjects implanted with intracochlear electrodes confirmed the asymmetric potential distributions predicted by the model in all five subjects. Psychophysical measures of the interaction between two electrodes stimulated simultaneously also exhibited asymmetries in these five subjects that were consistent with those predicted by the model.

This year we have continued to make measurements of scala tympani potentials and psychophysical measures of interaction in additional subjects. The results from these additional subjects are consistent with those of last year. We are currently preparing a paper that describes our work in this area.

We have also begun work to integrate the model of potential distribution with linear and nonlinear models of extracellular excitation of myelinated and unmyelinated nerve fibers (which have been developed this year).

1.9.2 Psychophysical Measures and Their Correlation with Speech Reception

Project Staff

Dr. Donald K. Eddington

One striking aspect of speech reception measurements made with subjects using cochlear implants is the wide range of performance. This project is designed to identify basic psychophysical measures that correlate with the subject's speech reception ability. Such correlations should help us both to identify basic performance deficits that might be overcome with alternative processing schemes and to relate correlations found between pathology and psychophysical measures in experimental animals to their potential effect on speech reception.

Last year we reported correlations of speech reception with four psychophysical measures [threshold ($r = -0.80$), dynamic range ($r = 0.78$), interaction ($r = -0.90$), and place pitch ($r = 0.83$)] in an initial set of eight

subjects. This year we have extended these measures to sixteen subjects and are preparing a paper that describes these results.

1.9.3 Cues Used by the Brain to Assign Pitch Based on Electrode Position

Project Staff

Dr. Donald K. Eddington

Subjects with intracochlear electrodes provide a unique opportunity to elicit activity patterns in the array of auditory nerve fibers that cannot be elicited in normal hearing individuals using acoustic stimuli. This opportunity to present novel inputs to the brain and to determine how human subjects perceive them provides a powerful tool to probe the processing mechanisms of the "central processor." I have been using this tool to identify cues that the brain uses to determine the relative pitch of perceptions produced by two electrical stimuli that are temporally but not spatially equivalent. Preliminary results in three subjects indicate that the subjects use the apical boundary of excitation when assigning relative pitch to these stimuli.

1.10 Anatomical Basis for the Relationships between Binaural Hearing and Brainstem Auditory Evoked Potentials in Humans

Project Staff

Dr. Jill C. Gardner, Dr. Robert A. Levine, Dr. Miriam Furst, Dr. Barbara Fullerton, Patricia A. Cuneo

Previous studies have shown that brainstem auditory evoked potentials and some lateralization phenomena are closely related in both normal subjects and subjects with multiple sclerosis (MS). We are currently investigating several features of binaural pro-

cessing, in normal and MS subjects, in order to determine the regions of the brainstem that are critical for sound localization and the evoked potentials. Our objective is to localize lesions in the brainstem, using magnetic resonance (MR) imaging, and to relate the location of the lesions to the subject's disturbances in auditory function.

During the past year, our primary focus was the development of a procedure to determine if an MS lesion, as detected by MR imaging, involved the brainstem auditory pathway. Toward that goal we: (1) constructed a model (atlas) of the auditory pathway in the human brainstem; and (2) developed an algorithm to map a specified section from the atlas to a corresponding section of an MR scan. The atlas was constructed from 40 mm, serial section histology of two adult human brainstems.²⁴

The locations of the nuclei and fiber tracts of the auditory pathway were determined with light microscopy and the data were digitized (see figure 2) for visualization. Outlines of each section and the auditory pathway were entered into a computerized anatomy system, which allows "resectioning" of the atlas in any plane.

An algorithm was developed to estimate the location of the auditory pathway in the MR scans from the computerized atlas (1) as follows. First, for each MR section a corresponding section (same plane, thickness, and distance from the midline) is generated from the atlas. Second, a few well defined landmarks appearing in the two corresponding sections are selected, so that a search procedure can be employed (from regions between adjacent landmarks, it finds points that most closely correspond). By using these two sets of points and a linear fitting procedure, a transformation matrix is derived which superimposes a section from the atlas onto the corresponding MR scan. In the last step, this same transformation is applied to the auditory pathway that lies within the atlas section. This transformed auditory pathway is then superimposed on the MR section to

²⁴ Part of this work was done in collaboration with John Sundsten and Jeff Prothero at the University of Washington, Seattle, Washington.



Figure 2. Computerized reconstruction of the auditory pathway in the human brain from the coronal view. The structures are color-coded according to the following abbreviations: cochlea (C), auditory nerve (AN), brainstem (BS), superior olivary complex (SOC), inferior olivary complex (IOC), nucleus reticularis (NR), nucleus reticularis, ventral part (NRV), nucleus reticularis, dorsal part (NRD), nucleus reticularis, lateral part (NRL), nucleus reticularis, medial part (NRM), nucleus reticularis, posterior part (NRP), nucleus reticularis, anterior part (NRA), nucleus reticularis, ventral part, lateral part (NRVL), nucleus reticularis, ventral part, medial part (NRVM), nucleus reticularis, ventral part, posterior part (NRVP), nucleus reticularis, ventral part, anterior part (NRVA), nucleus reticularis, ventral part, lateral part, medial part (NRVLM), nucleus reticularis, ventral part, lateral part, posterior part (NRVLP), nucleus reticularis, ventral part, lateral part, anterior part (NRVLA), nucleus reticularis, ventral part, lateral part, medial part, posterior part (NRVLMPL), nucleus reticularis, ventral part, lateral part, medial part, anterior part (NRVLMPLA), nucleus reticularis, ventral part, lateral part, medial part, posterior part, anterior part (NRVLMPLAP).

give an estimate of the auditory pathway's length (see Figure 2).

Publications

Lyda, M., C. Gannon, R. A. Lyda, B. Eppstein, and P. Tjebk, "Visualizing the Brainstem Auditory Pathway in Human Magneto-Resonance Images Using Application Mapping MRIs," in *Computerized Anatomy: Applications*, presented at the Association for Research in Computerized Anatomy, University of St. Petersburg, Russia, February 1994, p. 106.

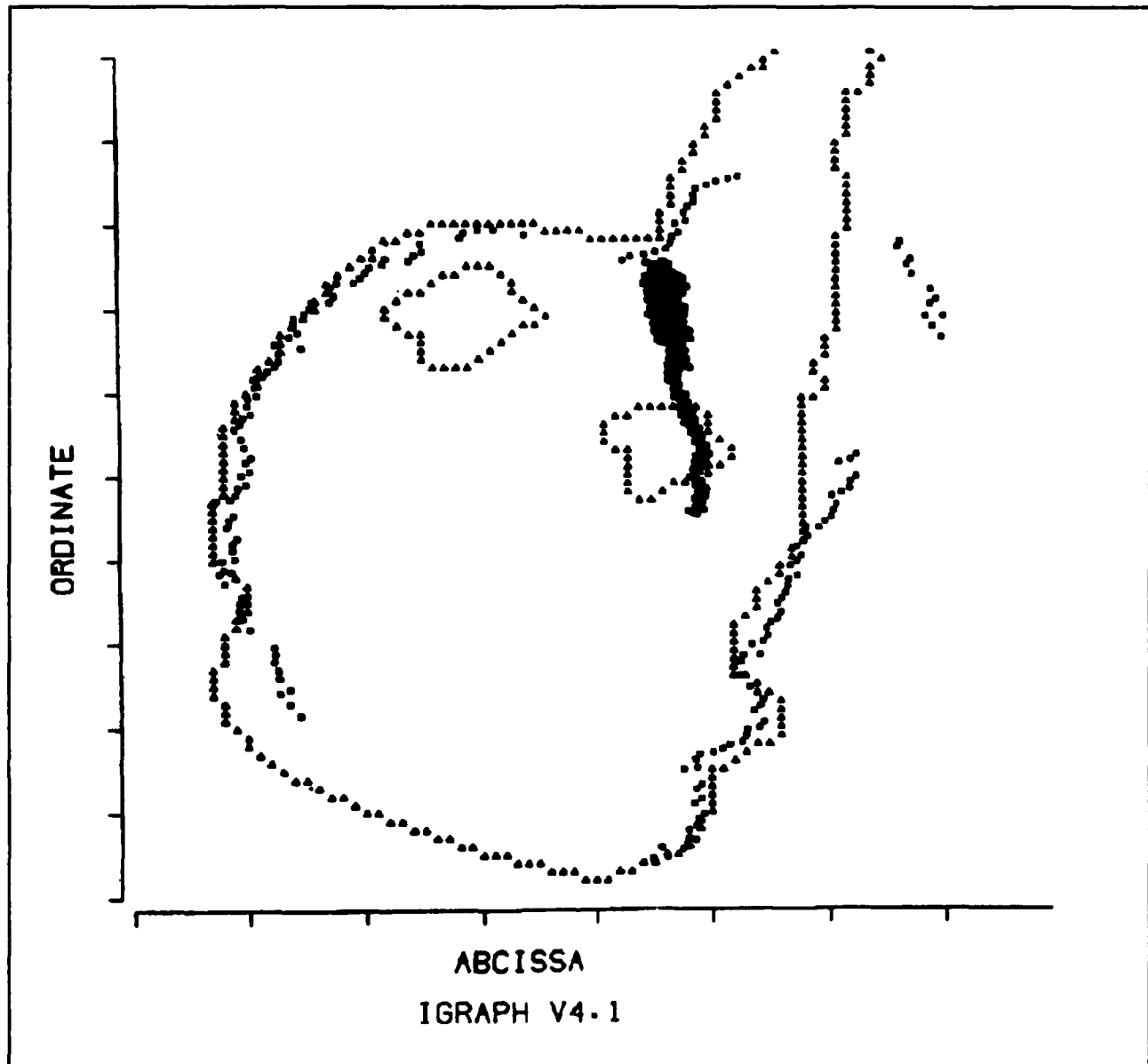


Figure 3. Results of the mapping algorithm. The outline of a sagittal magnetic resonance scan containing two multiple sclerosis lesions, is shown with triangles. A corresponding section from the anatomic atlas is represented with squares. The projection of the lateral lemniscus (dark area) of the auditory pathway overlaps one of the MS lesions.

Section 4 Linguistics

Chapter 1 Linguistics

Chapter 1. Linguistics

Academic and Research Staff

Professor Morris Halle, Professor Noam A. Chomsky

1.1 Introduction

The work of the Linguistics group is directed towards obtaining a better grasp of the mental capacities of human beings through the study of the nature, acquisition and use of language. Language is a uniquely human faculty in that only humans appear to be capable of learning and using a language and that every normal human acquires knowledge of one or more languages during his/her lifetime. This knowledge is represented somehow in the speaker's mind, which is a special organ located in the human brain. Viewed from this vantage point, the central issues of linguistics research are:

1. What is the nature of this knowledge? What do speakers of a particular language - Latvian, Spanish or Walpiri - know, and how does knowledge of one language differ from and resemble that of some other language?
2. How do speakers acquire this knowledge?
3. How do speakers put this knowledge to use in producing and understanding utterances?
4. What are the physiological mechanisms that provide the material basis for the storage, acquisition and utilization of linguistic knowledge?

There are considerable differences in our ability to answer these questions. It would seem that at present we have advanced more with regard to question 1 and least with question 4. These differences are also reflected in the research conducted by the group. At this time, it is most heavily concentrated on issues concerned with the nature of the knowledge that characterizes fluent speakers of various languages. Yet the other three questions have not been over-

looked, and significant efforts are being devoted to their solution.

The study of these topics is being carried out along a number of parallel lines. On the one hand, linguists have investigated the principles by which words are concatenated to form meaningful sentences. These principles have been the primary domain of inquiry of the disciplines of syntax and semantics. Phonology studies the sound structure of words while morphology examines the manner in which different languages combine different meaning-bearing units (specifically, stems, prefixes, suffixes and infixes) to form words. The latter topic has attracted increasing interest in recent years and is likely to become more prominent in the future.

1.2 Abstracts of Doctoral Dissertations

All of the following are abstracts of dissertations submitted to the Department of Linguistics and Philosophy in partial fulfillment of the requirements for the degree of Doctor of Philosophy in Linguistics.

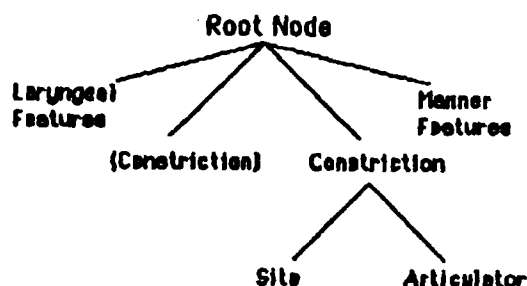
1.2.1 Phonology of Articulation

Alicja Gorecka

Abstract

In this thesis, I focus on the phonological representation of the articulatory component of speech production. I argue for a phonological constituent called the Constriction Node, which represents the constriction gesture. Within the segmental tree (cf. Clements (1985), Sagey (1986)), the Con-

struction Node is a daughter of the Root Node (in the sense of the Clements/Sagey model). It itself dominates the Site, which corresponds to the constriction location, and the Articulator, which corresponds to the organ executing the constriction gesture. The model of segment representation which includes the Constriction Node is represented as follows:



In this model, the Site ranges over the features Labial, Anterior, Palatal, Velar, and Pharyngeal. The Articulator can have either of the values: Lower Lip, Tongue Blade, Tongue Body, Tongue Root.

The constriction model reconciles two traditions of segment characterization: the IPA tradition, which stresses the importance of the constriction location features, and the SPE (Chomsky and Halle (1968)) tradition of giving priority to the features based on the active articulator. It adopts the hierarchical view of segment representation introduced by Clements (1985) and Sagey (1986). In particular, it adopts the concept of an Articulator as it is developed in Sagey (1986).

The constriction model offers a view of segment representation closely modelled on the physical reality which it represents: the constriction gesture is a necessary element of speech production.

On the phonological side, the main advantage of the constriction model is that it makes all articulation features equally available to consonants and vowels; this is what allows it to account for vowel/consonant interaction phenomena (e.g., mutual vowel/consonant palatalization, velarization, and pharyngealization, among others). Also, by offering more structured representations,

this model goes even further than the previous models in the direction of limiting the number of phonological processes which do not occur.

This thesis is organized as follows: Chapter 1 introduces the constriction model. Chapters 2 and 3 argue for the phonological constituent Articulator, and the phonological constituent Site (respectively) on the basis of the examples which can be analyzed only in terms of these features. Chapter 4 deals with the structure within the Constriction Node. In chapter 5, the articulatory basis of Site and Articulator features, and the phonological motivation for treating vowels in terms of such features are discussed. Chapter 6 discusses some residual questions in the representation of consonants. Finally, chapter 7 considers the consequences that follow from applying the constriction model in the analysis of various phonological processes.

1.2.2 A Case Study in the Syntax of Agreement: Hebrew Noun Phrases and Benoni Verb Phrases

Elizabeth Ann Ritter

Abstract

This dissertation investigates the role of number and gender agreement in two Hebrew contexts; present tense sentences and genitive noun phrases. As a point of departure, I adopt a recent proposal by Pollock (1987) that agreement projects a distinct syntactic category from tense. Thus, the analysis of S as IP, the maximal projection of inflection (I), is replaced by an analysis of S as TP, the maximal projection of tense (T). The complement of T on this view is AGRP, the maximal projection of agreement (AGR). In the spirit of this proposal, I assume that noun phrases are maximal projections of a functional category, determiner (D), and that the complement of D is a second functional category, which I call P. Although the position of P within the noun phrase parallels that of AGRP in the sentence, and AGR have distinct functions.

In chapter 2, I investigate the properties of present tense sentences in Hebrew. These

sentences contain *benoni* verb, which are distinguished from their past and future counterparts in that they are inflected for the number and gender, but not the person, of their subjects. The syntax of present tense sentences in Hebrew sheds light on the role of agreement in the assignment of nominative case and in the licensing of null subjects. I show that only an analysis which separates tense and agreement can account for the full range of construction in the present tense.

In chapter 3, I study the range of noun phrases containing postnominal genitives. These structures provide crucial evidence for the separate projection of a functional category, which I call #, and D. The head manifests grammatical number (and possible gender) of its nominal complement. A striking feature of derived nominals in Hebrew is that the subject always appears between the head noun and object. In order to account for the surface order of the constituents within these noun phrases, I posit functional projections which provide landing sites for movement of the head noun, analogous to verb movement in sentences. A comparison of different genitive constructions motivates the two distinct functional categories postulated.

1.2.3 Metrical Dependencies in Tone Assignment

Brian Mark Sietsema

Abstract

This thesis presents metrical analyses of tone assignment (tone shift, tone insertion, tone spread) in four Bantu languages of Tanzania. A constrained metrical system of rules and parameter (Halle and Vergnaud 1987) is introduced and applied to these languages in order to explain a variety of long-distance tone phenomena. The metrical analysis reduces these phenomena to a set of local operations within an autosegmental theory of phonology.

Along with the introduction to metrical theory (chapter 1), a theory of tone and morphology for the Bantu language as is sketched out and illustrated by partial analysis of Kimatuumbi and Ci-Ruri (chapter 2). Fuller analyses of Digo (chapter 3) and Sukuma (chapter 4) follow, building on the theoretical devices which were developed for the analyses of Kimatuumbi and Ci-Ruri. Metrical structure is shown to play a profound role in the tonology of these languages.

The study concludes by drawing out the theoretical implications of the previous analyses, with particular attention to the typology of tone-accent interactions.

Appendices

Appendix A RLE Publications and Papers Presented

Appendix B Current RLE Personnel

Appendix C RLE Research Support Index

Appendix A. Publications and Meeting Papers

The first section of this bibliography includes papers and talks presented by RLE faculty, staff and students during 1989, and is in alphabetical order by conference name. Reprints of these papers may be obtained by contacting the authors directly. Section 2 lists published meeting papers by author; section 3 is a list of meeting papers submitted for publication.

Sections 4, 5 and 6 are alphabetical listings by author of journal articles that were published, accepted or submitted for publication. Book chapters by RLE authors are listed in section 7. Section 8 of this bibliography lists RLE general publications and technical reports, while section 9 is a list of RLE theses submitted during 1989.

A.1 Meeting Papers Presented

Acoustical Society of America, 117th Meeting, Syracuse, New York, May 22-26, 1989.

Besing, J., M.J. Collins, and J.K. Cullen "Duration Effects on Vowel Perception by Hearing Impaired Listeners."

Delgutte, B. "Physiological Mechanisms of Masking and Intensity Discrimination."

Duchnowski, P., and P.M. Zurek. "Simulation of Sensorineural Hearing Loss."

Greenberg, J.E., and P.M. Zurek. "Reducing the Effects of Target Misalignment in an Adaptive Beamformer for Hearing Aids."

Payton, K.L., R.M. Uchanski, and L.D. Braida. "Speech Intelligibility as a Function of Environment and Speaking Style."

Acoustical Society of America, 118th Meeting, St. Louis, Missouri, November 27-December 1, 1989.

Greenberg, J.E., and P.M. Zurek. "Evaluation of a Real-Time Adaptive-Beamforming Hearing Aid."

Acoustical Society of America, Annual Meeting, Hawaii, November 14-18, 1989.

Grant, K.W., R.J. Renn, and J.S. Yu. "Amplitude Envelopes and Speechreading."

Advanced Research in VLSI, California Institute of Technology Conference, Pasadena, California, March 22, 1989.

Umminger, C.E., and S.P. DeWeerth. "Gradient Following in Analog VLSI."

American Astronautical Society, GSFL Symposium, Washington, DC, March 10, 1989.

Staelin, D.H. "Passive Microwave Technology: Present and Future."

American Chemical Society, National Meeting, Miami, Florida, September 10-15, 1989.

Ippen, E.P. "Recent Advances in Femtosecond Pulse Generation."

American Otologic Society Meeting, San Francisco, California, April 2-3, 1989.

Rosowski, J.J., P.J. Davis, S.N. Merchant, K.M. Donahue, and M.D. Coltrera. "Cadaver Middle-Ears as Models for Living Ears: Comparisons of Middle-Ear Input Immittance."

American Physical Society Division of Fluid Dynamics, 42nd Annual Meeting, Palo Alto, California, November 19-21, 1989.

Bers, A., G.S. Triantafyllou, and A.K. Ram. "Absolute Instabilities in Inhomogeneous Flows."

American Physical Society Division of Plasma Physics, 31st Annual Meeting, Anaheim, California, November 13-17, 1989.

Chow, C., V. Fuchs, and A. Bers. "An Analytic Theory of ICRF Heating."

Colborn, J.A., S.C. Luckhardt, K-I. Chen, R. Kirkwood, R. Parker, M. Porkolab, J. Squire, and J. Villasenor. "Combined ECRH and LHCD Experiments on the Versator II Tokamak."

Englade, R., and B. Coppi. "Transport Coefficients for the Plasma Thermal Energy."

Kupfer, K., A. Bers, and A.K. Ram. "Guiding Center Stochasticity by Electrostatic Waves in Toroidal Geometry."

- Migliuolo, S., B. Coppi, F. Pegoraro, and F. Porcelli. "Stability of $M=1$ Modes in the Reconnecting Regime."
- Ram, A.K., and A. Bers. "Kinetic Ray Tracing in Toroidal Plasmas."
- Squire, J.P., S.C. Luckhardt, M. Porkolab, K.I. Chen, J. Colborn, R. Kirkwood, and J. Villasenor. "Fast Magnetic Fluctuation Measurements of High Poloidal Beta Versator II Plasmas."
- Sugiyama, L.E. "Comparison of Thermal Transport in Ohmic Experiments."
- Sugiyama, L.E. "Time Dependent $D-3He$ Ignition and Burn."
- Tao, Z.C., A. Bers, and A.K. Ram. "Correlational Effects on the Time-Evolution of Plasma-Beam System."
- Villasenor, J., M. Porkolab, S. Luckhardt, K.I. Chen, and S. Squire. "Lower-Hybrid Fast Wave Current Drive on the Versator II Tokamak."
- American Physical Society Meeting*, St. Louis, Missouri, March 20-24, 1989.
- Antoniadis, D.A. "Surface Superlattice and Quasi-One-Dimensional Devices in GaAs."
- Bagwell, P.F., and T.P. Orlando. "Finite Voltage Tunneling in Ballistic Devices."
- Field, S.B., J.H.F. Scott-Thomas, M.A. Kastner, H.I. Smith, and D.A. Antoniadis. "Conductance Oscillations Periodic in the Density of a One-Dimensional Electron Gas."
- Liu, C.T., K. Nakamura, D.C. Tsui, K. Ismail, D.A. Antoniadis, and H.I. Smith. "Far-Infrared and Magneto-Capacitance Measurements on GaAs/AlGaAs Lateral Surface Superlattice."
- Scott-Thomas, J.F., S.B. Field, M.A. Kastner, D.A. Antoniadis, and H.I. Smith. "Periodic Oscillations in the Conductance of Si MOSFETs."
- Smith, H.I. "X-Ray Lithography and Nanostructure Fabrication."
- Walrod, D.B., S. Auyang, P.A. Wolff, R.E. Nahory, J.P. Harbison, L.T. Florez. "Four-Wave Mixing in S-Doped GaAs."
- American Physical Society Meeting*, Baltimore, Maryland, April 30 - May 4, 1989.
- Welch, G.R. "Chaos and a Small Quantum System: Experiments in Rydberg Atom Diamagnetism."
- American Society of Mechanical Engineers*, Winter Annual Meeting, San Francisco, California, December 10-15, 1989.
- Hagelstein, P. "Coherent Fusion Theory."
- American Speech, Language and Hearing Association*, St. Louis, Missouri, November 17-20, 1989.
- Besing, J., M.J. Collins, and J.K. Cullen. "Vowel Preference and Identification Behavior: Normal-Hearing and Hearing-Impaired Listeners."
- American Vacuum Society*, Boston, Massachusetts, October, 1989.
- Schulberg, M.T., M. McGonigal, D.J. Gladstone, K.B. Laughlin, and S.T. Ceyer. "The Etching of Si(100) with a Molecular Beam of F_2 ."
- Association for Research in Otolaryngology*, 12th Mid-Winter Research Meeting, St. Petersburg, Florida, February 5-9, 1989.
- Dynes, S.B.C., and B. Delgutte. "Phase Locking of Auditory-Nerve Responses to Electric Sinusoidal Stimulation of the Cochlea."
- Pang, X.D., and J.J. Guinan. "Effects of Stapedius Contractions on the Masking of Cat Auditory-Nerve-Fiber Responses to Tones."
- Association for Research in Vision and Ophthalmology*, Annual Meeting, Sarasota, Florida, April 30 - May 5, 1989.
- Fujimoto, J.G., B. Zysset, C.A. Puliafito, R. Birngruber, and T.F. Deutsch. "Picosecond Laser Photodisruption: Time Resolved Studies, Tissue Effects, and the Reduction of Collateral Damage."
- Bellcore and AT&T Laboratories Invited Seminar*, Holmdel, New Jersey, May 31 - June 1, 1989.
- Fujimoto, J.G. "Tunable Femtosecond Laser Techniques and Applications to all Optical Switching in Waveguide Devices."
- Boston Conference on Signal Processing*, Boston, Massachusetts, May 1989.
- Hardwick, J.C., and J.S. Lim. "Dual Excitation Speech Model."
- Canadian Workshop on X-ray Lithography*, First, Institute Nuclear Research Scientific, Quebec, Canada, April 27-29, 1989.
- Smith, H.I. "X-ray Nanolithography."

- Computer-Integrated Manufacturing of Integrated Circuits*, Semiconductor Research Corporation/Defense Advanced Research Projects Agency (DARPA), Fourth Annual, University of Michigan, Ann Arbor, Michigan, August 15-16, 1989.
- Troxel, D.E. "Process Control and the Cape Architecture."
- Condensed Matter Seminar*, University of Pennsylvania, Philadelphia, Pennsylvania, February 14, 1989.
- Fujimoto, J.G. "Femtosecond Processes in Semiconductors and Metals."
- Conference on Lasers and Electro-Optics*, Baltimore, Maryland, April 24-28, 1989.
- Anderson, K.K., M.J. LaGasse, H.A. Haus, J.G. Fujimoto, and C.A. Wang. "Femtosecond Pump-Probe Interferometry Studies of Optical Switching in AlGaAs Waveguides."
- Birngruber, R., V.P. Gabel, C.A. Puliafito, B. Zysset, and J.G. Fujimoto. "Intraocular Laser Tissue Interaction: Linear and Nonlinear Effects Produced with Nanosecond, Picosecond, and Femtosecond Pulses."
- Goodberlet, J.G., J. Wang, J.G. Fujimoto, P.A. Schulz, and S.R. Henion. "Modelocked Ti:Al₂O₃ Laser with a Nonlinear Coupled External Cavity."
- Hall, K.L., E. Ippen, J. Mark, and G. Eisenstein. "Sub-Picosecond Gain Dynamics in InGaAsP Diode Laser Amplifiers."
- Ippen, E., and K.L. Hall. "Ultrafast Optical Nonlinearities in Semiconductor Optical Amplifiers."
- Keith, D.W., M.L. Schattenburg, H.I. Smith, and D.E. Pritchard. "Diffraction Gratings for Atoms."
- Liu, L.Y., J. Mark, H.A. Haus, and E.P. Ippen. "Additive Pulse Mode Locking: A Mechanism for Femtosecond Pulse Generation with Coupled Nonlinear Resonators."
- Pritchard, D.E., K. Helmersson, M. Xiao, and K.-X. Sun. "Radio Frequency Spectroscopy of Trapped Neutral Atoms."
- Schoenlein, R.W., J.G. Fujimoto, G.L. Eesley, and T.W. Capehart. "Femtosecond Studies of Image Potential Dynamics in Metals."
- Zysset, B., J.G. Fujimoto, T.F. Deutsch, R. Birngruber, and C.A. Puliafito. "Time-Resolved Studies and Biological Effects of Picosecond Pulse Optical Breakdown."
- Custom Integrated Circuits Conference*, San Diego, California, May 15-18, 1989.
- Nabors, K., and J. White. "A Fast Multipole Algorithm for Capacitance Extraction of Complex 3-D Geometries."
- Defense Advanced Research Projects Agency (DARPA) Contractor's Meeting*, Snowbird, Utah, April 2-4, 1989.
- Troxel, D.E. "A Process Flow Language."
- Defense Advanced Research Projects Agency (DARPA)/VLSI Contractor's Meeting*, Washington, DC, November 2-3, 1989.
- Nabors, K., and J. White. "A Multipole-Accelerated 3D Capacitance Extraction Algorithm."
- Department of Energy Contractor's Meeting*, Germantown, Maryland, December 5-6, 1989.
- Hagelstein, P.L. "Coherent Fusion Theory."
- Electron, Ion and Photon Beam Symposium*, Monterey, California, April 22-26, 1989.
- Dubner, A.D., and A. Wagner. "Mechanisms of Ion Induced Deposition of Gold."
- Engineering Foundation Conference on Implantable Auditory Prostheses*, Potosi, Missouri, July 30 - August 4, 1989.
- Rabinowitz, W.M., and D.K. Eddington. "Effects of Channel-to-Electrode Mappings with the Symbion Cochlear Prosthesis."
- Engineering Foundation Conferences*, Molecular Electronics-Science and Technology, Keauhou Kona, Hawaii, February 19-24, 1989.
- Smith, H.I., K. Ismail, W. Chu, A. Yen, Y.C. Ku, and D.A. Antoniadis. "X-Ray Nanolithography and Quantum-Effect Electronics."
- Free Electron Laser Conference*, 11th International, Naples, Florida, August 28 - September 1, 1989.
- DiRienzo, A.C., G. Bekefi, C. Leibovitch, and B. Danly. "Cyclotron Autoresonance Maser Experiments."
- Future Directions for Lasers in Medicine and Surgery*, Palm Coast, Florida, February 26 - March 3, 1989.
- Zysset, B., T. Deutsch, C.A. Puliafito, and J.G. Fujimoto. "Time Resolved Studies and

- Biological Effects of Ultrashort Pulse Optical Breakdown."
- Gordon Conference on Dynamics of Gas-Surface Interactions*, Wolfeboro, New Hampshire, August 1989.
- Laughlin, K.B., D.J. Gladstone, M. McGonigal, and S.T. Ceyer. "Dynamics of the Reaction of F₂ with Si(100)."
- Gordon Conference on Nonlinear Optics and Lasers*, Wolfeboro, New Hampshire, July 24-28, 1989.
- Goodberlet, J., J. Wang, J.G. Fujimoto, and P.A. Schulz. "Femtosecond Passively Mode-locked Ti:Al₂O₃ Laser Using a Nonlinear External Cavity."
- Haus, H.A., and Y. Lai. "Quantum Theory of Soliton Squeezing - a Linearized Approach."
- IBM Laboratories Physics Seminar*, Endicott, New York, April 10, 1989.
- Fujimoto, F.G. "Femtosecond Processes in Semiconductors and Metals."
- IBM Research Laboratory*, Yorktown Heights, New York, July 5, 1989.
- Fujimoto, J.G. "Tunable Femtosecond Laser Techniques and Applications to All Optical Switching in Waveguide Devices."
- IEEE AP-S International Symposium and URSI Radio Science Meeting*, San Jose, California, June 26-30, 1989.
- Ali, S.M., T.M. Habashy, and J.A. Kong. "Probe Excitation of a Center-Fed Circular Microstrip Antenna Employing a Stratified Medium Formulation."
- Habashy, T.M., S.M. Ali, and J.A. Kong. "Probe Excitation of a Center-Fed Circular Microstrip Antenna Employing the Weber Transform."
- Poh, S.Y., M.J. Tsuk, and J.A. Kong. "Transient Response of Sources Over Layered Media Using the Double Deformation Method."
- Tsuk, M.J., and J.A. Kong. "Response of Layered Media to Current Sources with Arbitrary Time Behavior."
- Tulintseff, A.N., S.M. Ali, and J.A. Kong. "Resonant Frequencies of Stacked Circular Microstrip Antennas."
- Information Sciences and Systems Conference*, John Hopkins University, Baltimore, Maryland, March 23-24, 1989.
- Standley, D.L. "Criteria for Robust Stability in a Class of Lateral Inhibition and Related Networks Coupled Through a Resistive Grid."
- Integrated Factory Management-Integrated Circuit Workshop*, Semiconductor Research Corporation, College Station, Texas, November 15-17, 1989.
- Heytens, M.L., and M.B. McIlrath. "An Object-Oriented Interface to a Relational Database System."
- Kashani, A. "A Reservation-based Scheduler."
- McIlrath, M.B., and D.S. Boning. "Integrating Process Design and Manufacture."
- International Conference on II-VI Semiconductors*, Berlin, West Germany, August 21-25, 1989.
- Gunshor, R.L., M. Kobayashi, L.A. Kolodziejski, and A.V. Nurmikko. "Wide Gap II-VI Heterostructures."
- International Conference on Crystal Growth*, Sendai, Japan, September 11-15, 1989.
- Gunshor, R.L., M. Kobayashi, L.A. Kolodziejski, A.V. Nurmikko, and N. Otsuka. "MBE of Wide Bandgap II-VI Compounds."
- International Conference on Hot Carriers in Semiconductors*, Sixth Annual, Boston, Massachusetts, April 1989.
- Stanton, C.J., D.W. Bailey, K. Hess, M.J. LaGasse, R.W. Schoenlein, and J.G. Fujimoto. "Femtosecond Studies of Intervalley Scattering in GaAs and AlGaAs."
- International Conference on Laser Spectroscopy*, Ninth, Bretton Woods, New Hampshire, June 21-23, 1989.
- Pritchard, D.E. "Experimental Studies of Atom Diffraction and the Mechanical Forces of Light on Atoms."
- International Conference on Plasma Physics*, New Delhi, India, November 22-28, 1989.
- Ram, A.K., and A. Bers. "Kinetic Ray Tracing in Toroidal Geometry with Application to Mode-Converted Ion-Bernstein Waves."
- International Geoscience and Remote Sensing Symposium and 12th Canadian Symposium on Remote Sensing*, Vancouver, Canada, July 10-14, 1989.

- Melville, W.K., J.A. Kong, R.H. Stewart, W.C. Keller, A. Jessup, D. Arnold, and A. Slinn. "The Measurement and Modelling of Sea-State Bias in SAXON."
- International Laser Science Conference*, Stanford, California, August 27-31, 1989.
- Goodberlet, J., M.J. LaGasse, R.W. Schoenlein, M. Ulman, P. Schulz, J.G. Fujimoto. "Femtosecond Pulse Generation and Amplification in Ti:Al₂O₃."
- Haus, H.A. "Femtosecond Lasers with Fiber Optics."
- International Sherwood Theory Conference*, San Antonio, Texas, April 3-5, 1989.
- Chow, C., V. Fuchs, and A. Bers. "Analytic Studies of ICRF Heating."
- Kupfer, K., A. Bers, and A.K. Ram. "Transport of Charged Particles Interacting with Coherent Wave-Fields in a Tokamak Plasma."
- Ram, A.K., and A. Bers. "Ray Tracing of Mode-Converted Ion-Bernstein Waves in Toroidal Plasmas."
- Sugiyama, L.E. "Spatial Effects on the Ignition and Burn of D-³He Mixtures."
- International Symposium on Nanostructure Physics and Fabrication*, Texas A&M University, College Station, Texas, March 8-10, 1989.
- Smith, H.I., K. Ismail, W. Chu, A. Yen, Y.C. Ku, M.L. Schattenburg, and D.A. Antoniadis. "Fabrication of Quantum-Effect Electronic Devices Using X-Ray Nanolithography."
- International Test Conference*, Washington, D.C., August 28-30, 1989.
- Devadas, S. "Delay Test Generation for Synchronous Sequential Circuits."
- Devadas, S., H.-K.T. Ma, and A.R. Newton. "Redundancies and Don't Cares in Sequential Logic Synthesis."
- International Union of Radio Science Commission H Meeting*, Boulder, Colorado, January 4-7, 1989.
- Han, H.C., and J.A. Kong. "Self-focusing of a Radio Wave Beam During the Trans-ionospheric Propagation."
- International Workshop on High-Level Synthesis*, Kennebunkport, Maine, October 15-18, 1989.
- Fogg, D.C. "Operator Selection: Two Approaches."
- International Workshop on the Physics of Semiconductor Devices*, Fifth, New Delhi, India, December 10-13, 1989.
- Allen, J. "Fast and Parallelizable Techniques for High Accuracy Transient Device Simulation."
- Interuniversity Micro-Electronics Center-International Federation for Information Processing International Workshop on Applied Formal Methods for Correct VLSI Design*, Houthalen, Belgium, November 13-16, 1989.
- Van Aelten, F., and J. Allen. "Efficient Verification of VLSI Circuits Based on Syntax and International Semantics."
- Lasers '89*, New Orleans, Louisiana, December 3-8, 1989.
- Bam, S., and R.L. Byer. "Moving Slab Laser."
- Braud, J.P. "Adiabatic Whisper-Gallery Mirrors for EUV and Soft X-Ray Laser Cavities."
- Materials Research Society*, Spring Meeting, San Diego, California, April 24-29, 1989.
- Gunshor, R.L., L.A. Kolodziejski, M. Kobayashi, A.V. Numikko, and N. Otsuka. "Wide Gap II-VI DMS Superlattices: MBE Growth and Characterization."
- Materials Research Society*, Fall Meeting, Boston, Massachusetts, November 27-December 2, 1989.
- Bennett, B.R., and J.A. del Alamo. "Index of Refraction Anisotropy in Mismatched InGaAs/InP Heterostructures Measured by Ellipsometry."
- McGonigal, M., M.T. Schulberg, D.J. Gladstone, K.B. Laughlin, and S.T. Ceyer. "Reactions of F₂ with Si(100)."
- Melngailis, J. "Focused Ion Beam Induced Deposition for X-ray Mask Repair."
- Microwave Landing System User Forum*, Eastern Region, New York, New York, October 22-24, 1989.
- Yang, Y.-C.E. "Instrument Landing System/Microwave Landing System Frequency Management Assessment."
- Microwave Landing System User Forum*, Western Pacific Region, Honolulu, Hawaii, November 16, 1989.

- Yang, Y-C.E. "Instrument Landing System/Microwave Landing System Frequency Management Assessment."
- Military and Government Speech Technology Symposium*, Arlington, Virginia, November 13-15, 1989.
- Hardwick, J.C., and J.S. Lim. "A Real Time Implementation of a 4800 bps Improved Multi-Band Excitation Speech Coder."
- Mixed Signal Workshop*, Portland, Oregon, October 17, 1989.
- Kundert, K., and J. White. "Distortion Analysis of Switched-Capacitor Filters."
- NASECODE Conference*, Dublin, Ireland, June, 1989.
- Reichelt, M., and J. White. "Techniques for Switching Power Converter Simulation."
- National Radio Science Meeting*, University of Colorado, Boulder, Colorado, January 6, 1989.
- Han, H.C., and J.A. Kong. "Self-Focusing of a Radio Wave Beam During the Trans-ionospheric Propagation."
- Han, H.C., J.A. Kong, and T.M. Habashy. "VLF Beam Forming by a Phased Array in an Ionized Medium."
- Han, H.C., J.A. Kong, T.M. Habashy, and M.D. Grossi. "Principles of VLF Antenna Array Design in Magnetized Plasmas."
- New England Molecular Beam Epitaxy Workshop*, Fourth Meeting, Cambridge, Massachusetts, May 4, 1989.
- Bahl, S., W.J. Azzam, and J.A. del Alamo. "Fabrication of an InAlAs/n⁺ - InGaAs MIDFET."
- Nonlinear Guided Wave Phenomena: Physics and Applications*, Topical Meeting, Houston, Texas, February 2-4, 1989.
- Haus, H.A. "The Nonlinear Interferometer."
- Shirasaki, M., and H.A. Haus. "Broadband Squeezing with Cotraveling Waves."
- North American Sea Ice Workshop*, University of Massachusetts, Amherst, Massachusetts, June 25-28, 1989.
- Nghiem, S.V., J.A. Kong, R.T. Shin, and H.A. Yueh. "Application of Three-Layer Random Medium Model to Polarimetric Remote Sensing of Snow and Sea Ice."
- Optical Fiber Conference*, Houston, Texas, February 1989.
- Donnelly, J.P., L.A. Molter, G.S. Hopcraft, R.E. Smith, and H.A. Haus. "Extinction Ratio in Optical Two-Guide $\delta\beta$ Couplers."
- Optical Society of America*, Annual Meeting, Orlando, Florida, October 15-20, 1989.
- Haus, H.A. "Parametric Distributed Feedback Resonator and Unruh Radiation."
- Ippen, E.P. "Additive Pulse Modelocking."
- Ulman, M., R.W. Schoenlein, and J.G. Fujimoto. "Cascade High Repetition Rate Femtosecond Amplifier."
- Wong, N.C. "Optical Frequency Division using an Optical Parametric Oscillator."
- Optical Society of America Topical Meeting on Picosecond Electronics and Opto-Electronics*, Salt Lake City, Utah, March 7-12, 1989.
- Hall, K.L., E.P. Ippen, J. Mark, and G. Eisenstein. "Ultrafast Nonlinearities in InGaAsP Diode Laser Amplifiers."
- Physics and Chemistry of Semiconductor Interfaces Conference*, Bozeman, Montana, February 7-9, 1989.
- Alerhand, O.L., E. Kaxiras, J.D. Joannopoulos, G.W. Turner. "Model of Epitaxial Growth of GaAs on Si(100) - Nucleation at Surface Steps."
- Quantum Electronics and Laser Science Conference*, Baltimore, Maryland, April 1989.
- Keith, D.W., M.L. Schattenburg, H.I. Smith, and D.E. Pritchard. "Diffraction Gratings From Atoms."
- Radio Frequency Power in Plasmas*, Eighth Topical Conference, Irvine, California, May 1-3, 1989.
- Chow, C., A. Bers, and V. Fuchs. "Analytic Studies of ICRF Heating."
- Colborn, J., S.C. Luckhardt, J.P. Squire, K-I. Chen, R. Kirkwood, M. Porkolab, R. Parker, and J. Villasenor. "Combined ECRH and LHCD Experiments on the Versator II Tokamak."
- Kirkwood, R.K., I.H. Hutchinson, S.C. Luckhardt, and J.P. Squire. "Measurement of Suprathermal Current Carriers and Momentum Relaxation by Electron Cyclotron Transmission."
- Kupfer, K., A. Bers, and A. Ram. "RF Induced Transport in Tokamak Plasmas."

Remote Sensing Science Program, Annual Workshop, Santa Barbara, California, January 31, 1989.

Kong, J.A. "Polarimetric Models."

Rencontres de Moriond, Les Arcs, Savoie, France, March 5-12, 1989.

Burke, B.F. "Gravitational Lenses and the Determination of Cosmological Constants."

Rochester Conference on Coherence and Quantum Optics, Sixth, University of Rochester, Rochester, New York, June 26-28, 1989.

Gentile, T.R., B.J. Hughey, T.W. Ducas, and D. Kleppner. "Experimental Study of Two-Photon Rabi Oscillations."

Ho, S-T., N.C. Wong, and J.H. Shapiro. "Self-Focusing Limitations on Squeezed State Generation in Two-Level Media."

Hughey, B.J., T.R. Gentile, T.W. Ducas, and D. Kleppner. "Atom-Photon Interaction Modified by a Microwave Cavity."

Pritchard, D.E., and B.G. Oldaker. "Light Forces and Atom Diffraction - An Illustrated Summary."

Shapiro, J.H., S.R. Shepard, and N.C. Wong. "A New Number-Phase Uncertainty Principal."

Shapiro, J.H., S.R. Shepard, and N.C. Wong. "Coherent Phase States and Squeezed Phase States."

Sciences of Electronic Packaging Meeting, IBM Corporation, Endicott, New York, May 2-3, 1989.

Ali, S.M. "Microwave Design Techniques in Leading Edge Computer Packaging."

Signal Processing Conference, Boston, Massachusetts, May 1989.

Hardwick, J.C., and J.S. Lim. "Dual Excitation Speech Model."

SPIE Symposium on Lasers and Optics, Los Angeles, California, January 15-20, 1989.

DiRienzo, A., G. Bekefi, C. Leibovitch, and B.G. Danly. "Radiation Measurements from a 35GHz Cyclotron Autoresonance Maser (CARM) Amplifier."

Fujimoto, J.G. "Femtosecond Lasers and Ultrafast Measurement Techniques."

Nurmikko, A.V., R.L. Gunshor, and L.A. Kolodziejski. "Excitons and Phonons in Widegap II-VI Compound Semiconductor Superlattices."

Speech Research Symposium, Oklahoma State University, Stillwater, Oklahoma, March 13-15, 1989.

Hardwick, J.C., and J.S. Lim. "Dual Excitation Speech Model."

Symposium for Basic Research in a Clinical Environment, Dedham, Massachusetts, July 5-7, 1989.

Delgutte, B. "Does Suppression Result in Masking or Unmasking?"

Symposium on Electron, Ion and Photon Beams, 33rd International, Monterey, California, May 30 - June 2, 1989.

Blauner, P.G., Y. Butt, J.S. Ro, C.V. Thompson, and J. Melngailis. "Focused Ion Beam Induced Deposition of Low Resistivity Gold Films."

Chu, W., A. Yen, K. Ismail, M.I. Shepard, H.J. Lezec, C.R. Musil, J. Melngailis, Y-C. Ku, J.M. Carter, and H.I. Smith. "Sub-100 nm X-ray Mask Technology Using Focused-Ion-Beam Lithography."

Ismail, K., D.A. Antoniadis, and H.I. Smith. "A Lateral-Surface-Superlattice Structure on GaAs/AlGaAs for Far-Infrared and Magneto-Capacitance Measurements."

Ismail, K., W. Chu, R.T. Tiberio, A. Yen, H.J. Lezec, M.I. Shepard, C.R. Musil, J. Melngailis, D.A. Antoniadis, and H.I. Smith. "Resonant Tunneling Across and Mobility Modulation Along Surface-Structured Quantum Wells."

Moel, A., M.L. Schattenburg, J.M. Carter, and H.I. Smith. "Microgap Control in X-ray Nanolithography."

Symposium In Honor of N.Y.S. Kiang, Dedham, Massachusetts, July 5-7, 1989.

Peake, W.T., J.J. Rosowski, and T.J. Lynch III. "The Cat's Middle Ear: Measurements, Models, and Predictions."

Rabinowitz, W., and D.K. Eddington. "Effects of Channel-to-Electrode Mappings with the Symbion Cochlear Prosthesis."

Rosowski, J.J., W.T. Peake, and N. Yang. "A Simple Model for Level-Dependent Growth Rates of Auditory Distortion."

Transport Task Force Meeting, Institute for Fusion Studies, University of Texas, Austin, Texas, January 11-13, 1989.

Kupfer, K., A. Bers, and A.K. Ram. "Transport of Charged Particles Interacting with Coherent Wave-Fields in a Tokamak Plasma."

Sugiyama, L.E. "Predictive Transport Code Analysis."

US/Japan Workshop on Kinetic Modification of MHD Modes, Second Stability and Alpha Particles in Toroidal Systems, Princeton University, Princeton, New Jersey, January 12, 1989.

Luckhardt, S.C. "High Poloidal Beta Equilibria Generated by Means of Lower-Hybrid Current Drive."

Workshop on Compound Semiconductor Materials and Devices, Hilton Head, South Carolina, February 20-22, 1989.

del Alamo, J.A., and W.J. Azzam. "A Floating-Gate Transmission-Line Model (FGTLM) Technique for Accurate Measurement of Source Resistance in HFETs."

Workshop on Fracture Computations, Gaithersburg, Maryland, September 6-8, 1989.

Joannopoulos, J. "Total Energy Calculations in Solids."

Workshop on X-ray Lithography, Monterey, California, October 17-20, 1989.

Smith, H.I. "X-ray Mask Technology."

A.2 Published Meeting Papers

Ali, S.M., T.M. Habashy, and J.A. Kong. "Input Impedance of a Circular Microstrip Antenna Fed by an Eccentric Probe." *Progress in Electromagnetics Research Symposium*, Boston, Massachusetts, July 25-26, 1989.

Antoniadis, D.A., K. Ismail, and H.I. Smith. "Lateral Surface Superlattices and Quasi-One-Dimensional Structures in GaAs." *Proceedings of the Science and Engineering of 1- and 0-Dimensional Semiconductors NATO Advanced Research Workshop*, Cadiz, Spain, March 29-April 1, 1989.

Arnold, D.V., J.A. Kong, W.K. Melville, and R.W. Stewart. "Theoretical Prediction of EM Bias." *Progress in Electromagnetics Research Symposium*, Boston, Massachusetts, July 25-26, 1989.

Ashar, P., S. Devadas, and A.R. Newton. "Optimum and Heuristic Algorithms for Finite State Machine Decomposition and Partitioning." *Proceedings of the International Conference on Computer-Aided Design*, Santa Clara, California, November 5-9, 1989.

Bace, M.M., and J.S. Lim. "An Iterative Method for Designing Separable Wiener Filters." *Proceedings of the Second Acoustics, Speech, and Signal Processing Mini Conference*, Weston, Massachusetts, May 1989.

Bamji, C.S., and J. Allen. "GRASP: A Grammar-Based Schematic Parser." *Proceedings of the 26th Design Automation Conference*, Las Vegas, Nevada, June 1989.

Batchelor, D.B., E.F. Jaeger, B.A. Carreras, H. Weitzner, K. Imre, C. Stevens, V. Fuchs, and A. Bers. "Full-Wave Modeling of Ion-Cyclotron Heating in Tokamaks." *Proceedings of the 12th International Atomic Energy Agency Conference on Plasma Physics and Controlled Nuclear Fusion*, Volume 1:611-620, IAEA-CN-50/E-II-5 (Vienna: International Atomic Energy Agency, 1989), Nice, France, October 12-19, 1988.

Bekefi, G. "Coherent, Free Electron Radiation Sources." *Proceedings of the International Conference on Plasma Physics*, New Delhi, India, November 22-28, 1989.

Blauner, P.G., J.S. Ro, Y. Butt, C.V. Thompson, and J. Melngailis. "Direct Writing of Metallic Submicron Features Using Focused Ion Beams." *Proceedings of the Materials Research Society Symposium*, 129:483 (1989).

Borgeaud, M., J.A. Kong, R.T. Shin, and S.V. Nghiem. "Polarimetric Remote Sensing of Earth Terrain with Two-Layer Random Medium Model." *Progress in Electromagnetics Research Symposium*, Boston, Massachusetts, July 25-26, 1989.

Bossi, D.E., W.D. Goodhue, and R.H. Rediker. "Reduced-Confinement GaAlAs Tapered Waveguide Antenna." *Technical Digest Series Vol. 4:80-83 of the Integrated and Guided Wave Optics Topical Meeting*, Houston, Texas, February 6-8, 1989. (Optical Society of America, Washington, DC).

Chu, N.C., S.V. Nghiem, R.T. Shin, and J.A. Kong. "Phase Fluctuations of Waves Propagating Through a Random Medium." *Progress in Electromagnetics Research Symposium*, Boston, Massachusetts, July 25-26, 1989.

- Clevenger, L.A., C.V. Thompson, and R.R. deAvillez. "Kinetics and Thermodynamics of Amorphous Silicide Formation in Nickel/-Amorphous-Silicon Multilayer Thin Films." *Proceedings of the Spring Materials Research Society Meeting*, San Diego, California, April 24-29, 1989.
- Clevenger, L.A., C.V. Thompson, and K-N. Tu. "Controlled and Explosive Reactions in Nickel/Silicon Multilayer Thin Films." *Proceedings of the Materials Research Society International Meeting on Advance Materials* 10:431, Tokyo, Japan, 1989.
- Crow, M., J. White, and M. Ilic. "Stability and Convergence Aspects of Waveform Relaxation Applied to Power System Simulation." *Proceedings of the IEEE International Symposium on Circuits and Systems*, Portland, Oregon, May 9-11, 1989.
- Devadas, S. "Approaches to Multi-Level Sequential Logic Synthesis." *Proceedings of the 26th Design Automation Conference*, Las Vegas, Nevada, June 1989.
- Devadas, S. "Delay Test Generation for Synchronous Sequential Circuits." *Proceedings of the International Test Conference*, Washington, DC, August 1989.
- Devadas, S. "Optimal Layout Via Boolean Satisfiability." *Proceedings of the International Conference on Computer-Aided Design*, Santa Clara, California, November 5-9, 1989.
- Devadas, S. "General Decomposition of Sequential Machines: Relationships to State Assignment." *Proceedings of the 26th Design Automation Conference*, Las Vegas, Nevada, June 1989.
- Devadas, S., and K. Keutzer. "Boolean Minimization and Algebraic Factorization Procedures for Fully Testable Sequential Machines." *Proceedings of the International Conference on Computer-Aided Design*, Santa Clara, California, November 5-9, 1989.
- Devadas, S., H-K.T. Ma, and A.R. Newton. "Easily Testable PLA-Based Finite State Machines." *Proceedings of the Fault Tolerant Computing Symposium*, Chicago, Illinois, June 1989.
- Devadas, S., H-K.T. Ma, and A.R. Newton. "Redundancies and Don't Cares in Sequential Logic Synthesis." *Proceedings of the International Test Conference*, Washington, DC, August 1989.
- Devadas, S., H-K.T. Ma, A.R. Newton, and A. Sangiovanni-Vincentelli. "The Relationship Between Logic Synthesis and Test." *Proceedings of the VLSI '89*, Munich, West Germany, August 1989.
- Dubner, A.D., and A. Wagner. "In-Situ Measurement of Ion Beam Induced Deposition of Gold." *Proceedings of the Materials Research Society Symposium*, 147:155 (1989).
- Early, K., M.L. Schattenburg, and H.I. Smith. "Absence of Resolution Degradation in X-ray Lithography for λ from 4.5nm to 0.83nm." *Proceedings of the International Conference on Microlithography, Microcircuit Engineering*, Cambridge, England, September 26-28, 1989.
- Feder, M., and J.S. Jaffe. "Limited-Angle Reconstruction from Noisy Data Using Clustering of the Solution Space." *Proceedings of the IEEE International Conference on Acoustics, Speech, and Signal Processing*, Glasgow, Scotland, May 23-26, 1989.
- Feder, M., and E. Weinstein. "Sequential Algorithms FIR System Identification Based on the Kullback-Leibler Information Measure." *Proceedings of the IEEE International Conference on Acoustics, Speech, and Signal Processing*, Glasgow, Scotland, May 23-26, 1989.
- Ghosh, A., S. Devadas, and A.R. Newton. "Test Generation for Highly Sequential Circuits." *Proceedings of the International Conference on Computer-Aided Design*, Santa Clara, California, November 5-9, 1989.
- Gonsalves, J.M., N. Otsuka, J.Qui, M. Kobayashi, R.L. Gunshor, and L.A. Kolodziejski. "Electron Microscope Study of the Initial Stage of Growth of ZnSe on GaAs." *Proceedings of the Materials Research Society Symposia*, San Diego, California, April 24-29, 1989.
- Gu, Q., Y.E. Yang, and J.A. Kong. "Transient Analysis of Frequency-Dependent Transmission Lines with Nonlinear Terminations." *Progress in Electromagnetics Research Symposium*, Boston, Massachusetts, July 25-26, 1989.
- Gunshor, R.L., L.A. Kolodziejski, M. Kobayashi, A.V. Nurmikko, and N. Otsuka. "Metastable Zincblende MnTe and MnSe: MBE Growth and Characterization." *Proceedings of the Materials Research Society Symposium* 151:141-149 (1989).

- Hagelstein, P.L. "Coherent Fusion Theory." *Proceedings of The American Society of Mechanical Engineers Winter Annual Meeting*, San Francisco, California, December 10-15, 1989.
- Han, H.C., J.A. Kong, and T.M. Habashy. "Far Field Pattern of a VLF Antenna Array in the Ionospheric Plasmas." *Progress in Electromagnetics Research Symposium*, Boston, Massachusetts, July 25-26, 1989.
- Hardwick, J.C., and J.S. Lim. "The Dual Excitation Speech Model." *Proceedings of the Second Acoustics, Speech, and Signal Processing Mini Conference*, Weston, Massachusetts, May 1989.
- Jaffe, J.S., and J.M. Richardson. "Code-Division Multiple Beam Imaging." *Proceedings of the Oceans '89 Conference*, Seattle, Washington, September 17-21, 1989.
- Kiang, J.F., S.M. Ali, and J.A. Kong. "Analysis of Dielectric Strip Waveguides Using Integral Equation Formulation." *Progress in Electromagnetics Research Symposium*, Boston, Massachusetts, July 25-26, 1989.
- Ku, Y.C., H.I. Smith, and I. Plotnik. "Low Stress Tungsten Absorber for X-ray Masks." *Proceedings of the International Conference Microlithography, Microcircuit Engineering*, Cambridge, England, September 26-28, 1989.
- Kupfer, K., A. Bers, and A. Ram. "RF Induced Transport in Tokamak Plasmas." *Proceedings of the American Institute of Physics Conference 190*, Irvine, California, May 1-3, 1989.
- Lam, C.W., S.M. Ali, and J.A. Kong. "A New Finite-Difference Time-Domain Grid Model for Microstrip Problems in Anisotropic Media." *Progress in Electromagnetics Research Symposium*, Boston, Massachusetts, July 25-26, 1989.
- Lee, C.F., R.T. Shin, J.A. Kong, and B.J. McCartin. "Finite Difference Time Domain Techniques for Two Dimensional Triangular Grids." *Progress in Electromagnetics Research Symposium*, Boston, Massachusetts, July 25-26, 1989.
- Lee, C.F., R.T. Shin, J.A. Kong, and B.J. McCartin. "Absorbing Boundary Conditions on Circular and Elliptic Boundaries." *Progress in Electromagnetics Research Symposium*, Boston, Massachusetts, July 25-26, 1989.
- Li, K., R.T. Shin, and J.A. Kong. "Radar Cross Section Prediction of Slots in Ground Planes Using Method of Moments." *Progress in Electromagnetics Research Symposium*, Boston, Massachusetts, July 25-26, 1989.
- Lim, H.H., H.A. Yueh, J.A. Kong, R.T. Shin, and J.J. van Zyl. "Contrast and Classification Studies of Polarimetric SAR Images for Remote Sensing of Earth Terrain." *Progress in Electromagnetics Research Symposium*, Boston, Massachusetts, July 25-26, 1989.
- Lin, F.C., H.A. Yueh, J.A. Kong, and R.T. Shin. "Correlation Function Study for Random Media with Multiphase Mixtures." *Progress in Electromagnetics Research Symposium*, Boston, Massachusetts, July 25-26, 1989.
- Lumsdaine, A., J. Wyatt, and I. Elfadel. "Parallel Distributed Networks for Image Smoothing and Segmentation in Analog VLSI." *Proceedings of the 28th IEEE Conference on Decision and Control*, Tampa, Florida, December 13-15, 1989.
- Melngailis, J. "Focused Ion Beam Lithography and Implantation." *Proceedings of the Eighth Biennial University/Government/Industry Microelectronics Symposium*, Westboro, Massachusetts, June 1989.
- Melngailis, J., and P.G. Blauner. "Focused Ion Beam Induced Deposition." *Proceedings of the Materials Research Symposium*, San Diego, California, April 24-29, 1989.
- Nabors, K., and J. White. "A Fast Multipole Algorithm for Capacitance Extraction of Complex 3-D Geometries." *Proceedings of the Custom Integrated Circuits Conference*, San Diego, California, May 15-18, 1989.
- Nghiem, S.V., and J.A. Kong. "Faraday Polarization Fluctuations in Transionspheric Polarimetric VLF Waves." *Progress in Electromagnetics Research Symposium*, Boston, Massachusetts, July 25-26, 1989.
- Nghiem, S.V., F.C. Lin, J.A. Kong, R.T. Shin, and H.A. Yueh. "Three-Layer Random Medium Model for Fully Polarimetric Remote Sensing of Geophysical Media." *Progress in Electromagnetics Research Symposium*, Boston, Massachusetts, July 25-26, 1989.
- Phillips, J.M., J.E. Palmer, N.E. Hecker, and C.V. Thompson. "The Effect of Annealing on the Structure of Epitaxial CaF₂ Films on Si(100)." *Proceedings of the Materials Research Society*

- Spring Meeting*, San Diego, California, April 24-29, 1989.
- Ram, A.K., and A. Bers. "Kinetic Ray Tracing in Toroidal Geometry with Application to Mode-Converted Ion-Bernstein Waves." *Proceedings of the 1989 International Conference on Plasma Physics*, New Delhi, India, pp. 57-60. Eds. A. Sen, and P.K. Law, 1989.
- Reichelt, M., J. White, and J. Allen. "A Fast and Parallelizable Technique for Transient Device Simulation." *Proceedings of the International Conference on Computer-Aided Design*, Santa Clara, California, November 5-9, 1989.
- Reichelt, M., J. White, and J. Allen. "Waveform Relaxation for Transient Simulation of Two-Dimensional MOS Devices." *Proceedings of the International Conference on Computer-Aided Design*, Santa Clara, California, November 5-9, 1989.
- Segal, M., and E. Weinstein. "Spatial and Spectral Parameter Estimation of Multiple Source Signals." *Proceedings of the IEEE International Conference on Acoustics, Speech, and Signal Processing*, Glasgow, Scotland, May 23-26, 1989.
- Sheen, D.M., S.M. Ali, M.D. Abouzahra, and J.A. Kong. "Analysis of Multiport Rectangular Microstrip Structures Using a Three Dimensional Finite Difference Time Domain Technique." *Progress in Electromagnetics Research Symposium*, Boston, Massachusetts, July 25-26, 1989.
- Smith, H.I., K. Ismail, W. Chu, A. Yen, Y.C. Ku, and D.A. Antoniadis. "X-ray Nanolithography and Quantum-Effect Electronics." *Proceedings of the Molecular Electronics-Science and Technology, Engineering Foundation Conferences*, Keauhou Kona, Hawaii, February 19-24, 1989.
- Smith, H.I., K. Ismail, M.L. Schattenburg, and D.A. Antoniadis. "Sub-100nm Electronic Devices and Quantum-Effects Research Using X-ray Nanolithography." *Proceedings of the International Conference Microlithography, Microcircuit Engineering*, Cambridge, England, September 26-28, 1989.
- Staelin, D.H. "Passive Microwave Sensing of the Atmosphere from Space." *Proceedings of the Microwave Radiometry and Remote Sensing Applications*, Florence, Italy, March 9-11, 1989.
- Standley, D.L. "Criteria for Robust Stability in a Class of Lateral Inhibition and Related Networks Coupled Through a Resistive Grid." *Proceedings of the Conference on Information Sciences and Systems*, Johns Hopkins University, Baltimore, Maryland, March 22-24, 1989.
- Standley, D.L. "Design Criteria Extensions for Stable Lateral Inhibition Networks in the Presence of Circuit Parasitics." *Proceedings of the IEEE International Symposium on Circuits and Systems*, Portland, Oregon, May 1989.
- Tsuk, M.J., and J.A. Kong. "The Frequency-Dependent Resistance of Conductors with Arbitrary Cross-Section." *Progress in Electromagnetics Research Symposium*, Boston, Massachusetts, July 25-26, 1989.
- Tulintseff, A.N., S.M. Ali, and J.A. Kong. "Input Impedance and Radiation Fields of a Probe-Fed Stacked Circular Microstrip Antenna." *Progress in Electromagnetics Research Symposium*, Boston, Massachusetts, July 25-26, 1989.
- Van Aelten, F., and J. Allen. "Efficient Verification of VLSI Circuits Based on Syntax and Denotational Semantics." *Proceedings of the Interuniversity Micro Electronics Center-International Federation for Information Processing, Workshop on Applied Formal Methods for Correct VLSI Design*. Leuven, Belgium, November 1989.
- Weinstein, E., and M. Feder. "Sequential Algorithms Based on Kullback-Liebler Information Measure and their Application to FIR System Identification." *Proceedings of the IEEE International Conference on Acoustics, Speech, and Signal Processing*, Glasgow, Scotland, May 23-26, 1989.
- Xia, J., S.M. Ali, and J.A. Kong. "Analysis of Microstrip Discontinuities on Anisotropic Substrates." *Progress in Electromagnetics Research Symposium*, Boston, Massachusetts, July 25-26, 1989.
- Yang, W. "A Charged-Coupled Device Architecture for On Focal Plane Image Signal Processing." *Proceedings of the International Symposium on VLSI Technology, Systems, and Applications*, pp. 266-270, Taipei, Taiwan, R.O.C., May 1989.
- Yang, W., and A.M. Chiang. "VLSI Processor Architectures for Computer Vision." *Proceedings of the Image Understanding Work-*

- shop, pp. 193-199, Palo Alto, California, May 1989.
 - Yang, Y.E., and J.A. Kong. "Transient Analysis of Capacitively Loaded VLSI Off-Chip Interconnections." *Progress in Electromagnetics Research Symposium*, Boston, Massachusetts, July 25-26, 1989.
 - Yen, A., R.A. Ghanbari, E.H. Anderson, and H.I. Smith. "Fabrication of 100 nm-Period Gratings Using Achromatic Holographic Lithography." *Proceedings of the International Conference Microlithography, Microcircuit Engineering*, Cambridge, England, September 26-28, 1989.
 - Yueh, H.A., J.A. Kong, R.M. Barnes, and R.T. Shin. "Calibration of Polarimetric Radars Using In-Scene Reflectors." *Progress in Electromagnetics Research Symposium*, Boston, Massachusetts, July 25-26, 1989.
 - Yueh, H.A., J.A. Kong, J.K. Jao, R.T. Shin, and L.M. Novak. "K-distribution and Polarimetric Terrain Radar Clutter." *Progress in Electromagnetics Research Symposium*, Boston, Massachusetts, July 25-26, 1989.
 - Zissman, M.A., C.J. Weinstein, L.D. Braid, R.M. Uchanski, and W.M. Rabinowitz. "Speech State Adaptive Simulation of Co-channel Talker Interference Suppression." *Proceedings of the IEEE International Conference on Acoustics, Speech, and Signal Processing*, Glasgow, Scotland, May 23-26, 1989, pp. 361-364.
- ### A.3 Meeting Papers Accepted For Publication
- Asher, P., S. Devadas, and A.R. Newton. "A Unified Approach to Decomposition and Redecomposition of Sequential Machines." *Proceedings of the 27th Design Automation Conference*, Orlando, Florida, June 1990.
 - Asher, P., S. Devadas, and A.R. Newton. "Multiple-Fault Testable Sequential Machines." *Proceedings of the International Symposium on Circuits and Systems*, New Orleans, May 1990.
 - Beckmann, P., and B.R. Musicus. "Fault-Tolerant Round Robin A/D Converter System." *Proceedings of the IEEE International Conference on Acoustics, Speech, and Signal Processing*, Albuquerque, New Mexico, April 1990.
 - Bossi, D.E., W.D. Goodhue, M.C. Finn, K. Rauschenbach, and R.H. Rediker. "Fabrication and Enhanced Performance of Reduced-Confinement GaAlAs Tapered-Waveguide Antennas." *Technical Digest of the Topical Meeting on Integrated Photonics Research*, Hilton Head, South Carolina, March 1990. (Optical Society of America, Washington, DC).
 - Corcoran, C., and R.H. Rediker. "Operation of Five Discrete Diode Lasers as a Coherent Ensemble by Fiber-Coupling into an External Cavity." *Technical Digest of the Conference on Electoptics and Lasers, CLEO 90*, Anaheim, California, May 1990. (Optical Society of America, Washington, DC).
 - Davis, R.L. "Conditioning Lesions Promote Primary-Auditory Neurite Regeneration in Vitro." *Proceedings of the Association of Research for Otolaryngology*, St. Petersburg, Florida, February 4-8, 1990.
 - Devadas, S., and K. Keutzer. "Necessary and Sufficient Conditions for Robust Delay-Fault Testability of Logic Circuits." *Proceedings of the Sixth MIT Conference on Advanced Research on VLSI*, April 1990.
 - Devadas, S., and K. Keutzer. "A Unified Approach to the Synthesis of Fully Testable Sequential Machines." *Proceedings of the 23rd International Conference on System Sciences*, Hawaii, January 1990.
 - Devadas, S., and K. Keutzer. "Synthesis and Optimization Procedures for Robust Delay-Fault Testability of Logic Circuits." *Proceedings of the 27th Design Automation Conference*, Orlando, Florida, June 1990.
 - Devadas, S., and K. Keutzer. "Logic Synthesis and Testability." *Proceedings of the International Symposium on Circuits and Systems*, New Orleans, May 1990.
 - Devadas, S., and K. Keutzer. "Validatable Nonrobust Delay-Fault Testable Circuits Via Logic Synthesis." *Proceedings of the International Symposium on Circuits and Systems*, New Orleans, May 1990.
 - Devadas, S., K. Keutzer, and J. White. "Estimation of Power Dissipation in CMOS Combinational Circuits." *Proceedings of the Custom Integrated Circuits Conference*, Boston, Massachusetts, May 1990.
 - Devadas, S., H-K.T. Ma, A.R. Newton, and A. Sangiovanni-Vincentelli. "Irredundant Sequential Machines Via Optimal Logic Synthesis." *Proceedings of the 23rd International Confer-*

- ence on System Sciences, Hawaii, January 1990.
- Devadas, S., and A.R. Newton. "Exact Algorithms for Output Encoding, State Assignment and Four-Level Boolean Minimization." *Proceedings of the 23rd International Conference on System Sciences*, Hawaii, January 1990.
- Ghosh, A., S. Devadas, and A.R. Newton. "Verification of Interacting Sequential Circuits." *Proceedings of the 27th Design Automation Conference*, Orlando, Florida, June 1990.
- Ghosh, A., S. Devadas, and A.R. Newton. "Sequential Test Generation at the Register-Transfer and Logic Levels." *Proceedings of the 27th Design Automation Conference*, Orlando, Florida, June 1990.
- Lam, K., and S. Devadas. "Performance-Oriented Synthesis of Finite State Machines." *Proceedings of the International Symposium on Circuits and Systems*, New Orleans, May 1990.
- Nelson, K.A. "Impulsive Stimulated Raman Scattering with Single-Pulse and Multiple-Pulse Excitation." *Proceedings of the 12th International Conference on Raman Spectroscopy*, Columbia, South Carolina, August 13-17, 1990.
- Neto, H., L. Silveira, J. White, and L. Vidigal. "On Exponential Fitting for Circuit Simulation." *Proceedings of the International Symposium on Circuits and Systems*, New Orleans, May 1990.
- Weiner, A.M., D.E. Leaird, G.P. Wiederrecht, M.J. Banet, and K.A. Nelson. "Spectroscopy with Shaped Femtosecond Pulses: Styles for the 1990s." *Proceedings of the SPIE Conference on Optoelectronics and Lasers*, Los Angeles, California, June 14-19, 1990.
- and Wraparound Microstrip Structures." *IEEE Trans. Microwave Theory Tech.* 37(11):1773-1783 (1989).
- Alwan, A. "Perceptual Cues for Place of Articulation for the Voiced Pharyngeal and Uvular Consonants." *J. Acoust. Soc. Am.* 86(2):549-556 (1989).
- Arias, T.A., and J.D. Joannopoulos. "Re-Examination of Magnetic Effects in the Bose Gas." *Phys. Rev. B.* 39 (7):4071-4078 (1989).
- Atwater, H.A., and C.V. Thompson. "The Role of Point Defects in Ion-Bombardment-Enhanced and Dopant-Enhanced Grain Growth in Silicon Thin Films." *J. Nucl. Instrum. Meth. Phys. Res. B.* 39:64 (1989).
- Auyang, S.Y., and P.A. Wolff. "Free-Carrier-Induced Third Order Optical Nonlinearities in Semiconductors." *J. Opt. Soc. Am.* A6:2696 (1989).
- Bagnato, V.S., G.P. Lafyatis, A. Martin, K. Helmerson, J. Landry, and D.E. Pritchard. "Laser Deceleration and Velocity Bunching of a Neutral Sodium Beam." *J. Opt. Soc. Am. B.* 6(11):2171-2177 (1989).
- Bagwell, P.F., and T.P. Orlando. "Landauer's Conductance Formula and its Generalization to Finite Voltages." *Phys. Rev. B.* 40:1456 (1989).
- Bagwell, P.F., and T.P. Orlando. "Broadened Conductivity Sensor and Density of States for a Superlattice Potential in 1, 2, and 3 Dimensions." *Phys. Rev. B* 40:3735 (1989).
- Beckerle, J.D., A.D. Johnson, and S.T. Ceyer. "Observation and Mechanism of Collision-Induced Desorption: CH₄ on Ni(111)." *Phys. Rev. Lett.* 62(6):685-688 (1989).
- Bekefi, G., A. DiRienzo, C. Leibovitch, and B.G. Danly. "A 35 GHz Cyclotron Autoresonance Maser Amplifier." *Appl. Phys. Lett.* 54(14):1302-1304 (1989).
- Bekefi, G., A. DiRienzo, C. Leibovitch, and B.G. Danly. "A 35 GHz Cyclotron Autoresonance Maser Amplifier." *Nucl. Instrum. Methods Phys. Res. A* 285 :230-232 (1989).
- Bellissent, M.C., J. Teixeira, S.H. Chen, B. Dörner, H.D. Middendorf, and H.L. Crespi. "Low Frequency Collective Modes in Dry and Hydrated Proteins." *Biophys. J.* 56:713 (1989).

A.4 Published Journal Articles

- Alerhand, O.L., J.D. Joannopoulos, and E.J. Mele. "Thermal Amplitudes of Surface Atoms on Si(111) 2x1 and Si(001) 2x1." *Phys. Rev. B* 39(17):622-629 (1989).
- Alerhand, O.L., E. Kaxiras, J.D. Joannopoulos, and G.W. Turner. "Model of Epitaxial Growth of GaAs on Si(100): Nucleation at Surface Steps." *J. Vac. Sci. Technol. B.* 7(4):695-699 (1989).
- Ali, S.M., T.M. Habashy, J.F. Kiang, and J.A. Kong. "Resonance in Cylindrical-Rectangular

- Bers, A., G.S. Triantafyllou, and A.K. Ram. "Absolute Instabilities in Inhomogeneous Flows." *Bull. Am. Phys. Soc.* 34:2263 (1989).
- Blauner, P.G., Y. Butt, J.S. Ro, C.V. Thompson, and J. Melngailis. "Focused Ion Beam Induced Deposition of Low-Resistivity Gold Films." *J. Vac. Sci. Technol. B.* 7(6):1816-1818 (1989).
- Blauner, P.G., Y. Butt, J.S. Ro, C.V. Thompson, and J. Melngailis. "Focused Ion Beam Induced Deposition of Low-Resistivity Gold Structures." *J. Vac. Sci. Technol. B.* 7(6):609-617 (1989).
- Blauner, P.G., J.S. Ro, Y. Butt, and J. Melngailis. "Focused Ion Beam Fabrication of Submicron Gold Structures." *J. Vac. Sci. Technol. B.* 7(4):609-617 (1989).
- Blauner, P.G., J.S. Ro, Y. Butt, C.V. Thompson, and J. Melngailis. "The Microstructure of Gold Films Written by Focused Ion Beam Induced Deposition." *Mat. Res. Soc. Symp. Proc.* 129:483-488 (1989).
- Borgeaud, M., S.V. Nghiem, R.T. Shin, and J.A. Kong. "Theoretical Models for Polarimetric Microwave Remote Sensing of Earth Terrain." *J. Electromag. Waves Appl.* 3(1):61-81 (1989).
- Brock, J.D., D.Y. Noh, B.R. McClain, J.D. Litster, R.J. Birgeneau, A. Aharony, P.M. Horn, and J.C. Liang. "Hexatic Ordering in Freely Suspended Liquid Crystal Films." *J. Phys. B - Condensed Matter* 74:197-213 (1989).
- Cametti, C., P. Codastefano, A. Diasio, P. Tartaglia, and S.H. Chen. "Dynamic Scaling of Dielectric Relaxation in AOT/Water/decane Microemulsions Near the Percolation Threshold." *Phys. Rev. A* 40:1962 (1989).
- Carilli, C.L., J.W. Dreher, S. Conner, and R.A. Perley. "Broad- and Narrow-Band Imaging of the Giant Radio Galaxy Cygnus A." *Astron. J.* 98(2):513-523 (1989).
- Carilli, C.L., J.H. van Gorkom, and J.T. Stocke. "Disturbed Neutral Hydrogen in the Galaxy NGC 3067 Pointing to the Quasar 3C 232." *Nature* 338:134-136 (1989).
- Carvalho, B., G. Briganti, and S.H. Chen. "Lowering of the Miscibility Gap in the Dioctanoylphosphatidylcholine-Water System by Addition of Urea." *J. Phys. Chem.* 93:4282 (1989).
- Cassereau, P.M., D.H. Staelin, and G. de Jager. "Encoding of Images Based on Lapped Orthogonal Transform." *IEEE Trans. Comm.* 37(2):189-193 (1989).
- Chen, S.C., G. Bekefi, S. DiCecca, and R. Temkin. "Tunable MicroWigglers for Free-Electron Lasers." *Appl. Phys. Lett.* 54(14):1299-1301 (1989).
- Cho, J., and C.V. Thompson. "The Grain Size Dependence of Electromigration Induced Failures in Narrow Interconnects." *Phys. Lett.* 54:2577 (1989).
- Chow, C., V. Fuchs, and A. Bers. "An Analytic Theory of ICRF Heating" (abstract). *Bull. Am. Phys. Soc.* 34:2094 (1989).
- Chow, C., A.K. Ram, and A. Bers. "Damping of the Fast Alfvén Wave in Ion-Cyclotron Resonance Heating." *Phys. Fluids* B1(10):2018-2026 (1989).
- Chu, W., A. Yen, K. Ismail, M.I. Shepard, H.J. Lezec, C.R. Musil, J. Melngailis, Y.-C. Ku, J.M. Carter, and H.I. Smith. "Sub-100-nm X-ray Mask Technology Using Focused-Ion-Beam Lithography." *J. Vac. Sci. Technol. B* 7(6):1583-1585 (1989).
- Clifton, R.K., P.M. Zurek, B.G. Shinn-Cunningham, and N.I. Durlach. "Cross-Frequency Interactions in the Precedence Effect." *J. Acoust. Soc. Am.* 85:S83 (1989).
- Coffey, K.R., L.A. Clevenger, K. Barmak, D.A. Rudman, and C.V. Thompson. "Experimental Evidence for Nucleation During Thin Film Reactions." *Appl. Phys. Lett.* 55:852 (1989).
- Coppi, B. "Transport Coefficients for the Plasma Thermal Energy and Empirical Scaling 'Laws.'" *Comments Plasma Phys. Controlled Fusion* 12(6):319-327 (1989).
- Coppi, B., P. Detragiache, S. Migliuolo, F. Pegoraro, and F. Porcelli. "Quiescent Window For Global Plasma Modes." *Phys. Rev. Lett.* 63(25):2733-2736 (1989).
- Cornell, E.A., R.M. Weisskoff, K.R. Boyce, R.W. Flanagan, Jr., G.P. Lafyatis, and D.E. Pritchard. "Single-Ion Cyclotron Resonance Measurement of $M(\text{CO}^+)/M(\text{N}_2^+)$." *Phys. Rev. Lett.* 63(16):1674-1677 (1989).
- DeAvillez, R.R., L.A. Clevenger, and C.V. Thompson. "Relaxation Phenomena in Evaporated Amorphous Silicon Films." *J. Mater. Res.* 4:1057 (1989).

- del Alamo, J.A., and W.J. Azzam. "A Floating-Gate Transmission-Line Model (FGTLM) Technique for Measuring Source Resistance in Heterostructure Field-Effect Transistors." *IEEE Trans. Electron Devices* 36(11):2386-2393 (1989).
- del Alamo, J.A., and T. Mizutani. "A Recessed-Gate $\text{In}_{0.52}\text{Al}_{0.48}\text{As}/\text{n}^+ - \text{In}_{0.53}\text{Ga}_{0.47}\text{As}$ MIS-type FET." *IEEE Trans. Electron Devices* 36(4):646-650 (1989).
- del Alamo, J.A., and T. Mizutani. "An $\text{In}_{0.52}\text{Al}_{0.48}\text{As}/\text{n}^+ - \text{In}_{0.53}\text{Ga}_{0.47}\text{As}$ MISFET with a Modulation-Doped Channel." *IEEE Electron Device Lett.* 10(8):394-396 (1989).
- Devadas, S., H.-K.T. Ma, A.R. Newton, and A. Sangiovanni-Vincentelli. "A Synthesis and Optimization Procedure for Fully and Easily Testable Sequential Machines." *IEEE Trans. Comput.-Aided Des. Integr. Circuits* 8(10):1100-1107 (1989).
- Devadas, S., and A.R. Newton. "Algorithms for Hardware Allocation in Datapath Synthesis." *IEEE Trans. Comput.-Aided Des. Integr. Circuits* 8(7):768-781 (1989).
- Devadas, S., H.-K.T. Ma, A.R. Newton, and A. Sangiovanni-Vincentelli. "MUSTANG: State Assignment of Finite State Machines Targeting Multi-Level Logic Implementations." *IEEE Trans. Comput.-Aided Des. Integr. Circuits* 7(12):1290-1300 (1989).
- Devadas, S., and A.R. Newton. "Decomposition and Factorization of Sequential Finite State Machines." *IEEE Trans. Comput.-Aided Des.* 8(11):1206-1217 (1989).
- DiRienzo, A.C., G. Bekefi, C. Leibovitch, and B.G. Danly. "Radiation Measurements from a 35 GHz Cyclotron Autoresonance Maser (CARM) Amplifier." *SPIE Proc.* 1061:238-242 (1989).
- Dubner, A.D., and A. Wagner. "In Situ Measurement of Ion Beam Induced Deposition of Gold." *J. Appl. Phys.* 65(9):3636 (1989).
- Dubner, A.D., and A. Wagner. "The Role of Gas Adsorption in Ion-Beam-Induced Deposition of Gold." *J. Appl. Phys.* 66(2):870 (1989).
- Dubner, A.D., and A. Wagner. "Mechanism of Ion Beam Induced Deposition of Gold." *J. Vac. Sci. Technol.* B7:1950 (1989).
- Duchnowski, P., and P.M. Zurek. "Simulation of Sensorineural Hearing Loss." *J. Acoust. Soc. Am.* 85:S26 (1989).
- Durlach, N.I., L.A. Delhorne, A. Wong, W.Y. Ko, W.M. Rabinowitz, and J. Hollerbach. "Manual Discrimination and Identification of Length by the Finger-Span Method." *Percept. Psychophys.* 46(1):29-38 (1989).
- Durlach, N.I., H.Z. Tan, N.A. Macmillan, W.M. Rabinowitz, and L.D. Braida. "Resolution in One Dimension with Random Variations in Background Dimensions." *Percept. Psychophys.* 46(3):293-296 (1989).
- Englade, R.C. "Ignition and Anomalous Transport Processes." *Nucl. Fusion* 29(6):999-1012 (1989).
- Evans-Lutterodt, K., R.J. Birgeneau, E.D. Specht, J.W. Chung, J.D. Brock, M.S. Altman, P.J. Estrup, I.K. Robinson, and A.A. MacDowell. "X-ray Study of $\text{W}(001)$ With and Without Hydrogen." *J. Vac. Sci. Technol. A* 7(3):2209-2216 (1989).
- Feder, M., A.V. Oppenheim, and E. Weinstein. "Maximum Likelihood Noise Cancellation Using the EM Algorithm." *IEEE J. Acoust. Speech Sig. Proc.* 37(2):204-216 (1989).
- Fu, Q., D. Lee, A.V. Nurmikko, R.L. Gunshor, and L.A. Kolodziejski. "Isoelectronic Delta Doping in a ZnSe Superlattice: Te as an Efficient Hole Trap." *Phys. Rev. B.* 39(5):3173-3177 (1989).
- Gallagher, A., and D.E. Pritchard. "Exoergic Collisions of Cold $\text{Na}^+ - \text{Na}$." *Phys. Rev. Lett.* 63:957 (1989).
- Gasiewski, A.J., and D.H. Staelin. "Statistical Precipitation Cell Parameter Estimation Using Passive 118-GHz O_2 Observations." *J. Geophys. Res.* 94(D15):18,367-18,378 (1989).
- Gentile, T.R., B.J. Hughey, D. Kleppner, and T.W. Ducas. "Experimental Study of One- and Two-Photon Rabi Oscillations." *Phys. Rev. A.* 40(9):5103-5115 (1989).
- Glasser, L.A. "Frequency Limitations in Circuits Composed of Linear Devices." *IEEE Trans. Circuits Syst.* 35(10):1299-1307 (1989).
- Glenn, J.L., O. Sungki, M. Kobayashi, R.L. Gunshor, L.A. Kolodziejski, D. Li, N. Otsuka, M. Haggerott, N. Pelekanos, and A.V. Nurmikko. "Multiple Quantum Wells of InSb/CdTe Grown

- by MBE." *J. Vacuum Sci. Technol.* B7:249-252 (1989).
- Gomez-Santos, G., J.D. Joannopoulos, and J.W. Negele. "Monte Carlo Study of the Quantum Spin-1/2 Heisenberg Antiferromagnet on the Square Lattice." *Phys. Rev. B.* 39 (7):4435-4443 (1989).
- Goodberlet, J., J. Wang, and J.G. Fujimoto. "Femtosecond Passively Mode-Locked Ti:Al₂O₃ Laser with a Nonlinear External Cavity" *Optics Lett.* 14(20):1125-1127 (1989).
- Goodberlet, J., J. Wang, J.G. Fujimoto, P.A. Schulz, and S. Henion. "Passive Mode Locking of a Ti:Al₂O₃ Laser with a Nonlinear Coupled Cavity" *Proc. Opt. Soc. Am. Topical Meeting on Tunable Solid State Lasers* 5:16-19 (1989).
- Graybeal, A., J.J. Rosowski, D.R. Ketten, and A.W. Crompton. "Inner-Ear Structure in Morganucodon, an Early Jurassic Mammal." *Zool. J. Linn. Soc.* 96:107-117 (1989).
- Greenberg, J.E., and P.M. Zurek. "Evaluation of a Real-Time Adaptive Beamforming Hearing Aid." *J. Acoust. Soc. Am.* 86:S87 (1989).
- Greenberg, J.E., P.M. Zurek, and P.M. Peterson. "Reducing the Effects of Target Misalignment in an Adaptive Beamformer for Hearing Aids." *J. Acoust. Soc. Am.* 85:S26 (1989).
- Gu, Q., Y.E. Yang, and J.A. Kong. "Transient Analysis of Frequency-Dependent Transmission Line Systems Terminated with Nonlinear Loads." *J. Electromag. Waves Appl.* 3(3):183-197 (1989).
- Guinan, Jr., J.J., M.P. Joseph, and B.E. Norris. "Brainstem Facial-Motor Pathways From Two Distinct Groups of Stapedius Motoneurons in the Cat." *J. Comp. Neurol.* 289:134-144 (1989).
- Haroche, S., and D. Kleppner. "Cavity Quantum Electrodynamics." *Phys. Today* 42:24-39 (1989).
- Haus, H.A., and W.P. Huang. "Mode Coupling in Tapered Structures." *J. Lightwave Technol.* 7(4):729-730 (1989).
- Haus, H.A., W.P. Huang, and A.W. Snyder. "Coupled-Mode Formulations." *Optics Lett.* 14(21):1222-1224 (1989).
- Haus, H.A., K. Watanabe, and Y. Yamamoto. "Quantum Nondemolition Measurement of Optical Solitons." *J. Opt. Soc. Am. B.* 6(6):1138-1148 (1989).
- Held, G.A., J.L. Jordan-Sweet, P.M. Horn, A. Mak, and R.J. Birgeneau. "X-ray Scattering of the Deconstruction and Thermal Roughening of the Au(110)1x3 Reconstructed Surface." *Solid State Commun.* 72:37 (1989).
- Held, G.A., J.L. Jordan-Sweet, P.M. Horn, A. Mak, and R.J. Birgeneau. "Disordering Transitions of Metal Surfaces." *J. de Physique Colloque* C7(50):245 (1989).
- Hemmer, P.R., M.S. Shahriar, V.D. Natoli, and S. Ezekiel. "Ac-Stark Shifts in a Two-Zone Raman Interaction." *J. Opt. Soc. Am. B.* 6(8):1519-1528 (1989).
- Hong, H., C.J. Peters, A. Mak, R.J. Birgeneau, P.M. Horn, and H. Suematsu. "Synchrotron X-Ray Study of the Structures and Phase Transitions of Monolayer Xenon on Single-Crystal Graphite." *Phys. Rev. B.* 40(7):4797-4807 (1989).
- Hong, H., and R.J. Birgeneau. "X-ray Diffraction Study of the Structure of Xenon Multilayers on Single Crystal Graphite." *Z. Phys. B* 77:413-419 (1989).
- Huang, W-P., and H.A. Haus. "Power Exchange in Grating-Assisted Couplers." *J. Lightwave Technol.* 7(6):920-924 (1989).
- Hui, K., and A.N. Berker. "Random-Field Mechanism in Random-Bond Multicritical Systems." *Phys. Rev. Lett.* 62(21):2507-2510 (1989).
- Ippen, E.P., H.A. Haus, and L.Y. Liu. "Additive Pulse Mode Locking." *J. Opt. Soc. Am. B.* 6(9):1736-1745 (1989).
- Ippen, E.P., L.Y. Liu, and H.A. Haus. "Self-Starting Condition for Additive-Pulse Mode-Locked Lasers." *Opt. Lett.* 15(3):183-185 (1989).
- Ismail, K., D.A. Antoniadis, and H.I. Smith. "One-Dimensional Subbands and Mobility Modulation in GaAs/AlGaAs Quantum Wires." *Appl. Phys. Lett.* 54:1130 (1989).
- Ismail, K., D.A. Antoniadis, and H.I. Smith. "Lateral Resonant Tunneling in a Double-Barrier Field-Effect Transistor." *Appl. Phys. Lett.* 55:589 (1989).

- Ismail, K., D.A. Antoniadis, H.I. Smith, C.T. Liu, K. Nakamura, and D.C. Tsui. "A Lateral-Surface-Superlattice Structure on GaAs/AlGaAs for Far-Infrared and Magneto-Capacitance Measurements." *J. Vac. Sci. Technol. B* 7(6):2000-2002 (1989).
- Ismail, K., W. Chu, R.T. Tiberio, A. Yen, H.J. Lezec, M.I. Shepard, C.R. Musil, J. Melngailis, D.A. Antoniadis, and H.I. Smith. "Resonant Tunneling Across and Mobility Modulation Along Surface-Structured Quantum Wells." *J. Vac. Sci. Technol. B* 7(6):2025-2029 (1989).
- Ismail, K., W. Chu, A. Yen, D.A. Antoniadis, and H.I. Smith. "Negative Transconductance and Negative Differential Resistance in a Grid-Gate Modulation-Doped Field-Effect Transistor." *Appl. Phys. Lett.* 54:460 (1989).
- Ismail, K., T.P. Smith, W.T. Masselink, and H.I. Smith. "Magnetic Flux Commensurability in Coupled Quantum Dots." *Appl. Phys. Lett.* 55:2766-2768 (1989).
- Iu, C.-h., G.R. Welch, M.M. Kash, L. Hsu, and D. Kleppner. "Orderly Structure in the Positive-Energy Spectrum of a Diamagnetic Rydberg Atom." *Phys. Rev. Lett.* 63(11):1133-1136 (1989).
- Kalus, J., H. Hoffmann, S.H. Chen, and P. Lindner. "Correlations in Micellar Solutions Under Shear: A SANS Study of the Chain Surfactant N-Hexadecyloctyldimethylammonium Bromide." *J. Phys. Chem.* 93: 4267 (1989).
- Kash, M.M., G.R. Welch, C.-H. Iu, and D. Kleppner. "Diamagnetic Structure of Lithium, $n \sim 21$." *Spectrochim. Acta* 45A(1):57-61 (1989).
- Kawata, H., J.M. Carter, A. Yen, and H.I. Smith. "Optical Projection Lithography Using Lenses with Numerical Apertures Greater Than Unity." *Microelectron. Eng.* 9:31-36 (1989).
- Kaxiras, E., O.L. Alerhand, J.D. Joannopoulos, and G.W. Turner. "Microscopic Model of Heteroepitaxy of GaAs on Si(100)." *Phys. Rev. Lett.* 62(21):2484-2486 (1989).
- Kean, P.N., X. Zhu, D.W. Crust, R.S. Grant, N. Langford, and W. Sibbert. "Enhanced Mode Locking of Color-Center Lasers." *Opt. Lett.* 14(1):39-41 (1989).
- Kesler, M.P., and E.P. Ippen. "Femtosecond Time-Domain Measurements of Group Velocity Dispersion in AlGaAs Diode Lasers." *Electron. Lett.* 25(10):640-641 (1989).
- Kiang, J.-F., S.M. Ali, and J.A. Kong. "Propagation Properties of Striplines Periodically Loaded with Crossing Strips." *IEEE Trans. Microwave Theory Tech.* 37(4):776-786 (1989).
- Kiang, J.F., T.M. Habashy, and J.A. Kong. "Electrostatic Fields Due to an Electrode Mounted on a Conducting Pad of Finite Extent in a Planar Stratified Medium." *IEEE Trans. Antennas Propag.* 37(9):1140-1149 (1989).
- Kirkpatrick, D.A., G. Bekefi, and A.C. DiRienzo. "A Millimeter and Submillimeter Wavelength Free-Electron Laser." *Phys. Fluids B* 1(7):1511-1518 (1989).
- Kleinsasser, A.W., T.N. Jackson, G.D. Pettit, H. Schmid, J.M. Woodall, and D.P. Kern. "Prospects for Proximity Affect Superconducting FETs." *IEEE Trans. Mag.* MAG-25(2):1274-1277 (1989).
- Kundert, K., J. White, and A. Sangiovanni-Vincentelli. "A Mixed Frequency-Time Approach for Distortion Analysis of Switching Filter Circuits." *IEEE J. Solid-State Circuits* 24(2):443-451 (1989).
- Kupfer, K., A. Bers, and A.K. Ram. "Guiding Center Stochasticity by Electrostatic Waves in Toroidal Geometry" (abstract). *Bull. Am. Phys. Soc.* 34:1927 (1989).
- LaGasse, M.J., K.K. Anderson, H.A. Haus, and J.G. Fujimoto. "Femtosecond All-Optical Switching in AlGaAs Waveguides Using a Time Division Interferometer." *Appl. Phys. Lett.* 54(21):2068-2070 (1989).
- LaGasse, M.J., D.L.-Wong, J.G. Fujimoto, and H.A. Haus. "Ultrafast Switching with a Single-Fiber Interferometer." *Opt. Lett.* 14 (6):311-313 (1989).
- LaGasse, M.J., R.W. Schoenlein, J.G. Fujimoto, and P.A. Schulz. "Amplification of Femtosecond Pulses in Ti:Al₂O₃ Using an Injection-Seeded Laser." *Opt. Lett.* 14(24):1347-1349 (1989).
- Lai, Y., and H.A. Haus. "Quantum Theory of Solitons in Optical Fibers. I. Time-dependent Hartree Approximation." *Phys. Rev. A* 40(2):844-853 (1989).
- Lai, Y., and H.A. Haus. "Quantum Theory of Solitons in Optical Fibers. II. Exact Solution." *Phys. Rev. A* 40(2):854-866 (1989).

- Langston, G.I., D.P. Schneider, S. Connor, C. Carilli, J. Lehar, E.L. Turner, J.E. Gunn, and J.N. Hewitt. "MG1654+1346: An Einstein Ring Image of a Quasar Radio Lobe." *Astron. J.* 97:1283-1290 (1989).
- Lee, D., Q. Fu, A.V. Nurmikko, R.L. Gunshor, and L.A. Kolodziejski. "Widely Tunable Exciton Recombination Rate in ZnSe Based Superlattice Structures." *Superlat. Microstruct.* 5:345-348 (1989).
- Letalick, D., I. Renhorn, O. Steinvall, and J.H. Shapiro. "Noise Sources in Laser Radar Systems." *Appl. Opt.* 28(3):2657-2665 (1989).
- Lim, H.H., A.A. Swartz, H.A. Yueh, J.A. Kong, R.T. Shin, and J.J. van Zyl. "Classification of Earth Terrain Using Synthetic Aperture Radar Images." *J. Geophys. Res.* 94(B6):7049-7057 (1989).
- Liu, C.T., K. Nakamura, D.C. Tsui, K. Ismail, D.A. Antoniadis, and H.I. Smith. "Magneto-Optics of a Quasi Zero-Dimensional Electron Gas." *Appl. Phys. Lett.* 55:168 (1989).
- Luckhardt, S.C., K.-I. Chen, S. Coda, J. Kesner, R. Kirkwood, B. Lane, M. Porkolab, and J. Squire. "Production and Maintenance of High Poloidal Beta Tokamak Plasmas by Means of rf Current Drive." *Phys. Rev. Lett.* 62(13):1508-1511 (1989).
- Ma, H.-K.T., S. Devadas, R.-S. Wei, and A. Sangiovanni-Vincentelli. "Logic Verification Algorithms and Their Parallel Implementation." *IEEE Trans. Comput.-Aided Des. Integr. Circuits* 8(1):181-189 (1989).
- Magill, P.D., T.P. Scott, N. Smith, and D.E. Pritchard. "Level-to-Level Vibrationally Inelastic Rate Constants for Li₂-X (X=He,Ne,Ar,Xe) Collisions." *J. Chem. Phys.* 90(12):7195-7206 (1989).
- Malvar, H.S., and D.H. Staelin. "The LOT: Transform Coding Without Blocking Effects." *IEEE Trans. Acous. Speech Signal Process.* 37(4):553-559 (1989).
- Mark, J., L.Y. Liu, K.L. Hall, H.A. Haus, and E.P. Ippen. "Femtosecond Pulse Generation in a Laser with a Nonlinear External Resonator." *Opt. Lett.* 14 (1):48-50 (1989).
- Marko, J.F. "Exact Pair Correlations in a One-Dimensional Fluid of Hard Cores with Orientational and Translational Degrees of Freedom." *Phys. Rev. Lett.* 62 (5):543-546 (1989).
- Marko, J.F. "First-Order Phase Transitions in the Hard-Ellipsoid Fluid from Variationally Optimized Direct Pair Correlations." *Phys. Rev. A* 39(4):2050-2062 (1989).
- McCue, M.P., J.J. Guinan, Jr., J.B. Kobler, and S.R. Vacher. "Acoustic-Reflex Partitioning in the Stapedius." *Behav. Brain Sci.* 12:663-665 (1989).
- Meirav, U., M.A. Kastner, M. Heiblum, and S.J. Wind. "One-Dimensional Electron Gas in GaAs: Periodic Conductance Oscillations as a Function of Density." *Phys. Rev. B.* 40(8):5871-5874 (1989).
- Milios, E.E., and S.H. Nawab. "Signal Abstractions in Signal Processing Software." *IEEE Trans. Acoust., Speech, Signal Process.* 37(6):914-928 (1989).
- Moel, A., M.L. Schattenburg, J.M. Carter, and H.I. Smith. "Microgap Control in X-ray Nanolithography." *J. Vac. Sci. Technol. B* 7(6):1692-1695 (1989).
- Nelson, K.A., and E.P. Ippen. "Femtosecond Coherent Spectroscopy." *Adv. Chem. Phys.* 75:1-35 (1989).
- Palmer, J.E., G. Burns, C.G. Fonstad, and C.V. Thompson. "The Effect of As₄ Overpressure on Initial Growth of Gallium Arsenide on Silicon by MBE." *Appl. Phys. Lett.* 55:990 (1989).
- Payton, K., R. M. Uchanski, and L.D. Braida. "Speech Intelligibility as a Function of Environment and Speaking Style." *J. Acoust. Soc. Am.* 85:S55 (1989).
- Picheny, M.A., N.I. Durlach, and L.D. Braida. "Speaking Clearly for the Hard of Hearing III: An Attempt to Determine the Contribution of Speaking Rate to Differences in Intelligibility between Clear and Conversational Speech." *J. Speech Hear. Res.* 32:600-603 (1989).
- Qian, Q.-D., J. Qiu, M.R. Melloch, J.A. Cooper, L.A. Kolodziejski, M. Kobayashi, and R.L. Gunshor. "Low Interface State Density at an Epitaxial ZnSe/Epitaxial GaAs Heterointerface." *Appl. Phys. Lett.* 54(14):1359-1361 (1989).
- Qian, Q.-D., J. Qiu, M. Kobayashi, R.L. Gunshor, L.A. Kolodziejski, M.R. Melloch, J.A. Cooper, J.M. Gonsalves, and N. Otsuka. "Low Interface State Density at Pseudomorphic ZnSe/Epitaxial

- GaAs Interface." *Mater. Res. Soc. Symp.* 45:423-428 (1989).
- Ram, A.K., and A. Bers. "Kinetic Ray Tracing in Toroidal Plasmas" (abstract). *Bull. Am. Phys. Soc.* 34:2094 (1989).
- Ram, A.K., A. Bers, and K. Kupfer. "Periodic Interactions of Charged Particles with Spatially Localized Fields." *Phys. Lett. A.* 138(6,7):288-294 (1989).
- Rediker, R.H., C. Corcoran, L.Y. Pang, and S.K. Liew. "Validation of Model of External-Cavity Semiconductor Laser and Extrapolation from Five-Element to Multi-Element Fiber-Coupled High-Power Laser." *IEEE J. Quant. Electron.* 25(6):1547-1552 (1989).
- Reed, C.M., N.I. Durlach, L.D. Braid, and M.C. Schultz. "Analytic Study of the Tadome Method: Effects of Hand Position on Segmental Speech Perception." *J. Speech Hear. Res.* 32:921-929 (1989).
- Reed, C.M., N.I. Durlach, L.A. Delhorne, W.M. Rabinowitz, and K.W. Grant. "Research on Tactual Communication of Speech: Ideas, Issues, and Findings." *Volta Rev.* 91(5):65-78 (1989).
- Robinson, I.K., A.A. MacDowell, M.S. Altman, P.J. Estrup, K. Evans-Lutterodt, J.D. Brock, and R.J. Birgeneau. "Order-Disorder Transition of the W(001) Surface." *Phys. Rev. Lett.* 62(11):1294-1297 (1989).
- Rouch, J., A. Safouane, P. Tartaglia, and S.H. Chen. "The Critical Region of Water-in-Oil Microemulsions: New Light Scattering Results." *Progr. Colloid Polym. Sci.* 79:279-286 (1989).
- Rouch, J., A. Safouane, P. Tartaglia, and S.H. Chen. "Experimental Evidence of a Crossover in Critical Behavior of Water-in-Oil Microemulsions." *J. Phys.: Condens. Matter* 1:1773-1778 (1989).
- Rouch, J., A. Safouane, P. Tartaglia, and S.H. Chen. "Static and Dynamic Light Scattering Studies of Water-in-Oil Microemulsions in the Critical Region: Evidence of a Crossover Effect." *J. Chem. Phys.* 90:3756 (1989).
- Rouch, J., P. Tartaglia, A. Safouane, and S.H. Chen. "Reexamination of the Static and Dynamic Critical Phenomena in Water-amphiphile Micellar Solutions." *Phys. Rev. A* 40:2013 (1989).
- Schreiber, W.F., and A.B. Lippman. "Reliable EDTV/HDTV Transmission in Low-Quality Analog Channels." *SMPTE J.* 98(7):496-503 (1989).
- Schreiber, W.F., A.B. Lippman, A.N. Netravali, E.H. Adelson, and D.H. Staelin. "Channel-Compatible 6-MHz HDTV Distribution Systems." *SMPTE J.* 98(1):5-13 (1989).
- Schneider, B.A., and P.M. Zurek. "Lateralization of Coherent and Incoherent Targets Added to a Diotic Background." *J. Acoust. Soc. Am.* 85:1756-1763 (1989).
- Scott-Thomas, J.H.F., S.B. Field, M.A. Kastner, H.I. Smith, and D.A. Antoniadis. "Conductance Oscillations Periodic in the Density of a One-Dimensional Electron Gas." *Phys. Rev. Lett.* 62(5):583-586 (1989).
- Shapiro, J.H., S.R. Shepard, and N.W. Wong. "Ultimate Quantum Limits on Phase Measurement." *Phys. Rev. Lett.* 62(20):2377-2380 (1989).
- Sheu, E.Y., S.H. Chen, J.S. Huang, and J.C. Sung. "Non-Exponential Relaxations in Dense Microemulsions Near the Glass Transition." *Phys. Rev. A* 39:5867 (1989).
- Shirasaki, M., H.A. Haus, and D. Liu-Wong. "Quantum Theory of the Nonlinear Interferometer." *J. Opt. Soc. Am. B.* 6 (1):82-88 (1989).
- Shoucri, M., I. Shkarofsky, V. Fuchs, K. Kupfer, A. Bers, and S. Luckhardt. "A Quasilinear Fokker-Planck Code for the Numerical Solution of the Lower-Hybrid Current-Drive Problem in the Presence of Electron Cyclotron Heating." *Comput. Phys. Commun.* 55:253-268 (1989).
- Siegel, R.A., and H.S. Colburn. "Binaural Processing of Noisy Stimuli - Internal External Noise Ratios for Diotic and Dichotic Stimuli." *J. Acoust. Soc.* 86(6):2122-2128 (1989).
- Spaepen, F., and C.V. Thompson. "Calorimetric Studies of Reactions in Thin Films and Multilayers." *Appl. Surf. Sci.* 38:1 (1989).
- Srinivasan, M.A. "Surface Deflection of Primate Fingertip Under Line Load." *J. Biomech.* 22 (4):343-349 (1989).
- Standley, D.L., and J.L. Wyatt, Jr. "Stability Criterion for Lateral Inhibition and Related Networks that is Robust in the Presence of Integrated

- Circuit Parasitics." *IEEE Trans. Circuits Syst.* 36(5):675-681 (1989).
- Stern, D., W-Z. Lin, C.A. Puliafito, and J.G. Fujimoto. "Femtosecond Optical Ranging of Corneal Incision Depth." *Inv. Ophthalm. Vis. Sci.* 30:99-104 (1989).
- Stern, D., R.W. Schoenlein, C.A. Puliafito, E.T. Dobi, R. Birngruber, and J.G. Fujimoto. "Corneal Ablation by Nanosecond, Picosecond, and Femtosecond Lasers at 532 and 625 nm." *Arch. Ophthalm.* 107:587-592 (1989).
- Stevens, K.N. "On the Quantal Nature of Speech." *J. Phon.* 17:3-45 (1989).
- Stevens, K.N. "Response to Commentaries." *J. Phon.* 17:145-157 (1989).
- Stevens, K.N., and S.J. Keyser. "Primary Features and their Enhancement in Consonants." *Language* 65 (1):81-106 (1989).
- Tan, H.Z., W.M. Rabinowtiz, and N.I. Durlach. "Analysis of a Synthetic Tadoma System as a Multidimensional Tactile Display." *J. Acoust. Soc. Am.* 86(3):981-988 (1989).
- Tarnow, E., J.D. Joannopoulos, and M.C. Payne. "Antisites, Antistructures and Bond-Switching Reactions in Layered Chalcogenides." *Phys. Rev. B.* 39(9):6017-6024 (1989).
- Vacher, S.R., J.J. Guinan, Jr., and J.B. Kobler. "Intracellularly Labeled Stapedius-Motoneuron Cell Bodies in the Cat Are Spatially Organized According to Their Physiologic Responses." *J. Comp. Neurol.* 289:401-415 (1989).
- Vaziri, M., R.L. Gunshor, L.A. Kolodziejski, S. Venkatesan, R.F. Pierret, and R. Reifenberger. "Optical and Electrical Characterization of ZnSe Doped with Gallium." *J. Vac. Sci. Technol.* B7:253-258 (1989).
- Venkatesan, S., R.F. Pierret, J. Qiu, M. Kobayashi, R.L. Gunshor, and L.A. Kolodziejski. "Deep Levels in Ga-Doped ZnSe Grown by Molecular Beam Epitaxy." *J. App. Phys.* 66(8):3656-3660 (1989).
- Walrod, D., S.Y. Yuen, P.A. Wolff, and W. Tsang. "Optical Nonlinearities due to Subband Structures in $\text{Al}_{0.08}\text{In}_{0.92}\text{Sb}/\text{InSb}$ Superlattices." *Appl. Phys. Lett.* 56(3):218-220 (1989).
- Warwick, J.W., D.R. Evans, G.R. Peltzer, R.G. Peltzer, J.H. Romig, C.B. Sawyer, A.C. Riddle, A.E. Schweitzer, M.D. Desch, M.L. Kaiser, W.M. Farrell, T.D. Carr, I. de Pater, D.H. Staelin, S. Gulkis, R.L. Poynter, A. Boischot, F. Genova, Y. Leblanc, A. Lecacheux, B.M. Pedersen, and P. Zarka. "Voyager Planetary Radio Astronomy at Neptune." *Sci.* 246(4936):1498-1501 (1989).
- Weiner, A.M., D.E. Leaird, G.P. Wiederrecht, and K.A. Nelson. "Femtosecond Multiple Pulse Impulsive Stimulated Raman Scattering." *Opt. News* 15(12):29-31 (Optics in 1989 section).
- Welch, G.R., M.M. Kash, C-H. Lu, L. Hsu, and D. Kleppner. "Experimental Study of Energy Level Statistics in a Regime of Regular Classical Motion." *Phys. Rev. Lett.* 62 (8):893-896 (1989).
- Welch, G.R., M.M. Kash, C-H. Lu, L. Hsu, and D. Kleppner. "Positive-Energy Structure of the Diamagnetic Rydberg Spectrum." *Phys. Rev. Lett.* 62 (17):1975-1978 (1989).
- Wyatt, J.L., Jr., and D.L. Standley. "Criteria for Robust Stability in a Class of Lateral Inhibition Networks Coupled Through Resistive Grids." *Neural Comput.* 1:58-67 (1989).
- Xu, K., G. Bekefi, and C. Leibovitch. "Observations of Field Profile Modifications in a Raman Free-Electron Laser Amplifier." *Phys. Fluids B.* 1(10):2066-2072 (1989).
- Yokoyama, H., and S.D. Brorson. "Rate Equation Analysis of Microcavity Lasers." *J. Appl. Phys.* 66(10):4801-4805 (1989).
- Yueh, H.A., J.A. Kong, R.M. Barnes, and R.T. Shin. "Calibration of Polarimetric Radar Using In-scene Reflectors." *J. Electromag. Waves Appl.* 4(1):27-49 (1989).
- Yueh, H.A., J.A. Kong, J.K. Jao, R.T. Shin, and L.M. Novak. "K-Distribution and Polarimetric Terrain Radar Clutter." *J. Electromag. Waves Appl.* 3(8):747-768 (1989).
- Zysset, B., J.G. Fujimoto, and T.F. Deutsch. "Time Resolved Measurements of Picosecond Optical Breakdown." *Appl. Phys. B.* 48:139-147 (1989).
- Zysset, B., J.G. Fujimoto, C.A. Puliafito, R. Birngruber, and T.F. Deutsch. "Picosecond Optical Breakdown: Tissue Effects and Reduction of Collateral Damage." *Lasers in Surgery and Medicine* 9:193-204 (1989).
- Zysset, B., M.J. LaGasse, J.G. Fujimoto, and J.D. Kafka. "High Repetition Rate Femtosecond

Dye Amplifier Using a Laser-Diode Pumped Neodymium-YAG Laser." *Appl. Phys. Lett.* 54 (6):496-498 (1989).

A.5 Journal Articles Accepted for Publication

- Alerhand, O.L., A.N. Berker, J.D. Joannopoulos, D. Vanderbilt, R.J. Hamers, and J.E. Demuth. "Finite-Temperature Phase Diagram of Vicinal Si(100) Surfaces." *Phys. Rev. Lett.*
- Ali, S.M., T.A. Habashy, and J.A. Kong. "Dyadic Green's Functions for Multilayered Uniaxially Anisotropic Media." *J. Electromag. Waves Appl.*
- Atkins, R.G., R.T. Shin, and J.A. Kong. "A Neural Net Method for High Range Resolution Target Classification." *J. Electromag. Waves Appl.*
- Binder, B.T., P.T. Yu, J.H. Shapiro, and J.K. Bounds. "An Atmospheric Optical Ring Network." *IEEE Trans. Comm.*
- Borgeaud, M., S.V. Nghiem, R.T. Shin, and J.A. Kong. "Theoretical Models for Polarimetric Microwave Remote Sensing of Earth Terrain." *J. Electromag. Waves Appl.*
- Bossi, D.E., W.D. Goodhue, M.C. Finn, K. Rauschenbach, J.W. Bales, and R.H. Rediker. "Reduced-Confinement Antennas for GaAlAs Integrated Optical Waveguides." *Appl. Phys. Lett.*
- Brandstein, M.S., P.A. Monta, J.C. Hardwick, and J.S. Lim. "A Real-Time Implementation of the Improved MBE Speech Coder." *Proc. ICASSP-90.*
- Chow, C., V. Fuchs, and A. Bers. "The Dispersion Relation for $D(^3\text{He})$ Ion-Cyclotron Resonance Heating." *Phys. Fluids B.*
- Cornell, E.A., R.M. Weisskoff, K.R. Boyce, and D.E. Pritchard. "Mode Coupling in a Penning Trap: π -pulses and a Classical Avoided Crossing." *Phys. Rev. A.*
- Delgutte, B. "Physiological Mechanisms of Psychophysical Masking: Observations From Auditory-Nerve Fibers." *J. Acoust. Soc. Am.*
- Devadas, S. "Optimal Layout Via Boolean Satisfiability." *Int. J. Comput.-Aided VLSI Des.*
- Devadas, S., and K. Keutzer. "A Unified Approach to the Synthesis of Fully Testable Sequential Machines." *IEEE Trans. Comput.-Aided Des.*
- Devadas, S., and H-K.T. Ma. "Easily Testable PLA-based Finite State Machines." *IEEE Trans. Comput.-Aided Des.*
- Devadas, S., H-K.T. Ma, and A.R. Newton. "Redundancies and Don't Cares in Sequential Logic Synthesis." *J. Electron. Test.: Theory Appl.*
- Devadas, S., H-K.T. Ma, A.R. Newton, and A. Sangiovanni-Vincentelli. "Irredundant Sequential Machines Via Optimal Logic Synthesis." *IEEE Trans. Comput.-Aided Des.*
- Devadas, S., and A.R. Newton. "Exact Algorithms for Output Encoding, State Assignment and Four-Level Boolean Minimization." *IEEE Trans. Comput.-Aided Des.*
- DiRienzo, A., and G. Bekefi. "The M.I.T. 35 GHz Cyclotron Autoresonance Maser (CARM) Amplifier." *SPIE Proc.*
- Eugster, C.C., and P.L. Hagelstein. "X-ray Detection Using the Quantum Well Exciton Nonlinearity." *IEEE J. Quantum Electron.*
- Feder, M. "Parameter Estimation and Extraction of Almost Periodic Signals in a Wide Band Interference." *IEEE J. Acoust. Speech Sig. Proc.*
- Freeman, D.M. "Anatomical Model of the Cochlea of the Alligator Lizard." *Hear. Res.*
- Freeman, D.M., and T.F. Weiss. "Superposition of Hydrodynamic Forces on a Hair Bundle." *Hear. Res.*
- Freeman, D.M., and T.F. Weiss. "Hydrodynamic Forces on Hair Bundles at Low Frequencies." *Hear. Res.*
- Freeman, D.M., and T.F. Weiss. "Hydrodynamic Forces on Hair Bundles at High Frequencies." *Hear. Res.*
- Freeman, D.M., and T.F. Weiss. "Hydrodynamic Analysis of a Two-Dimensional Model for Micromechanical Resonance of Free-Standing Hair Bundles." *Hear. Res.*
- Gallagher, A., and D.E. Pritchard. "Exoergic Collisions of Cold Na^+-Na ." *Phys. Rev. Lett.*
- Gasiewski, A.J., J. Barrett, P.G. Bonanni, and D.H. Staelin. "Aircraft Based Radiometric Imaging

- of Tropospheric Profiles and Precipitation Using the 118.75 GHz Oxygen Resonance." *J. App. Meteor.*
- Gentile, T.R., B.J. Hughey, T.W. Ducas, and D. Kleppner. "Microwave Spectroscopy of Calcium Rydberg States." *Phys. Rev. A.*
- Gold, A. "Enhanced Plasmon Anomaly in the Dynamical Conductivity of Heterostructures with Large Spacer." *Phys. Rev. Lett.*
- Gould, P.L., P.J. Martin, G.A. Ruff, R.E. Stoner, J.-L. Picque, and D.E. Pritchard. "Momentum Transfer to Atoms by a Standing Light Wave; Transition from Diffraction to Diffusion." *Phys. Rev. Lett.*
- Grant, A.C., and J.Y. Lettvin. "The Nature of Electrical Transients Recorded in Frog Tectal Neuropil." *J. Neurosci.*
- Guinan, Jr., J.J., M.P. Joseph, and B.E. Norris. "Brainstem Facial-Motor Pathways from Two Distinct Groups of Stapedius Motoneurons in the Cat." *J. Comp. Neurol.*
- Guinan, Jr., J.J., and R.Y.S. Li. "Signal Processing in Brainstem Auditory Neurons Which Receive Giant Endings (Calyces of Held) in the Medial Nucleus of the Trapezoid Body of the Cat." *Hear. Res.*
- Habashy, T.M., S.M. Ali, and J.A. Kong. "Impedance Parameters and Radiation Pattern of Cylindrical-Rectangular and Wraparound Microstrip Antennas." *IEEE Trans. Antennas Propag.*
- Habashy, T.M., S.M. Ali, and J.A. Kong. "Input Impedance and Radiation Pattern of Cylindrical-Rectangular and Wraparound Microstrip Antennas." *IEEE Trans. Antennas Propag.*
- Hagelstein, P.L. "Neutron Tritium Production in Coherent DD Fusion." *Phys. Rev. Lett.*
- Haus, H.A. "Squeezing in Fibers Without Guided Acoustic Wave Brillouin Scattering." *Opt. Lett.*
- Haus, H.A., and Y. Lai. "Quantum Theory of Soliton Squeezing - a Linearized Approach." *J. Opt. Soc. Am. B.*
- Hemmer, P.R., H. Lamela-Rivera, S.P. Smith, and S. Ezekiel. "Observation of Ultra-Narrow Ramsey Raman Fringes in a Cesium Atomic Beam Using a Semiconductor Laser." *Opt. Lett.*
- Hettinger, J.D., A.G. Swanson, W.J. Skocpol, J.S. Brooks, J.M. Graybeal, P.M. Mankiewich, R.E. Howard, B.L. Straugh, and E.G. Burkhardt. "Flux Creep and High-Field Critical Currents in Epitaxial Thin Films of $\text{YBa}_2\text{Cu}_3\text{O}_7$." *Phys. Rev. Lett.*
- Ho, S.-T., P. Kumar, and J.H. Shapiro. "Quantum Theory of Nondegenerate Multiwave Mixing II: Coupled-Mode Equations and Spatial Propagation." *Phys. Rev. A.*
- Ho, S.-T., P. Kumar, and J.H. Shapiro. "Quantum Theory of Nondegenerate Multiwave Mixing III: Application to Single-Beam Squeezed-State Generation." *J. Opt. Soc. Am. B.*
- Hong, H., and R. J. Birgeneau. "X-ray Diffraction Study of the Structure of Xenon Multilayers on Single Crystal Graphite." *J. Phys. B.*
- Ismail, K., D.A. Antoniadis, and H.I. Smith. "A Lateral-Surface-Superlattice Structure on GaAs/AlGaAs for Far-Infrared and Magneto-Capacitance Measurements." *J. Vac. Sci. Technol.*
- Ismail, K., D.A. Antoniadis, and H.I. Smith. "One-Dimensional Subbands and Mobility Modulation in GaAs/AlGaAs Quantum Wires." *Appl. Phys. Lett.*
- Kastner, M.A., S.B. Fields, J.C. Licini, and S.L. Park. "Anomalous Magnetoresistance of an Electron Gas in a Restricted Geometry." *Phys. Rev. Lett.*
- Kaushik, S., and P. Hagelstein. "The Application of the Preconditioned Conjugate Gradient Algorithm to Rate Matrix Equations." *J. Comput. Phys.*
- Kaushik, S., and P. Hagelstein. "The Application of the Conjugate Gradient Methods to NLTE Rate Matrix Equations." *Appl. Phys. B.*
- Kiang, J.F., S.M. Ali, and J.A. Kong. "Integral Equation Solution to the Guidance and Leakage Properties of Coupled Dielectric Strip Waveguides." *IEEE Trans. Microwave Theory Tech.*
- Kiang, J.F., S.M. Ali, and J.A. Kong. "Modelling of Lossy Microstrip Lines with Finite Thickness." *J. Electromag. Waves Appl.*
- Kidd, R.C., and T.F. Weiss. "Mechanisms That Degrade Timing Information in the Cochlea." *Hear. Res.*

- Kim, E.J., D.H. Staelin, M. Shao, and M.M. Colavita. "Dispersed Fringe Group Astrometry with the Mk III Optical Interferometer." *Bull. Am. Astron. Soc.*
- Kirkpatrick, D.A., G. Bekefi, A.C. DiRienzo, H.P. Freund, and A.K. Ganguly. "A High Power, 600mm Wavelength Free Electron Laser." *Phys. Rev. Lett.*
- Klatt, D.H., and L.C. Klatt. "Analysis, Synthesis and Perception of Voice Quality Variations Among Female and Male Talkers." *J. Acoust. Soc. Am.*
- LaGasse, M.J., K.K. Anderson, C.A. Wang, H.A. Haus, and J.G. Fujimoto. "Femtosecond Measurements of the Nonresonant Nonlinear Index in AlGaAs." *Appl. Phys. Lett.*
- LaGasse, M.J., R.W. Schoenlein, and J.G. Fujimoto. "Amplification of Femtosecond Pulses in $\text{Ti:Al}_2\text{O}_3$ Using an Injection Seeded Laser." *Optics Lett.*
- Lam, C.W., S.M. Ali, and J.A. Kong. "The Propagation Characteristics of Signal Lines with Crossing Strips in Multilayered Anisotropic Media." *J. Electromag. Waves Appl.*
- Laurich, B.K., K. Elcess, C.G. Fonstad, C. Mailhoit, and D. Smith. "Optical Properties of (100) and (111) Oriented GaInAs/GaAs Strained Layer Superlattices." *Phys. Rev. Lett.*
- Lee, C.F., R.T. Shin, J.A. Kong, and B.J. McCartin. "Absorbing Boundary Conditions on Circular and Elliptic Boundaries." *J. Electromag. Waves Appl.*
- Leotta, D.F., W.M. Rabinowitz, C.M. Reed, and N.I. Durlach. "Preliminary Speech-Reception Results Obtained with the Synthetic Tadoma System." *J. Rehabil. Res. Dev.*
- Lin, F.C., J.A. Kong, and R.T. Shin. "Application of Three-Layer Random Medium Model for Microwave Remote Sensing of Snow-Covered Sea Ice." *J. Geophys. Res.*
- Liou, C-Y., and B.R. Musicus. "A Separable Cross-Entropy Approach to Power Spectral Estimation." *IEEE Trans. Acoust., Speech, Signal Process.*
- Liu, C.T., K. Nakamura, D.C. Tsui, K. Ismail, D.A. Antoniadis, and H.I. Smith. "Far-Infrared Transmission Measurements on Grid-Gate GaAs/AlGaAs Lateral-Surface-Superlattice Structures." *J. Surface Sci.*
- Magill, P.D., B. Stewart, and D.E. Pritchard. "Dynamics of Quasiresonant Vibrotational Transfer Explained by a Novel Use of Classical Trajectories." *J. Chem. Phys.*
- Marko, J.F. "Do Hard Spheres Freeze into HCP or FCC Crystals?" *Phys. Rev. Lett.*
- Rappe, A.M., K.M. Rabe, E. Kaxiras, and J.D. Joannopoulos. "Optimized Pseudopotentials." *Phys. Rev. B.*
- Rosenkranz, P.W., and D.H. Staelin. "Polarized Thermal Microwave Emission from Oxygen in the Mesosphere." *Radio Sci.*
- Rosowski, J.J., P.J. Davis, S.N. Merchant, K.M. Donahue, and M.D. Coltrera. "Cadaver Middle-Ears as Models for Living Ears." *Ann. Otol. Rhinol. Laryngol.*
- Rosowski, J.J., and A. Graybeal. "What Did Morganucodon Hear?" *Zool. J. Linn. Soc.*
- Saleh, R., J. White, A.S. Vincentelli, and A.R. Newton. "Accelerating Relaxation Algorithms for Circuit Simulation Using Waveform-Newton and Step-Size Refinement." *IEEE Trans. Comput.-Aided Des.*
- Schattenburg, M.L., C.R. Canizares, and H.I. Smith. "X-Ray/VUV Transmission Gratings for Astrophysical and Laboratory Applications." *Physica Scripta.*
- Scott, T.P., B. Stewart, P.D. Magill, N. Smith, and D.E. Pritchard. "Velocity Dependence of Quasiresonant Vibrotational Energy Transfer." *J. Chem Phys.*
- Segal, M. and E. Weinstein. "A New Method for Evaluating the Log-Likelihood Gradient, the Hessian, and the Fisher Information Matrix for Linear Dynamic Systems." *IEEE Trans. Inf. Theory.*
- Segal, M., E. Weinstein, and B.R. Musicus. "Estimate-Maximize Algorithms for Multi-Channel Time Delay and Signal Estimation." *IEEE Trans. Acoust. Speech, Signal Process.*
- Sheen, D.M., S.M. Ali, M.D. Abouzahra, and J.A. Kong. "Application of the Three Dimensional Finite Difference Time Domain Method to the Analysis of Planar Microstrip Circuits." *IEEE Trans. Microwave Theory Tech.*

- Shirasaki, M., and H.A. Haus. "Squeezing of Pulses in Nonlinear Interferometer." *J. Opt. Soc. Am. B*.
- Smith, H.I., K. Ismail, M.L. Schattenburg, and D.A. Antoniadis. "Sub-100nm Electronic Devices and Quantum-Effects Research Using X-ray Nanolithography." *Proceedings of the International Conference on Microlithography, Microcircuit Engineering*.
- Staelin, D.H., and S.S. Eikenberry. "Spectral Phenomenology of Uranian Radio Emission." *Bull. Am. Astron. Soc.*
- Stewart, B., P.D. Magill, and D.E. Pritchard. "Vibration-Rotation Resonance in Inelastic Li₂-Ne Collisions." *J. Chem Phys.*
- Thompson, C.V. "Coarsening of Particles on a Planar Substrate: Interface Energy Anisotropy and Application to Grain Growth in Thin Films." *Acta Metall.*
- Tulintseff, A.N., S.M. Ali, and J.A. Kong. "Resonant Frequencies of Stacked Circular Microstrip Antennas." *IEEE Trans. Antennas Propag.*
- Tulintseff, A.N., S.M. Ali, and J.A. Kong. "Input Impedance of a Probe-Fed Stacked Circular Microstrip Antenna." *IEEE Trans. Antennas Propag.*
- Vacher, S.R., J.J. Guinan, Jr., and J.B. Kobler. "Intracellularly Labeled Stapedius-Motoneuron Cell Bodies in the Cat are Spatially Organized According to Their Physiologic Responses." *J. Comp. Neurol.*
- Weiner, A.M., D.E. Leaird, G.P. Wiederrecht, and K.A. Nelson. "Femtosecond Pulse Sequences Used for Optical Manipulation of Molecular Motion." *Sci.*
- Weinstein, E., M. Feder, and A.V. Oppenheim. "A New Class of Sequential Algorithms for Parameter Estimation." *IEEE Trans. Inf. Theory*.
- Wurtele, J.S., G. Bekefi, R. Chu, and K. Xu. "Pre-bunching in a Collective Raman Free Electron Laser Amplifier." *Phys. Fluids*.
- Xu, K., and G. Bekefi. "Experimental Study of Multiple Frequency Effects in a Free Electron Laser Amplifier." *Phys. Fluids*.
- Yoo, B.S., X.C. Liu, A. Petrou, J-P. Cheng, A.A. Reeder, B.D. McCombe, K. Elcess, and C.G. Fonstad. "Optical and Infrared Studies of

(111) InGaAs/AlGaAs Strained-Layer Superlattices." *Superlatt. Microstruct.*

Yueh, H.A., J.A. Kong, R.T. Shin, H.A. Zebker, and T. Le Toan. "K-distribution and Multi-frequency Polarimetric Terrain Radar Clutter." *J. Electromag. Waves Appl.*

Yueh, H.A., R.T. Shin, and J.A. Kong. "Scattering from Randomly Oriented Scatterers with Strong Permittivity Fluctuations." *J. Electromag. Waves Appl.*

A.6 Journal Articles Submitted for Publication

- Braud, J.P. "Laser Cavities and Polarization Optics for Soft X-Rays." *Appl. Phys. B*.
- Chow, C., V. Fuchs, and A. Bers. "Reflection at the Resonance Layer of the Fast Alfvén Wave in Ion Cyclotron Heating." *Phys. Fluids B*.
- Delgutte, B. "Two-Tone Rate Suppression in Auditory-Nerve Fibers." *Hear. Res.*
- Gladstone, D.J., M.T. Schulberg, K.B. Laughlin, M. McGonigal, and S.T. Ceyer. "Design of a Power Supply for Resistive Heating of Semiconductor Crystals." *Rev. Sci. Instrum.*
- Hughey, B.J., T.R. Gentile, T.W. Ducas, and D. Kleppner. "A Split High Q Superconducting Cavity." *Rev. Sci. Instrum.*
- Hughey, B.J., T.R. Gentile, T.W. Ducas, and D. Kleppner. "Experimental Study of Small Ensembles of Atoms in a Microwave Cavity." *Phys. Rev. A*.
- Hui, K. "Domain Wall Study of the Stacked Frustrated Triangular Lattice." *Phys. Rev. Lett.*
- Kaushik, S., and P.L. Hagelstein. "The Application of the Method of Generalized Conjugate Residuals to NLTE Rate Matrix Equations." *J. Comp. Phys.*
- Kiang, J.F., S.M. Ali, and J.A. Kong. "Integral Equation Formulation of Inhomogeneous Slab Waveguides." *IEEE J. Quantum Electron.*
- Liu, C.T., D.C. Tsui, M. Shayegan, K. Ismail, D.A. Antoniadis, and H.I. Smith. "Observations of Landau Level Splitting of a Two-Dimensional Electron Gas in a Two-Dimensional Surface Superlattice." *Phys. Rev. Lett.*

- Nabors, K., and J. White. "FastCap-A Multipole Accelerated Capacitance Extraction Algorithm for Complex 3-D Geometries." *IEEE Trans. Comput.-Aided Des.*
- Oldaker, B.G., P.J. Martin, P.L. Gould, M. Xiao, and D.E. Pritchard. "Experimental Study of Sub-Poissonian Statistics in the Transfer of Momentum from Light to Atoms." *Phys. Rev. Lett.*
- Reichelt, M., J. White, and J. Allen. "WORDS - A Waveform Over-Relaxation Based Device Simulation Program." *IEEE Trans. Comput.-Aided Des.*
- Rosowski, J.J. "The Effects of External- and Middle-ear Filtering on Auditory Threshold and Noise-Induced Hearing Loss." *J. Acoust. Soc. Am.*
- Thompson, C.V., J. Floro, and H.I. Smith. "Epitaxial Grain Growth in Thin Metal Films." *J. Appl. Phys.*
- Weinstein, E., M. Feder, and A. Oppenheim. "Sequential Algorithms for Parameter Estimation Based on the Kullback-Liebler Information Measure." *IEEE Trans. Acoust. Speech Signal Process.*
- Wornell, G.W. "A Karhunen-Loeve-like Expansion for $1/f$ Processes via Wavelets." *IEEE Trans. Inf. Theory.*
- Yoon, P.H., and R.C. Davidson. "Alternate Representation of the Dielectric Tensor for a Relativistic Magnetized Plasma in Thermal Equilibrium." *J. Plasma Phys.*
- Yueh, H.A., J.A. Kong, R.T. Shin, H.A. Zebker, and T. Le Toan. "K-distribution and Multi-frequency Polarimetric Terrain Radar Clutter." *J. Electromag. Waves Appl.*
- Yueh, H.A., R.T. Shin, and J.A. Kong. "Scattering from Randomly Oriented Scatterers with Strong Permittivity Fluctuations." *J. Electromag. Waves Appl.*
- Chen, S.H., E.Y. Sheu, and J.S. Huang. "Non-Exponential Decay of Density Correlation Function in Dense Microemulsion." In *Dynamics of Disordered Materials*. Eds. D. Richter, W. Petry, J. Dianoux, and J. Teixeira. New York: Springer Verlag, 1989.
- Chow, C., A. Bers, and V. Fuchs. "Analytic Studies of ICRF Heating." In *Radio Frequency Power in Plasmas*, A.I.P. Conference Proceedings 190, 234-237. Ed. R. McWilliams. New York: American Institute for Physics, 1989.
- Clevenger, L.A., C.V. Thompson, A.J. Judas, and J.L. Olson. "Metastable Reactions and Explosive Silicidation in Nickel/ Amorphous-Silicon Multilayer Thin Films." In *Selected Topics in Electronic Materials*. Eds. B.R. Appleton et al. Pittsburgh, Pennsylvania: Materials Research Society, 1989.
- Gunshor, R.L., L.A. Kolodziejski, M.R. Melloch, N. Otsuka, and A.V. Nurmikko. "II-VI/III-V Heterointerfaces: Epilayer-on-Epilayer Structures." In *Growth and Optical Properties of Wide-Gap II-VI Low Dimensional Structures*. Eds. T.C. McGill, C.M. Sotomayor Torres, and W. Gebhardt. New York: Plenum Press, 1989.
- Gunshor, R.L., L.A. Kolodziejski, A.V. Nurmikko, and N. Otsuka. "Molecular Beam Epitaxy of II-VI Semiconductor Microstructures." In *Semiconductors and Semimetals*. Ed. R. Pearsall. Boston: Academic Press, 1989.
- Harris, J., C. Koch, J. Luo, and J. Wyatt. "Resistive Fuses: Analog Hardware for Detecting Discontinuities in Early Vision." In *Analog VLSI Implementation of Neural Systems*. Eds. C. Mead, and J. Ismail. Boston: Kluwer Academic Publishers, 1989.
- Ho, S-T., N.C. Wong, and J.H. Shapiro. "Self-Focusing Limitations on Squeezed State Generation in Two-Level Media." In *Coherence and Quantum Optics VI*. Eds. L. Mandel, E. Wolf, and J.H. Eberly. New York: Plenum Press, 1989.
- Klatt, D.H. "Review of Selected Models of Speech Perception." In *Lexical Representation and Process*. Ed. W.E. Marslen-Wilson. Cambridge: MIT Press, 1989.
- Kolodziejski, L.A., R.L. Gunshor, and A.V. Nurmikko. "II-VI Compound Strained-Layer Superlattices." In *Strained Layer Superlattices*. Ed. R.B. Biefeld. Switzerland: Trans Tech Publications, 1989.

A.7 Books/Chapters in Books

- Ceyer, S.T., D.J. Gladstone, M. McGonigal, and M.T. Schulberg. "Molecular Beams as Probes of Dynamics of Reactions on Surfaces." In *Physical Methods of Chemistry*. Eds. B.W. Rossiter, J.F. Hamilton, and R. C. Baetzold. New York: Wiley, 1989.

Kolodziejski, L.A., R.L. Gunshor, A.V. Nurmikko, and N. Otsuka. "Exciton Self-Trapping in ZnSe/ZnTe Superlattice Structures." In *Growth and Optical Properties of Wide-Gap II-VI Low Dimensional Structures*. Eds. T.C. McGill, C.M. Sotomayor Torres, and W. Gebhardt. New York: Plenum Press, 1989.

Kolodziejski, L.A., R.L. Gunshor, A.V. Nurmikko, and N. Otsuka. "MBE of Magnetic and Semimagnetic II-VI Semiconductors." In *Molecular Beam Epitaxy*. Eds. R.F.C. Farrow, and J.R. Arthur. New York: Noyes Publishers, 1989.

Kong, J.A., chief ed. *PIER 1: Progress in Electromagnetics Research*. New York: Elsevier, 1989.

Kong, J.A., chief ed. *PIER 2: Progress in Electromagnetics Research*. New York: Elsevier, 1989.

Kupfer, K., A. Bers, and A.K. Ram. "RF Induced Transport in Tokamak Plasmas." In *Radio Frequency Power in Plasmas*, A.I.P. Conference Proceedings 190, 434-437. Ed. R. McWilliams. New York: American Institute for Physics, 1989.

McKay, S.R., and A.N. Berker. "Magnetization of the d-Dimensional Random-Field Ising Model: An Intermediate Critical Dimension." In *New Trends in Magnetism*. Ed. S.M. Rezende. Teaneck, New Jersey: World Scientific, 1989.

Mead, C.A. *Analog VLSI and Neural Systems*. Reading, Massachusetts: Addison-Wesley, 1989.

Nelson, K.A. "Impulsive Stimulated Raman Scattering." In *Vibrational Spectra and Structure*. Ed. J.R. Durig. New York: Elsevier, 1989.

Oppenheim, A.V., and R.W. Schaffer. *Discrete-Time Signal Processing*. Englewood Cliffs, New Jersey: Prentice-Hall, 1989.

Shapiro, J.H., S.R. Shepard, and N.C. Wong. "A New Number-Phase Uncertainty Principle." In *Coherence and Quantum Optics VI*. Eds. L. Mandel, E. Wolf, and J.H. Eberly. New York: Plenum Press, 1989.

Shapiro, J.H., S.R. Shepard, and N.C. Wong. "Coherent Phase States and Squeezed Phase States." In *Coherence and Quantum Optics VI*. Eds. L. Mandel, E. Wolf, and J.H. Eberly. New York: Plenum Press, 1989.

Shin, R.T., and J.A. Kong. "Radiative Transfer Theory for Active Remote Sensing of Two-

Layer Random Medium." In *Progress in Electromagnetics Research* 1(5):359-417. Ed. J.A. Kong. New York: Elsevier, 1989.

Smith, H.I., K. Ismail, W. Chu, A. Yen, Y.C. Ku, M.L. Schattenburg, and D.A. Antoniadis. "Fabrication of Quantum-Effect Electronic Devices Using X-ray Nanolithography." In *Proceedings of the International Symposium on Nanostructure Physics and Fabrication*, 57-65. Eds. W.P. Kirk, and M.A. Reed. New York: Academic Press, 1989.

Yueh, H.A., R.T. Shin, and J.A. Kong. "Scattering from Randomly Perturbed Periodic and Quasiperiodic Surfaces." In *Progress in Electromagnetics Research* 1(4):297-358. Ed. J.A. Kong. New York: Elsevier, 1989.

Zurek, P.M. "Binaural Advantages and Directional Effects in Speech Intelligibility." In *Acoustical Factors Affecting Hearing Aid Performance II*. Eds. G.A. Studebaker, and I. Hochberg. Boston: College-Hill Press, forthcoming.

A.8 RLE Publications

To obtain copies of any of these materials, write: Research Laboratory of Electronics, Communications Office, Room 36-412, Massachusetts Institute of Technology, Cambridge, Massachusetts 02139 (617/253-2566).

Prepayment is required. Please include a check in U.S. funds payable to MIT RLE and allow six to eight weeks for surface mail. For foreign airmail, include an additional \$4.00 for each report ordered.

Bamji, C.S. *Graph-based Representations and Coupled Verification of VLSI Schematics and Layouts*. RLE TR-547. MIT, 1989. \$14.00.

Bickley, C.A. *Acoustic Evidence for the Development of Speech*. RLE TR-548. MIT, 1989. \$14.00.

Bose, A.G., and W.R. Short. *A Theoretical and Experimental Study of Noise and Distortion in the Reception of FM Signals*. RLE TR-540. MIT, 1989. \$7.50.

Covell, M.M. *An Algorithm Design Environment for Signal Processing*. RLE TR-549. MIT, 1989. \$17.00.

Fleisher, D. *RLE currents*. MIT, 1989. Biannual newsletter. No charge.

- Horn, B.K.P., H-S. Lee, T. Poggio, C. Sodini, and J. Wyatt. *The First Year of the MIT Vision Chip Project*. VLSI Memo No. 89-555. MIT, 1989.
- Hsu, S.C. *Moving-Object Reconstruction from Camera-Blurred Sequences Using Interframe and Interregion Constraints.* RLE TR-542. MIT, 1989. \$11.50.
- Joo, T.H. *Detection Statistics for Multichannel Data*. RLE TR-550. MIT, 1989. \$11.00.
- McCormick, S.P. *Modeling and Simulation of VLSI Interconnections with Moments*. RLE TR-543. MIT, 1989. \$8.00.
- Musicus, B.R., and E. Weinstein. *Iterative Maximum Likelihood Time Delay and Doppler Estimation Using Stationary Signals*. RLE TR-545. MIT, 1989. \$12.00.
- Pang, X.D. *Effects of Stapedius-Muscle Contractions on Masking of Tone Responses in the Auditory Nerve*. RLE TR-544. MIT, 1989. \$17.00.
- Passero, B., ed. *RLE Progress Report Number 131 (January — December 1988)*. MIT, 1989. No charge.
- Peterson, P.M. *Adaptive Array Processing for Multiple Microphone Hearing Aids*. RLE TR-541. MIT, 1989. \$9.00.
- Van Aelten, F. *Efficient Verification of VLSI Circuits Based on Syntax and Denotational Semantics*. RLE TR-546. MIT, 1989. \$11.00.
- ## A.9 Theses
- Aalberts, D.P. *Modelling the Behavior of the Relativistic Magnetron*. S.B. thesis. Dept. of Physics, MIT, 1989.
- Ajuria, S.A. *Photon Enhanced Grain Growth*. S.M. thesis. Dept. of Mater. Sci. and Eng., MIT, 1989.
- Anderson, K.K. *Disordered Quantum Well Waveguide Fabrication and Ultrafast Optical Characterization*. Ph.D. diss. Dept. of Electr. Eng. and Comput. Sci., MIT, 1989.
- Balent, L. *Study and Development of a Variational Method for Relativistic Atomic Structure Calculations*. S.B. thesis. Dept. of Physics, MIT, 1989.
- Bamji, C.S. *Graph-Based Representations and Coupled Verification of VLSI Schematics and Layouts*. Ph.D. diss. Dept. of Electr. Eng. and Comput. Sci., MIT, 1989.
- Brabson, A.R. *Nonlinear Optical Effects in a Single-Mode Fiber Mach-Zehnder Interferometer*. S.B. thesis. Dept. of Electr. Eng. and Comput. Sci., MIT, 1989.
- Brennan, T.A. *The Statistical Behavior of Coherent and Squeezed Phase States*. S.B. thesis. Dept. of Physics, MIT, 1989.
- Carpenter, R. *Material Characterization Techniques for SOI Devices*. S.M. thesis. Dept. of Electr. Eng. and Comput. Sci., MIT, 1989.
- Chang, I.Y., Jr. *Plane Electromagnetic Wave Scattering*. S.B. and S.M. thesis. Dept. of Electr. Eng. and Comput. Sci., MIT, 1989.
- Clevenger, L.A. *Controlled and Explosive Silicidation of Metal/Amorphous-Silicon Multilayer Thin Films*. Ph.D. diss. Dept. of Mater. Sci. and Eng., MIT, 1989.
- Covell, M.M. *An Algorithm Design Environment for Signal Processing*. Ph.D. diss. Dept. of Electr. Eng. and Comput. Sci., MIT, 1989.
- Donahue, K.M. *Human Middle-Ear Malleal Motion: Models and Measurements*. S.M. thesis. Dept. of Electr. Eng. and Comput. Sci., MIT, 1989.
- Duchnowski, P. *Simulation of Sensorineural Hearing Impairment*. S.M. thesis. Dept. of Electr. Eng. and Comput. Sci., MIT, 1989.
- Eide, E.M. *Extracting Stimulus and Response Center Locations from Confusion Matrices*. S.M. thesis. Dept. of Electr. Eng. and Comput. Sci., MIT, 1989.
- Evans-Lutterodt, K.W. *Synchrotron X-ray Diffraction Studies of Surface Phase Transitions*. Ph.D. diss. Dept. of Physics, MIT, 1989.
- Gentile, T.R. *Microwave Spectroscopy and Atom-Photon Interactions in Rydberg States of Calcium*. Ph.D. diss. Dept. of Physics, MIT, 1989.
- Gladstone, D.J. *Reaction Dynamics of Fluorine with Silicon (100): Design of a Molecular Beam Surface Reactive Scattering Chamber*. Ph.D. diss. Dept. of Chem., MIT, 1989.

- Grant, A.C. *The Nature of Electrical Transients Recorded in the Neuropil of the Frog's Optic Tectum*. Ph.D. diss. Dept. of Appl. Biol. Sci., MIT, 1989.
- Greenberg, J.E. *A Real-Time Adaptive Beam-forming Hearing Aid*. S.M. thesis. Dept. of Electr. Eng. and Comput. Sci., MIT, 1989.
- Henderson, D.R. *Tactile Speech Reception: Development and Evaluation of an Improved Synthetic Tadoma System*. S.M. thesis. Dept. of Electr. Eng. and Comput. Sci., MIT, 1989.
- Hengeveld, J.A. *Smooth Surface Reconstruction in VLSI*. S.B. thesis. Dept. of Electr. Eng. and Comput. Sci., MIT, 1989.
- Hilliard, Jr., J.E. *Monte Carlo Simulation of a One-Dimensional Ising System with Competing Interactions Using Domain Walls*. S.B. thesis. Dept. of Physics, MIT, 1989.
- Ho, S-T. *Theoretical and Experimental Aspects of Squeezed State Generation in Two-Level Media*. Ph.D. diss. Dept. of Electr. Eng. and Comput. Sci., MIT, 1989.
- Huang, W. *Modeling and Analysis of Guided-Wave Optoelectronic Devices*. Ph.D. diss. Dept. of Electr. Eng. and Comput. Sci., MIT, 1989.
- Hughey, B.J. *Cavity Modified Atom-Photon Interaction*. Ph.D. diss. Dept. of Physics, MIT, 1989.
- Hui, K.C-L. *Quenched Disorder and Competing Interactions in Spin Systems*. Ph.D. diss. Dept. of Physics, MIT, 1989.
- Im, J.S. *Experimental and Theoretical Investigation of Interface Morphologies Observed in Directional Solidification of Thin Si Films*. Ph.D. diss. Dept. of Mater. Sci. and Eng., MIT, 1989.
- Ismail, K. *The Study of Electron Transport in Field-Induced Quantum Wells on GaAs/GaAlAs*. Ph.D. diss. Dept. of Electr. Eng. and Comput. Sci., MIT, 1989.
- Joo, T.H. *Detection Statistics for Multichannel Data*. Ph.D. diss. Dept. of Electr. Eng. and Comput. Sci., MIT, 1989.
- Kaplan, J.T. *Pass and Restoring Logic Technology Mapping for the Efficient Automated Generation of Combinational Leaf Cells*. S.M. thesis. Dept. of Electr. Eng. and Comput. Sci., MIT, 1989.
- Keast, C.L. *A CCD/CMOS Process for Integrated Image Acquisition and Early Vision Signal Processing*. S.M. and E.E. thesis. Dept. of Electr. Eng. and Comput. Sci., MIT, 1989.
- Kiang, J-F. *On Fields and Propagation Characteristics of Guiding Structures in Stratified Media*. Ph.D. diss. Dept. of Electr. Eng. and Comput. Sci., MIT, 1989.
- Kim, E.J. *Dispersed Fringe Group Delay Astrometry Using the Mark III Stellar Interferometer*. S.M. thesis. Dept. of Electr. Eng. and Comput. Sci., MIT, 1989.
- Kuchnir, D.L. *Trapping and Detecting Two Different Single Ions at Once: A Step Towards Ultra-High-Precision Mass Comparison Measurements*. S.B. thesis. Dept. of Physics, MIT, 1989.
- LaGasse, M.J. *Femtosecond Optical Nonlinearities in AlGaAs*. Ph.D. diss. Dept. of Electr. Eng. and Comput. Sci., MIT, 1989.
- Lam, C-W. *Frequency-Domain and Time-Domain Methods for Analyses of Microstrip Structures in Anisotropic Media*. S.M. thesis. Dept. of Electr. Eng. and Comput. Sci., MIT, 1989.
- Lin, F.C-S. *Theoretical Models for Microwave Remote Sensing of Snow-Covered Sea Ice*. Ph.D. diss. Dept. of Physics, MIT, 1989.
- Maney, J.W. *Token Variability of Intra-Speaker Speech*. S.B. thesis. Dept. of Electr. Eng. and Comput. Sci., MIT, 1989.
- Marko, J.F.D. *On Structure and Scaling at First and Second Order Phase Transitions*. Ph.D. diss. Dept. of Physics, MIT, 1989.
- McCormick, S.P. *Modeling and Simulation of VLSI Interconnections with Moments*. Ph.D. diss. Dept. of Electr. Eng. and Comput. Sci., MIT, 1989.
- McGonigal, M. *Reactive Chemisorption of Molecular Fluorine on Si(100)*. Ph.D. diss. Dept. of Chem., MIT, 1989.
- Meyer, P.G. *Fabrication of Deep Submicron MOSFETs Using a Self-Aligned Cobalt Disilicide Process*. S.M. thesis. Dept. of Electr. Eng. and Comput. Sci., MIT, 1989.

- Miyanaga, H. *A Systematic Approach to VLSI Implementation for Real-Time Digital Signal Processing*. S.M. thesis. Dept. of Electr. Eng. and Comput. Sci., MIT, 1989.
- Moore, J.D. *Collisions of Orthogonally Polarized Solitary Waves*. S.M. thesis. Dept. of Electr. Eng. and Comput. Sci., MIT, 1989.
- Palmer, J.E. *Evolution of Microstructures in Ultra-Thin Films of GaAs and CaF₂ on Single Crystal Silicon*. Ph.D. diss. Dept. of Electr. Eng. and Comput. Sci., MIT, 1989.
- Pang, L.Y. *Polarization Effects on an External Cavity Controlled Ensemble of Fiber-Coupled Semiconductor Diode Lasers*. S.M. thesis. Dept. of Electr. Eng. and Comput. Sci., MIT, 1989.
- Petro, M.C. *An Autocorrelator for Determining the Temperature of the Upper Atmosphere*. S.B. thesis. Dept. of Electr. Eng. and Comput. Sci., MIT, 1989.
- Pickett, G.T. *Asymptotic Behavior of the Spectrum of Generalized Dimensions in Multifractal Tree Growth*. S.B. thesis. Dept. of Physics, MIT, 1989.
- Pratt, G.A. *Pulse Computation*. Ph.D. diss. Dept. of Electr. Eng. and Comput. Sci., MIT, 1989.
- Quek, H.M. *An Investigation of Graphoepitaxy in Thin Au and Bi Films*. S.M. thesis. Dept. of Mater. Sci. and Eng., MIT, 1989.
- Schoenlein, R.W. *Femtosecond Relaxation Dynamics of Image-Potential States in Metals*. Ph.D. diss. Dept. of Electr. Eng. and Comput. Sci., MIT, 1989.
- Shahidi, G.G. *Non-Stationary Transport Effects in Deep Sub-Micron Channel Si MOSFETs*. Ph.D. diss. Dept. of Electr. Eng. and Comput. Sci., MIT, 1989.
- Shinn-Cunningham, B.G. *Understanding the Precedence Effect: An Examination of Parameters Affecting its Strength*. S.M. thesis. Dept. of Electr. Eng. and Comput. Sci., MIT, 1989.
- Song, W.S. *A Fault-Tolerant Multiprocessor Architecture for Digital Signal Processing Applications*. Ph.D. diss. Dept. of Electr. Eng. and Comput. Sci., MIT, 1989.
- Tamir, T.J. *Characterization of the Speech of Tadoma Users*. S.B. thesis. Dept. of Electr. Eng. and Comput. Sci., MIT, 1989.
- Welch, G.R. *High Resolution Spectroscopy of Rydberg Atoms in a Magnetic Field*. Ph.D. diss. Dept. of Physics, MIT, 1989.
- Wong, S.B. *Magnetotransport Studies of the Magnetic Field Induced, Metal-Insulator Transition in Hg_{1-x}MnxTe*. Ph.D. diss. Dept. of Physics, MIT, 1989.
- Yang, Y.-C.E. *Time Domain Analysis of Electromagnetic Waves in Microelectronic Integrated Circuit Interconnects*. Ph.D. diss. Dept. of Electr. Eng. and Comput. Sci., MIT, 1989.
- Zangi, K.C. *A Novel QMF Design Algorithm*. S.M. thesis. Dept. of Electr. Eng. and Comput. Sci., MIT, 1989.
- Zirkind, N.E. *Adaptive Optics for Large Aperture Coherent Laser Radars*. Ph.D. diss. Dept. of Electr. Eng. and Comput. Sci., MIT, 1989.
- Zissman, M.A. *Co-Channel Talker Interference Suppression*. Ph.D. diss. Dept. of Electr. Eng. and Comput. Sci., MIT, 1989.

A.10 Miscellaneous Publications

- Chow, C., V. Fuchs, and A. Bers. *Reflection at the Resonance Layer of the Fast Alfvén Wave in Ion Cyclotron Heating*. MIT Plasma Fusion Center Report PFC/JA-90-2. Cambridge, MIT, 1990.
- Chow, C., V. Fuchs, and A. Bers. *The ICRF Dispersion Relation for D(³He)*. MIT Plasma Fusion Center Report PFC/JA-89-42. Cambridge, MIT, 1989.
- Chow, C., A.K. Ram, and A. Bers. *Damping of the Fast Alfvén Wave in Ion-Cyclotron Resonance Heating*. MIT Plasma Fusion Center Report PFC/JA-89-19. Cambridge, MIT, 1989.
- Durlach, N.I., C.M. Reed, C.E. Sherrick, and J.D. Miller. *Sensory Substitution: Visual and Tactile Methods*. Report Prepared for the Commission on Hearing and Bioacoustics (CHABA).
- Durlach, N.I., C.E. Sherrick, and J.D. Miller. "Sensory Substitution: Visual and Tactile Methods." In *Speech Communication Aids for the Hearing Impaired: Current Status and Needed Research*. (Report of CHABA Working Group 95). Eds. C.S. Watson, R.A. Dobie, N.I. Durlach, H. Levitt, J.D. Miller, C.E. Sherrick,

Appendix A. RLE Publications

- F.B. Simmons, G.A. Studebaker, R.S. Tyler, and Widin. Forthcoming.
- Keast, C.L., P. Tedrow, and C.G. Sodini. "A CCD/CMOS Process for Integrated Image Acquisition and Early Vision Signal Processing." Abstract presented at the VLSI Research Review, MIT, May 22, 1989.
- Lumsdaine, A., J. Wyatt, and I. Elfadel. "Parallel Distributed Networks for Image Smoothing and Segmentation in Analog VLSI." Abstract presented at the VLSI Research Review, MIT, December 18, 1989.
- Ram, A.K., and A. Bers. *Kinetic Ray Tracing in Toroidal Geometry with Application to Mode-Converted Ion-Bernstein Waves*. MIT Plasma Fusion Center Report PFC/JA-89-37. Cambridge, MIT, 1989.
- Shoucri, M., I. Shkarofsky, V. Fuchs, K. Kupfer, A. Bers, and S. Luckhardt. *A Quasi-linear Fokker-Planck Code for the Numerical Solution of the Lower-Hybrid Current Drive Problem in the Presence of Electron Cyclotron Heating*. Report No. CCFM-RI-298e. Varennes, Canada: Centre Canadien de Fusion Magnétique, Tokamak de Varennes, 1989.
- Standley, D., and J.L. Wyatt. "Stability Criterion for Lateral Inhibition and Related Networks that is Robust in the Presence of Integrated Circuit Parasitics." Abstract presented at the VLSI Research Review, MIT, December 18, 1989.
- Yang, W. *Method and Charge Coupled Apparatus for Algorithmic Computations*. Patent application submitted to U.S. Patent Office on May 1, 1989. Receipt number 07/352,765.

Appendix B. Current RLE Personnel

Director: Jonathan Allen

Associate Director: Daniel Kleppner

Professors

Jonathan Allen
Dimitri A. Antoniadis
Arthur B. Baggeroer
George Bekefi
A. Nihat Berker
Abraham Bers
Robert J. Birgeneau
Amar G. Bose
Louis D. Braid
Bernard E. Burke
Sylvia T. Ceyer
Sow-Hsin Chen
Bruno Coppi
Shaoul Ezekiel
Clifton G. Fonstad, Jr.

Lawrence S. Frishkopf
Hermann A. Haus
Albert Hill¹
Erich P. Ippen
John D. Joannopoulos
Marc A. Kastner
Nelson Y.-S. Kiang
John G. King
Daniel Kleppner
Jin A. Kong
Patrick A. Lee
Jerome Y. Lettvin¹
Jae S. Lim
Alan V. Oppenheim
William T. Peake

Miklos Porkolab
David E. Pritchard
William F. Schreiber
Campbell L. Searle
Jeffrey H. Shapiro
William M. Siebert
Henry I. Smith
David H. Staelin
Kenneth N. Stevens
Julius A. Stratton¹
Donald E. Troxel
Thomas F. Weiss
Jerome B. Wiesner¹
John L. Wyatt, Jr.
Henry J. Zimmermann¹

Associate Professors

James G. Fujimoto
Peter L. Hagelstein

Bruce R. Musicus

Keith A. Nelson
Carl V. Thompson III

Assistant Professors

Jesus A. del Alamo
Srinivas Devadas
John M. Graybeal

Jacqueline N. Hewitt
Qing Hu
Leslie A. Kolodziejski

Simon G.J. Mochrie
Jacob K. White
Jonathan S. Wurtele

Senior Research Scientists

Nathaniel I. Durlach
Joseph S. Perkell
Robert H. Rediker

Principal Research Scientists

H. Steven Colburn
John J. Guinan, Jr.
Stanley C. Luckhardt

John Melngailis
William M. Rabinowitz
Charlotte M. Reed

Philip W. Rosenkranz
Patrick M. Zurek

¹ Professor Emeritus.

Postdoctoral Fellows and Associates

Santanu Basu
Joan M. Besing
Suzanne Boyce
Robin L. Davis
Jill C. Gardner

Kenneth W. Grant
Marie K. Huffman
Kenneth B. Laughlin
Christine M. Rankovic
Mario A. Svirsky

Tao Tao
Rosalie M. Uchanski
Jyhpyng Wang
Xiu-Bing Wei
Min Xiao

Research Scientists and Research Specialists

Sami M. Ali
Giovanni Aliberti
Sunny Y.C. Auyang
John W. Barrett
James M. Carter
Bertrand Delgutte
Lorraine A. Delhorne
Donald K. Eddington
Ronald C. Englade
Carol Y. Espy-Wilson
Edward W. Fitzgerald

David W. Foss
Dennis M. Freeman
Seth M. Hall
Kazuhiko Kunitomi
Wilberto Martinez
Ivan Mastovsky
Melanie L. Matthies
Stefano Migliuolo
Xiao Dong Pang
Abhay K. Ram
Mark A. Randolph

John J. Rosowski
Giampiero Sciutto
Stefanie Shattuck-Hufnagel
Mark I. Shepard
Stephen C. Shepard
Mandayam A. Srinivasan
Linda E. Sugiyama
Giancarlo Trevisan
Ngai Chuen Wong
Ying-Ching E. Yang

Visiting Scientists

Sergio A. Angelini
Herbert J. Bernstein
Giuseppe Bertin
Corine A. Bickley
Charles S. Burrus
Tomaz Catunda
Stefano Coda
Alfred P. DeFonzo
Paolo Detragiache
Theodore W. Ducas
Richard L. Freyman
Bernard Gold
Qizheng Gu

Yan-an Han
Eli Jerby
Arthur K. Jordan
Philippe Kersale
Janet D. Koehnke
Jack Kotik
Pierandrea Lo Nostro
Neil A. Macmillan
Sharon Y. Manuel
Phylis Morison
Hidehito Nanto
Guilia A. Nassi
Marco Nassi

Kevin O'Neill
Karen L. Payton
Harold R. Raemer
Ramdas L. Ram-Mohan
Stanley J. Rosenthal
Bruce Schneider
Alexander Shlyakhter
Elias Snitzer
Arend M. Sulter
Makoto Tabei
Kongyi Xu
Tsuneki Yamasaki

Research Affiliates

John S. Barlow
Frank S. Cardarelli
John J. Donoghue
Giuseppe Gabetta
Richard S. Goldhor
Philip R. Hemmer
Robert E. Hillman
Jeannette D. Hoit
Eva B. Holmberg
Joseph A. Jarrell

Haruko Kawasaki
John D. Kierstead
Harlan Lane
John L. Locke
Debra S. Louison
John I. Makhoul
Michael B. McIlrath
Leonard L. Picard
Irving Plotnik
Soon Yun Poh

Carol C. Ringo
Jay T. Rubinstein
Michael Shao
Robert T. Shin
Richard J. Solomon
Frank J. Stefanov-Wagner
David A. Steffens
Kenneth P. Wacks
Jane W. Webster

Research Assistants

Khurram K. Afridi
 Sergio Ajuria
 Ashraf S. Alkhairy
 Abeer Alwan
 Tomas A. Arias
 Robert C. Armstrong
 David V. Arnold
 Robert G. Atkins
 Sandeep Bahl
 Donald G. Baltus
 David S. Barwick
 Paul E. Beckmann
 Keren Bergman
 Pierino G. Bonanni
 Kevin R. Boyce
 Andrew R. Brabson
 John P. Braud
 Tom P. Broekaert
 Stuart D. Brorson
 Michael J. Bryan
 Martin Burkhardt
 Pin-P. Chang
 William J. Chiarchiaro
 Warren H. Chou
 Carson C. Chow
 Kevin G. Christian
 Nelson C. Chu
 Daniel T. Cobra
 Samuel R. Conner
 Christopher J. Corcoran
 Eric A. Cornell
 Bruce G. Danly
 Steven J. Decker
 John T. Delisle
 Andrew D. Dubner
 Paul Duchnowski
 Kathleen R. Early
 Farzad Ehsani
 Christopher R. Ekstrom
 Ibrahim M. Elfadel
 Darin Ernst
 Jerrold A. Floro
 Dennis C.Y. Fogg
 Joseph A. Frisbie
 James G. Goodberlet
 Thomas J. Green, Jr.
 Mark E. Griffith
 Katherine L. Hall

Hsiu C. Han
 Jens-ole Hansen
 John C. Hardwick
 Michael B. Heflin
 Kristian P. Helmerson
 Michael L. Heytens
 Andrew W. Howitt
 Long Hsu
 Caroline B. Huang
 David Huang
 Charles T. Hultgren
 Janice M. Huxley
 Chun-Ho lu
 Michael A. Joffe
 Abbas Kashani
 Sumanth Kaushik
 David W. Keith
 Songmin Kim
 Richard Y. Kim
 Robert K. Kirkwood
 Wolfgang G. Knecht
 Kenneth C. Kupfer
 Yinchieh Lai
 Cheung-Wei Lam
 Kevin Lam
 Suzanne D. Lau-Shiple
 Check Fu Lee
 Joseph Lehar
 Darren L. Leigh
 Kin-Wai Leong
 Henri J. Lezec
 Harold H. Lim
 Ling-Yi Liu
 Jennifer A. Lloyd
 Hai P. Longworth
 Andrew Lumsdaine
 Robert I. Lutwak
 Cynthia R. McIntyre
 Robert E. Mentle
 Paul G. Meyer
 Alberto M. Moel
 Lynne Molter-Orr
 Peter A. Monta
 Keith S. Nabors
 Vasant Natarajan
 Son Van Nghiem
 Scott N. Paine
 Joyce E. Palmer

Lily Y. Pang
 Brian K. Pheiffer
 Mary R. Phillips
 Julien Piot
 Ashok C. Popat
 Matthew H. Power
 G.N. Srinivasa Prasanna
 Gill Pratt
 Khalid Rahmat
 Andrew M. Rappe
 Mark W. Reichelt
 George E. Rittenhouse
 Jae-Sang Ro
 Jon C. Sandberg
 Michelle T. Schulberg
 Hugh E. Secker-Walker
 Mohamad S. Shahriar
 Jerome M. Shapiro
 David M. Sheen
 Paul X. Shen
 Luis M. Silveira
 Richard A. Singer
 Stephen P. Smith
 David L. Standley
 Richard E. Stoner
 Howard R. Stuart
 Ke-Xun Sun
 Lon E. Sunshine
 Hong Z. Tan
 Mohammad A. Tassoudji
 Siang-Chung The
 Adam S. Tom
 Michael J. Tsuk
 Ann A. Tulintseff
 Morrison Ulman
 Murat E. Veysoglu
 Jesus Noel Villasenor
 David B. Walrod
 Robert J. Webster
 Lorin F. Wilde
 Timothy A. Wilson
 Dilys K. Wong
 Gregory W. Wornell
 Jiqing Xia
 Peter T. Yu
 Kambiz C. Zangi
 Farhad Zarinetchi

Teaching Assistants

Babak Ayazifar
 Charlotte E. Biber
 Christopher A. Crowley
 Yoshiko Ito

Joseph M. Jacobson
 Michael Orkisz
 John A. Rogers
 Mark N. Seidel

Andrew C. Singer
 Clay M. Thompson
 Michael L. Zerkle

Graduate Students

John J. Allen
John G. Apostolopoulos
Matthew M. Bace
David M. Baylon
Scott I. Berkenblit
Riccardo Betti
Bradley T. Binder
Michael Brandstein
John Buck
Stephen Buerle
Claudio L. Cesar
Claudio Chamon
Yoo Chan
Curtis S. Chen
Jerry C. Chen
Marilyn Y. Chen
Tak K. Cheng
Zandra H. Cheng
Shiufun Cheung
Michael W. Courtney
Christian E. de Graff
Kathleen M. Donahue
Anthony C. DiRienzo
San Duanmu
Ellen M. Eide
Andre B. Fletcher

Ethan B. Foxman
Seth A. Gordon
Julie E. Greenberg
Michael R. Haggerty
Ibrahim Hajjahmad
Helen M. Hanson
Yoshihisa Hara
William R. Hollaway
Alfred S. Hou
Jeung-Soo Huh
Steven H. Isabelle
Mark Jablonski
Jacek Jachner
Joseph V. Kaliszewski
David Kuo
David Leip
Kevin Li
Sandra I. Lugo
Rodney Marable
John A. Marroquin
Ignacio S. McQuirk
Scott E. Meredith
Michael C. Moldoveanu
John D. Moores
Martin Muendel
Christian R. Musil

Malini V. Narayanan
Julien J. Nicolas
James M. Njeru
Bruce G. Oldaker
Janet L. Pan
James C. Preisig
Timothy G. Reese
Michael D. Richard
Timothy T. Rueger
Scott R. Shepard
Philip Smith
Jared P. Squire
Kohichi R. Tamura
Lynore Taylor
Ricardo Telichevesky
Veena Trehan
Matthew D. Trevithick
Katherine S. Wang
Dan Wang
Susie Wee
Peter Woo
Xinglong Yan
Saed Younis
Herng-Aung Yueh
Marc Zissman

Undergraduate Students

Daniel P. Aalberts
Nasser A. Ahmad
Alfonso B. Amparan
Alexandar Angelus
Ellen Ballentine
Philip K. Baltz
Azizuddin A. Biyabani
Younes Borki
George Chen
Patrick Chou
Daniel J. Chung
Michael W. Connell
Charles Q. Davis
Desmond Davis
Alin D'Silva
Mark G. Duggan
Stephen S. Eikenberry
Mauricio A. Escobar
Leslie Fan
John M. Gachora
Rajiv Guha
JoAnne Gutierrez
Darby A. Hailes
Timothy J. Hawkey
Mary A. Hou

Rahat Husain
William W. Irving
Shaun Y. Kaneshiro
Farzana I. Khatri
Theodore T. Kim
Sarah I. King
Gloria W. Lau
Adnan H. Lawai
Wey Lead
Paula M. Lee
Alberto Leon
Gloria Leong
Stan Y. Liao
Yong Liu
Kenneth P. Lu
Keith S. MacKay
John D. MacKenzie
Laura Marmorstein
Michael L. McComas
Pablo Munguia
James L. Nagle
Quintin Ndibongo
Joel R. Phillips
Yaser A. Rehem

Rebecca J. Renn
William W. Roberts
Rahul Sarpeshkar
James P. Schwonek
Asif Shakeel
Lisa Su
Gary J. Tarnowski
Daniel Tauber
Colin J. Taylor
Lisa J. Tegeler
Flora S. Tsai
Quentin Turchette
Brian L. Vajda
Benjamin Van Roy
Bing Wang
Li-Fang Wang
Linus Wang
Shawn T. Williams
Diana Wong
Vincent Wong
David C. Wu
Derrick Yim
John Zeigler
Lori L. Zieran

Administrative Staff

Donald F. Duffy
Virginia R. Lauricella
Barbara J. Passero

John S. Peck
Gerrard F. Power
Anita T. Sloan

Vicky-Lynn Taylor
Donna Maria Ticchi

Support and Technical Staff

Robert W. Aalerud
Mary C. Aldridge
Margery E. Brothers
Mary Ellen Butts
Manuel Cabral, Jr.
Donald A. Clements
John F. Cook
Carol A. Costa
Francis M. Doughty
Laura B. Doughty
Toni Fischer
Dorothy A. Fleischer
Ann Forestell

Deborah A. Gage
Donna L. Gale
Mary S. Greene
Debra L. Harring
Maureen C. Howard
Wendy E. Hunter
Barbara A. King
Cynthia Y. Kopf
Kit-Wah F. Lai
Edward R. Lavalley
Cynthia LeBlanc
Anh Lieu
Wei Ming-Yu Lin

Catherine Lorusso
Eleanora M. Luongo
Rita C. McKinnon
Susan E. Nelson
Donald K. North
Robert Priest
Jeanne M. Prisbylla
Brian E. Ray
Susan M. Ross
Bruce A. Russell
Maxine P. Samuels
Clare F. Smith
Mary J. Ziegler

In Memoriam

Professor Richard B. Adler (1923 - 1990)
Jeremiah Brennan (1906 - 1989)
Robert M. Brown (1927 - 1989)
Professor Emeritus Harold E. "Doc" Edgerton (1903 - 1990)
George H. Leach (1922 - 1989)
Professor Emeritus Yuk Wing Lee (1904 - 1989)
John J. McCarthy (1915 - 1990)

Appendix C. RLE Research Support Index

- 3M Company 47-49
 Analog Devices, Inc. 275-279
 AT&T Research Foundation 47-49
 Battelle Laboratories 243-244
 Boston University 315-317
 California Institute of Technology
 Jet Propulsion Laboratory 212-215
 Center for Advanced Television
 Studies 258-264
 Defense Advanced Research Projects
 Agency (DARPA) 265-266
 Dennis Klatt Memorial Fund 302-311
 Digital Equipment Corporation 218-220
 Draper (Charles S.) Laboratory 31-33,
 73-74, 136-137, 241-242
 du Pont, de Nemours & Company
 279-283
 Hampshire Instruments Corporation 9
 International Business Machines Corporation
 24-26, 32, 80-82, 218-220, 275-279,
 288-292
 Johnson and Johnson Foundation 321-333
 Joint Services Electronics Program (JSEP)
 7-17, 21-23, 35, 41-45, 47-50, 53-57,
 59-62, 64-66, 73-83, 109-126, 139-142,
 148-153, 197-202, 275-279
 Lawrence Livermore National Laboratory
 93-94, 96-98, 167-169
 Maryland Procurement Office 267-269
 Massachusetts Eye & Ear Infirmary 316-317
 Massachusetts General Hospital 83-86
 National Aeronautics and Space Administration
 Goddard Space Flight Center 202-208,
 212-214, 232-234
 National Institutes of Health 83-86,
 302-311, 315-317, 321-333
 National Science Foundation 7-8, 47-49,
 61-65, 73-76, 78-83, 103-105, 143-149,
 167-181, 197-202, 225-230, 243-256,
 258, 260, 267-269, 279-283, 289-290
 Purdue University 47-51
 Sanders Associates, Inc. 245-246, 248, 251
 Schlumberger-Doll Research 197-202
 Simulation Technologies, Inc. 212-214
 SM Systems and Research, Inc. 231-232
 U.S. Air Force, Electronic Systems Division
 215-218, 253-255, 261
 U.S. Air Force, Office of Scientific Research
 21-24, 75-83, 272-273, 275-279
 U.S. Army Corps of Engineers 212-215
 U.S. Army Research Office 29-34, 149-153,
 197-202, 269-271
 U.S. Department of Energy 86-96, 98-101,
 169-194
 U.S. Department of Transportation 220-221
 U.S. Naval Research Laboratory 232
 U.S. Navy, Office of Naval Research 47-50,
 149-155, 208-211, 215-218, 232, 241-252,
 254-256, 271, 283-293
 WaveTracer, Inc. 212-214
 Woods Hole Oceanographic Institution 234
 X-Opt., Inc. 17

Project Staff and Subject Index

Project Staff and Subject Index

A

Aalberts, Daniel P. 167
 ABC 257
 Abernathy, Douglas A. 125
 Advanced Microwave Sounding Unit (AMSU) 231
 Advanced Television Research Program 257-264
 Afridi, Khurram K. 197, 218, 220
 Agarwal, Anant 247
 Airports
 Landing Systems 220
 Computer Simulation 220
 Safety 220
 Ajuria, Sergio A. 7, 21
 Akerson, Jerome J. 197
 Alcator C-MOD 181
 Aldridge, Mary C. 73
 Alerhand, Oscar L. 109, 115
 Ali, Sami M. 197, 215, 218
 Aliberti, Giovanni 241, 253, 257
 Alkhairy, Ashraf 225, 234
 Allen, Jonathan 275-279, 288, 301
 Alwan, Abeer A. 301
 Ampex 257
 Anderson, Kristen K. 73, 80
 Angelini, Sergio 181
 Angelus, Alexander 225, 231
 Antoniadis, Dimitri A. 7, 9-16, 30, 121, 275
 Arias, Tomas A. 115
 Ariel, Imadiel 109, 123
 Arman-Nassi, Giulia 301
 Armstrong, Robert C. 275
 Arnold, David V. 197, 202
 Astronomy, Radio
 See Radio Astronomy
 Atkins, Robert G. 197, 202
 Atom-Beam Interferometry 7
 Atomic Physics 131
 Precision Measurements 139, 155
 Auditory Physiology 321-333
 Auditory System 321-333
 BAEP 329
 Cellular Generators 329
 Evoked Potentials 329
 Nerves 325, 326
 Signal Transmission 321-333
 Auyang, Sunny 103
 Azzam, Walid 53

B

Bace, Matthew M. 257, 258
 Baggeroer, Arthur B. 241
 Bagwell, Phillip F. 7, 12, 13, 14
 Bahl, Sandeep 53
 Bahrani, Talal M. 225
 Baltus, Donald G. 275
 Bamji, Cyrus S. 275
 Barrett, John W. 225, 230, 232, 233
 Barwick, D. Shane 267, 271
 Basu, Santanu 73, 86, 88, 92, 96
 Bateman, Nicholas P.T. 225
 Baylon, David M. 257, 259
 Beckmann, Paul E. 241
 Bekefi, George 167-169
 Bekerle, John D. 35, 36, 37
 Bell Communications Research (Bellcore) 43, 67, 81
 Bergman, Keren 73
 Berker, A. Nihat 109-110
 Bers, Abraham 167, 169-181
 Besing, Joan 315
 Betti, Riccardo 167, 181
 Bickley, Corine A. 301
 Binder, Bradley T. 267
 Birgeneau, Robert J. 111-114
 Blanck, Herve 61, 66, 67
 Blauner, Patricia G. 29, 31
 Blum, Kenneth 111
 Bonanni, Pierino G. 225, 233
 Borgeaud, Maurice 197, 208
 Bossi, Donald E. 267, 272
 Boston University
 WBUR Radio Station 308
 Boyce, Kevin R. 139, 148
 Boyce, Suzanne E. 301
 Braid, Louis D. 315-317
 Brandstein, Michael S. 253
 Braud, John Paul 73, 86, 89, 90
 Brennan, Theresa A. 267
 Brock, Joel 111
 Broekaert, Thomas P.E. 61, 65, 66
 Brookhaven National Laboratory 111, 169
 Brorson, Stuart D. 64, 73, 76, 77
 Brothers, Margery E. 197
 Bryan, Michael J. 275, 283
 Buck, John R. 241, 243
 Burke, Bernard F. 225-231
 Burkhardt, Martin 7, 13, 14
 Burns, Geoffrey 21, 24, 61, 66, 67
 Burrus, Charles S. 241, 244

Project Staff and Subject Index

Butt, Yousaf 29, 31
Butts, Mary Ellen 73

C

CAF

See Computer-Aided Fabrication (CAF)

CAFE

See Computer-Aided Fabrication Environment (CAFE)

Cain, Gerald 35
California Institute of Technology 225, 231
Candell, Lawrence M. 241
Canizares, Claude R. 17
Carilli, Christopher 225
Carlin, Gregory A. 9
Carter, James M. 7
Carvalho, Bruce L. 157, 160
Ceyer, Sylvia T. 35-40, 68
Chamon, Claudio 80
Chang, Ike 197, 215
Chang, Pin P. 139, 146
Chang, Szu-Li 157, 160
Charles S. Draper Laboratory 242
Chen, Chenson K. 21, 25
Chen, Curtis S. 275, 283
Chen, George 167
Chen, John 157, 160
Chen, Judy 197
Chen, Kuo-in 167, 191
Chen, Marilyn Y. 301
Chen, Shien-Chi 167
Chen, Sow-Hsin 157-164
Cheng, Tak K. 73, 76
Cheung, Shiufun 225, 253, 254
Chiang, Alice 282
Chiarchiaro, William J. 225, 233
Cho, Jaeshin 21, 22
Choi, Woo-Young 61, 63
Chomsky, Noam A. 337-339
Chong, Tow 24
Chou, Warren 253
Chow, Carson 167, 169
Christian, Kevin G. 225, 234
Chu, Nelson C. 197, 202
Chu, William 7, 13, 14, 16
Chung, Daniel 197
Chung, Jee 225, 230
Circuit Design
 Process Flow Representation 265
Clevenger, Lawrence A. 7, 21, 24
Clifton, Rachel K. 315
Cobra, Daniel T. 241, 245
Cochlea 324
 Efferents 328

Cochlea (*continued*)

Implants 310, 316, 330

Cochlear Implant Laboratory

See Massachusetts Eye and Ear Infirmary (MEEI)

Coda, Stefano 167, 191

Colborn, Jeffrey A. 167, 191

Colburn, H. Steven 315

Columbia University 181

Communications

See Optical Communication

See Sensory Communication

See Speech Communication

Compact Ignition Experiment (CIT) 181

Computer Vision

Hardware 279

Computer-Aided Fabrication Environment (CAFE) 265

Computer-Aided Fabrication (CAF) 265

Conde, Manoel E. 167

Conner, Samuel R. 225

Coppi, Bruno 167, 181-191

Corcoran, Christopher J. 267, 271

Cornell, Eric A. 139, 148

Costa, Carol A. 139

Courtney, Michael W. 139, 143

Covell, Michele M. 241, 245

Cuneo, Patricia A. 321, 331

Custom Chips 279

Custom Integrated Circuits

See Integrated Circuits

D

Dally, William J. 292

Davis, Robin L. 321, 325

de Graff, Christian E. 167

DeAvillez, Roberto R. 21, 24

Decker, Steven J. 275, 279, 282

DeFonzo, Alfred P. 225

del Alamo, Jesus A. 7, 13, 14, 53-57

Delcroix, Jean-Loup 169

Delgutte, Bertrand 321, 326

Delhorne, Lorraine A. 315

Delisle, John T. 225, 234

Dennedy, Thomas 247

Detragiache, Paolo 167, 181

Devadas, Srinivas 275, 283-288

DiCecca, Salvatore 167

Digital Signal Processing 241-252

DiRienzo, Anthony C. 167

Dix, Ann 167

DNA Molecules 160

Donahue, Kathleen M. 321, 323

Donoghue, John 131
 Doughty, Francis M. 257, 265
 Doughty, Laura B. 167
 Dresselhaus, Mildred S. 76
 Dubner, Andrew D. 21, 25, 29, 32
 Ducas, Theodore W. 139
 Duchnowski, Paul 315
 Dupree, Thomas 167
 Durlach, Nathaniel I. 315

E

Ear 321-333
 Cochlear Implants 310
 External Ear 323
 Human Cadaver 323
 Middle-Ear 321, 323
 Early Mammal 321
 Muscles 327
 Structure and Function 321
 Early, Kathleen R. 7
 Eaton-Peabody Laboratory for Auditory
 Physiology 321
 Eddington, Donald K. 321, 330, 331
 Edell, David J. 21, 26
 Ehrnst, Darin 181
 Ehsani, Farzad 321, 324
 Eide, Ellen M. 315
 Eikenberry, Stephen S. 225, 232
 Einstein Rings 226
 Einziger, Pinchas D. 197, 202
 Ekstrom, Chris R. 139, 149
 Eldridge, Creighton 265
 Electromagnetic Waves 197-221, 267
 Electromagnetics
 Wave Theory 197
 Remote Sensing 197
 Electronic Devices 53
 MOSFETs 123
 Semiconductors 75, 121
 Si MOSFETs 121
 Superconductors 75
 Electronic Materials
 Films 157
 Thin Films 21, 111
 Focused Ion Beam Fabrication 29
 Molecular Beam Epitaxy 61
 Optical Systems 103
 Quantum Heterostructures 61
 Semiconductors 7, 35, 41, 47, 53, 59
 Submicron Structures 7
 Superconductors 59
 Surface Studies 35, 109, 115, 125
 Elfadel, Ibrahim M. 275, 279

Englade, Ronald C. 167, 181
 Espy-Wilson, Carol Y. 301
 Eugster, Cris 7, 73, 96
 Evans, Paul 21, 25
 Evans-Lutterodt, Kenneth 111
 Ezekiel, Shaoul 131

F

Feder, Meir 241, 243
 Fiber Optics 136
 Field, Stuart B. 10, 121
 Fischer, Toni 167
 Fitzgerald, Edward W. 167, 191
 Fleischer, Dorothy A. 275
 Fletcher, Andre B. 225
 Floro, Jerrold A. 7, 21, 23, 24
 Focused Ion Beam Fabrication 29
 Fogg, Dennis C. 241, 246
 Fonstad, Clifton G., Jr. 21, 24, 61-70
 Forestell, Ann F. 301
 France, Bureau des Longitudes 231
 Frank, Melissa 61
 Fraunhofer Institute (Berlin) 32
 Freeman, Dennis M. 321, 324
 Freyman, Richard 315
 Friedland, Lazar 167, 169
 Frisbie, Joseph A. 315
 Frishkopf, Lawrence S. 321, 324
 Frost, Harold J. 21
 Fu, J.K. 197
 Fuchs, Vladimir 167, 169
 Fujimoto, James G. 73, 78-86
 Fullerton, Barbara 321, 331
 Furst, Miriam 321, 331
 Fusion 190
 Coherent 98
 Cold 98

G

Gage, Deborah A. 241
 Gale, Donna L. 73
 Gardner, Jill C. 321, 331
 General Instruments 257
 General Motors Research Laboratories 82
 Gentile, Thomas R. 139
 Ghanbari, Reza A. 7, 13, 14
 Gharavy, Hassan 241, 253, 257
 Gilbert, Harvey R. 301
 Gladstone, David J. 35
 Glicksman, Laura B. 301

Project Staff and Subject Index

Gold, Alfred 123
 Goldhor, Richard S. 301
 Goodberlet, James G. 73, 78
 Gorecka, Alicja 337
 Grant, Arthur C. 295
 Grant, Kenneth W. 315
 Graybeal, John M. 59-60
 Green, Thomas J., Jr. 267, 269
 Greenberg, Julie 315
 Griffith, Mark 225
 Gu, Qizheng 197, 220
 Guinan, John J., Jr. 321, 327, 328
 Guo, Xuan-Hui 157, 158
 Gutierrez, JoAnne 7, 9

H

Habashy, Tarek M. 197, 215, 218
 Hagelstein, Peter L. 73, 86-101
 Hajjahmad, Ibrahim A. 257, 259
 Hakkarainen, Mikko 275, 279
 Hall, Katherine L. 73, 75, 76
 Hall, Seth M. 301, 315
 Halle, Morris 301, 337-339
 Han, Hsiu C. 212
 Hannon, Stephen M. 267, 269
 Hansen, Jens-Ole 225, 231
 Hara, Yoshihisa 197
 Hardwick, John C. 253, 254
 Harvard University, Museum of Comparative Zoology 321
 Haus, Hermann A. 62, 73-75, 80, 86
 Haystack Observatory 231
 HDTV
 See High Definition Television (HDTV)
 Hearing 315
 See also Ear
 Hearing Aids 315, 330
 Sensory Aids 330
 Hearing Impaired Individuals 321
 Tactile Aids 315
 Heflin, Michael B. 225
 Heiblum, Mordehai 121
 Helmerson, Kristian 139, 153
 Hemmer, Philip R. 131
 Henderson, Douglas H. 315
 Hendrix, Donna K. 321, 324
 Hewitt, Jacqueline N. 225, 231
 Heytens, Michael 265
 High Definition Television (HDTV) 259
 Hilliard, Joseph E. 109
 Hillman, Robert E. 301
 Ho, Seng-Tiong 267
 Hoit, Jeannette D. 301

Holmberg, Eva B. 301
 Hong, Hawoong 111
 Horn, Berthold K.P. 275, 279, 282
 Hoshiro, Isako 61, 63
 Hoston, William 109, 110
 Howitt, A. William 301
 Hryniewicz, J.V. 65
 Hsu, Long 139, 143
 Huang, Caroline B. 301
 Huang, David 83
 Huang, Wei-Ping 73, 74
 Huffman, Marie K. 301
 Hughey, Barbara J. 139
 Huh, Jeung-Soo 29, 31
 Hui, Kenneth 109
 Hultgren, Charles T. 73, 75
 Hunter, Wendy E. 225
 Huxley, Janice M. 73

I

Ignitor Experiment 181
 Im, James S. 21, 25
 Image Processing 241
 Indeku, Joseph O. 109
 Induced Stochasticity and Chaos 169
 Integrated Circuits 7, 21
 Computer-Aided Design 29, 265, 275-293
 Custom 275-293
 Fault Tolerance 283
 Reliability 283, 288
 VLSI 275
 International Business Machines Corporation 111
 Ippen, Erich P. 45, 73, 75-77, 83
 Isabelle, Steven H. 257, 260
 Ishii, Kenneth 265
 Ismail, Khalid 7, 13, 14, 16, 29, 30
 Ito, Yoshiko 315
 Iu, Chun-Ho 139, 143

J

Jablonski, Mark 167, 169
 Jachner, Jacek 241, 247
 Jacobson, Joseph M. 73, 78
 Jaffe, Jules 241, 250
 Japan, Institute for Science and Astronautics in Space 230
 Jerby, Eli 167
 Jet Propulsion Laboratory 212, 231
 Jiran, Eva 7, 21, 25

Joannopoulos, John D. 109, 115-120
 Joffe, Michael A. 139, 153
 Johnson, Andrew D. 35-39
 Joo, Tae H. 241, 248
 Jordan, Arthur K. 197

K

Kaes, Herbert D. 29, 33
 Kahn, Harold 7, 21, 22
 Kalisewski, Joseph 265
 Kashani, Abbas 265
 Kastner, Marc A. 7, 10, 12, 13, 14, 121-122, 123
 Kaushik, Sumanth 73, 86, 93, 96
 Kaxiras, Efthimios 115
 Keast, Craig 275, 279, 281
 Keith, David W. 139, 149
 Keyser, Samuel J. 301
 Kiang, Jean-Fu 218
 Kiang, Nelson Y.C. 321, 329
 Kierstead, John 131
 Kim, Edward J. 225, 232
 Kinaret, Jari 123
 King, Barbara A. 267
 Kirkwood, Robert J. 167, 191
 Kleppner, Daniel 139-148
 Knecht, Wolfgang G. 315
Knowledge-Based Signal Processing 241
 Ko, Weng-Yew 167, 169
 Kobler, James B. 321, 327
 Kodak 257
 Koehnke, Janet D. 315
 Kolodziejski, Leslie A. 47-52
 Kong, Jin Au 197-221
 Kopf, Cynthia Y. 73
 Koreman, Jacques 301
 Ku, Yao-Ching 7, 9
 Kuchnir, Deborah 139, 148
 Kuo, Charlene C. 225, 231
 Kuo, David 257, 260
 Kupfer, Kenneth C. 167, 169

L

LaGasse, Michael J. 73, 74, 80
 Lai, Kit-Wah 197
 Lai, Yinchieh 73, 76
 Lam, Cheung-Wei 197, 218
 Lam, Kevin 275, 283
 Lane, Harlan L. 301
 Langmuir-Blodgett Films 157

Laser Gyroscopes 136
 Lasers 86-96
 Femtosecond 78, 86
 Free Electron 167
 Medical Applications 83, 86
 Semiconductor 77
 Semiconductors 271
 X-Ray 93-96
 Lau, Gloria W. 197
 Lau-Shiple, Suzanne D. 267, 272
 Laughlin, Kenneth B. 35
 Laurich, B. 64
 Lawrence Livermore National Laboratory 88
 Le, H.Q. 65
 Leaird, Dan E. 41
 LeBlanc, Cynthia 253, 257
 Lee, Check-Fu 197, 215, 218
 Lee, Dana H. 47
 Lee, Hae-Seung 275, 279
 Lee, Patrick A. 123-124
 Lehar, Joseph 225
 Leibovitch, Chaim 167
 Leigh, Darren L. 225, 234
 Lenses 225
 Leon, Alberto 167, 191
 Leong, Kin-Wai 267
 Lettvin, Jerome Y. 295-296
 Leung, Vivian 157, 160
 Levine, Robert A. 321, 331
 Lezec, Henri J. 29, 30
 Li, Kevin 197
 Liao, Victor 197
 Lieu, Ahn 197
 Lim, Harold H. 197, 202
 Lim, Jae S. 253-256, 257-264
 Lin, Wei Ming-yu 197
 Linguistics 307
 Articulation 337
 Metrical Structure 339
 Phonology 337
 Syntax 338
 Liu, C.T. 14
 Liu, Ling-Yi 73
 Liu, Yachin 7, 21, 25
 Lloyd, Jennifer A. 275
 Lo Nostro, Pierandrea 157, 161
 Locke, John L. 301
 Longworth, Hai 7, 21, 22
 Lorusso, Catherine 167
 Louison, Debra S. 321
 Lu, Kenneth 7, 9
 Luckhardt, Stanley C. 167, 191
 Lugo, Sandra I. 301
 Lumsdaine, Andrew 275
 Luongo, Eleanora M. 315

Lutwak, Robert P. 139, 146

M

Ma, En 21, 24
 Machado, Michael E. 315
 Macmillan, Neil A. 315
 Mahoney, Leonard J. 29, 30, 31
 Mailhoit, Christian 64
 Mak, Alan 111
 Makhoul, John I. 301
 Maney, J. William 315
 Manuel, Sharon Y. 301
 Manufacturing Processes 234
 Marine Mammals 234
 Marko, John F. 109
 Marmorstein, Laura 197
 Marroquin, John A. 167
 Martinez, Donna 7, 29
 Masked Thresholds 326
 Massachusetts Eye and Ear Infirmary (MEEI)
 Cochlear Implant Laboratory 321
 Eaton-Peabody Laboratory for Auditory Physiology 321
 Mastovsky, Ivan 167
 Matthies, Melanie L. 301
 Maynard, Kevin J. 35, 38, 39
 McCabe, Margaret 131
 McClure, Timothy 7
 McCombe, Bruce D. 64
 McCormick, Steven P. 275
 McCue, Michael P. 321, 327
 McGonigal, Marianne 35
 McIlrath, Michael B. 265
 McQuirk, Ignacio 275, 279, 282
 Medard, Muriel 225
 Meirav, Udi 7, 10, 121
 Melcher, Jennifer R. 321, 329
 Melngailis, John 21, 25, 29-34
 Mentle, Robert E. 267, 269
 Meyer, Paul G. 7, 9
 Middle-Ear
 See Ear
 Migliuolo, Stefano 167, 181
 Miller, Debra 61
 MIT Lincoln Laboratory 74, 78, 79, 207, 241, 282
 MIT Microsystems Technology Laboratories 265
 MIT Plasma Fusion Center 167
 MIT Submicron Structures Laboratory 7, 31
 MIT-Woods Hole Joint Program 249, 250
 Mochrie, Simon G.J. 125-126
 Moel, Alberto 7
 Molecular Physics 157

Molter Orr, Lynne A. 74
 Monson, Eric 61
 Monta, Peter A. 257, 261
 Moores, John D. 73
 Morgenthaler, Ann W. 73, 86
 MOSFETs 123
 Motorola 257
 Muendel, Martin H. 73, 86, 88, 94
 Multiple Sclerosis 331
 Munguia, Pablo 7
 Murguia, James E. 29, 30, 31
 Musicus, Bruce R. 241, 243, 244, 246, 251, 275
 Musil, Christian R. 29, 30, 31

N

Nabors, Keith S. 275
 Nanto, Hidehito 47
 Nassi, Marco 167, 181
 National Aeronautics and Space Administration (NASA) 230
 Deep Space Net Program 230
 National Radio Astronomy Observatory 230
 National Synchrotron Light Source 111
 NBC 257
 Needels, Mark 115
 Nelson, Keith A. 41-45
 Nelson, Susan E. 275
 Netherlands Foundation for Radio Astronomy 230
 Netz, Roland 109, 110
 Neural Computation 295
 Neural Networks 249
 Neural Regeneration. 325
 Neurophysiology 295
 Neutron Scattering 157
 Nghiem, Son V. 197, 202, 208
 Noh, Do-Young 111
 Nonlinear Waves in Plasmas 169
 North, D. Keith 301
 Nuclear Magnetic Resonance
 Imaging 331
 Nuttall, William 111

O

Odoardi, Angela R. 47, 53, 61, 121
 Oldaker, Bruce G. 139, 149
 Olsen, James A. 247
 Oppenheim, Alan V. 241-252
 Optical Communication 53, 61, 75, 267-273
 Optical Physics 131

Optics 73–86, 103
See also Lasers
See also Optical Communication
 Femtosecond Pulses 82
 Guided-Wave 74, 75, 80, 272
 Nonlinear 103
 Orlando, Terry P. 7, 12, 13, 14
 O'Neill, Kevin 197

P

Paine, Scott 139, 146
 Palmer, Joyce E. 7, 21, 24
 Pang, Lily Y. 267, 271
 Pang, Xiao Dong 315, 321
 Park, Samuel L. 7, 10, 121
 Payton, Karen 315
 Peake, William T. 321–323
 Peng, Lung-Han 61, 66
 Perilli, Richard R. 61
 Perkell, Joseph S. 301
 Peterson, Kevin 247
 Peterson, Patrick M. 315
 Petro, Michael C. 225
 Phillips, Joel R. 275
 Phillips, Mary R. 62
 Photonics 131
 Picard, Rosalind W. 253, 255
 Pickett, Galen T. 109
 Piot, Julien 257, 261
 Plasma Physics 167, 194
 RF Heating 169
 Thermonuclear Plasmas 181
 Tokamaks 191
 Plotnik, Irving 7
 Poggio, Tomaso 275, 279, 282
 Poh, Soon Y. 197, 215, 218
 Popat, Ashok C. 257, 262
 Porkolab, Miklos 167, 189, 191–194
 Power, Matthew H. 315
 Prasad, Sheila 61
 Prasanna, G.N. Srinivasa 241, 246
 Pratt, Gill A. 296
 Preisig, James C. 225, 241, 249
 Prentiss, Mara G. 131
 Princeton University 225, 231
 Plasma Physics Laboratory 181, 186, 191
 Pritchard, David E. 17, 139, 148–155
 Production Engineering 234
 Prothero, Jeff 331
 Public Broadcasting System 257

Q

Quantum Optics 131, 139
 Quasi-Optical Communication 267
 Quek, Hui Meng 7, 21

R

Rabinowitz, William M. 315, 321
 Radar 212, 221, 267, 269, 271
 Radio Astronomy 225–235
 Very Long Baseline Interferometry (VLBI) 231
 Radio Telescopes
 Very Large Array (VLA) 231
 Raemer, Harold R. 197
 Rahmat, Khalid 275
 Rajan, Anita 301
 Ram, Abhay K. 167, 169
 Randolph, Mark A. 301
 Rankovic, Christine 315
 Rapoe, Andrew M. 115
 Ravicz, Michael E. 321
 Rediker, Robert H. 267, 271–273
 Reed, Charlotte M. 315
 Reichelt, Mark W. 275, 288
 Remote Sensing 202–221, 267
 Renn, Rebecca J. 315
 Richard, Michael D. 241, 249
 Richardson, John M. 241, 250
 Ringo, Carol Chapin 301
 Rittenhouse, George E. 59
 Ritter, Elizabeth Ann 338
 Ro, Jaesang 21, 25, 29, 31, 32
 Robotics 279
 Rosenkranz, Philip W. 225, 231, 233
 Rosowski, John J. 321, 323
 Ross, Susan M. 321
 Rouch, Jacques 157, 163
 Royter, Yakov 61, 63
 Rubenstein, Jay T. 321, 330

S

Salvucci, Elizabeth M. 111
 Sandford, Lorraine 301
 Savage, Kelly 197
 Sawin, Herbert H. 31, 68
 Schattenburg, Mark L. 7, 17
 Schneider, Bruce 315
 Schoenlein, Robert W. 73, 78, 82
 Schreiber, William F. 257–264
 Schroder, Kurt A. 167, 191

Schulberg, Michelle 35
 Schwonek, James P. 139, 146
 Sciutto, Giampiero 241, 253, 257
 Scott-Thomas, John H.F. 7, 10, 121
 Segal, Mordechai 251
 Seidel, Mark N. 275, 279
 Semiconductor Materials 41
 Chemical Beam Epitaxy 47
 Semiconductors 59, 82, 121, 123
 Surface Studies 35, 109, 111, 115, 125
 Sen, Aniruddha 301
 Sensory Communication 315-317
 Shahidi, Ghavam 7, 9
 Shahriar, M. Selim 131
 Shalvi, Ofir 252
 Shao, Michael 225
 Shapiro, Jeffrey H. 267-271
 Shapiro, Jerome M. 225
 Sharp, Julia 253, 257
 Shattuck-Hufnagel, Stephanie R. 301
 Sheen, David M. 197, 215, 218
 Shen, Paul 253
 Shepard, Mark I. 29, 30, 31
 Shepard, Scott R. 267
 Shepard, Stephen C. 47
 Shin, Robert T. 197, 202, 208, 212, 220
 Shinn-Cunningham, Barbara 315
 Siebert, William M. 321
 Sietsema, Brian Mark 339
 Signal Processing 61, 241-252, 253-256,
 257-264, 310, 311
 Silviera, Luis M. 275
 Singer, Andrew C. 241
 Singer, Richard 61, 64
 Slattery, Celia 21
 Smith, Daryl 64
 Smith, David A. 21
 Smith, Henry I. 7-20, 21, 23, 60, 121
 Smith, Stephen P. 131
 Smith, T.P. 14
 Snitzer, Elias 131
 Sodini, Charles G. 275, 279, 281, 282
 Sonar 245, 250
 Song, William S. 241
 Sorokin, Victor N. 301
 Speech Communication 301-311, 315
 Speech Perception 301
 Speech Physiology 301, 309
 Speech Processing 241, 253-256
 Spectrograms 254
 Vocoders 253, 254, 255
 Speech Production 301
 Speech Recognition 249
 Speech Therapy 310
 Squire, Jared P. 167, 191

Srinivasan, Mandayam A. 315
 Staelin, David H. 225, 231-235
 Standley, David L. 275, 279, 282
 Stanton, Timothy 241, 250
 Stapedius 327
 Stefanov-Wagner, Frank J. 321
 Steffens, David A. 321
 Stephan, Deborah A. 315
 Stevens, Kenneth N. 301-311
 Stoner, Richard E. 167
 Stuart, Howard R. 225, 232, 234
 Su, Lisa 7, 9
 Sugiyama, Linda E. 167, 181
 Sulter, Arend 301
 Sun, Ke-Xun 139, 153
 Sundsten, John 331
 Superconductors 59
 Supramolecular Solutions 157
 Suzuki, Noriko 301
 Svirsky, Mario A. 301

T

Tabei, Makoto 241, 250
 Tamir, Tali J. 315
 Tan, Hong Z. 315
 Tao, Tao 29, 33
 Tarnow, Eugen G. 115
 Tartaglia, Piero 157, 163
 Tassoudji, Mohammad A. 197, 212, 220
 Tauber, Daniel 73
 Tauber, Kaushik 86
 Tektronix 257
 Tel-Aviv University, Department of Electronic
 Systems 251
 Television
 Research 257-264
 Telichevsky, Ricardo 275
 The, Siang-Chun 7, 9
 Thermonuclear Plasmas 181
 Thin Films 21, 111
 Thompson, Carl V. 7, 18, 21-28, 31, 32, 66
 Tom, Adam S. 257, 263
 Towe, Elias D. 61, 65
 Trehan, Veena 301
 Troxel, Donald E. 265-266
 Tsai, Flora S. 7, 9
 Tsui, Dan 14
 Tsuk, Michael J. 197, 215, 218
 Tu, King-N. 21, 24
 Tulintseff, Ann N. 197, 215, 218
 Turchette, Quentin 139, 149

U

Uchanski, Rosalie M. 315
 Ulman, Morrison 73, 78, 82
 Umminger, Christopher B. 275, 279, 282
 Underwater Acoustics 241
 Underwater Sound
 Dolphins 234
 University of Texas, Linguistics Department 311
 University of Washington 331
 U.S. Department of Energy 88
 U.S. Geological Survey 245
 U.S.S.R. Institute for Space Research
 RADIOASTRON Mission 230

V

Vacher, Sylvette R. 321, 327
 Van Aelten, Filip 275
 Versator II 191
 Very Long Baseline Array (VLBA) 230
 Veysoglu, Murat E. 197, 220
 Villasenor, Jesus N.S. 167, 191
 Vlcek, James 61, 62, 63
 VLSI 279
 See also Integrated Circuits

W

Wagner, Alfred 29, 32
 Walrod, David B. 103
 Wang, Bing 267
 Wang, Jing 115
 Wang, Jyhpyng 73, 78, 83
 Wang, Katherine S. 253, 255
 Wang, Li-Fang 197, 220
 Weather Satellites 231
 Webster, Jane W. 301
 Webster, Robert C., Jr. 296
 Wei, Xiu-Bing 157
 Weiner, Andrew M. 41, 45
 Weinstein, Bern'e A. 64
 Weinstein, Ehud 241, 243, 244, 251, 252
 Weiss, Thomas F. 321-333
 Welch, George R. 139, 143
 White, Jacob 275, 288-293
 Wiederrecht, Gary P. 41
 Wilde, Lorin F. 301
 Wind, Shalom 121
 Wolff, Peter A. 103-105
 Wong, Ngai C. 267
 Wong, Vincent 7

Woo, Peter 167
 Woods Hole Oceanographic Institution 241, 245,
 249, 250
 Wornell, Gregory W. 241, 252
 Wurtele, Jonathan S. 167
 Wyatt, John L., Jr. 275, 279-283

X

X-Ray Detectors 96
 X-Ray Lithography 7-9
 X-ray Scattering 157
 X-Ray Spectroscopy 8, 17
 Xia, Jiging 197, 215
 Xiao, Min 139, 153
 Xu, Kongyi 167
 Xue, Ziling 29, 33

Y

Yamasaki, Tsuneki 197
 Yang, Qingyun 35, 36, 37, 38, 39
 Yang, Woodward 275, 279, 282
 Yang, Ying-Ching E. 197, 212, 215, 218, 220
 Yen, Anthony 7, 12, 13, 14
 Yim, Derrick 315
 Yokoyama, Hiroyuki 73, 77
 Yu, Jenny S. 315, 321, 326
 Yu, Peter T. 267
 Yueh, Herng A. 197, 202, 212

Z

Zamani, Susan 29
 Zangi, Kambiz C. 257, 264
 Zarinetchi, Farhad 131
 Zenith 257
 Zirkind, Naomi E. 267, 269
 Zissman, Marc A. 315
 Zolla, Howard 7, 21
 Zue, Victor W. 301, 315
 Zurek, Patrick M. 315
 Z;sett, Beat 73